Muscle physiology instrumentation

Whitlock, T. L.

Award date:
1990

Awarding institution:
University of Bath

Muscle Physiology Instrumentation

Submitted by
T. L. Whitlock M. Eng.
For the degree of
Doctor of Philosophy
of the
University of Bath
1990

T L Whitlock March 1990

ProQuest LLC
789 East Eisenhower Parkway
P.O. Box 1346
Ann Arbor, MI 48106-1346

Summary

The investigations described in this thesis are concerned with the development of muscle physiology instrumentation. The primary aim has been the development of surface sensors capable of providing feedback information suitable for closed loop control of muscle stimulators. These stimulators will be used for the restoration of muscle function to mid- and low-thoracic paraplegics.

The majority of the work has been concerned with electromyograms and a detailed discussion of the detection of these signals from the muscle surface is presented. It includes a review of a number of previous attempts to eradicate the stimulus artefacts. The investigation has led to the development of techniques for recording and analysing muscle Compound Action Potential trains evoked by stimulation systems. These are currently being developed by Bath University jointly with Odstock Hospital, Salisbury.

An initial analysis system based on a 68000 microcomputer and 'standard' instrumentation pre-amplifiers is presented. The analysis is achieved using Fast Fourier and Fast Hartley transforms. The system makes use of software filtering techniques to reduce the effect of the stimulus artefact distortion; the parameters that are monitored are the median frequency and total power. The system is shown to be slow but able to show some changes in the median and power signals with time. The major causes of the stimulus distortion are shown to be the stimulator and pre-amplifier combination.

An improved analysis system with new stimulator designs is then presented which uses a hardware technique to reliably detect CAP signals with minimum distortion whilst stimulating. The improved system makes use of a TMS320C25 digital signal processing card running in parallel with the 68000 system, in order to carry out the time to frequency transform and thus speeding the frequency analysis of the sampled CAP trains. The system is shown to be capable of detecting and analysing CAP trains. The parameters currently being derived from the signals detected using surface techniques, however are not suitable for feedback control.

The appendices describe the development of a strength-duration tester based on the designs reported in the main thesis. The discussion of twitch detection techniques concludes that the only method currently capable of detecting muscle twitches over the full pulse width range of the strength duration test is an accelerometer. A design

using this technique is presented and is shown to function successfully but with some system limitations.

Two designs for muscle fatigue monitoring are also presented with a review of previous muscle fatigue monitors reported in the literature. Both make use of the detection of the median frequency from voluntary muscle contractions. One system is based on analogue techniques and the other on digital techniques. Comprehensive tests of the analogue monitor are presented to show its effectiveness as a fatigue monitor in voluntary muscle contractions.

The thesis concludes with some suggestions for further work to improve the CAP analysis system so that it can be used to identify parameters that may be suitable as feedback signals when using surface detection. Suggestions as to how the various pieces of equipment described may be improved and made to conform to the required medical equipment standards are also presented and their possible uses are reviewed.

Table of Contents

Muscle Signals

Recording Muscle Responses

List of Principal Symbols

ACIA Asynchronous Communications Interface Adapter

ADC Analogue to Digital Converter

Ag Silver

AgCl Silver Chloride

AGC Automatic Gain Control

AP Action Potential

AR Autoregressive Model

ARIMA Autoregressive Integrated Moving Average Model

ARMA Autoregressive Moving Average

BIOS Basic Input Output System

$\chi(v)$ Amplitude scaling of SFAPs

C_1, C_2 Concentration of ions

$cas(2\pi ft)$ Short form of $\cos(2\pi ft) + \sin(2\pi ft)$

CAP Compound Action Potential

Cl^- Chlorine ion

CNS Central Nervous System

CR ASCII Carriage Return Character `13 decimal 0D hex.`

CTS Clear to Send

CV Conduction Velocity

$\delta_i(t)$ Dirac pulses

DAC Digital to Analogue Converter

DARMA Deterministic Autoregressive Moving Average

DMA Direct Memory Access

DSP Digital Signal Processor

E Electrode Voltage

e^- Electrons

ECG Electrocardio–gram –graph

EEG Electroencephalo–gram –graph

EMG Electromyogram

F Faraday Constant

f_1, f_2 Activity of coefficient of ions

f_{mean} Mean Frequency value

f_{med} Median Frequency value

$f_o(t,v)$ Extra Cellular reference SFAP waveshape

$F(f)$ Fourier Transform of a real function of time

FES Functional Electrical Stimulation

FFT Fast Fourier Transform

FHT Fast Hartley Transform

FNS Functional Neuromuscular Stimulation

GEM Graphics Environment Manager™

$h_i(t)$ 'Black Box' filters

H^+ Hydrogen ion

$H(f)$ Hartley Transform of a real function of time

H_2O Water

HPGL Hewlett Packard Graphics Language—as used by their range of plotters

ICU Intensive Care Unit

I^2C, **IIC, I2C** Inter-Integrated Circuit Bus

IPI Inter Pulse Interval

K^+ Potassium ion

$\lambda(t,F)$ Firing rate as a function of Time and Force

LCD Liquid Crystal Display

LED Light Emitting Diode

$\mu_{\bar{x}}$ Sample mean

MA Moving Average Model

ME, MES Myoelectric Signal

MF Median Frequency

MFM Muscle Fatigue Monitor

MU Motor Unit

MUAP Motor Unit Action Potential

MUAPT Motor Unit Action Potential Train

MVC Maximum Voluntary Contraction

Na^+ Sodium ion

O_2 Oxygen

OH^- Hydroxyl ion

$\varphi_e(t,v)$ SFAP for a fibre with propagation velocity v

$P_s(f)$ Power Spectra

PAL Programmable Array Logic

PIT Parallel Interface/Timer

Pn.m Port n bit m

Q_n Quartile n where n = 1 to 4

$R(\omega,d)$ Electrode filtering

R Gas Constant

RMS Root Mean Square

RTS Ready To Send

RUH Royal United Hospital, Bath

σ_x^2 Variance of the Population

$\sigma_{\bar{x}}$ Sample Standard Deviation

$S_m(f)$ Power density spectrum of EMG signal

$S_{\mathrm{m}}(\omega)$ Power density spectrum of EMG signal m(t)

$S_{\mathrm{u_i}}(\omega)$ Power density of MUAPT $u_{\mathrm{i}}(t)$

$S_{\mathrm{u_iu_j}}(\omega)$ Cross-power density spectrum of MUAPTs $u_{\mathrm{i}}(t)$ and $u_{\mathrm{j}}(t)$

T Absolute temperature kelvin

SEMG Surface Electromyogram

SFAP Single Fibre Action Potential

S/H Sample and Hold

SNR Signal to Noise Ratio

$\rho_x(x,t,F)$ Probability distribution function of the IPI histogram

$u_i(t)$ Random process of MUAPTs

$\omega(t,v)$ A weighting function, the effects of the volume conductor

Z Standardised Normal Random variable

Chapter 1

Introduction

In order to understand the engineering constraints placed on any system that is designed to monitor electrophysiological signals, it is necessary to have an understanding of the underlying anatomy and physiology involved. Here a brief introduction to the main principles involved in muscle movement is presented. The discussion is both in terms of the anatomical details that contribute to a muscle response and the physiological events that take place. Many of the common medical terms are introduced and the electrophysiological actions of long and short pulse muscle stimulation are summarised.

1.1 History

The history of Neurophysiology dates back to November 1786 when Luigi Galvani[1], anatomist and teacher, was studying the discharge of a Leyden jar. One of his pupils, dissecting a frog, noticed that every time the Leyden jar discharged sparks the frog twitched. He published his findings in 1791 in his monograph *De Electricitatis in Motu Musculari Commentarius*, in which he suggested that an inherent electricity exists in living tissue. Alessandro Volta[2] questioned Galvani's findings by proving that dissimilar metals in contact with an electrolyte—such as those present in body tissues—would generate an electric current.

It was not until after the 1820s when the galvanometer made its appearance, that Carlo Matteucci[3] proved that electrical currents did originate in muscles. The findings of Matteucci attracted the interest of DuBois-Reymond[4] who realised that skin impedance reduced the current which could be detected. He proved this by blistering the skin, removing the blistered skin and then by using the open wounds as his contact points he measured the electrical currents. He found that his technique improved the current reading by a factor of twenty.

Measurements from human musculature remained unwieldy until the metal surface electrode was employed by the German Piper[5]. Indeed it was Piper in his classic text *Electrophysiologie Menschlicher Muskeln* of 1911 who first commented on the slowing of the electromyogram with fatigue.

> Wenn der Rhythmus der Innervation und der Muskelvorgänge von der Kraft und der Dauer der Kontraktion sich unabhängig erweisen hat, so läßt sich doch zeigen.....
>
> ..... Das Auffallendste ist, daß die Frequenz der Hauptwellen auf 35—25 pro Sekunde in großen Strecken der Kurve heruntergeht.*

* If the rhythms of the innervation processes in the muscle prove independent of the force and duration of the contraction you can concluyde that....the most striking feature is the frequency of the main waves goes down to 35-25 per second over the major part of the curve

With the arrival of the oscilloscope in the 1920s action potentials could readily be studied and Gasser and Erlanger[3] earned a Noble Prize in 1944 for their work on this subject.

The first electrical engineer to become involved in these studies was the Englishman Baines in 1918[3]. He was the first to formalise the analogy between the propagation of pulses in the nerve trunk and an electric cable. He also suggested the idea of modelling the body as parts of an electrical circuit.

Clinical use of this information really started in the 1930s when Proebster[4] successfully managed to detect a signal from dysfunctional muscle. With the introduction of the needle electrode and improvements brought about with vacuum tube amplifiers, neurophysiology was really born.

Further advances have seen improvements in the amplifier designs, with first transistors, and then integrated circuits. The advances haven't been confined solely to the electronics. The electrically stable silver-silver chloride electrode has removed much of the variation due to electrode potential changes, and the non-obtrusive inserted wire electrode which appeared in 1960 has allowed more precise recording of single fibre Action Potentials[3].

Subsequent use of various neurological signals to control prostheses, to check muscle and nerves in kinesiological studies and as feedback for stimulators brings the subject up to modern times.

1.2 Muscle Anatomy

In terms of size, the most extensively developed organ in the body is the musculature, the "flesh". The muscles make up 40 to 50% of the total body weight. Their main function is to develop force and to contract. They are also, among other things, important for the thermal regulation of the body.

The method of operation of the muscle cells is better known than that of most other cells. The morphology and the chemical components and reactions as well as the physiological functions of muscle cells have been extensively researched, and in recent years various approaches have produced a unified theory of muscle contraction.

1.2.1 Skeletal Muscle

The skeletal muscle is probably the most important part of the musculature. It is composed of thread like highly specialised cells called muscle fibres. These fibres are arranged lengthways in the muscle. The ends of the fibres fuse into tendons at the ends of the muscle. These tendons in turn are attached to bones articulated by at least one joint.

Muscle fibres are the basic contractile units of muscle. Each fibre receives a neural event known as an action potential, at a highly specialised region known as the motor endplate. This region is usually located towards the centre of the muscle[6]. Once activated by a single action potential, a twitch of contractile force is generated by the muscle and transmitted through the tendons.

A number of fibres are innervated by a single alpha motorneurone. Thus, these fibres do not fire independently but are controlled by the same neural command. The fibres and motorneurone comprise the basic functional unit of the muscle, the *motor unit (MU).*

The input to the unit is the neural command originating in the spinal cord. The output is a twitch of force transmitted through the tendons which is the resultant sum of all the twitches of the individual fibres.

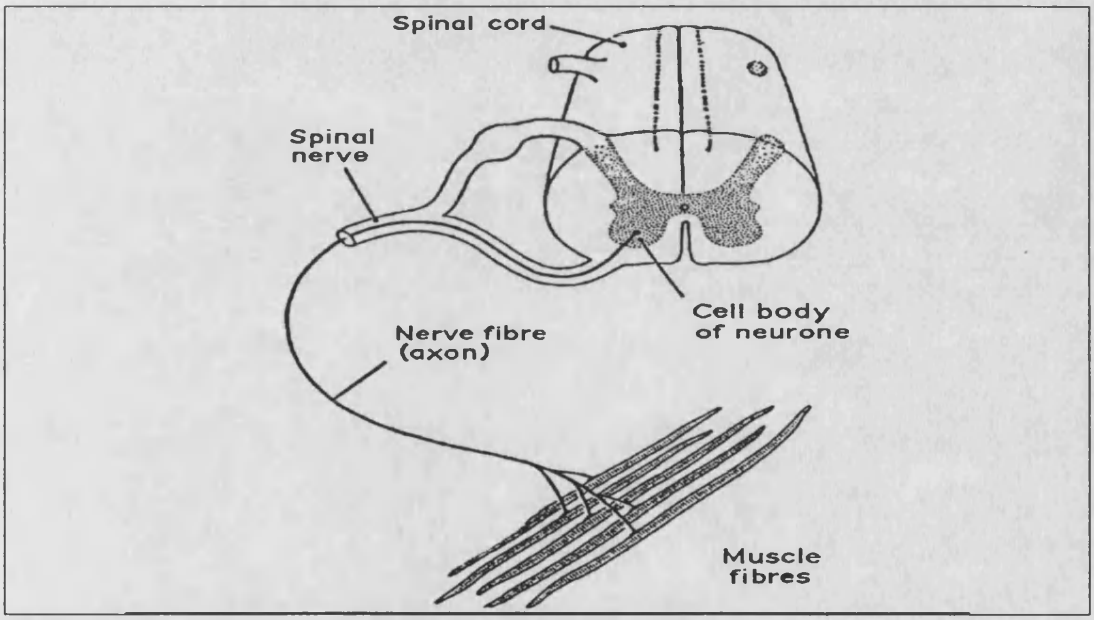

Figure 1.1 *Diagram of the Motor Unit*

1.2.2 The Motor Unit

Figure 1.1 shows a diagram of the basic muscle control loop. It consists of an axon (or nerve fibre) whose cell body is in the anterior horn of the spinal grey matter (spinal cord). The axon runs down the motor nerve to terminal branches which supply the muscle fibres. The number of fibres innervated by a single motorneurone varies greatly. It is generally accepted that the finer the control of the muscle, the fewer the number of muscle fibres. Ruedi[7] observed 2 to 3 fibres for the larynx and Bors[8] reported 5 to 6 for the human extraocular muscle. Both these muscles perform precise movements. In the large muscles which provide movement and strength, there may be thousands of fibres per motorneurone. Feinstein et al.[9] observed 2000 fibres per

motorneurone in the medial gastrocnemius. These fibres are innervated by the axon via a motor end-plate on each muscle fibre usually located near the middle of the fibre.

The fibres of a muscle are not clustered but are distributed randomly[10]. Buchthal et al.[11] determined that the fibres of a motor unit in the human biceps brachii are distributed over a circular region of about 5mm in diameter. They further suggested that this region may contain fibres belonging to 20 to 50 motor units. Milner-Brown and Stein[12] found that the motor units are distributed uniformly throughout the first dorsal interosseous muscle. The importance of this electrophysiologically is not the distribution, but that the fibres are intermingled.

Since all the fibres of one motor unit are controlled by a single axon, an impulse from the motorneurone will cause all the fibres to contract almost simultaneously. The delay between the fibres contracting has two main causes: the slight differences in the length and diameter of the axon branches innervating the individual fibres and the random delay of the discharge of acetylcholine packets released at the neuromuscular junction, as described in section 1.3.4. The branch delay is fixed but the chemical delay is a random function of time. This delay can be seen as jitter if the individual fibres are monitored. Each muscle will have a number of motor units which all fire independently. Each different motor unit will have fibres intermingled with other motor units within the muscle body.

1.2.3 Fibre Types

The muscle fibres of any one motor unit tend to display similar properties[13]. However within the muscle there tend to be two major types categorised by their appearance: the so called *Red* and *White* fibres. These two types also display differing properties. The red fibres when stimulated have a slower rising force twitch which is also longer lasting than that of a white fibre, ie red fibres are *slow twitch* and white fibres are *fast twitch*. They also differ in 'fatigueability'. Red fibres when repeatedly stimulated, generate the same peak tension in the twitch for a much longer time than white fibres which fatigue relatively quickly.

Many different measures of muscle fibres have also been found to be sensitive to fibre type. Not all of these are easily divisible between two groups[14] and there are some fibres that exhibit both red and white characteristics[15].

Motor units are often classified in terms of their fibre type with *slow twitch* and *fast twitch motor units* being common. Another possible description is *phasic* and *tonic motor units*, corresponding to fast and slow twitch motor units respectively.

It is however important to realise that different muscles have varying compositions of red and white fibres[16,17] depending on their function in the body. This obviously

will affect the signal produced by a given muscle when compared with that of a different muscle. Johnson et al.[16] observed that the muscles which are primarily used in *posture* are predominantly *red.* They also noted a high proportion of *white* in muscles performing quick *ballistic movements* such as in the eye where the orbicularis oculi contained over 80% white fibres.

1.3 Physiology

Movement is one of the essential characteristics of animal life. The muscles, in particular the skeletal muscle, generate the contractile force to accomplish this. Since the muscles can only provide a tension, they must work in *antagonistic pairs.* One muscle rotates the joint in one direction whilst the antagonist rotates the joint in the opposite direction. Usually in the human, one muscle does not act alone but in synergy with others, that is the *synergist* actively provides an additive contribution to a particular function during a contraction. The precise role of a muscle may change as the angle of the joint changes, thus over the entire range of motion, a single muscle may act as agonist, antagonist and synergist.

From this it is clear that the rotation of a single joint, such as the knee or elbow, results from the compound action of several muscles. To determine the percentage of force developed by individual muscles to obtain a desired motion, many assumptions must be made. This factor is particularly important when considering the control of stimulators for standing and walking systems, because not only must one consider which muscles are required, but also what level of stimulation is required during each stage of the stand or step.

The generation of the contractile force of an individual muscle is an equally complex process. As will be discussed in more detail in section 1.3.4, motor units produce a twitch in tension which is the sum of all the twitches of the muscle fibres which contribute to the motor unit. The total contractile force is the sum of all the twitch tensions of the active motor units. A continuous smooth contraction is the result of the repeated activation of the motor units. The twitches of the various motor units overlap, thereby summing spatially and temporally into a relatively smooth constant force.

The other prominent feature of muscle is the ability to grade contractile force. The graduation of tension is accomplished primarily by two mechanisms. One is the increase of the rate of stimulation of the active motor units which is referred to as *rate coding.* The other is to increase the number of active motor units which is known as *recruitment.* The neural control system uses both these processes[18]. The third possible method is synchronisation of concurrently active motor units.

Henneman[19] et al. reported that for decerebrate cats the order of recruitment is from smallest to largest motorneurones. This is known as the *size principle*, and many motor unit properties have been shown to depend on the size of the motorneurone. Henneman[20] and Olson suggested that the type of motor unit—red or white fibres—also depends on the size of the motorneurone. Milner-Brown et al.[21] have suggested that the motorneurones that are recruited last correspond to fast twitch motor units or white fibres. Grimby[22] and Hannerz along with other authors have suggested that during abrupt forceful contractions the fast twitch motor units are recruited first. This suggests the central nervous system adjusts the order of recruitment to match the task.

Recruitment is most significant at controlling low force levels[23]. Gydikov and Kosarov[24] presented evidence that very little recruitment occurs above 60% of the maximal voluntary contraction —MVC— of the biceps brachii. Clamann[25] did not find recruitment above 75% MVC in the same muscle.

In order to sustain a contraction the motor unit must be fired repeatedly. In normal muscle, the firings do not occur at equal intervals but at random intervals. The discharges are characterised by statistics of their interpulse intervals—IPI*—the most common statistic is that of the reciprocal of the average IPI which is referred to as the *firing rate.*

It is the change in firing rate which accounts for the increase in force at higher MVCs. Milner-Brown et al.[21,26] found in linearly-varying contractions of the first dorsal interosseous muscle, that when first recruited the firing rates were 8.4±1.3 pulses per second. The firing rates then increased by a factor of 1.4±0.6 pulses per second for each 100 grams increase in force. It was also found that the initial rate and the rate-force factor were independent of the force level at which they were recruited.

More recently LeFever et al.[27] have noted not only rate coding of motor units in linearly-varying contractions but also firing rate *modulation.* They noticed that with constant force contractions, the firing rate can achieve rapid changes to keep the force constant.

Up to now the contributions of individual motor units to contractile properties have been assumed independent, however, some investigators have presented evidence that at least some active motor units become synchronised during a contraction. That is, the firing rate of one motor unit is not statistically speaking independent of another.

* This term and abbreviation, adopted by the electromyographers, should not be confused with the same term and abbreviation used to describe muscle stimulator parameters. For a muscle stimulator, interpulse interval refers to the time between the stimulus pulses.

The presence of this synchronisation may increase or decrease the level of the myoelectrical signal[28].

Increased synchronisation has also been suggested as the cause of physiological tremor which occurs near the end of a sustained contraction in normal muscle and also the accentuated tremor associated with diseased muscle.

1.4 Electrophysiology of Muscle and Nerve

A full account of the electrical and chemical processes involved in the contraction of a muscle is beyond the scope of this report. However a brief account of how an action potential is generated and propagates down a nerve axon to the neuromuscular junction and along each muscle fibre will be given. The nature and ionic basis of the electrical activity of striated muscle fibres are qualitatively similar to that of nerve cells. The following description, therefore may be applied to both cell types.

1.4.1 The Resting Membrane Potential

The inside of a muscle or nerve cell is electrically negative with respect to its exterior. This potential difference is known as the *resting membrane potential* or *resting potential*, and is of the order of –90 mV for striated muscle cells and –70 mV for lower motor neurones; the sign indicates the polarity of the inside of the cell with respect to the outside. This potential is due to the differences in ionic concentration that exist across the cell membrane.

The cell membrane separates the intracellular and interstitial fluid, each of which contains ions. These two fluids are in osmotic equilibrium with each other, that is, in each fluid the total number of anions and cations is equal, so both fluids are electrically neutral. However the distribution of ions between the two solutions is unequal. The intracellular fluid has a relatively high concentration of potassium ions (K^+) ions and the concentration of sodium chloride (Na^+Cl^-) is relatively low when compared with the concentration of these ions outside the cell membrane. This membrane readily allows K^+ and Cl^- ions to pass through but blocks the passage of Na^+into the cell. The effect of the membrane is to leave the outside of the membrane, as described above, with a higher concentration of sodium ions. To try and counteract the effects of this external positive charge, positively charged potassium ions enter the cell. However they will never match the external positive charge leaving the potential difference, described above, due to the potassium ion imbalance.

A cell that is in this state of equilibrium, which it maintains until some kind of disturbance upsets it, is said to be *polarised.* It should be noted that the cell membrane has the electrical characteristics of a capacitor which is believed to contribute to its overall biophysical properties[29].

1.4.2 The Action Potential

When a section of the cell membrane is excited by the flow of an ionic current or by some form of externally applied energy, the membrane characteristics change and it begins to allow Na^+ ions to enter. This movement of Na^+ ions into the cell is an ionic current flow which further reduces the barrier to Na^+ ions. The effect of this is an avalanche of Na^+ ions rushing into the cell. At the same time the K^+ ions, which are in a higher concentration inside the cell, try to leave, but do so more slowly than the Na^+ ions rush in. The net result is that the inside of the cell becomes slightly positive with respect to the outside of the cell due to the imbalance of potassium ions. This potential is known as the *Action Potential* and is of the order of +20 mV. A cell that has been excited and displays an action potential is said to be *depolarised*; and the process of changing from the resting state to the action potential is called *depolarisation.*

When the influx of Na^+ions through the cell membrane ceases, that is a new state of equilibrium has been reached, the ionic currents that lowered the barrier to sodium ions are no longer present and the membrane returns to its selectively permeable state, blocking the passage of Na^+ions from the outside into the cell. As a result of this a high concentration of Na^+ions is trapped in the cell which would prevent, or slow considerably, the returning of the cell to its resting potential. By an active process known as the *Sodium Pump*, the sodium ions are quickly transported to the outside of the cell, and the cell again becomes *polarised* and assumes its *resting potential.* The exact chemical process of the sodium pump is not known, however it is known that the rate of pumping is directly proportional to the concentration of Na^+ ions in the cell.

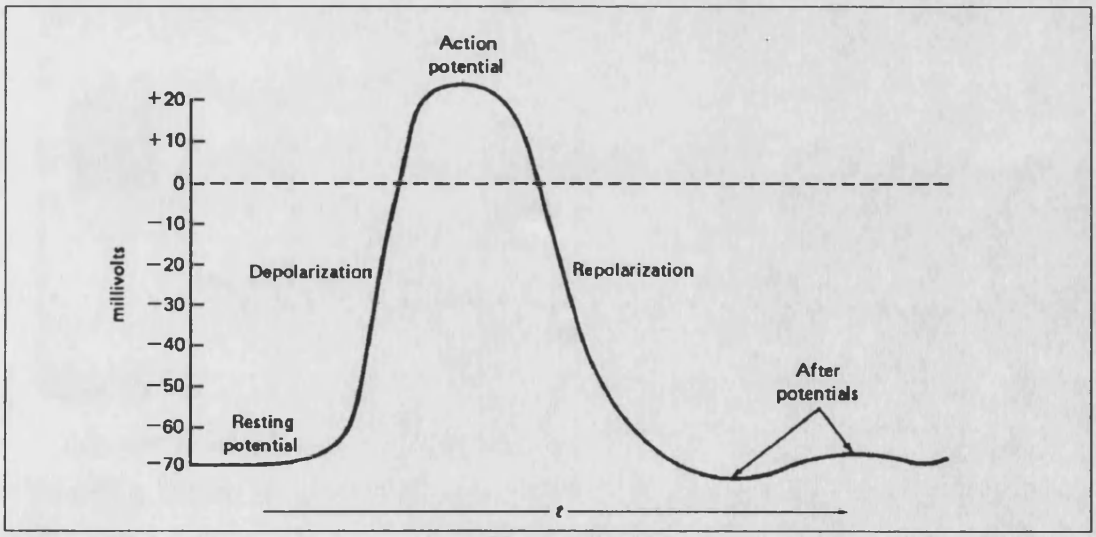

Figure 1.2 *Typical Action Potential*

Figure 1.2 shows a typical action potential beginning at its resting potential, depolarising and returning to its resting potential, after repolarising. The time scale is

dependent on the type of cell producing the action potential. In nerve and muscle the repolarisation occurs so rapidly that the action potential appears as a spike of as little as 1 ms in width. Heart muscle is much slower in repolarising giving action potentials of 150 to 300 ms in width making them more easily detected.

For any given cell regardless of the method by which it was excited, or the intensity of the stimulus—provided it is sufficient to activate the cell—the action potential is always the same. This is known as the *All-or-Nothing Law.*

Following the generation of an action potential there is a short period of time during which the cell cannot respond to any stimulus. This is known as the *absolute refractory period.* This period is about 1 ms in nerve cells. After the absolute refractory period there occurs a *relative refractory period* during which another action potential can be triggered, but a much stronger stimulation is required. In nerve cells this period lasts for several milliseconds and is believed to be due to after potentials that follow the action potential.

1.4.3 Propagation of Action Potentials

When a cell generates an action potential ionic currents begin to flow. These currents can, in turn, excite neighbouring cells or adjacent areas of the same cell. In the case of a nerve with a long fibre the action potential is generated over a small segment of the fibres length but is propagated in both directions from the original point of excitation. As the action potential travels down the fibre, it cannot re-excite the portion of fibre that it has just propagated from, because of the refractory period that follows the action potential. Figure 1.3 gives a schematic charge diagram of the action potential flow along a nerve fibre.

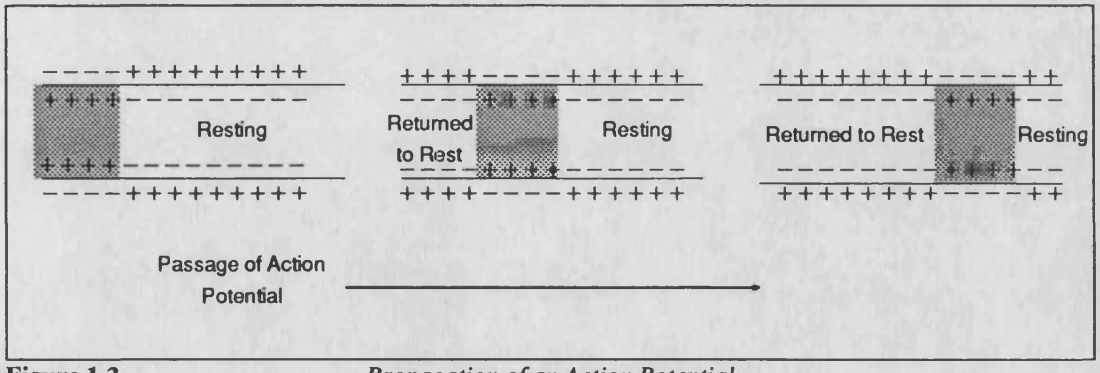

Figure 1.3 *Propagation of an Action Potential*

The rate at which an action potential moves down a fibre or is propagated from cell to cell is known as the *propagation rate.* In nerve fibres the propagation rate is called the *nerve conduction rate* or *conduction velocity* . Its value is correlated to several of the nerves morphological features. The conduction velocity is directly related to the diameter and is inversely related to the internal electrical resistance of the fibre, with

the conduction velocity increasing as electrical resistance reduces. Myelinated fibres conduct faster than unmyelinated fibres because the local current circuits are confined to regions some distance ahead. The usual velocity range for a nerve is from 20 to 140 m/s.

1.4.4 Motor Unit Action Potential

The term Motor Unit Action Potential is used to describe the electrical signal generated by a Motor Unit. When a nerve impulse arrives at the motor end-plate the electrical disturbance leads to the release of a neurotransmitter- acetylcholine. This quickly diffuses across the synapse where it binds to receptors in the muscle fibre membrane and opens channels in that membrane. The muscle fibre like any neurone tries to maintain its intracellular environment at a potential of 80—90mV negative with respect to its surroundings. The effect of the acetylcholine is to reduce this potential (depolarisation). This depolarisation propagates in both directions along the fibre. It is this depolarisation accompanied by a movement of ions, which causes the contraction, that generates an electromagnetic field in the vicinity of the fibres. A recording electrode in this field would detect the potential with respect to ground whose time excursion is known as the action potential.

In order to sustain a muscle contraction the motor units must be repeatedly activated. The resultant sequence of MUAPs is known as a Motor Unit Action Potential Train (MUAPT). The repetition rate of the action potentials is random and controlled by the spinal grey matter. The shape of the MUAPs within a MUAPT will remain constant only if the geometric relationship between the electrodes and active muscle fibres remains constant, if the properties of the recording electrode do not change and if there are no significant biochemical changes in the muscle tissue.

Clearly when a muscle is contracted a number of Motor Units are activated each by its own unrelated train of pulses so that the surface EMG is in fact the spatial and temporal summation of a number of MUAPTs. This is why the typical EMG muscle response looks like a random noise signal.

1.5 Types of Muscle Contraction

There are a number of different types of muscle contraction that are associated with skeletal muscle. The particular type of contraction the muscle performs usually depends on the stimulus.

1.5.1 Twitch

The *Twitch Contraction* is a rapid, jerky response to a single stimulus. It is these types of contractions, usually artificially induced, that are used to study muscle responses. A recording of the twitch contraction is the usual way to illustrate the different phases of

a single contraction. Figure 1.4 is a graph of such a contraction. This type of recording is often referred to as a ***myogram*** and should be distinguished from an electromyogram.

Figure 1.4 shows that there is a brief period between the application of the stimulus and the beginning of the contraction; the *latent period*, which usually lasts about 10 milliseconds. The second phase, the *contraction period*, lasts about 40 milliseconds. The last phase is the relaxation period and usually lasts around 50 milliseconds. The duration and exact shape of these responses depends on the muscle and where it is situated. In the eye the latent and relaxation periods are very short. In the leg muscles the periods are much longer.

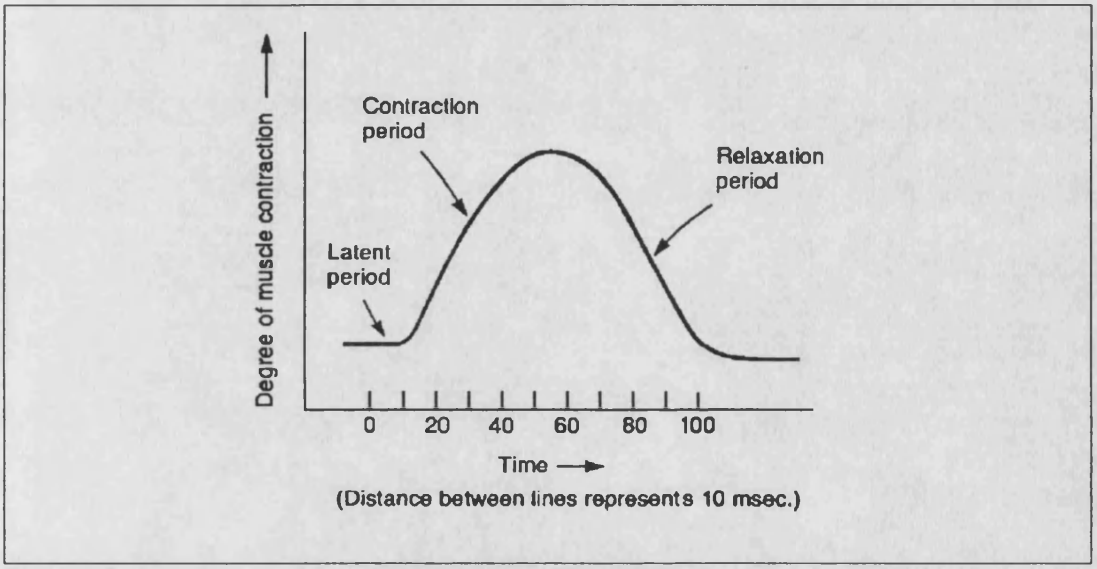

Figure 1.4 *Myogram of a Twitch Contraction*

If two stimuli are applied one immediately after the other, the muscle will respond to the first stimulus but not the second. This is because the muscle temporarily loses its irritability after the first contraction and cannot respond again until it is regained. This period is known as the *refractory period*. Its duration is also muscle dependent.

1.5.2 Treppe

The *Treppe contraction* is the condition when the muscle contracts more forcefully in response to the same strength of stimulus. It is usually demonstrated by stimulating an isolated muscle with a series of *threshold* or *liminal* stimuli. Figure 1.5 shows the myogram for the muscle of a frog stimulated at 2 Hz. Here the first few responses show treppe contractions. It is the principle athletes use in warming up. After the first few stimuli the muscle reaches its peak of performance and undergoes its strongest contractions.

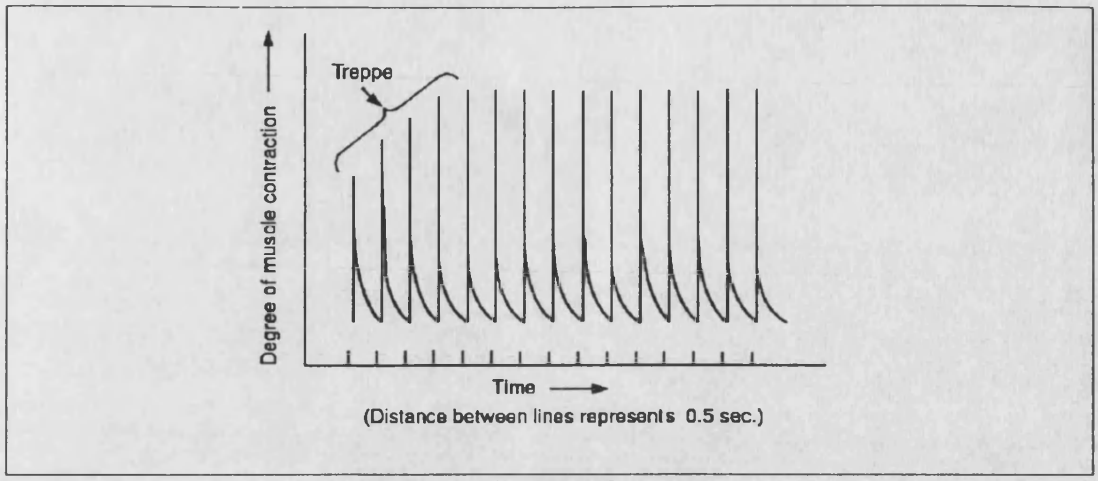

Figure 1.5 *Myogram of a Treppe Contraction*

1.5.3 Tetanic

When two stimuli are applied and the second is delayed until the refractory period is over, the skeletal muscle will respond to both stimuli. In fact, if the second stimulus is applied after the refractory period but before the muscle has finished contracting, the second contraction will be stronger than the first. This effect is known as *summation of twitches* or *wave summation* and is shown in Figure 1.6.

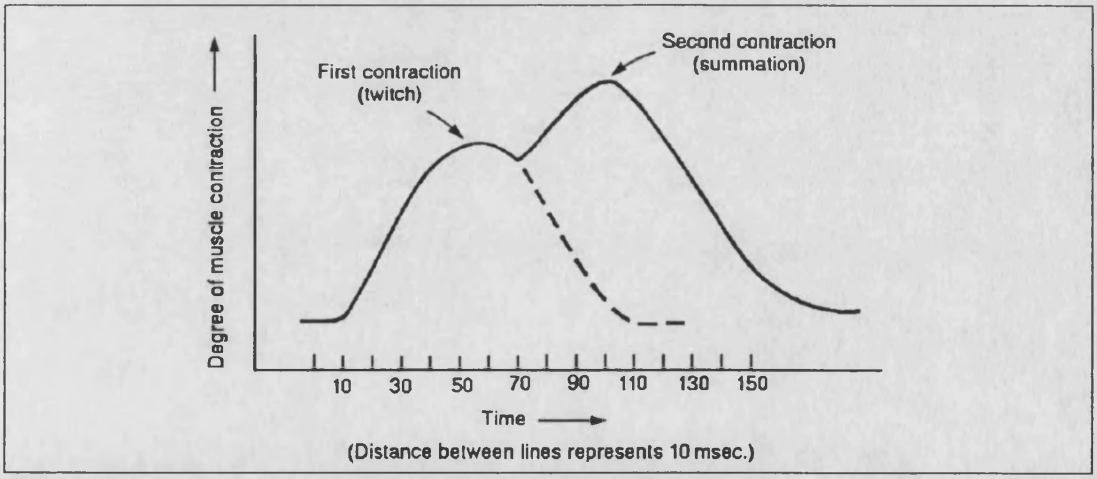

Figure 1.6 *Myogram of Summation of Twitches*

In frog muscle a stimulus of 20 to 30 stimuli per second permits the muscle to partly relax. This results in the muscle maintaining a sustained contraction known as an *incomplete tetanus* Figure 1.7a. Increasing the stimulus rate to 35 to 50 stimuli per second results in *complete tetanus*, a sustained contraction which lacks even partial relaxation Figure 1.7b. Voluntary contractions, such as contraction of the biceps to flex the forearm are tetanic contractions. Tetanic contractions are one of the requirements to successfully stand a paraplegic patient. It has been found that a stimulus of 20 to 30 pulses per second gives a good tetanic contraction with most paraplegics. The exact frequency is usually patient dependent, with some patients requiring a lower frequency to permit better recruitment control.

1.5.4 Tonic (Tonus)

A sustained partial contraction of portions of a skeletal muscle in response to stretch receptors is called a *tonic contraction (tonus).* At any given time normal muscle contains some cells that are contracted and others that are relaxed. This contraction tightens a muscle, but not enough fibres are contracting to produce movement. The same group of motor units does not function continuously. Instead, there is asynchronous firing of alternating motor units that relieve one another so smoothly that the contraction can be sustained for long periods. Tone is essential for the maintenance of posture.

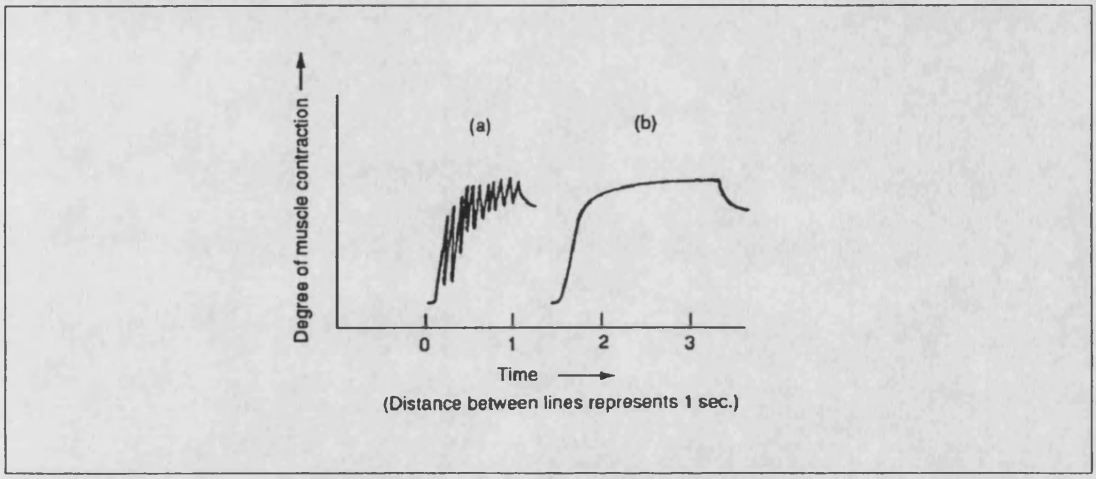

Figure 1.7 *Myograms of (a) incomplete (b) complete Tetanus*

In paraplegics and patients with various diseases of the nerve there is a loss of tone because the 'tone' impulses do not get through to the muscle. The term that is applied to such muscle is *flaccid.* If this occurs for a long period, as is the case with paraplegics, the muscle progresses from flaccidity to *atrophy*, a state of wasting away. One of the major benefits that paraplegics have found with regular use of muscle stimulation has been an improvement in tone and a reduction of flaccidity/atrophy. It is because of this effect that the subjects taking part in the standing and walking programme, are required to do considerable exercise stimulation, to re-build their muscle bulk so that they can once again use their muscles functionally before standing and walking with FES.

1.5.5 Isotonic and Isometric

Isotonic (iso =equal; tonos = tension) *contractions* are ones in which the muscle shortens and pulls on another structure, such as a bone, to produce movement. During such a contraction the tension remains constant and energy is expended.

In an *Isometric Contraction*, there is minimal shortening of the muscle. That is the muscle remains almost the same length but the *tension* greatly increases. An example of an isometric contraction would be to carry an object with the arm extended. The

weight of the object pulls the arm down, stretching the shoulder and arm muscles. The isometric contraction of the shoulder and arm muscles counteracts the stretch force.

1.6 Stimulation of Muscle

Stimulating muscles by use of an external electrical impulse of voltage—or current—has many uses within medicine. In particular it is being used to try and restore standing and walking function to paraplegics who no longer have any voluntary control in their legs. Another area where muscle stimulation is used is in the diagnostic technique known as the strength-duration test. A full discussion of the strength-duration test is presented in Appendix A, where the development of an automated strength-duration tester is described.

1.6.1 Electrical Stimulation of Nerves

A nerve impulse may be initiated by an electrical stimulus[30]. In order to achieve this a current of sufficient intensity must be applied. The cell membrane of the fibre forms a series resistance with the other tissues so there is a potential difference across it as the current flows. The surface of the membrane closest to the cathode becomes negative with respect to the opposite surface. On the side of the nerve nearest the anode this increases the resting potential across the membrane, but on the side nearer the cathode the effect is to reduce the resting potential. If the resting potential falls below the level at which the membrane becomes permeable to the Na^+ ions, the ions enter the axon causing an ionic current which further increases the permeability, as described in section 1.4.2, and an action potential is initiated.

The impulse is initiated if the potential difference falls sufficiently across *any* part of the cell membrane of the nerve. If the cathode is applied over a superficial nerve, the side of the nerve nearest to the cathode is activated, but the anode can equally well cause the initiation of a nerve impulse. In this case, it is the aspect of the nerve furthest from the anode that is activated. Since the current spreads out from the electrodes, the current density is less on the further surface of the nerve fibre than the nearer surface, thus the anode is less effective than the cathode is at initiating an impulse. This means that less current is required to produce a contraction of innervated muscle at the cathode than the anode.

Once an action potential has been initiated—more than one nerve will be activated if the current density is sufficiently great—it will travel down the nerve fibres to the motor endplates and the contraction of the innervated fibres occurs as in a normal voluntary contraction. The field strength required to cause the depolarisation will depend on a number of factors including electrical contact, nerve position and fibre

size. Usually voltages in the range 30 to 100 volts are sufficient and pulse widths in the range 100-300μs.

This type of muscle firing is clearly not the same as that described for voluntary muscle contractions. The regular firing rate is fixed by the pulse repetition rate of the stimulator and if the stimulus level is kept constant, the same fixed number of muscle fibres contract with each stimulus pulse. This does not mean however that muscle signals are not present, since clearly if the muscle contracts, it must generate electromagnetic fields due to the depolarisation wave. What it does mean is that the MUs are synchronised to fire almost simultaneously. This means that instead of picking up the result of a large number of MUAPTs added together, one single train is picked up. This is often referred to as the *Compound Action Potential or M Wave.*

1.6.2 Accommodation

When a constant current flows, the nerve adapts itself to the altered conditions, this effect is known as *accommodation.* As a consequence a constant current is not effective in initiating a muscle response.

When the current rises, a response is initiated, similarly a fall in current can initiate a response. While the current is constant, accommodation of the nerve takes place and the potential difference across the nerve no longer affects the excitability of the nerve fibre, which adapts itself to the altered conditions. When the constant current ceases, the potential difference which was altering the potential difference across the plasma membrane suddenly disappears. The potential difference during the accommodation period augments the resting membrane potential, its sudden loss causes a fall in resting potential. If this falls below the level at which the membrane is permeable to sodium ions, a response is initiated. A fall in current is not as effective as a rise in initiating a response.

The effects of accommodation mean that if the rise time of the stimulating impulse is too slow, a response is never initiated, since the nerve just accommodates. This sets finite limits on the rise time for stimulus pulses to initiate a response, with a slower rise time requiring a greater current change.

1.6.3 Effects of Nerve Stimulation

When a nerve impulse is initiated at a nerve cell or an end organ, there is only one direction in which the action potential can travel along the axon. If the action potential is initiated at some point on the nerve fibre, it is transmitted in both directions from the point of stimulation.

When a *sensory* nerve is stimulated, the downward travelling action potential has no effect, but the upward travelling impulse is 'felt' when it reaches the conscious levels

of the brain. If impulses of constant level but varying pulse widths are applied, it is found that long pulses (>1ms) produce uncomfortable, stabbing sensations. Short pulses reduce this effect to a mild pricking sensation.

When a *motor* nerve is stimulated, the upward-travelling impulse is unable to pass the synapse, as it is travelling in the wrong direction. The downward travelling impulses pass to the muscle fibres innervated by the nerve, causing them to contract.

When a stimulus is applied to a motor nerve trunk, impulses pass to all the muscles that the nerve supplies below the point at which the stimulus is applied.

When the stimulus is applied directly over an *innervated* muscle, the nerve fibres are stimulated in the same way. The maximum response is obtained at the motor point, which is the point at which the main nerve enters the muscle.

1.6.4 Effects of Frequency of Stimulation

When a single stimulus is applied, the impulses pass simultaneously to a number of motor units so in normal circumstances there is a sudden twitch, followed by immediate relaxation. If the rate at which the stimulus is applied is increased there is no time for relaxation leading to a tetanic contraction.

1.6.5 Strength of Contraction

The strength of contraction depends on the *number of motor units* activated, which is dependent on the intensity of the stimulus, and the *rate of change of current.* If the intensity of the current rises suddenly, no accommodation can take place so a muscle contraction takes place. If the current rises more slowly, as with triangular, saw-tooth and trapezoidal impulses, some accommodation takes place and a greater intensity is required to produce a contraction.

1.7 Physiological Effects of Stimulation

The tissues of the body can conduct by virtue of the fact that the tissue fluids are ionic, that is contain ions. Consequently when a current flows there is a two-way migration of ions, and the conductivity of any given section of tissue is dependent on the amount of fluid they contain. Muscle, by virtue of its good blood supply, is a good conductor, whilst fat is a poor conductor. Current will flow through the path of least resistance. At the skin electrode contact there is a high resistance because the epidermis has a high resistance of about 1KΩ because it contains little fluid—this is discussed in greater detail in Chapter 4. The passage of currents and hence ions may result in chemical changes.

1.7.1 Stimulation of Sensory Nerves

Short pulse stimulation leads to a mild prickling sensation. This is due to the stimulation of the sensory nerves, and is not very marked because of the short duration of the pulses. The sensory stimulation can cause a reflex vasodilatation of the superficial blood vessels, so there is a slight reddening of the skin, *erythema.* It is usually confined to the superficial tissues, and is of little practical significance.

1.7.2 Stimulation of Motor Nerves

Short pulse or *faradic stimulation,* will stimulate the motor nerves and, if the current is of sufficient intensity, will cause a contraction in the muscles it innervates. If a tetanic stimulation is maintained for more than a short period, the muscle fatigues. The only way to overcome this is to increase the intensity such that further fibres are recruited.

1.7.3 Effects of Muscle Contraction

When a muscle is induced to contract by electrical stimulation, the changes that occur in the muscle are similar to those associated with voluntary contractions. There is an increased rate of metabolism, with the consequent increase in demand for oxygen and foodstuffs, and an increased output of waste products, including metabolites. The metabolites cause dilatation of capillaries and arterioles, and there is a considerable increase in the blood supply to the muscle.

As the muscles contract and relax they exert a pumping action on the veins and lymphatic vessels lying within and around them. The valves in these systems ensure that their contents can only flow towards the heart. If the muscle contracts sufficiently strongly to cause joint movement this also exerts a pumping effect. This leads to increased veinous and lymphatic return.

1.7.4 Stimulation of Denervated Muscle

The current required to produce contraction of denervated muscle is significantly greater than that for innervated muscle, with faradic type stimulation. The level is in fact too painful on subjects who still have sensory feeling to be of practical use.

1.7.5 Chemical Effects of Faradic-Type Current

When a direct current is passed through an electrolyte there is a net flow of ions to the electrodes where chemical changes can take place. There is a possibility of the formation of compounds which could cause electrolytic burns in contact with the tissue, though the short period of the pulses prevents a large build-up of chemicals. If the current alternates—biphasic pulses—the net flow of ions reverses so, if the two phases are equal no build up of chemicals occurs. If unequal phases are used there is a net build up but it is reduced.

1.8 Long Pulse Stimulation

In denervated muscle it is not possible to use the short pulse stimulation (<10ms) because this will only provide sufficient energy to stimulate motor nerves. In order to stimulate denervated muscle the muscle fibres themselves must be depolarised. Thus, if a pulse provides sufficient current intensity for a sufficient duration a contraction of denervated muscle can be initiated. The contractions and relaxations are slower than when the motor nerve is stimulated. Since denervated muscle tissue does not have the same property of accommodation as motor nerves, the rise time of the current is not critical when trying to elicit a contraction. Moreover, a slowly rising current can often produce a contraction in denervated muscle with a current that is insufficient to stimulate selectively the motor neurone. 100 ms is the usual pulse width used to ensure that all the denervated muscle fibres are stimulated; if shorter pulse widths are used some of the muscle fibres may fail to contract. It is sometimes necessary to lengthen the pulse width in order to eliminate contractions of innervated muscles or if the muscle has been denervated for some time.

When long pulse stimulation is used the *sensory nerves* are stimulated. The pulse widths are long so the effect is noticeable, giving a stabbing or burning sensation. There is usually reflex dilation of the superficial blood vessels and consequent erythema of the skin.

On innervated muscle the motor nerves can still be stimulated but no significant advantages are gained over short pulse stimulation. The strength-duration test described in Appendix A is one area where this phenomenon is used in order to assess the recovery of muscle lesions.

1.8.1 Effects of Long Pulse

When a muscle is deprived of its nerve supply, changes occur in its structure and properties. There is a marked wasting of the muscle fibres and if the degeneration is of long-standing they tend to become fibrossed and lose their properties of irritability, contractility, extensibility and elasticity. Electrical stimulation may slow this process down though no conclusive evidence has been published to support this.

1.9 Summary

The study of muscle physiology using only surface contact with the muscle significantly reduces the number and nature of the signals available for deriving information about the state of muscle.

The most frequently used signal for studying muscle physiology is the electromyogram (EMG) or myoelectric (ME) signal. This is the electrical

manifestation of the neuromuscular activation associated with a contracting muscle. It is a very complicated signal, which is affected both by the anatomical and physiological properties of muscles, the control scheme of the peripheral nervous system, as well as the characteristics of the recording instrumentation used to detect it. It is the detection and analysis of this signal, particularly whilst using chronic stimulation, that the bulk of this thesis is concerned with.

Chapters two and three discuss the published data on the analysis of EMGs with Chapter two describing the generation of EMG signals in terms of various models that have been reported in the literature. It considers not only the generation of the voluntary EMG signal but also the modelling of compound action potentials. Applications of the models are reviewed and their possible use in the work described in this thesis is discussed. Chapter three considers the natural feedback mechanisms of the muscle and then goes on to describe the parameters chosen by researchers in the literature to try and quantify muscle function in terms of force and fatigue. Throughout this chapter these parameters are discussed in the context of their application as feedback signals within closed loop standing and walking systems.

Chapter four concludes the introductory discussion by describing the various aspects of picking up and recording the EMG signals. This includes: models for stimulating and recording electrodes and body tissue, the effects of interference on the signal quality and maximisation of the signal to noise ratio. The discussion of interference focuses particularly on the effects of the stimulating voltage on the recording of Compound Action Potentials and suggests some ways of reducing the interference.

Chapter five describes the new stimulator designs that have been produced as part of the new stimulus artefact reduction system described in this thesis. It includes a description of the software written to control the stimulator and provide the necessary synchronistaion signals for the other hardware described in the subsequent chapters. Chapter six details the EMG pre-amplifier designs and isolation amplifier used to amplify the CAP action potentials and remove the stimulus artefacts. Chapter seven describes the new on-line realtime sampling system for closed loop control of FES that makes use of the artefact removal/suppression hardware. This includes both the hardware arrangements and the analysis and display software.

Chapter eight discusses various aspects of the setting up and calibration of the software and hardware and presents calibration graphs showing how effective and accurate the frequency analysis system is.

Chapter nine presents results from the original CAP analyser system and some results from the new improved version that uses hardware artefact suppression

techniques. It includes some results that show how the application of the system can be used to improve the systems ability to analyse CAP trains.

Chapter ten discusses the results presented in Chapter 9 and summarises the results of this research in the wider context of practical muscle physiology instrumentation.

Chapter eleven discusses the further work that could be done to improve the systems presented and suggests some new areas that may be opened up with a fully developed system.

Another recently revived muscle signal is the sound generated by the contracting muscle fibres. These sounds are normally inaudible because they are low frequencies, around 20 Hz, which is near the lower threshold of hearing. The sounds produced may easily be demonstrated in the following manner: place the thumbs gently over the ear openings so as to cover the ear canal; with the elbows raised make a fist. The sound perceived, which becomes louder the tighter the fist is made, resembles the rolling of distant thunder. This signal is discussed further in Appendix A where it is considered for use in an automated Strength-Duration Tester. The design of an automated strength-duration tester using an accelerometer is also presented along with some preliminary results that suggest the automation of the strength-duration test is feasible.

Appendix B discusses a number of muscle fatigue monitors that have been described in the literature in recent years. It then describes two stand alone muscle fatigue monitors aimed primarily at the monitoring of fatigue in voluntary muscle contractions by monitoring the change in the frequency content of the electromyogram. One system uses analogue techniques and the other digital techniques. Results are presented for the analogue system and a comparison with the digital version is made.

Appendix C presents a copy of a paper presented at the 7^{th} Congress of the International Society of Electrophysiological Kinesiology at Enschede in June 1988.

Appendix D gives a glossary of medical terms used in this thesis and within many of the papers referenced throughout this thesis.

Appendix E gives some anatomical diagrams of the major muscles in the arm and leg as a ready reference.

Appendix F contains photographs of the various pieces of equipment that have been designed and built as part of this project. They show views of the item and its front panel and where appropriate the internal circuitry.

Appendix G contains the circuit diagrams for the various pieces of equipment that have been designed. These, as with the photographs, are in the same order as the sections which describe them in the body of the report.

Chapter 2

EMG and Muscle Models

Much research effort has been directed towards the modelling of the body's electrophysiological signals such as the ECG, EEG and EMG. Of the many electrophysiological signals the EMG is probably one of the most complex. Not only is it non-stationary but when using surface detection techniques it is filtered by the body tissues which are an anisotropic and non-homogeneous medium.

The models that have been developed fall into a number of categories. Until recently the main use was in the control of artificial limbs[31, 32, 33, 34, 35] such as the Utah Arm[36]. More recently the identification of muscle parameters by models has been used to control muscle stimulators for patient controlled walking[37, 38, 39].

Another area where the model has been put to good use is in the understanding of the observed effects such as fatigue. Here the changes to parts of the models lead to an understanding of the physiological changes that may be occurring. Lindström[40] and others have produced comprehensive models that include the modelling of the detection system. These have helped to show how the information content of the signal may be altered by the detection technique. More recently the modelling of stimulated muscle and in particular the compound action potential has occurred[41, 42]. These not only aid in the understanding of the more deterministic stimulated muscle response but the so called Inverse Problem may lead to some new diagnostic techniques. The use of stimulated muscle models allows the optimal design of control strategies for closed loop FES systems[43].

This chapter is intended to give a brief overview of the types of model in use and their particular application and to detail the principle equations used in one of the most common stochastic type models used to simulate the various observed EMG features[3, 28, 44, 45, 46]. A brief review is given of some other types of model that have recently been reported in the literature. Finally the chapter concludes with a discussion of possible applications of the models in the work described in this thesis.

2.1 Types of Model

The models that have been used in EMG modelling fall into 3 main groups:

- The Autoregressive (AR), Moving Average (MA), Autoregressive Moving Average (ARMA) Autoregressive Integrated Moving Average (ARIMA) types now commonly used as signature discriminators for prosthetics control and more recently for stimulator control.

- The Volume Conductor types which have recently been used to model compound action potentials for the Inverse Problem—the analysis of a CAP in order to determine the active fibres involved.
- The stochastic model usually used to simulate EMG signals to improve understanding of surface and intracellular EMG. The model essentially generates action potential trains that are added to obtain interference EMG patterns.

2.1.1 Autoregressive and Moving Average Type Models

This type of modelling, that is AR, MA, ARMA and ARIMA, was originally used for signature discrimination in prosthetics control though now it is being considered as a means of monitoring fatigue in muscle by using some of the parameters of the model as the fatigue indicator[47]. Before the application of this type of model the prosthetics were controlled by an assessment of EMG signal strength which required some non-linear processing—such as rectifying—because the EMG signal does not contain zero frequency components[48, 49, 50]. Often this technique meant that a separate detection site was required for each degree of freedom required. Examples of these systems are the Utah-Arm and the Swedish arm[36]. This type of model also benefits from muscle crosstalk since the way a group of muscles contribute to the signal will help define more clearly the intended limb function.

The AR model expresses the value of a single measurement of an observed process or a discrete signal at any instant of time as a linearly weighted sum of its past values. The difference between that predicted by the model and the true value is called the residual error. That is, an AR model describes an all-pole filter driven by a white noise input and yielding an output equal to the values of the observed signal.

Moving average models differ from autoregressive ones in that they express the time series as the linearly weighted sum of a sequence of random shocks rather than as a linear combination of its past values. MA models specify an all-zero filter as defined by the MA parameters.

Mixed or differenced models ARMA and ARIMA contain both autoregressive and moving average terms, to remove certain nonstationarities from the process under study by taking repeated difference samples.

Time series modelling is a powerful tool for spectral estimates. All time series models of this type relate a stochastic input sequence to the output observations by a linear difference equation of past values of the signal or input.

Statistics of the surface EMG should dictate the form of the model which best describes the process under conditions simulating normal operation. The statistics of

surface EMG are much debated. Most researchers[51, 52, 53] have noted a certain amount of stationarity in the voluntary response though the degree has differed depending on quite which technique the author wishes to support. Essentially the EMG is nonstationary, thus the models above cannot be used except possibly the ARIMA which does take into account nonstationarity. Stationarity tests have been carried out by many researchers using the tests proposed by Bendat and Piersol[54, 55]. They have found quasi-stationarity or stationarity over short periods and have even found that if the patient is trained in the required muscle function the stationarity can be improved[36], that is, although the EMG signal may be globally nonstationary it may be locally stationary, or quasi-stationary. Although Shwedyk[56] suggests otherwise, if the EMG signal is locally stationary the use of these models is justified.

2.1.2 Volume Conductor Models

These models appear more suited to the modelling of the nerve fibres[57]. Recently they have been used to model evoked Compound Action Potentials in peripheral nerves which have latterly been applied to the inverse problem, that is, the interpretation of actual recorded CAPs.

Although a number of authors have been using volume conduction models for the simulation of CAPS, Lindström et al.[40] made use of volume conduction theory in a very comprehensive model that not only modelled the generation of EMG but also modelled the filtering effects of the detection electrodes[see Section 4.1.1.9]. They started by describing muscle fibres as long cylinders and assuming the medium to be isotopic, homogeneous and to have a linear current-voltage characteristic. With their model they were able to show the effects of electrode spacing and a relationship between conduction velocity and the myoelectric spectrum. Using their model they were able to explain a number of observed phenomenon seen in the voluntary EMG spectrum. Gootzen et al.[58] have used a similar modelling scheme to estimate the total number and the size of motor units involved in a given EMG signal.

Schoohoven et al.[59] provide a detailed review of a number of recent CAP models. The CAPs are modelled as the linear summation of temporally dispersed single fibre action potentials SFAP[60]. It is the definition of the SFAP that is one of the main differences between models. Some models base their SFAP on physical data, others on idealised forms or equations[59].

Schoohoven et al.[59, 61] show that all the models reduce to a single equivalent form which makes comparison easier. If the propagation velocity v of a SFAP is assumed constant over the propagation distance l between stimulation site and recording site and neglecting activation times and virtual cathode effects[60] then CAP $y(t,l)$ is given by:

$$y(t, l) = \sum_{j=1}^{N} \varphi_e\left(t - \frac{l}{v_j}, v_j\right) \qquad 2.1$$

where $\varphi_e(t,v)$ *is the SFAP for a fibre with propagation velocity* v.
l *is the propagation distance between stimulation site and recording.*
N *is the number of active fibres.*

They then show that $\varphi_e(t,v)$, the SFAP, can be represented by:

$$\varphi_e(t,v) = \chi(v)[\, \omega(t,v) * f_o(t,v)\,] \qquad 2.2$$

where $*$ *denotes convolution over the variable* t.
$f_o(t,v)$ *represents the underlying source of reference to that actually observed, that is, the intracellular transmembrane SFAP or the extracellular reference SFAP waveshape.*
$\omega(t,v)$ *is a weighting function that gives the variations in* $\varphi_e(t,v)$, *that is, the effects of volume conduction or modifications to the reference SFAP.*
$\chi(v)$ *is any additional amplitude scaling of the SFAPs.*

Stegman et al.[42] in a later paper following on from the Schoohoven work presented a statistical technique to interpret the recorded CAP and by using an *a priori* SFAP description they can reduce the chances of completely erroneous interpretations.

2.1.3 Typical Stochastic Model

Variations of this type of model are frequently reported in the literature[44, 46, 62, 63]. De Luca[3, 62, 64] and others have given comprehensive descriptions of this technique. The intention here is to give a brief resumé of the key equations in order to show how the various controlling properties of the muscle affect its output as described by the model.

The MUAPT train can be characterised by its IPI[62] and the shape of the MUAP. The firing rate of a motor unit is dependent on the time duration force and possibly the rate of contraction[28, 62]. In a typical model the firing rate $\lambda(t,F)$ is considered a function of time t and force F. De Luca and others obtain an expression for $\lambda(t,F)$ by fitting a probability distribution function $\rho_x(x,t,F)$ to the IPI histogram, such that the inverse mean value of $\rho_x(x,t,F)$ is the firing rate, that is:

$$\lambda(t,F) = \left[\int_{-\infty}^{\infty} x\, \rho_x(x,t,F)\, dx\right]^{-1} \qquad 2.3$$

The MUAPT train is conveniently represented by a pulse random process. The random process is conveniently generated by decomposing the MUAPT sequence into dirac pulses $\delta_i(t)$ which pass through a 'black box' filter $h_i(t)$, where:

$$\delta_i(t) = \sum_{k=1}^{n} \delta(t - t_k) \qquad 2.4$$

The impulses occur at time t_k where t is a real continuous variable. Passing these pulses through a black box with an impulse response of $h_i(t)$ gives the random process $u_i(t)$. If $h_i(t)$ is the equation of a MUAP the random process $u_i(t)$ represents MUAPTs, where i denotes a particular MUAPT:

$$u_i(t) = \sum_{k=1}^{n} h(t - t_k) \qquad 2.5$$

and where $t_k = \sum_{l=1}^{k} x_l$ for $k,l = 1, 2, 3, 4, \ldots, n$

The real, continuous, random variable x represents the interpulse interval and n is the total number of interpulse intervals in a MUAPT.

The definition of $h_i(t)$ and the probability distribution used to describe the dirac impulses are the two main areas of difference between the various models reported in the literature. Hermens et al.[44] use a library of recorded SFAPs, others use equation-based approximations[65] or even linear piece-wise approximations[28]. The choice of probability distribution differs greatly[28, 44, 46, 66]. De Luca and Forest[66] used a Weiball Distribution after considering a number of other possible distributions.

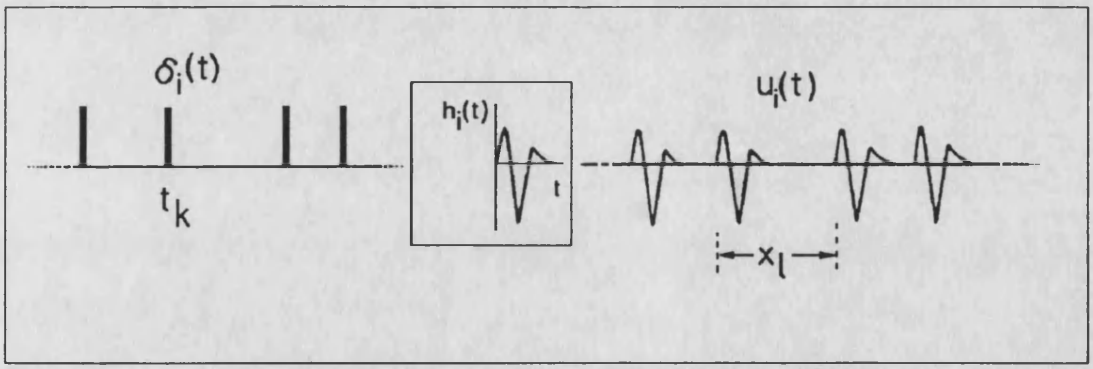

Figure 2.1 *Schematic of the Model for a Motor-Unit Action Potential Train*

The EMG waveform itself is formed by a spatial and temporal summation of MUAPTs[3, 62, 67] thus:

$$m(t) = \sum_{i=0}^{p} u_i(t) \qquad 2.6$$

where p *is the number of active Motor Units*

$m(t)$ *is the EMG signal at the detection point*

When considering the frequency response in a model it is more convenient to carry out the modelling in the frequency domain[46, 64]. From equation 2.6 the power density spectrum of the EMG signal m(t) may be expressed [46] as:

$$S_m(\omega) = \sum_{i=1}^{p} S_{u_i}(\omega) + \sum_{\substack{i,j=1 \\ i \neq j}}^{q} S_{u_i u_j}(\omega) \qquad 2.7$$

where $S_{u_i}(\omega)$ *is the power density of MUAPT* $u_i(t)$

$S_{u_i u_j}(\omega)$ *is the cross-power density spectrum of MUAPTs* $u_i(t)$ *and* $u_j(t)$*This value will be non-zero iff the firing rates of any two active motor units is non-zero*

q *is the number of MUAPTs with correlated discharges*

If equation 2.7 is expanded to allow for the fact that:

i) During a sustained contraction the characteristic of the MUAP shape may change as a function of time t[64]. An increase in time duration of the MUAP is common[66].

ii) The number of MUAPTs present in the EMG signal will be dependent on the force of the contraction F.

iii) The detected EMG signal will be filtered by the electrode before it can be observed. This electrode filtering, $R(\omega,d)$, will be a function of frequency ω and distance d between the pick up points on bipolar electrodes[40]:

$$S_m(\omega,t,F) = R(\omega,d)\left[\sum_{i=1}^{p(F)} S_{u_i}(\omega,t) + \sum_{\substack{i,j=1 \\ i \neq j}}^{q(F)} S_{u_i u_j}(\omega,t)\right] \qquad 2.8$$

The equation 2.8 can only be usefully applied if an expression for the power density spectrum for a MUAPT is known. To calculate this the statistics of the IPI and the actual MUAP shape must be considered. The IPIs may be considered as a real-continuous random variable, that is the MUAPT may be represented as a renewal pulse process. Thus the IPI is independent of all other IPIs. This approach is overwhelmingly supported in the literature[62, 64].

Thus the power density spectrum of the MUAPT is given by:

$$S_{u_i}(\omega) = S_{\delta_i}(\omega) \cdot |H_i(j\omega)|^2 \qquad 2.9$$

where $S_{\delta_i}(\omega)$ *is the power spectrum of* $\delta_i(t)$ *the impulse train*

$H_i(\omega)$ *is the fourier transform of* $h_i(t)$

From this LeFever and De Luca[68] have derived the following expression for the power density spectrum of a MUAPT:

$$S_{u_i}(\omega,t,F) = \frac{\lambda_{i(t,F)} \cdot \{1 - |M(j\omega,t,F)|^2\}}{1 - 2 \cdot \mathrm{Re}\{M(j\omega,t,F)\} + |M(\omega,t,F)|^2} \{|H_i(j\omega)|^2\} \qquad 2.10$$

for $\omega \neq 0$

where λ_i *is the firing rate of the ith motor unit*

$M(j\omega,t,F)$ *is the Fourier Transform of the probability distribution function* $\rho_x(x,t,F)$ *of the IPIs.*

Equation 2.10 shows how the power density spectrum depends on the statistical properties of the motor unit discharges. Although the MUAP shape is represented by $H_i(j\omega)$, changes in the shape during a sustained contraction would not be represented. One factor that is significant is the conduction velocity of the EMG signal along the muscle fibres. This has been included by De Luca[62] in his derivation and is given in equation 2.11:

$$S_m(\omega,t,F) = R(\omega,d)\left[\frac{1}{v^2(t,F)} G\left(\frac{\omega d}{2v(t,F)}\right)\right] \qquad 2.11$$

where v is the average conduction velocity of active muscle fibres contributing to the EMG signal

G is the shape function which is implicitly dependent on anatomical, physiological and experimental factors.

As the velocity decreases, the depolarisation current would take longer to travel along the muscle fibres in the area of the recording electrodes, and thus the recorded MUAPs would have a longer duration. The MUAPs frequency spectrum and hence the EMG signal would thus have an increase in low frequency components and a reduction in high frequency. Equation 2.11 clearly shows that as the reduction in conduction velocity occurs, as is known to happen as a muscle fatigues, the amplitude of the EMG would increase. From the equations it can be shown[68] that if the EMG signal contains several independent MUAPTs with MUAPs of about the same amplitude but differing firing rates, the region below 40 Hz is relatively smooth: the peaks and troughs that exist in the individual power spectra are smoothed out by cancellation. LeFever and De Luca[68] and others have noted that large peaks can be observed in the 8 to 20 Hz range with no significant muscle tremor. From a model using the technique described above it can be shown that this situation can arise in two ways: if the EMG Signal contains a predominance of regularly firing MUAPTs with somewhat similar firing rates or if the EMG signal is dominated by a high amplitude MUAPT.

These types of model help resolve some of the ambiguities as well as to give some insights into the information contained in the EMG signal.

2.2 Different Approaches

Some recent effort has been given over to modelling EMG signals without making assumptions about the EMG signal such as its stationarity, or in the case of stimulated muscle, allowing for the deterministic nature of the CAP trains that result. Here a brief review of the work carried out in this field is given.

2.2.1 Nonstationary Models

Non-stationary signal processing methods are poorly developed[69] and it is probably for this reason that very few researchers have used non-stationary models. Shwedyk et al.[56] use a technique very similar to that described in section 2.1.3 to generate their model where they assume the controlling factor in force production is the number of active motor units $n(t)$ showing that the EMG can be represented as an amplitude modulation process of the form:

$$\text{EMG} = [Kn(t)]^{1/2} w(t) \qquad 2.12$$

where $w(t)$ has the spectral and probability characteristics of the EMG during a constant contraction.

Meanwhile Xiong and Shwedyk[69] used a Midpoint Moving Average Estimator (MMAE) which intuitively compensates for the EMGs nonstationarity. They compare the MMAE results to the standard EMG processing method of squaring and low-pass filtering and found that with proper interpretation the traditional method could be made to perform just as well as the MMAE.

2.2.2 Stimulated Muscle Models

These models fall into two categories;

- The modelling of the electrophysiological effects of the stimulation so as to relate stimulation to CAP response.
- The modelling of a stimulated mechanical response such as the force which is a commonly controlled response in FES systems.

The CAP modelling is generally based on volume conductor models as described in section 2.1, although it is possible to use the stochastic type models described above. The difference between the voluntary and the stimulated response is the repetitive and deterministic waveform that is elicited. This would require that equation 2.4 use a fixed value of t_k which would be defined by the stimulator repetition rate. The CAP models are currently being used to help in the diagnosis of various neurological problems.

The modelling of the mechanical response of the muscle or limb when subjected to stimulus is another new area of interest as the research into FES systems moves on from its initial open-loop type of stimulus to a closed loop system using position and/or force feedback. The identification of the 'plant' is an important part of the design of a closed loop control system in order to ensure that an optimal controller is used[70, 71, 72, 73].

Allin and Inbar[43, 74] developed a model for the elbow flexion/extension and wrist pronation/supination, using as the input the surface stimulation of the biceps, triceps and pronator teres muscles. Their model was third-order with one simple pole and one complex pair at 1.4 Hz for the elbow and 1.8 Hz for the wrist. They also found large variations between individual subjects. This model was then used to design a feedback controller using a third order feed forward and a model reference adaptive controller. They found the two types comparable in performance but that the third order feed forward controller had the disadvantage of requiring a lengthy set-up time for the *a priori* identification which is implicit in the adaptive controller.

Beronatas et al.[70] produced a model describing the input/output properties of electrically stimulated muscle using a second order, discrete-time, deterministic, autoregressive, moving average (DARMA) model. The stimulator is modelled as an ideal sampler and the model separates the static recruitment non-linearity and linear dynamics. They use this model in closed loop control of muscle in FES orthoses where the tasks are carried out isometrically, such as grasp. Unfortunately most muscle actions are not isometric. In a later paper Beronatas et al.[71] present an adaptive controller that is able to respond to a range of load conditions, muscle length and command signals.

Hatwell and Inbar[72] have modelled the leg joints under electrical stimulation to design loop joint position controllers. They found a third-order system was required to model the joint, as with the arm. Their model once again uses a DARMA model.

2.3 Application of Models

The description of the models already includes a certain amount of application information detailing how the models reported in the literature have been put to use. It is intended here to give a short summary of areas relevant to the work described in this thesis where the various types of model could be applied.

2.3.1 Standing and Walking Systems

The main part of this work has been aimed at the detection, identification and feeding back of muscle EMG derived signals for the control of muscle stimulators to provide

standing and walking functions for paraplegics. The application of the models in this case can be in three distinct areas:

Command; The standing and walking systems require some means of initiating the required function. Ewins[75] uses switches in the standing support which are controlled by the user. In the standing system the user presses one button to stand and the other to sit. Clearly for a complete system some means of controlling this by just starting the action would seem preferable, especially for an implanted system. Graupe et al.[76, 77] are currently working on this type of function using ARMA modelling.

Feedback; In order that the controller can make the best decision on how to adjust the stimulators[78] to achieve the required function from the paralysed limb, it requires as comprehensive information as possible about the physical state of the muscle such as the force it is exerting, the state of fatigue and the position of the limb/muscle. The models can not only be used in helping to identify the optimal parameters to determine the required information from the EMG, but models such as the AR model of Paiss and Inbar[47] can be used to provide a measure from one of its parameters of fatigue. Some authors have derived equations for a number of the commonly used muscle parameters from simple stochastic models which allow for the testing of these parameters' integrity under a number of conditions such as noise[79, 80, 81].

System Modelling; A sufficiently complex model of the stimulator input to muscle output/limb function would allow the testing of controller types and feedback combinations before application to the subject. This technique is common for control problems of large machines and the like, but has significant problems here since there is significant variation between subjects, such that either a very complex model is required or the testing of the closed loop system can only be very general.

2.3.2 Strength Duration Testers

An EMG based strength-duration tester would provide the clinician with a set of CAPs for a range of pulse widths and even a range of voltages. If a suitable model of the compound action potential generation is available—such as the one used by Stegeman et al.[42]—these CAPs may be made part of a more comprehensive muscle and nerve analysis system.

By converting the CAPs of the recovering lesion back into a fibre type distribution or conduction velocity distribution the clinician may find that there is more information to be found on the lesion recovery than currently can be determined from the traditional strength-duration curve.

2.3.3 Muscle Fatigue Monitors

The muscle fatigue monitors such as those described in Appendix B can make use of muscle EMG models to optimise the control loop of the detector. Stulen[79], in his original MFM design, modelled the MFM and muscle signals in order to maximise the system response to changes in the monitored fatigue parameter.

Stability of the chosen fatigue parameter to external noise influences may also be tested[80, 81]. The models can be used to identify the best theoretical parameter for the fatigue aspect of interest.

Chapter 3

Muscle Signals

When a muscle contracts it regulates its movements and positioning by use of a number of feedback signals. These signals and their specific function as far as they are understood are first summarised. Attempts to use these signals for feedback, especially with surface detection techniques have been the subject of little, if any, published work.

Having discussed the muscle feedback signals, a review of current research into both stimulated and voluntary muscle responses is given. From this review a few possible parameters are suggested that could or already have been used as feedback signals to control muscle.

3.1 Peripheral Control System

Within the body there are a number of specialised receptors located in muscles, tendons and skin (*fascia*), which provide information on the state of the force and length of muscles to the appropriate part of the nervous system. There is also a nonreceptor system, the Renshaw system which reside in the anterior horn cell of the spinal cord. Under the traditional system for distinguishing between the peripheral and central nervous system the Renshaw system is in the Central Nervous System (CNS) but because it plays a role within the peripheral feedback mechanism it will be considered along with the peripheral nervous system.

The concept of the peripheral nervous system is based around a central pool of motorneurones, which is the aggregate of the interacting neurones, located in the anterior horn of the spinal cord. The effect of the motorneurone pools is the control of a function in either one muscle or a specific group of muscles. The output of the pool consists of the (*efferent*) information transmitted down α–motorneurones, γ-motorneurones and possibly the β–motorneurones. The presence of β–motorneurones is still to be clearly established for humans. The input to the motorneurone pool consists of the (*afferent*) information from the peripheral receptors, the Renshaw system and the drive from higher centres such as the brain.

Figure 3.1 gives a simplified block diagram of the major elements of the peripheral control system. In the diagram the arrows and signs indicate excitory (+) and inhibitory (–) action on the pool. The thickness of the lines represents the dominance of the contributions, the dotted line represents force interactions. An excitory action is one where either the disposition of an α- or γ-motorneurone to start discharging (*recruiting*), or to increase its firing rate if already active, is increased. An inhibitory

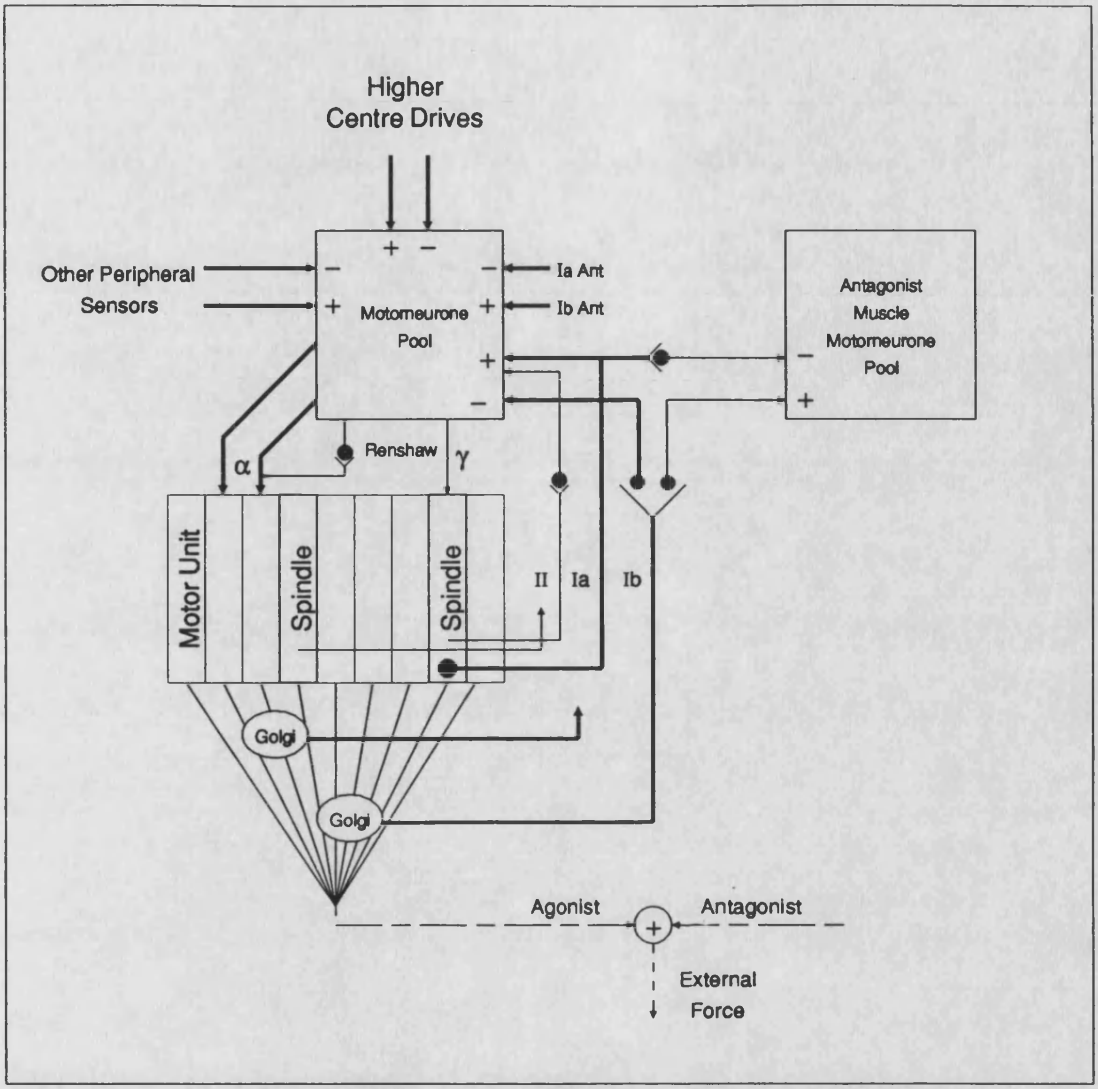

Figure 3.1 *Simplified Block Diagram of Peripheral Control System*

contribution has the opposite effect. In the block diagram the Ia and II afferent fibre discharges are shown as being excitory. However, when a spindle slackens during a muscle contraction, the discharges of these fibres decrease, which is the opposite to that shown.

3.1.1 Muscle Spindle

The muscle spindle is the most studied muscle sensor organ. It is located within the muscle body and consists of a capsule that is spindle shaped, attached at both ends to muscle fibres. It is believed to be arranged in parallel with the fibres of adjacent muscles. The arrangement is such that it can monitor length and changes in length. Internally the spindle is made up of *intrafusal* muscle fibres, which number from 5 to 25. They have contractile properties similar to normal *extrafusal* fibres. There are three types of fibre distinguished by the arrangement of their nuclei in the middle of the fibre. They are referred to as *bag 1*, *bag 2*, and *chain fibres*. The bag and chain fibres are distinguished because bag fibres are more dynamic. Bag 1 and bag 2 fibres

are distinguished by their content. Two distinct types of efferent motorneurone innervate these fibres: the gamma dynamic, which innervates bag 1 fibres and the gamma static which innervates the bag 2 and chain fibres. The γ-motorneurones are much smaller than their functionally similar α-motorneurones. Wrapped around the interfusal fibres are the endings of two groups of afferent nerve, the group Ia and the group II, with the former being the larger group. The Ia afferent fibres connect directly with an excitory projection on the motorpool of the same muscle (*monosynaptic*) and through an interneurone (*dysynaptic*) to an inhibitory projection on the motor pool of the antagonist muscle(s). The group II afferent fibres also connect to the motor pool of the same muscle via an excitory projection; however, the connection is dysynaptic.

The Ia and II group fibres modify their discharge rate as the mechanoreceptor endings of these fibres are elongated. These receptors can be elongated either by stretching the muscle which stretches the spindle capsule, or by contracting the intrafusal fibres via γ fibre excitation. As the receptors shorten, their discharge rate decreases and as they lengthen, it increases. It is also thought that the rate of change affects the discharge rate. The Ia afferents have been shown to respond to length and velocity, the II afferent fibres to mainly length[3].

The α– and γ–systems are coactivated during a muscle contraction, that is, both the extrafusal and intrafusal fibres contract. The main aim of this, it seems, is to set the length of the spindle appropriately, with respect to the length of the contracting muscle fibres. This is equivalent to setting the operating point of the Ia mechanoreceptors so that their sensitivity remains high over the length variability of the extrafusal fibres.

The usual way to conceptualise the functioning of the muscle spindles is as a servocontroller for compensations of loads applied to the muscle tendons. More recent work has shown that this is an incomplete model because it appears that muscle receptors also generate a sensory partitioning of the muscle[3].

3.1.2 The Golgi Organ

These organs are located in the *aponeuroses* which are tendon-like fibrous tissues that connect the muscle to the bone. Since the aponeuroses are relatively stiff, the Golgi Organs provide almost no information concerning muscle length. Instead they are sensitive to muscle tension. Like the muscle spindle they are fusiform in shape, and are innervated by group Ib afferent fibres. They have an inhibitory effect on the motorneurone pool of the agonist muscle and a less pronounced effect on the motorneurone pool of the antagonist muscle(s). They are very sensitive to minute changes in tension because they are inserted into the muscle such that several motor units attach to any one Golgi organ. This arrangement provides the Golgi sensor with the capability of responding to the force contribution from the whole muscle.

3.1.3 Function of Muscle Spindle and Golgi Organs during Contractions

The Golgi organ is basically a force sensor and will respond in a similar fashion during a stretch resulting from an externally applied tension, or during a voluntary contraction, resulting from an internally applied tension. The muscle spindle is sensitive to length and velocity. This means it will respond differently, depending on whether it is being elongated by a stretch or shortened by a voluntary contraction.

When an external load stretches a muscle, almost all the muscle spindles are stretched and respond by having an excitory effect on the motorneurone pool of the stretched muscle and an inhibitory effect on the motorneurone pool of the antagonist muscle. During the stretch, the Golgi organs will also be stimulated and respond by an inhibitory influence on the motorneurone pool of the agonist muscle and an excitory effect on the motorneurone pool of the antagonist muscle. Thus the responses of the Golgi organs are in conflict with those of the muscle spindles. If the applied stretch is brisk, the result is a reflex contraction response counteracting the displacement results.

This shows that under these conditions the Ia afferent fibre stimulation provides the dominant effect; this is consistent with the fact that the Ia fibre endings detect motion changes. Thus in the case of the stretch reflex, due to external disturbances, the muscle spindles provide a mechanism for load or displacement compensation.

When a muscle is contracted by a voluntary contraction or via electrical stimulation, the spindles are slackened as the muscle fibres shorten. But unlike the case of a rapidly applied stretch, not all of the spindles are disturbed at any given force level—unless all the motor units are excited—thus, the discharge of the spindles will be reduced. This will cause a decrease in the excitory influence on the agonist motorneurone pool (*disfacilitation*). The Golgi organs will respond to the increasing tension and increase their discharge rate. This will have an inhibitory effect on the agonist muscle and an excitory effect on the antagonist muscle(s). Thus, during a voluntary contraction the behaviour of the muscle spindles and Golgi organs is complementary.

3.1.4 Renshaw Cells

These cells were discovered by Renshaw in 1946[3]. They are interneurones in the ventral horn and are triggered by impulses in the motorneurone moving towards the cell body (*antidromic*) and appear to inhibit neighbouring motorneurones. The Renshaw cells receive collateral branches from motorneurones and their axons terminate on the motorneurones themselves. This link forms a feedback circuit with recurrent inhibition whose precise purpose is not fully understood.

The Renshaw cells have been found to inhibit not only α-motorneurones but also other Renshaw cells: the γ-motorneurones and the interneurones mediating group Ia

reciprocal inhibition. They may be triggered by a single motorneurone discharge rate. The precise role of the Renshaw cells is unclear but it has been suggested that they act as a variable gain regulator at the motorneuronal level.

3.1.5 Other Muscle Feedback Sensors

There are a number of other sensory fibres that have been identified in muscle. Afferent fibres with free nerve endings and a wide range of diameters have been identified. Skin sensors sensitive to touch and pressure have been identified (*Pacinian Corpuscles*), along with a number of others sensitive to light, touch or temperature changes. The action of these receptors is unclear: several withdrawal reflexes which may arise in response to the possibility of injury seem to originate in these fibres.

3.2 External Use of Internal Feedback Signals

Of all the various feedback sensors[82, 83] that the body uses to control muscle contractions and movement, the two that could provide useful information in a closed loop control stimulator system are the muscle spindles and the golgi organs. In order to use these signals it would be necessary to detect the feedback fibre signals of the afferent type Ia, Ib and possibly II fibres. These signals, on a single fibre basis, would be very small because these fibres are small and the differentiation of these signals at the muscle surface, where they would be swamped by the electromyogram from the muscle fibres, would be extremely difficult.

The only way that it may be possible to detect these signals is with needle electrodes which would have to be very precisely placed in order to get the signals required. If an implanted system is considered, cuff electrodes around individual fibres or groups of fibres may be possible, but once again identifying the fibres and connecting cuff electrodes to such small fibres could be difficult. Clearly, in a surface electrode-based standing and walking system none of the possible routes to detecting the internal feedback signal would be very practical, especially since the precise positioning of electrodes could not be guaranteed[84].

Looking towards the future, assuming suitable electrodes exist as a means of connecting to the afferent fibres, it seems likely that the feedback system of the body could be used as part of a closed loop control system for standing and walking. The use of these signals also relies on the fact that they remain intact, so the precise cause of the paraplegia could have an effect. If it is due to upper nerve lesions rather than lower motorneurone damage, the natural feedback signals are likely to be functioning. If lower motorneurone damage exists, the muscle will be denervated and the functioning of the sensor organs is unclear[84].

3.3 Motor Units Control of Muscle Function

The precise details of how the nervous system and the motor units combine in the control is beyond the scope of this thesis. However, a brief overview of a number of control strategies that have been described in the literature will be given.

As has already been described each motor unit innervates a number of muscle fibres. Each of these motor units are fired at random by a series of action potentials, the Motor Unit Action Potential Train (MUAPT). The interpulse interval (IPI) of the individual MUAPTS in a MUAPT is irregular and can be described as a random variable with characteristic set of properties[36, 79, 85, 86]. As the force required from a given muscle increases, the rate of discharge of the motor unit increases and the IPI becomes shorter.

Besides describing a MUAPT by the distribution of its IPI it can also be described by its IPI interdependence, the greatest amount of dependence being expected between adjacent intervals. In order to test for this it is necessary to have a stationary waveform (time invariant) since samples are to be compared. For the MUAPT, this requires that the sample time be sufficiently small so that stationarity of the MUAPT is valid. If the IPIs are independent then a scatter plot will be defined by the IPIs' probability distribution function. If they are dependent it will have statistically dependent co-ordinates when plotted on a scatter graph.

Synchronisation of MUAPTs, that is, the tendency for two or more motor units to discharge at a fixed time interval with respect to each other, is another property of MUAPTs. Piper[5] noted this originally when he saw surface EMG showing an oscillatory activity. It still remains to be fully proven. Mori and Ishida[3] have shown that if the feedback from the muscle spindle is large enough the MUs will become synchronised.

The random nature of the IPIs leads to the use of the average firing rate to describe the discharges of MUs which is the reciprocal of the average IPI. In order for the value to be reasonable it is normally taken over 400 to 1000ms.

Much work has been done to show how the firing rate modulates muscle force[23, 27]. These studies have found that the firing rates increase with the force required up to a maximum. Depending on which muscle is involved, the smaller muscles, such as in the hand, have higher rates than the MUs in larger limbs, such as the leg.

With time, the firing rate of MUs tends to decrease independently of the force output of the muscle[21, 22, 66] and is thought a reflection of the motorneuronal adaption process. This decrease in firing rate with sustained contraction is associated with twitch potentiation, that is, an increase in the twitch tension produced by a motor unit.

The overall strategy that the nervous system uses to control MUs for the purpose of generating and modulating the force of a muscle has been the subject of many investigations. De Luca[87] has described a unison behaviour of the firing rates of motor units, both as a function of time and force. The property has been termed common drive. The existence of this property implies that the nervous system does not control the firing rates of motor units individually but rather acts on a group of motorneurones in a uniform way. Thus, a demand for modulation of the excitation of a muscles force output may be seen as a modulation of the excitation and/or inhibition of a motorneurone pool.

Common drive has been observed[3, 87] when two antagonist muscles are activated to stiffen a joint; the nervous system views them as one unit and controls them as one. Thus, the controlling motorneurone pool consists of motorneurone pools from both muscles.

The order of recruitment of motor units has also received much attention. It has been found consistently[3] that the recruitment is in order of size. The derecruitment occurs in the opposite order to the recruitment.

The orderly progression of the recruitment may be altered, for example when the muscle performs a different task, but the order is consistent for the same task though these results are not fully confirmed. It is known that the order of recruitment of motor units can be artificially changed by electrical stimulation leading to an order reversal that persists sometime after the end of stimulation.

The actual recruitment schemes vary from muscle to muscle with some muscles having all their motor units recruited well below maximal stimulation level, while in others, recruitment continues up to maximal. This again appears to be split between the small muscles, such as in the hand where all the MUs are recruited below 50% MVC, and large muscles, such as in the legs which recruit MUs throughout the full range of voluntary force. The small muscles also rely much more on modulation of the firing rate to modulate their force whilst larger muscles rely mainly on recruitment.

3.4 Muscle Force

The measurement of the exerted force of a muscle is difficult: to provide a correct measure, the force transducer would need to be placed in line with the muscle. This is clearly only really possible in animal experiments. It is in this line of research where much of the reported research on the muscle force-EMG relationships has been carried out.

When carrying out experiments with human subjects it is usual to carry out the tests in terms of the maximum voluntary contraction (MVC) of the subject. The subject is

usually restrained in some form of harness such that in exerting the force only the muscles under test are used and often the contraction is constrained to be of an isometric type. The force measurement is usually carried out by a transducer in the harness which provides a visual feedback to the subject via a DC level on an oscilloscope. To maintain an isometric contraction of say 50% MVC the subject would be asked to maintain the DC level at some level that has been previously calibrated as 50% of the MVC of the subject.

Before reviewing some of the findings concerning the relationship found between muscle force and EMG signal amplitude some of the common parameters used in the literature will be defined.

3.4.1 Time Domain Processing Techniques

The EMG signal, as has already been discussed, is a time and force dependent signal whose amplitude varies randomly around zero. The signal is often recorded via AC coupled amplifiers, as discussed in Chapter 4, which guarantees that the signal is centred around a zero average level. In order to derive some useful signal from the EMG signal it is common to use some form of non-linear processing to remove the zero average.

Rectification is a common method used to non-linearly process the recorded EMG signal. The rectification could be either full– or half-wave; the best for this work being full-wave rectification because it would retain all the energy content of the signal; half-wave rectification, on the other hand, would lead to a serious alteration of the energy content. Having rectified the EMG signal it is usually smoothed to enhance the trends in amplitude and remove the high frequency transients and fluctuations, that is low pass filtered. The smoothing can be achieved either by analogue or digital techniques. Most modern analysis systems use microprocessors to manipulate the recorded EMG signal and it is in the choice of the smoothing function that researchers differ[88].

With an analogue filter, the lower the cut-off frequency is, the greater the smoothing that may be achieved. This is equivalent to smoothing over a greater time period. Clearly this can be directly emulated in the digital time domain by implementing a digital low-pass filter. The smoothing may be defined mathematically as:

$$\overline{|m(t)|}_{t_j-t_i} = \frac{1}{t_j - t_i}\int_{t_i}^{t_j} |m(t)|dt \qquad 3.1$$

where t_j *and* t_i *are the points over which the average is performed.*

$t_j - t_i$ *defines how much smoothing will occur; the greater the difference the smoother the output.*

Equation 3.1 will only provide one point in time for the period $T = t_j - t_i$. To gain the time varying average the window must be moved along the signal record thus giving a moving-average. The movement may be in steps of any value of t up to a maximum of T. If the steps are less than T the average is said to be biased, that is, it shares some common values because of the overlap. If the steps are in T this may be expressed mathematically as:

$$\overline{|m(t)|} = \frac{1}{T}\int_{t}^{t+T} |m(t)|\, dt \qquad 3.2$$

The operation produces a time lag T in the transfer from input to output as with any filter. Common values for T are 100 or 200 ms.

One of the most often used terms is the Integrated EMG (IEMG). Not only is this often used, but it is often misused[88]. Taking the strict mathematical definition, it may be defined as:

$$I\{|m(t)|\} = \int_{t}^{t+T} |m(t)| dt \qquad 3.3$$

This is a subset of the average/mean function given in equation 3.2, except there is no division by T. The original use of the term was in the description of an envelope detector[88, 3]. The mathematical procedure is a calculation that gives the area under a curve and the units are V·s or mV·ms and not, as has been reported, mV/s or mV[88]. Since the normal EMG signal has a mean of zero it will also have an integrated value of zero, hence the integrated EMG must always be applied to a rectified waveform (non-linearly processed). Integrating the rectified EMG will not give any extra information. As with averaging it is common to integrate over a fixed time period; the period may be a fixed time such as 150 ms or until the output reaches a fixed voltage[88, 89].

Derivation of time and force dependent parameters from models similar to those presented in Chapter 2 indicate that the Root-Mean-Square value would provide more information[62, 3] though currently its use is rare. It is defined as:

$$\mathrm{RMS}\{m(t)\} = \left(\frac{1}{T}\int_{t}^{t+T} m^2(t)\, dt\right)^{1/2} \qquad 3.4$$

The final method that has been used is zero crossing and turns counting, that is the counting of the number of times per unit time that the signal contains a peak or crosses the zero line. Basmajian and De Luca[3] do not recommend this method for force evaluation, they prefer the RMS.

Figure 3.2 gives a comparison of these techniques for a raw EMG signal recorded from the biceps brachii during a constant force isometric contraction.[3]

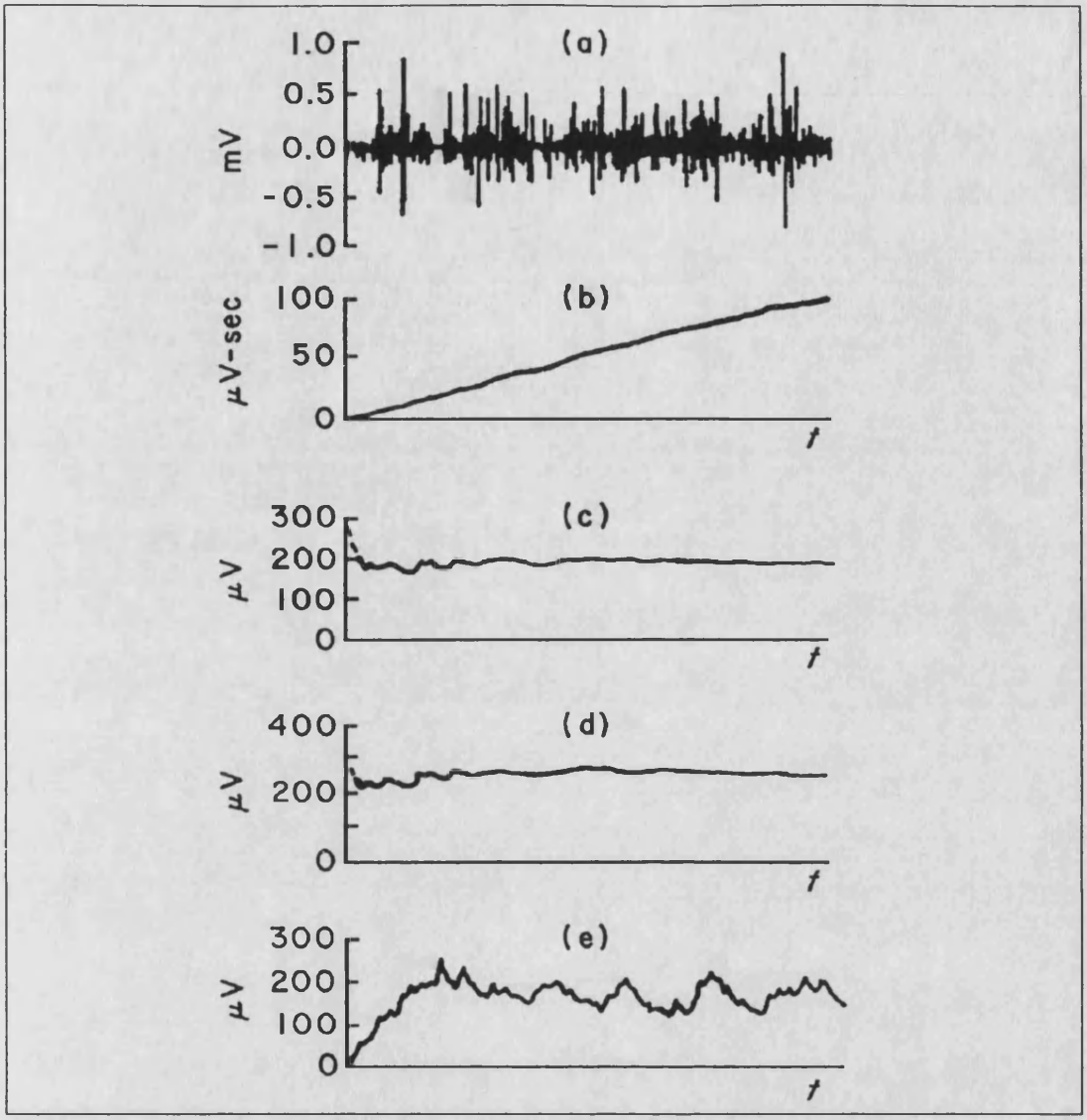

Figure 3.2 *Four of the Processing Techniques (a) raw EMG signal; (b) the integrated rectified signal; (c) the average rectified signal; (d) the root-mean square signal; (e) smoothed rectified signal—RC filter 25ms; Time base is 0.5ms*

3.4.2 EMG Force Relationships

The precise relationship between the myoelectric signal and the exerted force is a subject of much debate. It is already clear that a number of different methods are available for quantifying the EMG signal. Basmajian and De Luca[3 p188] present an extensive list of recently published data on the subject. The relationships vary from linear to non-linear for both isometric, isotonic and isokinetic contractions, using all the measurement parameters discussed above. Rather than replicate the data presented by Basmajian and De Luca, a few selected papers will be cited: these offer suggestions for the differing results. Application of these results to stimulated muscle will also be discussed where appropriate.

The most common problem recorded by researchers in obtaining their results is that the surface recorded EMG signal is much more difficult to obtain consistently and reliably than the intramuscularly recorded response[63,89,90]. Calvert and Chapman noted significant problems in getting consistent estimates of dynamic changes in the active state of the biceps brachii using surface recording in their tests. In fact they found the inconsistency increased with the speed of contraction.

In an extensive study of surface EMG-force relationships using the Integrated rectified EMG (TC=150ms) Woods and Bigland-Ritchie[89] investigated the linearity of this relationship for a number of different muscles. They used three groups of muscles: a uniform slow fibre muscle (soleus), an even mix of fast and slow fibre muscles—(brachial flexors) and mixed muscles (dorsal interosseous). Their results for isometric voluntary contractions showed significant variation in the relationship between integrated rectified EMG and muscle force which appeared to depend on the physiological characteristics of the muscle.

For muscles with a predominantly uniform fibre type composition such as the soleus, the relationship was linear; a roughly even fibre type combination such as in the biceps brachii produced a non-linear relationship; muscles that rely on rate coding (that is, the variation of the IPI) for force modulation, such as the adductor policis, gave a linear response, whilst non-linear relationships were obtained from the biceps brachii which recruits throughout its force range. The curves all showed a discontinuity around 30% MVC with the curve tending to be more linear above this level.

An anomaly is noted for the quadriceps muscle tested (vastus lateralis), where both linear and non-linear relationships were observed. This supports the literature where both even and uneven fibre compositions have been recorded[89]. They also note that a variation of surface recording configuration, electrode placement and limb position did not change the non-linearity of the relationships. This is in conflict with some explanations of the reason for the non-linearities found.

Lawrence and De Luca[90] in a similar study compared normalised surface recorded EMG signal amplitude with normalised force. By using normalised values they were able to compare different subjects and so assess how exercise affected the biceps brachii, deltoid and first dorsal interosseous for pianists, long distance swimmers, power lifters and normal subjects during voluntary isometric linearly force-varying contractions. Instead of using the IEMG they used the RMS voltage. As with Woods and Bigland-Ritchie they found quasi-linearity for the first dorsal interosseous, non-linearity for the biceps and deltoid, with the EMG and amplitude increasing faster than force. They also noted these curves were partially affected by the different motor

unit firing rate and recruitment properties of different muscles. They also found a large intersubject variation but smaller intrasubject variation for the same muscle. The relationship was independent of subject group, suggesting that it was possibly not affected by the type of exercise, with the exception of one or two muscles of the power lifters and the deltoid of swimmers.

Heckathorne and Childress[91] in an attempt to overcome the problems of actual force measurements used amputees with cineplastic biceps which allowed direct force measurements. They made use of the integrated rectified EMG and their results compared well with those of Woods and Bigland-Ritchie. They also found that for static force the relationship was independent of muscle length, but for dynamic force it increased with respect to the static case as the muscle length decreased.

Lloyd[92], in a series of endurance tests, found an apparent linearity in the EMG force relationship but had too few points to say conclusively. In the endurance tests he found the EMG amplitude consistently increased as the test continued with each muscle showing a differing variation. The biceps showed the greatest change whilst the triceps, deltoids and contralateral triceps showed very small increases.

Explanations for the observed features may be derived by considering the way the muscle fibres are recruited, the firing patterns and the muscle fibre composition of the muscles. Both Woods et al.[89] and Lawrence et al.[90] offer explanations which are in agreement with other authors[3]. The effects that occur with fatigue mean that the use of the EMG amplitude as a force indicator would be modified by how fatigued the muscle gets, so care must be taken in interpreting the EMG amplitude.

The stimulated EMG signal has not seen much use in the time domain analysis, often because of the effects of stimulus artefacts contaminating the recorded muscle responses. Solomonow et al.[93, 94] have made use of the rectified CAP response from stimulating cat muscle to show that the EMG-Force relationship of stimulated muscle can be linear. The muscle was stimulated using cuff electrodes and by cutting the muscle tendon a force transducer was attached in-line. By a careful choice of stimulating parameters they showed that there was a linear EMG (rectified, smoothed TC=120ms) force relationship but also found that this did vary with muscle fibre composition.

Graupe et al.[76, 76] have investigated the stimulated muscle EMG as a signal to use as feedback in standing and walking systems of fatigue. They have shown that the filtered CAP (filtered to remove the stimulus artefacts) may be used to show fatigue and when fast and slow fibres come in and out of firing during various stages of fatigue. They have also been able to detect spasms within the CAP train which is a

common problem when standing paraplegics. Recently Graupe[96] published details on the practical use of this information in a walking system.

3.5 Muscle Fatigue

The uses of the term fatigue when discussing the deterioration of performance of a human operator has often been ambiguous. This is because the many disciplines that study 'fatigue' have their own definition. The measurement of fatigue relies both on the subject to perform the task and the observer assessing the task since it is possible for the researcher to persuade the subject to exert a little extra effort beyond their normal fatigue point. This effect has in fact been noted for the tests carried out on the muscle fatigue monitor described in Appendix B.

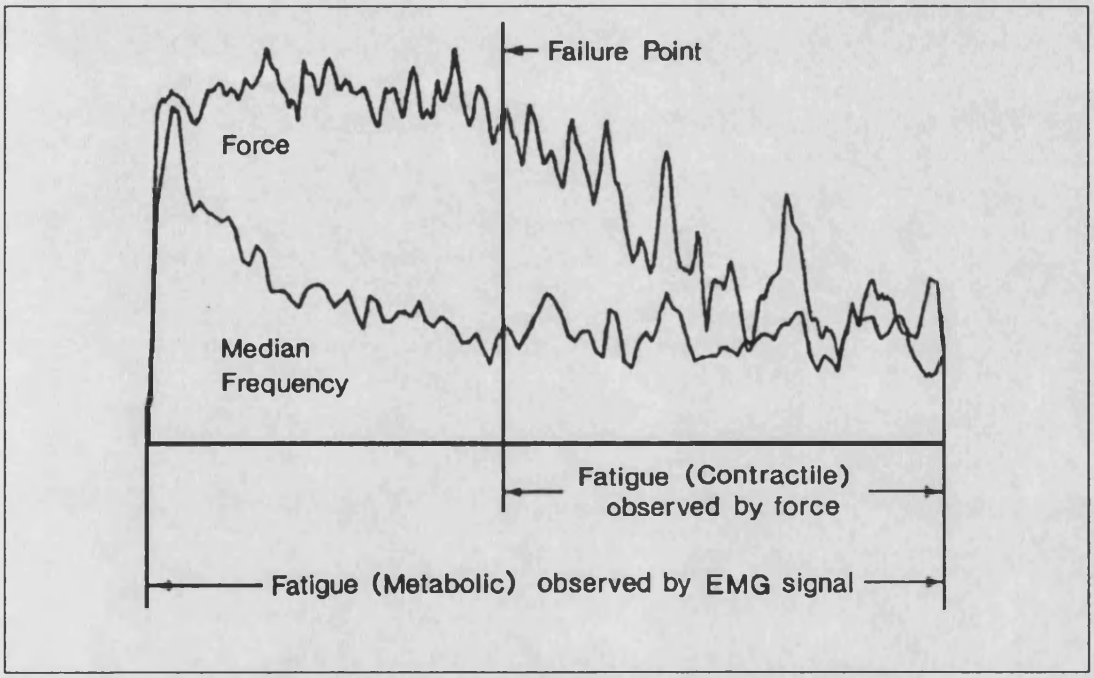

Figure 3.3 *Plot showing the Force exerted by the First Dorsal Intersosseous Muscle whilst trying to maintain a 50% MVC and the corresponding Median frequency.[64]*

In this thesis the definition of the term will be that given by Basmajian and De Luca[3, 62]. They use a definition based on the engineering definition. The engineering example is that of a steel girder supporting a bridge. The bridge may remain in place for 50 years then suddenly a fracture develops and the girder fails and the bridge collapses. If the bridge is observed from a distance then no sign of fatigue is seen until the point of failure is reached and the bridge collapses. However there will be progressive changes over the years in the crystalline structure of the steel which could only be seen if samples of the girder are tested.

Forming an analogue with muscle function, it is similar to the task of maintaining a muscle contraction constant for as long as possible. Throughout this task the muscles

are continuously fatiguing but at some point they will no longer be able to maintain the desired output force and the failure point will have been reached. Thus contractile fatigue can be seen.

Internal biochemical and physiological changes within the muscle and/or the nervous system could reveal time dependent changes that indicate that fatigue is taking place though externally observable mechanical performance would not be affected until the failure point. Figure 3.3 demonstrates this for the first dorsal interosseous muscle during an attempt to maintain 50% MVC. The force and median frequency of the EMG power spectrum are plotted against time. Here it can be seen that the median frequency (biochemical, physiological data) is continuously dropping even though the force is constant up to the failure point.

3.5.1 Frequency Domain Monitoring

The most notable feature of muscle fatigue is its frequency compression and it is this feature or a parameter derived from the power spectrum that is often used to monitor the fatiguing muscle. A discussion of the signal processing and sampling aspects of frequency analysis of EMG signals is given in Chapter 4. Here it is intended to give a brief outline of the common parameters reported in the literature.

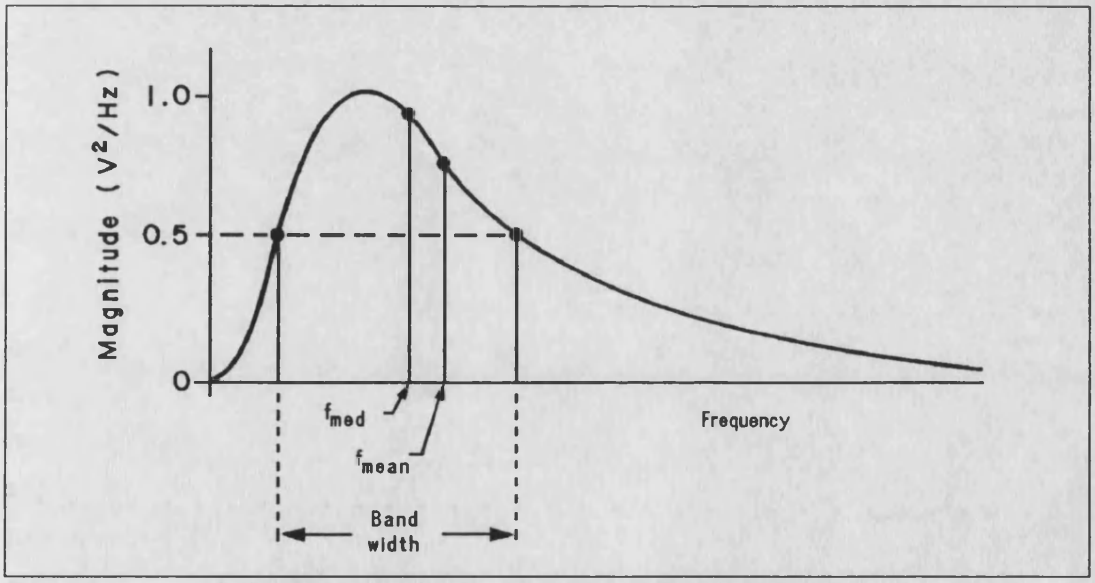

Figure 3.4 *Idealised Spectrum showing some common Frequency Parameters*

Figure 3.4 presents, on an idealised EMG spectrum, the most common of the parameters used to characterise the frequency changes that are observed in fatiguing muscle. The choice of a linear scale for the power is a matter of some debate, with some authors preferring the more common log scales. A number of authors prefer the linear scale because 'it provides a more direct expression of the power distribution'[3].

The parameters most often used are the *median frequency* f_{med} which is the frequency at which the spectrum is divided into two regions with equal power. This may be defined mathematically[88] as:

$$\int_0^{f_{med}} S_m(f)\,df = \int_{f_{med}}^{\infty} S_m(f)\,df = \frac{1}{2}\int_0^{\infty} S_m(f)\,df \qquad 3.5$$

The *mean frequency* f_{mean} which is the average frequency is defined[3] as:

$$f_{mean} = \frac{\int_0^{\infty} f\,S_m(f)\,df}{\int_0^{\infty} S_m(f)\,df} \qquad 3.6$$

and the bandwidth of the spectrum is defined as the difference between the 3dB frequency points. Some investigators have used the mode which is the frequency at the maximum of the power spectrum—the most probable frequency—others have used ratios of segments of the power density spectrum.

Paiss and Inbar used the parameters of an AR model to try and track the changes in the surface EMG as the subject fatigued. With their model they concluded it would only track changes in the MUAP shape because the order of the model was not great enough to track the low frequency components due to the MUAPT firing rate.

3.5.2 Choice of Trend Parameter

Stulen and De Luca [80] and Hary et al.[97] have performed mathematical analysis to investigate the restrictions on estimating various parameters of power density spectrum. They all found the mean and median frequencies to be the least sensitive to noise. However they differed on which of the two were best.

Stulen and De Luca[80] analysed the mean, median and the ratio of low-frequency components to high-frequency components of the spectrum. The mode parameter is theoretically the most effective estimate, because even with a relatively poor signal to noise ratio a perfect estimate can be made. It is not considered because the EMG signal is a stochastic signal which does not have a smooth and sharply defined region near the peak value of its spectrum.

From their analysis Stulen and De Luca found that both the mean and the median are only slightly effected by noise for a SNR of greater than 100. With the median frequency showing a lower error for low SNRs, for a SNR of 2 the error in the median frequency is 20%[79]. They also found that the ratio parameter was sensitive to the shape of the EMG spectrum. This is a significant problem: as motor units with significantly different action potential shapes are recruited, as is likely during varying-force contractions, the frequency components of the EMG signal in some

muscles could vary . The parameter is also dependent on the frequency at which the spectrum is divided.

Hary et al.[80] found that the mean (centroid) frequency was the most reliable measure of spectral shifts, because it demonstrated low variability and small thresholds of significance. This is in conflict with the findings of Stulen and De Luca which is based on added white noise interference. Hary et al. confirmed the effects of noise but suggest that a high sensitivity to added white noise is desirable to reliably track changes in the underlying spectrum. They did however agree that the ratio parameter is the least reliable due to its high sensitivity to variation in signal amplitude.

Maranzana Figini et al.[98] have experimentally confirmed the repeatability of the mean frequency with respect to the median frequency. Their tests were aimed at the evaluation of the intra-experiment, inter-experiment and inter-subject variations within the normal population.

3.5.3 Changes in the Spectrum due to Fatigue

Figure 3.5 presents diagrammatically the changes that occur to the idealised spectrum with time for a differentially detected EMG signal. The diagram also includes the changes that occur with force, as has been discussed earlier in this chapter. The features of interest have been accentuated. The peak in the low frequency components is associated with the MUAPT firing rate, the dip in the high frequency components is associated with the conduction velocity along the muscle fibres. The shading indicates the range over which these features normally occur.

As with the EMG force relationships there is variability between choice of parameter and precise relationships between EMG and fatigue. This review is primarily concerned with frequency based assessments but it is worth noting that a number of authors have tried to make use of the EMG amplitude[92] or similar time domain technique to monitor the fatigue. The reason for this is that the signal tends to increase as the muscle fatigues. This observation is consistent with the expected results, especially for surface recorded EMGs, since, as has already been stated, the frequency content shifts to a lower frequency, that is, it tends towards DC. Since the recorded signal is low-pass filtered there is an effective increase in the energy in the lower frequency band which, once rectified, will lead to a larger signal.

The use of frequency shifts to monitor force is another technique that has been tried. It has little support because no consistent relationships could be found. Stulen[79] has shown that the absolute values of the mean and median frequency vary inconsistently as a function of force. Some authors[64] have found a slight increase in mean

frequency with low level contractions, that is, below 25% MVC. Above this level of contraction the mean was independent of force.

As with the EMG amplitude-force relationship, authors differ on the nature of the change in characteristic (mean or median) with time. Both the median[79, 80] and the mean[3, 64] have been shown mathematically to be linearly related to the average conduction velocity.

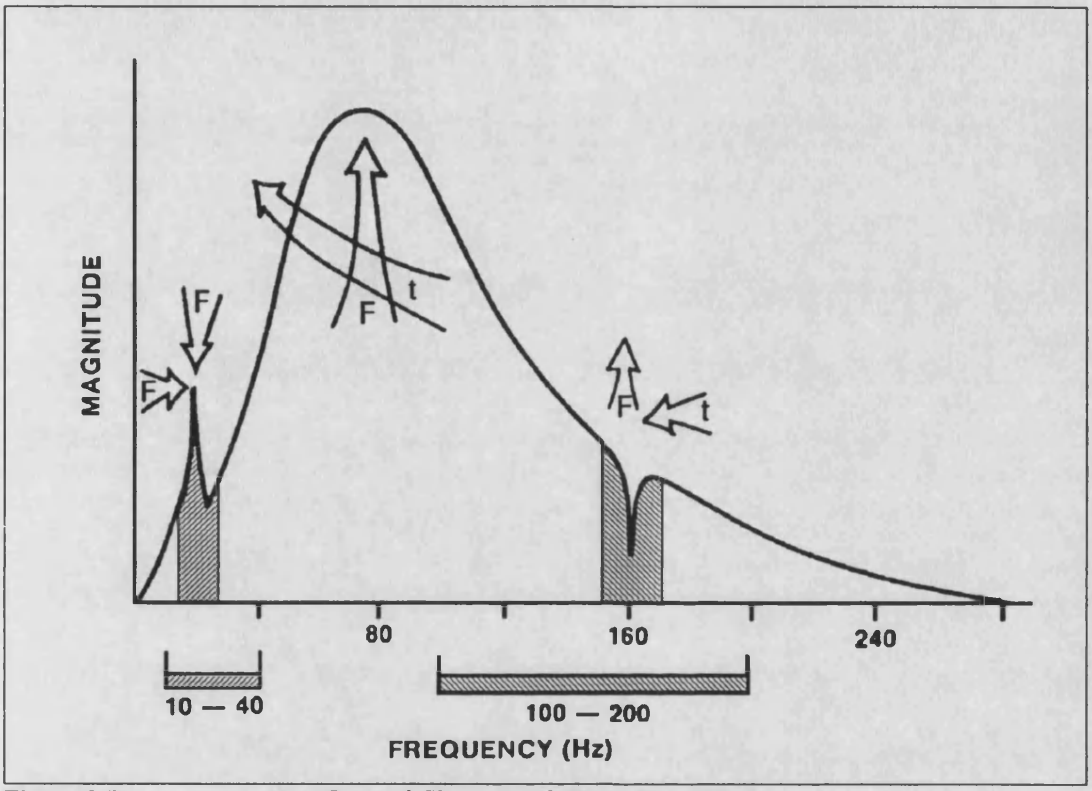

Figure 3.5 *Spectral Changes with Force F and Time t*

During sustained constant-force contractions the rate of decrease has been found to be quasi-linear[99] or quasi-exponential[79, 80]. As with the force relationships these differences may be explained by the different muscles chosen for the test and the methods used to calculate the characteristic frequency. As an example of this, if the time constant of the system used to calculate the characteristic frequency is long relative to the period of the test, an exponential curve will appear as if it were a quasi-linear curve.

The mean- or median-frequencies may decrease by as much as 50%[3, 64] in value from the beginning to the end of sustained isometric constant-force contraction. The actual amount appears to depend on the actual muscle being investigated. Stulen[79] found in the first dorsal interosseous muscle and deltoid muscles that they gave the greatest decrease in the value of median frequency for a 50% MVC. Inbar et al.[100] investigated the changes in the median frequency that occurred as the length of the muscle changed. Using the biceps and extensor digitorum they recorded the surface

EMG and calculated the median frequency using an FFT. They observed a decrease in median frequency with muscle length; this was also observed in stimulated muscle responses. Larsson[101] found using needle electrodes for the recording of the EMG signal, found that the frequency content of the EMG could be used to characterise lesions of the motor nerve. With doubtful neurogenic lesions and old lesions there was an increase in low frequency—*'Bass' displacement*—and lesions of only a few months gave an increase in higher frequencies—*'Descant' displacement.*

It is well known that a stimulated muscle fatigues much quicker than a voluntary controlled muscle, because of the fact that the same muscle fibres are recruited throughout the stimulation period. A number of authors[102, 103, 104, 105] have looked at this as part of their tests and compared the results with those obtained from voluntary muscle responses.

Merletti et al.[102] have investigated spectral changes with fatigue for both voluntary and stimulated isometric contractions of the tibialis anterior, using the mean, median and conduction velocity to assess the changes. For the stimulation they used two levels of stimulation which were measured as about 4% MVC and 16% MVC respectively, showing that they could only manage to excite a small part of the muscle.

Their voluntary results for increasing force showed an increase in mean, median and conduction velocity. This is the expected result since, as has already been discussed, the muscle fibres recruit the small units (lower conduction velocity) followed by the larger units (high conduction velocity). These results are supported by Broman et al.[106] and Roy et al.[107].

With the electrical, results recruitment order would be expected to reverse because the thresholds are related[108] to the unit size. The results of Merletti et al. showed that 60% of the tests displayed an increase in conduction velocity with stimulated force and 40% of the tests showed a decrease in conduction velocity showing that the electrical excitability threshold of motorneurones is not always the dominant factor.

With the sustained contraction there was a faster decrease of the mean and median than the conduction velocity, which would suggest that other factors beside conduction velocity contribute, such as ischemia. They show a repeatability in their median and mean plots and they all show a decrease with time for both the low level and high level stimulation. Mills[99] has shown similar curves to those presented by Merletti et al.[102]. The conduction velocity changes with fatigue are supported also by Lindström et al.[109] and Naeije et al.[110].

3.6 Stimulating Muscle

A number of reviews[108, 111, 112] have appeared in the literature giving reasons for the use of and discussing the practical application of muscle stimulation. The most common practical use being in the provision of function to paralysed limbs. In order to do this, closed loop control is probably the safest solution. However, until recently most available systems have been open loop[113, 114], that is, the control of the stimulator is not determined by any feedback, such as the knee angle, when standing. Closed loop systems have been used in the laboratory but have not been available for use outside of this controlled environment until recently.

Recently a number of authors have reported new techniques to control muscle force and to minimise the rate of fatigue by controlling the stimulating waveform. Since this is closely related to the work described in this thesis a brief review of these is given.

3.6.1 Stimulating for Minimal Fatigue

Using the typical stimulation parameters of 200-300μs and stimulating rate of 20-25 Hz, when a muscle fatigues the only way to maintain the tetanic contraction is to increase the stimulus. In the typical open loop system it has been up to the user to decide that they are tiring and turn the voltage up. In a feedback system the feedback circuit would determine this and increase the voltage as necessary. Since functions such as standing require the majority of muscle force to stand and sit, when the subject is actually standing very little muscle force is required. This means that a closed-loop stimulator system may be made to ramp down the output voltage when the feedback indicates the subject is stable. This technique has been used successfully by Ewins et al.[115, 116] to increase standing time in his closed loop stimulating system. Mulder et al.[117] present a similar standing system using state feedback which also includes the ramping down.

In an attempt to emulate the natural firing of muscle, Pournezam et al.[118] have made use of multiple stimulation sites on a single muscle or muscle group. In their experiments they tried to maintain knee extension by the sequential stimulation of the quadriceps, that is the rectus femoris, vastus lateralis and vastus medialis muscles. They found three benefits: there was a prolonged time until the knee extension was said to have fatigued because the work load is shared between a number of muscles. Coupled with this there was an improved recovery time and finally the individual muscle performance is improved. They quote improvements of 500% over the normal continuous stimulation techniques. This system is obviously far easier to implement using internal stimulation rather than surface stimulation as was used here.

The other technique that has been reported for the improvement of fatigue is eutrophic stimulation which is 'an electrotherapy based on the natural sequence of motor unit action potentials'[119]. This technique uses a pre-recorded sequence of pulse widths and interpulse intervals which are derived from a voluntary muscle contraction MUAPT. This sequence of pulsewidths and interpulse intervals is used to control the stimulator such that it is firing the muscle in a similar way to the normal motor unit. The use of this technique has been found to give fatigue resistance but use of pseudorandom sequences using sequences with similar spectral composition do not give such a marked improvement[119, 120, 121].

3.6.2 Controlled Stimulation

Solomonow et al.[93, 94, 122, 123] have already been mentioned with regard to their studies of cat muscle and its force EMG relationships. In order to achieve this they developed a new technique for stimulation which allowed the control of recruitment of the muscle fibres. Zhou et al.[124] describe the technique in detail. Essentially they use a dual stimulator, that is, there are two stimuli, one is essentially the typical stimulus (pulse width 100 μs and firing rate of 10-75 pps) which is combined with a second high frequency stimulus of around 600pps. With the typical stimulation techniques, it is well known that as the stimulus is increased, the larger diameter axons are stimulated first, since they have a lower threshold, followed by the smaller diameter axons[21, 108]. The effect of the high frequency stimulus is that with a 600pps supramaximal stimulus the neuromuscular junction can be prevented from conducting action potentials elicited by the firing rate stimulus. As the high frequency pulse amplitude is reduced, the smallest diameter axons, that is, the smallest motor units, escape the block and conduct action potentials. As the pulse amplitude is decreased, progressively larger motor units become active.

This technique is claimed to allow far greater control over the muscle force and can be used to ensure a linear force relationship. The system has particular application in muscle where more precise control is required such as the hand. There is increased fatigue resistance since not all the fibres fire at once. It should be noted however that this work has been carried out using cuff nerve electrodes on the muscles of a cat and not as yet in humans.

Chapter 4

Recording Muscle Responses

The recording of muscle signals is probably one of the greatest sources of error within any muscle analysis system. The causes of these errors can be due to a number of different effects. In this chapter it is intended to review the problems associated with recording EMGs both from voluntary muscle contractions and from stimulated muscle. Possible sources of error will be described and the minimisation or elimination of them discussed, such that the reasons for the designs described in Chapters 5, 6 and 7 will become clear. Where there are choices other than those suggested by this discussion of skin and electrode modelling, specific explanations are offered in the appropriate chapter.

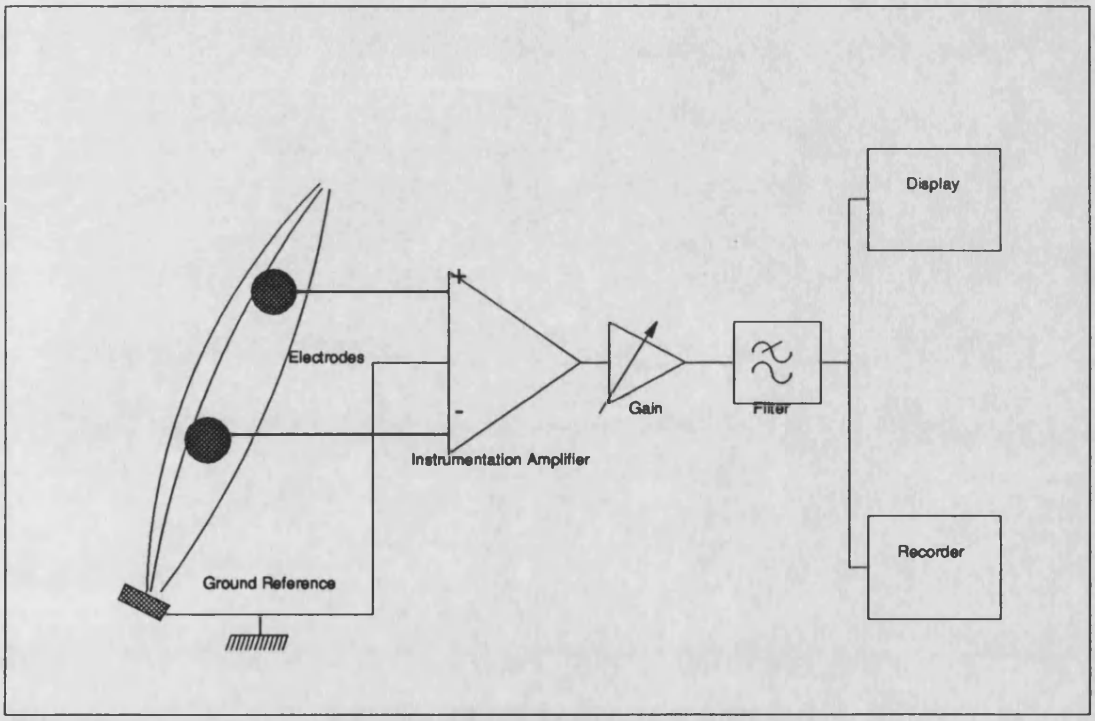

Figure 4.1 *Schematic of Basic EMG Detection System*

When discussing the detection and analysis of muscle EMGs it is important to define the detection method since this has a large effect on the type and quality of the detected EMG and CAP. All the systems described in this report make use of surface detection techniques. Percutaneous techniques such as needle electrodes have not been used because the aim is to develop systems that require no specific medical training to apply. The percutaneous techniques have an inherently higher SNR and signal bandwidth but will not be explicitly discussed here because the techniques cannot be applied readily as part of a feedback control system at this stage.

The basic EMG pickup system consists of four main elements as shown in Figure 4.1. It consists of electrodes which make an electrolytic contact with the body. These are fed into an amplifier which is usually configured as some form of instrumentation amplifier. The output of the pre-amplifier then passes through an adjustable gain and low-pass filter stage, which will amplify and filter the small detected signal to a level where the display and analysis system can process the muscle responses. The various parts of this basic system will now be considered in more detail.

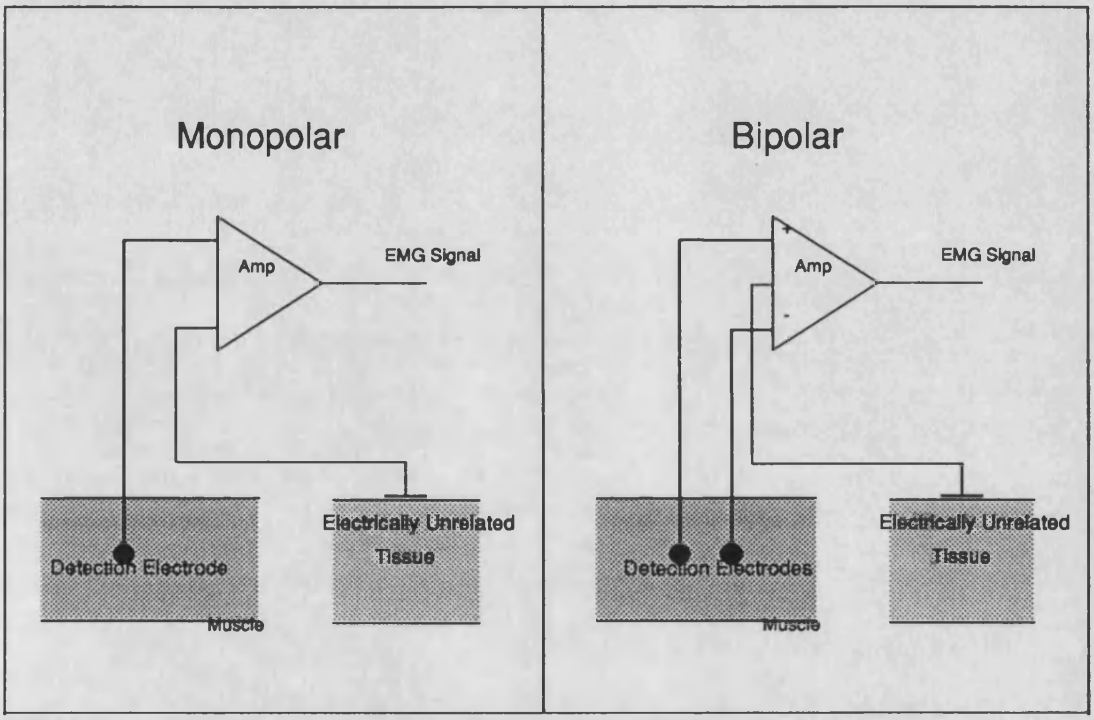

Figure 4.2 *Diagram showing Monopolar and Bipolar Electrode Configurations*

4.1 Electrodes

Over the years many different types of electrodes have been developed for the various electromyographic investigation techniques. The choice of electrode is determined by such factors as required selectivity, size, or ease of use in a particular situation. The section of the electrode that makes contact is usually referred to as the detection surface. The electrodes are either used singularly in a monopolar configuration or in pairs in a bipolar configuration, as assumed in Figure 4.1. Figure 4.2 shows these two configurations both of which require some form of reference or ground electrode.

As has already been mentioned there are two main types of electrode that are used to study muscle behaviour: surface (or skin) electrodes, and inserted (wire and needle) electrodes. Figure 4.3 shows a picture of some typical needle electrodes and surface

electrodes. Two types of surface electrode are shown: "stick-on" ones and electroencephalogram silver disc electrodes. The electrodes act as metal-electrolyte half-cells because the electrode forms an interface between a system in which conduction occurs by ion movement and a system involving electronic-type conduction.

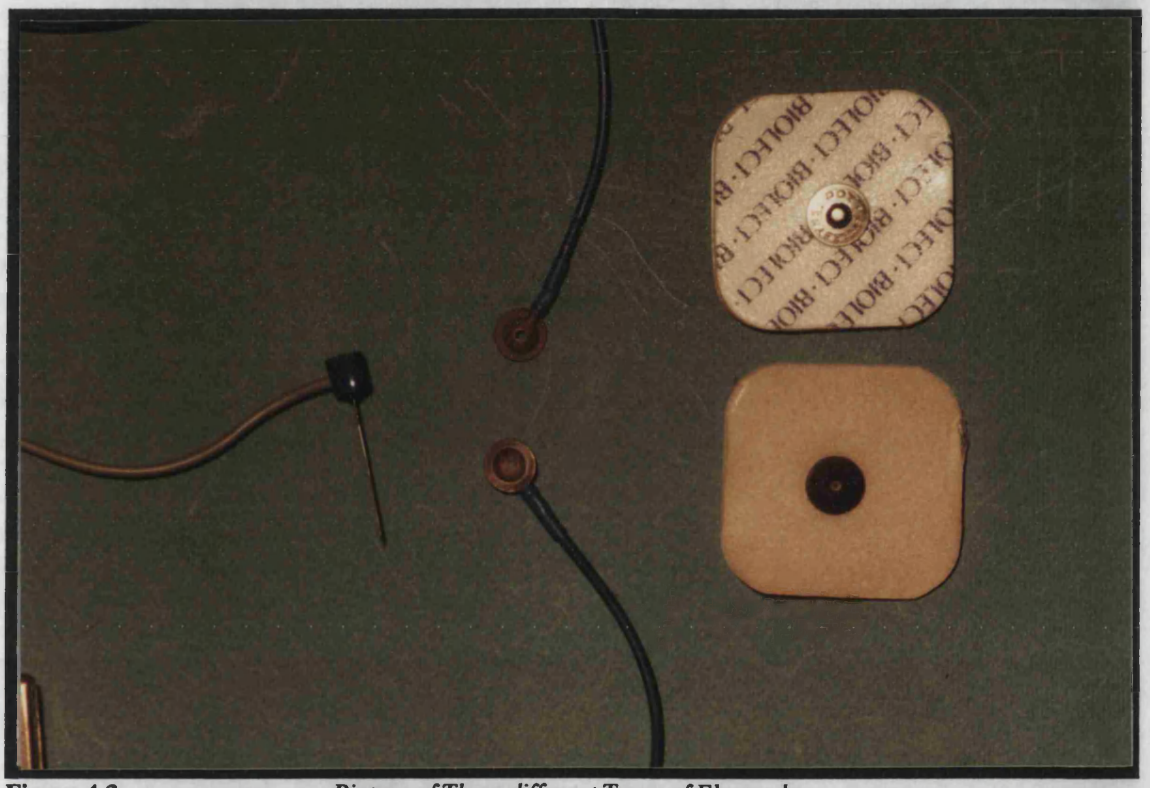

Figure 4.3 *Picture of Three different Types of Electrodes*
a) Needle Electrode, b) Silver Disc Electrode c)Stick on Ag-AgCl

The properties, design and application of potential sensing electrodes is not a straightforward topic and complete books have been written on this topic alone [125, 126]. The important question when considering EMG electrodes is whether the potential appearing between the terminals of the electrodes is totally bioelectric in origin.

4.1.1 Electrode-Electrolyte Interfaces

It is the characteristics of this phase boundary that give an electrode many of its properties. Although electrophysiologists have been using electrodes since the 1850s, an accurate description of the nature of the electrode-electrolyte interface has been slow to evolve. Up until the 1920s when the valve amplifiers appeared with their relatively high input impedances the only way the electrode-electrolyte-subject impedances could be reduced was by using large area electrodes and strong electrolytes[127, 128 pp69-71].

At the electrode-electrolyte interface there is a tendency for ions in the electrode to exchange with ions in the electrolyte and vice-versa. Electron transfer and a state of equilibrium results, which leads to a charge distribution that is characteristic of both the metal and the electrolyte. This region was conceptualised by Helmholtz[125 p3, 127] as a double layer of electric charges of one sign at the electrode surface in equilibrium, with a sheet of charges of the opposite sign in the electrolyte. This configuration has the properties of both a capacitor and a voltage source. This description, though possibly simpler than the real process, provides a good model for the components of an electrode-electrolyte interface. Nernst[129 p45, 130 p145] subsequently defined an equation relating the potential across the membrane and the two concentrations of the ions, known as the Nernst Equation, which can be stated as:

$$E = -\frac{RT}{nF} \ln \frac{[C_1 f_1]}{[C_2 f_2]} \qquad 4.1$$

where R = *Gas Constant* (8.31441 *J/K×mole*)

T = *Absolute Temperature Degrees Kelvin*

n = *Valence of ion*

F = *Faraday Constant* (9.648456×10^4 *C/mole*)

C_1, C_2 = *Concentrations of ions on the two sides of the membrane*

f_1, f_2 = *Respective activity coefficient of the ions*

This equation permits the calculation of the finite electrode potential due to the half-cell at the electrode-electrolyte interface.

4.1.2 Warburgs Law

Warburg[127] demonstrated that an electrode-electrolyte interface could be equated to a series resistance and capacitance circuit. He also showed that for a single frequency the reactance of the capacitance is approximately equal to the resistance and over a limited frequency range, the values for resistance and capacitance vary inversely and almost as the square root of the frequency.

These findings however have limitations. Although the reactance is almost equal to resistance both do not always vary as $1/f^{0.5}$. Often the exponent is less than 0.5 so a better approximation is X=R and both vary as $1/f^{\alpha}$ where $\alpha \leq 0.5$. This is only valid for sinusoids over ≈10 Hz and even then it is only valid for a limited range. The second factor affecting this model is that for a given metal-electrolyte interface the magnitude of the capacitance depends not only on the frequency but also on the magnitude of the current employed for measurement. That is, equivalent series capacitance increases with increasing current density. It has also been shown that the series equivalent resistance decreases with increasing current density. From the above

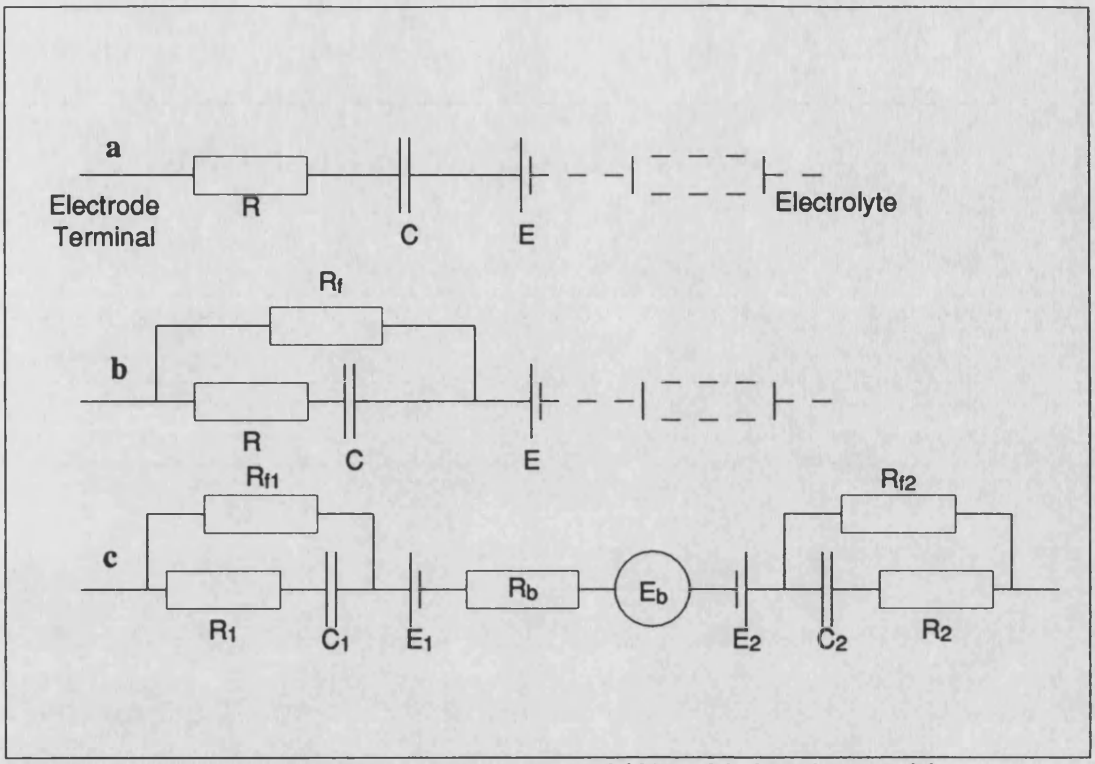

Figure 4.4 *Equivalent Circuits of the a) Warburg Model b) Modified Warburg Model to allow for finite DC resistance c) Model showing the Electrode to Electrode Components*

discussion it is clear that empirical formulae cannot be readily applied to the modelling of the electrode-electrolyte interface.

4.1.2.1 Electrode-Electrolyte Model

From the discussion above it can be seen that a model for a metal electrode placed in contact with an electrolyte—such as body fluid (needle) or electrolyte paste (surface)—can be formed as a series circuit consisting of a battery to represent the half-cell potential, and a resistor and a capacitor in series to represent the Warburg impedance, see Figure 4.4a. At a given frequency the value of the resistance approximately equals the reactance of the capacitance. Both resistance and capacitance decrease with increasing frequency. In addition, the values of resistance and capacitance are dependent on the electrode current density. At a low current density the series equivalent reactance and resistance vary as $1/f^{\alpha}$ where α is 0.5 or slightly less as has been discussed.

This model is incomplete because it has an infinite resistance to DC. To account for the finite DC resistance a resistance R_f is required across the Warburg Impedance as shown in Figure 4.4b. This parallel resistance is neither simple nor linear and is called the 'Faradic Admittance' by electrochemists.

This simple model has electrical properties consistent with the electrical characteristics measured between the terminals of a large number of electrodes used in

bioelectric event measurement extracellularly. Thus for a typical bipolar detection system the impedances between a pair of electrodes would be as shown in Figure 4.4c.

There are three potentials: two due to the half cell potentials of the electrodes, E_1 and E_2 and one due to the bioelectric generator E_b—muscle in the case of EMG. There are also three impedances: $R_1C_1R_{f1}$ and $R_2C_2R_{f2}$ due to the electrode impedances and one due to the equivalent bioelectric generator R_b.

The model predicts that there is a finite DC resistance between the electrode terminals which will be high in the low frequency region and decrease with increasing frequency until it tends to match the impedance of the equivalent bioelectric event generator.

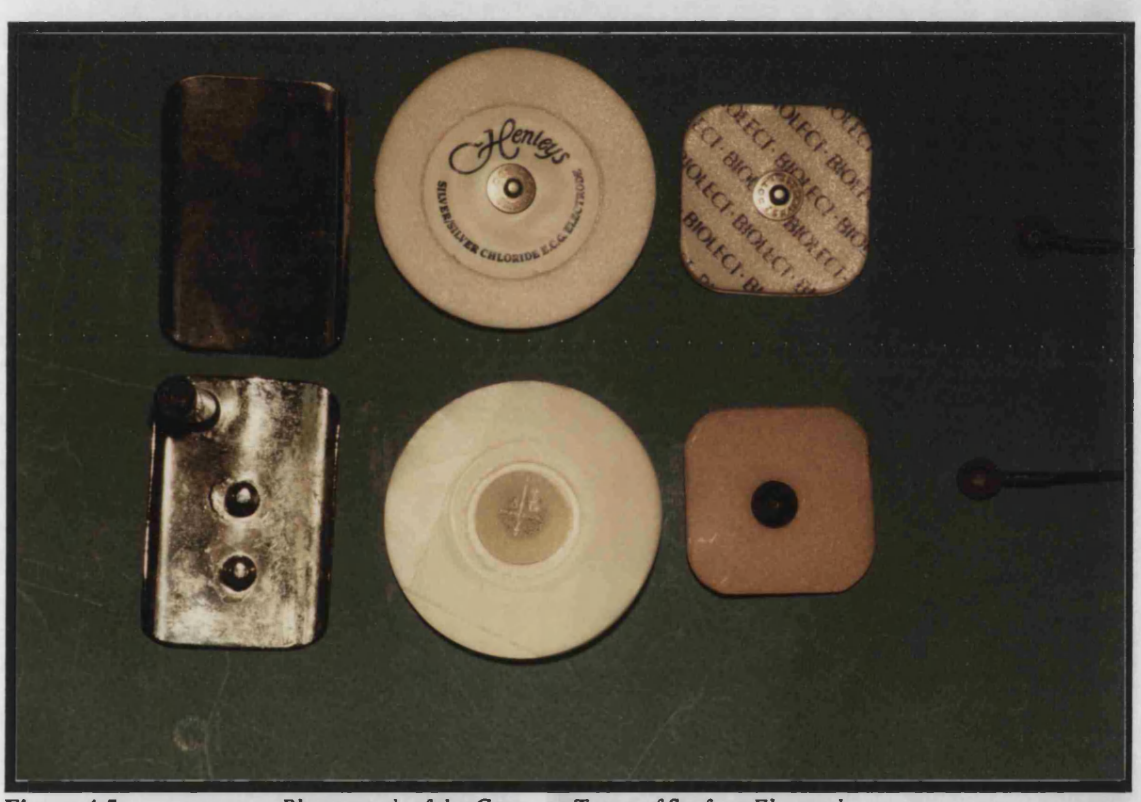

Figure 4.5 *Photograph of the Common Types of Surface Electrode*

4.1.3 Types of Surface Electrodes

From the discussion on an equivalent model for the electrode-electrolyte interface it is clear that the choice of metal and electrolyte will contribute significantly to the extraneous noise in the recorded waveform. The original surface electrodes were plate electrodes. These were separated from the subject's skin by cotton or felt pads soaked in saline. Later a conductive jelly—electrolyte paste—replaced the felt; in fact some electromyographers still use this system today. Figure 4.5 shows this type of electrode and the other types that are described below. The metal plate electrodes are usually made of, or plated with, silver, nickel or similar alloy.

One of the major problems with using plate electrodes is the possibility of slippage or movement. These movements will introduce artefacts due to changes in the electrode impedances and their respective electrode potentials. Often these changes are so severe that they completely hide the bioelectric potential that the electrodes are trying to measure. A number of attempts to reduce the effect have been made and the relatively recent *floating electrode* is probably one of the most successful to date[126, 128, 130, 131].

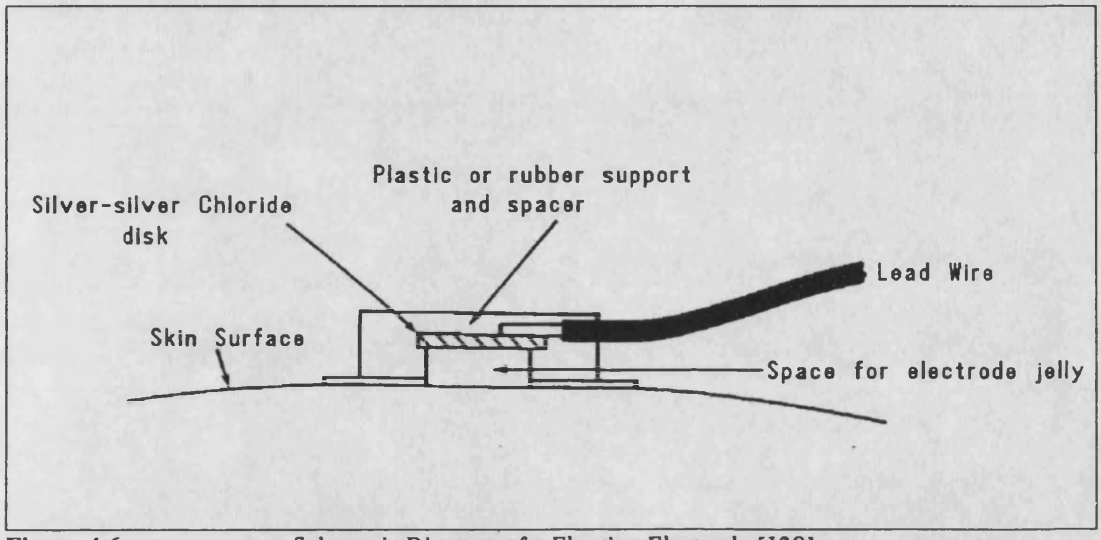

Figure 4.6 *Schematic Diagram of a Floating Electrode [128]*

The floating electrode comes in various forms but all are based on the same principle. The aim is to eliminate movement artefacts by avoiding any direct contact between the metal electrode and the skin. The only conductive path is the electrolyte paste which forms an electrolyte bridge. It is now this electrolyte bridge that must be maintained to ensure performance is not impaired. Figure 4.6 shows a cross section of a typical floating electrode and the other electrodes in Figure 4.5 are all variations of the floating electrode; they are two disposable versions and a Silver-SilverChloride ECG reusable electrode. The Floating Electrode is usually attached to the skin by means of double sided adhesive rings—collars—which adhere to both the skin and the electrode.

Special problems are associated with long term monitoring such as astronauts ECG or as in the FES programme. This has led to the development of special flexible spray on electrodes[125, 126]. More recently, in the search for minimal preparation electrodes, combined electrode and preamplifiers have been used. Some of these have used electrode gel and some have relied on the good design of the amplifier to ensure that the use of gel is not required. Most of these pre-amplifier combinations use stainless steel in preference to the now standard Ag-AgCl electrodes used in the floating electrodes. Geddes[125] gives a full discussion on various metal combinations

and their relative merits. Essentially the choice of electrode is determined by its electrochemical properties. The stability of silver electrodes is well known and the coating of chloride increases the stability significantly thus making the Ag-AgCl electrode the most stable of the easily constructed electrodes. With care, a pair of Ag-AgCl electrodes can have a difference of a few micro volts as can be seen from Figure 4.7.

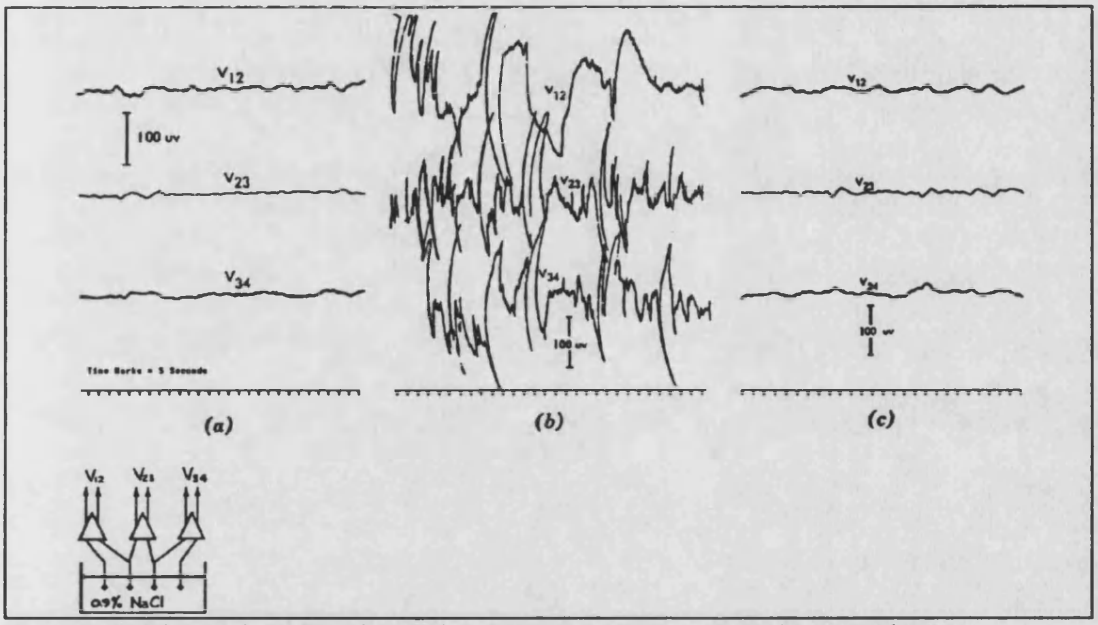

Figure 4.7 *Electrical stability of chlorided silver electrodes: (a) electrode noise voltages after chloriding; (b) electrode noise voltages after removing silver chloride coating with emery paper; (c) electrode noise voltage after rechloriding. [125 p12]*

4.1.3.1 Dry Electrodes

Up to now the electrode descriptions have assumed that some form of electrolyte is used to maintain the electrical contact. Recent advances in electronics have enabled alternative approaches in which the electrodes are applied directly to the skin without any electrolyte paste. The main feature of these electrodes is that they are self contained and have a very high input impedance.

A metal electrode placed directly against the skin establishes some contact with the skin. An equivalent circuit similar to the Warburg circuit of Figure 4.4c, still exists despite the lack of electrolyte. In this case the impedance is mainly resistive but there is still some capacitance due to the metal plate being in contact with the stratum corneum which has a very high resistance. The dermis has a much higher conductivity than the stratum corneum and thus a capacitor exists. The dermis and metal electrode are the two plates with the stratum cornea as the dielectric.

The spacing between the plates is considerably greater than for the double layer with the wet electrodes and thus the capacitance is much lower. If there is any moisture such as perspiration on the skin it can establish a half cell potential but is usually

neglected. Thus the effective equivalent circuit is mainly resistive but of a considerably higher resistance than is the case with the wet electrodes. By using an impedance converting amplifier—buffer—mounted directly on the electrodes the biopotential can be detected with minimal distortion despite the high source impedance. The input impedance required is of the order of 0.1 to 1 GΩ.

Various investigators have built electrodes based on these principles [3, 132, 133, 134]. It is also possible to make dry electrodes in the form of insulated electrodes where there is no metal-electrolyte interface at all[135, 136]. Richardson[137] describes electrodes that are really capacitors consisting of a metal electrode on which is grown a thin surface of the oxide of the metal. This is placed against the skin such that the skin forms one plate of a parallel-plate capacitor and the metal electrode forms the other, the oxide film is the dielectric. These electrodes have a capacitance of the order of 1nF to 5nF between the metal and the body. As long as the input impedance of the amplifier is high enough the high pass filter effects due to the RC circuit formed by the electrode and the amplifier input impedance are minimised. As with dry metal electrodes the amplifier should be located as close to the electrodes as possible to reduce noise from electrostatically detected signals. Several authors[132, 138, 139, 140] have built the electrodes and amplifier into a single unit to reduce the effects described above.

Although the dry electrodes do offer advantages there are some inherent disadvantages. For the metal type dry electrodes, care must be taken to ensure any half cell potentials that might exist do not saturate the amplifier. With the capacitive dry electrode, impedance can be less than predicted if the electrode is not in good contact with the skin. This has two effects: the low frequency response of the amplifier can be reduced due to the reduced capacitance or if there is a change in capacitance, as usually happens, there will be a changing voltage which will cause an artefact.

The very high impedance of these electrodes makes them very susceptible to picking up extraneous voltages due to external electromagnetic fields and hence a combined preamplifier and electrodes is the preferred form[3, 107, 138].

4.1.4 Electrode Configuration

The EMG may be easily detected on the surface by placing an electrode with one detection surface on the muscle and detecting the electrical activity with respect to a reference electrode located in an environment which is electrically quiet or contains electrical signals unrelated to those being detected. The reference electrode is often another surface electrode or a felt strap soaked in saline. This arrangement is called monopolar and is shown in Figure 4.2a.

The monopolar configuration has the disadvantage that it will detect all the electrical signals in the area of the electrode. That is, it will detect both bioelectric potentials and unwanted electrical signals from sources other than the muscles under investigation. This configuration is used more for historical than rational reasons in modern practice.

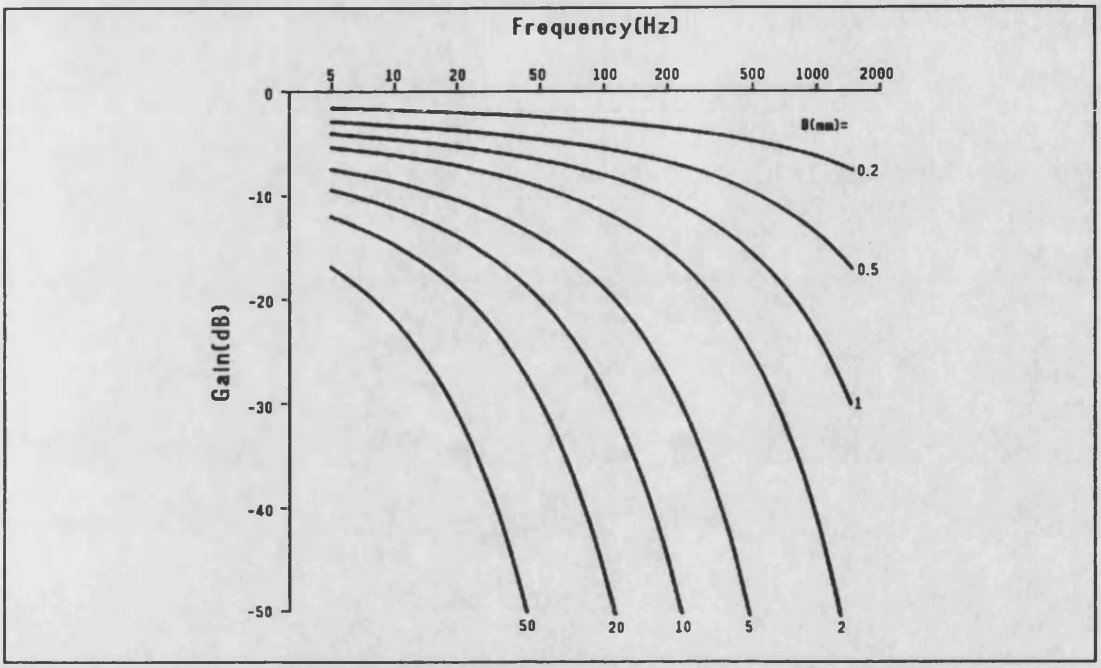

Figure 4.8 *Representation of the Tissue Filter Function [3 p40]*

The bipolar configuration overcomes these limitations. Here two detection surfaces are used to detect two potentials from the muscle of interest each with respect to the same reference electrode. These two signals are then fed to a differential amplifier which amplifies only the difference and eliminates the common mode components, such as the electrode potentials. Signals from the muscle will differ at the two detecting surfaces whilst AC noise signals such as mains 'hum' will be detected with approximately equal amplitude and thus will be subtracted before being amplified. This results in reduced noise with respect to the bioelectric signal of interest.

4.1.5 Tissue and Skin Filtering Effects

The muscle tissue appears as a filter to the propagation of the biocurrents. The output signal is greater for lower frequencies than for higher frequencies; it is also a function of the distance of the EMG sources to the detection surface of the electrodes. Thus the muscles and adjacent tissues appear as a distance-dependent low pass filter as shown by Figure 4.8. Extensive modelling of this has been carried out by a number of investigators[97, 126, 130, 141, 142]. Figure 4.8 gives some typical curves showing the effect of the attenuation with distance from the EMG source.

Unfortunately these effects are neither simple nor isotropic; in fact the effects are highly directional. This anisotropy is due to the non-homogeneity of the anatomical construction of a muscle. The muscle fibres are usually arranged lengthways and the

surrounding extracellular fluid forms lengthways channels running parallel to the muscle fibres. These channels have a much lower impedance giving the highly anisotropic property. The modelling of these factors becomes considerably more complex when the effects of passing through the fatty tissue and the skin to reach the skin surface are added in.

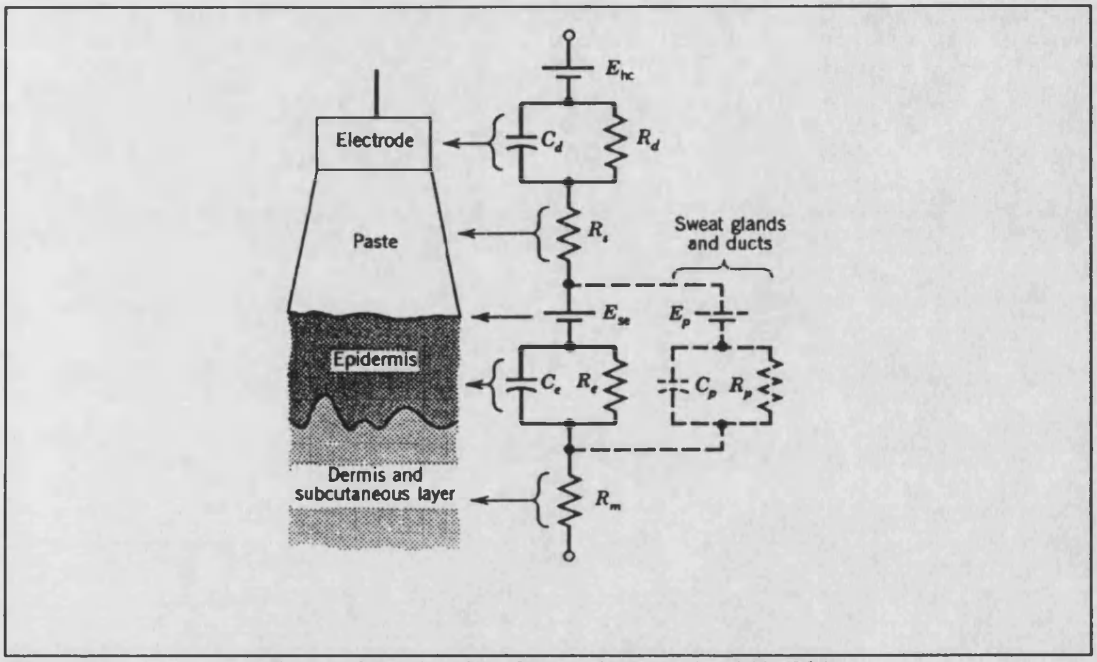

Figure 4.9 *Electrical Model of the Skin and Electrodes[141 p204]*

A number of authors have produced models for the skin impedance[130, 144, 145], all of which follow a very similar form. A model for the electrode-electrolyte interface has been already discussed. This will now be used along with a typical skin model, to produce an equivalent circuit for the signal paths in a bipolar differential amplifier configuration. First it should be noted that the original modified Warburg circuit can be rationalised into a single resistor and capacitor in parallel using standard circuit manipulation techniques and it is this form that will be used in the discussion.

Expanding the original bipolar configuration to include a skin model produces the circuit of Figure 4.9. The electrode-electrolyte model of Geddes[127] is shown adjacent to the electrode-paste interface. The resistance R_S is the effective resistance of the paste between the skin and electrode. The stratum cornea—the horny layer of dead material on the surface of the epidermis—acts as a semi-permeable membrane so that if there is an ionic concentration difference between the two sides, a potential E_{se} will exist and its value is defined by applying the Nernst equation. The epidermal layer itself has an impedance that behaves as a parallel resistor and capacitor combination. The dermis and subcutaneous layers behave much more as a pure resistance with conduction—it is thought—via the blood which is ionic and has a very low resistivity of 120-160 Ωcm. These layers are modelled by a resistor R_m.

The stratum cornea gives an added artefact effect which could be reduced or even eliminated by removing the stratum cornea by vigorous rubbing or even light sanding. The removal of the protective barrier makes this region more susceptible to irritation[144, 146]. This tends to short out all the effects of the stratum cornea and the epidermis. Tam and Webster[146] showed that this is not a significant source of motion artefact in Ag-AgCl skin electrodes.

The dashed lines represent contributions from the sweat glands and sweat ducts. Their effect is usually ignored except when considering special responses such as the galvanic skin response.

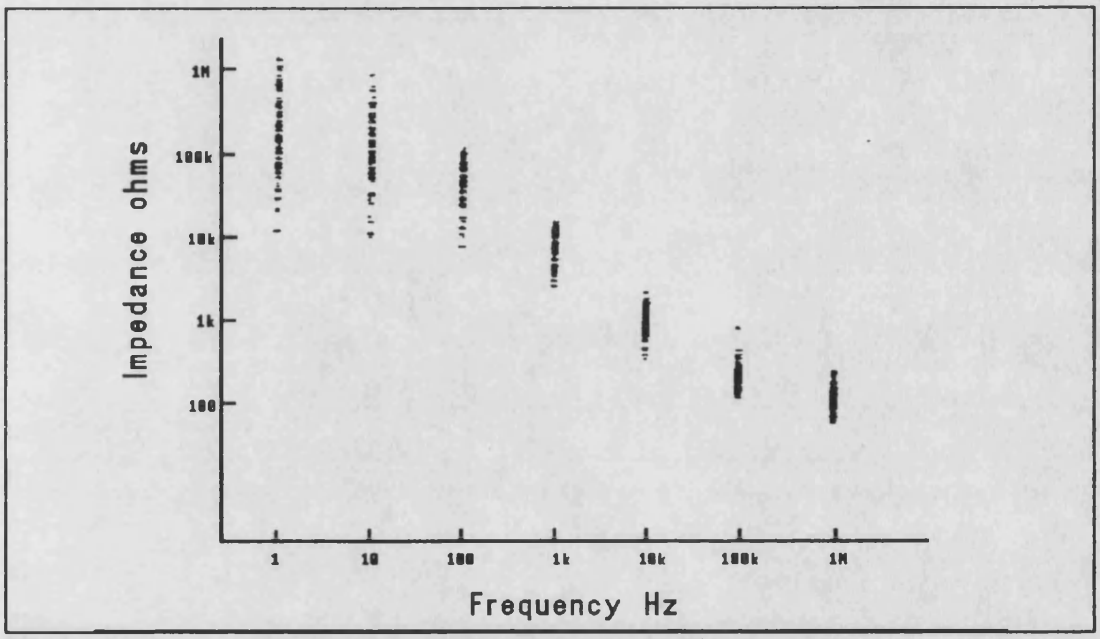

Figure 4.10 *Results obtained by Rosell showing the Filter Response*

Rosell and Webster[147] have carried out impedance measurements to characterise the skin filter model from 1 Hz to 1 MHz, Figure 4.10. They found a 20 dB/decade drop at high frequencies which compares well with the results of Wood[144] who found the 3dB point occurring at 100 kΩ at a frequency of 500 Hz. Assuming a pure low pass filter response, Wood finds values for the resistors of $R_1 = 100k\Omega$ and $R_2 = 100\Omega$. For the capacitor he calculates a value of 3 nF. A model for the overall filter is given in Figure 4.11, where z_1 is the electrode-skin interface impedance, z_2 is the surface sweat layer, z_3 is the epidermal (including sweat glands) and z_4 the dermal resistance.

4.1.6 Changes in the Model when applied to Stimulating Electrodes

The stimulating electrodes are very similar in principle to the pick up electrodes. They differ in that currents of several milliamps flow across the electrode skin interface.

When considering changes to the model it is important to realise that the net current flow across the electrode-electrolyte is not always zero. Even if Biphasic stimulation is

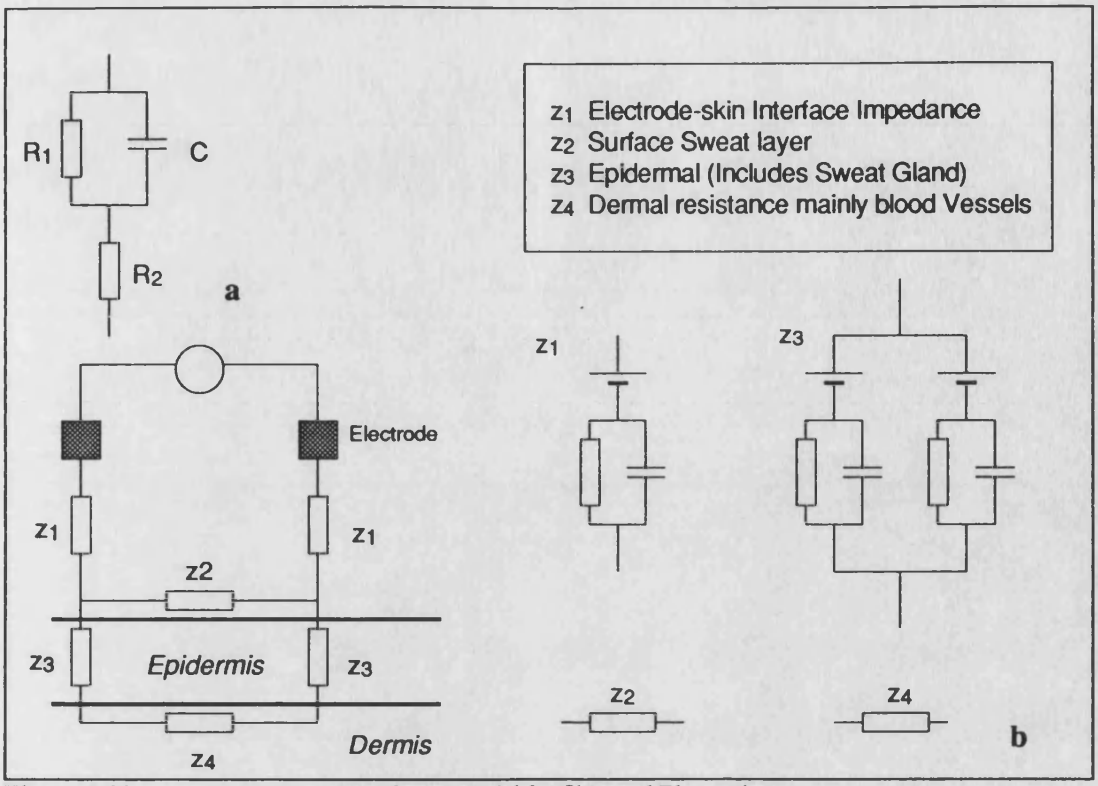

Figure 4.11 *Impedance Model for Skin and Electrodes*

used the average currents over a long time period will be zero but over a single period there are points when the net current is in one direction and periods when it is in the opposite direction. Since the currents in the two directions may also differ, the electrical properties of the electrode-electrolyte interface will change both during the pulse and over the time in which the stimulation is being carried out. Thus the electrodes equivalent circuit is determined by both the current and the duration of the stimulus.

Figure 4.12 shows some typical waveform plots of constant current and constant voltage stimulation showing the voltage and current waveforms and how the electrode polarisation can affect the shape. For the constant current pulse it can be seen that the voltage pulse is not constant. This finding is not unreasonable from the model since there is a large reactive element. In other words, polarisation occurs. The initial rise is due to the voltage drop across the resistive components of the electrode-electrolyte interface. The voltage then continues to rise due to a redistribution of charge, that is, there is a change in the polarisation due to the unidirectional current. In the discussion of the Warburg model this polarisation is represented by a capacitor. The size of this capacitor is determined by several factors, one of which is the current density. Thus the equivalent circuit will change as the stimulus intensity is increased. When the current falls back to its low value the voltage drops rapidly until it reaches a voltage equivalent to the polarisation which decays away at a much slower rate.

In the case of the constant-voltage stimulus, the current has a large jump as the polarisation charge establishes itself, then falls back to a lower steady-state value. When the voltage pulse falls, the current changes direction then slowly returns to its initial value. This is a result of the dissipation of the polarisation charge built up at the electrode-electrolyte interface.

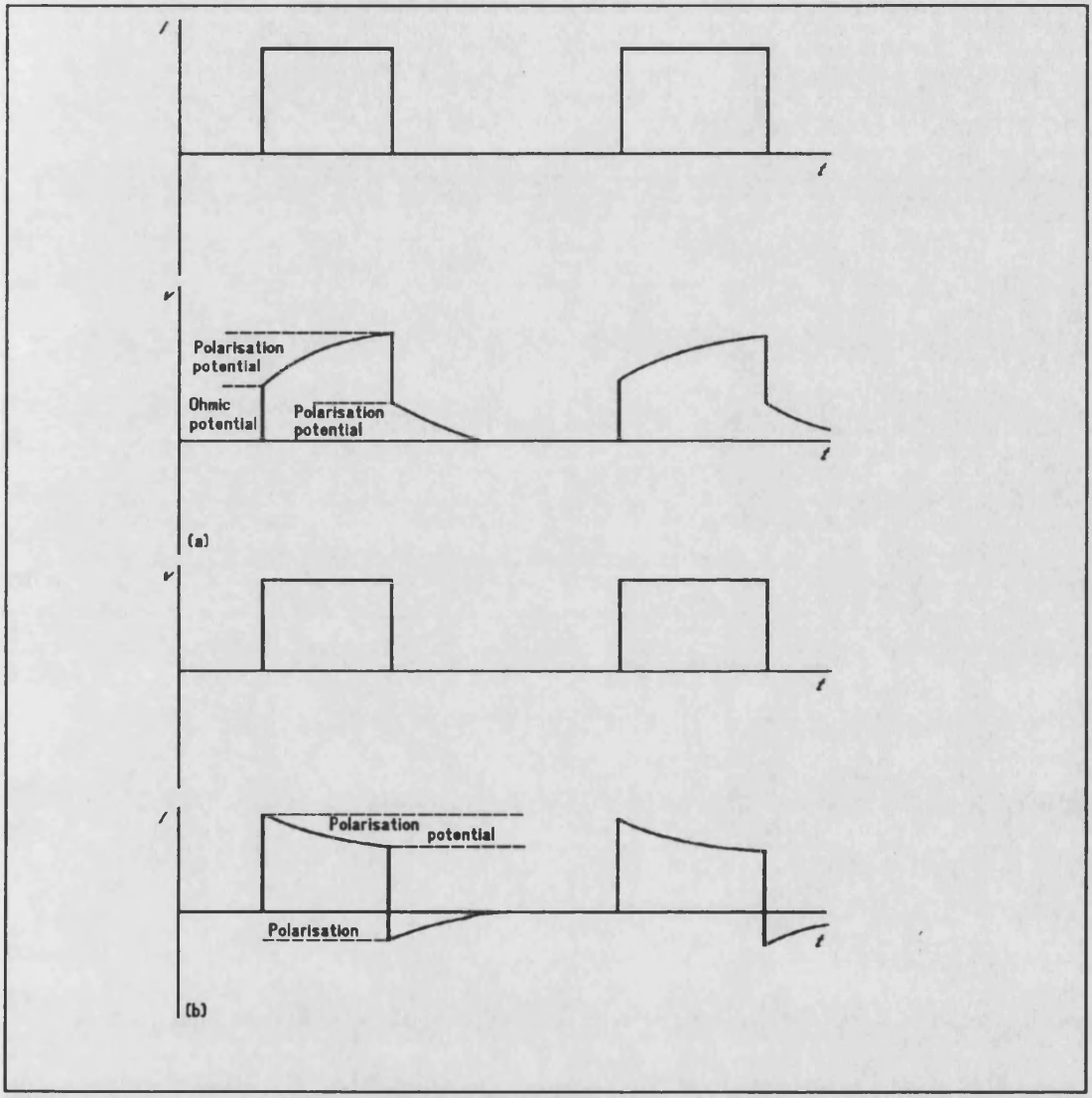

Figure 4.12 *a) Voltage waveform for a Constant Current Stimulator*
b) Current Waveforms for a Constant Current Stimulator [130 p266]

Choice of materials for the stimulus electrodes must take into account the chemical reactions that occur at the electrode-electrolyte interface. If the stimulating current causes the oxidation of the electrode, the electrode will be destroyed with use and there will be an increase of ions from the electrode in the vicinity of the electrode which may well be toxic to the tissue. If Ag-AgCl electrodes are used there will be a creation of Cl^- ions or the reduction of what is already formed thereby changing the electrode characteristics.

Stainless steel electrodes—as when they are used for detection—will irreversibly dissolve at a very slow rate—much less than 10^{-3} to 10^{-6} times the reaction rate of Ag-AgCl electrodes. In addition one or more of the following *electronation reactions* [141 p204] exist:

$$O_2 + 4H^+ + 4e^- \rightarrow 2H_2O \quad \text{(acid solution)} \qquad 4.2$$

$$O_2 + 2H_2O + 4e^- \rightarrow 4OH^- \quad \text{(alkaline solution)} \qquad 4.3$$

$$2H_3O^+ + 2e^- \rightarrow 2H_2O + H_2 \quad \text{(acid solution)} \qquad 4.4$$

$$2H_2O + 2e^- \rightarrow H_2 + 2OH^- \quad \text{(alkaline solution)} \qquad 4.5$$

The current due to the O_2 generation of equation 4.3 will be affected by surface blockage on the electrode caused by various organic and inorganic gel constituents if an electrode gel is being used.

It is thought[141] that there are two sets of reactions that cause the polarisation of stainless steel electrodes. At the cathode, O_2 reduction occurs according to equations 4.2 or 4.3, H_2 evolution according to equations 4.4 or 4.5, and gel impurity reductions occur. At the anode, O_2 evolution, gel impurity oxidation, and the formation of metal oxides, hydroxides, and complexes occur. Since the nature and rate of these two sets of reactions are changed, the electrode is somewhat permanently polarised. The gas evolution is only likely to occur with stimulating voltages, that is, voltages above a volt.

The best stimulating electrodes are made from noble metals or stainless steel[148] which undergo minimal reactions. The polarisation of these electrodes is large and this leads to greater distortion of the waveforms.

Conductive rubber stimulating electrodes are a fairly recent addition to the electrode market[141]. These function in an similar way to a metal electrodes. The models used previously for the metal electrodes apply in a similar way but there are no half cell potentials. The reactions of equations 4.2 to 4.5 apply and lead to a circuit equivalent similar to the Warburg circuit described earlier.

At higher current densities there is a possibility of water electrolysis with both metal and rubber electrodes. The reaction rate is limited however by the diffusion of the reactants to the conductor surface, surface blocking from gel ingredient adsorption and the gas evolution reactions of equations 4.2 to 4.5.

4.1.7 Positioning of Electrodes

The positioning of the electrodes has been a subject of much discussion over the years. Basmajian[3] states that the common practice of electromyographers of locating the detection electrode in the vicinity of the motor point of the muscle—the surface

projection of the anatomical centre of the innervation zone of the muscle—is wrong. The reasons offered to support this argument are that the motorpoint is to some extent an electrically and anatomically definable point.

Masuda et al.[149] have shown for the biceps brachii muscle that the number of innervation points varies from subject to subject, although general areas for the position of innervation zones could be identified. Thus, the only way to guarantee that a certain individual has an innervation zone in a defined area is to locate them experimentally before carrying out the test of interest. The second reason often used to support the use of the innervation zone is that because the motorpoint is the position at which an externally applied electric current causes maximal excitation of the muscle, it should be the position at which the greatest signal would be found.

Basmajian[3] presents results that show the least reliable results for surface electrodes are obtained around the innervation zone when recording the EMG as a muscle is shortened. The results were made more reliable by applying pressure. He notes that the variation obtained as the muscle contracts/shortens causes the electrode to move relative to the active fibres in the muscle and therefore is itself a source of signal changes that are not related to physiological aspects of the muscle contraction. This type of effect is particularly likely to occur in EMG signals during anisometric contractions such as those that occur in gait.

Roy et al.[107], using the tibialis anterior muscle in tests on the median frequency and conduction velocity using electrical stimulation, found as many as five motor points, contrary to the common belief of one motor point and in support of Masuda et al.[149]. In subjects with more than one motor point a 5-10% variability in stimulation thresholds was found. When comparing electrode position with respect to the motor points and measuring the CV and median frequency, they found the CV estimates were unstable close to the motor points and that both MF and CV varied as a function of location. They noted that a 'stable zone' between the distal motor point and the tendon provided the best estimate of the median frequency and conduction velocity.

The distance between the two electrodes in the bipolar configuration also has a filtering effect on the observed EMG[3, 62, 150, 151, 152]. Lynn[153] proposed a rule of thumb of an interelectrode spacing of 1 cm. They also noted[153] that the bandwidth of the detected signal increases as the interdetection surface distance decreases.

Lindström[3, 62] has derived an equation to define the filter function $R(\omega,d)$ for bipolar electrodes as a function of the interelectrode distance d, and the mean conduction velocity v and the signal frequency ω:

$$R(\omega,d) = K \sin^2\left(\frac{\omega d}{2v}\right) \qquad 4.6$$

where K is a scaling factor representing various gain factors of the electrode- electrolyte interface.

This equation is plotted out for surface electrodes assuming an interelectrode spacing of 1 cm and a conduction velocity of 4 m/s in Figure 4.13 . From the graph shown in Figure 4.13 it is clear that the electrodes will impose a bandwidth limit on the recorded signal for the given example of about 400 Hz. Clearly with needle electrodes, where d is of the order of 0.5 mm, the bandwidth is much higher and is of the order of 10 kHz. This is one of the reasons that needle electrodes provide an increased signal quality when compared to surface electrodes.

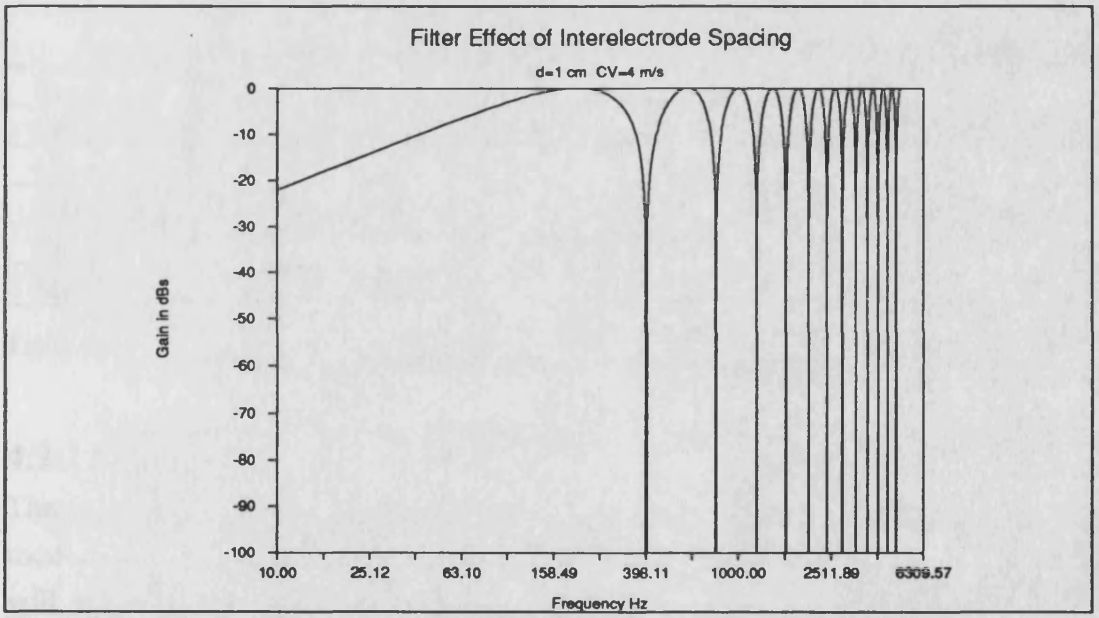

Figure 4.13 *Filtering Effect of Bipolar Recording Electrodes as defined by Equation 4.6*

4.2 Amplifier Design

The amplifier[154, 155, 156] is the second most important part of the detection system and it is the matching of the amplifier to the electrodes that usually decides the quality of the detected signal. It is clear from the discussion above that the electrodes and body tissue distort—filter—the electromyogram even before it reaches the amplifier. If the amplifier is not designed with its loading and output impedance properly matched for the load then it too will modify the frequency characteristics of the recorded signal.

4.2.1 Bandwidth

The bandwidth required from an amplifier depends on how the muscle signals are detected. The actual muscle signals have a bandwidth of the order of ten kHz.

However in order to detect a signal of this bandwidth the detector has to be close to the signal source and this would require needle electrodes. A summary of bandwidth versus detection electrode is given in Table 4.1 where the frequencies are given in terms of required amplifier response. When amplifying the EMG signal it is usual not to use a DC coupled amplifier for a number of reasons:

- The DC polarisation potential present at the electrode-electrolyte interface may be as large as the EMG signal being detected.
- Motion Artefacts in the lead wire will generally lead to low frequencies (<20 Hz) and these would be amplified.
- The frequency components below 20 Hz are unstable and fluctuate unpredictably.

Electrode Types	Bandwidth (Hz) 3 dB points for 12 dB/octave rolloff
Surface Electrodes	20—500
Wire Electrodes	20—1000
Monopolar and Bipolar Needle Electrodes	20—1000
Needle Electrodes for Signal Decomposition	1000—10000
Single Fibre Electrodes	20—10000
Macroelectrode	20—10000

Table 4.1 *Bandwidth Requirements of Various Electrode Types*

4.2.2 Input Impedance and Input Bias

The input bias current is the minimal current required to keep the amplifier active. In modern operational amplifiers it is of the order of hundreds of picoamps. The current will either flow into the input or out of the input depending on the input stage configuration, that is, whether it is made up of npn or pnp transistors or FETs. This current will cause polarisation in the electrodes and if it is too large lead to significant electrode capacitance.

The input impedance of the amplifier is the load seen by the biopotential source. Thus in order that the amplifier does not load or distort the signal, it must have a high input impedance. As has already been discussed, loading on the electrodes can affect their characteristics and lead to signal distortion. This means that the input impedance required is of the order of $10^{12}\ \Omega$.

The bias current becomes even more significant when using small needle electrodes which have a very small contact area. This means that even with currents of 100 pA the current density is high, resulting in a change of the electrode-electrolyte filter characteristics.

4.2.3 Common Mode Rejection Ratio

The common mode rejection ratio (CMRR) of a differential amplifier such as is used in a bipolar pickup configuration is a measure of its ability to reject common mode signals.

Considering Figure 4.2b, the differential amplifier will detect a signal at each electrode from the muscle combined with the ambient noise. The noise will be common to both inputs whilst the muscle signal will differ slightly because the electrode is in a slightly different place relative to the active fibres. Defining the signals at the two electrodes as m_1+n and m_2+n where m_1 and m_2 are the responses seen by electrodes one and two respectively and n is the ambient noise, then for a perfect differential amplifier with a gain of A:

$$\begin{aligned} amplifier\ output &= A\left[(m_1+n)-(m_2+n)\right] \\ &= A(m_1-m_2) \end{aligned} \qquad 4.7$$

The noise signal—the so called common mode signal—which is common to both inputs is cancelled out. In the case of practical differential amplifiers the cancellation is not quite perfect and there is a small residual error voltage E_e. This is due to the two input stages not being perfectly matched. The ratio of the common mode voltage applied, E_{cm} to the error voltage is defined as the CMRR and is a measure of the effectiveness of the differential amplifier. Thus:

$$CMRR = \frac{E_{cm}}{E_e} \qquad 4.8$$

The importance of a good common mode rejection-ratio can be seen from equation 4.8 where as long as the externally induced noise signals—such as the power line induced interference or EM radiation—is equal at the two electrodes they will not appear at the output. There is an obvious flaw in this requirement and that is that the two noise signals need to be the same. Since the noise is mostly radiated noise it will only be approximately equal at the two electrodes and hence the output will have an error signal due to the CMRR being finite and another due to the difference signal of the two noise components. In practice a CMRR >100dB is used and the tests should preferably be carried out in an area of minimal EM radiation.

4.3 Filtering

It is now clear that by the time the bio-signal reaches the filter it is already bandlimited by the detection method and the amplifier configuration. The filtering serves two purposes: it reduces the out of band noise so that energy is not wasted in amplifying noise that is not in the bandwidth of interest and it ensures that if the display and

storage process involves some form of sampling, as is the case for the system developed here, the Nyquist sampling criterion is met.

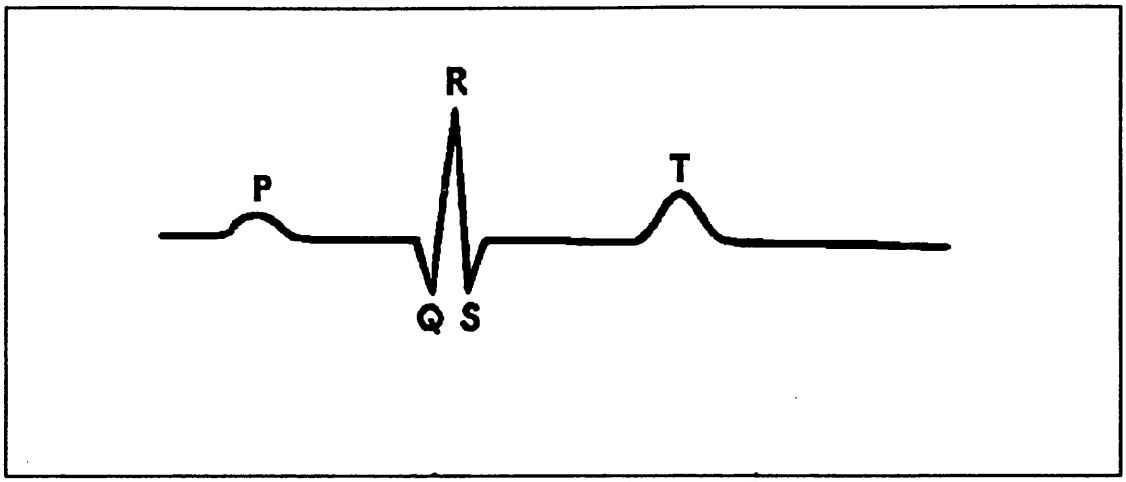

Figure 4.14 *Typical ECG Waveform showing the P, Q, R, S, T waves*

For surface electrodes, the signal is already bandlimited by the electrode spacing and tissue filtering to around 400 Hz so that a low-pass filter of 500 Hz or at most 1 kHz is required. The low frequency cut-off is somewhat harder to define because it has some conflicting constraints depending on the type of muscle response to be detected. For voluntary muscle responses 20 Hz is a reasonable cut-off but as will be seen later in this chapter stimulated muscle responses pose a new set of criterion on the precise cut-off point required.

If one wishes to measure signal power the signal must be amplified by a known gain. Sufficient gain is also required to ensure that the muscle response can be reliably measured and if trying to monitor changes with time it needs to be sufficient to ensure that a clearly measurable change can be recorded. Depending on the source of the myoelectric activity and the electrode type the muscle response can range in value from a few microvolts to tens of millivolts. Thus to get a reasonable output signal the gain required will range from hundreds to tens of thousands depending on the signal source and detection technique used, some authors quote using up to 2×10^5[157].

4.4 Common Problems

There are many factors that must be considered when trying to reliably record biopotential signals[130, 141, 158, 159, 160]. These affect both the design and use of the biopotential pickups. There now follows a discussion of the common problems associated with using an EMG pickup before considering the specific artefact problems associated with stimulated muscle responses. In order to demonstrate these effects, plots of typical ECG waveforms will be used because they are available and because they have a repeatability that can only be obtained with EMGs using stimulation. This will be shown later to provide a whole host of extra problems. The

repetitive nature of the ECG enables the comparison of the various effects to be seen readily.

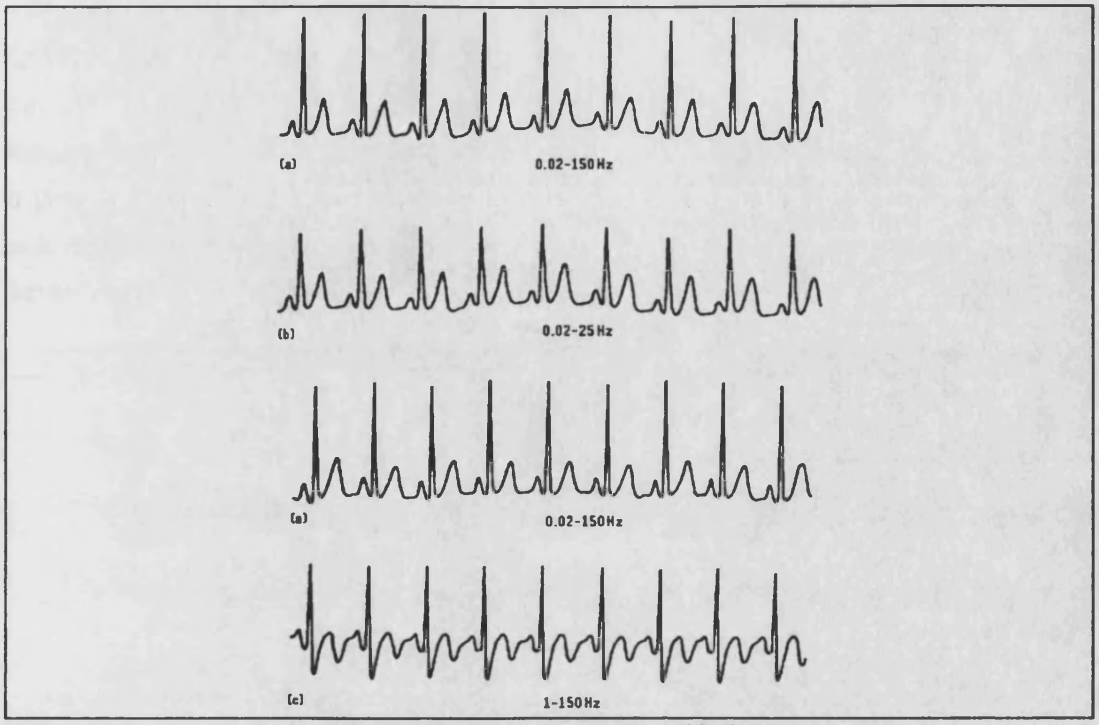

Figure 4.15 *Effects of Frequency Distortion [130 p285]*

Figure 4.14 shows a typical ECG waveform consisting of five waves which by convention have been called the P, Q, R, S and T waves. The P wave is caused by the impulse of contraction which sweeps over the atria. The Q, R and S waves are indicative of the spread of the impulse of contraction from the atrioventricular node, through the atricular bundle to the ventricular muscle. The T wave is recorded whilst the ventricular muscle is relaxing.

4.4.1 Frequency Distortion

If the amplifier bandwidth is insufficient for the bandwidth of the detected signal, the biopotential signal will be distorted. Figure 4.15 shows 3 ECG traces each taken with a different amplifier bandwidth. The normal signal of Figure 4.15a is taken with a bandwidth from 0.05 Hz to 150 Hz which is greater than the normal frequency range of 0.05 Hz to 100 Hz. Figure 4.15b has a bandwidth where the high frequency cut-off is considerably reduced. This causes *high frequency distortion* leading to the sharp edges being more rounded and the QRS complexes having a reduced amplitude. Figure 4.15c shows *low frequency distortion*, the base line is no longer horizontal and the more monophasic P and T waves appear biphasic.

4.4.2 Saturation and Cut-off Distortion

High offset voltages at the electrodes due to polarisation or improperly adjusted amplifiers, can cause the signal to be cut-off by the saturation of the amplifier. The

result is a greatly modified waveform where not only does the waveform look different but its frequency content can be quite significantly altered.

Figure 4.16 shows a set of waveforms where Figure 4.16b has its positive going QRS complex cut-off by saturation and Figure 4.16c has its most negative elements cut-off. This saturation, though apparently easy to see on the ECG, may well be hidden by subsequent filtering that rounds off the sharp cut-off corners. In modern digital systems where sampling is carried out, narrow saturated pulses may only have one or two samples to describe them. Thus all that would be seen at the output would be a reduced amplitude.

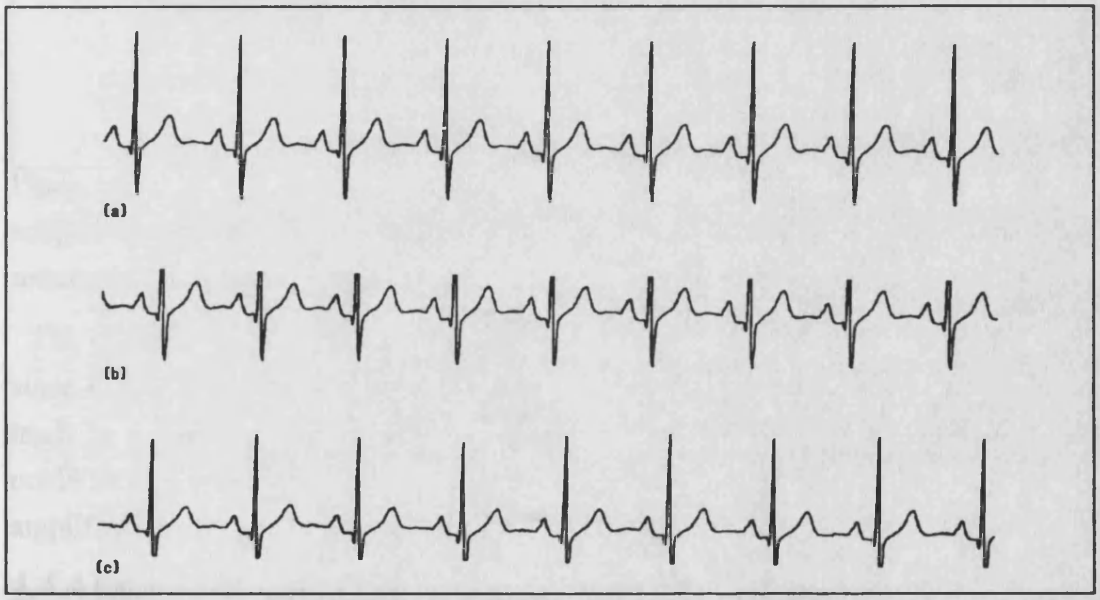

Figure 4.16 *Effects of Saturation and Cut-off Distortion [130 p286]*

4.4.3 Ground Loops

The ground loop can exist when more than one piece of equipment requires a ground reference on the subject. The problem is most likely to occur when using two pieces of mains powered equipment. Figure 4.17 shows two different pieces of equipment both using a reference ground on the ankle of the subject. Equipment A is earthed at one mains socket and equipment B is earthed at its power socket somewhere else in the room. If the ground voltage for equipment B (V_B) is slightly larger than the ground voltage for equipment A (V_A) a current will flow from ground B to ground A via the earth straps on the subject. Not only does this create the hazard of an unknown current flow through the body, especially if one of the pieces of equipment has an earth fault, but it can change the subjects resting potential with respect to earth, leading to large common mode voltages and increased artefacts.

Figure 4.18 shows the set up rewired to ensure that no ground loop currents can flow. This is achieved by only having one ground point via device A and ensuring the

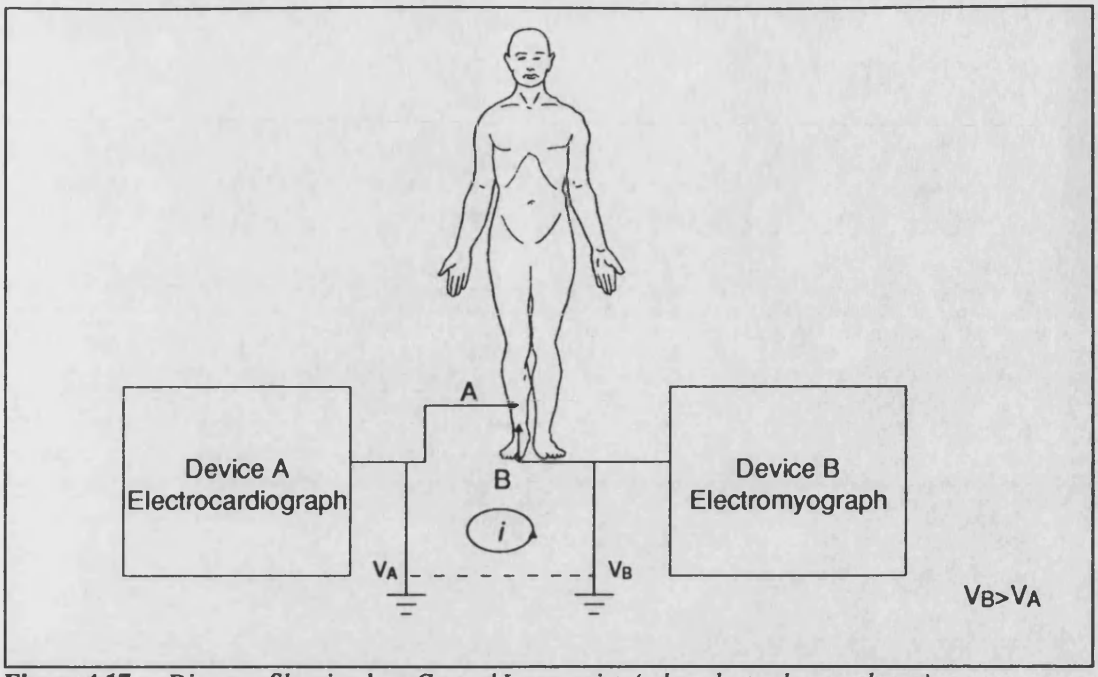

Figure 4.17 *Diagram Showing how Ground Loops exist (other electrodes not shown)*

subject is only grounded by one of the pieces of equipment. This way a common reference is ensured and no ground current should flow except in a fault condition.

The other problem that can be caused by ground loops is due to induced artefacts, since it is usual, when using discrete electrodes, to run the reference lead and signal leads in a common cable to the amplifier. Any current flowing in the ground wire could induce a voltage in the detection leads leading to an artefact at the output of the amplifier.

4.4.4 Broken Wires

When using electrodes and electrode wires with a separate differential amplifier it is not uncommon for breaks to occur in the cables particularly where they connect to the electrodes, such that one of the electrodes is no longer connected. The unterminated wire can then act as an aerial and large potentials can be induced by the ambient electromagnetic field. This can usually be seen as a mains frequency waveform with the biopotential of interest superimposed. This same effect can also be caused by bad electrode contact so care must be taken to determine the correct source of the error signal.

4.4.5 Interference from Electrical Devices

Mains based interference is one of the most common sources of interference in biopotential measurements. It is for this reason normal that clinical biopotential tests are carried out as far as possible in a *quiet*—electromagnetically speaking—environment where the radiated fields from other equipment have been minimised by

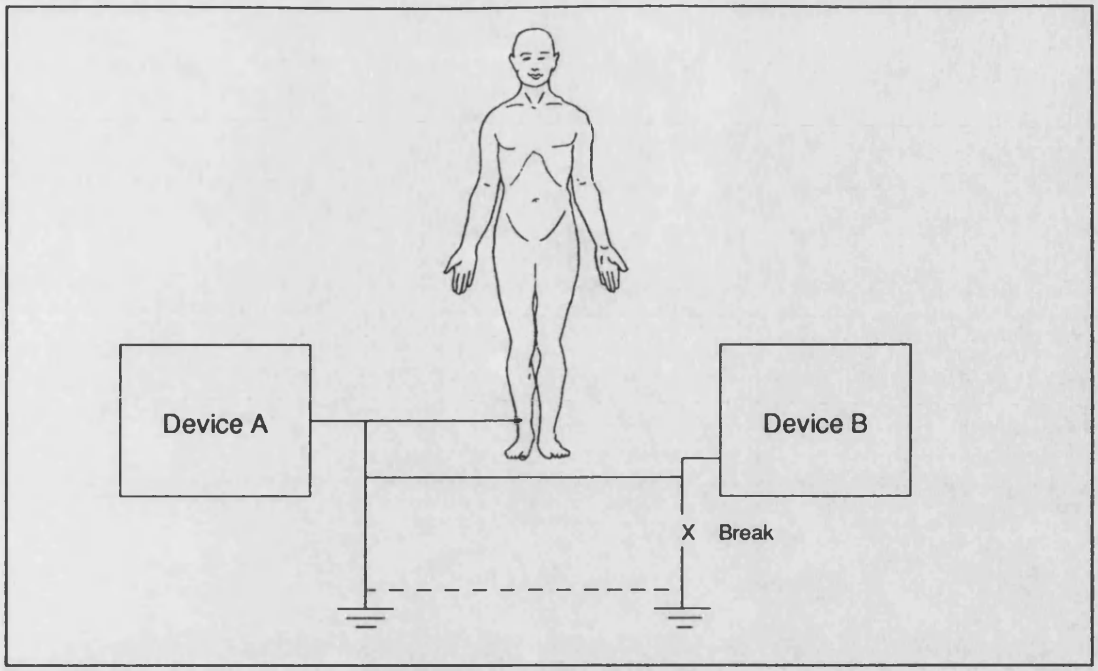

Figure 4.18 *The Elimination of the Ground Loop*

screening. Clearly this cannot always be achieved as in the case of ECG machines in the operating theatre or ICU.

There are two mechanisms by which other electrical devices can interfere: *Electric Field Coupling* between the power lines and *Magnetic Induction.*

The Electric field coupling is the result of the electric fields that surround mains leads, connecting different pieces of electrical equipment to the mains outlets. These fields could be present even when no current is actually flowing in the cables. They couple into the patient and the electrode leads. It may be considered as capacitors connected between the power lines to the various coupled items. The effect is to generate a very small current flow of the order of 6nA[130 p293]. The combination of this, coupled with slightly differing path impedances, leads to difference voltages of the order of 120μV. In order to minimise these effects the electrode leads are shielded and grounded at the amplifier end. Lowering the skin impedances which are the major variable will ensure that the difference voltages are minimal.

Coupling to the body of the subject causes a common mode voltage throughout the body as shown in Figure 4.19. The displacement current i_{db} flows through the ground impedance Z_G to ground. The result of this is a voltage drop across the body leading to a common mode voltage v_{cm}. That is:

$$v_{cm} = i_{db} Z_G \qquad 4.9$$

Typical values would be 0.2 μA for the current and 50 kΩ for the impedance giving a voltage v_{cm}=10mV. In cases where there is a high electric field i_{db}>1μA, this results in common mode voltages of 50 mV. Since real differential amplifiers have a finite

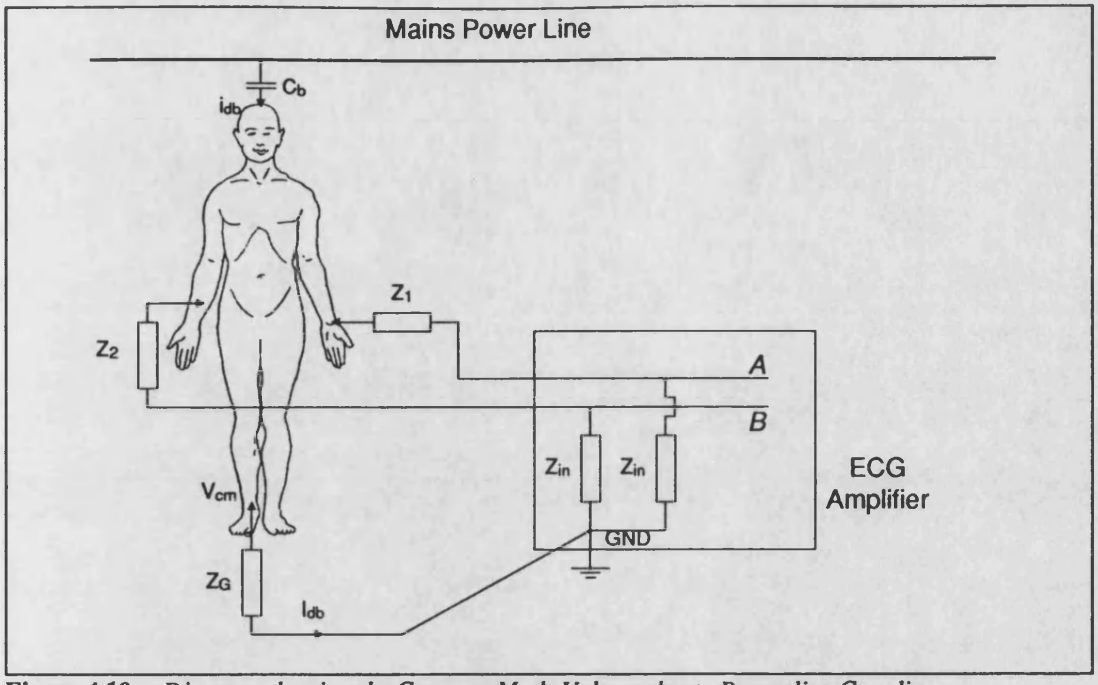

Figure 4.19 *Diagram showing the Common Mode Voltage due to Power line Coupling*

input impedance Z_{in}, this means that v_{cm} is reduced by the attenuator created by the skin-electrode impedance and Z_{in}. Thus:

$$v_A - v_B = v_{cm}\left(\frac{Z_{in}}{Z_{in}+Z_1} - \frac{Z_{in}}{Z_{in}+Z_2}\right) \qquad 4.10$$

Since Z_1 and Z_2 are much smaller than Z_{in}:

$$v_A - v_B = v_{cm}\left(\frac{Z_2 - Z_1}{Z_{in}}\right) \qquad 4.11$$

Taking typical values of v_{cm} = 10 mV, Z_2-Z_1=20 kΩ and Zin=5 MΩ yields an error voltage of 40 μV which is still noticeable but not as significant as the original figures. Clearly increasing the amplifier input impedance and reducing the skin-electrode impedance will reduce this figure still further.

From this it can be seen that the difference between the skin-electrode impedances plays an important roll in the detection of biopotential signals. The input imbalance coupled with the amplifier input impedance are critical factors in determining the common mode rejection ratio of a biopotential amplifier in use. This is independent of the value for the differential amplifier by itself.

Current flowing in the power lines establishes a magnetic field. These fields can also come from the ballasts in fluorescent lights and from transformers. If this field passes through the effective single turn coil created by the two electrode leads and the patient, a voltage will be induced in the loop. The voltage is proportional to the effective area of the single turn coil. To reduce this effect either the magnetic field

must be reduced by shielding or the effective area of the coil must be reduced by twisting the two leads together.

4.4.6 Reduction of Artefacts in Voluntary Muscle Response

Frequency distortion can be avoided by simply ensuring the amplifier combination has a sufficient bandwidth for the biopotential under investigation. The skin and limb tissue act as a low-pass filter and combine with the filtering effects of the differential detection, before the signal ever reaches the amplifier. This means the EMG signal bandwidth from surface detection is not more than 1 kHz. Various authors quote figures in the range 300 Hz to 1 kHz for the bandwidth[3, 161, 162, 163]. The low frequency cut-off is a figure that varies much more in the literature, with its value depending on the precise use to be made of the EMG response. If the cut-off is greater than 50 Hz then the problems due to mains 'hum' would be limited to the mains harmonics which some authors have considered[164 106 Hz]. However a cut-off that's high enough to filter out mains would also filter out a significant proportion of the EMG spectrum, in particular the components that relate to the MUAPT firing rate. Values of the order 10—20 Hz are common[3, 132, 138] and prevent the low frequency movement artefacts and dc components from appearing at the output. Some authors propose significantly lower; Knaflitz and Merletti[165] used 6 Hz.

Saturation or cut-off distortion will not only introduce extra harmonics to the spectrum due to the squaring of the spikes but could lead to false results. The effect can only be avoided by ensuring the amplifier gain is such that saturation does not occur. Some authors have made use of forms of AGC to maintain the signal at maximum size with no saturation[166, 167].

Ground loop problems can be readily removed not only by the rewiring shown in Figure 4.18 but may also be avoided by using battery powered isolated front end amplifiers.

Interference due to broken wires or bad electrode contact can readily be detected by careful checking of equipment and monitoring the detected muscle responses for tell-tale signs such as increased mains 'hum'[168]. Several authors include circuits to check electrode contact[130, 169, 170]. These are usually based around a high—relative to the frequency band of interest—frequency signal source that drives a small current of the order of microamps through the electrodes and skin tissue. By monitoring the voltage drop across the electrodes and allowing for some variation due to sweating or drying of the skin surface, a significant increase in voltage would suggest a breaking lead or bad electrode contact.

Another technique used to reduce the 'hum' is the use of the driven guard[171, 172]. In this technique the ground electrode is active and is driven by the common mode

signal via a unity gain amplifier. The effect of this is that the subject being tested now 'sits' at the common mode voltage thus reducing interference. The subject is protected from hazardous electric shock by referencing the unity gain amplifier to true ground by a large impedance. This technique used to be popular in cardiology. The benefit of the technique is that the placement of the ground electrode is not so critical because excessive common mode voltage is removed by the active ground.

Interference from other electrical devices is a difficult problem to eradicate especially in the work being described where the ultimate purpose of the sensors is to provide feedback for standing and walking systems[see 159 Fig. 2]. Placing constraints on subjects as to where and when they can use their systems is not a viable option so clearly techniques that are capable of reducing the effect of electric field coupling are required. The problem of electric field coupling can be reduced by shielding the electrode leads and making them as short as possible with the shields being grounded at the amplifier end[130, 141, 159, 173]. In order to make the leads as short as possible some authors have proposed amplifiers or just buffers mounted on the detection electrodes[132, 133, 138]. This would reduce actual electrode leads to nothing, or at least increase the signal size in the leads if a buffer is used, thus reducing the effect of the coupling. As might be expected the reduction of the electrode-skin impedance and in particular the imbalance between the electrode impedances will reduce the significance of the displacement currents.

Magnetic field coupling is reduced by twisting the electrode leads together thus reducing the area of the coil formed by the electrode leads. Using electrode mounted amplifiers will effectively reduce the coil area to zero. These amplifiers must have a high input impedance with respect to the electrode impedance. Leads should be short and screened to reduce the effects of external fields. High frequency effects will be filtered out by the limited bandwidth of the system.

Thus to determine the voluntary muscle EMG most effectively the literature suggests the use of electrode mounted differential amplifiers with a very high input impedance.

4.5 Stimulated Muscle

In order to detect the muscle response from a stimulated muscle exactly the same procedure as that described for a voluntary muscle response is required. The major difference is that there is a conflicting voltage source present on the 'muscle', namely the stimulating voltage. The effect of the secondary source will depend on its proximity to the point at which the muscle response is being recorded. From the preceding chapter it is clear that as long as the muscle response is well separated from the time of the stimulus the two signal sources will not affect each other significantly.

4.5.1 Contamination Artefacts

The artefacts present in a stimulated muscle response or Compound Action potential stem from two sources: one group are the sources already described above and the second group are due to the interference effects of the stimulating voltage.

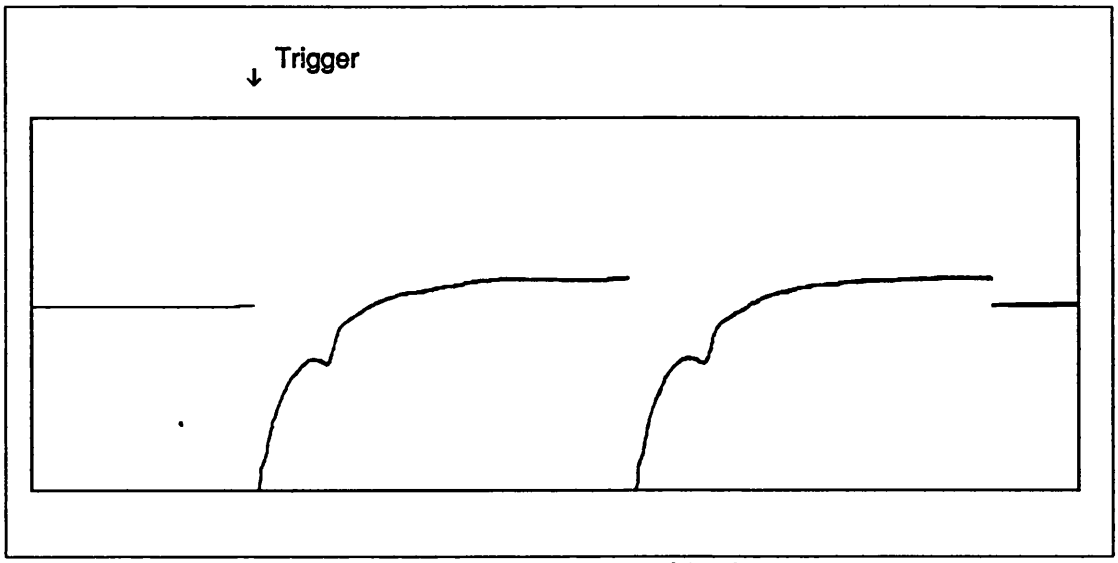

Figure 4.20 *Compound Action Potential showing Bad Artefact Distortion*

The nature of the artefact contamination is very dependent on the stimulation techniques used. Several authors have discussed its elimination when using invasive electrodes such as wires, needle or cuff electrodes [3, 157, 173, 174]. In these cases the current field is limited to a very small volume of tissue and rarely, if ever, extends to the region of space that contributes to the voltage sensed by the detection electrodes. Solomonow[161] found that stimulation pulses ten times supramaximal when applied directly to the nerve, generate artefacts of about twice the intramuscularly detected M wave (CAP) amplitude. These techniques effectively reduce the seriousness of stimulus artefacts such that they are readily manageable.

The systems described in this thesis are non-invasive and this means that the problem is entirely different. In the case of surface stimulation and especially the monopolar configurations, where the active electrode is placed over the motor point, the current field extends over a large tissue area which often includes the detection volume of the EMG surface electrodes.

CAPs detected by surface electrodes on a muscle stimulated by surface stimulation are usually, if not always, contaminated by stimulus artefacts whose amplitude can be several orders of magnitude larger than the elicited muscle response. The duration of the artefact can be several milliseconds[96, 145, 165].

Figure 4.20 shows a typical contaminated muscle response obtained from a commercial Medelec EMG machine. The small arrow indicates the point at which the

stimulus pulse was applied. The fast exponential rise and slow exponential tail are due to artefact contamination and the small biphasic pulse in the middle is the actual CAP response.

Although the contamination does not hamper simple analysis of the CAP, such as measurement of the latency, it does interfere with any analysis requiring accurate knowledge of the CAP waveform such as the estimation of fibre conduction velocities[145]. Broman, Bilotto, and De Luca[175] showed that small artefacts below 1 mV can affect estimates of muscle fibre velocity since they can provide synchronous contributions to the double differential signals and lead to false delay estimates.

4.5.2 Sources of Stimulus Artefact

As has been described in Section 1.6, the stimulator injects a charge into the nerve/muscle of sufficient intensity to cause a depolarisation and ultimately the recorded compound action potential. In order to do this a voltage/current pulse is applied across the stimulating electrodes. This pulse effectively charges up the capacitors that exist between the two electrodes as described by the model in Section 4.1. When the stimulators switch off, the capacitors are left charged up to the stimulating voltage. Because of the design of stimulators there is usually no active drive off so the charge on the capacitors is left to disperse through whatever low impedance path it can find[145, 165, 176]. The result of the discharging of the electrodes is that the artefacts can be present several milliseconds after the actual stimulus has been removed. The artefact size and shape is affected by a number of factors:

- the type of stimulator output stage.
- the stimulus intensity.
- the relative geometry of the stimulating and detection electrodes.
- the properties of the signal amplifier input stage.

Each of these topics will now be discussed to give an indication how they affect the generation of the stimulus artefacts.

4.5.2.1 Stimulator Output

There are two basic types of muscle stimulator: the so called *Constant-Current* and *Constant-Voltage* types. The essential difference between these two types is the controlled parameter: current or voltage. The choice of stimulator type is a subject of much debate with each type having its good and bad facets. The stimulators described in this thesis are of the constant-voltage type because it has been found that the patients 'prefer the stimulus output' in comparison to constant-current.

The constant-current stimulator is characterised by having a high output impedance thus ensuring that changes in the interelectrode resistance do not affect the output current. Since membrane depolarisation is related to current density, a constant-current stimulator is preferred by some researchers because they believe that they allow better response reliability and repeatability[165, 177]. Between the stimulus pulses, the output stage across the stimulating electrodes appears as an open circuit when compared with the body path. This high impedance leads to long transients in the recorded CAPs due to the discharge of the electrodes and skin tissues through the body[145, 176]. The disadvantages of this type of stimulator are two fold. Patients have said that the constant-current stimulus is more painful than constant-voltage. This may be due to the second disadvantage which is that the current is the controlled parameter. If the electrodes start to peel off, so reducing the surface contact area, the constant-current stimulator will continue to try and output the same current up to its voltage limit. The effect of this is that the current density at the stimulator electrode is increased, leading to the possibility of current burns and injury to the subject.

The constant-voltage stimulator has a controlled voltage output and is characterised by having a low output impedance somewhat lower than the interelectrode resistance[145, 165]. If the interelectrode impedance changes then the current and the effects of the stimulus may be modified. This can be a serious disadvantage with certain tests such as the strength-duration test where the alteration of the stimulus effects during the test can result in a false curve. The stimulation current from one of these stimulators is likely to be a non-linear function of the stimulation voltage. When the stimulator switches off, the output stage appears as a low impedance path, so the tissue and electrode capacitances discharge via the stimulator output stage giving very short spikes as the stimulus artefacts. These will be considerably shorter than obtained from a constant-current stimulator[166, 176, 177].

Since the constant-current stimulator has certain advantages to researchers when stimulating muscles, yet displays disadvantages during the interpulse period because of its slow discharge, several authors have proposed a hybrid stimulator[165, 177]. This is essentially a current stimulator that switches to a low impedance across the electrodes between the stimulus pulses so that it appears as a constant-voltage stimulator. In the case of the Del Pozo[177] stimulator this is achieved using a FET switch to short out the electrodes when a stimulus pulse is not present. This produced short discharge transients whose parameters were not reported but provided no control over the rate of discharge. This system however could not be easily applied to biphasic pulses. Knaflitz and Merletti[165] use feedback to control the voltage fall such that either monophasic or biphasic output pulses may be used.

4.5.2.2 Stimulus Intensity

The effect of the stimulus intensity is two fold. During the stimulation it sets up an electric field whose area of influence and hence strength of stimulus is dependent on the stimulus. Clearly the larger the stimulus the greater the stimulus voltage seen by the pick up amplifier during the stimulating pulse. The artefact discharge tail is not only determined by the stimulator output impedance but also the amount of charge on the electrodes at switch off.

4.5.2.3 Electrode Geometry and Position

The stimulus electrode geometry will determine how the stimulus field initially disperses within the body tissue. Similarly the detection electrode geometry will determine how the stimulus field is picked up. As has been described in the stimulator section, changes in electrode contact will, depending on the stimulator type, change the effect of the stimulus and subsequent artefact.

The position of the pickup electrodes relative to the stimulating electrode positions will determine the size of the voltage gradient artefacts. This artefact is a voltage difference between the two recording electrodes of the differential amplifier and is produced by current flowing through the limb[145, 178]. The stimulus voltage sets up a voltage gradient at the recording site which contributes to two features of the artefact. The stimulus pulse itself contributes to the initial spike and the subsequent discharge of the electrodes through the limb will contribute to the long tail.

4.5.2.4 Amplifier Effects

The amplifier will contribute a common mode voltage proportional to the electrode imbalance as described by equation 4.10, where v_{cm} is the sum of the voltage difference dropped across the grounding and recording sites by the stimulus current and the voltage dropped across the ground electrode by the escape current[145]. The escape current is caused by stray stimulator capacitances. At the rising and falling edges of the stimulus pulse, the stray stimulator capacitances must be charged and discharged. Unless the capacitances and the stimulating electrode impedances are perfectly balanced there will be a current flow through the ground electrode[145, 178] which is called the escape current. It should be noted that these effects are dependent on a transformer coupled stimulator.

If the stimulating and recording leads are closely coupled there will be some capacitive coupling of the stimulus into the amplifier. This is because the stimulating leads are usually not screened in order to reduce lead capacitance.

The major effects on the amplifier are due to the stimulus pulse causing saturation effects. Figure 4.21 shows some of the effects caused by passing the stimulus through

the amplifier. The passage of the stimulus pulse through the high-pass filter of the amplifier introduces a slow exponential tail into the signal[145, 179, 180]. The low-pass filter used to limit the recorded signal would cause an exponential decay of the rising and falling edges of the pulse. The diagram Figure 4.21 demonstrates these effects. In the quiescent state there is a charge on the coupling capacitors that are usually used in this type of amplifier to eliminate any DC effects such as electrode potential, which is set by the DC voltage differences between the stages. If the first stage saturates, as is often the case, the charge on the coupling capacitor to stage two will change by the input stage of section 2 being driven out of its linear range, reducing the coupling time constant; or, even if the stage 2 input remains linear, the charging of the coupling circuit to the saturation potential leads to a voltage difference across the coupling capacitor which is much greater than the normal signals encountered at this stage. When the overload ends and the first stage returns to normal, the voltage difference, amplified by the succeeding stages, results in a large or even saturated output from the amplifier. This offset decays away very slowly at a rate set by the linear coupling time constants. (This description assumes that the recovery of a stage from overload is instantaneous).

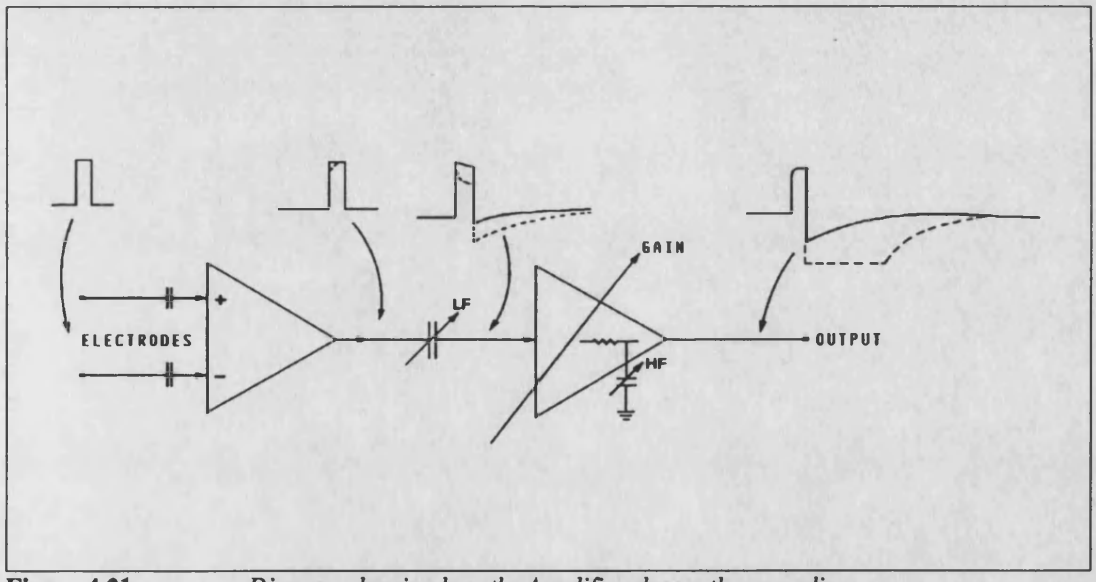

Figure 4.21 *Diagram showing how the Amplifier shapes the recording*

4.6 Artefact Reduction

The artefact can never be totally eliminated but there are a number of methods by which the size and effect of the stimulus can be reduced. In most circumstances this will be sufficient. A number of techniques based on post-processing or secondary processing of the contaminated CAPs will also be discussed which, when used with the practical techniques, can all but eliminate the CAP interference. To minimise the stimulator discharge effects it is clearly better, at least during the period between

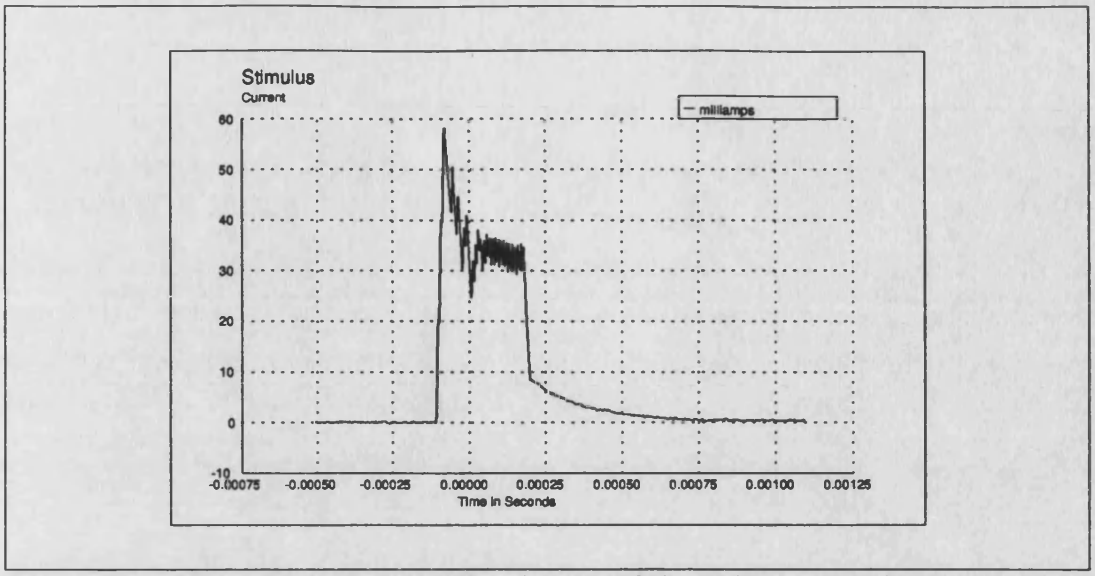

Figure 4.22 *Current Discharge through Stimulating Leads for High Impedance Output*

pulses, to have a low output impedance to speed up the discharge of the electrodes and body tissue capacitance. This will ensure the electrodes discharge through the low output impedance stage of the stimulator in preference to the body. There is however a problem with this type of system; the lower the output impedance, the faster the discharge, but also the larger the negative spike due to the reversal of the stimulating current flow. Figure 4.22 shows the current that flows through the stimulating leads for an output impedance of around 10kΩ with Figure 4.23 showing the same output voltage pulse but with the output impedance reduced to around 12Ω in between the stimulating pulses. If, however, an active switch-off is used, the current spike can be controlled with a slight increase in the fall time, thus reducing the size of the negative spike though not necessarily eradicating it[165].

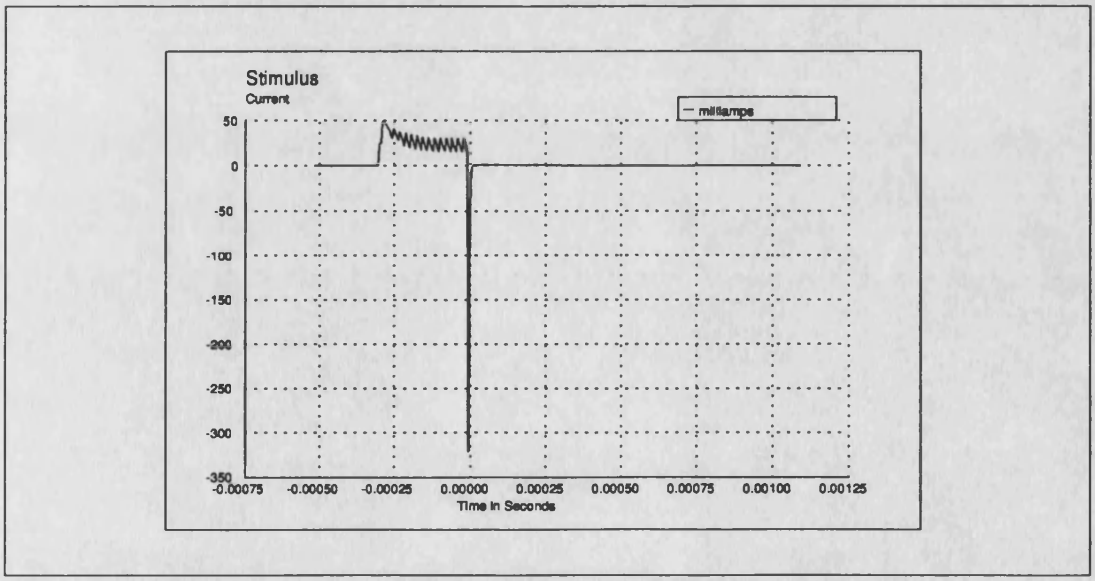

Figure 4.23 *Current Flowing through Stimulating Leads for Low Impedance Output*

Pickup electrode positioning can have a significant effect on the size of the recorded artefact, particularly during the stimulus pulse. The effect of the voltage gradient set up in the limb by the stimulus, can be reduced by placing the detection electrodes on equipotential lines. The electric field due to the stimulus will spread out from the electrodes through the anisotropic limb tissue creating a set of field contours around the electrodes[148]. If the electrodes are on one of these contours, the difference voltage seen at the detection amplifier will be almost zero. Since the field will change during the stimulus pulse the difference voltage can never be eliminated but it can be reduced as shown by Figure 4.24.

In the amplifier stage, as with problems associated with the normal voluntary muscle response recording, the effects of the stimulated artefacts effects can be reduced by ensuring a low electrode impedance relative to a high amplifier impedance coupled with a good CMRR.

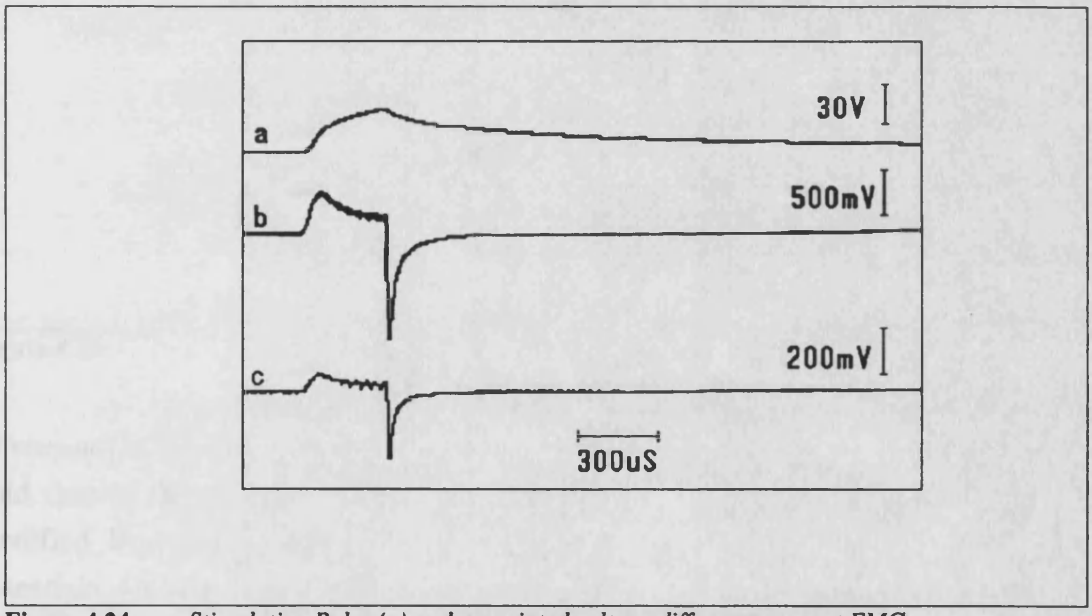

Figure 4.24 *Stimulating Pulse (a) and associated voltage difference seen at EMG Electrodes; (b) Electrodes not on Equipotential Line; (c) Electrodes on Equipotential Line*

Coupling effects between stimulating and recording electrodes can be reduced by ensuring that they are well separated. Once again moving the amplifier as close to the electrodes as possible will ensure that any coupling will be reduced with respect to the signal of interest. A good electrode contact reduces the electrode imbalance contribution[145].

The effects due to the high-pass filter of the amplifier can be reduced by reducing the time constant and hence the high-pass cut-off, to as low a value as possible. DC coupling is a possible solution, but then the polarisation of the electrodes will lead to DC offsets which could cause saturation of the amplifier in the later gain stage.

Careful positioning of the electrodes can reduce the stimulus spike size but may lead to CAP distortion due to the proximity to the point of innervation as occurs in voluntary muscle responses[107].

The prevention of the stimulus artefact from entering the equipment is a technique that a number of authors have used. This can be achieved in a number of ways: the amplifier could be short-circuited at the input, or disconnected from the signal source during the stimulation. These two methods however would lead to an artefact because of the DC voltage difference of the electrodes due to the input being switched to zero. A better solution is to maintain the DC level using sample and hold circuits.

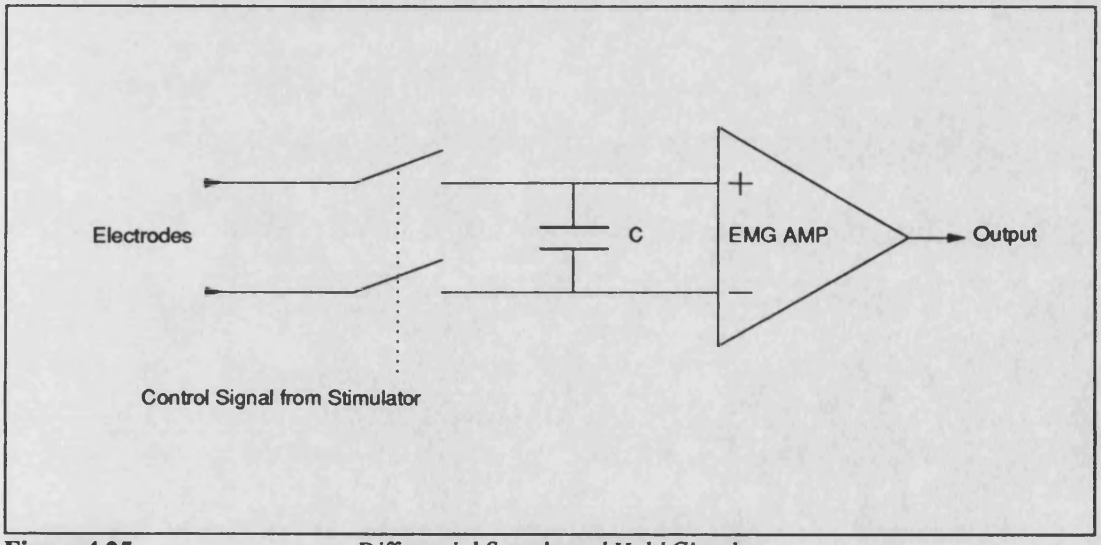

Figure 4.25 *Differential Sample and Hold Circuit*

Freeman[181] used a sample and hold circuit in his amplifier that was switched to hold during the stimulation artefact. Roby and Lettich and Babb et al.[182, 183] modified Freeman's circuit with some pre-stimulus blanking for use on evoked potentials. During measurements the output impedance of the source and the hold capacitor form a low-pass filter whose cut-off must be high enough to ensure the required signal bandwidth 'passes'. During the stimulation, or just a short time before the sample and hold is switched to hold, and as long as the input current of the next stage amplifier is very small, the capacitor will remain charged. Peper and Grimbergen[176] moved their sample and hold into the electrode leads such that a differential sample and hold was required as shown in Figure 4.25.

Once again this system is for EEG using a biphasic stimulus. The effect of the capacitor is to make the input impedance capacitive though Peper states that this did not produce an observable effect. Babb[183] observes the need for a second sample and hold further down the signal path due to switching transients on the differential sample and hold circuit.

Roškar and Roškar[184] used a different technique of digitally controlling the amplifier gain. They switched between a gain of ×1000 during the interpulses interval and ×1 during the stimulus period and the stimulus after tail. They provide no details of any amplifier transients caused by switching, though they do show a linked sample and hold circuit on the amplifier output which may be because of the transients.

In a very recent paper, Knaflitz and Merletti[165] present a system that is similar in function to the system described in this thesis. They make use of a double differential amplifier-electrode module designed by Broman, Bilotto and De Luca[175] whose output is fed through a slew rate limiter which limits the rate to 5V/s. The 5V/s limit means that sine waves with an amplitude frequency product of up to 800 mV·Hz are undistorted. This allows maximal M waves, as well as myoelectric signals from maximal voluntary contractions whilst limiting a 1 ms stimulation pulse to 5mV. This avoids saturation of the variable gain amplifier allowing high gains to reduce noise effects. A CMOS switch is then used to blank the signal from the input of the low-pass filter during the blanking time window, which means the switch is opened before the stimulus and closed after the stimulus once the artefact is below the noise threshold. The results presented show some very clean CAPs with the stimulus being kept below the noise thresholds.

4.6.1 Software Reduction of Artefacts

Several authors[145, 185] have proposed methods of artefact reduction that could be readily done using software in a sampled system. Some of the proposals of McGill et al.[145] could be done with special hardware as well but are really more suited to the software approach.

Kovacs[185] uses a least squares technique to generate a model for the artefact from the recorded data. This model is then used to generate the values to subtract from the recorded data to leave just the peripheral nerve response. He states that he has applied it successfully to 60 sensory nerve response measurements.

McGill et al. use inverse filtering to remove the effects of the high-pass filter of the amplifier. He quotes a discrete-time inverse filter for a single pole high-pass filter with time constant τ

$$V_R(t) = V_{art}(t) + \frac{1}{\tau}\sum_{k=0}^{t} V_{art}(k)\,\Delta t \qquad 4.12$$

where $V_{art}(t)$ *is the average distorted signal.*

$V_R(t)$ *is the reconstructed signal.*

Since the sampling is unlikely to be fast enough to accurately define the spike, the reconstructed signal will be inaccurate in that region.

The second method proposed by McGill et al.[145] is to record a subthreshold stimulus signal which would be CAP free. Then by assuming that this can be linearly scaled, a scaled version of the subthreshold CAP can be subtracted from contaminated CAP to give an artefact free CAP response. The subthreshold value is very small, so many responses are required to average out the noise. The noise will be accentuated by the scaling so some resultant smoothing may be required.

The third technique is the Off-Nerve method which is similar to the second method except that an artefact-only signal is picked up from a second site. It is then assumed that the two signals are linearly related, even though this is not 100% guaranteed. McGill et al provide formulae to calculate the scaling factors required. The major disadvantage of the method is the difficulty of finding a suitable location for the recording of the artefact only signal.

The final technique suggested is the Double-Stimulus method. In this method a second stimulus is applied during the refractory period. This means the first stimulus will evoke a CAP and artefact and the second will evoke only an artefact. If it is assumed that the double pulse is the linear superposition of two single pulse artefacts, the signal evoked by the double stimulus (V_{DS}) can be used to cancel the artefact from the normally evoked CAP (V_R) by

$$\hat{V}_N(t) = V_R - [V_{DS}(t+T) - V_R(t+T)] \qquad 4.13$$

Graupe[96], in a very recent paper, takes an alternative approach in his software treatment of the contaminated CAP by assuming its presence and monitoring the shape of the CAP with respect to the artefact. It should be noted however that his interest is in trying to get a fatigue feedback signal rather than calculating muscle or nerve parameters such as conduction velocity.

4.7 Sampling of Muscle Signals

The sampling of muscle signals is in itself a fairly simple task. The signal is already bandlimited by the detection system, so the choice of sampling frequency, such that it satisfies the Nyquist criteria is a simple matter. The value chosen usually being determined by the constraints in the post-sampling processing system. The problem comes with sample size and whether the samples of the muscle signal are a truly representative sample of the overall muscle signal.

In order to discuss the statistical properties required of the EMG signal to ensure that a set of results derived from the sampled muscle signal give a reasonable estimation of the muscle response at the time of the sample, the various statistical properties will be discussed individually. The definition[186, 187, 188] of the random properties of EMG signals will dictate the processing techniques required.

4.7.1 Deterministic and Non-Deterministic Processes

If the properties of a signal are a random function of time, such that its future values cannot be exactly predicted from the observed past values, it is said to be a *Nondeterministic* random process. A EMG signal recorded from a voluntary contraction is an example of such a process. Given a set of previous samples it is not possible to predict the next value accurately. This can be seen by the number of different techniques used to model voluntary EMG signals.

If it is possible to predict exactly the future values of a process based on a knowledge of the past values, then the random process is said to be *Deterministic.* A classic example of such a random process is given in equation 4.14.

$$X(t) = A\cos(\omega t + \theta) \qquad 4.14$$

where A *and* ω *are constants*

θ *is a random variable with a specified probability distribution*

If $X(t)$ represents the sample value at time t then for any one sample function, θ has the same value for all t but different values for the other members of the ensemble. That is, the only random variable is with respect to the ensemble and not time. The muscle response from a stimulated muscle may be considered a deterministic function since the position of the CAP is determined by the stimulator settings and so it can be predicted. The signal is not truly deterministic since the CAP shape changes with fatigue, that is, time.

4.7.2 Stationarity

A random signal is said to be stationary if all the marginal and joint density moments of the signal do not depend on the choice of the time origin. If any of the probability density functions do change with time then the process is nonstationary.

Clearly in the strictest sense of the word the EMG cannot be considered stationary since it will have differing spectral properties with respect to time. In the case of a voluntary contraction, that is a nondeterministic process, the process can be considered pseudo- or quasi-stationary if the right time duration is chosen. Bendat and Piersol[54, 55] give a simple test by which this time may be estimated. From the literature, the time is dependent on the muscle and the recording technique. However, values of the order of 500 ms to 1 s have been quoted[52, 100].

A deterministic waveform is only usually stationary under certain special conditions. If the stimulated muscle response is considered, it is a train of CAPs repeating at or very close to the stimulator repetition rate. If the sample period is chosen to be a multiple of the stimulator repetition rate and the sampling always starts at the same point with respect to the waveform, for example at the falling edge of the stimulus,

then the stationarity of the waveform is now independent of its deterministic nature, being only determined by the stationarity of the changing CAPs.

4.7.3 Ergodicity

Ergodicity is a property of stationary random processes. That is, if a process is ergodic it must be stationary; the corollary is not necessarily true. However all nonstationary processes are nonergodic. *Ergodicity* means that almost every member of the ensemble exhibits the same statistical behaviour as the whole ensemble. Thus the statistical behaviour may be examined by examining only one sample function.

Chapter 5

Muscle Stimulators

As described in section 1.6, muscle recruitment is induced by artificially creating a polarisation. In innervated muscle the nerve fibre is polarised, in the case of denervated muscle the muscle fibres themselves are polarised. In order to achieve this the muscle stimulator must be capable of generating a field of sufficient intensity to cause this polarisation. As has already been stated the current waveform is the critical factor in assessing the capabilities of a stimulator, even though a constant voltage stimulator is usually preferred.

Two stimulators, both of the constant voltage type, have been designed: one based on the new Bath University Stimulator design; the other based around a high voltage operational amplifier, the BurrBrown 3583.

5.1 The Microcontroller Card

In order that the signal analysis hardware and software can be correctly synchronised to the stimulator, it is necessary to provide a number of control signals not available with the original fixed frequency Bath University Stimulators[75]. To overcome this, both stimulators have a custom programmed microcontroller card to provide the necessary programmability. The microcontroller is chosen in preference to the 65C02 based design used in the standing system[115, 116], because of the limited control and programmability provided by the processor in this configuration. This processor card has since been redesigned as part of the walking system research programme so could now provide most of the required programmability.

5.1.1 The Microcontroller

The controller card is based around a Philips PCB83C552, which is a derivative of the PCB80C51 microcontroller family using the same instruction set. Additional special function registers are incorporated to control the on chip peripherals. Figure 5.1 shows a general block diagram of the device.

There are two versions: the romless version which is used here, and the masked rom version. The PCB83C552 contains a volatile 256×8 read/write data memory, six 8-bit I/O ports, two 16 bit timer/event counters (as per the PCB80C51), an additional 16 bit timer coupled to capture and compare latches, a fifteen source, two priority level nested interrupt structure, an 8 input ADC, a dual DAC pulse width modulated interface, two serial interfaces (UART and I^2C bus) and a 'watchdog timer'.

In the romless version one of the I/O Ports acts as a multiplexed data and low order address bus and the another as the high order address bus. A memory map of the device is shown in Figure 5.2.

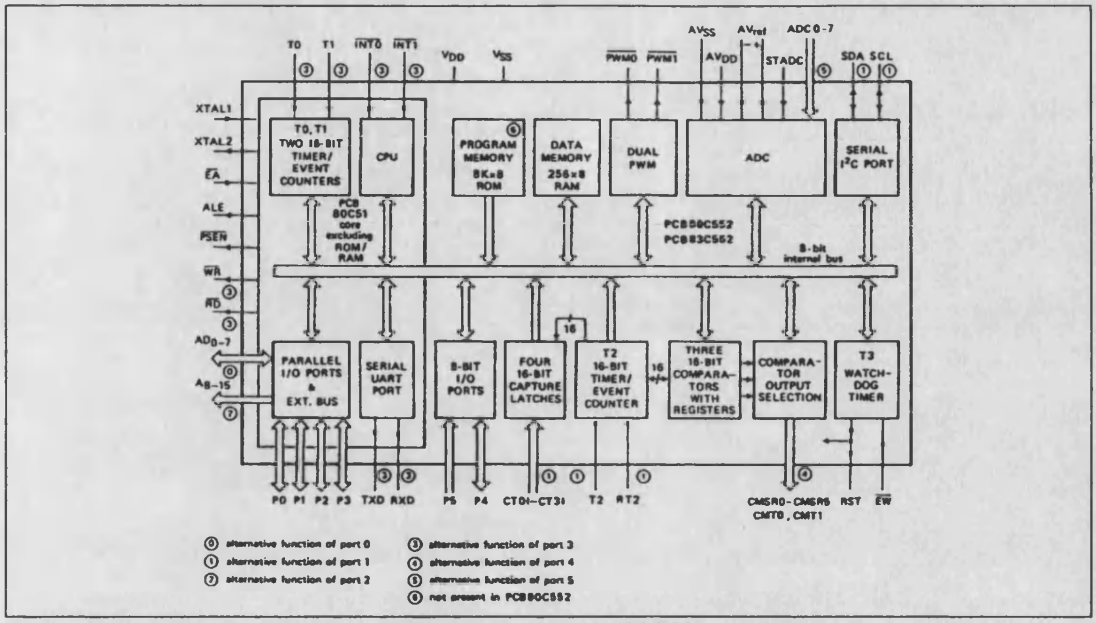

Figure 5.1 *Block Diagram of the 80C552*

5.1.2 Hardware Configuration

Two stimulator control cards have been built, both based on the same basic design but tailored to the needs of the stimulator output stage. For the purposes of this description the dual channel controller card, which is used with the Bath University Standing System[115, 116] output stage, is described. The differences between this card and that used for the operational amplifier based stimulator are described separately in section 5.1.3.

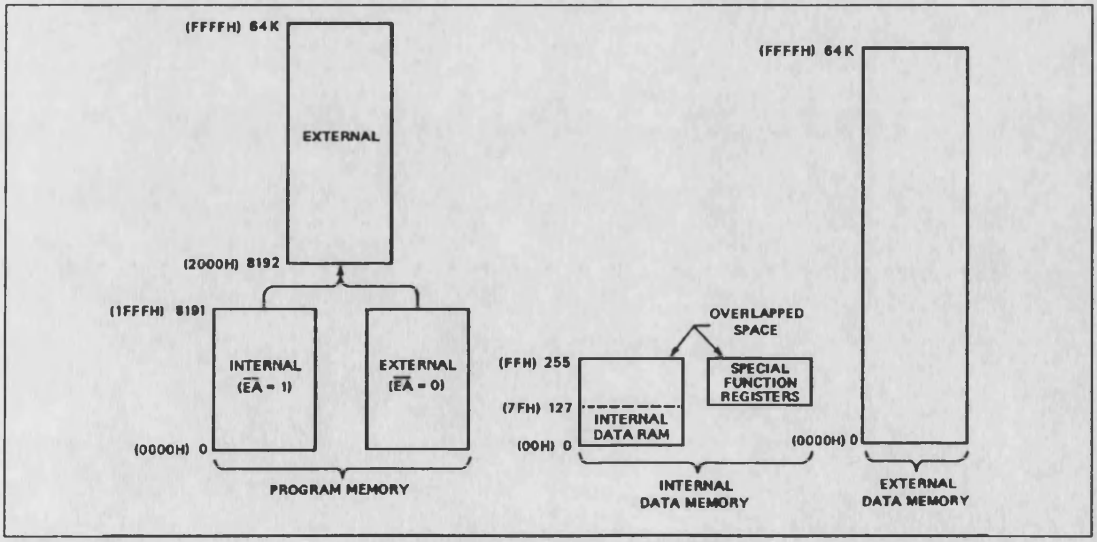

Figure 5.2 *General Memory Map of 80C552*

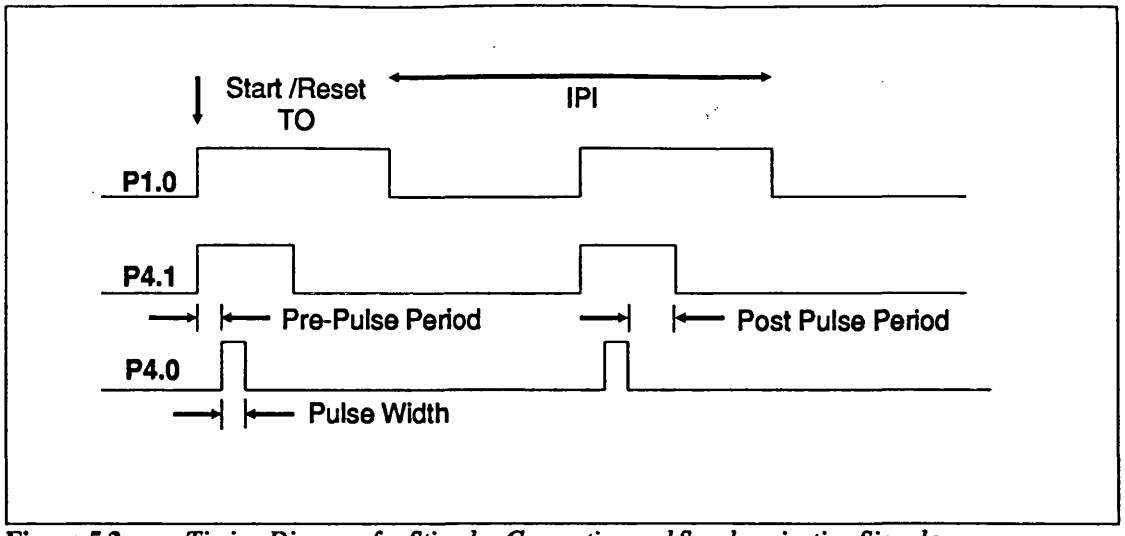

Figure 5.3 *Timing Diagram for Stimulus Generation and Synchronisation Siganls*

Figures G.3 and G.4 show the circuit diagram of the microcontroller card. It is configured for a maximum of 16 kbytes of external ROM and 8 kbytes of external RAM. The serial port pins P3.0 and P3.1 are brought out to a 25-way D-type connector to provide an RS423 voltage level serial interface. Control of the stimulator output voltage is provided by a memory mapped 2 channel Digital to Analogue(DAC) converter with the two channels mapped at addresses 04000H and 04001H. The display is provided by a 20 character LCD alphanumeric display mapped in at 08000H with its control signals being derived from Port 3. Input to the stimulator is provided for by a 4x4 matrix keyboard which is directly connected to Port 5 and strobed P1.2 and P1.3. It should be noted that the addresses for the hardware are not completely decoded so that both the DAC and the alphanumeric display image through the upper memory map. The I^2C interface is made available but not used in the current configuration.

The other section of the circuit consists of the actual stimulus pulse and associated timing signals buffer circuitry. Figure 5.3 shows a timing diagram for the various port pins involved.

Port 1 Bit 0 generates a square wave with a period equal to the required interpulse period, IPI, by using Timer T0. On the low to high transitions of this signal the 16 bit timer T2 is reset, via RT2, Port 1.5. At the same time T2 is started and by using the compare registers to cause interrupts, the sample and hold pulse on Port 4.1 is generated and the actual stimulus pulse on Port 4.0.

All the signals are buffered and level shifted by using VMOS FETs switching between 0 and 10V, which is the voltage required by the stimulator card. The clamp control signals derived from the stimulus pulse are used to drive clamp circuits that are connected to the outputs of the stimulator. Their function is to maintain the thyristor

that is across the output stage (QC1 Figure G.1) in the 'on' state whilst no stimulus is being outputted. This effectively clamps the output to ground. Since the thyristor will stop conducting when the current flowing through it drops below its threshold, the thyristor spends most of its time enabled but not conducting, since any remaining voltage between the electrodes at the end of the stimulus pulse quickly discharges.

5.1.3 Changes to OpAmp Controller Card

The circuit diagram for this card is given in Figures G.7 and G.8. The circuit is essentially the same as that for the dual channel card already described.

The DAC, though present cannot be used to control the output stimulus level in the current implementation. Stimulus output level can only be controlled manually. The clamp control signals are not required and therefore are not present. The regulator and inverter are unnecessary because voltages of ±5 V are available from the power supply board Figure G.6. The 'watchdog timer' is enabled so that it may be used to ensure that mains glitches cannot lock-up the processor.

5.2 Stimulator Output Stages

The interface between the microcontroller card and the stimulator output cards is very similar no matter which output stage is being used. A PCB has been produced for the Bath University Standing system output stage and also the original version of the operational amplifier, later versions were built on matrix board.

5.2.1 Bath University Standing System

The two channel output stage is based on the 2 channel standing stimulator as described in references 75 and 115. The two channel standing stimulator is made up of an output stage card, which is used here, and a 6502 based processor card which has been replaced by the microcontroller card. The circuit diagram for the output stage is

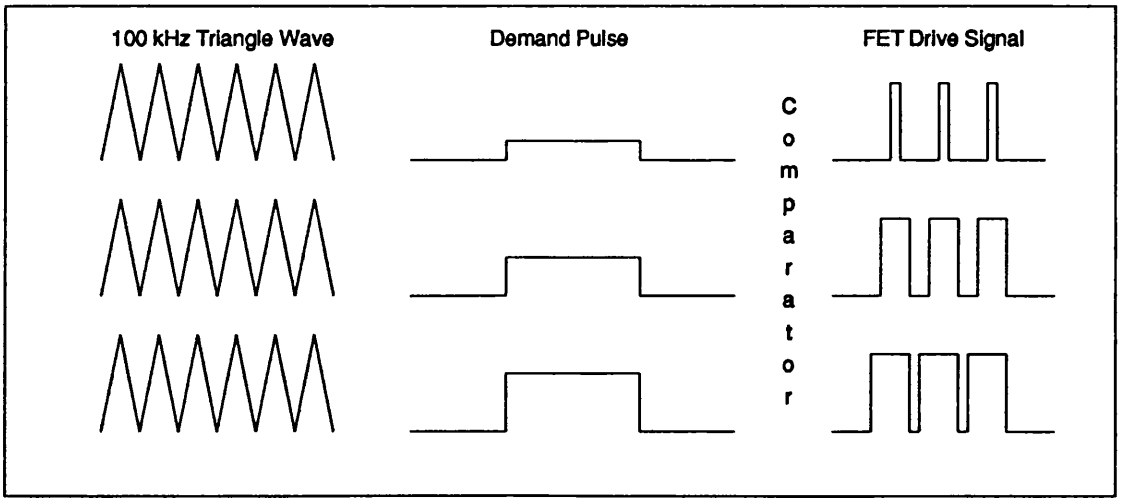

Figure 5.4 *Diagram Showing how Varying the Demand Pulse Modulates the FET gate Drive Signal*

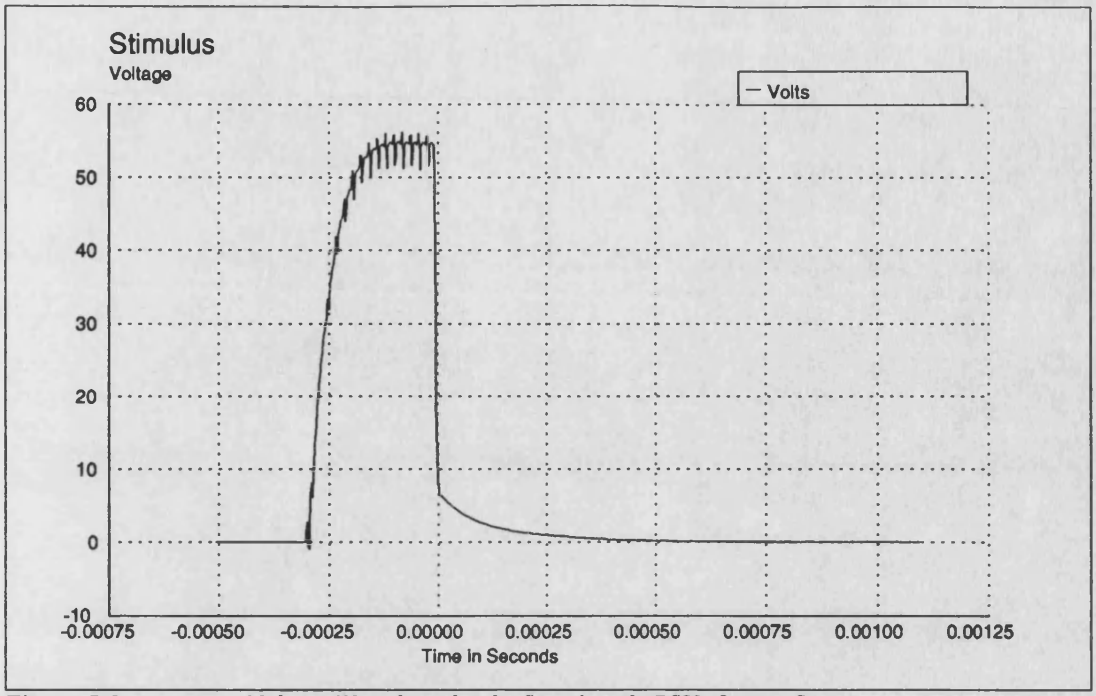

Figure 5.5 *Voltage Waveform for the Switchmode PSU Output Stage*
Clamped Output on a Standard Load of 1 kΩ in parallel with 100 nF

shown in Figures G.1 and G.2. Plate F.2 shows a populated output stage PCB with the 96 way connector used to connect to the 65C02 processor card on the left.

In the original stimulator design, as used in the standing system, timing is provided by half of an NE556. The other half is used to control the timings of the cyclic functions which are provided for exercise purposes in the original system. In this

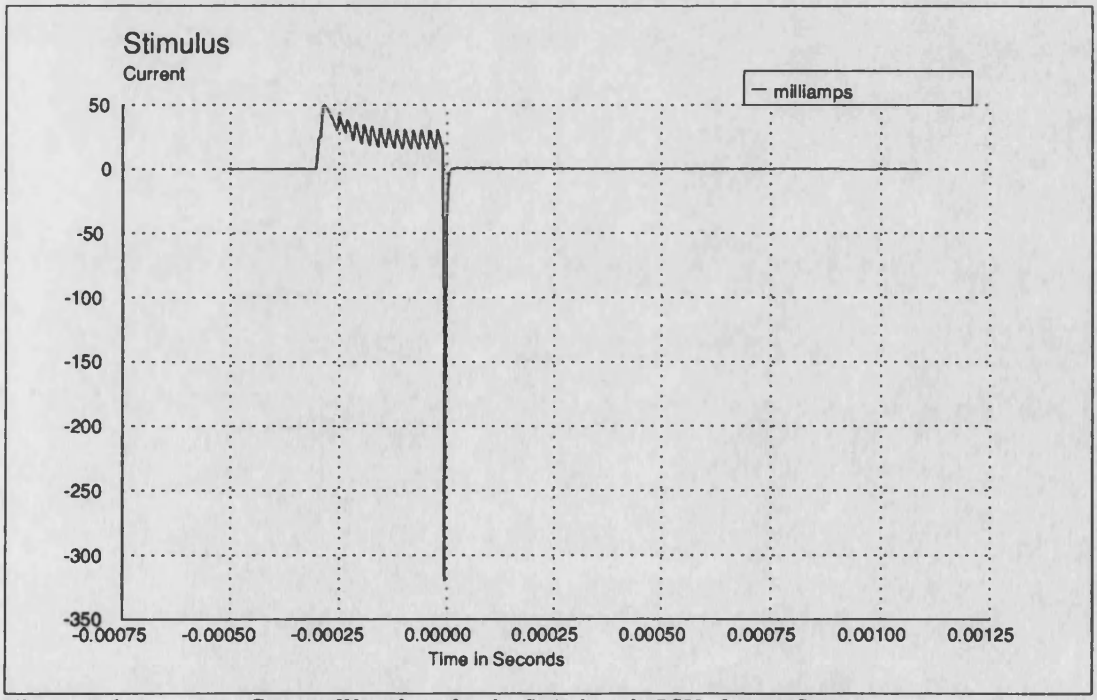

Figure 5.6 *Current Waveform for the Switchmode PSU Output Stage*
Clamped Output on a Standard Load of 1 kΩ in parallel with 100 nF

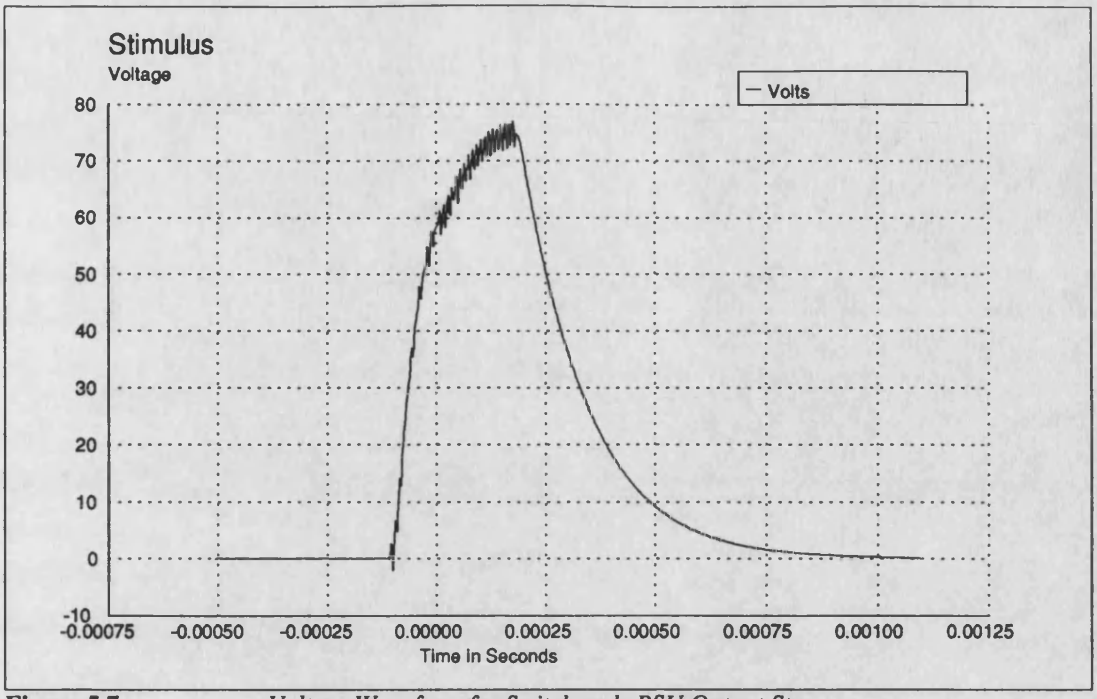

Figure 5.7 *Voltage Waveform for Switchmode PSU Output Stage*
Clamp Disabled and Standard Load 1 kΩ in parallel with 100nF

configuration the cyclic/continuous and alternate/simultaneous functions are still enabled, but only in Manual mode. In Micro mode both timing and output voltage are controlled by the microcontroller.

The output stage is essentially a switch mode power supply forward converter, switching at 100 kHz. This clock is generated by the NE555 U1 in Figure G.1. The

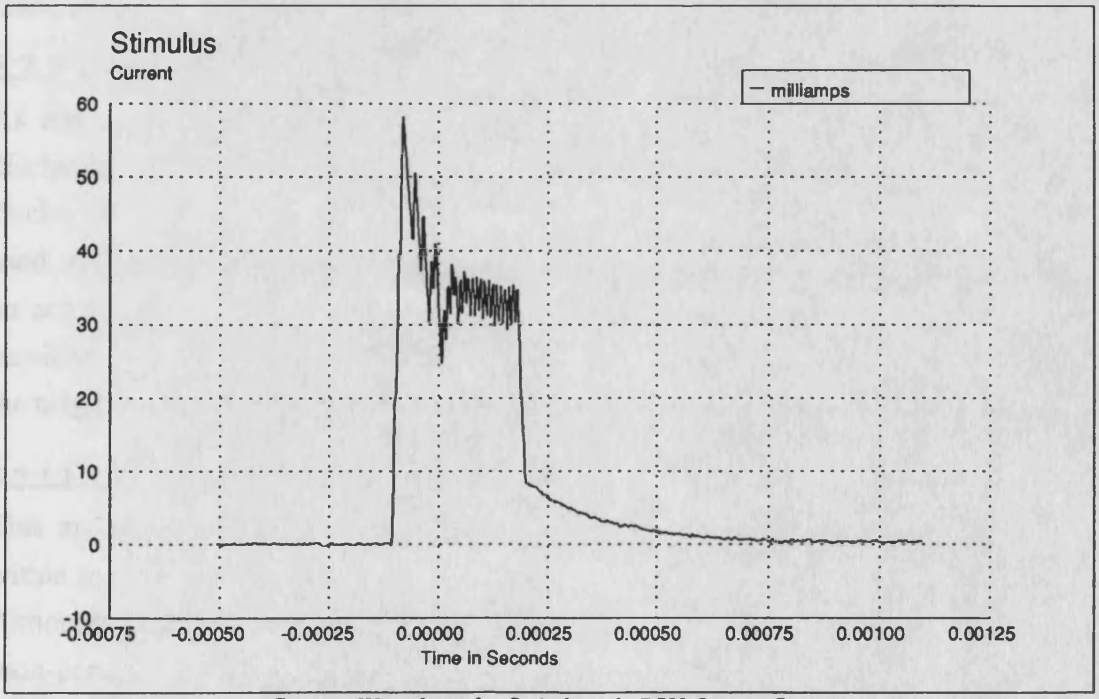

Figure 5.8 *Current Waveform for Switchmode PSU Output Stage*
Clamp Disabled and Standard Load of 1kΩ in parallel with 100 nF

demand signal generated by the pots VR1 and VR2, or the DAC output if the Micro/Manual switch position is in the Micro position, is first converted into a pulse train where the pots vary the amplitude of the pulse. This is then compared with the 100 kHz triangle wave derived from the 100 kHz clock. The result of this comparison is a series of 100 kHz pulses whose width is proportional to the required output as shown in Figure 5.4. These pulses then switch the FET to generate the output via the standard transformer diode inductor forward converter configuration.

An opto-isolated feedback signal is used to ensure a good rise time on the voltage pulses and maintain the demanded output level. This feedback does not affect the discharge, so when the demand goes to zero the output stage discharges via the body. As described earlier (section 4.5) this leads to artefact contamination of the recorded compound action potentials. To reduce this effect an additional clamp circuit has been added to the original design. This is in the normally on state with the thyristor triggered and is switched off when a stimulus is present. Output smoothing is achieved mainly by relying on the body's capacitance when the stimulator is connected to the subject.

Figures 5.5, 5.6, 5.7 and 5.8 show the current and voltage waveforms for the clamped and non-clamped output. The effect of the clamp circuit can clearly be seen with the voltage dropping rapidly down to a few volts. The penalty of the rapid discharge of the voltage can be seen in the current curves; which exhibit a very narrow negative going spike of about six times the positive going current pulse but for a very much shorter time.

5.2.2 The Opamp Based Output Stage

As has already been mentioned, the Bath University Stimulators do not actively discharge the stimulus voltage when switching off. This leads either to a slow discharge or a large negative discharge spike if the clamp circuit described above is used. An operational amplifier however will actively drive the signal on and off with an active control thus reducing the large negative spikes to a small overshoot. Two versions of the operational amplifier stage have been built because of problems with the original design.

5.2.2.1 Original Power Operational Amplifier

This makes use of a power operational amplifier design that was already available within in the department. The circuit diagram for this amplifier is given in Figure G.5. Although this stimulator appeared to function well in tests on normals (non-paraplegics), it was found not to be very well controlled when used on paraplegics. Investigations into the output waveforms with differing loads revealed some strange properties when driving capacitive loads, which gave a very spiky

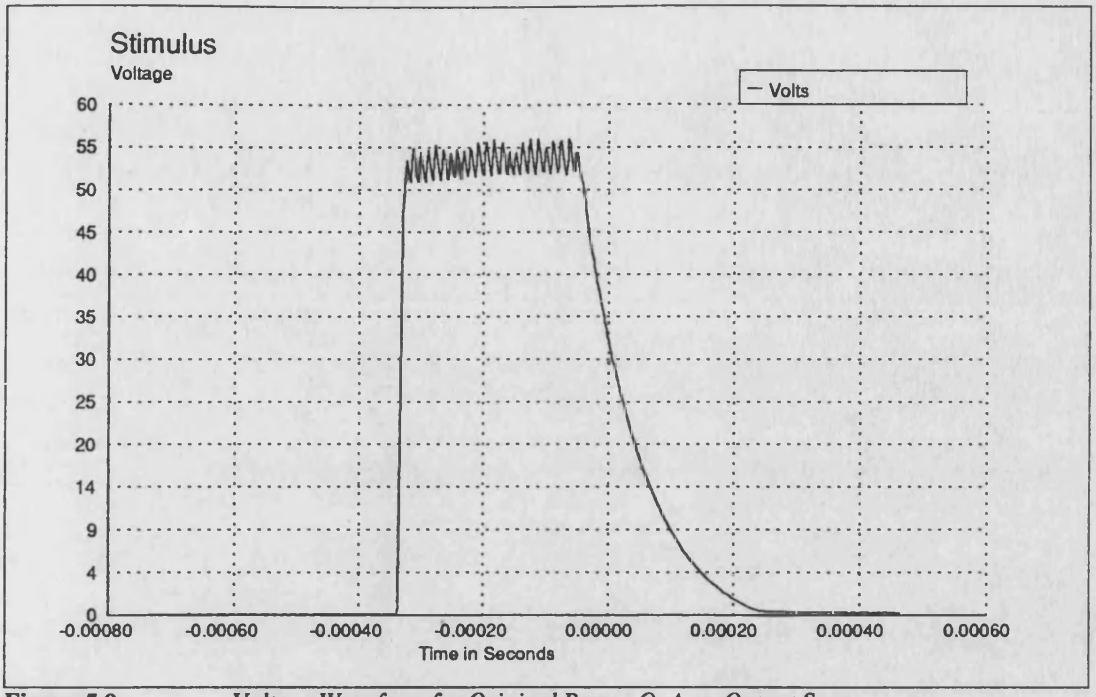

Figure 5.9 *Voltage Waveform for Original Power OpAmp Output Stage*
Standard Load of 1 kΩ in parallel with 100 nF

current waveform as shown in Figures 5.9, 5.10, 5.11 and 5.12. This did not seem to affect normals adversely, except that stronger contractions could be achieved at lower thresholds. However, on paraplegics, very strong contractions were obtained with very little control available from the voltage level pot. The effect of this was that the stimulator could not be used on paraplegics successfully, so a second version has been built.

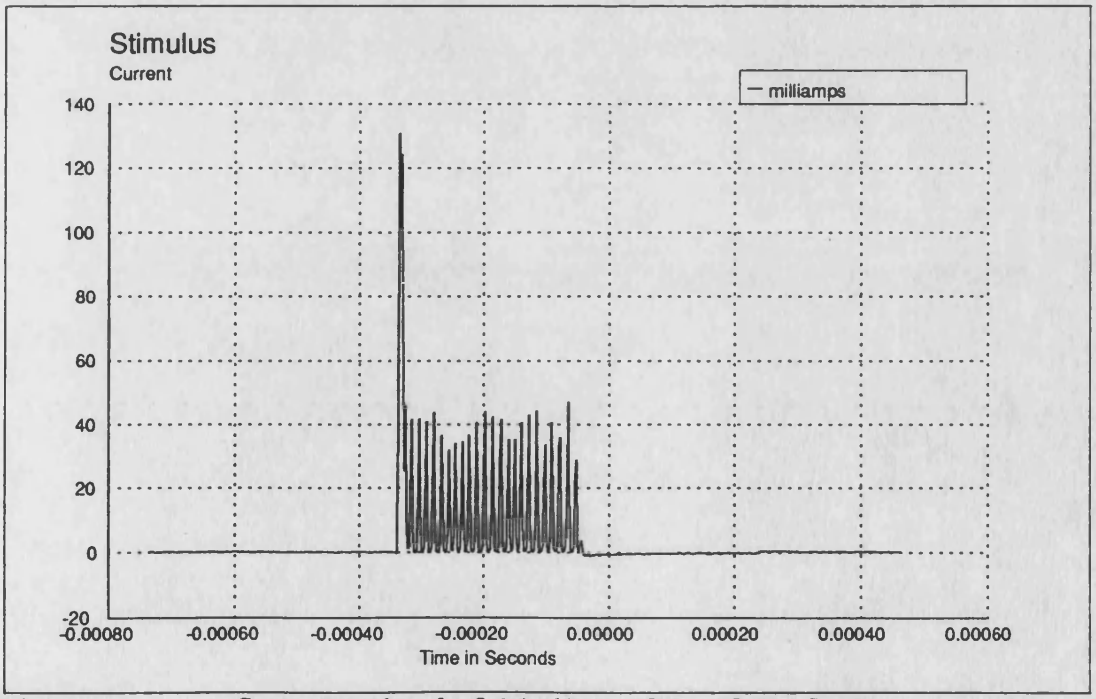

Figure 5.10 *Current Waveform for Original Power OpAmp Output Stage*
Standard Load of 1 kΩ in parallel with 100 nF

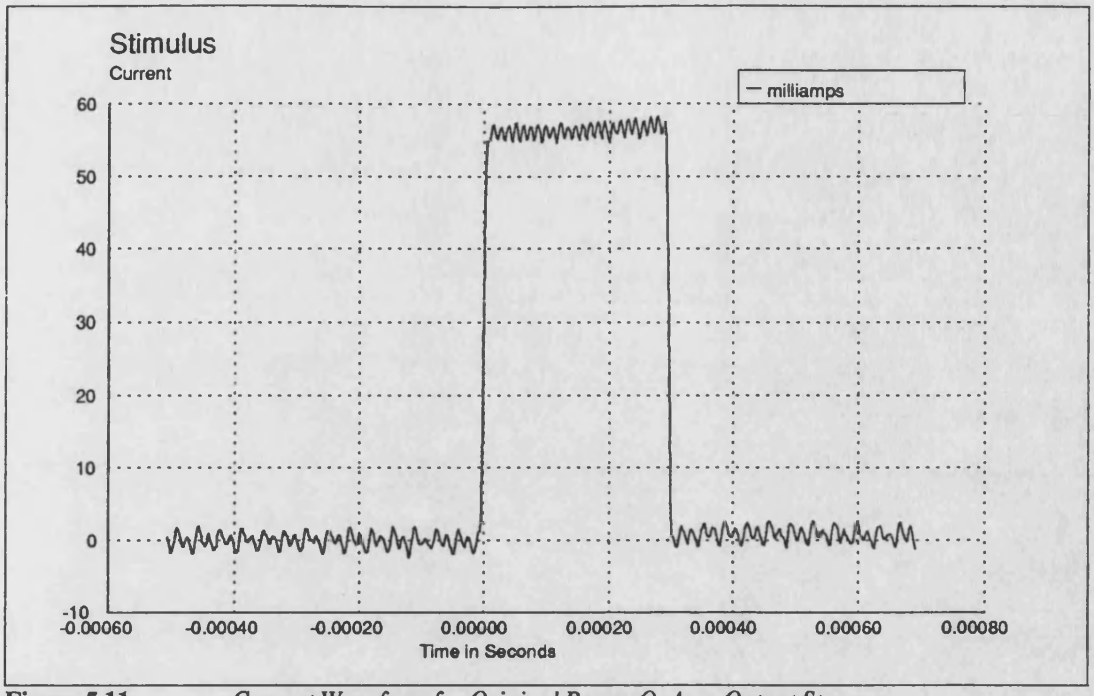

Figure 5.11 *Current Waveform for Original Power OpAmp Output Stage Resistive Load of 1 kΩ*

5.2.2.2 The Improved OpAmp Stimulator

The improved design makes use of a high voltage–high current power operational amplifier. The one chosen for this design is the BurrBrown 3583, which operates from rails of up to ±140V with a load current of up to ±75 mA. The other important features of this device are: it has a 5 MHz unity gain bandwidth and a slew rate of 30 v/μsec.

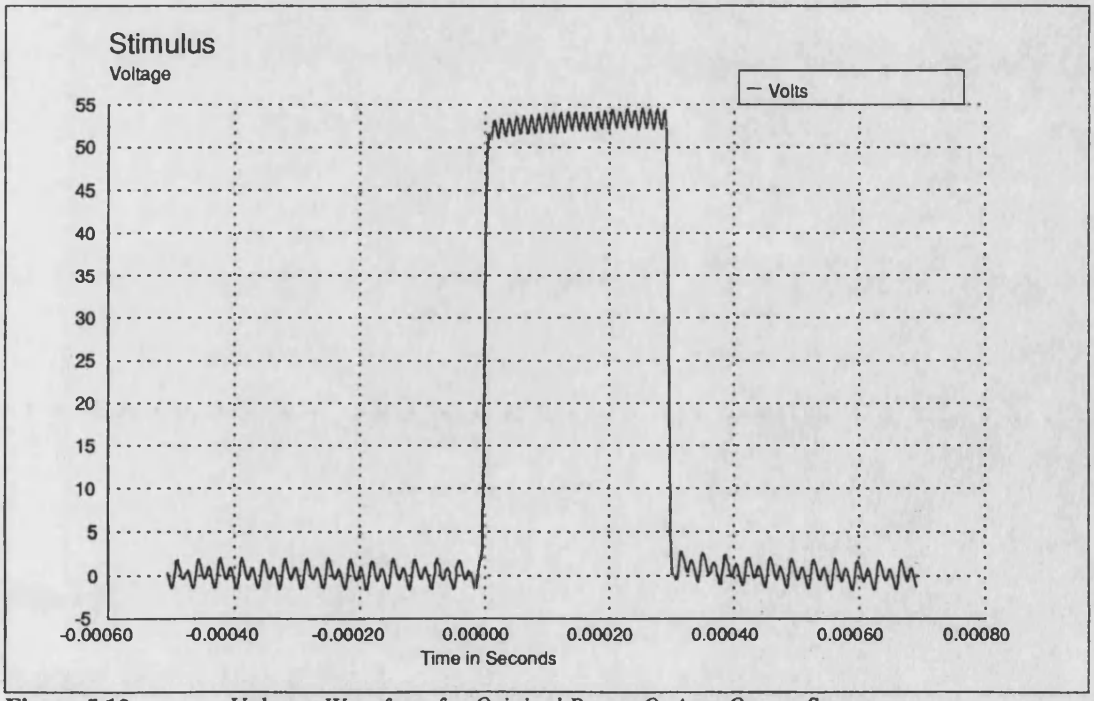

Figure 5.12 *Voltage Waveform for Original Power OpAmp Output Stage Resistive Load of 1 kΩ*

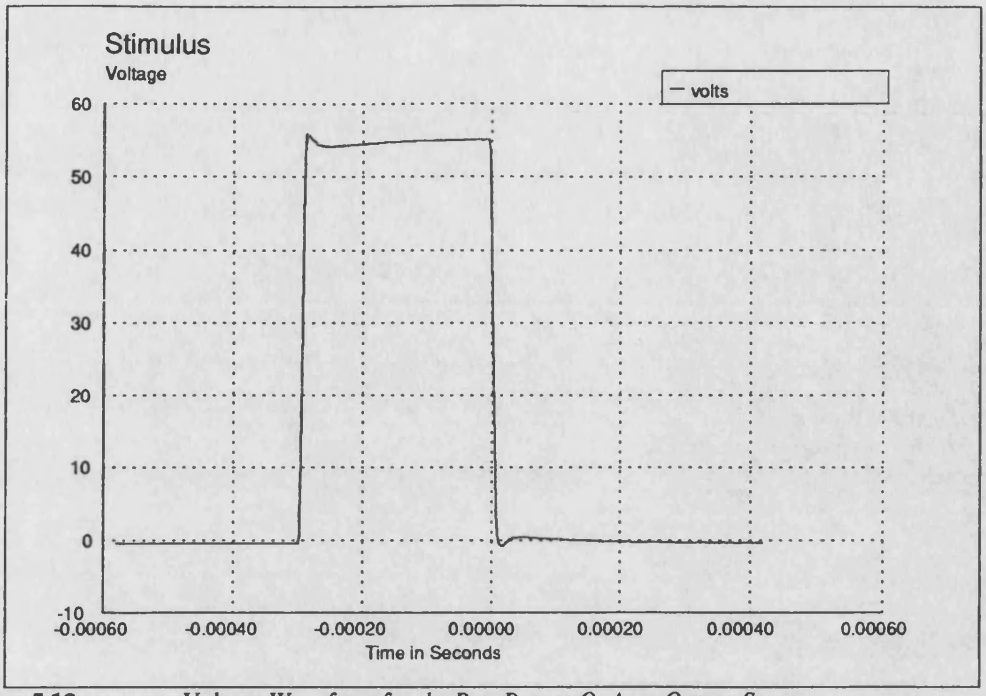

Figure 5.13 *Voltage Waveform for the BurrBrown OpAmp Output Stage*

The revised circuit diagram is given in Figure G.9. Figure 5.13 and 5.14 show the current and voltage output waveforms for this stage using a 'real' human load and 3M rubber electrodes.

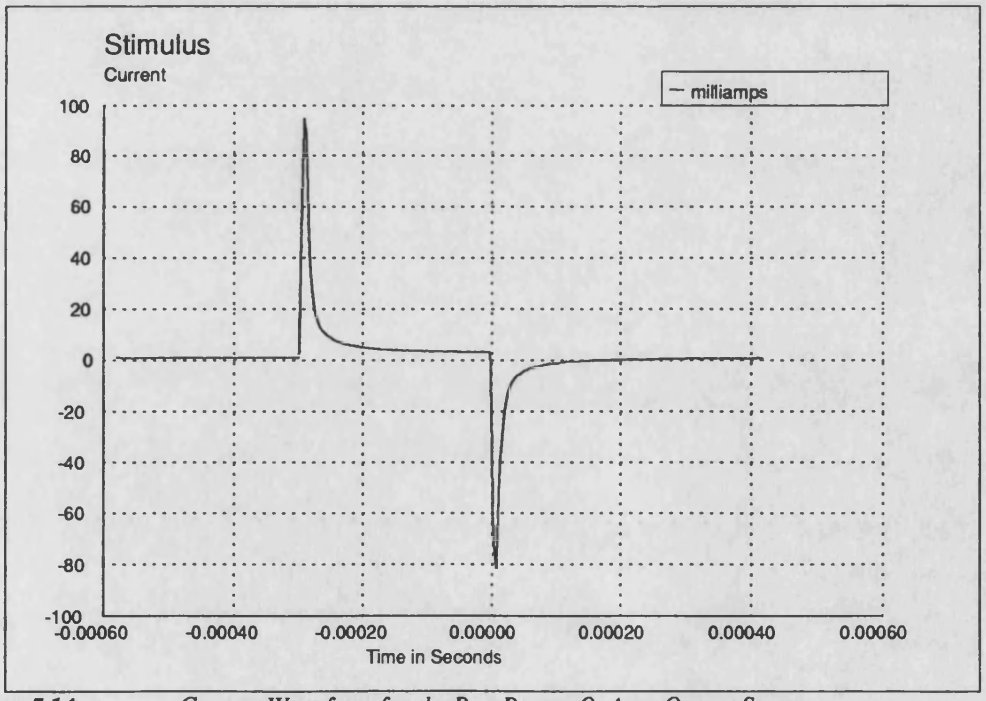

Figure 5.14 *Current Waveform for the BurrBrown OpAmp Output Stage*

5.2.2.3 The Pre-processing Board

The output stage is made up of two sections: a pre-processing and isolation stage, and an amplification stage. The pre-processing stage takes the 5V pulse train from the

microcontroller card and amplifies it, via a variable gain amplifier, to give a pulse train that can be varied between 0 and 10V. This is shown in Figure G.5.

The pre-processing stage also provides a DC offset adjust, which is used to offset the output to the negative rail, to give the full 100V range. This is required because the stimulator output stage is powered from ±50V.

This section also contains a number of safety features to ensure that on power up the operational amplifier output is not connected to the stimulator output socket. This is achieved by relays, which must be enabled by pressing a reset button before they will connect the opamp output to the output socket. This ensures that if the variable gain amplifier is left turned to its maximum setting it will not be immediately connected to the subject at switch on. The current system does not ensure that the output voltage is turned to zero before enabling the relays.

5.2.2.4 Power Amplifier

The variable stimulus pulse from the pre-processing card is amplified by the power amplifier, which has a fixed gain of 10, giving a maximum output voltage of 100V.

Both power amplifier stages function as described above, except that the original output is a non-inverting amplifier—as oppose to the opamp circuit, which is configured as an inverting amplifier. This difference has necessitated the changes between the two circuits that can be seen in the circuit diagrams of Figures G.5 and G.9.

5.2.2.5 OpAmp Power Supply

The power supply board provides regulated ±5V, ±15V DC supplies and an unregulated ±50V DC supply. The 5V supply is used by the microcontroller card, the 15V supply is used by both the pre-processing and the original power operational amplifier stage. The 50V supply is only used by the power operational amplifier. On the output socket GND is in fact –50V relative to the ground (0V) of the main circuit and maximum stimulus output is +50V relative to the ground of the rest of the circuitry. The power supply circuits are shown in Figure G.6.

5.3 Stimulator Enclosures

The original two channel exercise stimulator used for the initial tests is described elsewhere[75]. It is shown in Plate F.1. The only modification made to this stimulator is that a buffered version of the stimulus pulse is brought out to a 3.5mm socket mounted on the back of the case. This provided the synchronisation for the original analysis configuration.

The stimulators that have been designed have been boxed in two separate types of casing. The switchmode power supply based stimulator has been boxed in a standard instrument case measuring 220 by 105 by 230 mms. This casing style has been adopted within the Medical Electronics laboratory for most of the standalone equipment that has been developed here. Plates F.3 and F.4 show the final boxed stimulator and a close-up view of the front panel respectively. The sixteen key keypad is mounted in the top of the stimulator case above the LCD display. Plate F.5 shows a view of the internal circuitry showing the processor card on the left and the two PP9 ni-cad batteries on the right. Plate F.6 shows the LCD Display whilst re-programming the pulse width.

The operational amplifier stimulator has been built into a metal case. Plates F.7 and F.11 show the fully cased operational amplifier stimulator and the top panel respectively. Plates F.8 and F.9 show views of the internal circuitry from the side and top respectively. On the left hand end of Plate F.8, two 25 way D connectors can be seen. The top one of these is a 25 way female connector and provides the connection to the keypad and LCD display shown in Plate F.10. The other connector is for the RS232 link.

5.4 Stimulator Control Software

The stimulators are required to be readily programmable so that the various stimulating parameters can be adjusted during the stimulation tests. As suitable parameters are identified the programmability will be a key feature in the closing of the feedback control loop in standing.

The 8051 series microcontrollers have an RS232 compatible serial port available as standard, so it is logical to make use of this to set the stimulator parameters. To ensure the stimulator can be programmed without recourse to a terminal, a keypad has been provided. Since the stimulator is a potentially dangerous piece of equipment, it is important that the stimulator displays what it thinks the current programmed mode is. When using a terminal this can be on the display of the terminal, but the addition of a keypad requires that separate display be provided, which in this case is the 2 line 20 character LCD display.

The two stimulators run almost identical versions of the stimulator code. The one difference is due to the types of power supply. The operational amplifier stimulator is currently mains powered. This means there is the possibility of 'mains glitches' crashing the microcontroller. The 80C552 has on board a 'watchdog' timer which will reset the processor if allowed to time out. Use is made of this timer so that should the 80C552 software fail to regularly reset the timer the processor is reset. This means that

regularly throughout the operational amplifier stimulator code there are calls to reset the watchdog timer.

The main control routine initialises all the system variables and control lines to their default states. Then it enters a loop that regularly polls the keyboard on the stimulator awaiting a key being pressed. This occurs in both Manual and Micro mode. In Micro mode however, control of the stimulus level is only possible via the RS232 link. All other functions may be programmed from either the key pad or via a dumb terminal.

5.4.1 Debugging and Monitor Software

The only system available for the programming of 8051 based processors could not provide any debug capabilities. In order that the 8051 code could be readily debugged and to provide a simple method for analysing any problems that may occur whilst using the various 80C552 based processing cards, a simple debug monitor program has been incorporated into all the software. The monitor program is invoked by sending a character to the processor via the RS232 link. The code is readily incorporated with any other RS232 facilities, so it can exist even though the serial port is used to program the processor, as is the case with the stimulator.

The facilities provided are given in Table 5.1: the standard register dump, internal ram dump, external ram dump, function test and hardware register display. Though it is possible to add in functions for writing to the registers and memory locations it has not been found necessary to do so.

Command	Function
R	Register Dump for all four Memory Banks
D	Internal Ram Dump
MXXXX	Dump External Ram from XXXXH
SXX	Display Contents of Special Function Register at XXH
H or ?	Help Message
X	Exit Monitor and Return to main Program
T(XXXX)	Test a subroutine XXXXH should be entered if required

Table 5.1 *Debug Monitor Functions*

The monitor module is self contained and only requires the availability of the RS232 receive interrupt, whether directly or indirectly. All the commands are single letters and may be followed by a hexadecimal address if required. The internal ram of the 80C552 has been divided up into defined sections such that minimal interference between the various software modules occurs. This means that register bank 4 is allocated to the debug monitor and for input it makes use of the input buffer used by all other input. On entry to the monitor, which is by a single CR sent via the RS232, all the registers are saved. This allows the monitor to be entered at any point in the

flow of the main program. Registers of interest can be viewed and then control can be returned to the main program without it crashing.

The monitor program also provides a simple hexadecimal display of the accumulator contents by a subroutine called DISPL, which may be called from within the main program to output variables. It will send the current accumulator contents as hexadecimal digits for display on a terminal using the RS232 link. The routine saves all the registers it uses on entry and restores them all on exit, so appears transparent to the main routine.

5.4.2 Stimulus Generating and Timing

The stimulus pulse, and S/H pulse are generated by interrupts which run at high priority level. This means the stimulator will continue to function from within the serial port routine, which is an interrupt routine in the current software. After the setting up of the timers and interrupt routines in the initialisation code, the stimulus generation continues under interrupt control. The only time that stimulus generation is stopped is when the pre-pulse width, pulse width, post-pulse width and interpulse interval are being updated.

The interpulse interval is generated by timer T0. This is clocked by the processor machine-cycle clock which is one twelfth of the processor clock, i.e. 1 MHz. The timer itself is configured as a 16 bit counter. In this mode, when the timer count rolls over from all '1's to all '0's it causes an interrupt. Using this the slowest interrupt rate is every 65 ms. This time is equivalent to half the interpulse interval as can be seen from the timing diagram of Figure 5.3. To allow for interpulse intervals greater than 130 milliseconds, an extra count is used within the timer interrupt routine T0INT. By using the count, DELAY, the interpulse half period may be extended to 16 seconds, that is, an interpulse interval of upto 32 seconds.

The timer 0 interrupt routine carries out several tasks as detailed in the pseudocode of Figure 5.15. DELAY and DSET are calculated by the routine that sets up the IPI pulse width (SETFREQ). Essentially it is a count of how many times the counter T0 must time out before toggling P1.0. Generally these values are zero unless the IPI is greater than 130 ms.

Included in this listing are the two other interrupts that are used. T2OVFL is an interrupt that occurs if T2 overflows. Generally T2 is reset before it overflows but for long interpulse intervals it may overflow. This routine ensures that there is no chance of an overflow causing an extra stimulus pulse. COMP2 is an interrupt generated by the second compare register forming a match with the contents of Timer T2.

The stimulus pulse on P4.0 is generated purely by hardware matches of the compare 1 and compare 0 registers. These hardware registers will automatically toggle selected port pins (P4.0 in this case) when matches of the T2 count and the compare register contents occur. Timer T2 is clocked by the machine cycle clock via a divide by 8 pre-scalar, thus the timer resolution is 8 μsecs. The various pulse parameters are scaled within the routine GET_NUM which is called by all the pulse setting routines. The binary number returned by GET_NUM is thus the time in microseconds inputted divided by 8. The pre-pulse width is stored as a 16 bit value in PREL and PREH, the pulse width is stored as a 16 bit number in PWL and PWH and the post-pulse width is stored as a 16 bit number in POSTL and POSTH. These values are used by the routine SETUP to set-up the hardware compare registers as defined in Figure 5.16.

```
;Timer T0 Interrupt Routine T0INT
Save processor Status
Decrement DELAY
If DELAY = 0FFH
   Complement P1.0
   Reset DELAY = DSET
   If P1.0 High
      Set P4.1
      Start Timer 2
Stop Timer T0
Re-Load TL! and TH1
Restore Processor Status
Re-Start Timer T0
Return
;Timer T2 Interrupt Routines COMP2 T2OVFL
;COMP2
Clear P4.1
Clear Compare Interrupt Flag CMI2
Return
;T2OVFL
Switch off Timer T2
Clear Overflow Flag T2OV
Return
```

Figure 5.15 *Pseudocode for the Interrupt Routines*

5.4.3 Keyboard

The keyboard software uses a double buffering technique to provide a buffered and debounced key pressed table. The key pressed is returned in the two byte buffer Keys. A second buffer monitors whether the Dokey routine has carried out the key function yet. This allows for a debounced auto-repeat function. The keyboard layout is given in Figure 5.17; the keys on the right are dual function, their primary function is to select the programming mode. Once the programming mode has been selected they take on their secondary function as shown below the keys in Figure 5.17. (BS is the backspace or rubout key for when an error is made whilst entering the new data.)

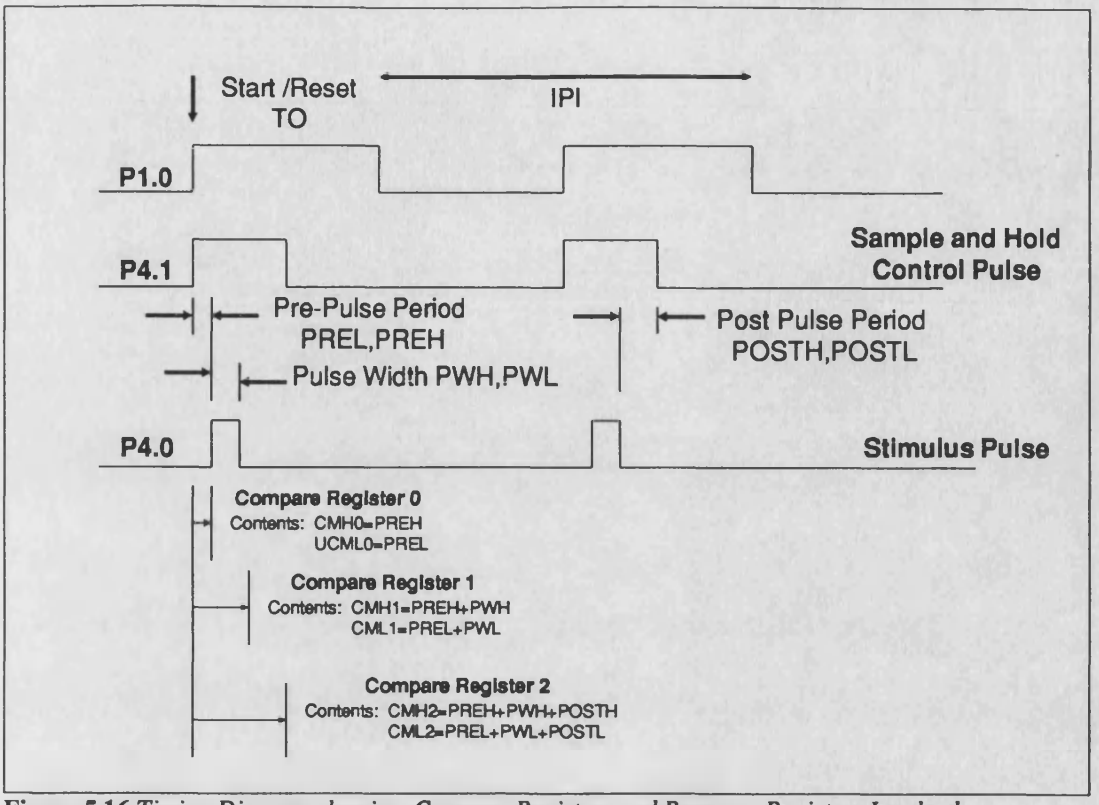

Figure 5.16 *Timing Diagram showing Compare Registers and Program Registers Involved*

The key subroutines for the keyboard are given in pseudocode form in Figure 5.18. These routines ultimately return the equivalent ASCII codes so that the data can be processed by the same routines as are used for the serial port programming mode.

5.4.4 LCD

The LCD can be read from and written to because the data is passed via a common 8 bit port which is read by the LCD display processor when it has time. The effect of

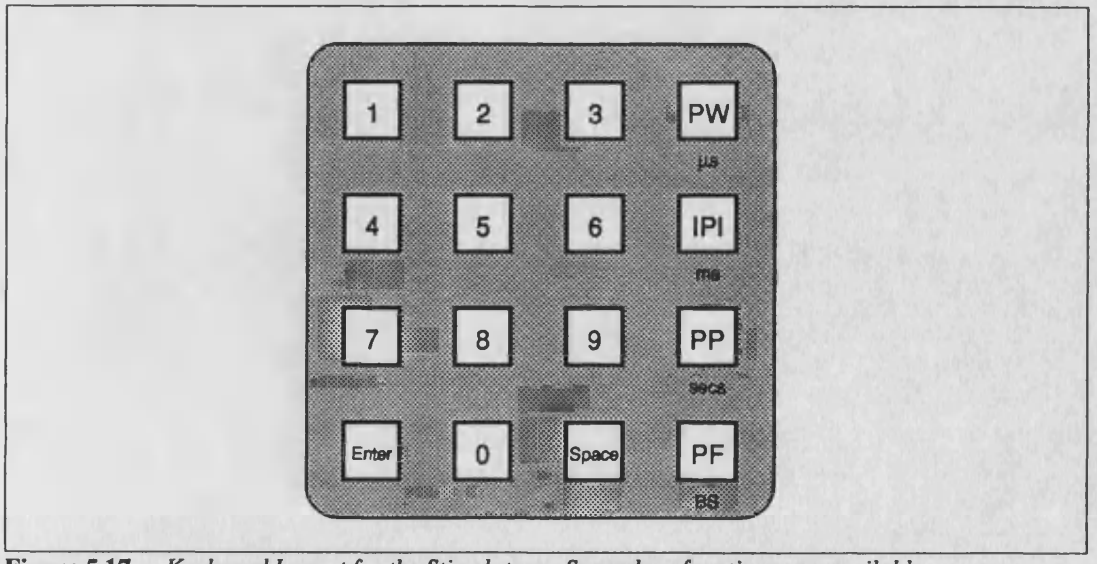

Figure 5.17 *Keyboard Layout for the Stimulators ; Secondary functions are available as soon as one of the program Modes has been sel;ected*

```
;KBRD Identifies if key pressed
Read Keydata into Newkey for each nibble of selector
       ie P1.2 and P1.3 = 00, 01, 10, 11
If Newkey <> Oldkey
   Oldkey = Newkey
   Newdat = FALSE
Else
   Oldkey = NewKey
   Keys = Oldkey
   Newdat = TRUE
Endif
Return

;DOKEY Returns key pressed
Newdat = FALSE
Repeat
   If Keys(Bits) = 1 And Done(Bits) = 0
      Done(Bits) = 1
      Do a Keyclick
      Call KEYCONV ;Convert value to Equivalent ascii
      Return
   Endif
   If Keys(Bits) = 0 And Done(Bits) = 1
      Done(Bits) = 1
      ;Call to do something on key release
   Endif
   Increment Bits
Until Bits = 15
Return
```

Figure 5.18 *Pseudocode for the Key Keyboard Subroutines*

this is that it is necessary to ensure the previous data has been acted on before sending new data. This is the so called busy 'test'.

In order to reliably write to the LCD, all the control signals are toggled by the software. The LCD module has two registers which are selected by the RS line P3.3. One register is the Instruction register which when read returns the 'busy' state in bit 7, the other is the Data register which is the register to which the display data is written. Writing to the display follows a simple pattern; the data is set up by writing to the memory location 08000H, the register select line is set in the appropriate state and the R / W line, P3.5 is cleared. Then the Enable pin, P3.4 is pulsed high. Reading is similar except the data is read from memory location 08000H after the Enable has been pulsed.

The LCD display has two modes of display: the default mode in which the current pulse width and interpulse interval are displayed as may be seen in Plate F.4 and the program mode. In the program mode the LCD will display a question appropriate to the function being programmed. This may be seen in Plates F.6 and F.10.

5.4.5 RS232 Programming

The serial port programming of the stimulator is currently entered from within the Monitor program by entering P(rogram) at the Debug Monitor prompt. This then allows for a number of programming functions as listed in Table 5.2. On entering a command letter the stimulator prompts for the appropriate parameter. The time units are microseconds unless an alternative time unit is entered using the commands given in the table preceded by a space (20H).

Command Letter	Function
R r	Pulse Repetition Rate Setting in µsecs
W w	Pulse Width Setting in µsecs
P p	Pre-Pulse Period Setting in µsecs
F f	Following(Post)-Pulse Period Setting in µsecs
A a	Output Value as DAC Value on Channel A
B b	Output Value as DAC Value on Channel B
X x	Exit Stimulator Program Mode
Unit Abbreviations	Units (preceeded by a space) may be used instead of Entering Times in µsecs
SPC S	Seconds
SPC m	Milliseconds
SPC u	Microseconds

Table 5.2 *Commands available in Stimulator Programming Mode using RS423*

Serial programming is the only means by which the output stimulus may be remotely programmed. (In the case of the operational amplifier stimulator where DAC control is currently not available this function is unavailable). The stimulating voltage is non-linearly related to the DAC value as may be seen from the detailed discussion in Appendix A.

5.5 RS232 Isolation Box

In order to ensure complete isolation of the stimulator from any controlling computer, that is using the RS232 link to program the parameters of the stimulator, it is necessary to provide an isolation unit. This has been achieved using opto-isolators. The circuit for the opto-isolating RS232 box is given in Figure G.10. The unit has two twenty-five way D-type (male and female) connectors on both sides of the isolation to provide maximum flexibility.

Since the RS232 link is bi-directional it is necessary to have an isolated power supply on both sides of the isolation. This can be achieved either by a single power supply with some means of transmitting the power across the isolation to power the isolated side or by using two isolated power sources. Since this unit has a wide range of applications within the medical laboratory it needs to be small and portable. Thus

the simplest option is to power the two sides of the isolation from separate PP3 batteries. From the circuit diagram it can be seen that power LEDs are provided to indicate the battery state. These LEDs visibly dim as the voltage drops to levels at which the isolator will not function reliably.

The box has been wired as a Reverser, that is, the transmit and receive and the RTS and CTS lines are swapped. This not only makes the isolator simpler to implement but also allows the use of Null Modem cables for connection to the stimulator and terminal.

Chapter 6

EMG Amplifiers

The EMG amplifier is one of the most important parts of the analysis system so a number of stringent requirements are placed on it. When the work reported here commenced, knowledge within the group about EMG amplifiers was sketchy and their interaction with stimulus artefacts was largely unknown, having been largely ignored by the medical community for most of their tests. The was because the tests then being carried out on the paraplegics were of the diagnostic type such as the H reflex. Section 4.5 has already discussed the problems in picking up and amplifying the CAPs.

In this chapter the various designs that have been used for this research are presented. These amplifiers fall into two broad categories; pre-amplifier modules for use with 'disposable' surface electrodes and combined electrode/preamplifier modules. In order to isolate the subject from the mains powered analysis equipment, an adjustable gain isolation amplifier is presented. This serves two purposes in that it isolates the subject and also bandlimits and amplifies the muscle response to the required level for the ADC input.

6.1 The Requirements

As has already been stated, the bandwidth of the surface EMG is limited by the low-pass filtering effect of the body tissues. Authors disagree as to quite how low the cut-off is, ranging from 200 Hz to 500 Hz and even 1 kHz. It was decided that the optimal bandwidth would be of the order of 500 Hz since this would allow sampling at around 1 kHz so giving a frequency resolution of 1 Hz from the analysis system.

Gain is a significant problem in these systems, since the compound action potential from a healthy subject could be of the order of several millivolts, whilst from the wasted leg muscle of a paraplegic this may be reduced to a few hundred microvolts. The system, though primarily aimed at the testing of the stimulated muscle responses from paraplegics, is also used for testing normal voluntary muscle responses so a flexible gain system is required.

After some experimentation it was found that the best solution to the gain problem was to have two versions of the preamplifier: one that has a minimum gain up to one thousand for use on voluntary muscle recording and one that has a much reduced gain of the order of one hundred for use on compound action potential recording. Although these requirements have been found to be adequate for most of the subjects within the

standing program, it has been found that some subjects whose muscles are particularly wasted have required greater gains in order to detect the CAPs.

The pre-amplifiers having buffered and amplified the small biopotential signals, feed into a variable gain isolating and filtering unit such that they make maximum use of the sampling systems ADC range. As is described in Chapter 7 three different ADC input stages have been used. Each of these has had an improved resolution and differing input voltage range.

The original Printer Port interface described in Section 7.1 requires an input signal to its filter of ±4.5V max. This is achieved with a simple switchable gain amplifier whose circuit diagram is given in Figure G.19.

For the 12 Bit ADC80 used in the Mega Expansion version, described in Section 7.2.2 the input to the analogue filters have a maximum range of ±5V. This again is achieved using the same switchable gain amplifier shown in Figure G.19.

The DSP card requires an input signal in the range of ±10V at its ADC input. This is achieved by using the switchable filter and gain stage described in Section 6.6 which incorporates the isolation stage electrical isolation.

6.2 "Stick On" Electrode Amplifiers

Initial studies were carried out using traditional Ag-AgCl surface ECG/EMG electrodes. These electrodes consist of a small 1 cm diameter Ag-AgCl electrode and either a sticky jelly that not only sticks the electrode to the skin but also ensures a good contact, or it consists of a sticky surrounding ring to attach the electrode and a conductive electrode jelly which goes between the electrode and the skin surface. Figure 4.6 shows two examples of these electrodes.

The first versions of the EMG amplifiers were conceptually based on the systems currently in use in the hospitals. These systems made use of a pre-amplifier connected via short electrode leads to the surface electrodes. As has been discussed in Chapter 4 this affords some protection from a large number of the common interference artefacts.

All the pre-amplifiers described in this section followed this philosophy and so were powered from a single PP3 ni-cad battery and built into a screening case. Early versions used diecast boxes as shown in Plate F.13. Later the boxes were changed to plastic cases with internal screens. This was found necessary because of problems caused by the screening case of the diecast boxes. Plate F.12 shows the latest casing along with the electrode lead and electrodes.

Another important factor in the pre-amplifier design is the electrode lead. This lead acts like an aerial to radiated interference and was found to be a significant factor in the generation of interference and artefacts. The original lead consisted of a screened multi-core cable with the screen grounded at the pre-amplifier end. The last six inches of the core leads were unscreened to allow sufficient lead for the connection to the electrodes. It was found that this lack of screening led to significant motion artefacts and mains frequency interference.

The improved lead that can be seen in the Plates F.13 and F.12 uses a multi-core cable, but one in which the individual leads are screened; this afforded much better screening. The screen now extends up to the connection to the electrodes. These leads gave a significant reduction in the interference and artefacts. At the pre-amplifier end the lead is terminated in a 5 pin DIN plug which has been adopted as the connector for EMG electrodes and probes.

6.2.1 Straight Pre-amplifiers

The design of these amplifiers was based on a design published by Burger and Rugh[164]. This is a combined instrumentation amplifier and bandpass filter and served as the initial point for the EMG amplifier designs and the EMG tests. Figure G.11 gives the circuit diagram of the original design.

This pre-amplifier consists of the standard three operational instrumentation amplifier but with zero DC gain. This is achieved by using the capacitor C1 in series with the gain setting resistor R5 between the two high impedance buffers U1A and U1B. The CMRR is adjusted to its optimal figure by using preset R10 which ensures that the two buffer amplifiers have matched gains. This original design had a gain of 21 and the band-pass filter made by U3B and U3A has a low frequency cut-off of 9.7 Hz and a high frequency cut-off of 1000 Hz.

The low frequency cut-off is well below mains frequency which means that significant amounts of mains hum could, and in fact were, produced in the early designs. In order to reduce this a notch filter was introduced between the instrumentation amplifier and the bandpass filter. Figure G.12 gives the revised circuit diagram. It uses a 'Twin-T' bandstop filter where the notch depth may be adjusted by the preset R15. This change was combined with attempts to improve the dynamic range of the amplifier by using an inverter to generate a –9 V rail from the battery. This gave an output range of practically ±9 V.

To protect the input of the amplifier from excessive stimulating voltages, back to back diodes are placed across the input. This limits the maximum input differential voltage to around 1.4 V. The two 1 nF capacitors C12 and C13 were required to

reduce the increased noise associated with the diodes across the input and they also served to reduce all high frequency noise.

The final revision of the basic instrumentation amplifier is shown in Figure G.13. The input instrumentation amplifier and twin-tee notch filter remain largely the same but the band-pass filter was replaced by a fourth-order Sallen and Key based Butterworth filter. As had been done previously two versions were built: one using a split rail supply and the other using an inverter to give a –9 V rail from the +9 V rail.

The original versions of these amplifiers were built on veroboard as may be seen in Plates F.14 and F.15 which show views inside one of the pre-amplifier modules. Later modules have made use of PCBs with the top surface acting as a ground plane to reduce noise and interference further.

6.2.2 Precision Instrumentation Amplifier

A number of investigators have also made use of precision Instrumentation amplifiers as the basis of their EMG or ECG detection systems. These devices incorporate in a single integrated circuit a complete adjustable gain differential amplifier. The common features of these devices are very high common mode rejection ratio, high gain, high input impedance and good linearity. Often they incorporate input protection for both power on and power off fault conditions.

A number of manufacturers make instrumentation amplifiers suitable for inclusion in EMG amplifiers. The device used here was chosen because it was already being used within ECG analysis equipment in the hospital and had been found very suited to the task[169].

The AD524 instrumentation amplifier is used to replace the discrete component instrumentation amplifier used in the final pre-amplifier design of Figure G.13. The complete circuit diagram is given in Figure G.14 and has the back to back diodes used previously to protect the inputs. The signal then feeds into the amplifier which has both the input and output offset null circuitry incorporated. The amplifier output then feeds through a fourth order low-pass Butterworth filter built from two cascaded Sallen and Key second order stages. The cut-off of the low-pass filter is set at 500 Hz.

This pre-amplifier has been built on a double-sided PCB with the top surface acting as a ground plane. The circuit board is mounted in a small diecast box, sized 89 by 35 by 30 mm. The power is supplied by two externally mounted PP3 ni-cad batteries.

6.2.3 Specific Modifications for Artefact Suppression

Two modified EMG amplifiers have been designed, specifically aimed at trying to reduce the effects of stimulus voltage on the recorded CAP. These were introduced after the initial investigations with the amplifiers, described in section 6.2.1, indicated

that a major cause of the artefacts was the stimulus waveform saturating the amplifiers. This, as has already been discussed, is not the whole problem but can be significant with the wrong electrode and input impedance combination. Both designs were built on double-sided PCBs where the top surface acted as a ground plane.

The two designs have been used to try and prevent the stimulus voltage entering the pre-amplifier and saturating the front-end. The first approach is the differential sample and hold as discussed by Babb et al.[183]. The control signal for the sample and hold switches is derived from the stimulator trigger pulse.

The circuit for the differential sample and hold is given in Figure G.15. Essentially the circuit is the instrumentation amplifier, as described earlier, with the differential sample and hold place between the electrodes and the amplifier. In order that there is space in the casing for the extra circuitry required, the filter has been removed and an adjustable gain amplifier replaces it. The analogue switches, U2, are controlled by a control signal generated by a monostable U4A. The monostable is triggered via an opto-isolated pulse from the muscle stimulator. The stimulator was originally the small 2 channel exercise stimulator Plate F.1 where the stimulus trigger pulse matched the stimulus pulse. The monostable lengthens the trigger pulse so that the hold state is held after the stimulus has finished but before the CAP appears. Power is provided by a a single PP3 ni-cad and a voltage inverter provides the negative rail.

The second design uses a combination of a sample and hold stage on the output of the instrumentation stage and an on-off switch on the power rail to the instrumentation amplifier stage. The circuit diagram is given in Figure G.16. The generation of the clamp and switch control signals is exactly the same as that used in the differential sample and hold amplifier. The on-off switch on the front end either connects the operational amplifier U1 to the power rail or, when in the hold mode, it connects the positive rail to ground. The idea is to maintain the instrumentation amplifiers quiescent charge whilst disabling its functioning, thus reducing the switching transients. The sample and hold provides a second filter to remove the effects of switching the instrumentation amplifier on and off. As with the previous pre-amplifier the filter circuitry had to be removed to make space for the additional clamping circuitry and a fixed gain of ten amplifier.

Power is once again provided by a single PP3 ni-cad battery with both a split rail power supply version and a ±9 V supply by using an inverter version being designed. Both of these versions were built on double sided PCBs with the top surface acting as a ground plane.

6.3 Electrode Pre-amplifier Modules

The investigations with the "stick on" electrodes made it clear that the skin-electrode and electrode-pre-amplifier interfaces were the major sources of extraneous noise. Mains interference, as discussed in section 4.4.6, is particularly significant when the electrodes are making bad contact due to the impedance mis-match problems.

Since the purpose of the analysis system was to provide feedback information, signal integrity is particularly important. A number of authors have found that the combination of the electrodes with the pre-amplifier stage in a single unit improves signal integrity and permits greater variations in electrode-skin impedance. Using a design based on one developed at the RUH in Bath a number of small electrode mounted pre-amplifiers have been made.

The circuit for the original design is given in Figure G.17. This design used two silver electrodes inset into the small perspex case to allow the application of electrode gel to ensure there is a good contact between electrode and skin. The amplifier used a dual operational amplifier. One half configured as a 'single operational amplifier' high gain differential amplifier, the other as an inverting amplifier. The input stage is AC coupled to the electrodes to remove the electrode voltages before the differential amplification. This is then AC coupled to a times ten gain to drive the output lead. The differential amplifier used 100M resistors to give a high gain (100) and high input impedance. The high impedances involved mean that low input bias currents are required to ensure DC offsets are kept to a minimum.

The pre-amplifier designed uses two stainless steel electrodes 1 cm apart as the detection surfaces. These protrude slightly from the casing in order that there is no need for the electrode gel to maintain a good electrode skin contact. Plate F.17 shows the perspex case in which the amplifiers are built. Two basic versions of the amplifier have been built. Figure G.16 gives the circuit diagrams for the two basic amplifiers. The two designs are in fact copies of the RUH design with the gain stage adjusted to reduce the gain from one thousand to one hundred. A number of variations have been designed where the various capacitors have been changed to adjust the bandwidth of the amplifier and to speed up the recovery of the amplifier from saturation.

Plate F.16 shows a built electrode pre-amplifier in its case. The power is supplied via the screened multicore cable. The power is provided by two PP3 ni-cad batteries and the detected signal is returned via the same multi-core cable. A 5 pin DIN plug is used as the connector for the unit and its pin connections are given in the circuit diagram of Figure G.18.

6.4 Gain Stage

The gain stage is essentially a non-inverting amplifier with a switched feedback resistor to set the gain. It offers gains of 2, 3, 5, 10, 20, 30, 40, 50 via a multi-way switch. The circuit diagram is shown in Figure G.19. This unit is built into a small diecast box using phono sockets for input and output. Power is supplied from a second diecast box containing the batteries which are two PP3 ni-cad batteries.

Included within the power supply box is a 5 pin DIN connector for powering the EMG probe and a sample and hold buffer which is controlled by the S/H pulse from the stimulators described in Chapter 5. The purpose of this is to allow the clamping of the output of the pre-amplifier whilst it recovers from the effects of the stimulus as discussed in section 4.6. The circuit diagram for this unit is included in Figure G.19.

6.5 Isolation Amplifier

The isolation is provided by a switching modulator based Analog Devices Isolation amplifier. This provides isolation of ±1000 Vpk and has a bandwidth of 5 kHz. Power is provided to the device via a clock module that generates a 25 kHz 15V pk-pk square wave from a 15 V DC power supply.

Figure G.20 gives the circuit diagram for the isolation amplifier and input filter. The ±15 V power supplies are derived from two PP3 batteries in series. The +15 V is derived from the nominal 18 V supply by a low dropout regulator. A 7661 inverter generates a –15V negative rail from the +15V positive rail to power the output buffer amplifier.

The filter circuits on the input side of the isolating amplifier are powered from the isolated ±7.5 V power supply generated by the isolating amplifier. The low-pass input filter is a sixth order Butterworth with a cut-off of 1 kHz. The gain of the filter is 4.2, so in order that the isolation unit has a fixed gain from input phono connector to output, there is a buffer amplifier between the filter and the isolation amplifier to adjust the filter gain to be times five.

The output of the isolation amplifier is amplified by a times two buffer amplifier to make the overall gain of the isolation unit ten. The amplifier is built into a large plastic cased box with an internal conductive screen. Care has been taken to ensure isolation between the input and isolated output is maintained by removal of the screen around the isolated section.

6.6 Combined Front End Unit

The gain unit, sample and hold unit, filter and isolation amplifier described above have been combined into a single boxed unit. This amplifies the EMG signals from

either the EMG probes or the pre-amplifier modules to a level suitable for the DSP card. The combined unit has a choice of three low-pass filters of 500 Hz, 1 kHz and 5 kHz and switchable gains of 1, 2, 3, 4, 8, 12, 16, 20, 40, 60, 80, 100. This gain is the overall box gain and takes into account the gain provided by the filter which is a sixth order Butterworth based on the Sallen and Key circuit. The gain of the filter is 4.2 and this is amplified to a value of five using an additional buffer amplifier before the isolation unit. The box has a choice of input connector, the standard 5 pin DIN or a phono socket, selectable by a single pole switch and the sample and hold circuit may be optionally by-passed.

The circuit diagrams for the complete unit including the isolation amplifier are given in Figures G.23, G.22 and G.21. The isolated input side is supplied by two PP9 ni-cad batteries with the output side and isolating circuitry being supplied by a ±15 V DC power supply in place of the original battery based supply as is discussed in Chapter 8. Low power LEDs are used to indicate battery state, as may be seen in the view of the front panel Plate F.18. The subminiature connector has been adopted as the standard control and synchronising connector and is used on the stimulator to output the synchronising signals. The output from the unit is on the isolated back panel which is shown in Plate F.19. Maximum output is ±10 V peak to peak which matches the input requirements of the DSP card described in Section 7.3. To allow for other input requirements to be met the output is provided with a variable attenuator allowing an output of ±10 V to 0 V. This is however an uncalibrated attenuator.

Chapter 7

Signal Processing Hardware

As has already been stated, very few papers have been published on the information content of CAPs. It is only recently that Merletti et al.[102] have published on the subject. To discover if any of the well documented features of voluntary muscle response could be found, albeit with some modification, in the response of stimulated muscle, a means of analysing and recording the CAPs was required which could also provide a means of assessing the EMG amplifiers and their ability to amplify CAPs without undue distortion from the stimulation.

The requirements for the analysis system in the first instance were fairly simple; to sample an analogue signal with a bandwidth of of no more than 5 kHz and then to transform the sampled data from the Time Domain to the Frequency Domain. A simple analysis system has been built around an Atari ST computer.

This system has recently been improved by using a TMS320C25 digital signal processor as the front-end to speed up the sampling and transformations. This leaves more time for the Atari to do the display tasks. This has also required a move from the standard Atari 520ST system to an Atari Mega System.

7.1 The Initial System

The primary aim of this system was to establish whether Compound Action potentials could provide useful information about the muscle state using simple frequency analysis.

The Atari ST series of computers are based around an 8 MHz Motorola 68000 microprocessor with a minimum of 512 kbytes of RAM, a 3 ½ inch floppy disk drive and a high resolution, 640x400 pixels, black and white display. They have one serial port, one bidirectional parallel port, midi ports, and a cartridge slot. The cartridge port is read only, writing to this address space causes a Bus Error.

Since the basic Atari has no access to the 68000 bus, the analogue to digital interface has been built to interface via the bidirectional parallel port. This port provides 8 bidirectional data lines, one input only *Busy* line and one output only *Strobe* line. Figure G.24 shows the circuit; it consists of a ZN448 ADC configured to free run. The output of the ADC is latched after each conversion by the 74LS373, U3, using the end of conversion signal. The latching is disabled by the *Strobe* line of the printer port being taken high, thus ensuring stable data during a read by the computer.

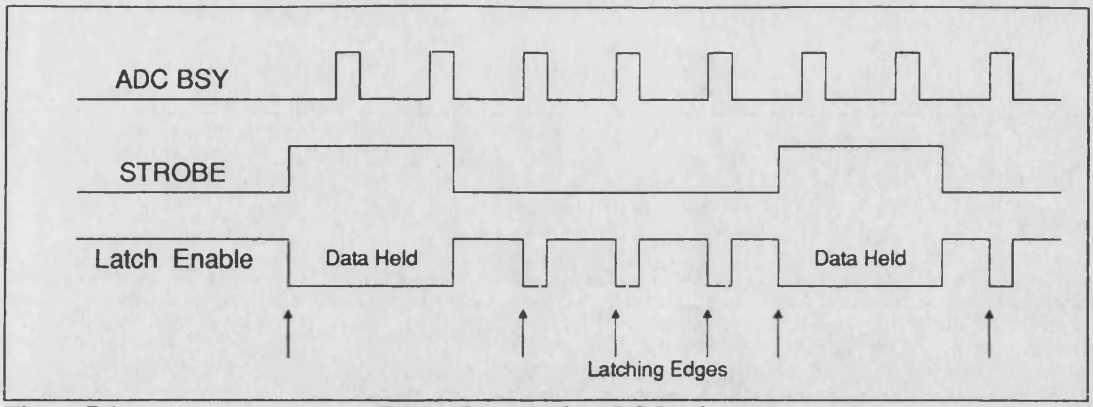

Figure 7.1 *Timing Diagram for ADC Reads*

The ADC is fed from an anti-aliasing filter, based around an MF10 switched capacitor filter, configured as a 4th Order Butterworth filter with a switchable cut-off of 10 kHz, 2 kHz and 1 kHz. The clock for the filter is derived from a 2 MHz crystal divided down to provide an equal mark space ratio clock of 500 kHz, 100 kHz, 50 kHz. The choice of filter cut-off is selected manually via a multi-way switch.

Power is provided from an external 12V source, with a negative rail for the switched capacitor filter being generated by a single chip voltage inverter.

The *Busy* input of the printer port is used to provide an opto-isolated synchronising pulse from the stimulator to the computer for triggering the sampling. This ensures that the samples always start at the same point in the stimulated pulse train.

Figure 7.1 shows the timing diagram for the ADC control signals. As can be seen this system relies entirely on the Atari system for all timing and control. When the Atari Mega series became available it gave access to the 68000 bus so enabling direct memory mapping of the ADC.

7.2 The Mega Expansion

The Atari Mega is functionally the same as the original Atari ST series but with more memory, 2 or 4 megabytes, and an internal 64 way connector providing direct access to the 68000 bus.

7.2.1 Mega Bus Buffering

The internal bus access provided in the Mega ST does not have any buffering so for practical use with a rack based expansion buffering is required. An internally mounted PCB has been designed and its circuit diagram is given in Figure G.26. This card buffers all the signals on to a 96 way a/c connector mounted on the back of the Atari Mega case. This board also provides some high level decode allowing the choice of one of two 524 kbyte blocks at address ranges $C00000-$C7FFFF and $C80000-$CFFFFF, which covers the block of memory specified by Atari for use by

outside developers. Only interrupts of level 7, 5 and 3 are permissible via this expansion connector so they are the only interrupts decoded on the buffer card.

```
PAL16L8
BUFDEC                                          PAL DESIGN SPECIFICATION
MEGA BUFFER BOARD DECODER VERSION 1                              16-AUG-88

/AS FC0 FC1 FC2 A1 A2 A3 A19 NC GND
A20 /DBECORK A21 /IACK A22 /CORKY A23 /LIPPO /DBELIP VCC

IF (VCC)  DBELIP = LIPPO + IACK
IF (VCC) DBECORK = CORKY + IACK
IF (VCC)     IACK = FC0*FC1*FC2*A1*A2*A3*AS + FC0*FC1*FC2*A1*/A2*A3*AS
                  + FC0*FC1*FC2*A1*A2*/A3*AS
IF (VCC)    LIPPO = A23*A22*/A21*/A20*/A19*AS
IF (VCC)    CORKY = A23*A22*/A21*/A20*A19*AS

DESCRIPTION:
DATA BUFFER ENABLE SIGNAL THAT ALLOWS LEVEL 7,5 AND 3 INTERRUPT ACKS
 TO ENABLE THE BUFFER. ALSO PROVIDES TWO PARTIAL DECODES FOR ADDRESS
 RANGES LIPPO=$C00000-$C7FFFF AND CORKY=$C80000-$CFFFFF
```

Figure 7.2 *PAL Equations for the Buffer Board Pal*

The decoding on board is achieved with a 16L8 PAL whose logic equations are given in Figure 7.2. Since a high level decode is carried out on the buffer board A23 pin 26 on the 96 way connector becomes DBELIP, the enable signal for the data buffers during an interrupt acknowledge cycle for level 7,3,2 interrupts. The GND on pin 27 is replaced on the output connector by LIPPO, the enable signal for memory block $C00000-$C7FFFF. Figure G.26 gives the 64 way and 96 way connector signal specifications.

The Bus signals are then fed via a 64 way ribbon card to another buffer card that buffers the signals on to the back plane. Figure G.27 gives the circuit for this backplane driver card.

7.2.2 ADC Card

The ADC card replaces the parallel port ZN448 ADC with a memory mapped ADC80 12 bit ADC with computer switchable analogue anti-aliasing filters. This card also provides a 16 bit input port, 16 bit output port, and two fixed baud rate RS232 serial ports.

Figures G.28, G.29, G.30 and G.31 give the full circuit diagrams. The ADC80 is configured as a free running ADC with reads of the output latch disabling latch updating for the duration of the read. Memory decoding is via a PAL16L2 to give two address blocks in the ranges $C00100-$C0010F and $C00110-$C0011F. Figure 7.3 gives the logic equations for the PAL decoding. The ADC80 is specifically decoded to the two addresses $C00100-$C00101.

The ADC80 is fed from one of two Sallen and Key based 4th Order Butterworth filters, with cut-offs at 1000 Hz and 500 Hz respectively. Selection of input filter is via an eight-way multiplexer controlled by the three low-order bits of the 16 bit parallel port. This port is decoded at addresses $C00102 and $C00103. Reading from these addresses accesses the 16 bit input port which has the opto-isolated stimulus synchronising pulse input on its least significant bit.

```
PAL16L2
ADCDEC                                          PAL DESIGN SPECIFICATION
ADC DECODER LOGIC PAL VERSION 1                                 01-AUG-88

A4 A5 A6 A7 A10 A11 A12 GND
A13 A14 A15 A16 /ADC1 /ADC2 A17 A18 /LIPPO VCC

ADC1  = /A4*/A5*/A6*/A7*A8*/A9*/A10*/A11*/A12*/A13*/A14
      */A15*/A16*/A17*/A18*LIPPO

ADC2  = A4*/A5*/A6*/A7*/A8*/A9*/A10*/A11*/A12*/A13*/A14
      */A15*/A16*/A17*/A18*LIPPO

DESCRIPTION:
    DECODER FOR TWO ADC CHIPS ON THE ATARI
    ADDRESSES C00100 AND C00110 HEX
```

Figure 7.3 *PAL Logic Equations for the ADC PAL*

The serial ports are based on two 6850 asynchronous communications interface adapters, ACIA, deriving their clocks from a 1.8432 MHz crystal giving them fixed data rates of 2400 and 9600 baud. The 2400 baud-rate is the maximum serial rate that can be generated by the PCB80C552 when using a 12 MHz crystal so that by using the RS232 isolation box, Figure G.10, they can be used to directly communicate with and control the stimulators described in Chapter 5. The two 6850s are decoded to reside one at odd addresses and one at even addresses using $\overline{\text{ADC2}}$ from the PAL decoder. The receive/transmit registers are decoded at $C00112 and $C00113, and the control/status registers are decoded at $C00110 and $C00111 respectively.

7.3 Digital Signal Processor Coprocessor System

Since the initial ADC interface hardware was both slow and had shown some clear indications that stimulated muscle signals did show some similar trends to those documented for voluntary muscle contractions, it was decided to speed up the processing system. The system has been upgraded by introducing a TMS320C25 signal processor to act as a front end pre-processor. This card carries out the sampling and the transformation from Time to Frequency Domains.

In order to implement the system as quickly as possible a readily available DSP card has been used. This card is made by Loughborough Sounds and will plug directly into a standard IBM PC slot. Using the IBM the system can be programmed and may be configured to run totally independently of the IBM, which just provides the power for the card.

The Loughborough Sounds card contains a TMS320C25 digital signal processor running at a clock rate of 40 MHz, and provides sockets for the full addressable memory range, that is, 64 kwords data and program memory. This ram may be full speed 35 ns ram, which permits the processor to run with zero wait states or 120 ns access ram, which requires one wait state.

Input and output to the DSP card memory is possible independently of the DSP by using the IBM port. This means that any device with an IBM compatible card slot can make use of this feature. The TMS320C25 is connected via its Port 0 to a 16 bit bidirectional latching port which provides a link between the DSP and IBM slot. On Port 1 the DSP has a 16 bit interval timer arranged to provide sample pulses for the ADC and DAC, which is clocked at 5 MHz. The ADC and DAC use Ports 2 and 3, writes go to the DAC and reads come from the ADC. The choice of port for accessing the ADC and DAC depends on which type of sample clock is used.

The IBM PC interface centres on dual-port access to the memory of the TMS320C25. This is achieved via a block of 8 I/O Port addresses on the IBM. The address of the TMS320C25 memory location is set up on one port. For speed of operation, the address is on a 16 bit up/down counter, allowing blocks of data to be transferred using just one IN or OUT instruction on the PC per transfer. Each access by the IBM introduces just one extra wait state to the TMS320C25 if both processors are working in memory. This is all controlled by a PAL state machine on the card[191].

Figure 7.4 gives a block diagram for the DSP card and Figure G.33 gives the pinouts for the PC Connector and 50 way expansion connector on the DSP card. The system comes with 8 kwords of 35 ns program RAM and 8 kwords of 35 ns data RAM.

7.3.1 DSP Interface Card

The DSP interface card, Figure G.32 contains two MC68230L8 Parallel Interface/Timers (PITs). These devices contain three 8 bit parallel ports, two of which may be configured as bit I/O, unidirectional 8 bit or 16 bit, and bidirectional 8 bit or 16 bit modes. The third port is a dual purpose port which may be configured as bit I/O or their secondary functions may be used. These are interrupt handshake lines and timer input and output lines. To control data flow there are four programmable handshake lines. There is also a 24 bit programmable timer with 5 bit pre-scalar.

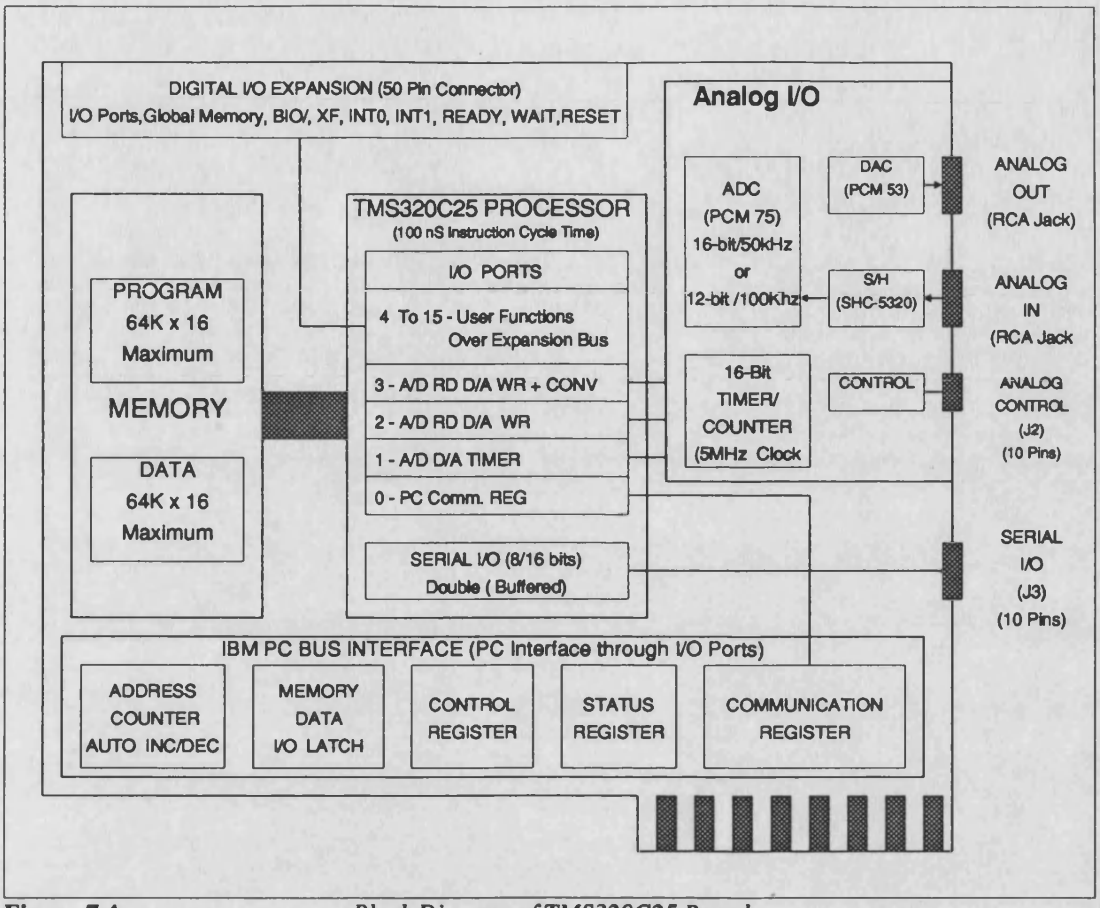

Figure 7.4 *Block Diagram of TMS320C25 Board*

The PIT allows use of vectored or autovectored interrupts, and also provides a DMA request pin for connection to a DMA controller. Programming of the device is via a set of memory mapped registers occupying a block of 64 bytes, these registers are addressed for the MOVEP type instructions of the Motorola 68000 series microprocessors.

The two PITs are mapped into the LIPPO address space at addresses $C00000 to $C0003F and $C00040 to $C0007F. The decoding is performed by a 16L8PAL chip whose logic equations are given in Figure 7.5.

Both timer and handshake interrupts are permitted from the PITs at level 5. In order to decode this, the interrupt request signals from the two PITs are decoded by another 16L8PAL to give a four level daisy chain. The order of priorities is PIT1 Handshake interrupt, PIT2 Handshake interrupt, PIT1 Timer interrupt, PIT2 Timer interrupt. The prioritised acknowledge signals for the level 5 interrupts are generated by the PAL. The logic equations for this PAL are given in Figure 7.6.

The circuit diagram for this card is given in Figure G.32. PIT1 is used as a unidirectional, handshake controlled, 16 bit double buffered input port and is

```
PAL16L8
PITDEC                                          PAL DESIGN SPECIFICATION
68230 DECODER LOGIC PAL VERSION 1                              01-AUG-88

/LDS A6 A7 A8 A9 A10 A11 A12 A13 GND
A14 /SPO1 A15 A16 A17 A18 /LIPPO /PIT1 /PIT2 VCC

IF (VCC) PIT1  = /A6*/A7*/A8*/A9*/A10*/A11*/A12*/A13*/A14
               * /A15*/A16*/A17*/A18*LDS*LIPPO
IF (VCC) PIT2  = A6*/A7*/A8*/A9*/A10*/A11*/A12*/A13*/A14
               * /A15*/A16*/A17*/A18*LDS*LIPPO
DESCRITION:
    PIT DECODER FOR TWO 68230 PIT CHIPS ON THE ATARI
    ADDRESSES C00000 AND C00040 HEX
```

Figure 7.5 *Logic Equations for the PITDEC PAL*

connected directly to the DSP Port decode circuitry. This acts as a unidirectional link with Port 4 of the DSP.

PIT2 is connected to the JAM pins of a 74HCT4059 programmable divide by N counter. The counter is driven by a 6.5536 MHz crystal controlled clock. The pre-divider of the 74HCT4059 is hard-wired to divide by 2 giving a maximum

```
PAL16L8
INTCOD                                          PAL DESIGN SPECIFICATION
68230 INTERRUPT LOGIC PAL VERSION 1                            01-AUG-88

/LDS /PIRQ1 /TOUT1 /PRIQ2 /TOUT2 FC0 FC1 FC2 A1 GND
A21 /PITINT A3 /PIAK1 /PIAK2 /TIAK1 TIAK2 /INTEN SPO1 VCC

IF (INTEN)  PITINT = PIRQ1 + PIRQ2 + TOUT1 + TOUT2

IF (VCC)    INTEN = PIRQ1 + PIRQ2 + TOUT1 + TOUT2

IF (VCC)    PIAK1 = FC0*FC1*FC2*A1*/A2*A3*LDS*PIRQ1*/TIAK1*/PIAK2
                  * /TIAK2 + PIAK1*LDS

IF (VCC)    PIAK2 = FC0*FC1*FC2*A1*/A2*A3*LDS*PIRQ2*/TIAK1*/PIAK1
                  */TIAK2 + PIRQ1
                  + PIAK2*/PIAK1*LDS

IF (VCC)    TIAK1 = FC0*FC1*FC2*A1*/A2*A3*LDS*TOUT1*/PIAK2*/PIAK1
                  */TIAK2 + /PIRQ1*/PIRQ2
                  + PIAK2*/PIAK1*/PIAK2*LDS

IF (VCC)    TIAK2 = FC0*FC1*FC2*A1*/A2*A3*LDS*TOUT2*/PIAK2*/PIAK1
                  */TIAK1 + /PIRQ1*/PIRQ2*/TOUT1
                  + PIAK2*/PIAK1*/PIAK2*/TIAK1*LDS

DESCRIPTION:
  FOUR LEVEL DAISY CHAIN FOR TWO 68230 PIT CHIPS SHARING THE
  SAME INTERRUPT LEVEL (5). PROVIDES OPEN COLLECTOR INTERUPT OUTPUT
```

Figure 7.6 *Logic Equations for the PIT Interrupt Cycles*

programmable divide factor of 15999. The output of the divide by N counter is an uneven mark-space ratio so it is fed through a divide by 2 flip-flop to give a square wave at the programmed frequency. The choice of crystal enables clock frequencies in powers of 2 to be output such as 1024 Hz. By using a 1024 Hz clock to trigger sampling by the ADC on the DSP card jitter, in the sampling is reduced. This clock would also ensure that for a 1024 point FFT the frequency bins represent 1Hz precisely.

The JAM codes that set the precise divide ratio are set by the output state of ports A and B on PIT2. The 74HCT4059 output is also brought out to the front panel to allow triggering of external equipment such as oscilloscopes.

7.3.2 DSP to Atari Interface

In the new configuration the Atari has become an intelligent display unit, capable of collecting the data from the DSP in real-time and displaying it in a number of different forms after any further processing has been carried out. These displays may then be recorded on disc for further analysis.

The current link between the DSP card and the Atari display unit makes use of Port 4 of the DSP and PIT1 with handshaking with the DSP being controlled by the XF and BIO pins of the TMS320C25. This link permitted the debugging of the DSP card in parallel with the Atari display software. With the provision of an IBM compatible PC-Slot on the Atari rack this link can be replaced and the direct access provided to the data memory of the DSP made use of.

The link uses the 50 way expansion connector on the DSP card. The 50 way connector is brought out from the IBM on ribbon cable to the Atari MEGA rack. Here decode circuitry, Figure G.34, decodes the outputs from the DSP to provide a 16 bit bidirectional port and handshake lines. The output port from the DSP interfaces directly to Ports A and B of PIT1 on the same card which are configured as a unidirectional 16 bit input port. The input port of the DSP has an opto-isolated input for the synchronisation signal provided by the stimulator on bit 0. This allows the DSP sampling to be synchronised with the end of the stimulus pulse. The connections for the stimulator are brought out in a subminiature connector on the front panel of the card to maintain compatibility with the connectors used on the stimulators.

The handshake lines are provided by the DSP's XF and BIO lines. XF is a single bit output line and BIO is a single bit input line that have their own individual checking and setting instructions associated with them, within the TMS320C25 instruction set.

7.4 Signal Processing Software

The signal processing makes use of digital signal processing techniques to initially extract the median frequency and total power from the sampled data. These parameters as described in Chapter 3 are two of the most common measures of fatigue and muscle force in voluntary muscle contractions and more recently in stimulated muscle responses.

Before describing the software that has been developed to analyse the muscle signals the algorithms used to transform the data from the Time to the Frequency domain will be briefly described.

7.4.1 The Fourier Transform

The Fourier transform has been used for a long time for identifying the frequency components making up a waveform. When a waveform is sampled it is the discrete Fourier Transform (DFT) that is used. Although most of the properties of the Continuous Fourier Transform (CFT) are retained several differences result from the constraint that the DFT must operate on sampled waveforms sampled over a finite interval. The Fast Fourier Transform (FFT), originally described by Cooley and Tukey in 1965[192,193], is simply an efficient method of computing the Discrete Fourier Transform.

The Continuous Fourier Transform is defined by:

$$F(f) = \frac{1}{2\pi}\int_{-\infty}^{\infty} x(t)e^{-j2\pi ft}dt \qquad 7.1$$

$$x(t) = \int_{-\infty}^{\infty} F(f)e^{j2\pi ft}df \qquad 7.2$$

$$\text{for } -\infty < f < \infty$$
$$-\infty < t < \infty$$

where $F(f)$ *represents the Frequency domain function.*
$x(t)$ *represents the Time domain function.*

The equivalent Discrete Fourier Transform pair is given by:

$$F(f) = \frac{1}{N}\sum_{t=0}^{N-1} x(t)e^{-j2\pi ft/N} \qquad 7.3$$

$$x(t) = \sum_{f=0}^{N-1} F(f)e^{j2\pi ft/N} \qquad 7.4$$

$$\text{for } f = 0,1,...,N-1$$
$$t = 0,1,...,N-1$$

where in general $F(f)$ *and* $x(t)$ *are complex series.*

It is usual to replace the term $e^{j2\pi/N}$ by W_N which gives for equations 7.3 and 7.4:

$$F(f) = \frac{1}{N}\sum_{t=0}^{N-1} x(t) W_N^{-ft} \qquad 7.5$$

$$x(t) = \sum_{f=0}^{N-1} F(f) W_N^{+ft} \qquad 7.6$$

In order that the Fast Fourier Transform may be compared with the FastHartley Transform a simple derivation of the Cooley-Tukey algorithm[192] will be presented for N=8. Deriving for the transform direction of equation 7.6. If equation 7.5 is re-written:

$$F(f) = \frac{1}{N}\left[\sum_{t=0}^{N-1} x(t)^* W_N^{ft}\right]^* \qquad 7.7$$

where * *refers to the complex conjugate operation.*

Then the derivation of the forward transform can easily be derived. The FFT algorithm involves the evaluation of:

$$\hat{F}(f) = \sum_{t=0}^{N-1} A(t) W^{ft} \qquad 7.8$$

where $f = 0,1,...,N-1$

$W = e^{j2\pi/N}$

$\hat{F}$ *and A may be interpreted as* F^* *and* $\frac{x^*}{N}$ *for the forward problem and as* x and F *for the inverse problem.*

Consider the case of N=8, f and t may be represented by binary numbers thus for:

$$f = 0,1,....,7 \quad \text{and} \quad t = 0,1,....,7 \qquad 7.9$$

f and t can be written:

$$f = f_2 4 + f_1 2 + f_0 \quad \text{and} \quad t = t_2 4 + t_1 2 + t_0 \qquad 7.10$$

where $f_0, f_1, f_2, t_0, t_1, t_2$ *can take the values 0 and 1 only.*

Thus equation 7.8 becomes:

$$\hat{F}(f_2 f_1 f_0) = \sum_{t_0=0}^{1}\sum_{t_1=0}^{1}\sum_{t_2=0}^{1} A(t_2,t_1,t_0) W^{(f_2 4 + f_1 2 + f_0)(t_2 4 + t_1 2 + t_0)} \qquad 7.11$$

Now since $W^{m+n} = W^m . W^n$ the twiddle factors can be rewritten:

$$W^{(f_2 4+f_1 2+f_0)(t_2 4+t_1 2+t_0)} = W^{(f_2 4+f_1 2+f_0)t_2 4} . W^{(f_2 4+f_1 2+f_0)t_1 2} . W^{(f_2 4+f_1 2+f_0)t_0} \qquad 7.12$$

which gives:

$$W^{(f_2 4+f_1 2+f_0)t_2 4} = [\, W^{8(f_2 4+f_1)t_2} \,]\, W^{f_0 t_2 4} \qquad 7.13$$

$$W^{(f_2 4+f_1 2+f_0)t_1 2} = [\,W^{8f_2 t_1}\,]\,W^{(f_1 2+f_0)t_1 2} \qquad 7.14$$

$$W^{(f_2 4+f_1 2+f_0)t_0} = W^{(f_2 4+f_1 2+f_0)t_0} \qquad 7.15$$

And

$$W^8 = [e^{2\pi i/8}] = e^{2\pi i} = 1 \qquad 7.16$$

Thus substituting equations 7.13, 7.14, 7.15, 7.16 into equation 7.12 gives:

$$\hat{F}(f_2,f_1,f_0) = \sum_{k_0=1}^{1} \sum_{t_1=0}^{1} \sum_{t_2=0}^{1} A(t_2,t_1,t_0)\; W^{f_0 t_2 4}\; W^{(f_1 2+f_0)t_1 2}\; W^{(f_2 4+f_1 2+f_0)t_0} \qquad 7.17$$

$$\underline{\qquad\qquad A_1(f_0,t_1,t_0)}$$

$$\underline{\qquad\qquad\qquad\qquad A_2(f_0,f_1,t_0)}$$

$$\underline{\qquad\qquad\qquad\qquad\qquad\qquad A_3(f_0,f_1,f_2)}$$

From equation 7.17 it can be seen that it is quite convenient to perform each of the summations as separate groups and to label the intermediate results as shown. Each set consists of eight terms and only the latest need be saved. Thus rewriting the equations:

$$A_1(f_0,t_1,t_0) = \sum_{t_2=0}^{1} A(k_2,t_1,t_0)\; W^{f_0 t_2 4} \qquad 7.18$$

$$A_2(f_0,f_1,t_0) = \sum_{t_1=0}^{1} A_1(f_0,t_1,t_0)\; W^{(f_1 2+f_0)t_1 2} \qquad 7.19$$

$$A_3(f_0,f_1,f_0) = \sum_{t_1=0}^{1} A_2(f_0,f_1,t_0)\; W^{(f_2 4+f_1 2+f_0)t_0} \qquad 7.20$$

$$\hat{F}(f_2,f_1,f_0) = A_3(f_0,f_1,f_2) \qquad 7.21$$

A signal flow diagram is shown in Figure 7.7. Each small number represents the power of W applied along the adjacent path. The last operation shown is the reordering due to the bit reversal in the argument of equation 7.21. The speed of the FFT is due to the redundancy inherent in equation 7.8. The direct calculation of equation 7.8 requires 64 complex multiplications and add operations; the FFT requires 48, however, the first multiply in each summation is by +1 thus reducing this to 24.

Since $W^0 = -W^4$, $W^1 = -W^5$ etc., the number of multiplications reduces to 12. These reductions for the general case of $N = 2^m$ reduces the number of operations from N^2 to $(N/2)\log_2 N$ complex multiplications, $(N/2)\log_2 N$ complex additions and $(N/2)\log_2 N$ subtractions. Figure 7.8 gives a pseudocode implementation of the basic FFT algorithm.

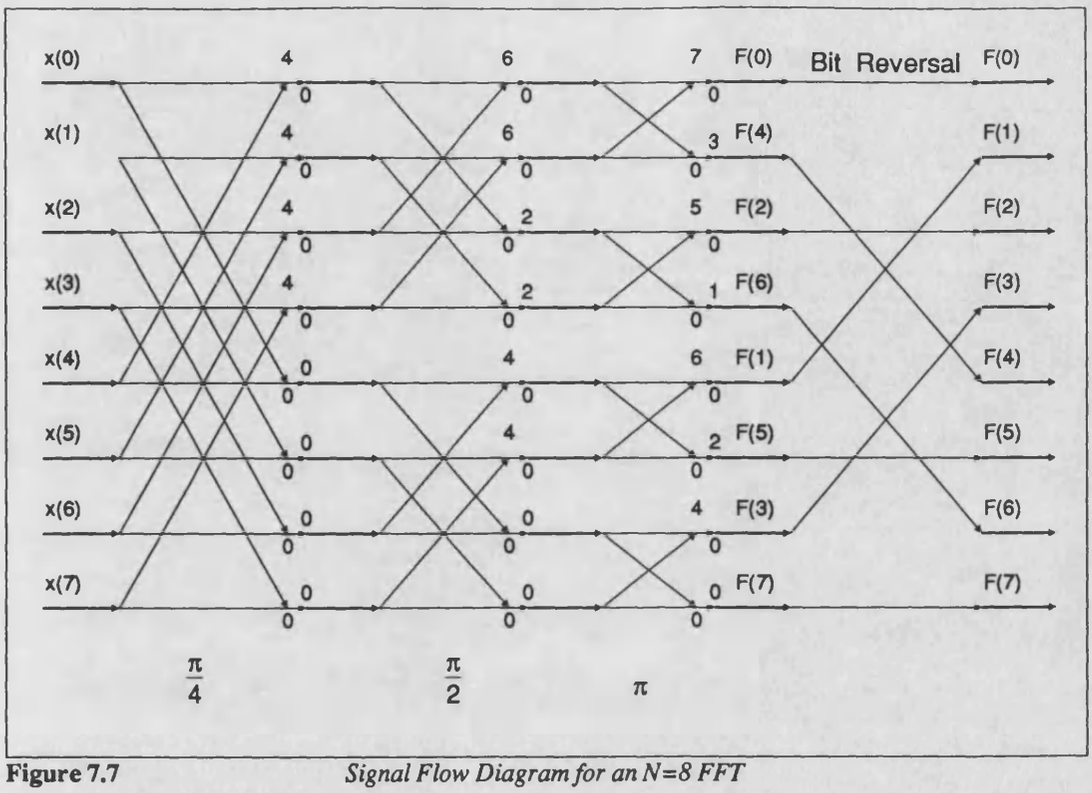

Figure 7.7 *Signal Flow Diagram for an N=8 FFT*

7.4.2 The Hartley Transform

The Fast Hartley Transform was first described by Bracewell[194]. It is analogous to the Fast Fourier Transform but is purely real and as a result is faster. Both the FHT and FFT map a contiguous signal over time on to a frequency function.

The Fourier Transform maps a real function of time x(t) onto a real function of Frequency F(f), whilst the Hartley Transform maps a real function of time x(t) on to a real function of frequency H(f). Since the Hartley Function is real, it only requires arithmetic operation to compute it. This also means that only real data arrays are required, taking only half the memory of complex data arrays. Thus to calculate Hartley Transforms requires less memory for a given data set than the Fourier Transform.

However, this does not mean that the size of the transform is any smaller since the relationship between transform size and frequency resolution is unchanged. That is a 256 point FHT would give the same resolution as a 256 point FFT.

7.4.2.1 Definition of the Hartley Transform

Hartley first formulated a real integral transform in 1942[195] though it wasn't until recently with publications by Bracewell[194, 196] that it started to be thought of as a practical alternative to the Fourier Transform[197, 198].

The Hartley Transform is defined as:

```
;Pseudcode FFT Radix 2 Decimation in Time
;Bitreversal Routine
; Input data in array....A(1...N)+jB(1...N)
; Output data in array...X(1...N)+jY(1...N)
For I=0 to N
    X(Bitrev(I)) = A(I)
    Y(Bitrev(I)) = B(I)
Next I
;Actual FFT routine calculations done in place
set N2 = N
For K=1 to M
    N1 = N2
    N2 = N2 / 2
    E  = 2 * pi / N
    A  = 0
    For J=1 To N2
    ; Twiddle Factor Calculation
        C = cos(A)
        S = -sin(A)
        A = J * E
        For I=J To N step N1
        ; Butterfly Loop for each Summation
            L = I + N2
            XT = X(I) - X(L)
            X(I) = X(I) + X(L)
            YT = Y(I) - Y(L)
            Y(I) = Y(I) + Y(L)
            X(L) = XT*C - YT*S
            Y(L) = XT*S + YT*C
       Next I
     Next J
Next K
; Results in  X(1...N) + jY(1...N)
```

Figure 7.8 *Pseudo code for a Typical FFT*

$$H(f) = \frac{1}{2\pi}\int_{-\infty}^{\infty} x(t)\,\mathrm{cas}(2\pi ft)\,dt \qquad 7.22$$

and the inverse as:

$$x(t) = \int_{-\infty}^{\infty} H(f)\mathrm{cas}(2\pi ft)\,df \qquad 7.23$$

where $\mathrm{cas}(2\pi ft) = \cos(2\pi ft) + \sin(2\pi ft)$

Comparing with the equivalent Fourier Equations:

$$F(f) = \frac{1}{2\pi}\int_{-\infty}^{\infty} x(t)e^{-j2\pi ft}\,dt \qquad 7.24$$

$$x(t) = \int_{-\infty}^{\infty} F(f)e^{j2\pi ft}\,df \qquad 7.25$$

where $e^{j2\pi ft} = \cos(2\pi ft) + j\sin(2\pi ft)$

$e^{-j2\pi ft} = \cos(2\pi ft) - j\sin(2\pi ft)$

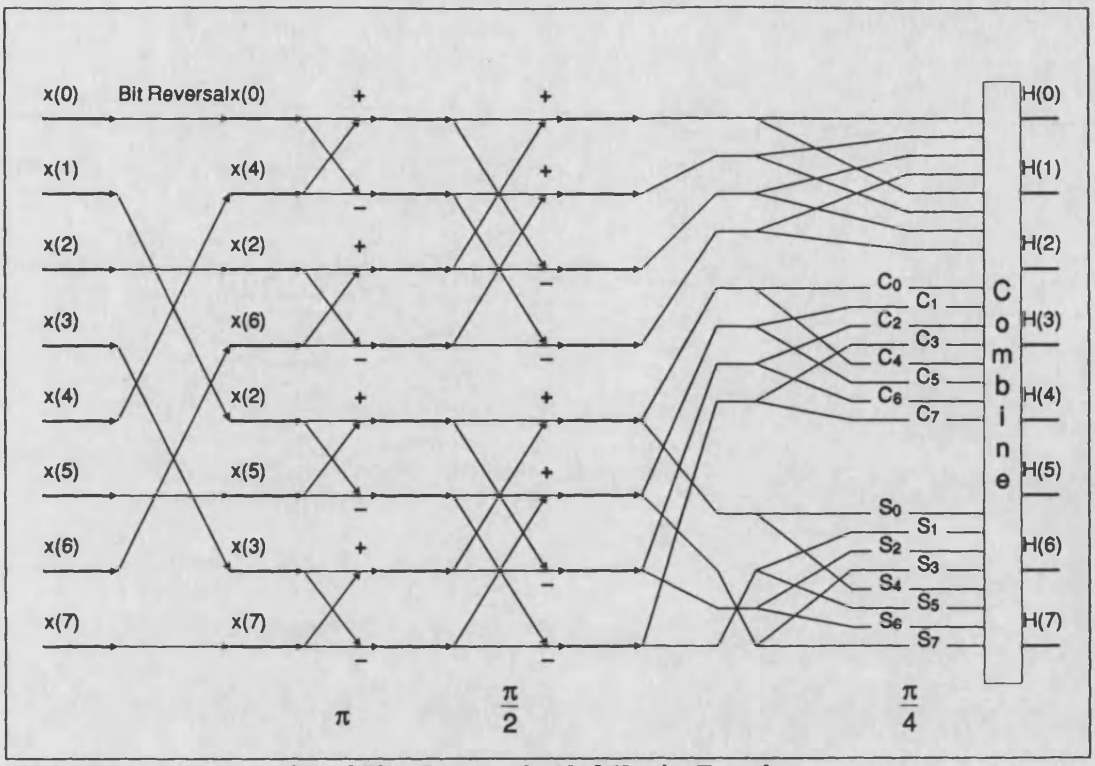

Figure 7.9 *Signal Flow Diagram for N=8 Hartley Transform*

Comparing equation 7.22 with 7.24 and equation 7.23 with 7.25 it can be seen that the essential difference is the substitution of the complex exponential term $e^{\pm j2\pi ft}$ by the cas function. Equations 7.22 and 7.23 describe the transforms for the continuous variables. For sampled data as with the Fourier Transform the discrete form is required which is defined for the Hartley Transform pair as:

$$H(f) = \frac{1}{N}\sum_{t=0}^{N-1} x(t)\,\mathrm{cas}(2\pi ft/N) \qquad 7.26$$

$$x(t) = \sum_{f=0}^{N-1} H(f)\,\mathrm{cas}(2\pi ft/N) \qquad 7.27$$

Bracewell's FHT uses a process analogous to the FFT routine, described above, to gain speed improvements over the direct implementation of equations 7.26 and 7.27. Bracewell shows that the butterfly is defined as the decomposition formula:

$$H(f) = H_1(f) + H_2(f)\cos(2\pi f/N_s) + H_2(N_s - f)\sin(2\pi f/N_s) \qquad 7.28$$

The equivalent form of the Fourier Equation is:

$$F(f) = F_1(f) + F_2(f)\,e^{j2\pi f/N_s} \qquad 7.29$$

where N_s *is the number of elements in the half length sequence.*

i.e. $N_s = N/2$ *for a dataset of* N elements.

Figure 7.9 shows the signal flow diagram for the calculation of an N=8 Hartley Transform. The FHT decomposition formula differs from the FFT in one important

```
; Pseudocode FHT Radix 2 Decimation in Time
; Bitreversal Routine
; Input Data Array.....A(N)
; Output Data Array....X(N)
; N is the number of elements
; 2 L = N
For I=0 to N
    X(Bitrev(I)) = A(I)
Next I
; Actual FHT routine
; Because the twiddle factors for stages one are +1 or -1
; The N=2 DHT for stage one becomes
For I=0 to N-2 step 2
    temp = X(I)
    X(I) = temp + X(I+1)
    X(I+1) = temp + X(I+1)
Next I
; Because the twiddle factors for stage two are +1, -1 or 0
; The N=4 DHT for stage two becomes
For I=0 to N-4 step 4
    temp = X(I)
    temp1 = X(I+1)
    X(I) = temp + X(I+2)
    X(I+1) = temp1 + X(I+3)
    X(I+2) = temp - X(I+2)
    X(I+3) = temp1 - X(I+3)
Next I
; Stages 3 and above have none trivial sine and cosine twiddles
L = N DIV 2
U = L-1 : S = 4
For L1=2 to L-1
    S2 = S+S            ;Pairs index
    U=U-1 : S0 = 2^U-1
    For Q = 0 to N-1 step S2
        I = Q
        D = I + S
        tempI = X(I)
        X(I) = temp + X(D)
        tempD = X(D)
        X(D) = temp - X(D)
        K = D - 1
        For J=S0 to N/4
            I = I + 1
            D = I + S
            E = K + S
            X = X(E) * cos((2*pi*J)/N) - X(D) * sin((2*pi*J)/N)
            Y = X(D) * cos((2*pi*J)/N) + X(E) * cos((2*pi*J)/N)
            tempI = X(I)
            tempD = X(K)
            X(I) = tempI + Y
            X(D) = tempI - Y
            X(K) = tempD - X
            X(E) = tempD + X
            K=K-1
      Next J
      E = K + S
  Next Q
  S = S2
Next L
;Hartley Transform Results in X(0...N-1)
```

Figure 7.10 *Pseudocode for a Fast Hartley Transform*

respect, the elements multiplied by trignometric terms are not symmetric. In the FFT formula the terms multiplied by the trignometric coefficients involve terms in F(f) only. In the FHT case both H(f) and H(N_s–f) have sine coefficients. This asymmetry makes calculation of the FHT slightly harder.

To obtain the inverse Hartley it is only necessary to apply the same code as is used to do the forward transform. There is however a slight asymmetry between the FHT and its inverse. In the case of the time to frequency transform the results of the butterfly need to be scaled by N, where N is the size of the input data set. For the frequency to time transform this is not necessary. Figure 7.10 gives a pseudocode example of the equivalent FHT to the FFT.

7.4.2.2 Relationship between FFT and FHT

The Hartley Transforms may be used to get the Fourier components directly by the following equations. The proof may be found in reference [196 pp17-19]

$$F_r = H(f) + H(N-f) \qquad 7.30$$

$$F_{im} = H(f) - H(N-f) \qquad 7.31$$

where F_r *is the real portion of the* Complex Fourier Transform.

F_{im} *is the imaginary portion of the* Complex Fourier Transform.

and the Power Spectra may be calculated directly

$$P_s(f) = \frac{[H(f)^2 + H(N-f)^2]}{2} \qquad 7.32$$

where P_s *is the Power Spectrum.*

7.4.2.3 Advantages of the Hartley Transform

The Fast Hartley is intrinsically faster than the Fast Fourier Transform because it does not require any complex mathematics to calculate. Agbinya[199] has shown that when using the FHT to carry out interpolation he not only had to carry out fewer mathematical operations but got a reduced mean squared error. Bold[200] shows that the maximum speed increase that can be achieved is two over the traditional FFT, but also suggests that optimised FFT routines show a similar speed improvement.

Further advantage may be gained from the fact that the same routine may be used for the forward and inverse transform unlike the FFT. This would be combined with the reduced storage the FHT takes. Since in signal processing the sampled data is real, the advantages of a purely real transform can clearly be seen.

7.5 Atari Stand-alone Software

The software for the Atari has been developed entirely in assembly language to try and ensure the fastest possible execution times. The assembly language programming has

been carried out using FastBasic which, as an integral part of its instruction set, has a built in assembler.

FastBasic is a very structured version of BASIC and as such provides a very simple means for testing the assembly language algorithms. It provides simple indirection facilities within its dialect of BASIC to access and set the assembly language variables. This permits simple BASIC test routines to be written 'around' the assembly routine to allow full testing of individual subroutines before inclusion in the main code.

Further run-time testing and debugging can be achieved by using the FastBasic option of assembling the code into an executable program. This executable code can then be run from within a debugger which permits single stepping of the instructions and break point setting.

The facilities provided by the combination of FastBasic and its in built assembler provided a much faster development time than with a conventional assembler and debugger combination. This is mainly due to the ease of testing the assembler code.

Two versions of the analysis software have been produced with the only major difference between them being the means of moving from time domain to frequency domain. Thus the code for both the Fast Fourier Transform based frequency analysis software and the Fast Hartley Transform based frequency analysis software may be readily split into a number of common sections. It is convenient to consider each of the major parts of the two pieces of analysis software separately before discussing the main control of the two programs.

7.5.1 Interrupt and Sampling Routine

The Atari ST uses an MFP68901 multifunction peripheral chip for various tasks. This chip contains a number of useful peripherals such as a serial port and parallel port. It also contains 4 timers of which timer A is available for user applications. It is driven from a 4 MHz clock and may be programmed using the extended BIOS call *xbtimer* provided by the Atari operating system. This call will set the appropriate timer registers from the data supplied and install the specified interrupt routine.

Two sample rates have been used: 1024 Hz and in later versions of the software 2048 Hz. The interrupt routine checks to see if the sample to be taken is the first and if so will await the synchronisation pulse from the stimulator. It then latches the ADC data and reads it. Having read the data the routine converts it to a signed 16 bit number, applies the windowing function if necessary and stores the data. It then updates the counts and sets a flag if a complete block of samples has been taken. Finally it clears the interrupt flag of the MFP68901 and returns from the interrupt.

7.5.2 Windowing

The problem of leakage is inherent in the Fourier, or Hartley, analysis of a finite data record. The record is formed by looking at the actual signal for a period of T seconds and by neglecting everything that happened before or after this sample period. This is equivalent to multiplying the sampled signal by a rectangular data window to give the data block.

The continuous Fourier Transform of a pure cosine wave as shown in Figure 7.11a would appear at only one point on the frequency axis. The effect of multiplying the data by the rectangular data window in the time domain is equivalent to convolution in the frequency domain. This means that the single spectral line of the input is convolved by the Fourier Transform of the rectangular data window. This results in a function with an amplitude of the $\frac{\sin x}{x}$ form centred about f_1 as shown in Figure 7.11b and 7.11c.

This function has a number of spurious side lobes. The usual way to deal with this is by trying to localise the contribution of a given frequency by reducing the amount of *leakage* through these sidelobes. The way this is done is by applying a data window to the sampled data which has lower sidelobes in the frequency domain than the rectangular data window.

There are a large number of different window functions that have been described in the literature[203, 204, 205]. They all involve the tailoring of at least the first few and last few samples of the data set such that they smoothly drop to zero. Their effect may be described as the reduction of the discontinuity at the boundary of the periodic extension. That is, at the boundary, as many orders of derivative of the weighted data as possible are matched, which is most easily accomplished by setting the value of the derivatives to zero or close to zero. Thus the windowed data is smoothly brought to zero at the boundaries so that the periodic extension of the data is continuous in many orders of the derivative.

It is the way these windows fall that determines the precise effects the windowing function has. One of the most commonly applied windows is the Hanning* window (cosine squared or raised cosine window), which is one of the best general purpose windows. This is defined[206] as:

$$w(n) = \cos^2\left[\frac{n}{N}\pi\right]$$

* The Hanning Window should not be confused with the Hamming window which may be thought of as a modified Hanning Window where the in exact cancellation of sidelobes is improved by adjusting the relative size of the three kernels that add to form the window[Harris]

$$= \frac{1}{2}\left[1.0+\cos\left[\frac{2n}{N}\pi\right]\right] \qquad 7.33$$

where $n = -\frac{N}{2},\ldots,-1,0,1,\ldots,\frac{N}{2}$

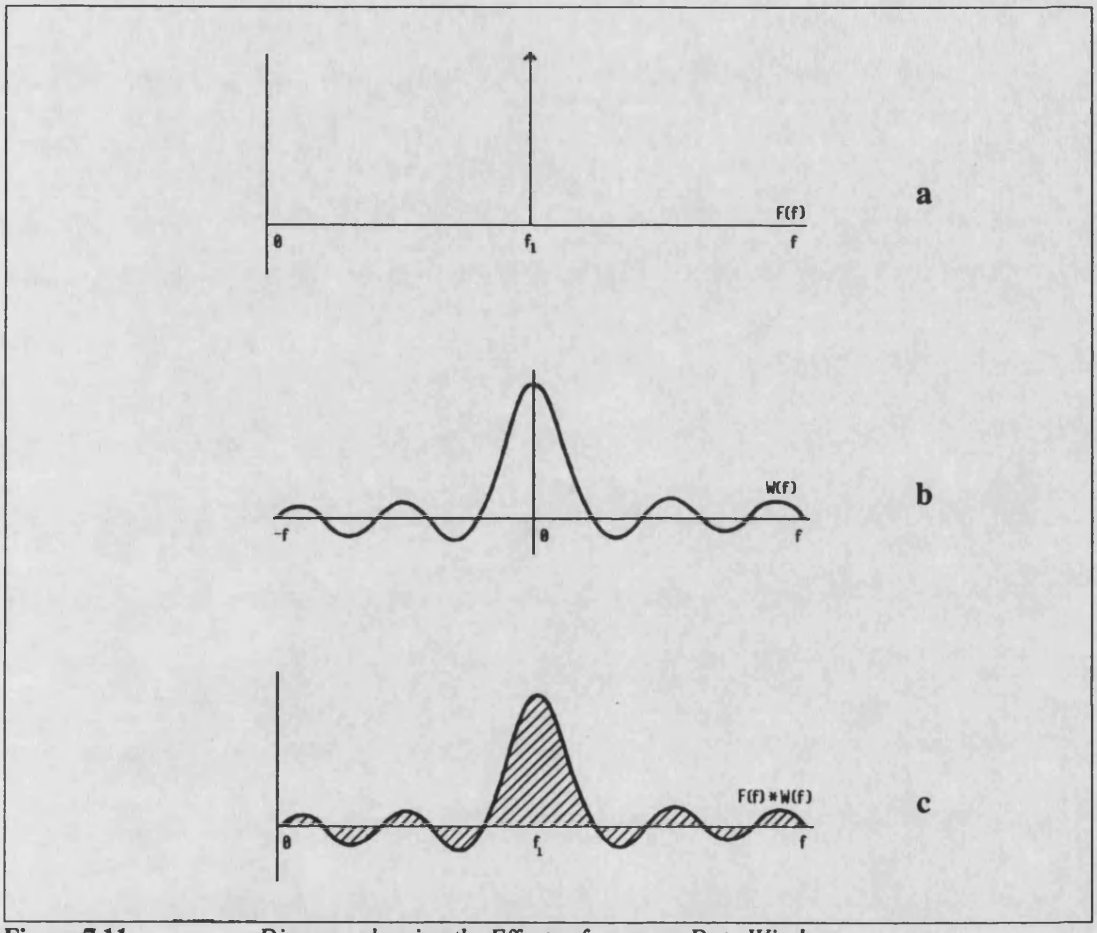

Figure 7.11 *Diagram showing the Effects of a square Data Window*

The only problem with applying the Hanning window is that it requires that every sample be weighted, which adds a significant overhead to the sampling routine, thus a simplified form is used in this software. The effect of simplifying the window is to increase slightly the sidelobes and at the same time widen the central lobe so increasing slightly the leakage. The simplified version is known as the extended cosine-bell data window which is defined:

$$w(n) = \begin{cases} \frac{1}{2}(1-\cos\pi\frac{t}{0.1T}) & \text{for} \quad 0 \le t \le T \\ 1 & \text{for } 0.1\,T \le t \le T \\ \frac{1}{2}(1-\cos\pi\frac{T-t}{0.1T}) & \text{for } 0.9T \le t \le T \end{cases} \qquad 7.34$$

This window only requires a weighting other than one for the first 10% and last 10% of the data. This routine is implemented by using a coefficient lookup table of fixed point where +1 is equivalent to 128. The window is applied in the interrupt routine

that is used to read the samples. The data having been read from the ADC is first converted to a twos complement number, then multiplied by the scaling coefficient, before being scaled back to take into account the fixed point integer of the window coefficient. It is this windowed data that is then stored for the spectral calculation.

7.5.3 The Fast Fourier Transform Algorithm

The Fast Fourier Transform routine used for the stand-alone Atari system was based on the 6800 based FFT algorithm used by Tooley et al.[169, 207] in their ECG analyser. This algorithm is a signed 8 bit, decimation in time radix 2 algorithm and has been refined by the Medical Physics Department at Odstock hospital for use on a 6809 microprocessor.

The version implemented on the 68000 of the Atari microcomputer closely follows the structure of the 8 bit version but uses signed 16 bit integers instead of the original 8 bits. It is a decimation in time radix two algorithm using a sine and cosine lookup table. The first pass, where the twiddle factors are ±1 or 0, is carried out separately to the main loop to speed up the processing by by-passing the table lookup. The routine matches very closely that shown in the pseudocode of Figure 7.8, except the bit-reversal is done first because the number of points to swap is less. This occurs because the sampled data in this case is purely real, so the imaginary half of the data need not be swapped as would be the case if the bit-reversal were carried out after the transform.

The sine and cosine data is stored as fixed point integers where unity is represented by 32768, that is, the cosine and sine factors are stored as the INT(sine(angle) × 32768). The effect of this on the overall routine is to add a scaling factor of 2^{15} which must be removed after each multiplication.

7.5.4 The Fast Hartley Transform Algorithm

The Hartley transform routine is very similar to the FFT routine already described, in fact it is derived from the same code. It is a 1024 point 16 bit integer radix 2, decimation in time Fast Hartley transform. It follows quite closely the form of the pseudocode given in Figure 7.10. It also makes use of a lookup table configured as fixed point signed integers as used by the FFT algorithm.

Overflows are prevented by regularly checking the data for values greater than 8192 and if these occur all the data is halved. A count is kept of the number of scalings required so that this can be taken in to account at the end of the calculation.

7.5.5 Software Filtering Algorithm

The software filtering algorithms are aimed at reducing two artefact effects. These are: mains interference and stimulus artefacts. The filtering is carried out in the frequency

domain since it is much easier to filter selected frequencies in this domain. The mains interference is characterised by a major harmonic at 50 Hz and reduced harmonics at 100 Hz, 150 Hz etc.. The stimulus artefact is dependent on the interpulse interval. For the standard exercise and standing stimulus the IPI is 40 ms which is equivalent to a frequency of 25 Hz. Assuming the exercise and standing stimulator is used, the stimulus artefact produces a major frequency component at 25 Hz and its harmonics. The actual harmonics contribution is defined by the shape of the stimulus artefact pulse in the sampled data. If it is a square pulse then the only major harmonics would be odd. However, this is rarely the case so both odd and even harmonics are likely.

The filter itself may be implemented in two ways. The frequency components produced by the transformation software could be scaled down by a value representative of the ratio of interference to valid signal. This is essentially a frequency domain version of the technique described by McGill et al.[145]. Its major problem is the identification of the scale factor to use. If, as is the case here, the stimulus voltage and hence artefact change with time it is likely that the interference proportions will change. A similar situation exists with the mains interference which may be affected by the changes that occur in the EMG electrode contact. The alternative method is to zero the frequency components at the artefact frequencies and its harmonics. This reduces the frequency information about the muscle response of interest but does remove the swamping effects of the artefacts.

It is the second technique that is used within the software here. The routine steps through the calculated spectrum and zeros 25 ±1 Hz and its harmonics ±1 Hz. The ±1 Hz is required to allow for leakage and inaccuracies in the system, which could lead to the most significant swamping component not being at precisely the theoretical harmonic. The stimulator used with this test has a fixed frequency which conveniently covers the frequency and harmonics of the mains interference.

7.5.6 Display and Post-processing Routines

There are two displays used by the software. One displays the calculated spectrum plotting spectral power against frequency. The other display has a split screen and on the left plots the calculated median frequency and on the right hand half plots the total power. Each new calculation the display scrolls up, thus giving time on the y-axis. This gives an indication of how the median frequency and total power vary with time.

The choice of display is determined by the version of the software that is run. Both display routines make use of screen switching to ensure that the user doesn't see any writing to the screen. Screen switching is a simple technique where the displayed memory is not the same as the memory the graphics routines are currently writing to. On the Atari this is controlled by two system variables; PHYSBASE and LOGBASE.

```
;Spectrum Plot
Initialise
   Timer
   Memory Pointers
   Counts
   Start Sampling
Repeat
   Do FFT(FHT)
      Bit Reversal
      Start New Samples
   Calculate Spectrum
   Plot Spectrum
   Calculate Median Frequency
   Display Median Frequency at top of Screen
Until ESC
CleanUp
   Remove Timer Interrupt
   Tidy Screen

;Median Frequency Plot
Initialise
   Timer
   Memory Pointer
   Counts
   Start Sampling
Repeat
   Do FFT(FHT)
      Bit Reversal
      Start New Samples
   Calculate Spectrum
   Scroll Screen Up
   Draw new Timing Tick if Required
   Calculate Median Frequency
   Plot Median Frequency
   Plot Total Power
Until ESC
CleanUp
   Remove Timer Interrupt
   Tidy Screen
```

Figure 7.12 *Pseudocode for the Control of the Stand-Alone Atari Programs*

PHYSBASE is the address to the 32 kbyte block that is currently being displayed. LOGBASE is the address of the 32 kbyte block the graphics routines will write to. If these two values are the same then the screen updates are visible as they occur.

7.5.7 Median Frequency Calculation

The median frequency calculation may be expressed mathematically as:

$$\sum_{i=0}^{median} f_i \geq \frac{\sum_{i=0}^{512} f_i}{2} \qquad 7.35$$

where f_i *represents the power of each spectral component.*

$median$ *represents the median frequency value.*

This equation is implemented using two simple loops: one to sum the spectral components and one to repeat the summing operation until the value of the sum is

greater than or equal to half the total. The result of this calculation also gives the value for the total power.

7.5.8 Spectral Plot Control

The pseudocode for the control of this program is given in Figure 7.12. The display is just a plot of the spectral lines where their height is proportional to the power, with the median frequency printed in the corner. No power scale is available with this display and the spectrum can only be used to show the spectrum shape.

7.5.9 Median and Power Plot Control

An example of the median frequency plot is shown in Figure 7.13. This is the display that has been used for most of the tests using the stand-alone Atari system. It shows the variation of the total signal power and median frequency.

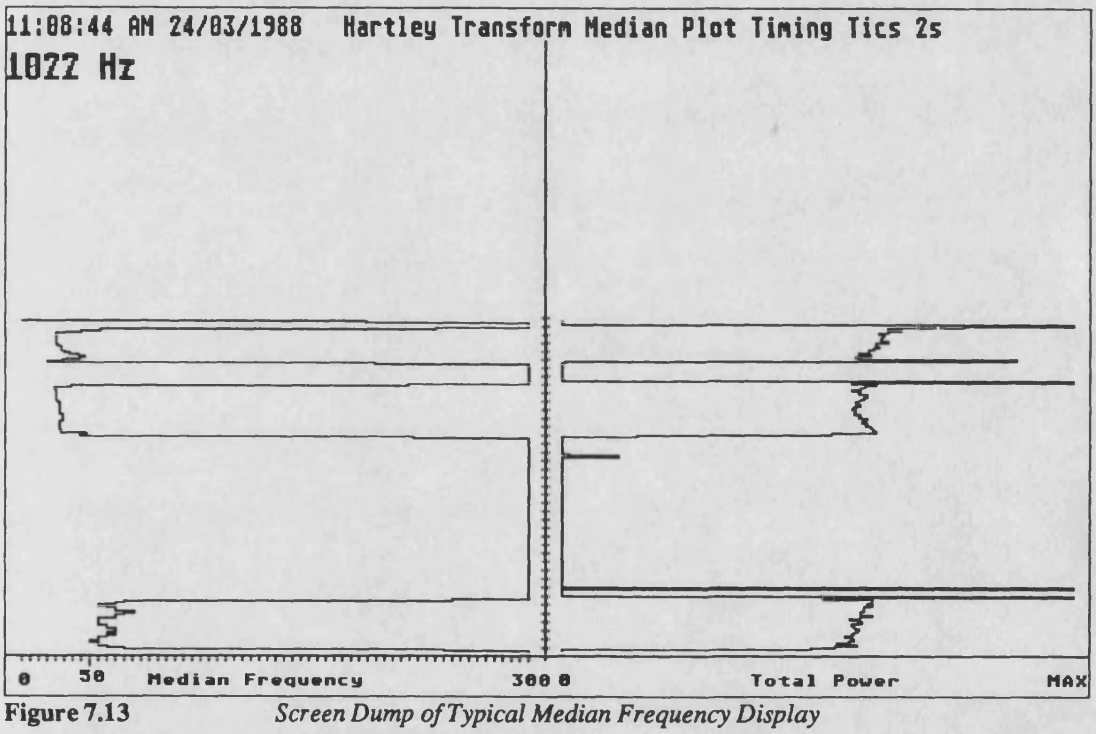

Figure 7.13 *Screen Dump of Typical Median Frequency Display*

Time ticks are used on the y-axis to indicate 2.5 second steps. With a sample rate of 2048 Hz this system provided an update rate of 0.5 seconds.

7.5.10 Modifications for ADC80 Card

The only alterations required for the programs to function with the ADC80 card are to the interrupt routine read. The original ADC is 8 bit and makes use of the parallel port. The ADC80 is 12 bit and is directly addressable by carrying out a word read from $C00100. This speeds up the interrupt routine because there is no need to toggle port pins as required with the printer port based ADC. The synchronisation pulse may be checked by reading the 16 bit port at $C00102. The synchronisation pulse is on the least significant bit of the port.

The effect of changing to a memory mapped ADC card reduces the overhead of accessing the ADC via interrupts. This is mainly due to the reduction in complexity accessing the ADC.

7.6 DSP Based System Software

This system is intended to be a single unit based around the Atari Mega ST but currently still makes use of the IBM to host the DSP card. This means the IBM may be used to 'grab' data from the DSP card and hence record calculated results on its hard disk with minimal overhead to DSP and Atari.

The system thus contains three components: the Atari display software and receiver interface software; the DSP sampling, calculating and transmitting software; and the IBM results display and save software. Within this multi-processor environment the DSP card acts as the master signalling the IBM and Atari when data is available for capturing.

7.6.1 DSP Fourier Transform Software

The fastest form for the FFT calculation would be achieved using in-line code. Unfortunately this is not possible with the current DSP configuration due to the limited program memory. A highly optimised 1024 radix 2 decimation in time FFT routine would require approximately 24 kwords[208] and would take around eight milliseconds to execute. This would be preferable since it gives the processor as much time as possible to carry out secondary processing tasks on the calculated spectrum. This could include the total power and median calculation that are currently carried out by the display processor.

The current limit of 8 kwords of program memory and 8 kwords of data memory have prevented an optimal implementation. The current implementation uses looped code. It makes use of a fast internal RAM 256 point FFT routine which it calls four times to carry out the first eight stages of the 10 stage 1024 point FFT. It then carries out two more passes to sort out the results. This algorithm is not optimal and takes about five times longer but can just be squeezed into the available memory. The algorithm is based on one described in the DSP applications manual[209].

The current DSP code does not do any post-processing of the calculated spectrum. As it becomes clearer which parameters should be calculated these calculations can be readily carried out by the DSP before transmitting the data to the Atari display processor.

A pseudocode description of the main control code and the interrupt routine is given in Figure 7.14. The main control loop waits for a block of 1024 samples to be taken, then calculates the FFT using method described above. Having carried out the

transformation to the frequency domain, power components are calculated. In this processor, maximum use is made of the 16 bit storage by calculating the maximum power in the internal 32 bit accumulator. Then using the normalisation instruction which will right shift the number to fit in 16 bits, maximal use of the 16 bits is made. The normalised power spectrum is then transmitted as the next 1024 samples are taken.

```
;DSP Main Routine
Initialise
Repeat
   Do FFT
   Find Max Power Value
   Find Normalisation factor for Max Power
   Normalize Spectral Power Data
   Bit Reverse Data
   Move to Output Array
   Wait for 1024 samples to be taken
   Reset Counts
Until FALSE

;DSP Interrupt Routine
If first sample
   Wait for synch pulse to go Low to Hogh
   Wait for synch pulse to go High to Low
Endif
Get ADC value and Store
If first sample
   Get Normalisation Factor
   Make it Negative
   Wait BIO high
   Output Synchronisation Pulse
   Pulse XF Low
Endif
If count is Odd
   Send a Result to the Atari
Endif
Decrement Count
If Got all Samples
   Signal IBM
Endif
Return from Interrupt
```

Figure 7.14 *Pseudocode for DSP and Interrupt Routine*

There are two versions of the interrupt routine: one which waits for a stimulus pulse before starting to sample and one which doesn't. The selection is made within the IBM loading program described in Section 7.6.3. Essentially the interrupt routine will take a sample every interrupt and then every other sample it will also transmit one word of the previous spectra result to the Atari. The Atari is synchronised by the sending of a single negative word on the first sample of every block, that is, sample one. Combined with this negative number, which can be identified because it has its most significant bit set, is the value of the normalisation factor used to normalise the data in order that the Atari can display the correct scales. Transmission to the Atari is

controlled by the XF and BIO pins. The Atari is informed of the presence of new data by a pulse on the XF line. The DSP ensures the previous data has been removed by checking the BIO line is high before transmitting.

The IBM software is flagged via the IBM port link once the DSP completes the sampling of a block of data. The byte transmitted via the port link is the normalisation factor. The IBM then grabs the sampled data and its calculated spectrum via the shared ram link.

7.6.2 Atari Display Software

The display software is all written in assembler code and implements the same format displays as were used in the Atari stand-alone software. The difference however is that the plots of the spectrum display a true power scale and some simple routines are included to save the displays to disk. One single program also provides all the displays selectable from the keyboard. Extra key functions are provided for changing the scales and for identifying frequency components using a small pointer when viewing the spectrum display.

The pseudocode for this software is given in Figure 7.15. Plates F.25 and F.26 show the spectrum screen and the median frequency and power screen during the recording of a voluntary muscle response.

```
;DSP Display Software for the Atari
Initialise
Repeat
   Check for a Key
      Arrow keys move Cursor Sprite
      f1 set max scale of Power 1 V²/Hz
      f2 set max scale of Power 10 V²/Hz
      f3 set max scale of Power 100 V²/Hz
      f10 select Power/Median Frequency Display
      Shift f10 Select Spectrum Display
      Help Save current screens
      ESC exit program
   Move Sprite
   Plot Spectrum Screen
   Plot Spectrum
   Display Frequency and power at Sprite on Spectrum
   Calculate Median Frequency and Total Power and Display on Spectrum
   Update Median and Power Screen
   Scroll up
   Plot new Median and Power
   Show selected screen
Until Esc
   Cleanup
      Remove Interrupt
```

Figure 7.15 *Pseudocode for the Atari Display Processor with the DSP Card*

7.6.3 IBM Download and Data Capture Software

The IBM software is written in Turbo C and serves two functions. Its primary use is the setting up and configuration of the DSP card. The Turbo C routine down loads the

DSP code to the card and sets up the sample rate that the DSP will use for sampling. The down load code also permits the choice of synchronisation of the sampling with the falling edge of the stimulus pulse as is required if stimulated muscle signals are to be compared reliably.

The second function included in the code is a facility to grab the sampled data and calculated FFT from the data memory of the DSP. This allows the IBM to display a plot of the last sampled waveform. This is useful when setting up the system to prevent ADC overload. Included in this routine is a facility to save the captured data to hard disc. The data grabbing is controlled by the DSP card which writes to the IBM/DSP port link to indicate a new block of data is available. When the IBM software detects the flag it grabs the sampled data block and calculated spectrum from the shared RAM. The sampled data is displayed on the screen and may be saved along with its associated spectrum to disc. Included in the software is the ability to expand sections of the recorded waveform for closer examination.

Plate F.24 shows a typical display obtained from this program whilst recording voluntary muscle responses.

7.6.4 Display and Plot Software

The display and plot routine on the IBM allows the post processing and plotting of data. Currently the only plotter supported is the Watanabe plotter. However it is a simple alteration to convert the output codes to be HPGL or even postscript. A typical display from this program is shown in Plate F.27. The program is designed to display data recorded using the IBM DSP loader program. It is written in Turbo C and uses similar routines to those used for the other program.

The display is split into two sections. The top half is a scaled down version of the display provided by the loader program. As with the loader program the time base may be expanded and the expanded data scrolled through by using the number keys and <> keys respectively. The bottom half of the display gives a plot of the recorded spectrum with a true scale. Plotter output is provided via the P key and outputs at 9600 baud via the serial port a copy of what is currently displayed on the screen.

Chapter 8

System Calibration

The accuracy required in the calibration of an EMG system is very dependent on the precise configuration of the component parts and the type of EMG source. The EMG amplifiers are required to be low noise because of the low level signals that they usually have to amplify. However their signal to noise ratio is much improved when amplifying the typical CAP because of the higher signal energy in the CAP. The sampling system is another part where apparent improvements in signal to noise ratio will not be transferred to the output because once the noise is below the quantisation levels of the ADCs any further improvement will not be measured. Quantisation levels affect the accuracy of the FFT or FHT since integer calculations lead to rounding errors and these errors translate to inaccuracies in the least significant bits. This effectively increases the permissible signal to noise ratio on the input since the noise is lost in the FFT calculations.

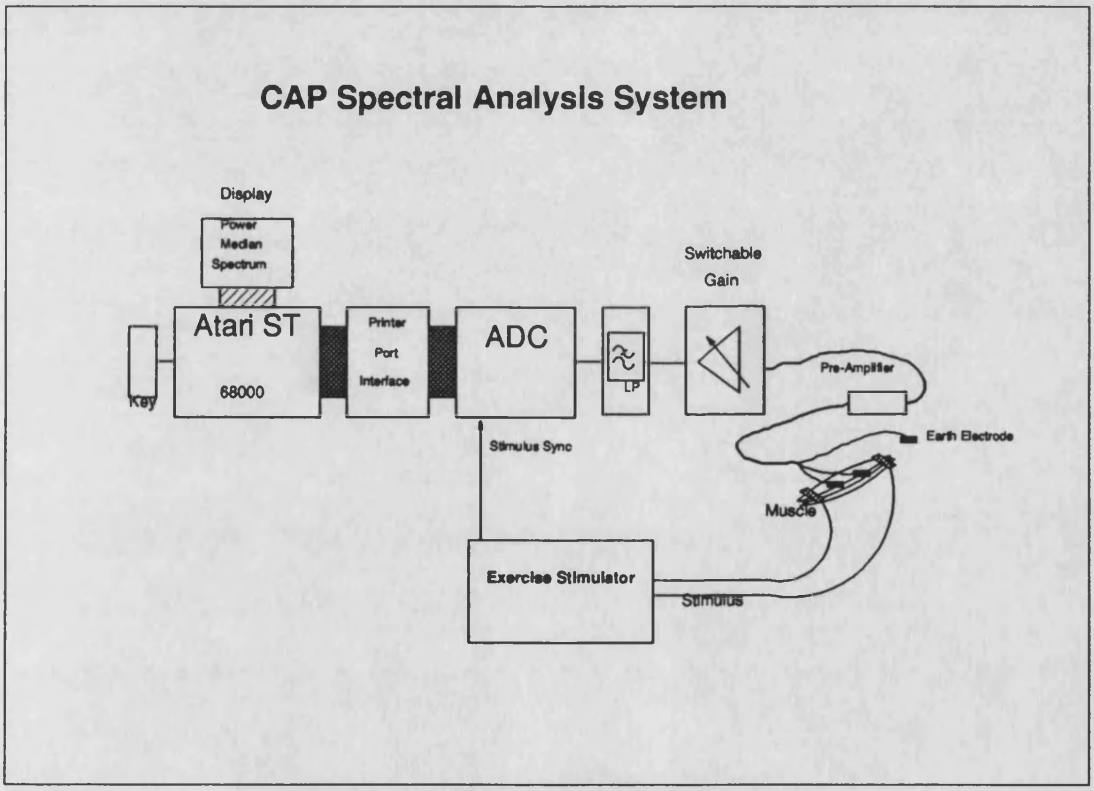

Figure 8.1 *Block Diagram of the Original Atari System Setup*

In this chapter the system configurations used for carrying out the tests discussed in Chapter 9 will be described. The original and improved systems are described, followed by a discussion of the setting up of some specific parameters. For the improved system some more comprehensive calibration tests are presented.

8.1 Atari Only System

A block diagram of the original Atari sampling and analysis system is shown in Figure 8.1. This configuration used the printer port based ADC card described in Section 7.1. This was controlled by the standard Atari 520ST microcomputer. The stimulator used was the original two channel exercise stimulator which provides a pulse that matches the stimulus. The input is provided by the original EMG pre-amplifier modules, some of which included clamping circuitry. The pre-amplifiers were connected to the body via a screened multi-core lead and silver-silver chloride 'stick on' electrodes. In later configurations an extra earth strap that could be connected to a remote earth point was added. With the advent of the Atari Mega computers the printer port ADC card was replaced by the memory mapped ADC card, interfaced via the expansion bus described in Section 7.2.2.

8.1.1 Input Signal Noise

The major contribution to input noise in the original system was generated by the EMG amplifier modules. This is because the original ADC was 8 bits, giving only 256 quantisation levels on a 5 V input signal which is equivalent to a 19 mV step size. Figure 8.2 shows the typical input noise measured at the ADC for this system with the electrode leads disconnected and the inputs to the pre-amplifier shorted together.

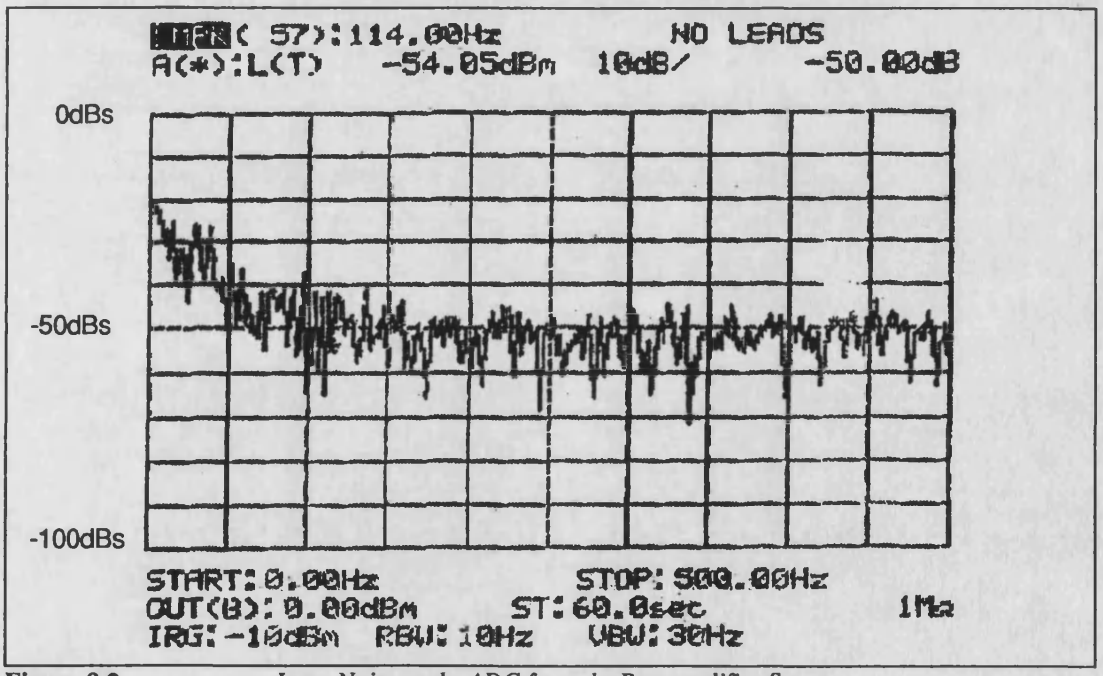

Figure 8.2 *Input Noise at the ADC from the Pre-amplifier Stage*

Figure 8.3 shows the input noise for the system but this time with the electrode leads connected and shorted together. From these it can be seen that the actual threshold level remains approximately constant at 50 dBs down though there appears to be slightly more fluctuation.

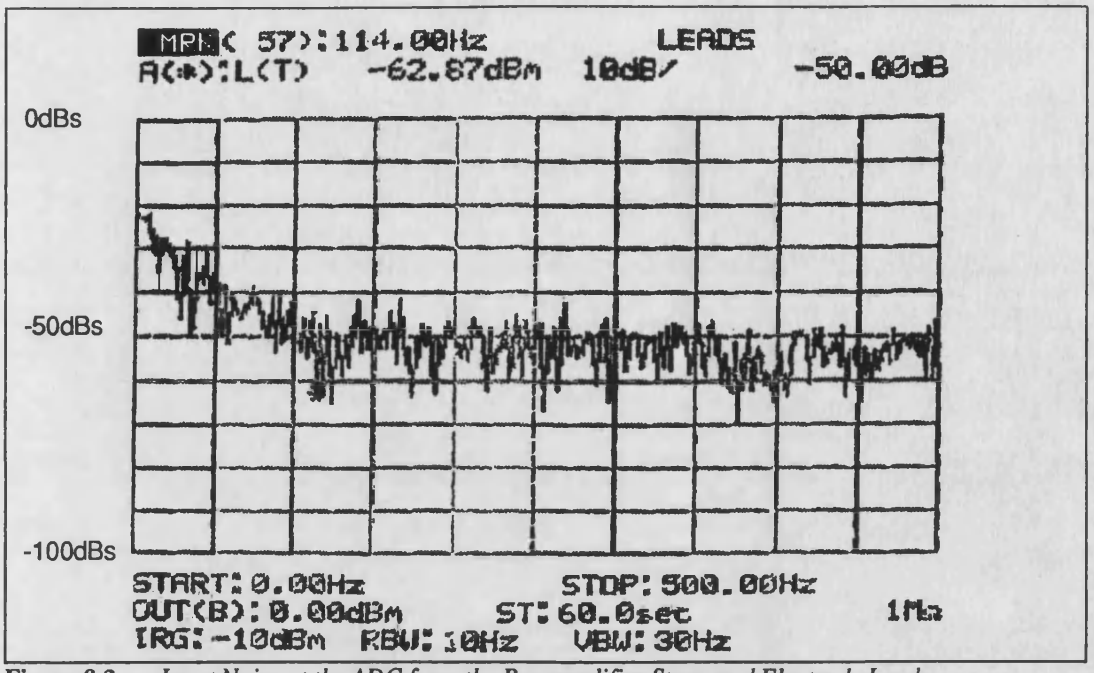

Figure 8.3 *Input Noise at the ADC from the Pre-amplifier Stage and Electrode Leads*

This noise is below the thresholds detectable using an 8 bit ADC so there is little effect on the recorded signals. It should also be noted that the noise is quite evenly spread across the signal bandwidth of interest, except at very low frequencies where motion artefacts usually occur and the input amplifiers thus have a low frequency cut-off.

8.1.2 EMG Module Bandwidths

Each of the EMG modules have had their bandwidth tested to determine how well they conform to the original design specification. Plots were obtained using a scanning

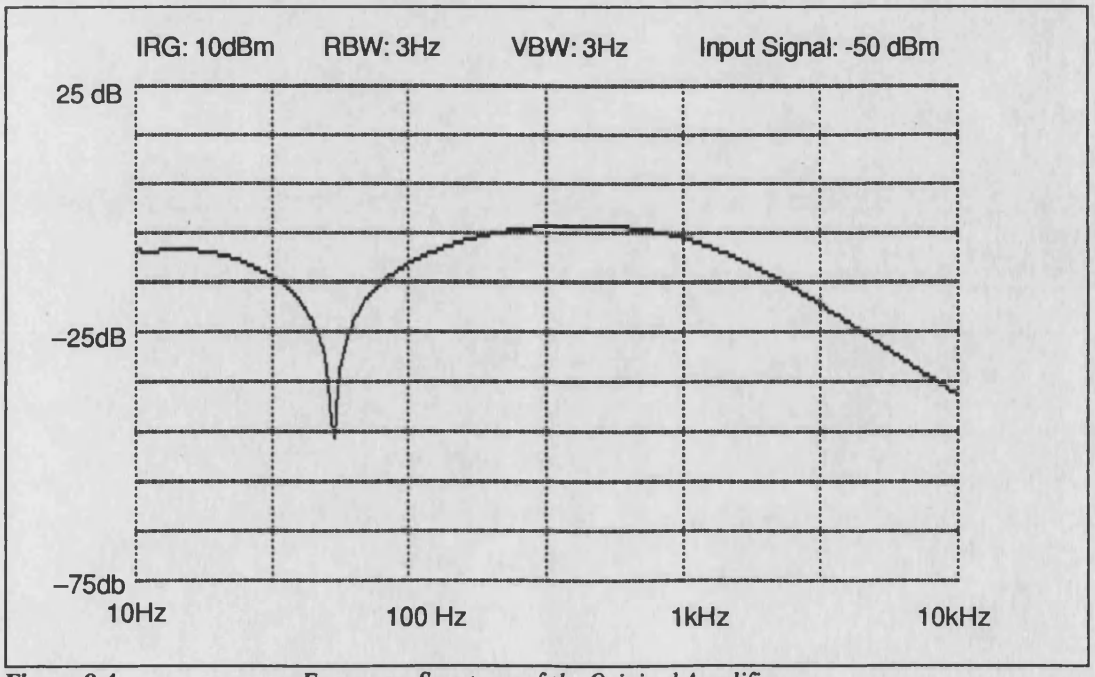

Figure 8.4 *Frequency Spectrum of the Original Amplifiers*

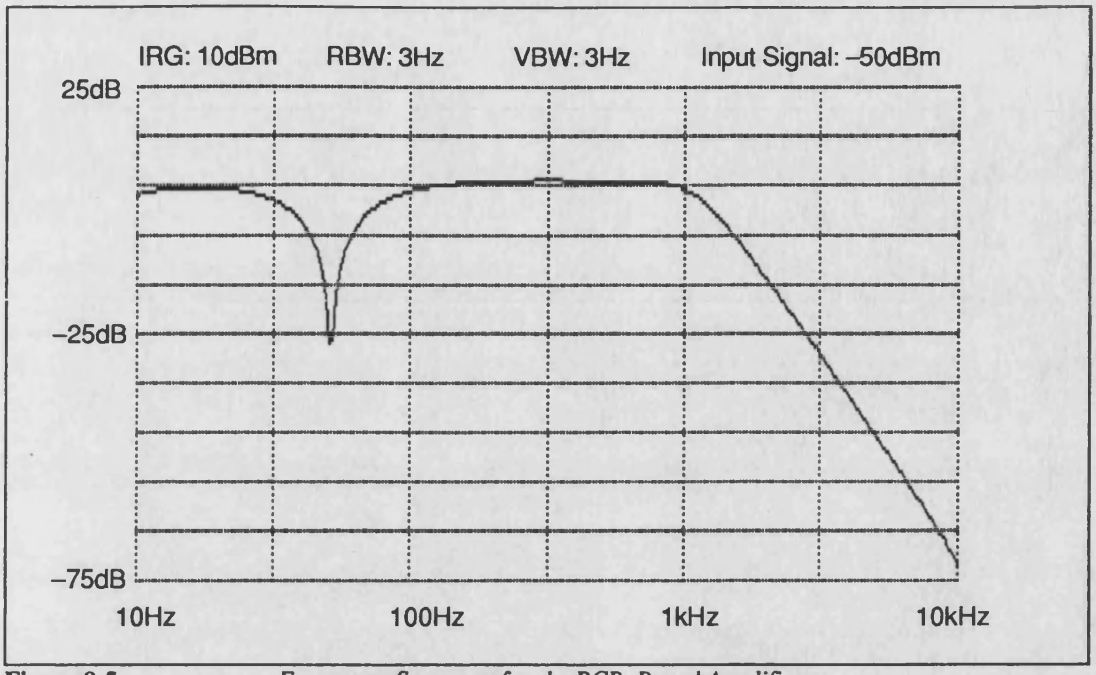

Figure 8.5 *Frequency Spectrum for the PCB Based Amplifiers*

spectrum analyser. The input signal used was of -50dBm and the spectra were plotted on a log scale from 10 Hz to 10 kHz.

8.1.2.1 Original Pre-Amplifier

A plot of the spectrum for the original pre-amplifier is shown in Figure 8.4. The frequency response of the original design shows the notch filter and the slow tail off 1 kHz cut-off. The notch is 40 dBs down on the main gain of the amplifier at -15 dB.

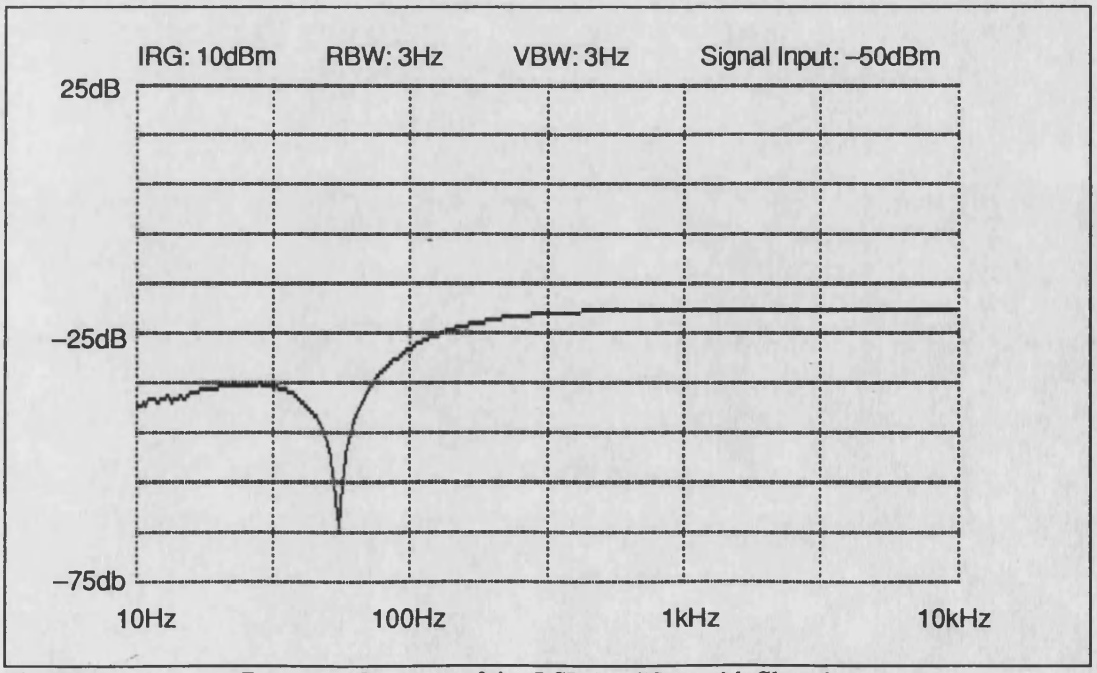

Figure 8.6 *Frequency Spectrum of the PCB Amplifiers with Clamping*

8.1.2.2 PCB based Pre-Amplifiers

A typical frequency response for the PCB amplifier is given in Figure 8.5 and Figure 8.6 shows the response of the PCB amplifiers that include clamping hardware for the removal of the stimulus artefact. The PCB amplifiers show an improved noise threshold and sharper frequency cutoffs. The gain is increased by 5 dBs over the original amplifiers with a much flatter passband and sharper low-pass cut-off at 1 kHz.

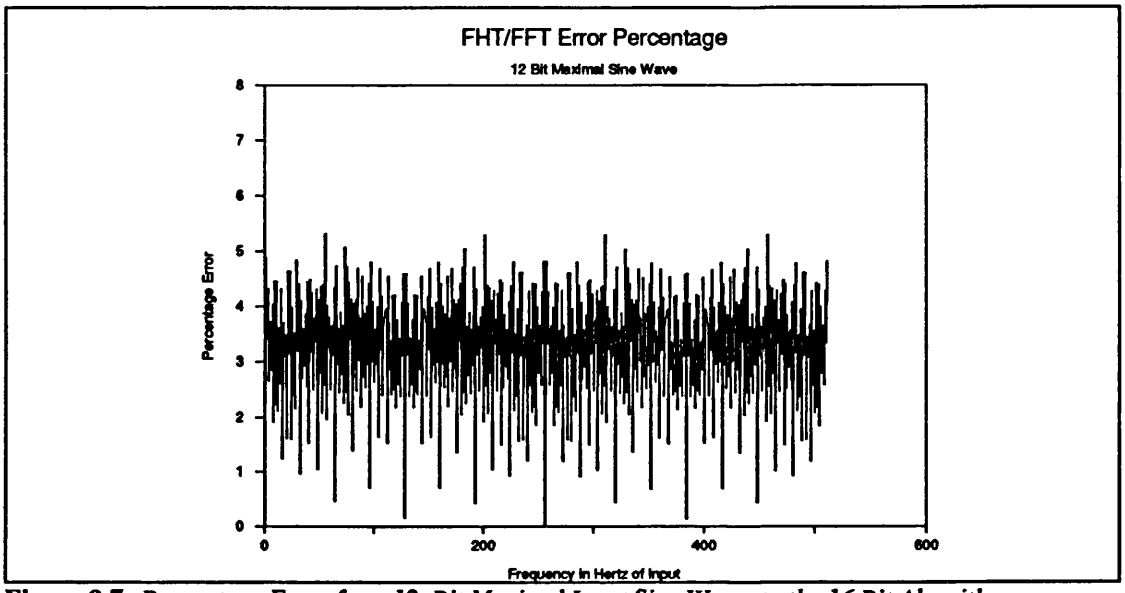

Figure 8.7 *Percentage Error for a 12 Bit Maximal Input Sine Wave to the 16 Bit Algorithm*

The clamping amplifier spectrum shows the effects of AC coupling the input which produces a large reduction in the low frequency band below 50 Hz. The gain of this amplifier shown is deliberately reduced to cope with the saturating effects of the stimulating voltage.

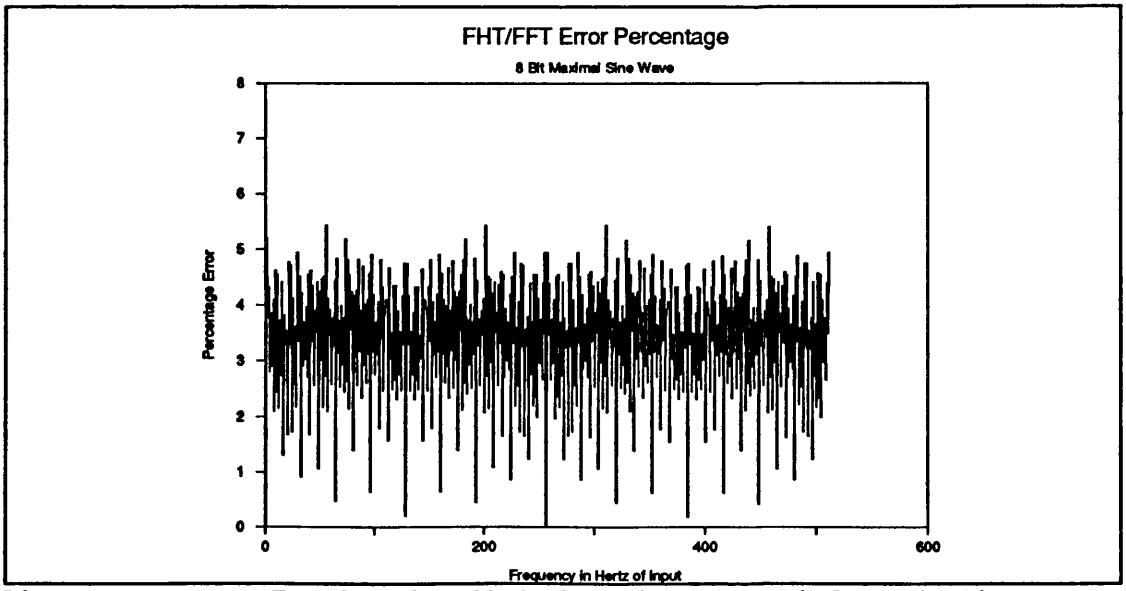

Figure 8.8 *Percentage Error for an 8 Bit Maximal Input Sine Wave to the 16 Bit Algorithm*

8.1.3 FFT and FHT Accuracy

The accuracies of the FFT and FHT algorithms in the original system are exactly the same because they are both based around a simple 16 bit arithmetic algorithm. As explained in Chapter 7, the sine and cosine tables are scaled up by 2^{15}; a 32 bit register is used for the multiplication and scaling. Automatic scaling between passes prevents any overflow and reduces the maximum bit significance still further. The results are output as 32 bit integers, thus removing the problems encountered with DSP card necessitating the normalisation to 16 bits.

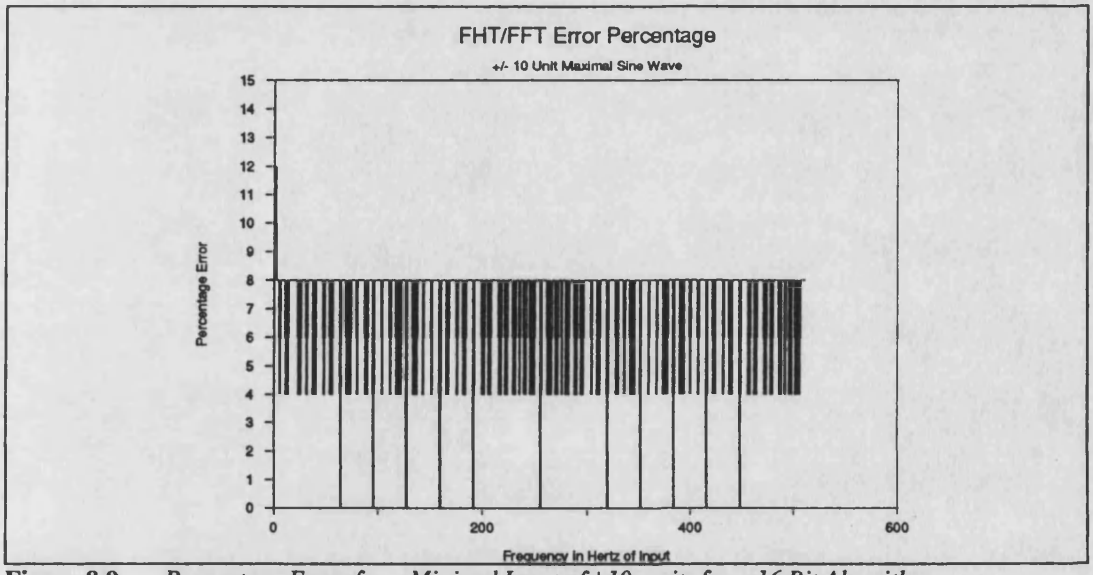

Figure 8.9 *Percentage Error for a Minimal Input of ±10 units for a 16 Bit Algorithm*

The algorithms have been tested with two sets of data. One set is the equivalent of a maximal 8 bit data sinewave, the other is a maximal 12 bit data sinewave. Figures 8.7 and 8.8 plot the percentage error in the calculated spectral line as a percentage of the correct value for these two input signals.

The tests were then repeated for the smallest quantisation level that could produce a result, which is a ±2 unit* sine wave. This is because the spectral power is reflected around zero frequency so that each spectral component except the DC level is $\frac{V^2}{4}$.

Tests using this value gave a result of mainly zero except for every 20 or so Hertz when a value of one was produced. This is due to the way an FFT(FHT) approximates the repetitive waveform. This means that an input signal of as much as ±10 units is required before the rounding errors, caused by using integer arithmetic, become reasonably insignificant, that is, less than 25%. Figure 8.9 shows a plot of the error

* A unit in this context is used to refer to the actual value returned by the ADC. Its actual physical value in volts would depend on the ADC input range and the number of bits the ADC uses. Since the FFT(FHT) algorithm does not know the physical value, its accuracy in real terms would have to be scaled by the ADC input requirements.

using an input of ±10 units. The error is calculated as a percentage of the required value. This value is equivalent to a 390 mV peak to peak input on the Atari printer port ADC and 195 mV peak to peak input on the Atari Mega Expansion ADC.

Software Routine	Basic Speed	Speed in Use	Degradation
FFT Routine	0.58	0.885	52%
Display Routines	—	1.24	—
FHT Routine	0.395	0.59	49%
Display Routines	—	1.24	—
Percentage Improvement offered by Hartley	31%	33%	—

Table 8.1 *Table of Software Timings on the Original Atari System*

8.1.4 Software Timings

The timings for the software are given in Table 8.1. These were measured using the internal timing function of the Atari ST. This is a 200 Hz interrupt driven counter and so will vary depending on the interrupt load. Two sets of timings have been carried out. One set has been recorded with the extra interrupts required to sample data disabled, which means that the timings given reflect quite accurately the software timing when running with just the normal system overheads. The second set of figures represent the changes that occur when the sampling overhead is introduced. As can be seen, the calculation of the median and screen display routines are in fact the slowest part of the software. It can also be seen that the relative speeds of the two routines are scaled evenly by the back ground interrupt tasks.

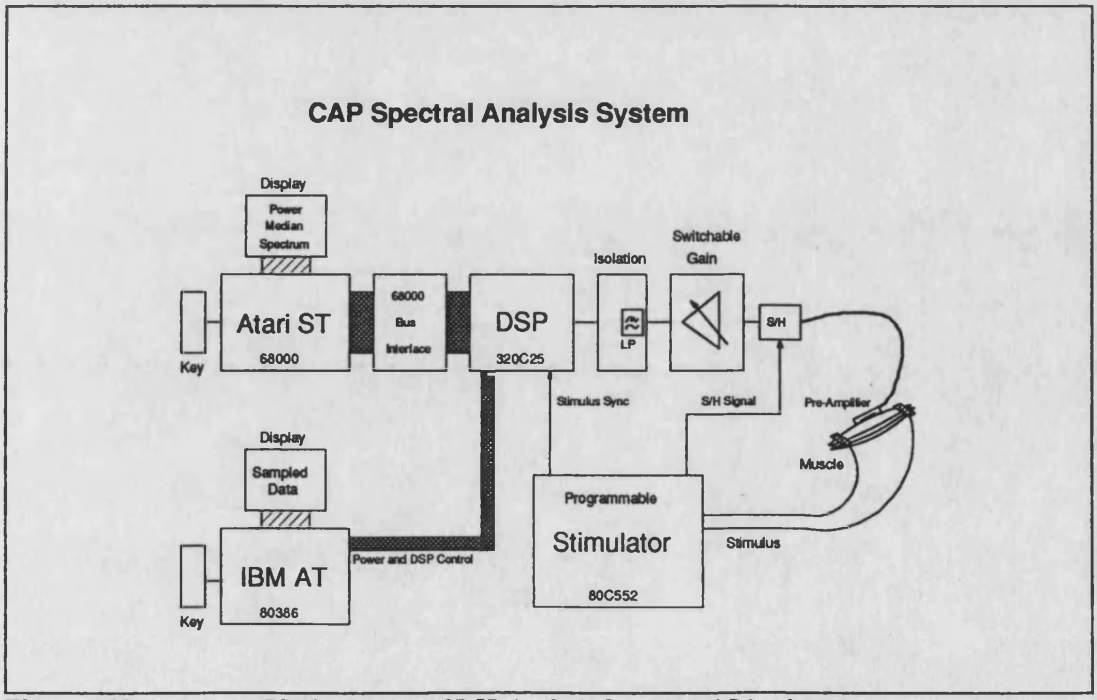

Figure 8.10 *Block Diagram of DSP Analysis System and Stimulator*

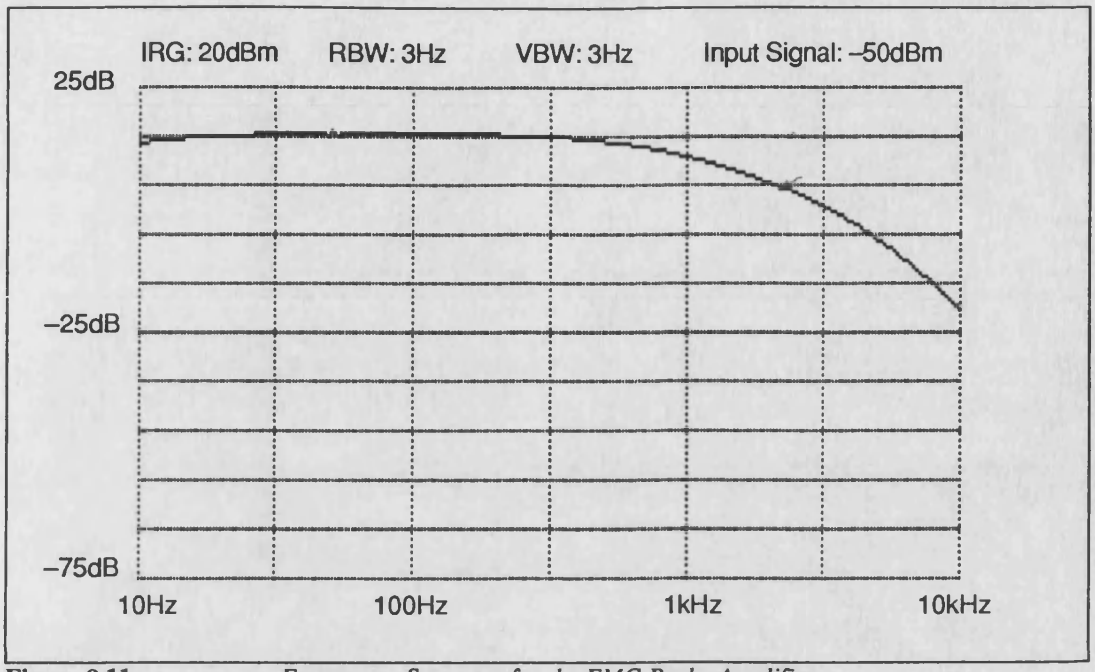

Figure 8.11 *Frequency Spectrum for the EMG Probe Amplifier*

Significant speed advantages are thus gained from the use of the Hartley Transform over the Fourier Transform.

8.2 DSP System

A block diagram of the complete system is shown in Figure 8.10. Plate F.22 shows the actual equipment. The configuration shown is for the testing of the biceps muscle. Plate F.23 shows a close up of the stimulator electrodes on the biceps. The EMG probe is placed between the electrodes with the EMG contacts running along the muscle length. The probe is held on using elasticated straps. When testing the leg muscles a similar configuration is used except there is a larger separation between the electrodes allowing the EMG probe to be placed where the optimal signal can be detected. In both these tests the earth strap is connected at some convenient point. For the biceps this is usually the wrist and for the leg the knee or ankle.

8.2.1 EMG Probe Bandwidth

The frequency response of the EMG probe is given in Figure 8.11. The later version is shown here. In these versions the electrodes are DC coupled to reduce the tail produced by the stimulus artefacts. The Bandwidth is nominally set to 500 Hz and is a simple 6dB/octave rolloff.

8.2.2 Isolation Amplifier Bandwidth

The Isolation amplifier combines both amplification and filtering. The amplifier provides three filter cut-off frequencies and each of these was tested using the spectrum analyser. As with the EMG pre-amplifiers the input signal is -50 dBs and a

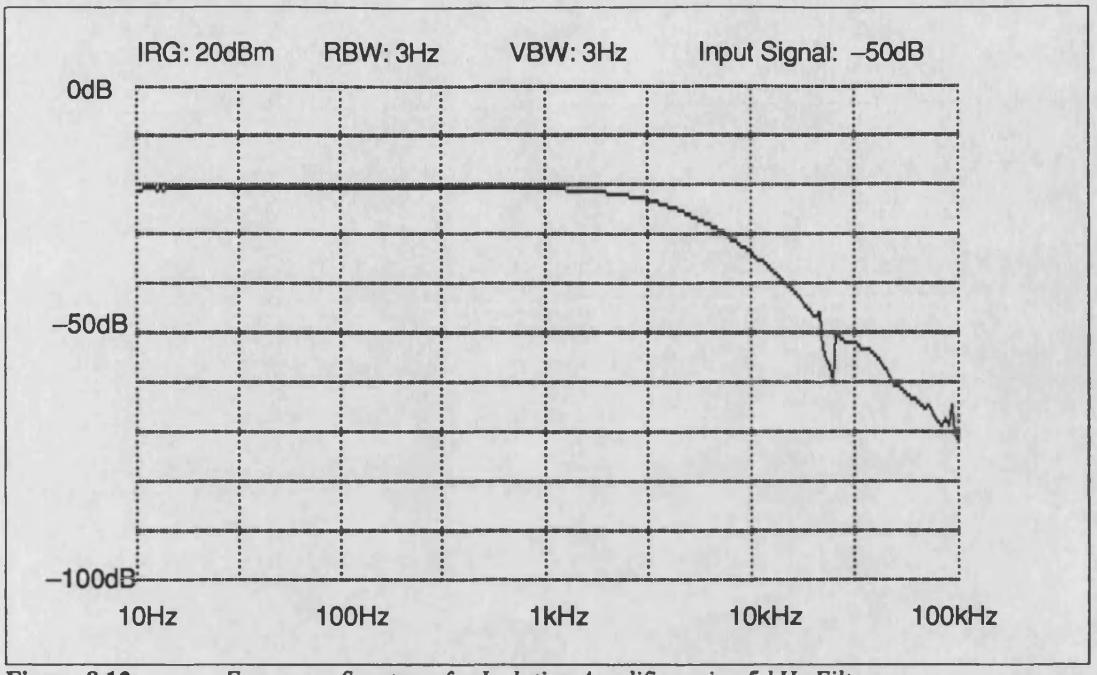

Figure 8.12 *Frequency Spectrum for Isolation Amplifier using 5 kHz Filter*

slow scan rate and narrow resolution band width have been used in order to guarantee the integrity of the plots.

Figure 8.12 shows the spectrum of the 5 kHz filter which is in fact the filtering of the isolating amplifier itself which has a guaranteed bandwidth of 5 kHz. The cut-off at 5 kHz is not as sharp as that obtained from the actual filter circuits and has noticeable interference at 25 kHz. The interference is due to the way the isolation amplifier derives its clock signal from a 25 kHz 15 V square wave and is a good 30 dBs down on the signal passband.

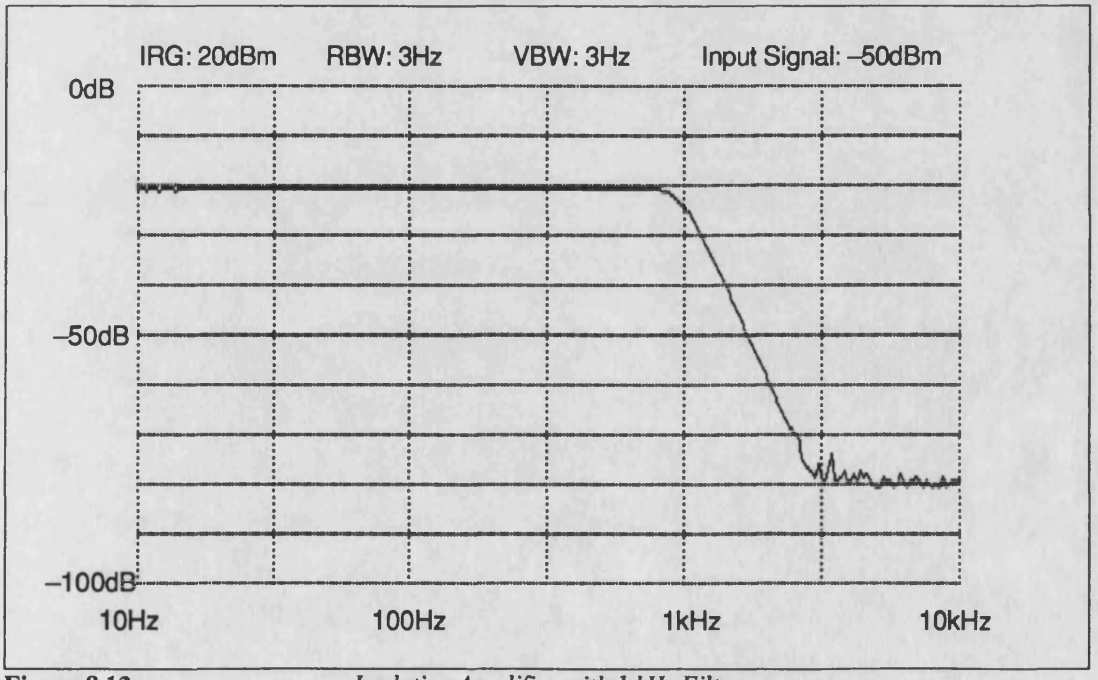

Figure 8.13 *Iso lation Amplifier with 1 kHz Filter*

Figure 8.13 shows the spectrum of the 1 kHz filter and it clearly shows the sharp cut-off achieved using the 6th Order Butterworth filter circuitry. The signal rapidly drops to the noise threshold of –100 dBs.

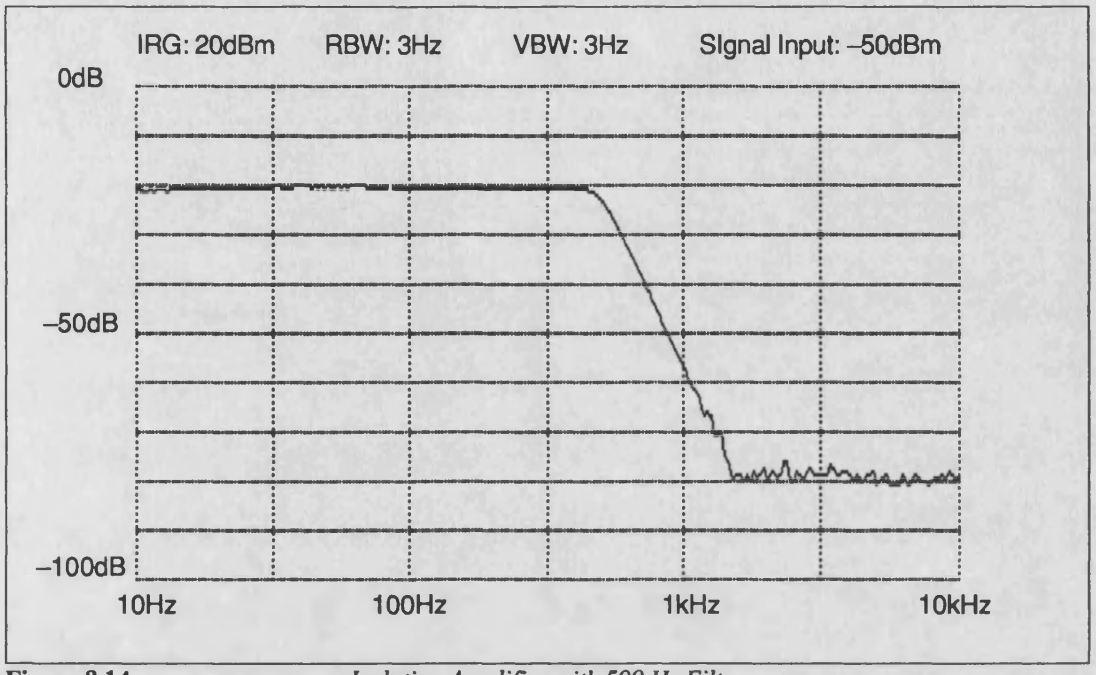

Figure 8.14 *Isolation Amplifier with 500 Hz Filter*

Figure 8.14 shows the spectrum for the 500 Hz filter. As might be expected this very closely follows the typical curve of the 1 kHz filter but shifted in frequency by 500 Hz. This, like the 1 kHz filter drops to a noise floor of –100 dBs.

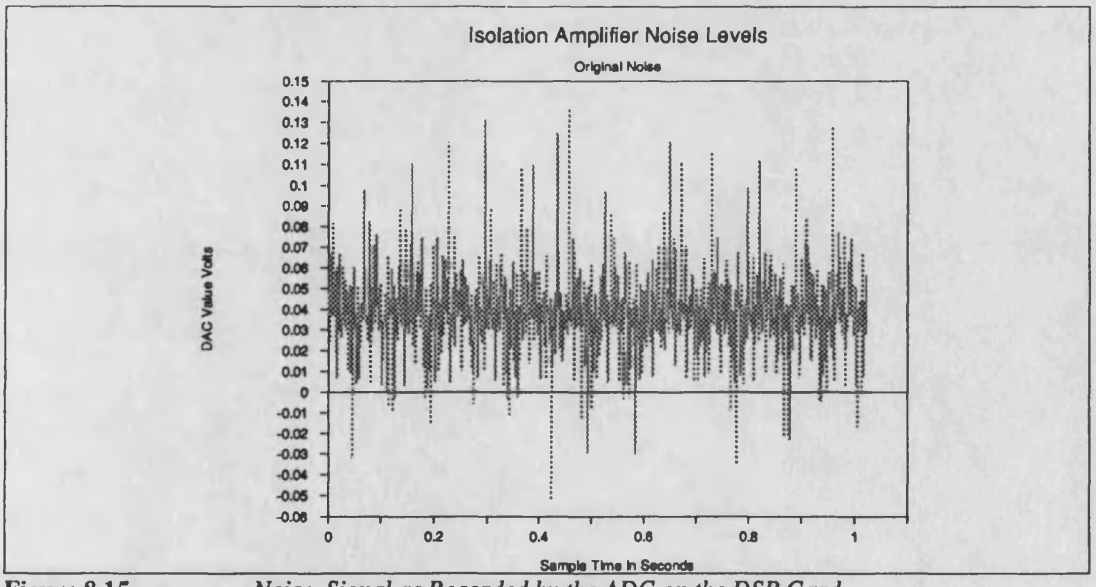

Figure 8.15 *Noise Signal as Recorded by the ADC on the DSP Card*

8.2.3 Isolation Amplifier Noise

As shown in the circuit diagram Figure G.21, two different schemes have been used for powering the output stage. The reason for the second design is excessive noise at

the ADC input. As can be seen in the spectral plot for the 5 kHz band limited signal there is a clock signal at 25 kHz. In the original design the positive rail was provided by a regulated 18 V battery supply which fed the clock generator for the isolation

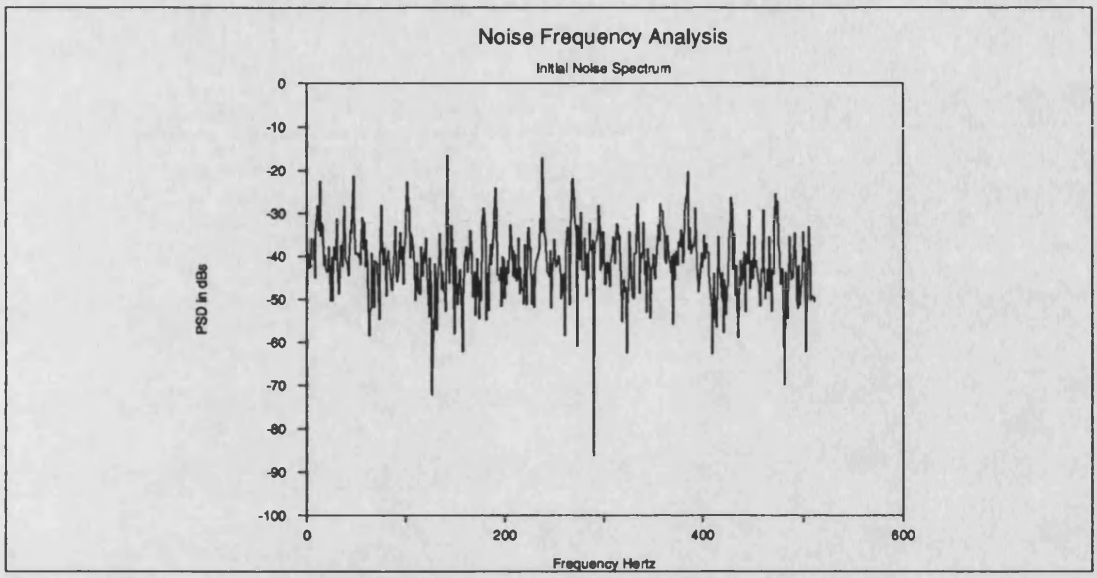

Figure 8.16 *The Frequency Spectrum of the Original Noise Signal*

amplifier. The output buffer amplifier was powered from this regulated 15 V supply and a –15 V supply generated using a single chip inverter clocking at 10 kHz. The effect of this was excessive noise at the output when the input of the isolation box was shorted. Figure 8.15 shows the noise as recorded at the ADC of the DSP card with the isolation amplifier inputs grounded. Figure 8.16 shows the spectrum of this noise.

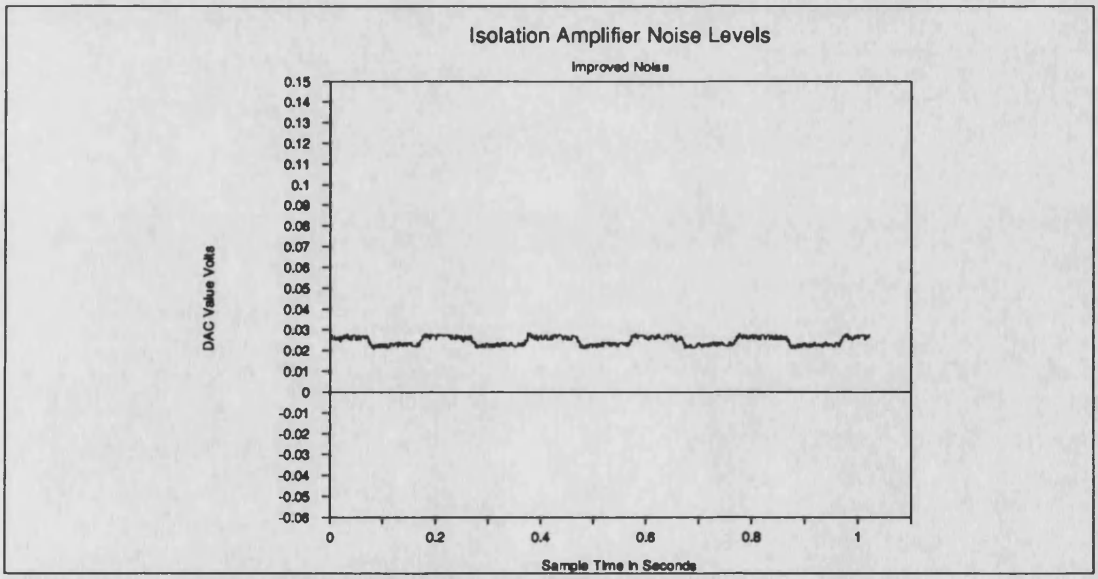

Figure 8.17 *Plot of the Noise at the ADC of the DSP Card after the Circuit Changes*

The problems were found to be mainly attributable to the power supply. This not only introduced noise due to the way the negative rail was generated but also was unable to maintain a stable 15 V rail with the 25 kHz clock generator connected. As

can be seen in the circuit diagram, Figure G.21, the solution was to replace the batteries by a a 'solid' ±15 V power supply. This reduced the noise quite significantly to a small ripple which was well below the threshold of the FFT algorithm though it could be recorded by the ADC.

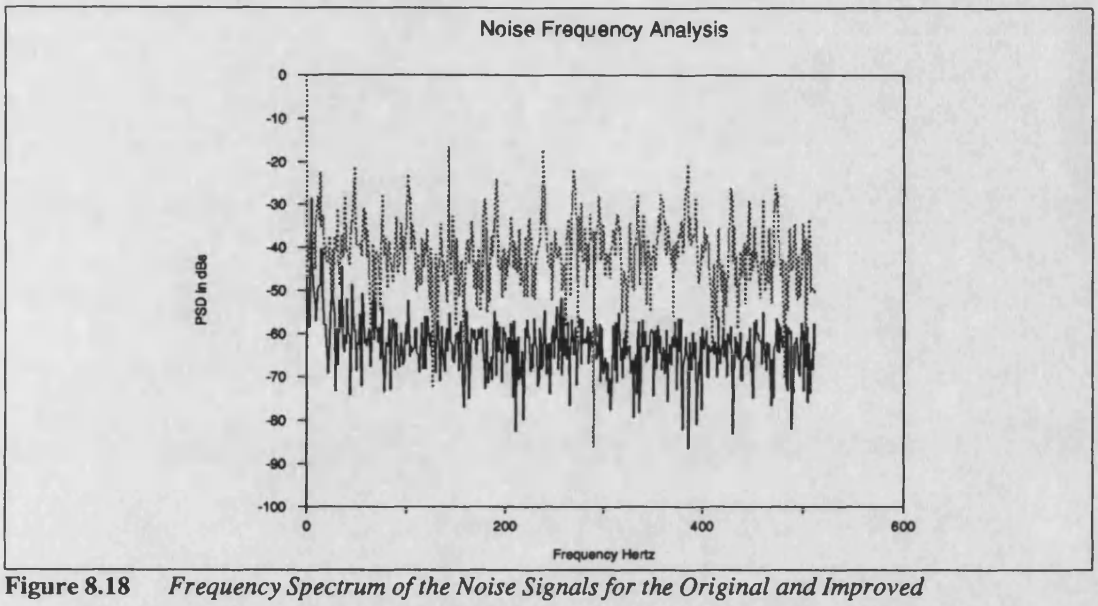

Figure 8.18 *Frequency Spectrum of the Noise Signals for the Original and Improved Amplifier Circuit*

Figure 8.17 is a plot of the final improved version showing the marked reduction in circuit noise. Figure 8.18 is a plot of the spectrum of this noise signal along with that of the original noise signal. As can be seen the noise is reduced by a factor of 20 dBs. It should be noted that the spectra were calculated using a floating point FFT algorithm rather than the 16 bit algorithm of the DSP card which was unable to produce a spectrum from this level signal.

8.2.4 FFT Accuracy

As has been described in Chapter 7 the DSP card FFT software currently runs a non-optimised and non-windowed input FFT routine. In order to test the integrity of the FFT results two sets of test have been carried out.

8.2.4.1 Frequency Accuracy and Mathematical Noise

The first test uses a signal generated sine wave which was fed via the isolation amplifier into the DSP. The frequency of the sine wave was set using a frequency counter to a number of different frequencies covering the band of interest. The values chosen being; 10, 50, 100, 200, 300, 400 and 500 Hz. The sinewave was a maximal ±10 V, i.e. 20 volts peak to peak sinusoid. The calculated spectrum was then recorded. The sample data was also recorded and fed into a floating point based FFT algorithm running on the IBM PC. The two calculated spectra were then compared and any differences noted.

Since the IBM PC calculation made use of floating-point arithmetic it is reasonable to consider this the best result that could be achieved by the DSP card. The difference therefore may be considered the arithmetic noise due to the inaccuracies of the 16 bit integer arithmetic.

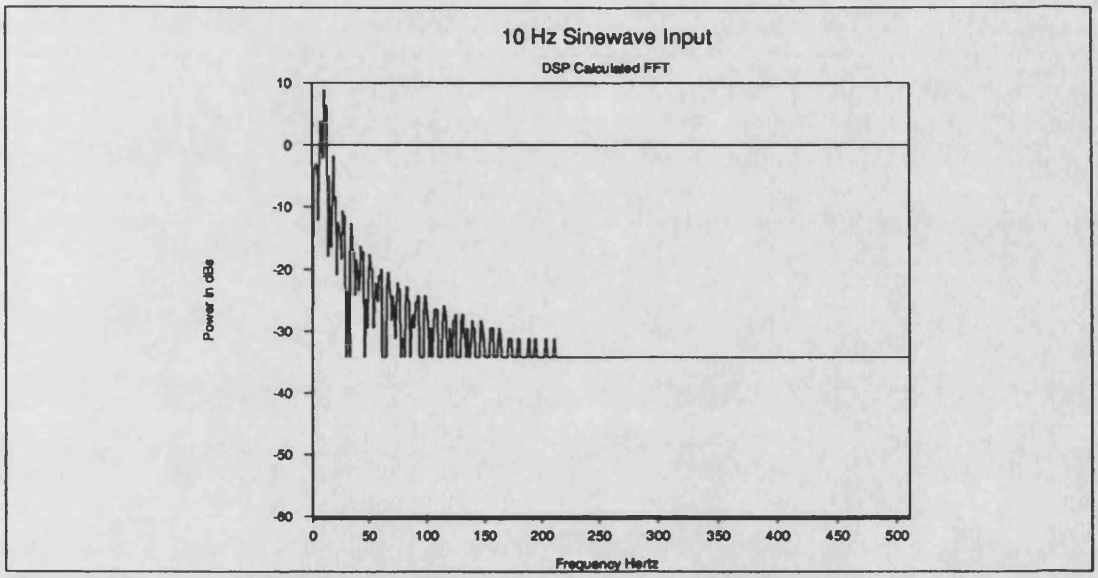

Figure 8.19 *DSP Calculated Frequency Spectrum for a 10 Hz Sinewave*

The results that follow do not plot the two spectra superimposed, but rather plot the difference or 'error'. Except for the odd spectral line the top edge of it may be thought of as the spectrum from the DSP card and the bottom edge as the best achievable spectrum.

To demonstrate this better the plots for the 10 Hz input are presented first as separate plots then as a difference plot. Figure 8.19 is a plot of the DSP generated FFT of a 10 Hz sine wave from the signal generator. The reason that the plot has a horizontal line from about 250 Hz is that the power calculated by the DSP was equal to zero. To prevent attempts at plotting the log of zero, these values were set to 1 unit as calculated by the DSP which is equivalent to the FFT threshold in this calculation. The actual value of 1 DSP FFT unit will vary depending on the scaling factor as described in Section 7.6.1. Figure 8.20 is a plot of the frequency spectrum generated from the same sample data as used by the DSP card but this time using the floating-point algorithm. Since floating point calculations have been used there are no zeros in the calculated spectrum and thus the signal tails rapidly to some 40 dBs down.

The difference of these two spectra is plotted in Figure 8.21. It can be seen that the two spectra match well close to 10 Hz, but start to differ markedly further from the peak.

Figures 8.22, 8.23, 8.24, 8.25, 8.26 and 8.27 plot the difference spectra for 50, 100, 200, 300, 400 and 500 respectively. Figure 8.28 is a plot of the spectra obtained with

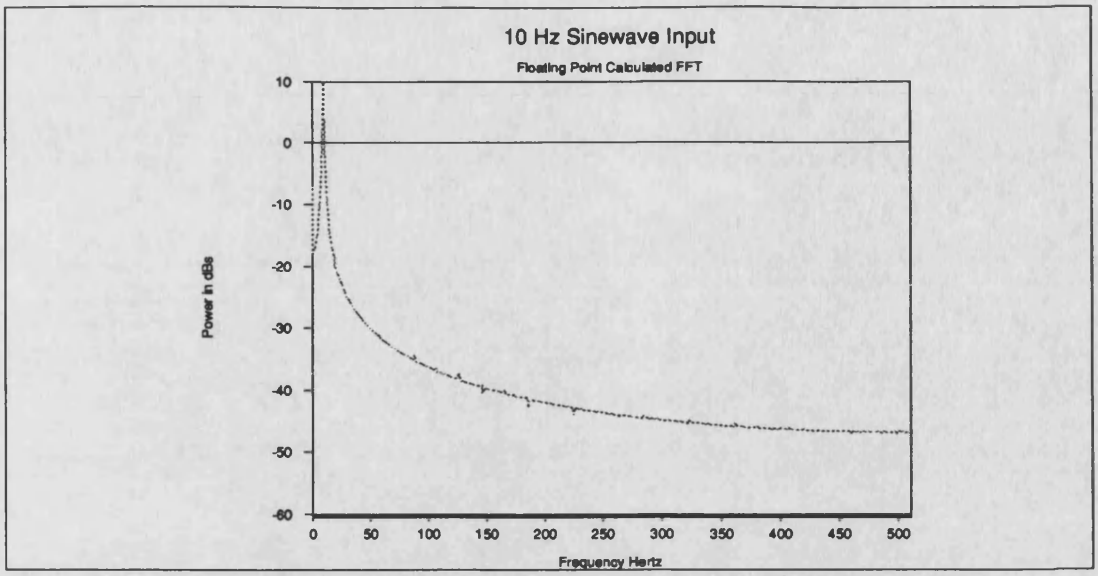

Figure 8.20 *Frequency Spectrum of the 10 Hz Sinewave Input using a Floating-point FFT*

the isolation amplifier filter set to a 1 kHz cut-off as opposed to a 500 Hz cut-off which is used for all the previous tests. It is quite noticeable how the noise thresholds fluctuate across the various plots, although the peaks at the frequencies of interest remain quite consistent. The DSP values also match quite well those calculated by the floating point algorithm.

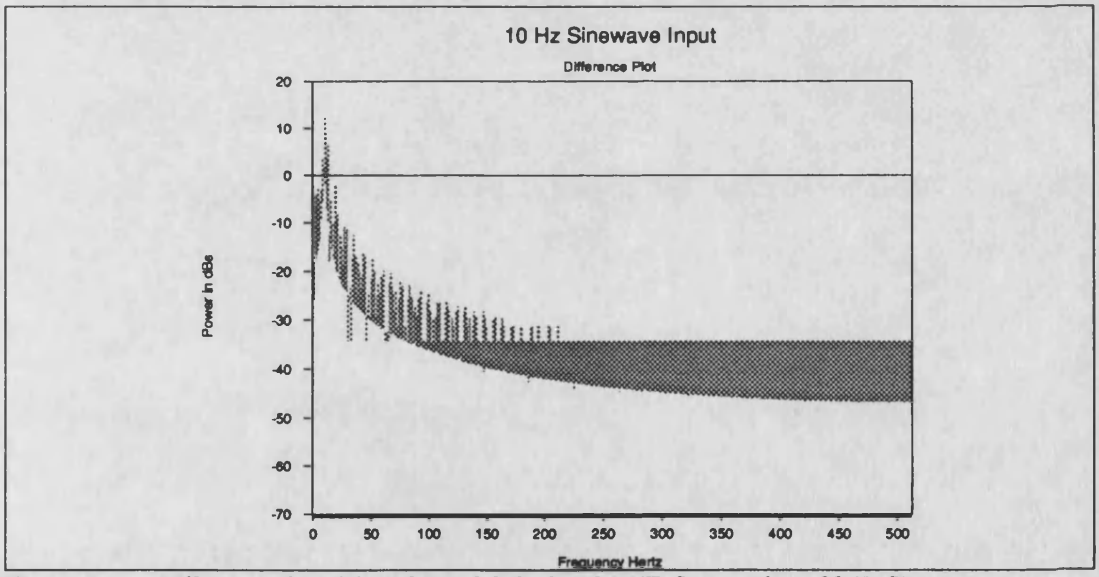

Figure 8.21 *Difference Plot of the DSP and Calculated FFT Spectra for a 10 Hz Sinewave*

8.2.4.2 Signal Power Accuracy

The signal power accuracy was measured using a similar technique to that used to measure the FFT frequency accuracy and noise thresholds. This time, instead of sweeping the frequency across the sampling bandwidth, the frequency was kept constant at 250 Hz and the signal power was adjusted. The voltages used were 2, 6, 12 and 20 V peak to peak. As before the sample data and calculated spectrum were recorded. An FFT using a floating point algorithm was used to calculate the optimum

spectrum and the two spectra, one from the DSP and one from the floating point algorithm, were plotted as a difference plot for each of the input voltages.

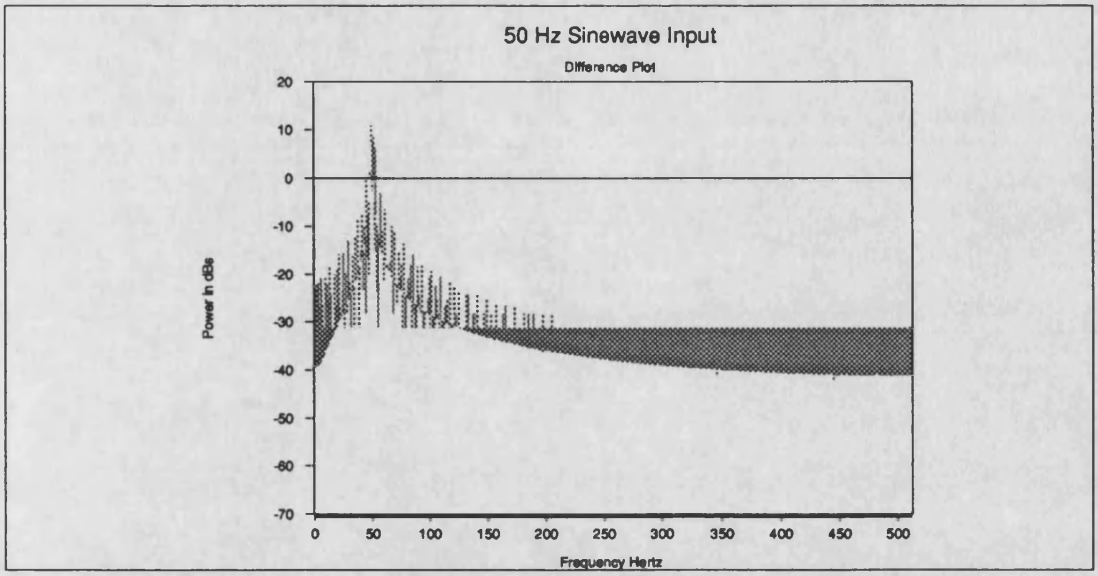

Figure 8.22 *Difference Plot of the DSP and Calculated FFT Spectra for a 50 Hz Sinewave*

Figures 8.29, 8.30, 8.31 and 8.32 are plots of the difference spectra for each of the test voltages, that is 2, 6, 12, 20 V peak to peak sinewaves at a frequency of 250 Hz. The figures show that the spectral lines in the vicinity of 250 Hz for the DSP calculated spectra and floating-point spectra match each other quite closely in terms of peak power level. Where they do differ is in the precise frequency that the peak power

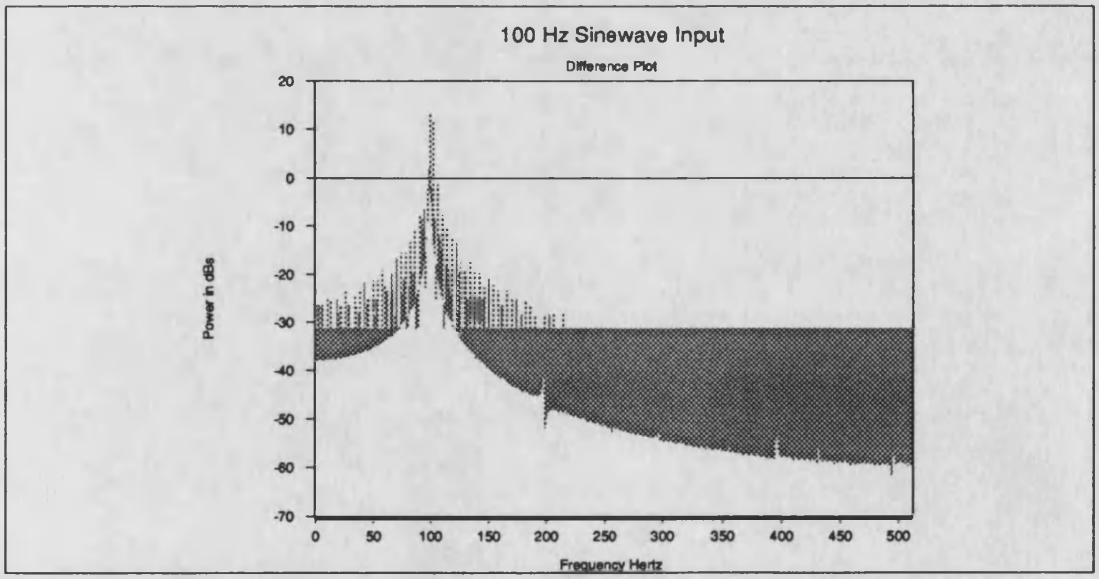

Figure 8.23 *Difference Plot of the DSP and Calculated FFT Spectra for a 100 Hz Sinewave*

is attributed to. This is due to the spectral spread caused by using real data derived from a fairly noisy signal generator. If the sinewave data had been generated by calculation, as in the case of the Atari system tests, the spectral lines could be guaranteed to fit neatly in the frequency bins, thus reducing the ambiguity. Tests using

the lookup table data and similar higher frequency data returned the correct frequencies. The tests that have been carried out show the ambiguities that are introduced into the frequency transform when using real data.

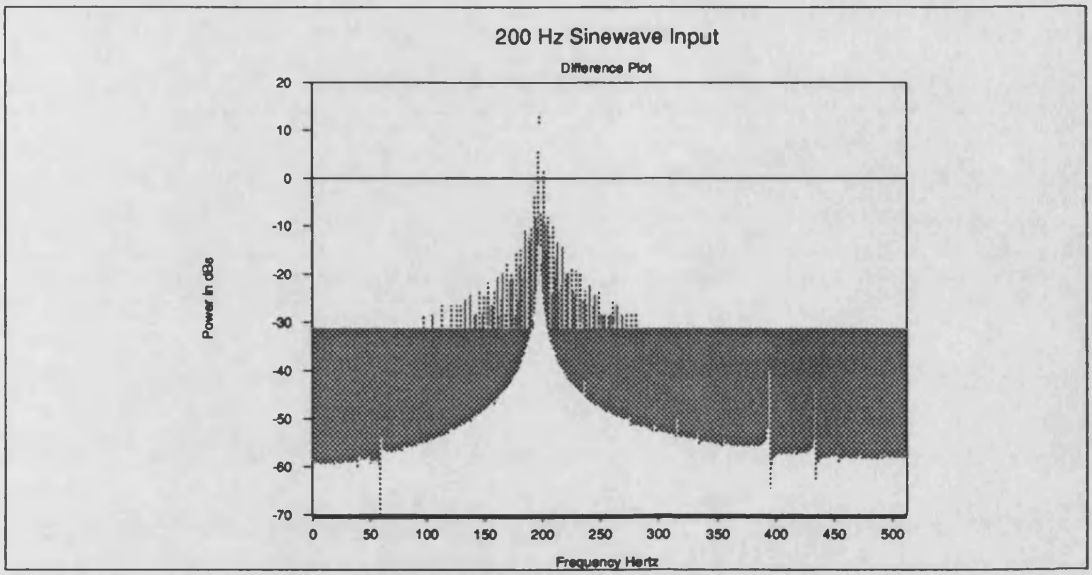

Figure 8.24 *Difference Plot of the DSP and Calculated FFT Spectra for a 200 Hz Sinewave*

8.2.4.3 Systems Ability to Analyse Real Muscle Data

The final set of tests were aimed at testing the systems integrity with real muscle data. For this test real data recorded using the analysis system from the biceps muscles has been used. There are two forms of muscle data that the system has to be able to analyse; voluntary muscle responses and stimulated CAP trains.

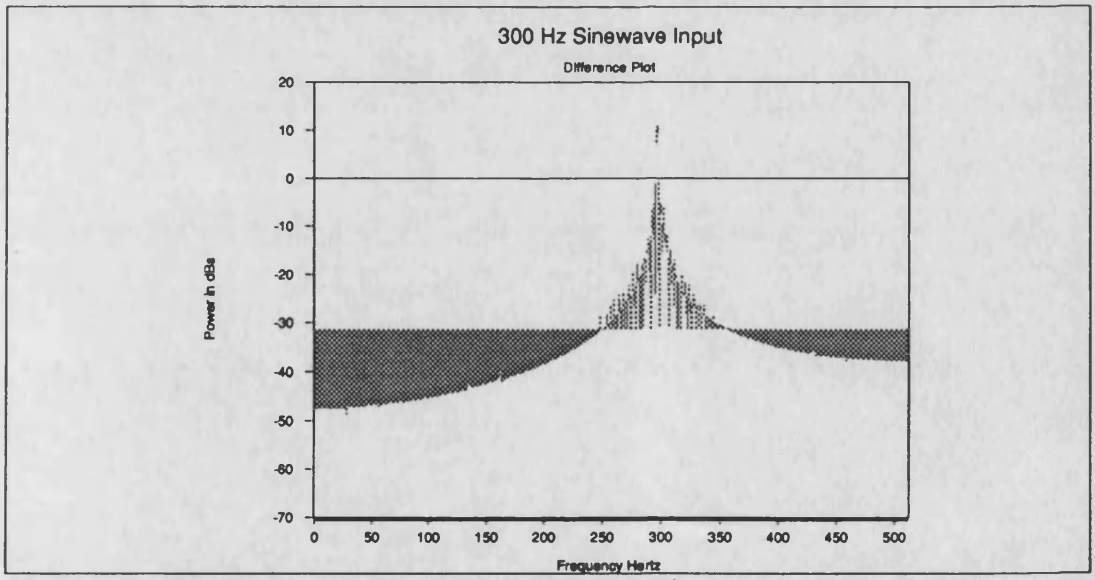

Figure 8.25 *Difference Plot of the DSP and Calculated FFT Spectra for a 300 Hz Sinewave*

These two tests are aimed at ensuring the calculated responses displayed by the analysis system are a true reflection of the data. The tests involved the recording of some muscle responses from voluntary and stimulated muscle. The sampled data

recorded by the DSP is then used to calculate the expected spectrum which is compared with the DSP FFT algorithm calculated spectrum.

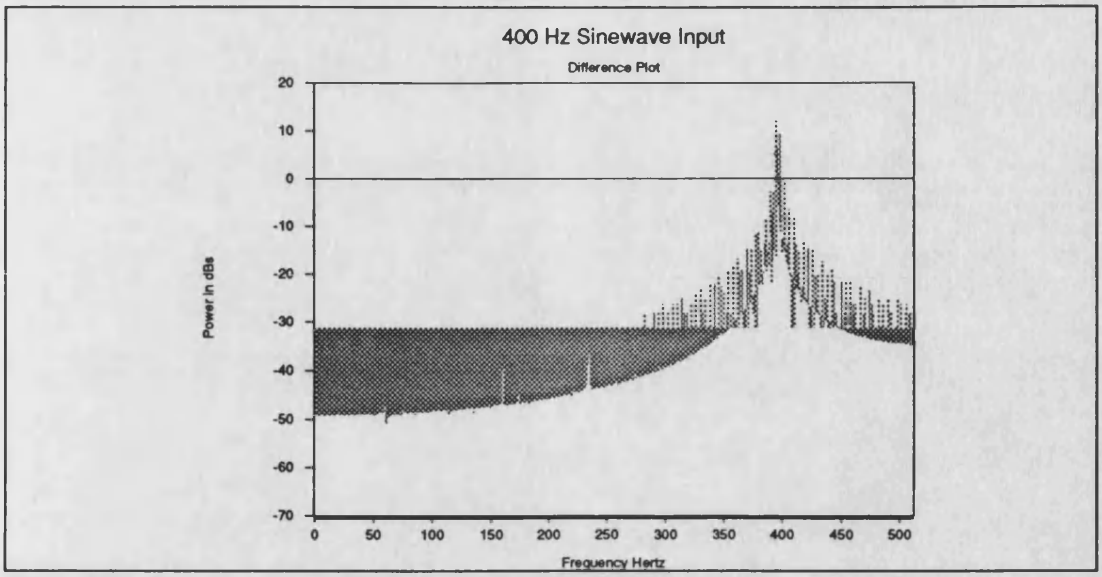

Figure 8.26 *Difference Plot of the DSP and Calculated FFT Spectra for a 400 Hz Sinewave*

Figure 8.33 is a copy of the results as presented by the DSP program for a typical voluntary contraction of the biceps muscle. This is recorded using the facilities provided by the IBM loader program. The actual screen is produced by the record playback program described in Section 7.6.4. The top half of the screen shows the recorded data and the lower half shows the DSP calculated spectrum. Figure 8.34 shows the spectrum calculated from the same data using the floating point FFT routine. As can be seen the two spectra match each other quite closely. The frequency spectrum displays the characteristic envelope shape associated with EMG signals.

Two sets of results are presented for the stimulated muscle. The first results shown in Figures 8.35 and 8.36 are the screen dump and floating point calculated spectrum for a

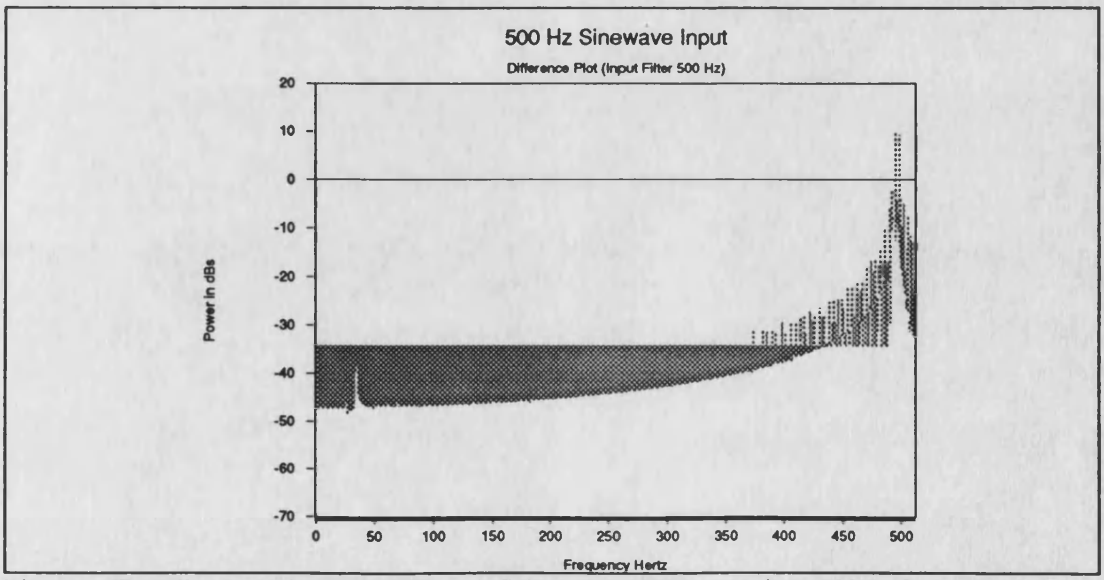

Figure 8.27 *Difference Plot of the DSP and Calculated FFT Spectra for a 500 Hz Sinewave*

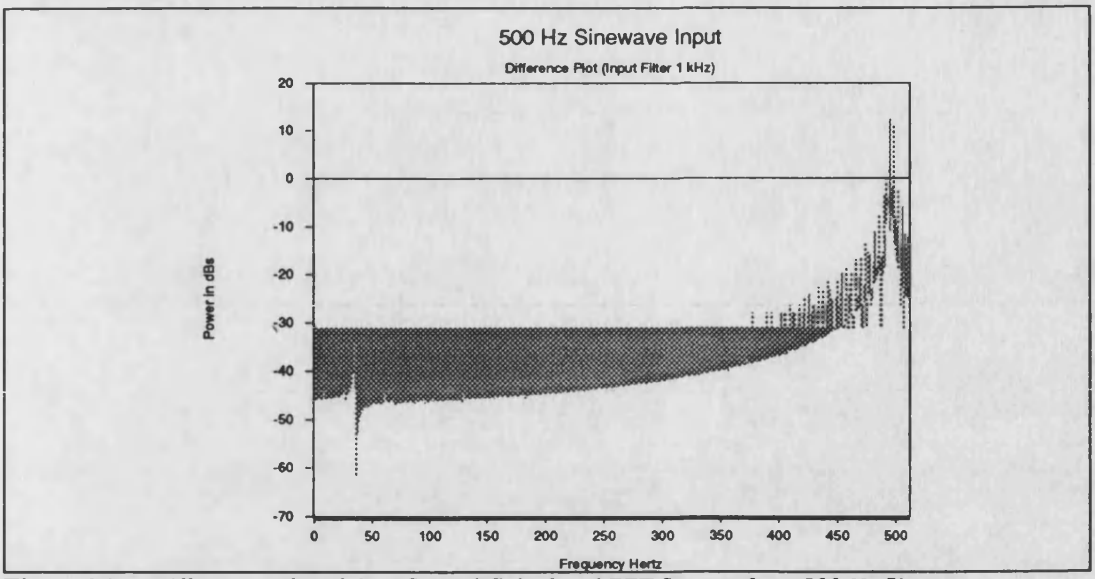

Figure 8.28 *Difference Plot of the DSP and Calculated FFT Spectra for a 500 Hz Sinewave and the Isolation Amplifier Filter set to 1 kHz*

typical CAP train. The stimulus parameters were 300μs pulse width and 40 ms interpulse interval and the level was just sufficient to produce a tetanic contraction. The spectrum is characterised by strong spectral components at the pulse repetition rate, 25 Hz in this case. This is what would be expected given that this is the fourier transform of a repetitive waveform. As can be seen once again there is a close match

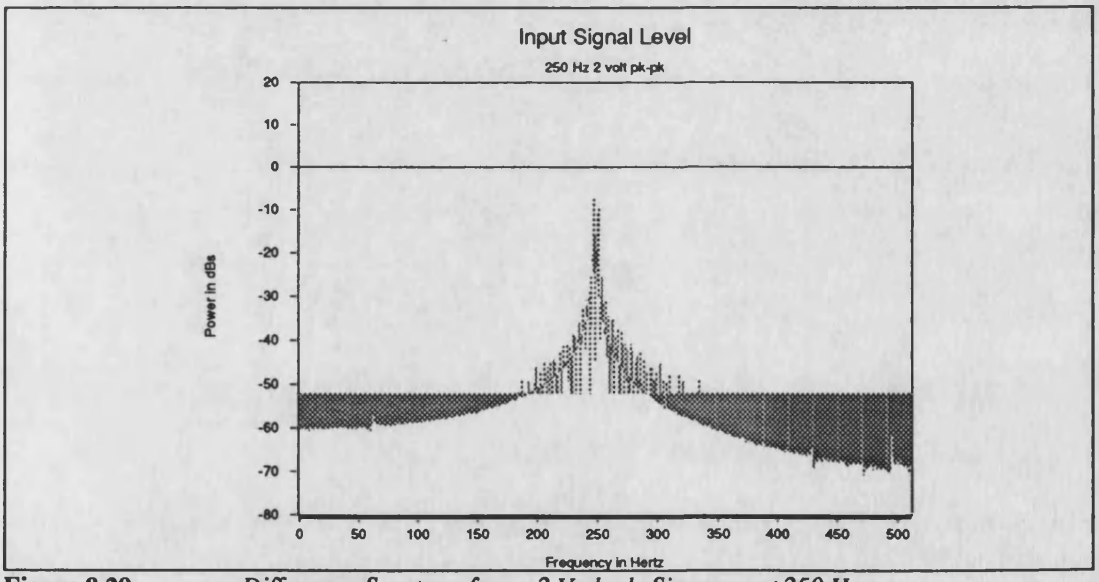

Figure 8.29 *Difference Spectrum for a 2 V pk-pk Sinewave at 250 Hz*

between the recorded DSP spectrum and the calculated spectrum. Besides the spectral lines at 25 Hz there are also frequency components between. There are two possible explanations for this. The first is that since the recordings were from a normal biceps they could be voluntary EMG breaking through because the muscle was not fully relaxed. the second cause which seems more likely is that the CAPs in the CAP train are not identical and this combined with the small sample size leads to the spectral

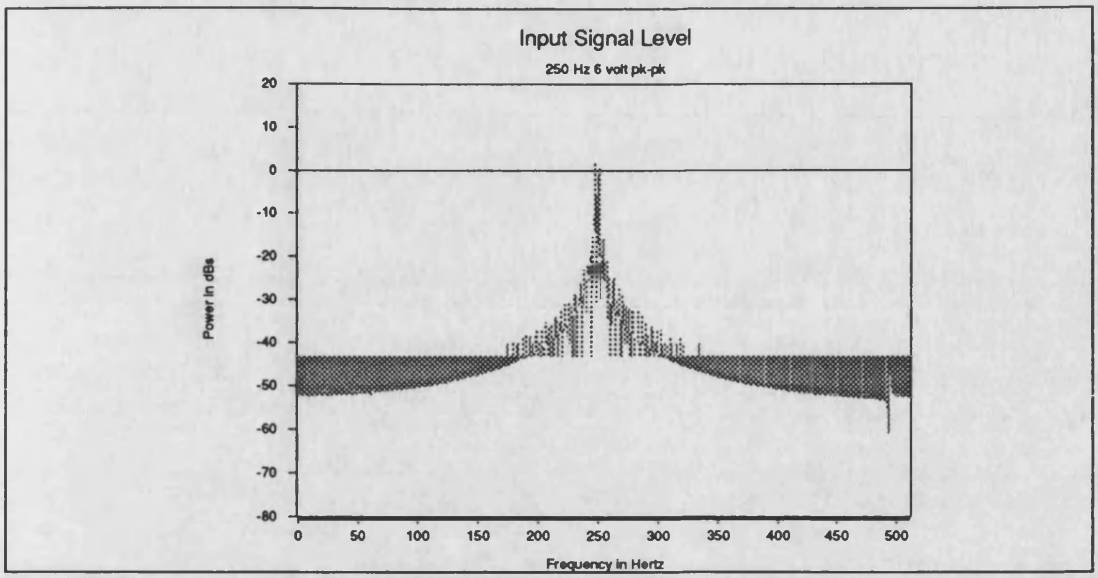

Figure 8.30 *Difference Spectrum for a 6 V pk-pk Sinewave at 250 Hz*

components between the spectral lines at 25 Hz and its harmonics. If the number of CAPs in the sample set is increased the spectral lines would tend to dominate and hide this background effect.

Figures 8.37 and 8.38 show the results for a pair of recorded CAPs produced by reducing the pulse repetition rate to 2 Hz, an interpulse interval of 0.5 seconds. The reasons for reducing the number of CAPs per sample period are discussed in detail in Chapter 9. It is obvious from the spectrum that the effects of the repetition rate are now hidden and instead the shape of the spectrum is defined by the CAP shape. The calculated spectrum is again very similar to that produced by the DSP FFT.

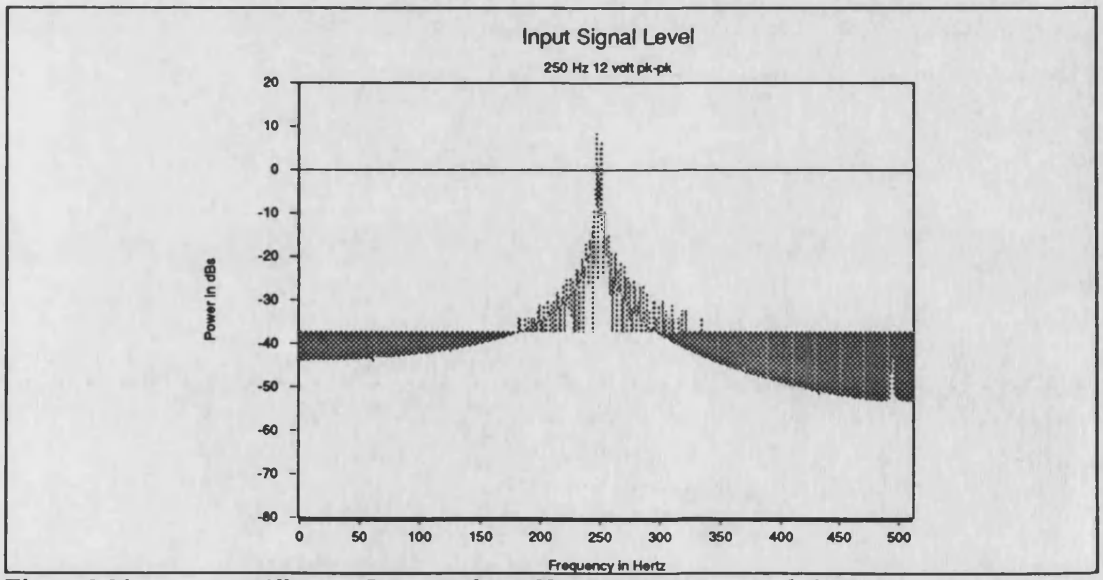

Figure 8.31 *Difference Spectrum for a 12 V pk-pk Sinewave at 250 Hz*

8.2.4.4 FFT Timings

Tests on the DSP card using the toggling of the XF bit indicate that the FFT takes around 40 milliseconds to complete the 1024 point FFT. This means that it is sitting dormant just collecting the data for the next sample and transmitting the results of the previous calculation to the Atari display for some 960 milliseconds. Clearly this means that the DSP card has the potential to do considerably more pre-processing before sending the data to the Atari for display.

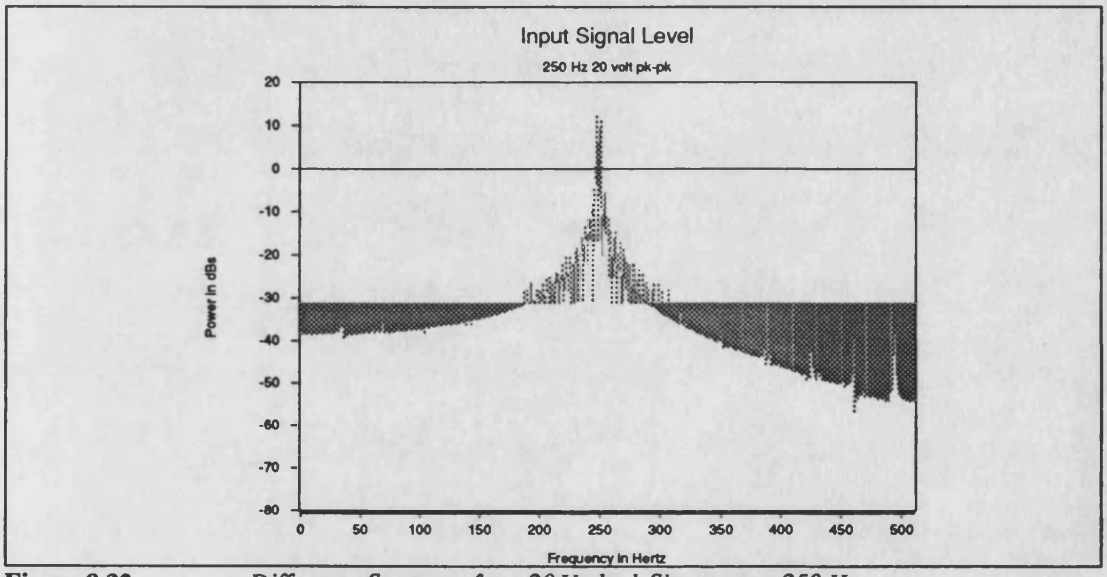

Figure 8.32 *Difference Spectrum for a 20 V pk-pk Sinewave at 250 Hz*

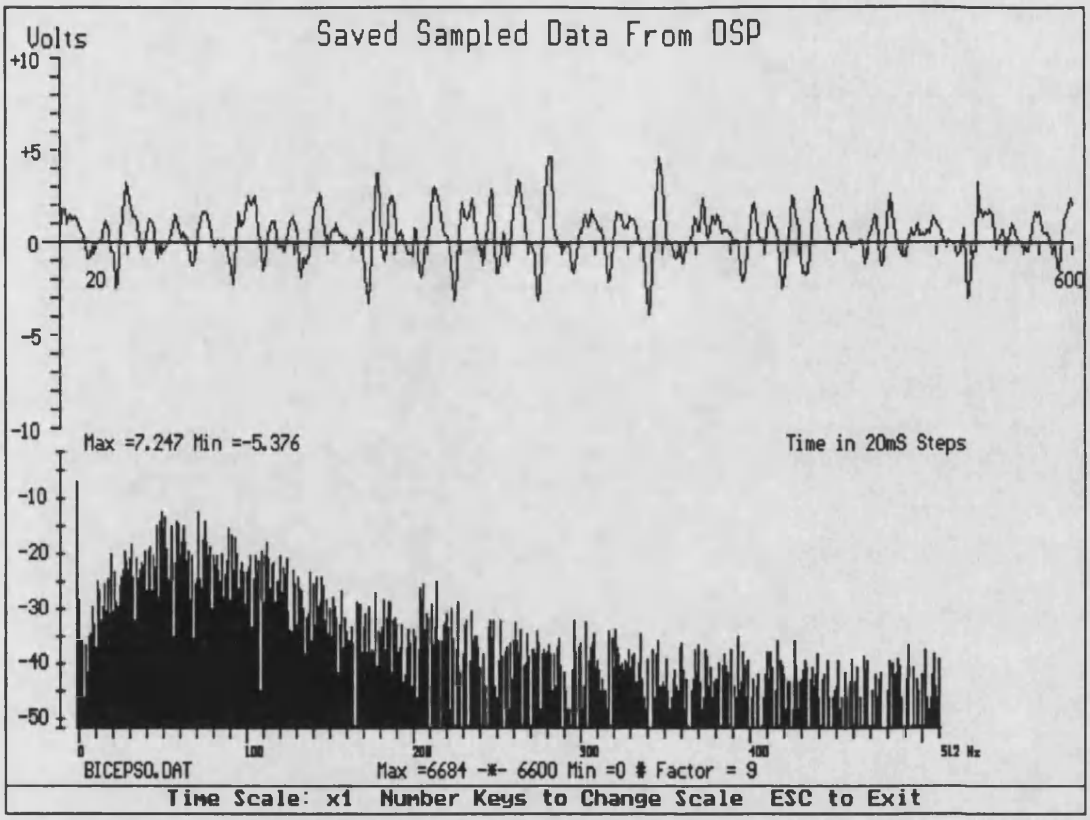

Figure 8.33 *DSP Data for a Voluntary Muscle Response*

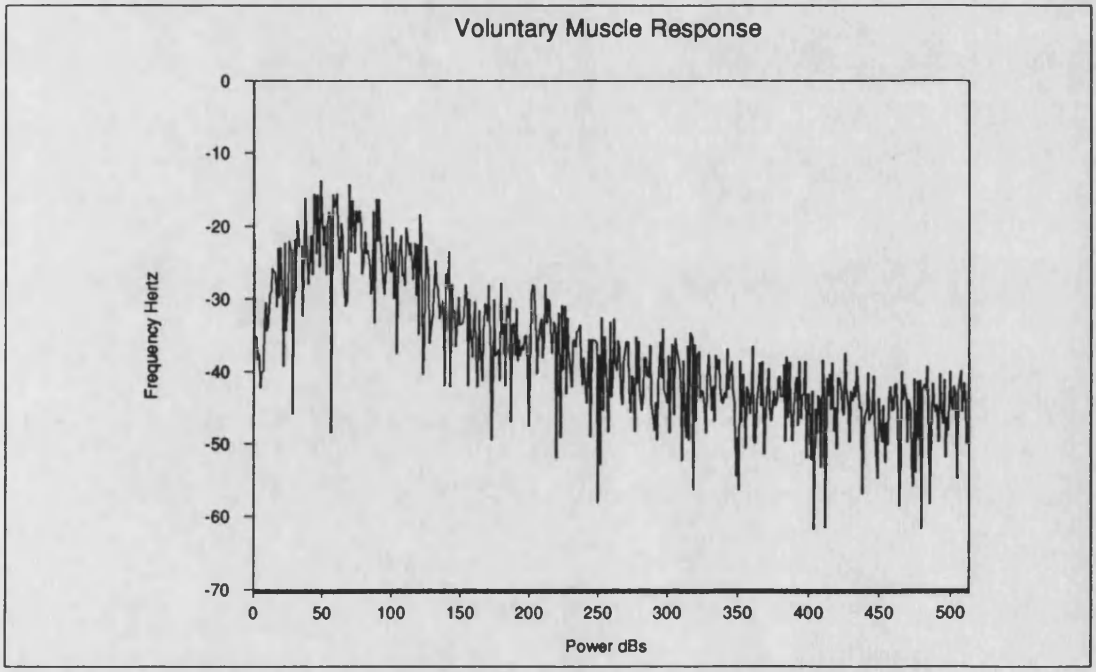

Figure 8.34 *Calculated Spectrum for the Voluntary Muscle Contraction shown above*

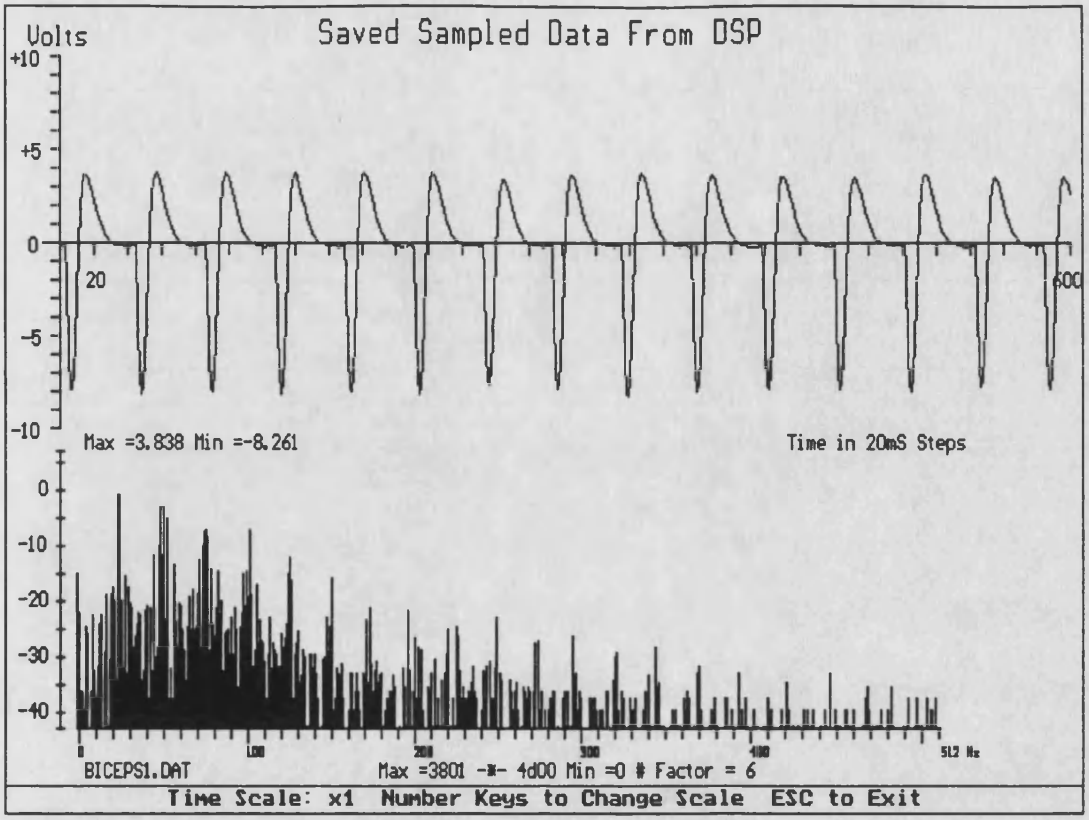

Figure 8.35 *DSP Data for a CAP Train*

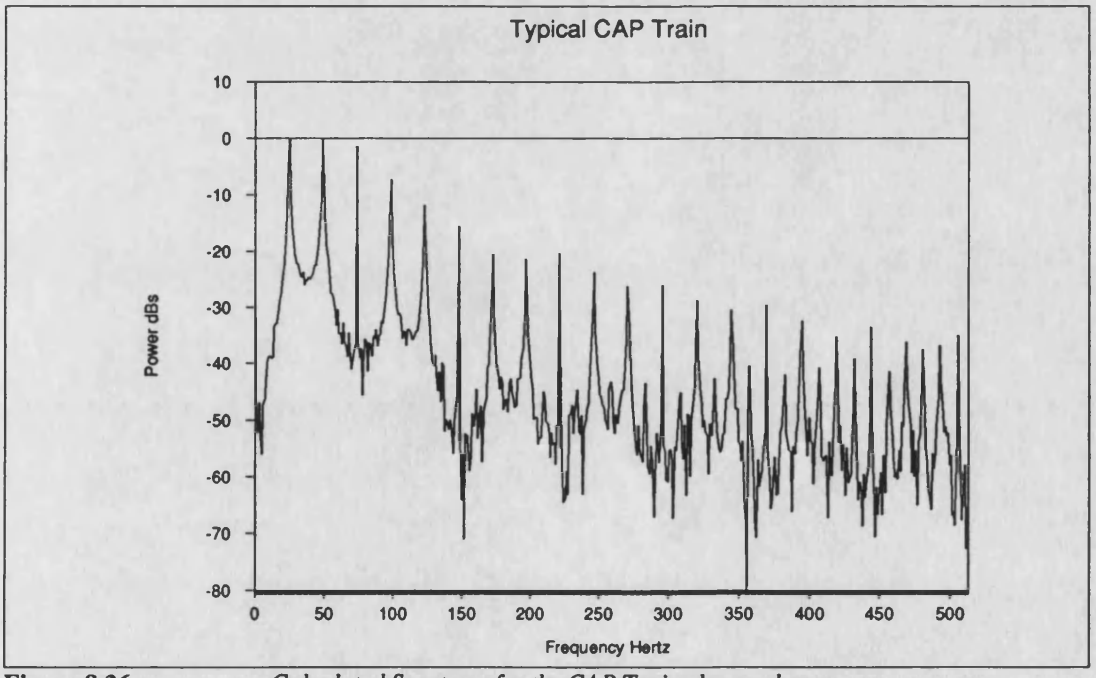

Figure 8.36 *Calculated Spectrum for the CAP Train shown above*

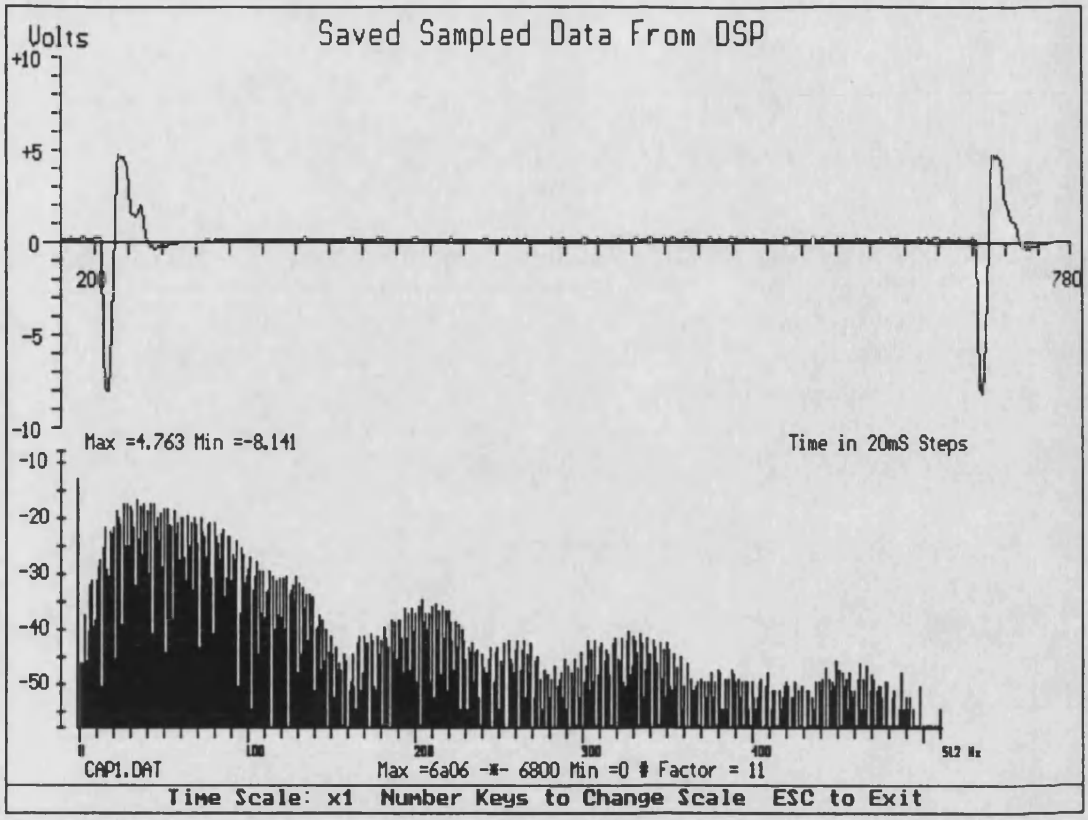

Figure 8.37 *DSP Data for a CAP Pair*

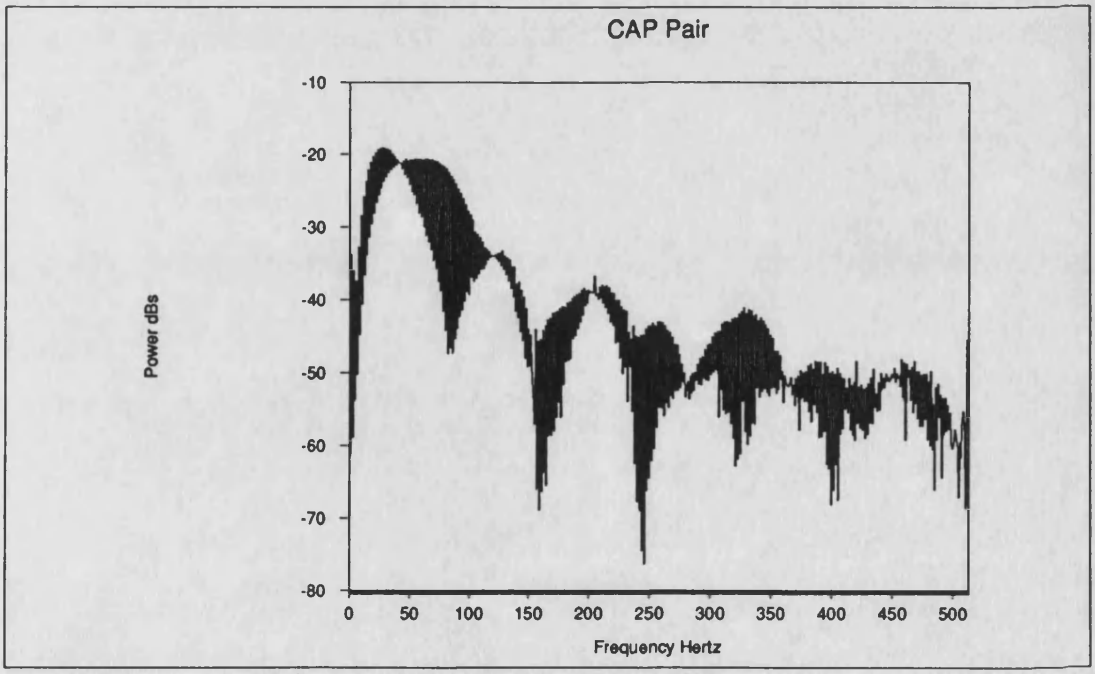

Figure 8.38 *Calculated Spectrum for the Single CAP shown above*

Chapter 9

Results

The purpose of this chapter is not to provide conclusive medical evidence of muscle biopotential changes with fatigue during stimulation. Instead it aims to demonstrate the effectiveness of the equipment designs. At this stage of the research, equipment has been built that has been shown to give a good indication of the input signals median frequency and power with time. The parameters chosen being the ones suggested in the literature and discussed in Chapters 2 and 3 as being signals, possibly suitable for the derivation of feedback information for closed loop FES systems. The new equipment provides a means to suppress the artefact contamination of the CAP trains, thus permitting a more accurate calculation of parameters. The results are intended to show that the equipment is capable of giving some indications of fatigue and force changes but that further investigations need to be carried out to identify whether the repeatability and reliability are sufficient for a closed loop controller.

The results fall into two main categories:-

Qualitative Results. The original printer port Atari system was not really capable of functioning as much more than a qualitative system. That is the results obtained would indicate trends based on a known time scale but the values of the power signals could only be considered relatively because of the lack of linear calibration. The software provides no means of autoscaling the power display so that results would often overflow the display range. Similarly, the absolute values of the frequency components would only be of value when being compared to the other components in the sample and within the test. Comparison of these values with previous and future tests in other than a qualitative manner was not valid.

Quantitative Results. The new system, described in section 7.3, set out to improve on the qualitative results and provide a means of quantifying the values in terms of signal power so that the results obtained from different individuals could be compared. The results obtained from this system therefore give a quantifiable measure of the signal power as well as the frequency. This allows the results from different sets of tests and even different subjects to be compared.

9.1 Atari System

At the start of this research it was assumed that a 'standard' stimulator would be used for the eliciting of a tetanic muscle contraction. Thus for the original Atari system the stimulation was provided by the standing stimulators described by Ewins[75] and Welch[210] as part of their research into closed loop standing. The synchronisation

pulses in this system being pulses equivalent to the stimulus pulse, but of a CMOS logic level. It is because of the use of 'standard' stimulators, that the original stimulation test results presented here, were all carried out on paraplegic subjects.

9.1.1 Protocol

The subjects were all paraplegics taking part in the standing program either based at Odstock Hospital, Salisbury or at Marie Thérèse House, Hayle. The tests were carried out in two ways:

- By recording the CAP train from the quadriceps during a normal stimulated stand session.
- By recording the CAP train from the quadriceps whilst the subject remained seated in their chair. The quadriceps were stimulated until the leg extended approximately horizontal then this stimulus level was maintained until the muscle was completely fatigued and no tetanic contraction obtained ie the leg dropped to the floor.

9.1.2 Results

The results are presented as screen dumps taken from the median frequency display program. This method for the recording of results was all that was available in the original Atari system. Since the aim was to show trends this is exactly what this form of display could do.

Figure 9.1 shows a series of four separate stands which are marked by the arrows. After each stand the subject was allowed ten to fifteen minutes to recover before attempting a another stand. The plot does not show this because the system would only record results if the stimulator was functioning, thus the display looks as if the results were recorded back to back. All four stands show very similar trends in the

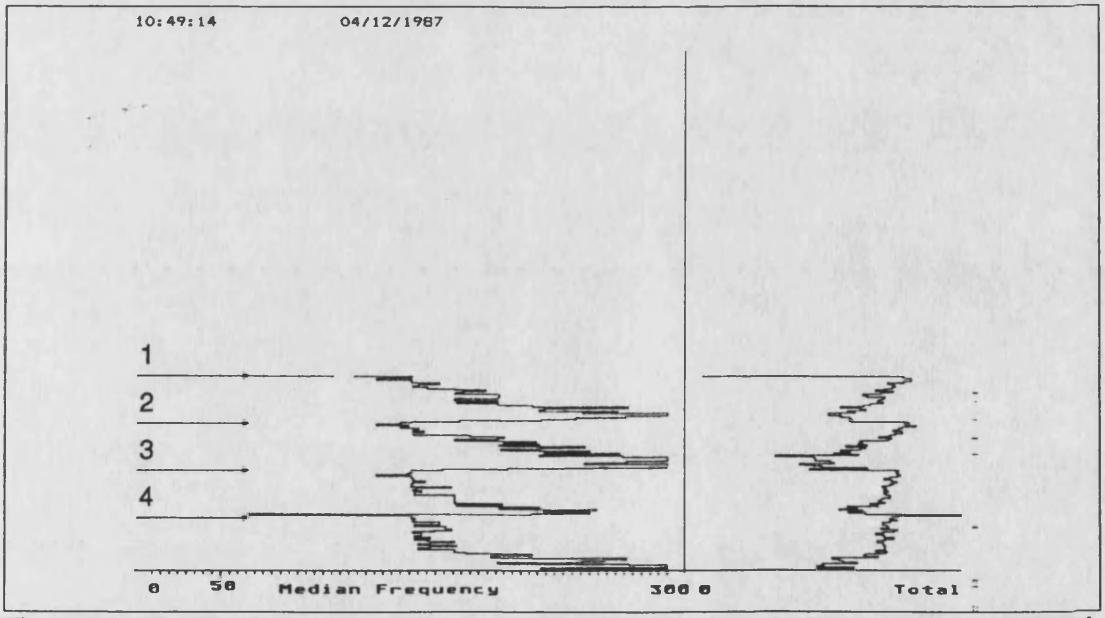

Figure 9.1 *First Results showing a Clear Frequency Shift in the Opposite Direction to that Expected*

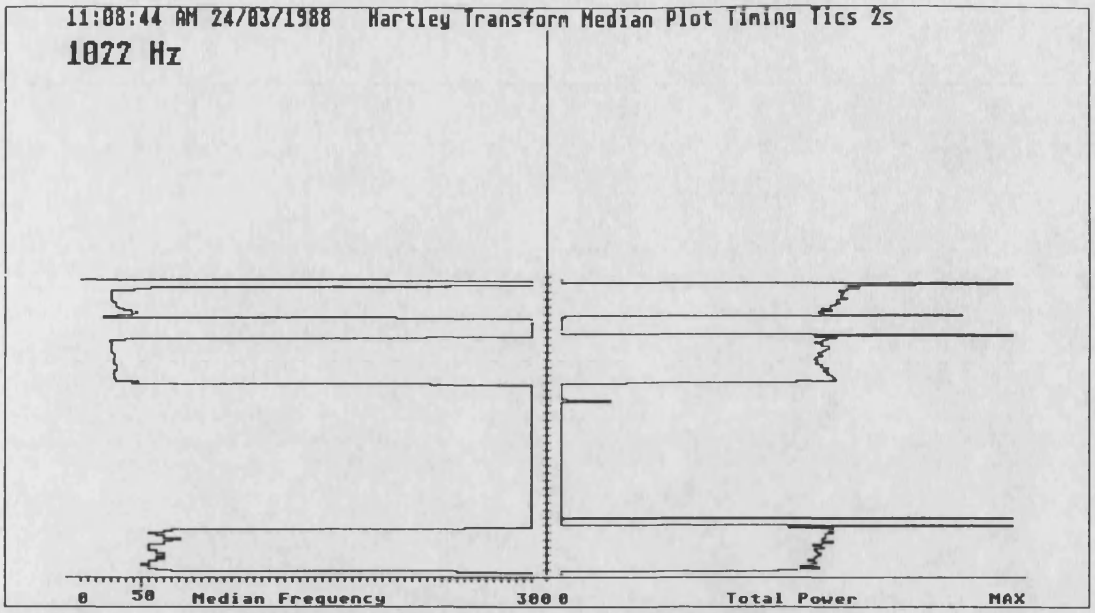

Figure 9.2 *Plot Showing Other trends in Power and Median Frequency*

median frequency, with each starting at approximately the same frequency then rapidly rising. The power also shows a similar pattern, falling rapidly off in each case although the peak starting power does reduce with the later stands.

Figure 9.2 shows three further sessions on the same male subject as in the previous figure. These results are from the latest version of the Atari system software using the Hartley transform and providing a time scale. The number in the top left is the last calculated median frequency value. These results were obtained from the horizontal

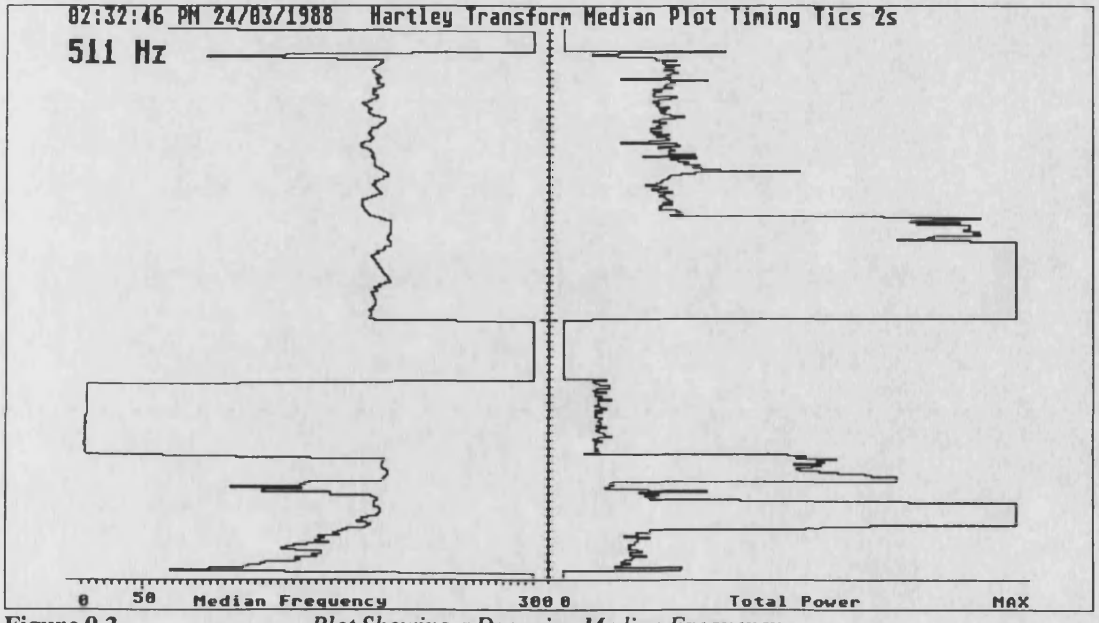

Figure 9.3 *Plot Showing a Dropping Median Frequency*

leg test and not from the subject whilst he was standing. The gap in the recordings now reflects the time between tests. In the first two tests the median frequency rises whilst in the last, where the electrodes had been adjusted, the median frequency

reverses direction. The other interesting point about these results is that the median frequency was much lower than previously recorded. This may have been due to the tests being carried out after a morning of standing tests so the subject's muscles were already fatigued.

Figure 9.3 shows the results for a different subject to the previous tests. The plot shows two tests carried out using the horizontal leg test with weights added to the ankle to increase the fatigue rate. The first test shows a fluctuating median frequency in which no real trend is discernible. The second test shows a quite rapid drop in the median frequency of the subject as would be expected from the literature for voluntary responses. The rate of change is faster than for voluntary muscles but this would also be expected, since stimulated muscle fatigues far faster than voluntarily contracted muscle. The power shows a gradual drop not as pronounced as in the previous subject.

Figure 9.4 shows the results from a third subject once again doing the horizontal leg test with weights. Here there are three tests where the median frequency rises throughout the test but peaks each time at a lower value. However, the power drops during each stand but starts at a high level in each test. This could be due to the increased stimulus level required each time to get the leg into the horizontal position. Actual values for the stimulating voltage could not be recorded with this configuration.

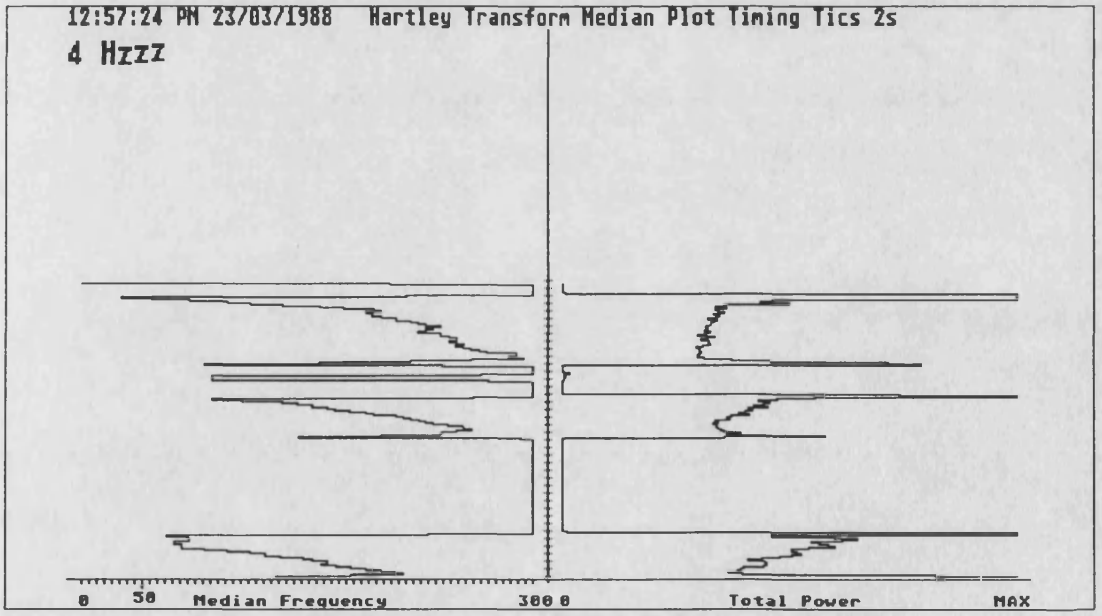

Figure 9.4 *Second Subject Displaying Rising Median Frequencies with Fatigue*

A feature of the horizontal leg tests that was repeatedly observed was that as the leg fatigued it would slowly drop to the floor but then it would suddenly start to rise again towards the horizontal position before dropping again. This could be repeated a number of times before the leg finally fatigued. These observations were usually in the

period when the leg could no longer provide sufficient force for the subject to stand. There were no obvious changes in median frequency to match this but it was observed in more than one subject.

9.2 DSP System

The investigations carried out with the original system indicated a number of sources for the artefact effects. These were discussed in detail in Section 4.5 and lead to the designs described in Chapter 5, Section 6.3, Section 7.3. The tests that are described in this section are aimed at showing:

- The correct functioning of the analysis system for voluntary muscle responses.
- The effectiveness of the artefact removal system and how the two different stimulator output stage designs have a bearing on this.
- The correct functioning of the analysis system for stimulated CAP train analysis.
- The relationship between stimulus rate and sample size.

9.2.1 Voluntary Muscle Responses

In assessing the Bath University Muscle Fatigue Monitor described in Appendix B, a series of fatigue tests were carried out to investigate the systems ability to track the changes in median frequency. For the tests described here on the analysis system the same protocol has been used. Two subjects were tested: one female and the other male. This is important because of the differing distribution of fat in the two sexes which can give differing effects due to the impedance changes caused by fat layers as discussed in Section 4.1.5. Since only 2 people have taken part in these tests they only serve as an indicator of trends.

9.2.1.1 Protocol

Two muscle groups have been tested using isometric contractions. The muscle groups chosen were the biceps and quadriceps muscle groups.

For the biceps test, the subjects were required to stand upright whilst holding either a 5 kilogram dumb-bell or using up to two wrist weights of 1.1 kilogram each. The forearm was required to be maintained at the horizontal with the palm supinated—facing upwards—for the duration of the test. That is, the arm was bent at right angles at the elbow with the forearm extended in front of the body. This arm positioning is shown in Figure 9.5. The weight is held in the hand or wrapped around the wrist, with its force acting as shown. The muscle signals were detected by the EMG probe which is placed along the length of the muscle over the belly of the biceps with the earth strap being connected to the wrist of the subject. The test was considered complete when the subject was unable to continue to maintain the forearm horizontally. The male subject was able to use both the 5 Kg dumb-bell and 2.2 Kgs of

wrist weights for two separate tests. The female could only manage the 1.1 Kg wrist weight for her two tests one on each arm.

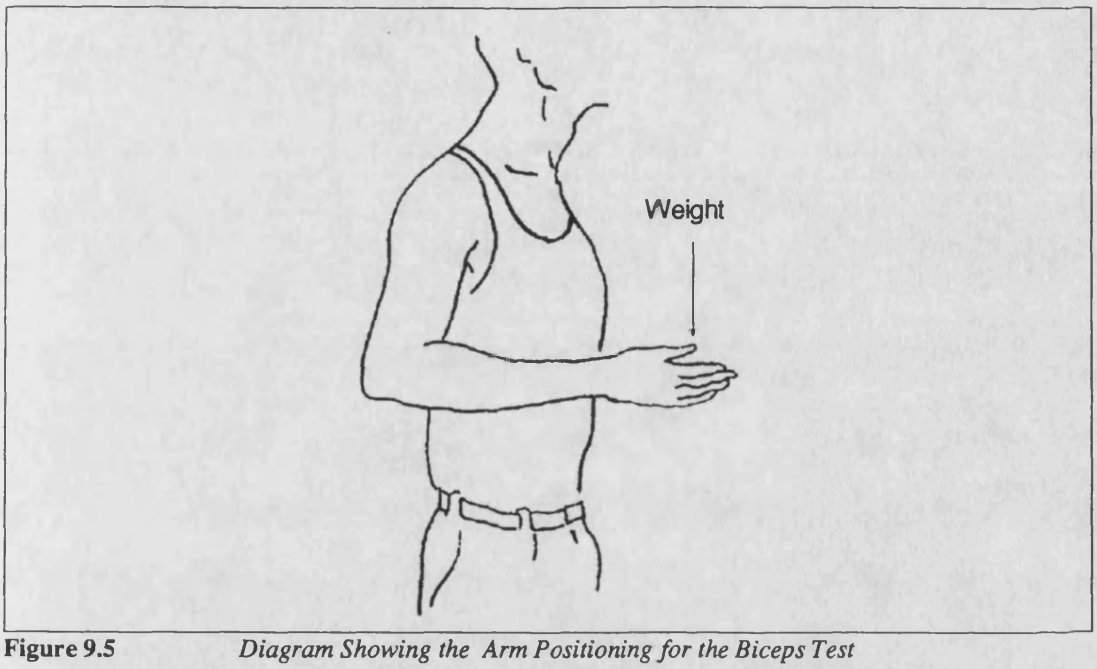

Figure 9.5 *Diagram Showing the Arm Positioning for the Biceps Test*

For the quadriceps test, the subject sat on a chair with the thigh resting on the chair. The lower leg was then extended horizontally out in front and loaded at the ankle with weights up to 2.2 kilograms. The knee was acting as the fulcrum in this test. Once again the subject was required to maintain this position for as long as they could. The EMG signal was recorded from the belly of the most prominent quadriceps muscle which would usually be either the vastus lateralis or rectus femoris muscle. The earth strap was connected to the ankle of the subjects. In this case the male was tested with 1.1 Kgs of weight and 2.2 Kgs of weight whilst the female was tested with just the 1.1 Kg weight. Both subjects were tested on both their left and right legs.

9.2.1.2 Fatigue Results

The results are presented as a set of three plots. The first two are 0.5 second plots of the sampled EMG taken at the start and end of each of the tests. These serve as a visual indicator of some of the more obvious changes in the EMG signal. The third plot is a screen dump of the Atari median frequency and power display screen taken at the end of the test. These show the trends in the median and power over the duration of the test. Two of the scale options available on the power scale have been used for these recordings. The scales are governed by a log scaling algorithm, thus there is only the choice of a full scale display of 1 V^2/Hz or 10 V^2/Hz and neither of these have matched the signal size well.

9.2.1.3 Results from Female Subject

The results for the left and right leg of the female are shown in Figures 9.6 to 9.11 inclusive. Figures 9.6 and 9.9 show the recorded EMG at the start and Figures 9.7 and 9.10 show the recorded EMG at the end of the tests for the left and right leg respectively.

The trend in the median frequencies is clearly visible in both the right and left leg for the female subject with her left leg lasting about a minute longer than the right leg. The power plots were plotted on the 10 V^2/Hz plot and show no real trend on this scale.

The EMG 'snapshots' for the legs both show a clear reduction in signal size and in the 'spikiness' of the EMG signal. The right leg has generally a slightly larger amplitude when compared with the left leg at the end, which may suggest it was not as tired. However it is difficult to make such deductions from two 500 msec samples from a total time of 4 and 3 minutes for the left and right leg respectively.

Figures 9.12 to 9.17 show the results from the left and right arm of the female subject. In these tests the female subject could only manage the 1.1 Kg wrist weight with the 2.2 Kg weight being too heavy for her. This unfortunately meant that the fatigue rate was slower than the display range of the median and power display. This display is tailored to match a typical stand time for the paraplegics which is usually no more than ten minutes and often less.

The EMG waveforms for the left and right arms of the female subject show little change over the duration of the test. In the case of the left arm results, shown in Figures 9.12 and 9.13, the sample recorded at the end of the test shows a spikier and slower waveform when compared to the one at the start. As explained above these samples are not very representative and as is seen in the median plot described below, the reduced frequency is not reflected by a clear droop.

The median frequency plots of Figures 9.14 and 9.17 show no visible trend which is probably due to the lightness of the load used. The power display this time uses the 1 V^2/Hz max display and shows a great deal of variability. The left arm power does show a slight trend upwards in power over the duration of the test.

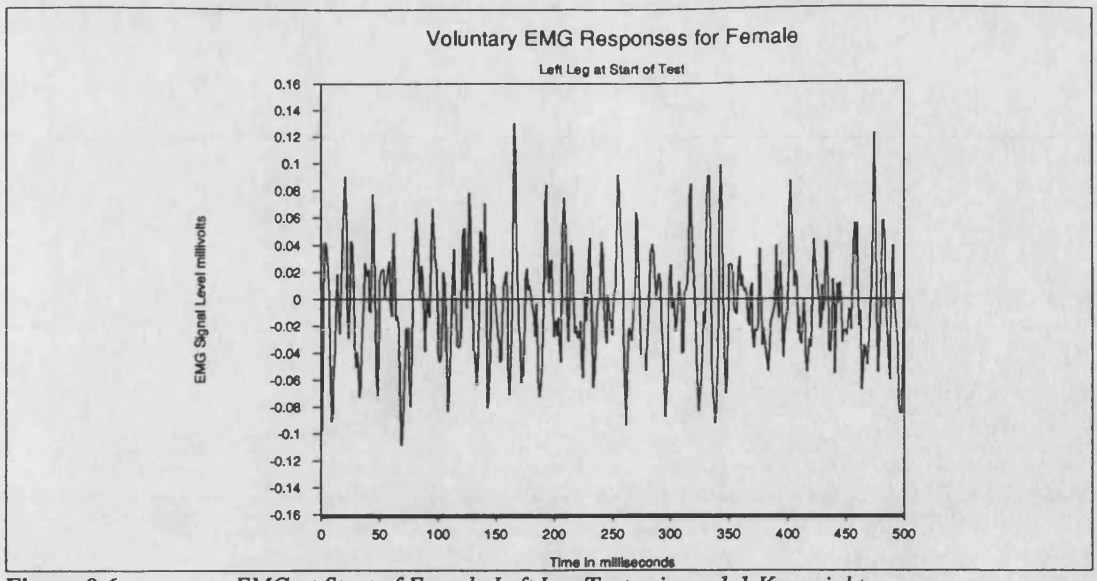

Figure 9.6 *EMG at Start of Female Left Leg Test using a 1.1 Kg weight*

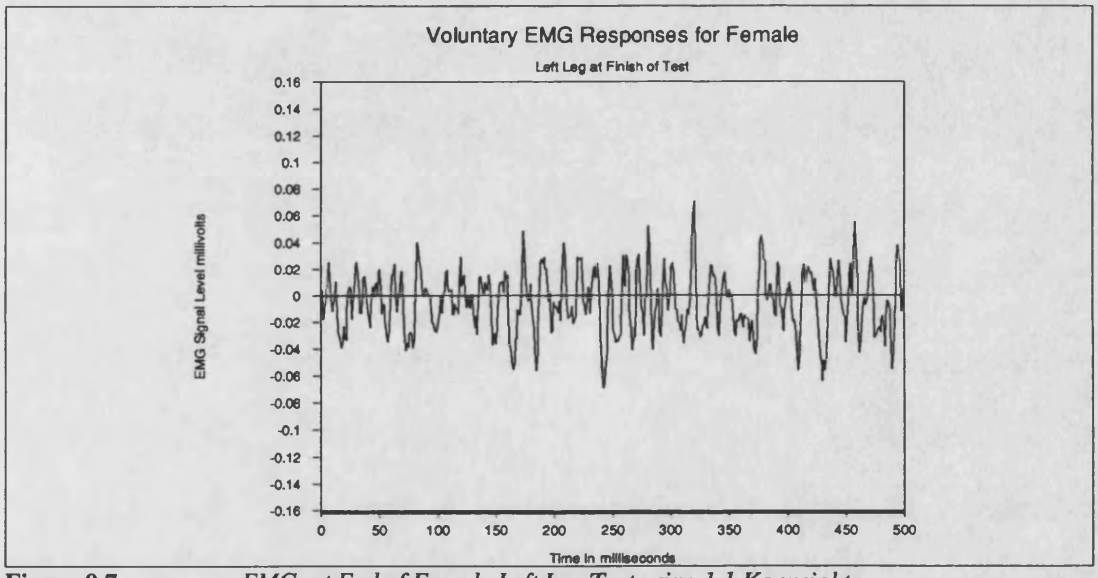

Figure 9.7 *EMG at End of Female Left Leg Test using 1.1 Kg weight*

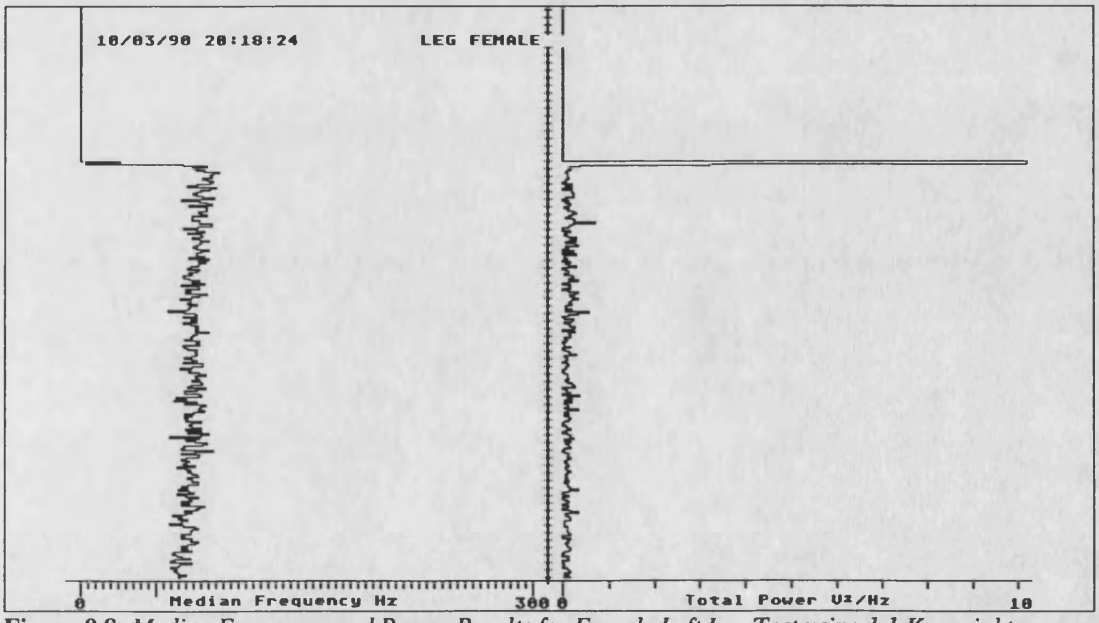

Figure 9.8 *Median Frequency and Power Results for Female Left Leg Test using 1.1 Kg weight*

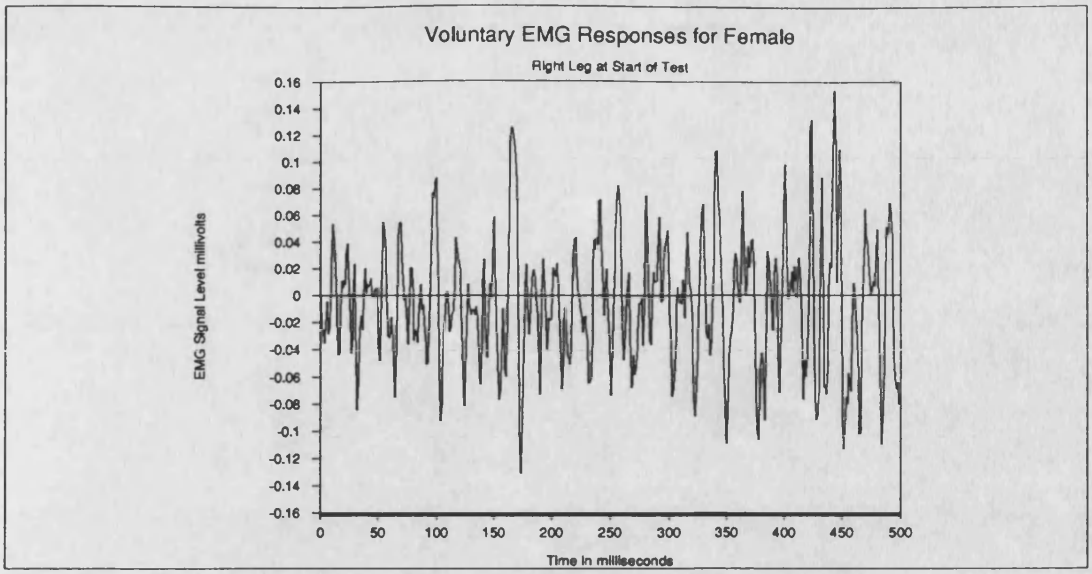

Figure 9.9 *EMG at Start of Female Right Leg Test using 1.1 Kg weight*

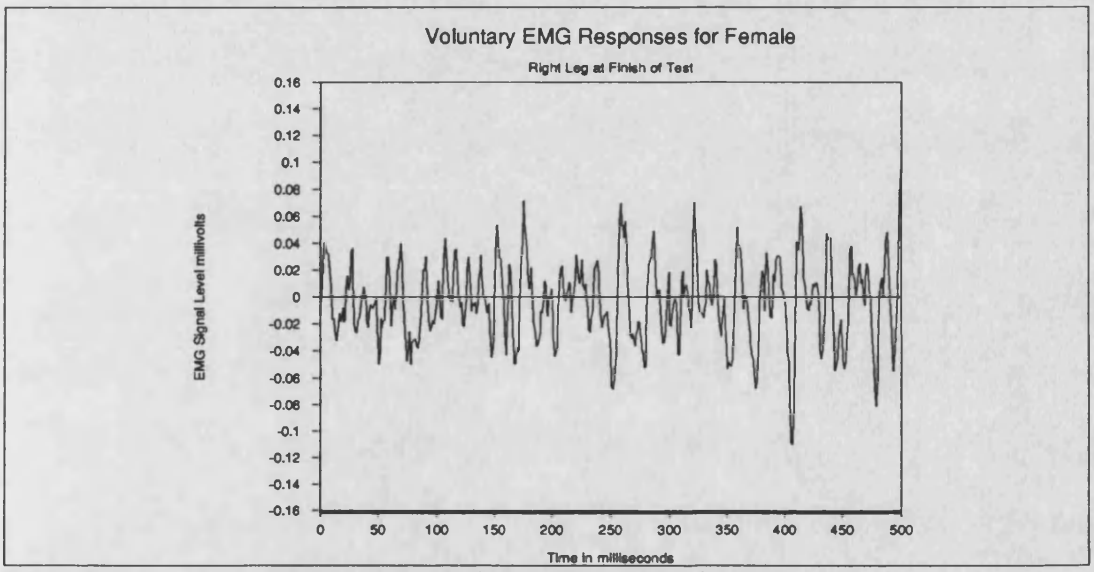

Figure 9.10 *EMG at End of Right Leg Test using 1.1 Kg weight*

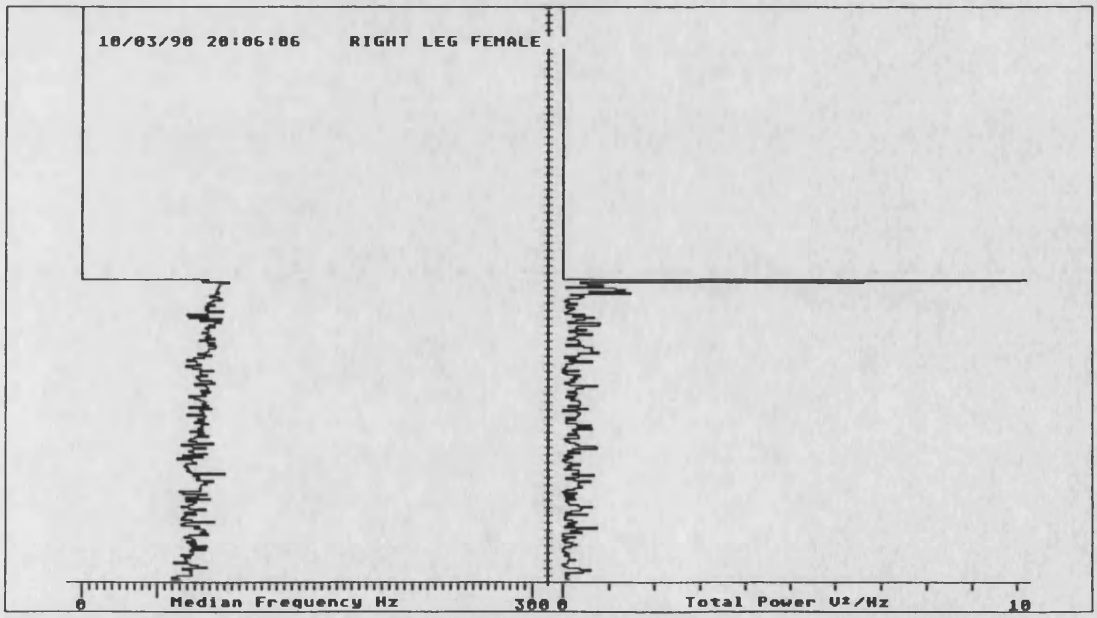

Figure 9.11 *Median Frequency and Power Results for Female Right Leg Test using 1.1 Kg weight*

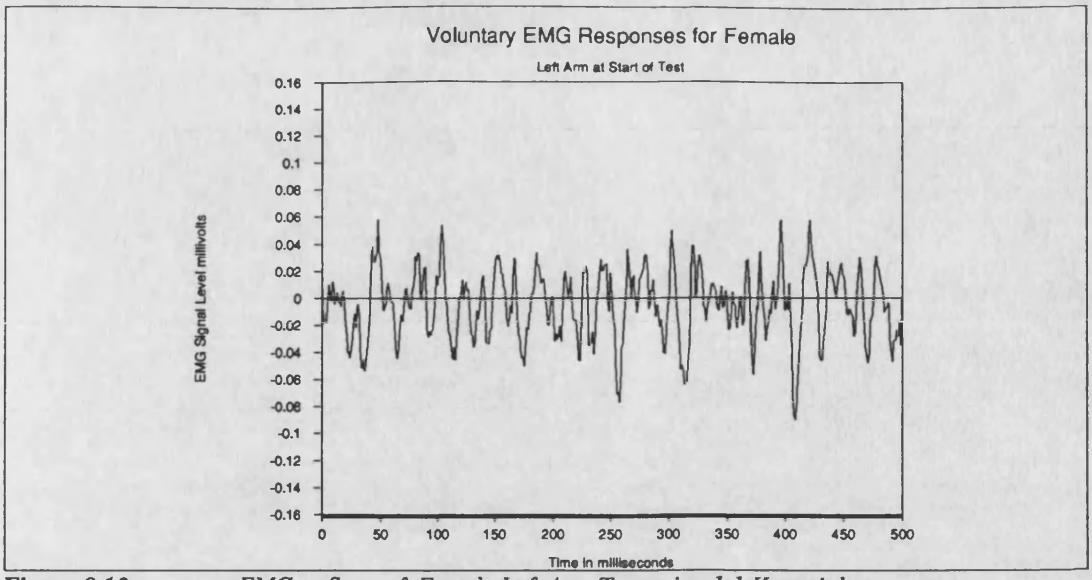

Figure 9.12 *EMG at Start of Female Left Arm Test using 1.1 Kg weight*

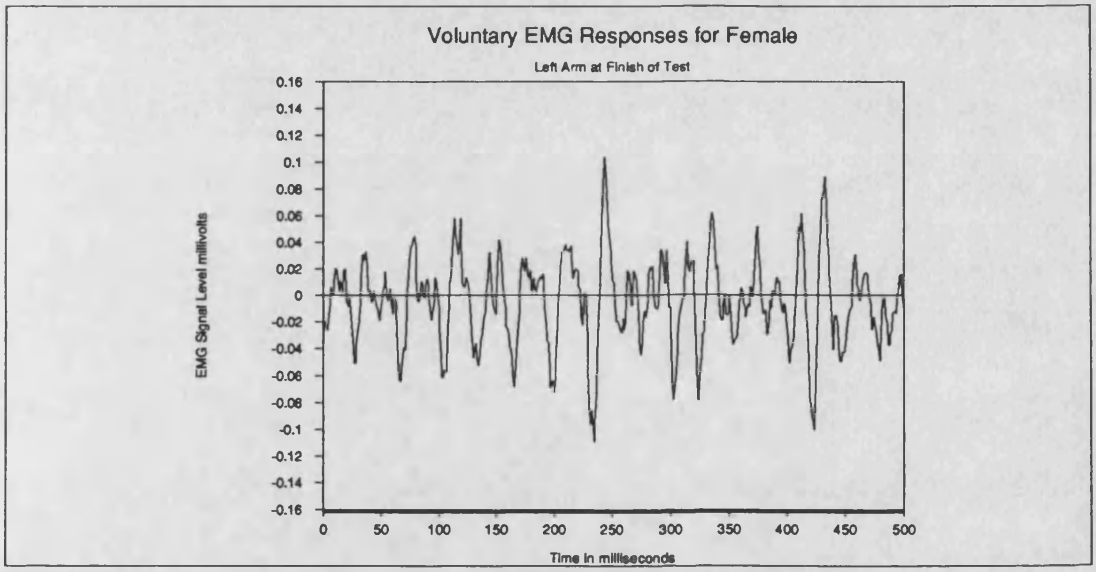

Figure 9.13 *EMG at End of Female Left Arm Test using 1.1 Kg weight*

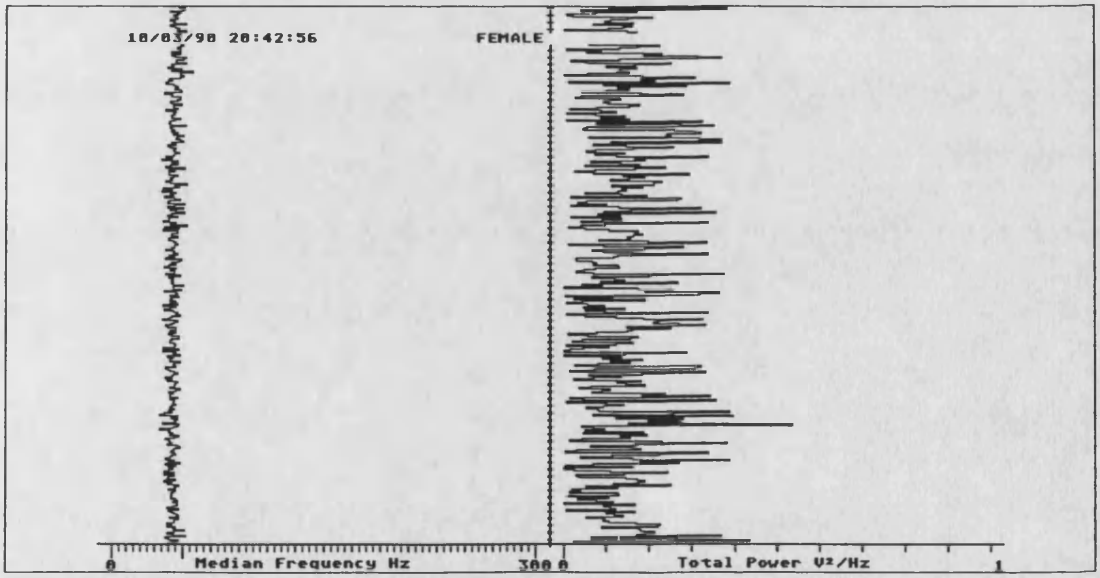

Figure 9.14 *Median Frequency and Power Results for Female Left Arm Test using 1.1 Kg weight*

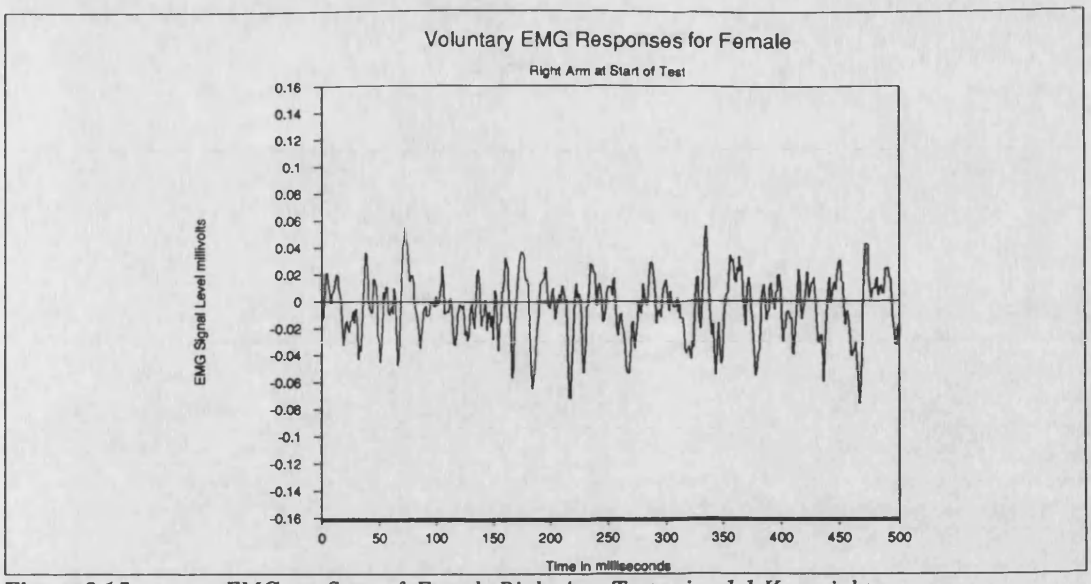

Figure 9.15 *EMG at Start of Female Right Arm Test using 1.1 Kg weight*

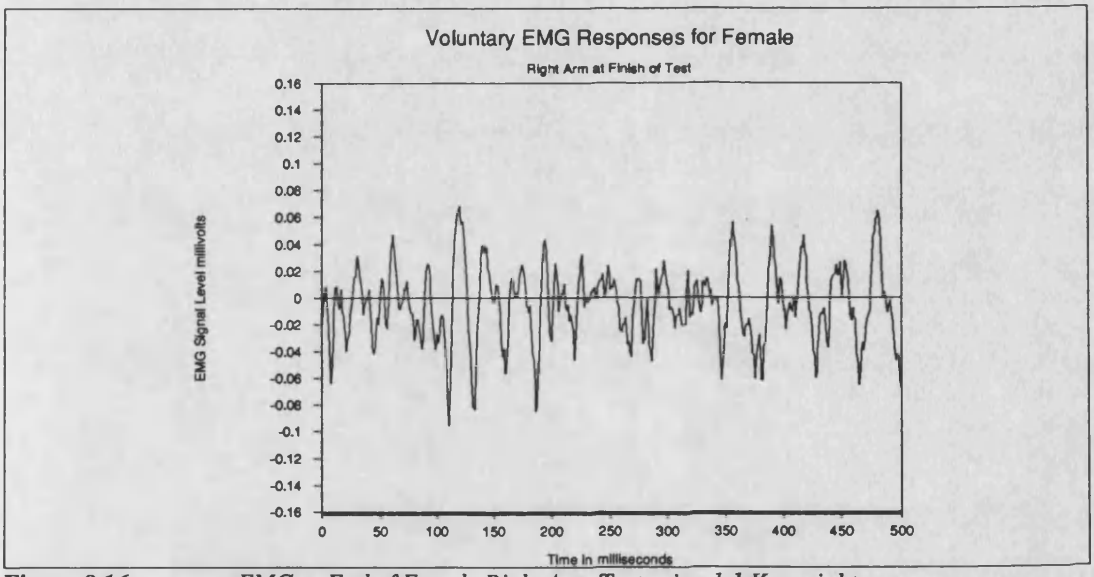

Figure 9.16 *EMG at End of Female Right Arm Test using 1.1 Kg weight*

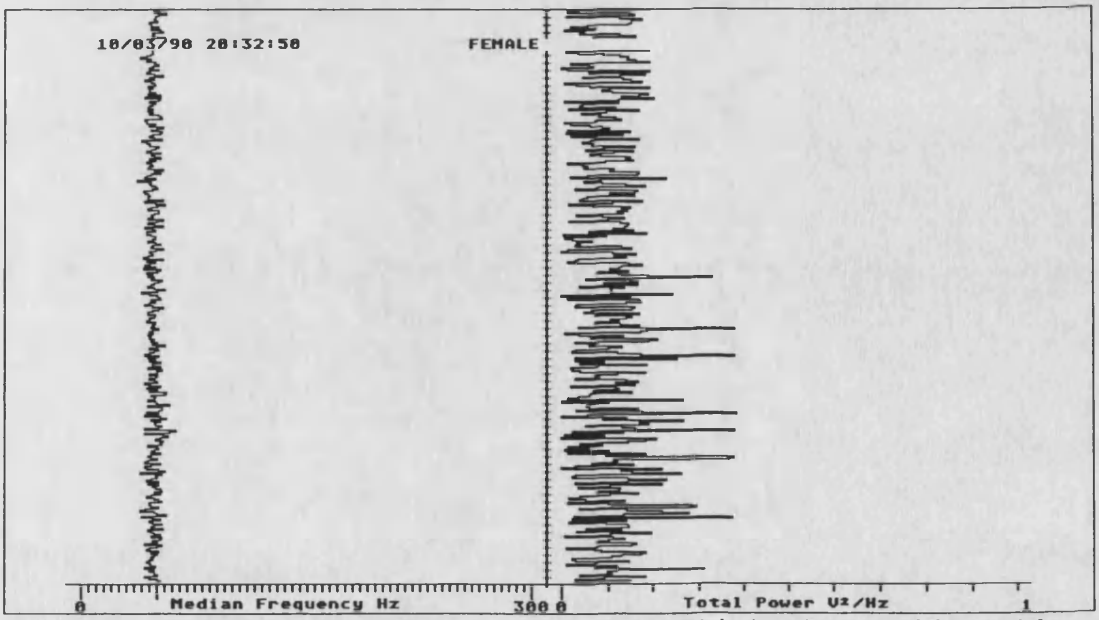

Figure 9.17 *Median Frequency and Power Results for Female Right Arm Test using 1.1 Kg weight*

9.2.1.4 Results from Male Subject

Included with the male results are just two sets of plots of the EMG signal. These are included because they show some slightly different features to those observed with the female subject. Figures 9.21 and 9.22 show the start and end of the extra right leg test using the heavier weight and Figures 9.24 and 9.25 show the EMG at the start and end of the right arm test.

The male fatigue tests on each leg as described in the protocol were carried out using two different weights. The lighter 1.1 Kg load was used for the first tests and the results are shown in Figures 9.18 and 9.19 for the left and right leg respectively. The median frequency for the left leg shows a drop in frequency over the 5 minutes of the test whilst the right leg shows no significant change for the eight minutes displayed.

The power from leg muscle of the male subject is significantly higher than for the female subject. The power display for the left leg shown in Figure 9.18, uses the 1 V^2/Hz display. It can be seen that the left leg results show a a great deal of power variation with the general trend being towards an increased signal size. The right leg results using the 1.1 Kg weight are shown in Figures 9.19. This tess uses a power scale of 10 V^2/Hz and the signal does not appear to be as variable as the left leg, however there is an increase in signal fluctuations as the test ends.

The results for the 2.2 Kg weight tests on the left and right leg of the male subject are shown in Figures 9.20 and 9.23 respectively. The start and end EMG samples for the right leg tests are shown in Figures 9.21 and 9.22 respectively.

The results for the median frequency plots for both legs show a drop in frequency as would be expected. The right leg, which showed very little change with the lighter load, showed a clear trend with the increased load. The power display once again uses the 1 V^2/Hz scale for the left leg and the 10 V^2/Hz for the right leg. The left leg power shows a rise and a fall but with massive variations which tend to hide the trend. The right leg shows a consistent increase in power throughout the test.

With both of these tests the muscles of the subject showed significant trembling towards the end of the test. The EMG signals for the right leg test reflect this. The results for the start of the test show a relatively low signal level of quite a high frequency with sporadic spikes. By the end of the test this had changed to bursts of spikes followed by periods of relative quiet. This could explain the trembling that the fatiguing muscle showed, though it is possible some of the effect is due to artefacts caused by the trembling muscle.

Figures 9.24 to 9.29 show the results of the two weight tests on the right arm of the male subject. The median frequency plots show a much greater frequency drop with

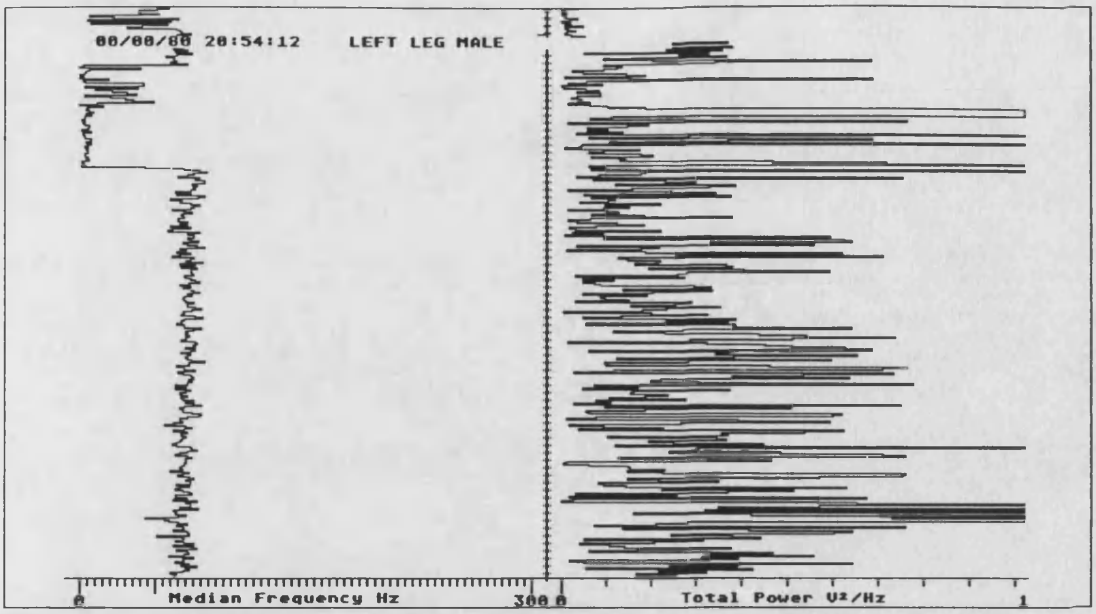

Figure 9.18 *Median Frequency and Power Results for Male Left Leg Test using 1.1 Kg weight*

the 2.2 Kg weight than when using the 5 Kg weight, which may be due to the electrode positioning in the former case being better. The sudden increase in the median frequency at the end of the 2.2 Kg test shown in Figure 9.26 is due to the subject being allowed sight of his results which was avoided in all the other tests until the test was completed. As is discussed in greater detail in Appendix B this was found to effect the rate of decay of the median frequency. Once again the 10 V^2/Hz scale was used and no discernible trends can be seen.

The EMG plots for the 2.2 Kg weight shown in Figures 9.24 and 9.25 show a remarkably spikey waveform at the start of the test which is considerably reduced in amplitude by the end of the test. The two particular samples taken here would suggest

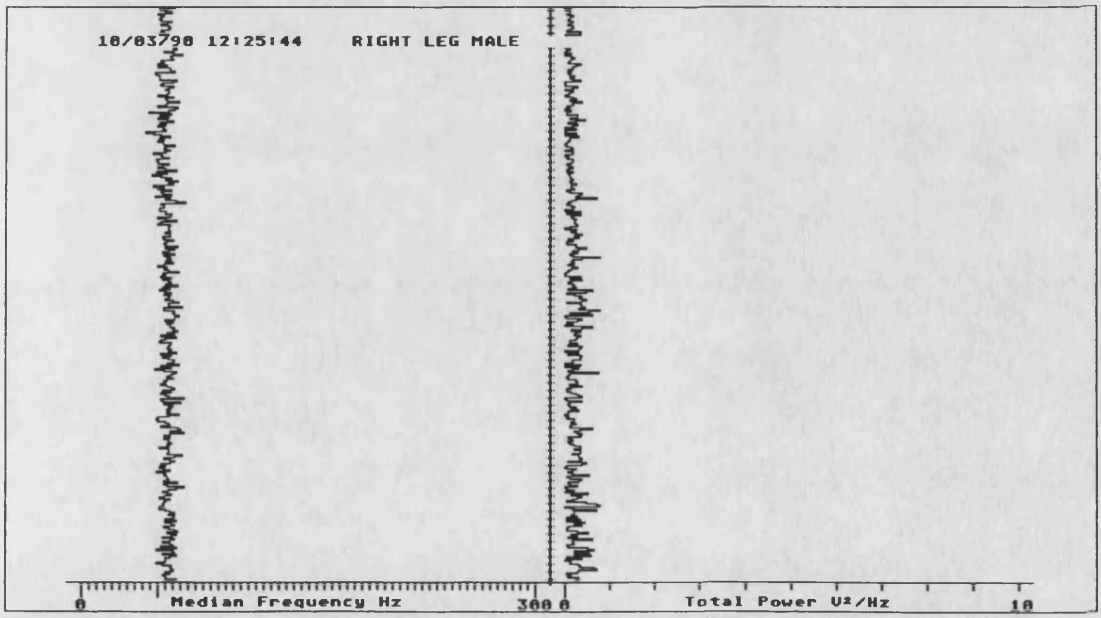

Figure 9.19 *Median Frequency and Power Results for Male Right Leg Test using 1.1 Kg weight*

that the EMG may have increased frequency but as explained earlier this is more likely due to the particular time the sample was taken.

The EMG plots for the 5 Kg weight shown in Figures 9.27 and 9.28 a significant increase in the spikiness of the recorded samples between the start and the finish of the test. This increased spikiness is associated with a reduction in the frequency of the zero crossings as would be expected.

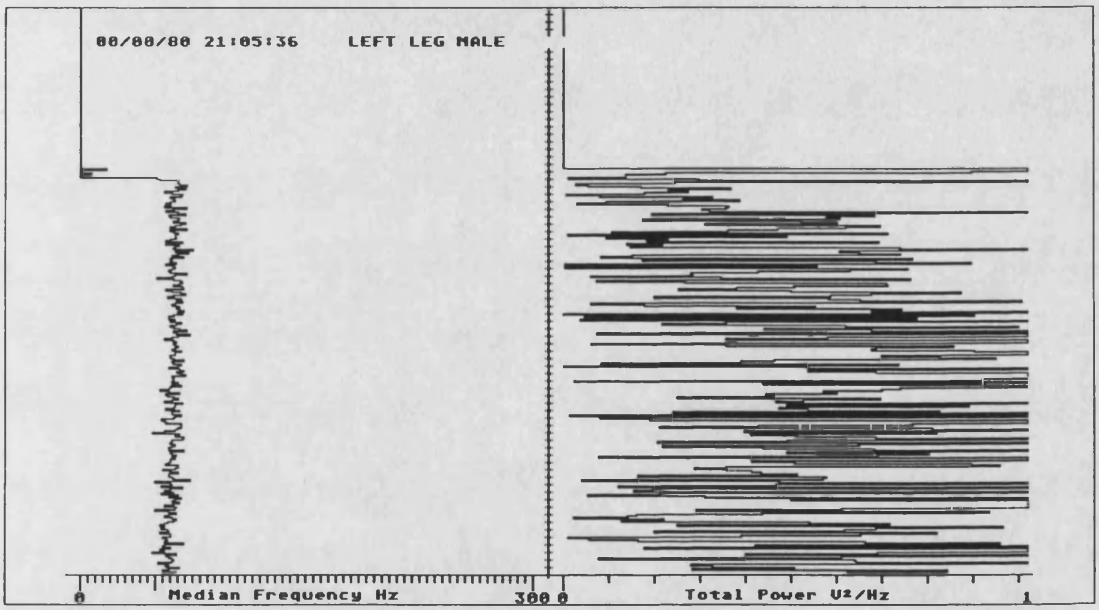

Figure 9.20 *Median Frequency and Power Results for Male Left Leg Test using 2.2 Kg weight*

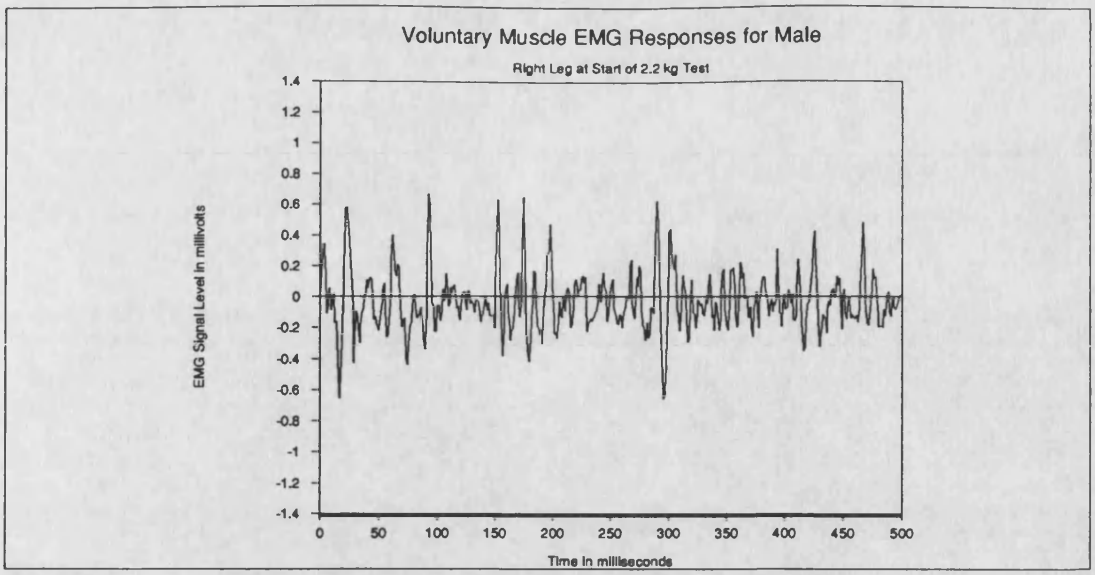

Figure 9.21 *EMG at Start of Male Right Leg Test using a 2.2 Kg weight*

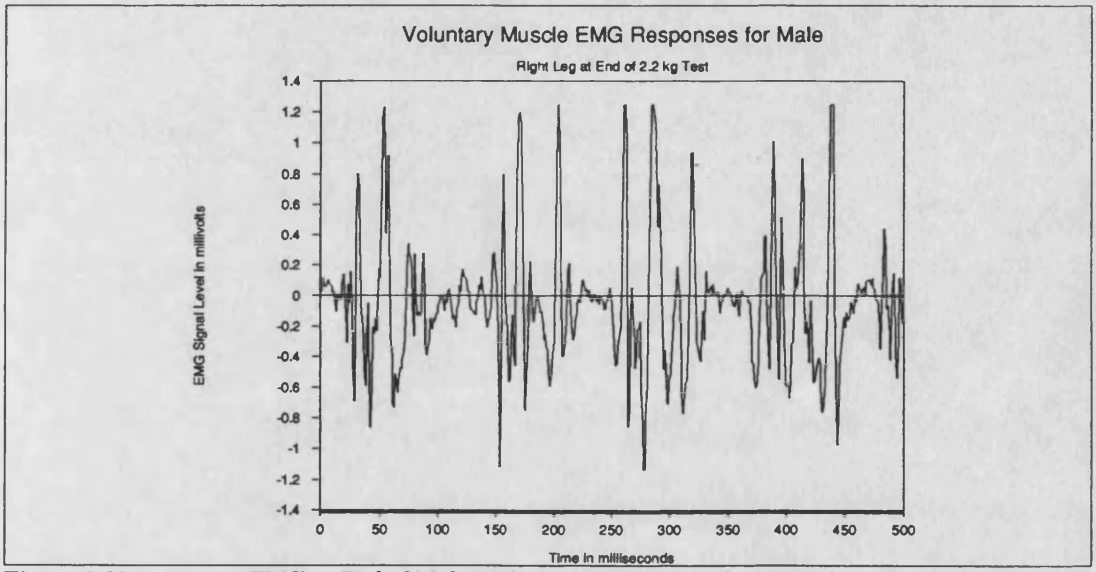

Figure 9.22 *EMG at End of Male Right Leg Test using 2.2 Kg weight*

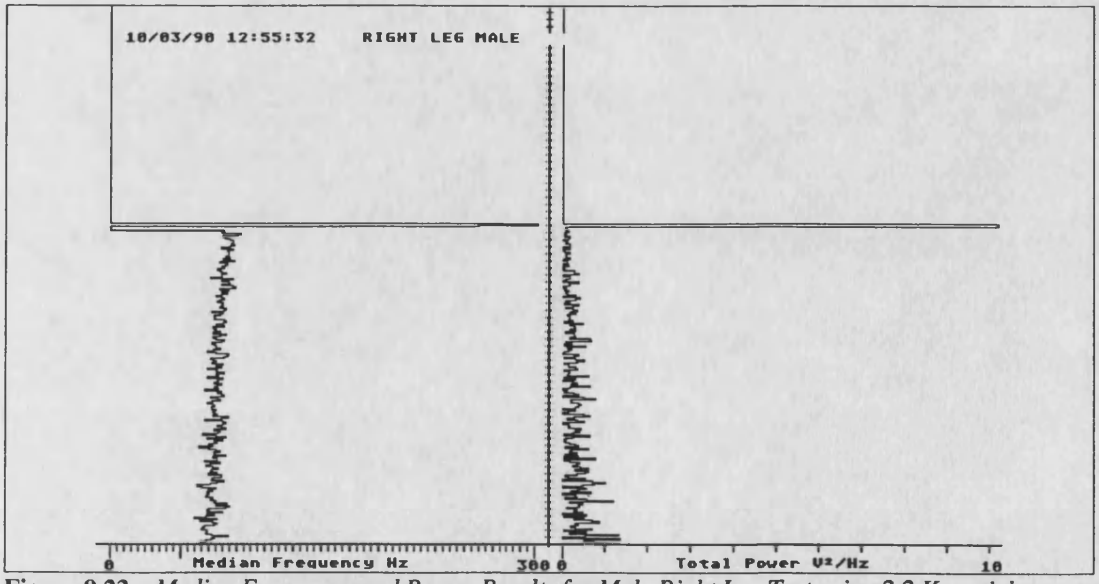

Figure 9.23 *Median Frequency and Power Results for Male Right Leg Test using 2.2 Kg weight*

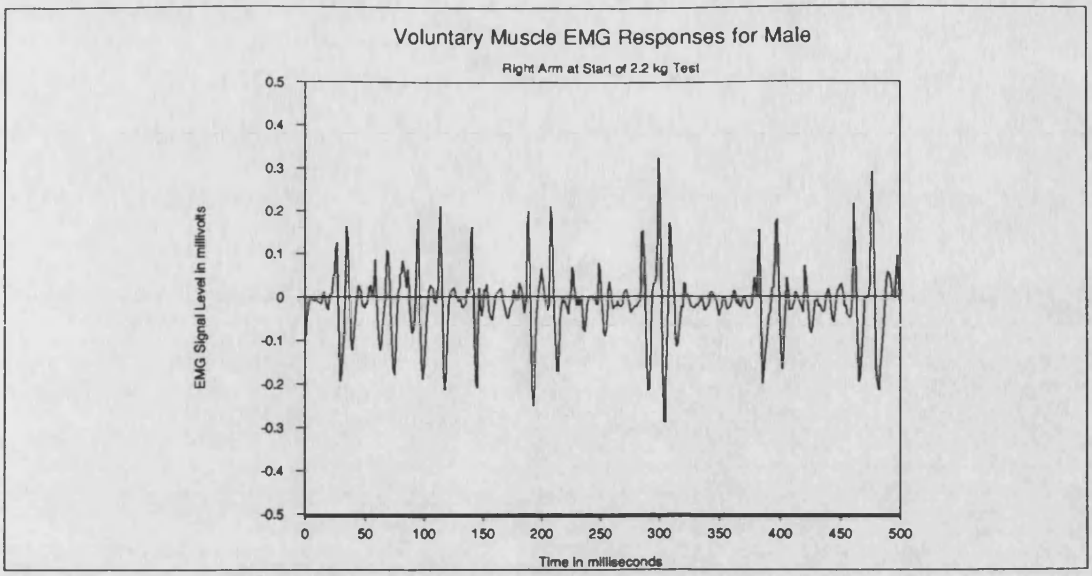

Figure 9.24 *EMG at Start of Male Right Arm Test using 2.2 Kg weight*

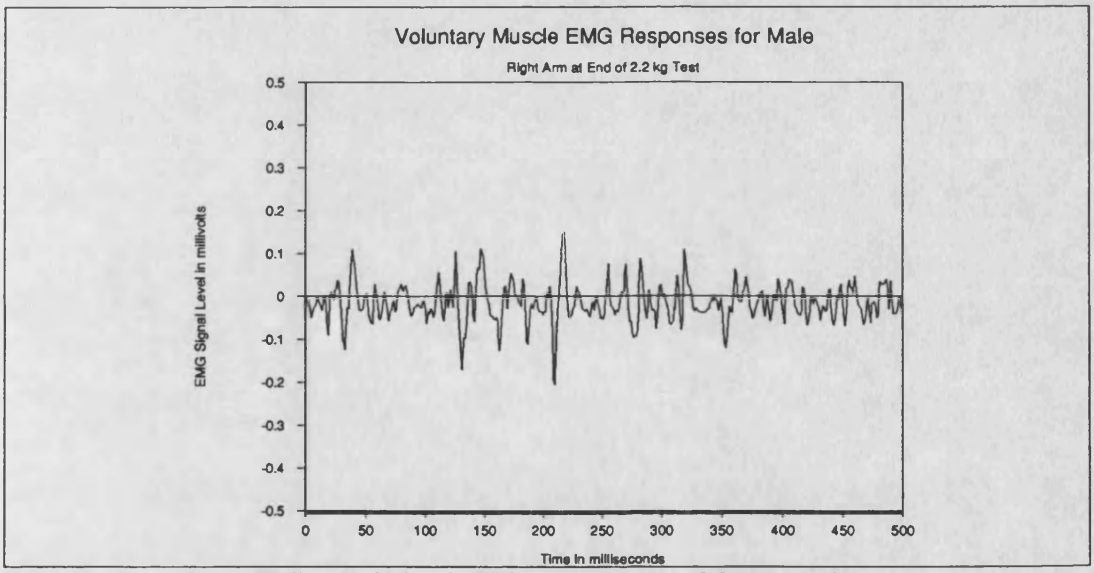

Figure 9.25 *EMG at End of Male Right Arm Test using 2.2 Kg weight*

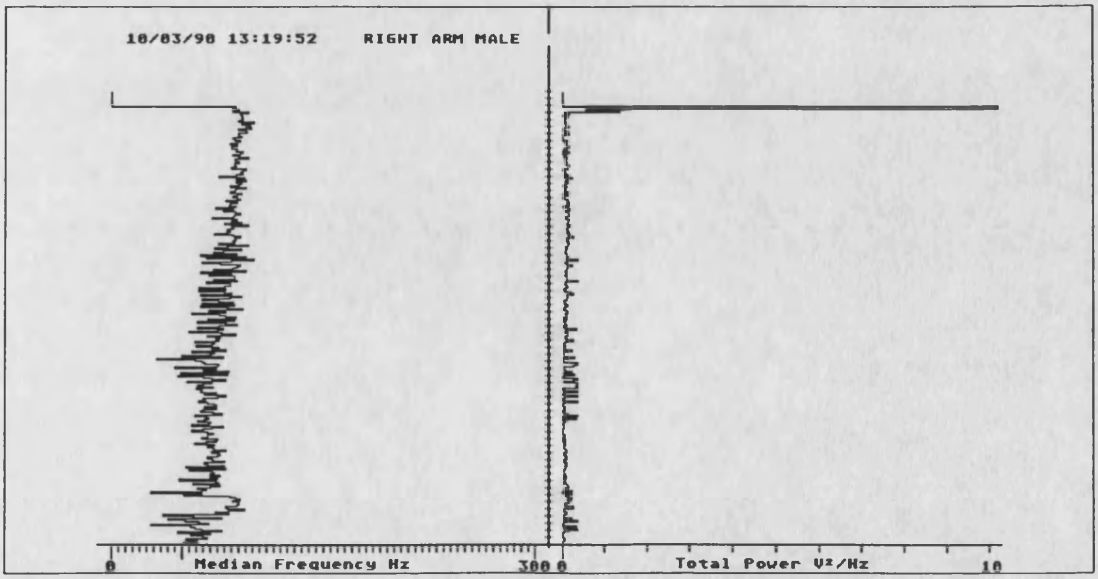

Figure 9.26 *Median Frequency and Power Results for Male Right Arm using 2.2 Kg weight*

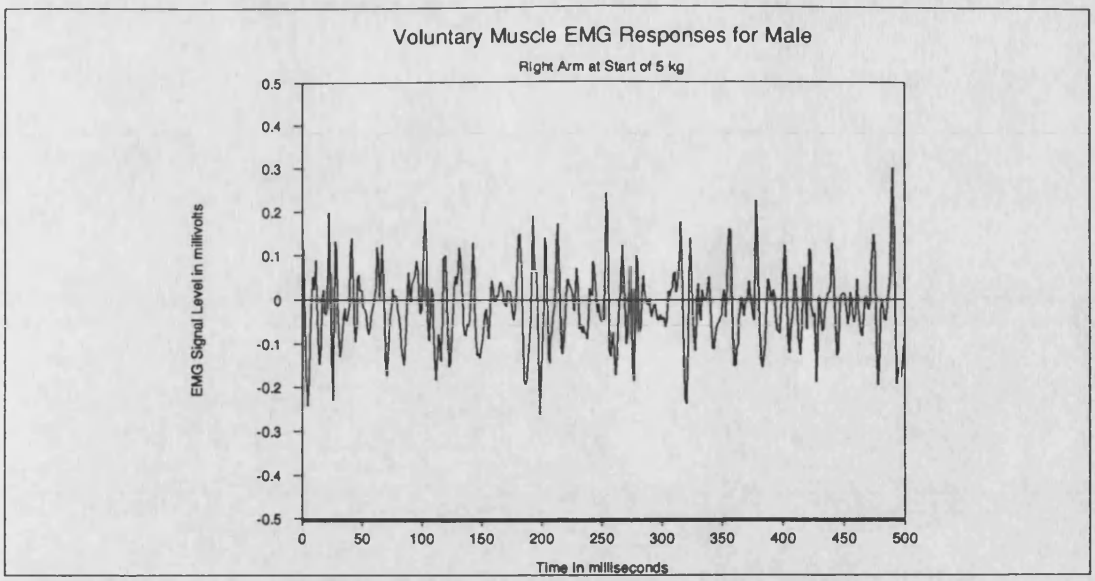

Figure 9.27 *EMG at Start of Male Right Arm Test using 5 Kg weight*

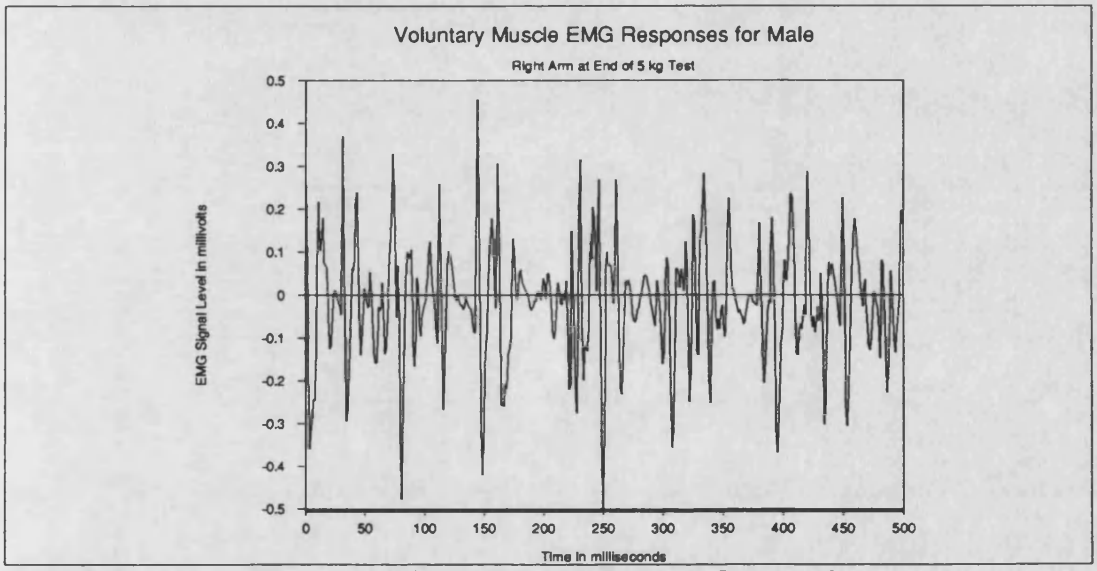

Figure 9.28 *EMG at End of Male Right Arm Test using 5 Kg weight*

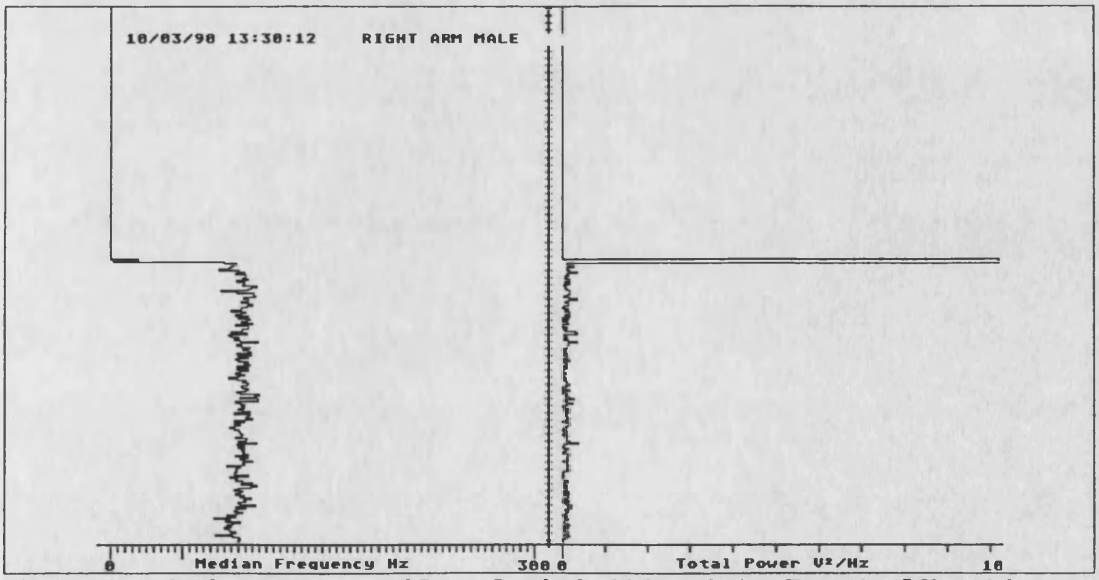

Figure 9.29 *Median Frequency and Power Results for Male Right Arm Test using 5 Kg weight*

9.2.2 Stimulators and the Artefact Suppression Hardware

These tests show the effective working range of the artefact suppression system. They also serve as a comparison of the two stimulators described in Chapter 5. The important factor in the comparison of the stimulator output stage is the post-pulse hold time which reflects the time that the EMG probe is saturated, combined with the time the stimulator takes to return to zero. The shape of the recorded CAP is more an indicator of the effectiveness of the stimulator.

9.2.2.1 Protocol

These tests were all carried out on the biceps brachii muscle of the arm on the same subject. The stimulation rate was reduced as necessary in order that a single CAP could be recorded without after potential effects, using a stimulus pulse width of 300μs.

The stimulating electrodes were placed such that the active electrode was over the motor point and the indifferent electrode was at the end of the muscle body. The EMG probe was placed along the length of the muscle body of the muscle belly between the stimulating electrodes. The earth strap was placed around the wrist of the arm being stimulated.

For each of the two stimulators the standard strength-duration test set of pulsewidths was used. As described in Section A.2.1 these range from 10μs to 300ms in a logarithmic progression. Using the slow repetition rate, the stimulus was applied and the voltage increased until the muscle was producing a visible twitch. Then the pre-pulsewidth and post-pulsewidth hold periods were adjusted to give a minimally distorted CAP. The values of these and the CAP were then recorded. This process was repeated for each of the pulse widths and for each of the stimulators.

9.2.2.2 Suppression Hardware Results

Before the results from the test described in section 9.2.2.1 , the effects of the artefact suppression hardware will be shown by displaying the recorded CAP as the post-pulse hold time is increased.

The three plots shown in Figures 9.30 to 9.32 show the effects of the increasing post-pulse hold time using a data sample rate of 5 kHz. Figure 9.30 shows the distorted CAP recorded with no hold time. Figure 9.31 shows the effects of a hold time of 1 ms after the end of the stimulus pulse and Figure 9.32 shows an almost optimal setting of 1.5 ms post-pulse hold time showing just the large CAP response.

Figures 9.33 to 9.35 show a similar set of data to the previous set of plots except the sample rate is 2 kHz and the final hold time is increased to 1.6 ms to eliminate the final glitch. This sample rate is two times that usually used and as can be seen, the

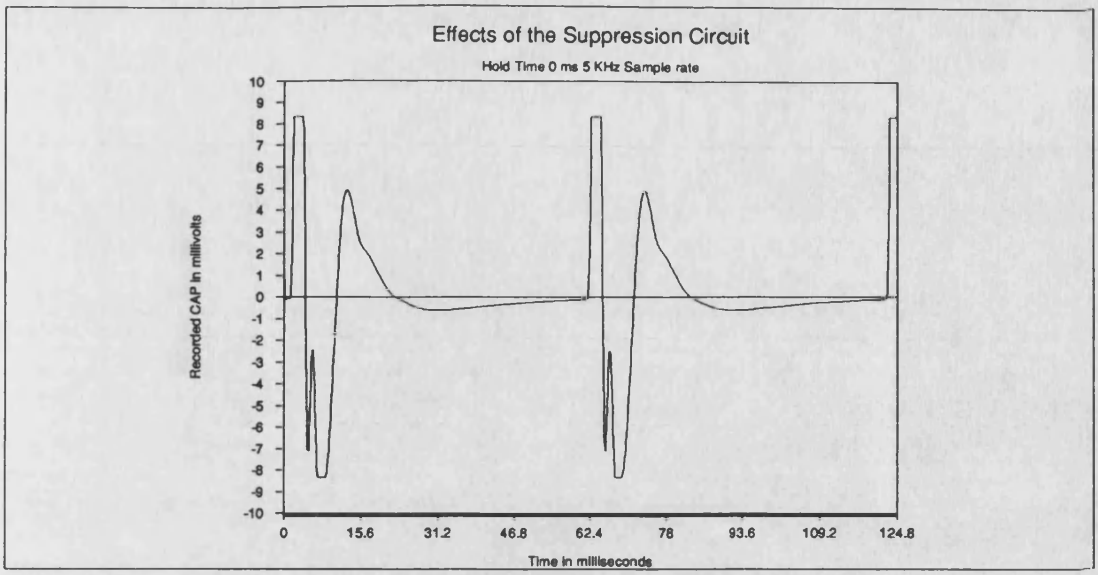

Figure 9.30 *CAP response with no Suppression Circuit Sampled at 5 kHz*

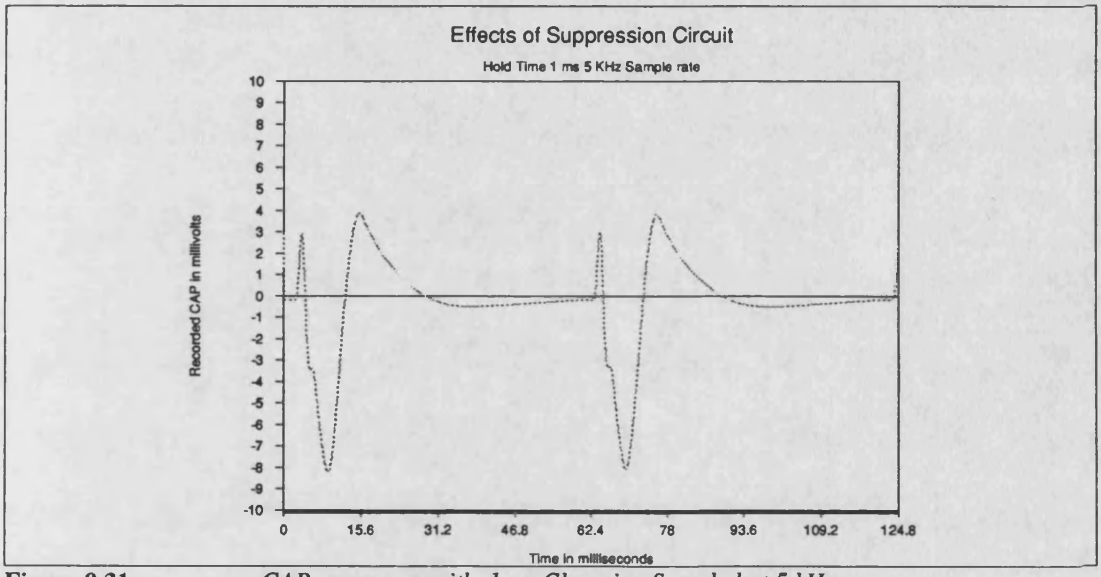

Figure 9.31 *CAP response with 1 ms Clamping Sampled at 5 kHz*

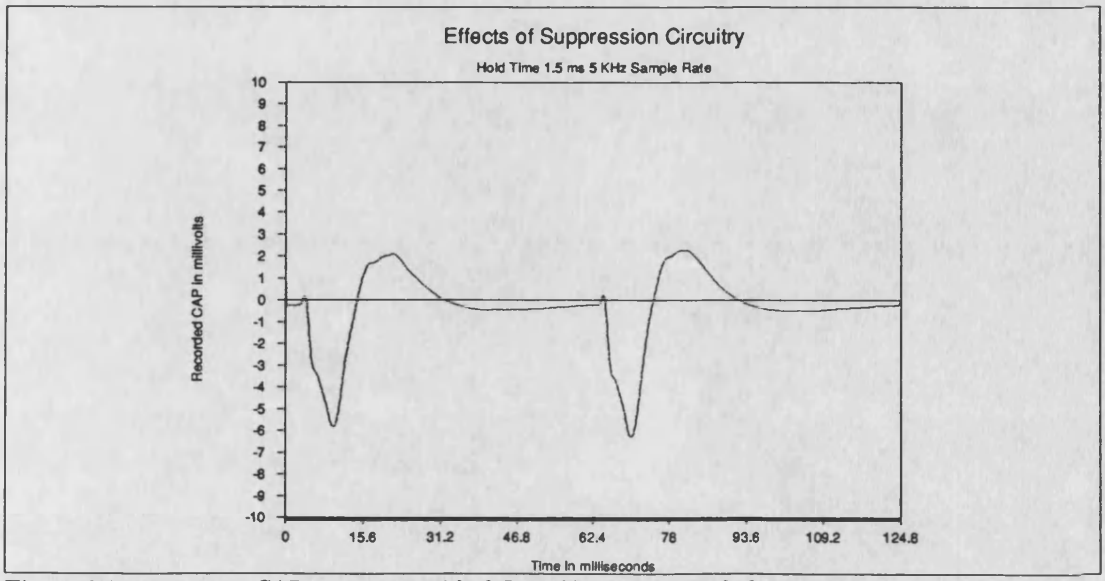

Figure 9.32 *CAP response with 1.5 ms Clamping Sampled at 5 kHz*

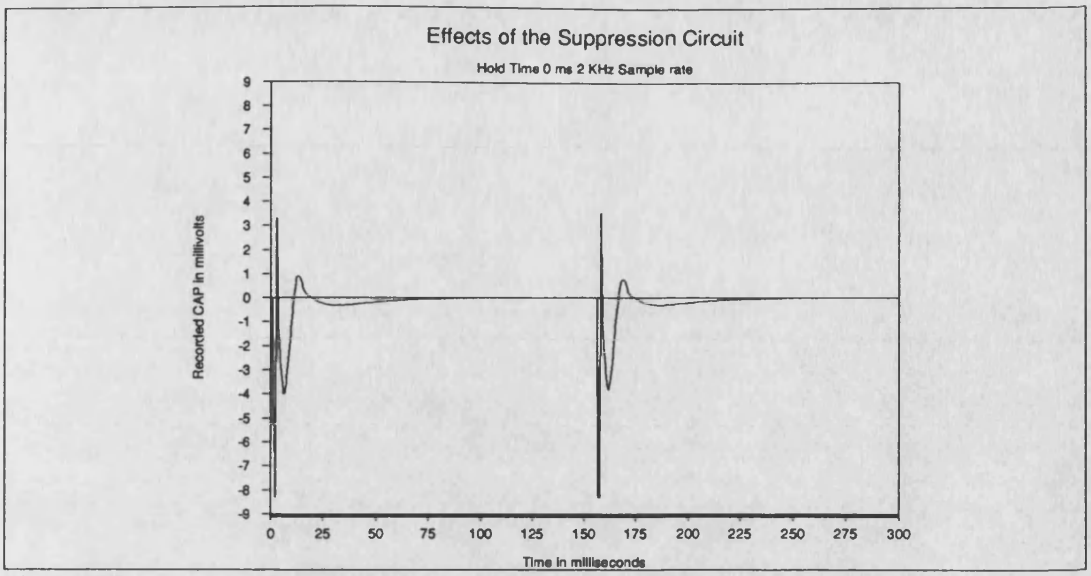

Figure 9.33 *CAP response with no Suppression Circuit Sampled at 2kHz*

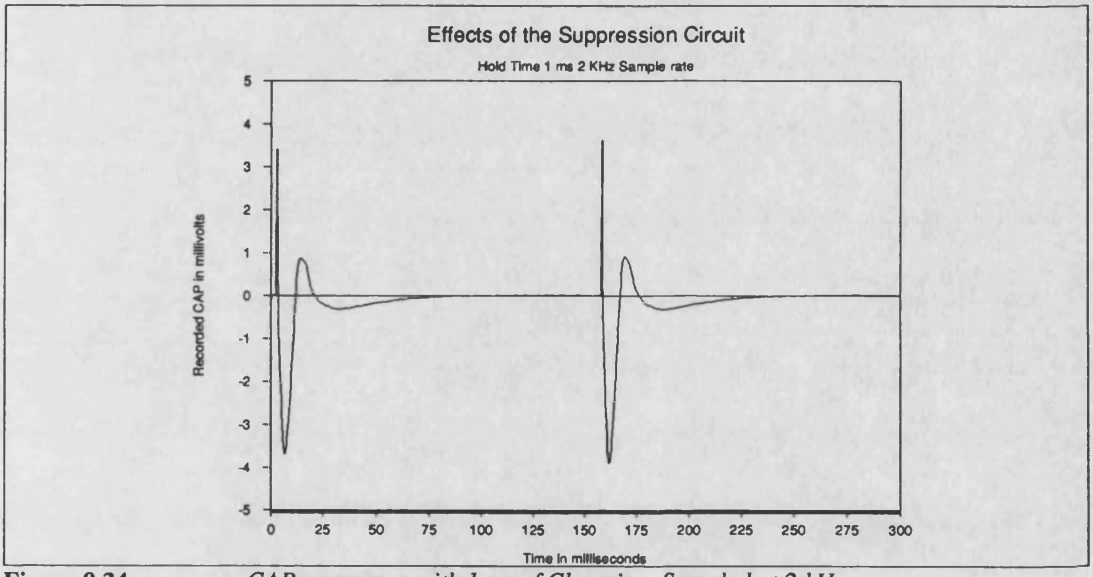

Figure 9.34 *CAP response with 1 ms of Clamping Sampled at 2 kHz*

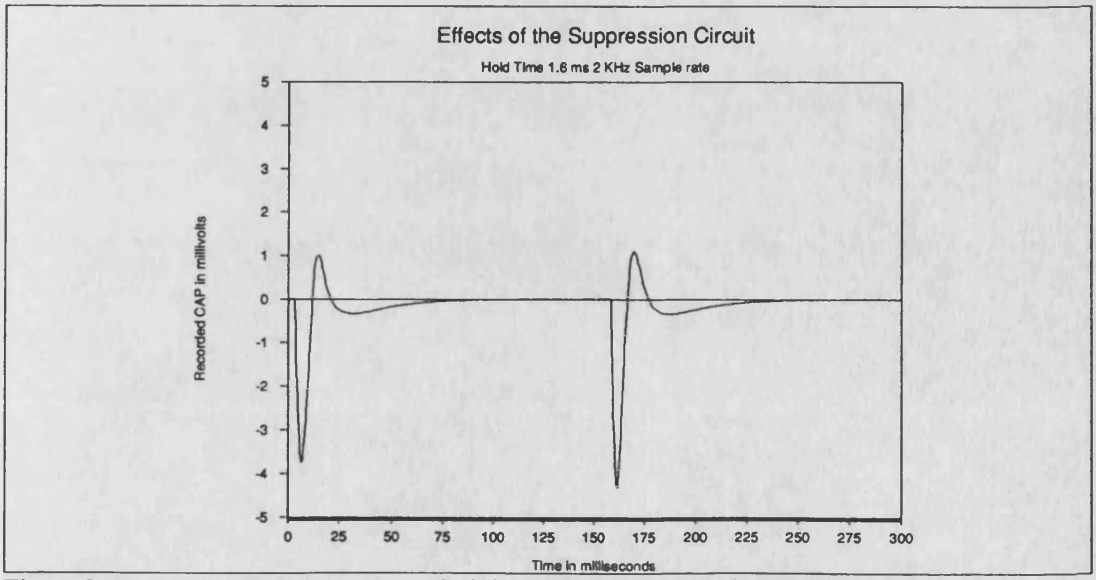

Figure 9.35 *CAP response with 1.6 ms of Clamping Sampled at 2 kHz*

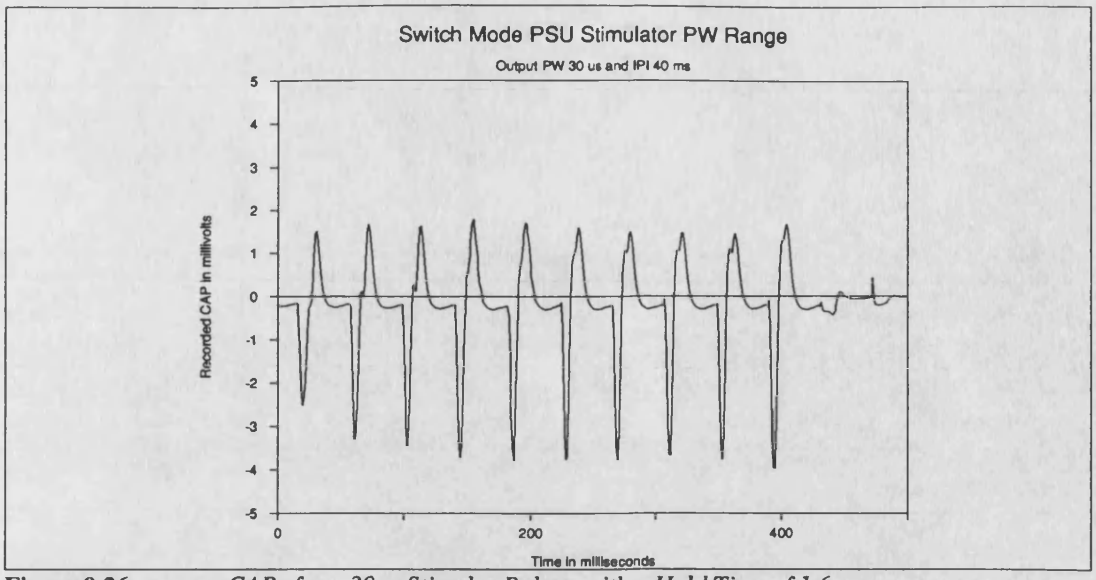

Figure 9.36 *CAPs from 30μs Stimulus Pulses with a Hold Time of 1.6 ms*

effects of the stimulus using the new probe amplifiers lead primarily to spikes. This is because the sample time is every 500μs relative to the stimulus pulse of 300μs, thus there can be no more than one sample during the stimulus period. If a saturation time of 4 ms is considered there will be at most eight samples to describe the saturation period. The no-hold plots both show an improvement over the original pre-amplifier design with a reduced distortion. The 5 kHz no-hold plot in Figure 9.30 clearly shows the point at which the CAP starts to overcome the distortion effects.

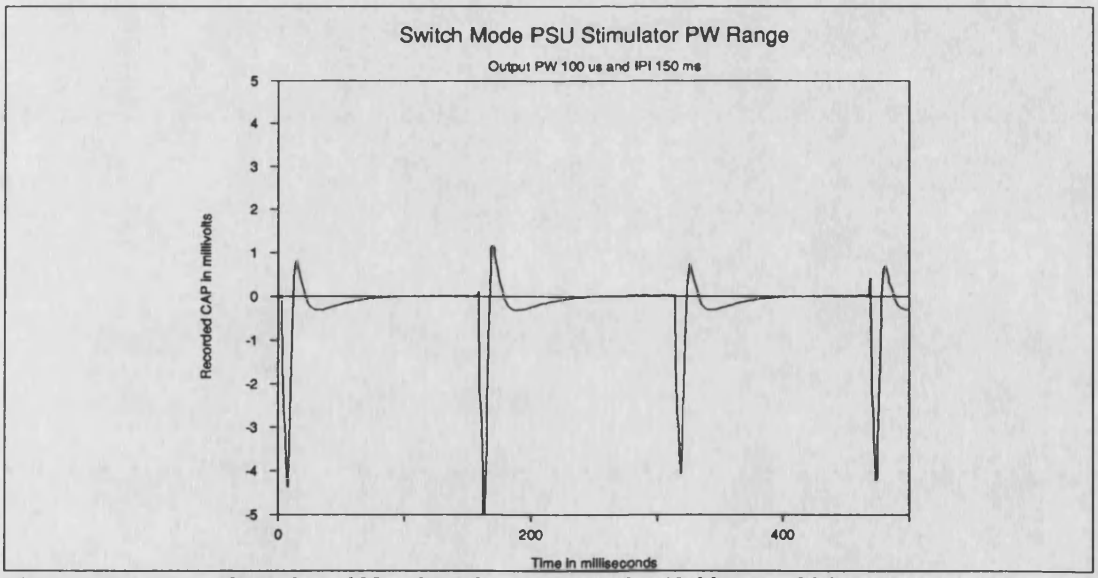

Figure 9.37 *CAPs from 100μs Stimulus Pulses with a Hold Time of 1.2 ms*

Figures 9.36 to 9.40 show the results for the switchmode power supply output stage stimulator. The plots show the recorded CAP with the post-pulse hold period adjusted for the best CAP response. The stimulus level is not necessarily the same because of the difficulty in determining the output voltage and because the pulse width will determine the minimum voltage required to produce a suitable muscle response. The

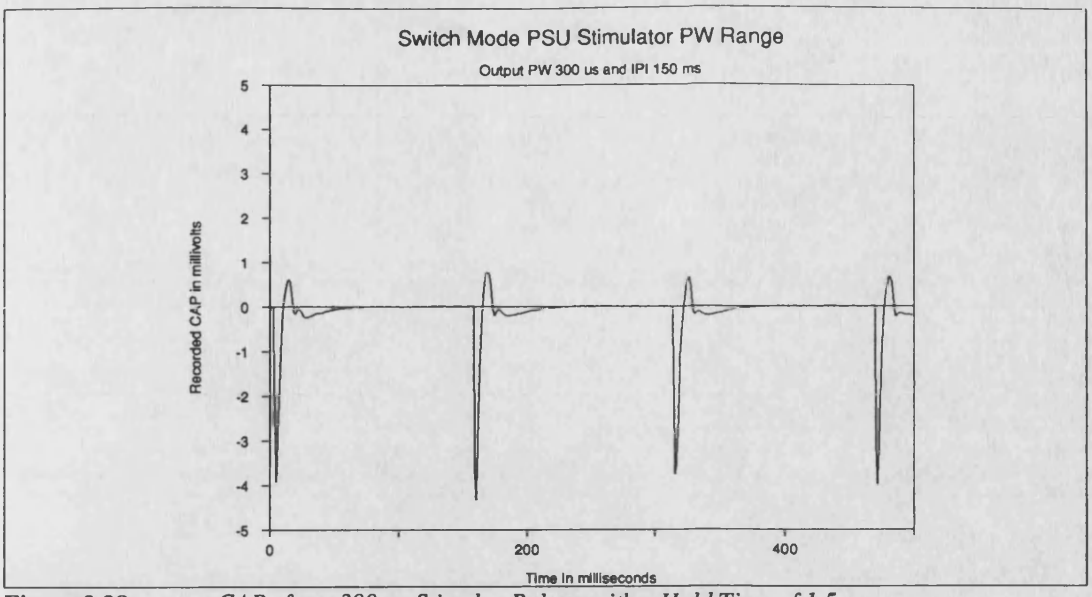

Figure 9.38 *CAPs from 300 µs Stimulus Pulses with a Hold Time of 1.5 ms*

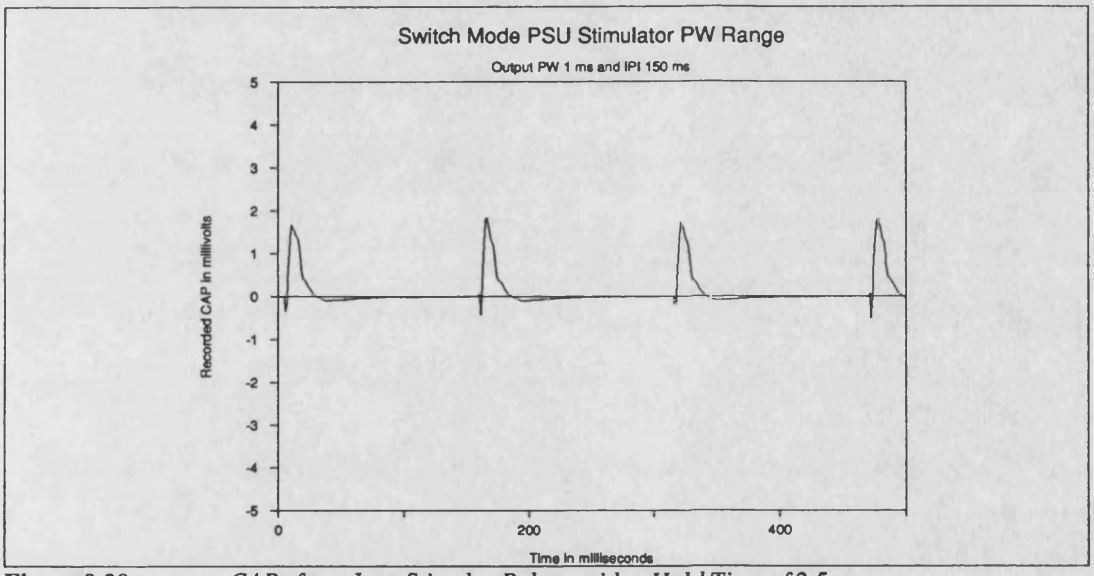

Figure 9.39 *CAPs from 1 ms Stimulus Pulses with a Hold Time of 2.5 ms*

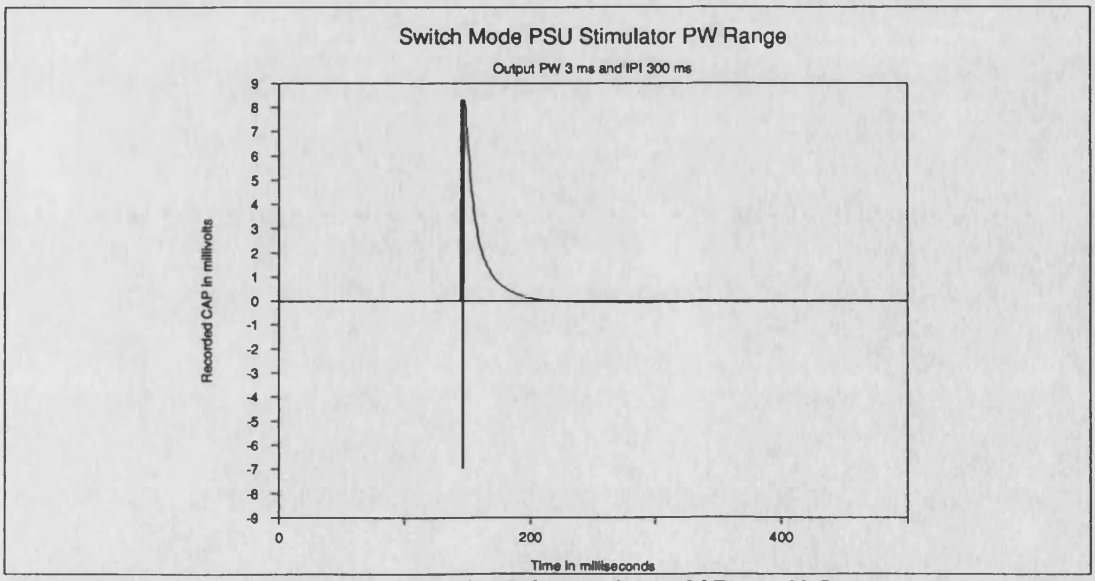

Figure 9.40 *CAPs from 3 ms Stimulus Pulses with a Hold Time of 2.5 ms*

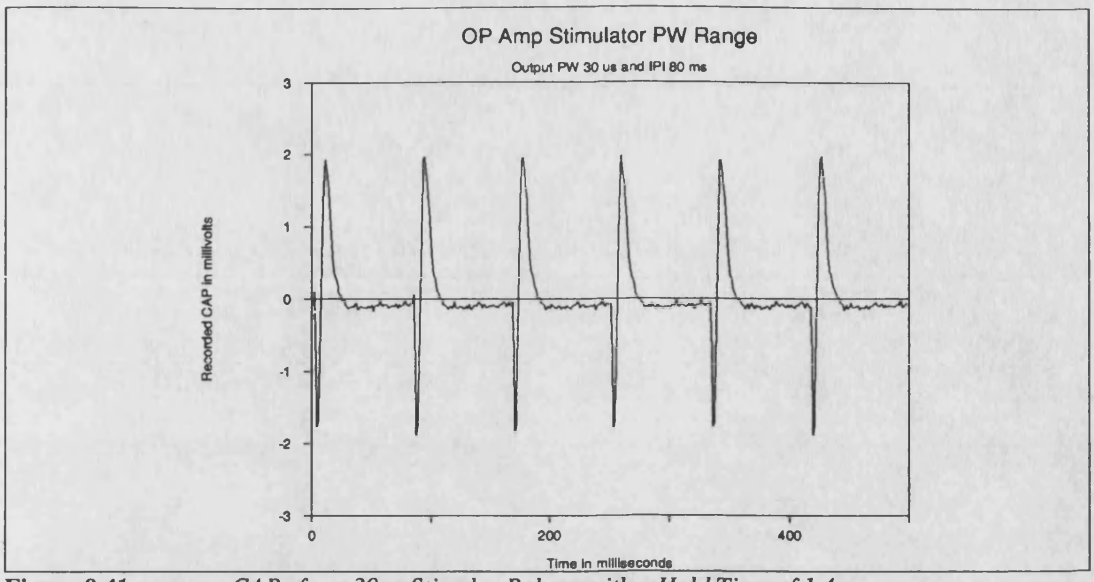

Figure 9.41 *CAPs from 30μs Stimulus Pulses with a Hold Time of 1.4ms*

results for the 30μs stimulus pulse show a great deal of variation. This is caused by the stimulator design as is discussed in Appendix B. The suppression circuitry can be seen to be effective up to about the 1 ms stimulus pulsewidth shown in Figure 9.39, at which point the CAP is significantly affected by the distortion. The 3 ms stimulus pulse shown in Figure 9.40 shows no CAP and significant distortion due to saturation that the suppression circuitry is unable to suppress.

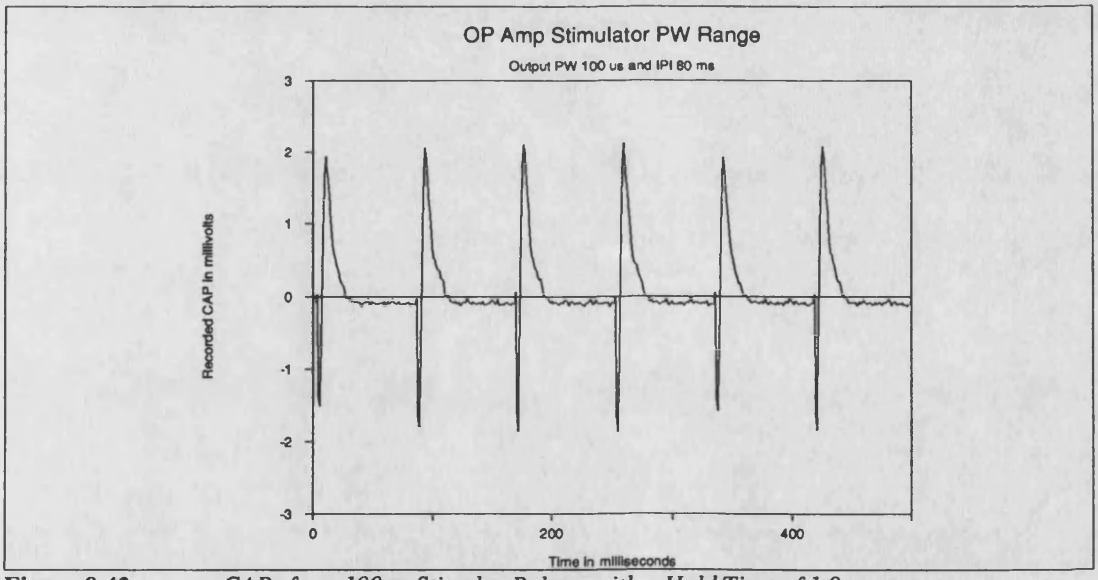

Figure 9.42 *CAPs from 100μs Stimulus Pulses with a Hold Time of 1.8 ms*

Figures 9.41 to 9.45 show the results for the operational amplifier output stage stimulator. With this stimulator it was possible to use a constant stimulator frequency of 80 ms. The results for the 30μs pulse width show the improved reliability available with this stimulator on the lower pulse widths. The results for the 1 ms pulse width shown in Figure 9.44, show that the opamp stimulator gives an improved range for the suppression circuitry. The 3 ms stimulus pulse is once again the limiting pulse width

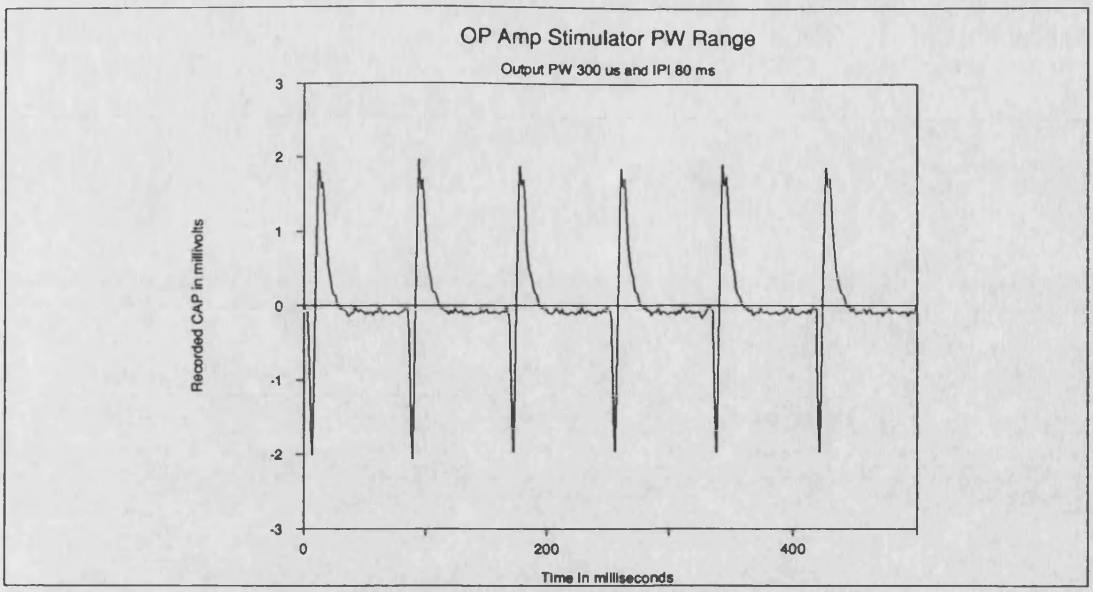

Figure 9.43 *CAPs from 300μs Stimulus Pulses with a Hold Time of 1.6 ms*

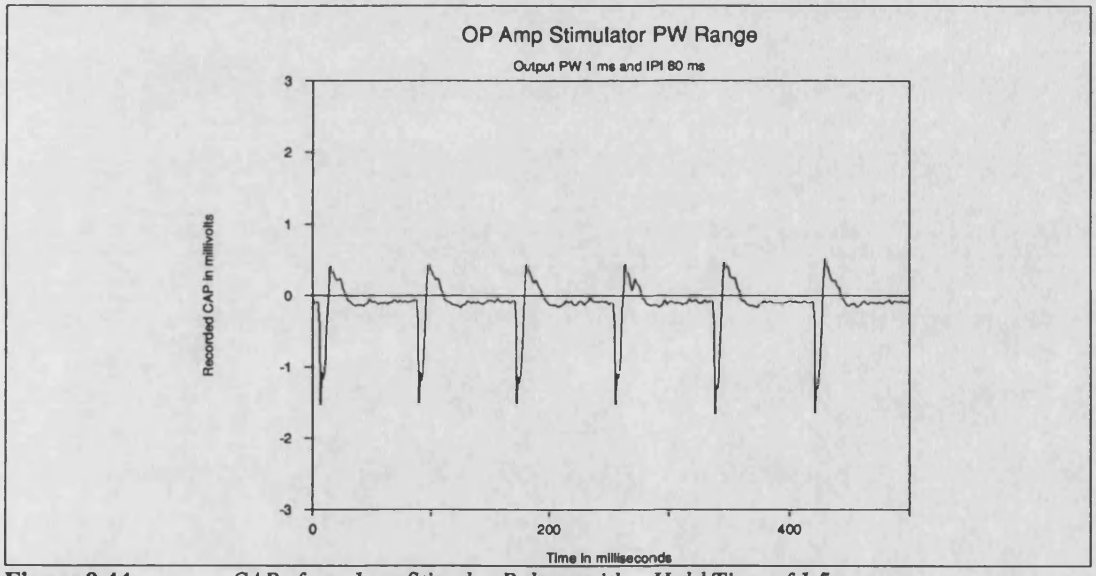

Figure 9.44 *CAPs from 1 ms Stimulus Pulses with a Hold Time of 1.5 ms*

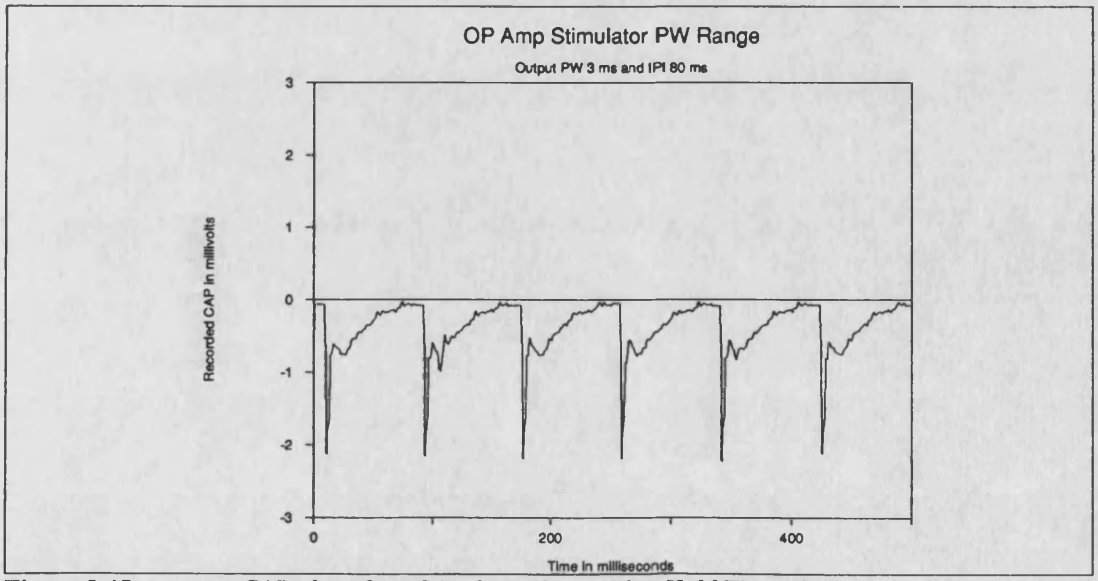

Figure 9.45 *CAPs from 3 ms Stimulus Pulses with a Hold Time of 4 ms*

except the combination of the opamp stimulator and suppression circuitry still elicits a small CAP. The distortion is not as great as with the switchmode output stage stimulator and suggests that this system may lead to an effective long pulse system. The subject noted that the opamp stimulator 'felt' more comfortable when compared to the switchmode power supply stimulator. This may be due to the effects of the clamping circuit used on the switch mode stimulator.

9.2.3 Tetanic Stimulation

These tests aim to show how the analysis system currently performs on typical CAP trains. It is CAP trains similar to these that will require reliable analysis if a feedback sensor is to be developed using this technique. The subjects for these tests are described beside their respective results. This set of tests is intended to show how the system is currently functioning and some of the limitations of the current analysis software.

9.2.3.1 Protocol

The tests have been carried out on two subjects, one a paraplegic the other a healthy subject. The muscle groups were stimulated in the normal way using the usual stimulus parameters of 300μs pulses and 40ms IPI time. The voltage level was adjusted to give a strong tetanic contraction. The EMG probe was placed along the body of the muscle and between the stimulation electrodes. The earth strap is connected either to the wrist or the ankle depending on which limb the muscles being tested are in.

The quadriceps muscles of the paraplegic subject were tested using a protocol similar to that used for the voluntary test. The difference is that the contraction was generated by the stimulator and the leg was unloaded. Fatigue was said to have occurred when the foot had dropped to the floor.

The biceps brachii muscle of the healthy subject was tested by increasing the stimulus level until a strong contraction was obtained. The fatigue was said to have been reached when the biceps muscle was no longer showing a good tetanic contraction. In this case it was found necessary to change the stimulus interval to 80 ms which tended to give a more vibratory contraction. The reason for this was that the analysis software would almost immediately lock on to the stimulator frequency when using a 40 ms IPI interval.

Having adjusted the pre-pulse and post-pulse periods such that the stimulus artefacts are minimised, the median frequency was recorded until the muscle had fatigued whilst keeping the stimulus voltage constant. The CAP train at the start and finish of the test were also recorded to show how their shape had changed.

9.2.3.2 Tetanic Results

The results for the paraplegic subject are presented in a similar form to those for the voluntary muscle case but with CAP trains from the start and the end of the test. As in the voluntary case the median and power plots are shown as a screen dump.

Figures 9.46 to 9.50 show the results from the right and left leg of the paraplegic subject, which required a gain of 5000 to produce an appreciable muscle response.

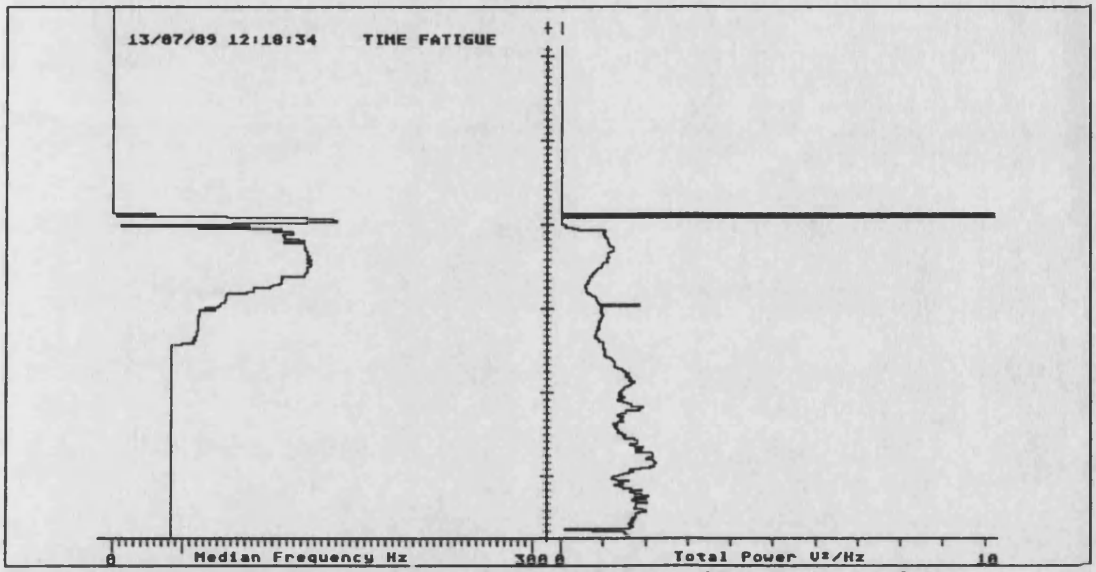

Figure 9.46 *Median Frequency and Power Results for Left Leg of Paraplegic Male Subject*

Figure 9.46 shows the median frequency plot from the left leg and Figures 9.47, 9.48 and 9.49 show the recorded CAP train at the start, halfway through and at the end of the test. The median frequency shows a drop in frequency as would have been expected. The median frequency starts significantly higher than for the voluntary muscle tests but rapidly drops to a lower figure where it appears to stay for the rest of the test. This is a pattern that is also seen in the results of tests on the healthy subject. The power signal however shows a gradual increase in power with less variation than was the case with the voluntary tests. The CAP trains show the typical CAP shape but are of a much lower signal size. The paraplegic subject tended to suffer from muscle spasms, which can be seen in some of the plots between the CAP trains. The CAP train at the end of the test shows a lot of variation as the number of muscle fibres that respond to the stimulus changes due to the fatigue effects.

Figure 9.50 shows the median and power plot for the right leg of the paraplegic. The signal obtained off the leg in this case was significantly smaller than the left leg so that even though the equipment was working at its maximum gain—which has since been increased—the CAP responses were barely visible. The median frequency results show no real consistent trends and this may be due to the signal size. The power plot does however show a steady increase in power for the full 3 minutes of the test.

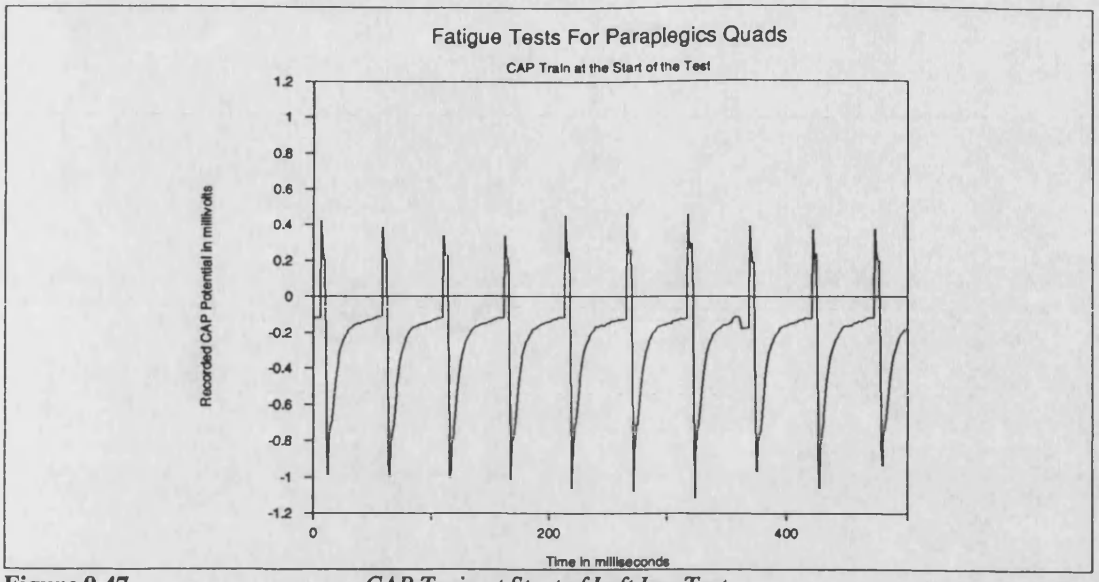

Figure 9.47 *CAP Train at Start of Left Leg Test*

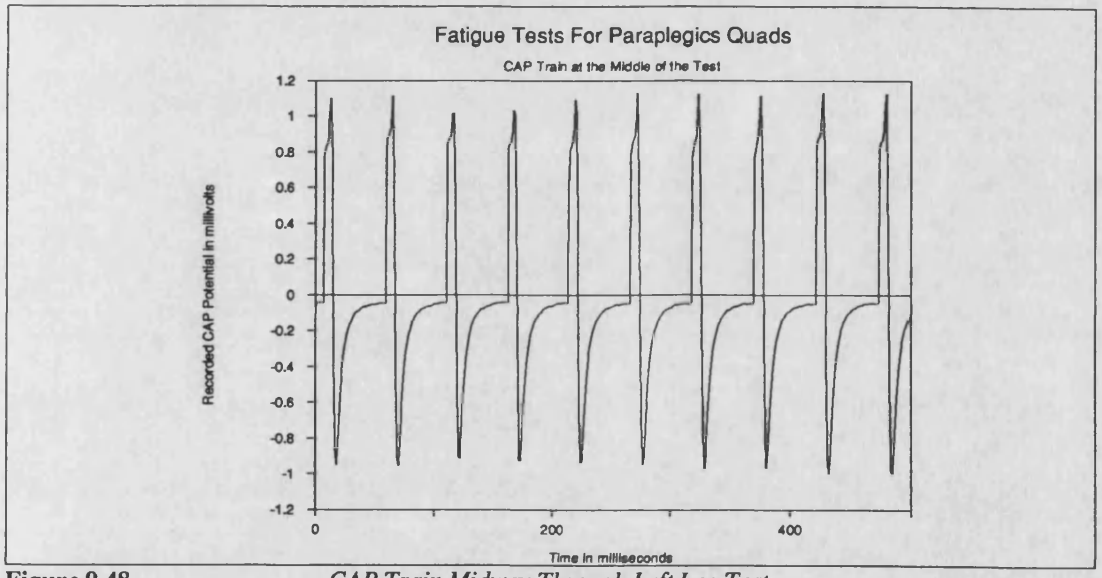

Figure 9.48 *CAP Train Midway Through Left Leg Test*

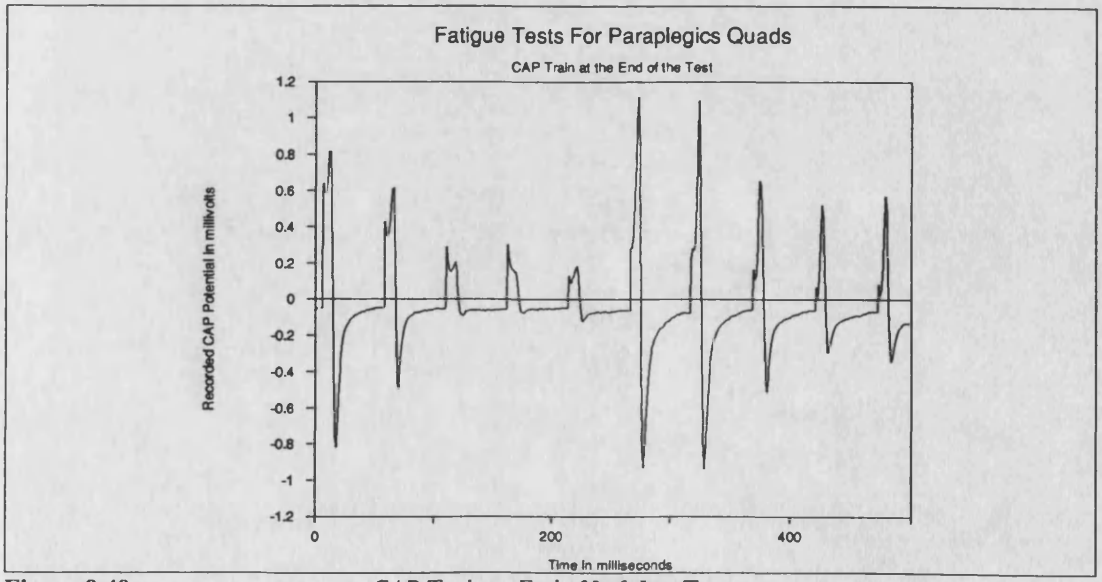

Figure 9.49 *CAP Train at End of Left Leg Test*

The results shown in Figures 9.51 to 9.56 are for a normal subjects right arm. Two sets of results are shown one with the power scale on 10 V^2/Hz and the other with a power scale of 1 V^2/Hz.

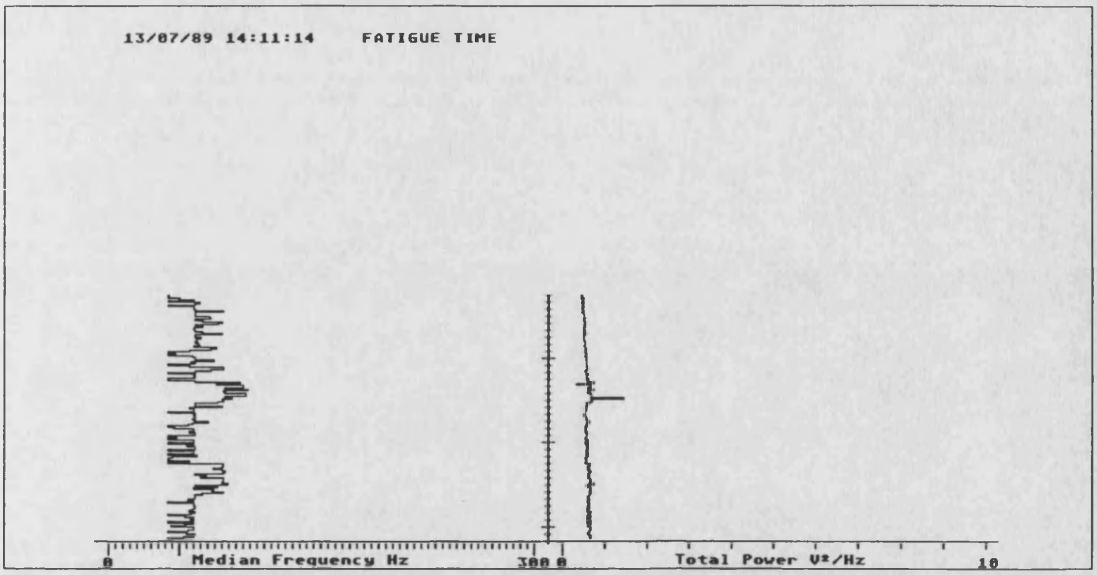

Figure 9.50 *Median Frequency and Power Results for Right Leg of Paraplegic Male*

Figures 9.51, 9.52, 9.54 and 9.55 show the CAP train recorded at the start and end of each of the biceps muscle tests. The two sets of results show a great deal of similarity with the CAP train reducing in size and having a longer duration towards the end of the test. The CAP train for the end of the first test shown in Figure 9.52 also shows significant fluctuations in CAP size which matches in with the physical observation of more trembling in the muscle at the end of this test.

Figures 9.51 and 9.52 are the median and power plots for the two tests. They both have a similar shape with the median frequency dropping rapidly to a plateau in the first half a minute, then dropping at the end of the first minute to a second plateau at 25 Hz which is the second harmonic of the stimulus rate. The power also shows a similar pattern rising and falling during the first minute before rising again and dropping throughout the rest of the test.

9.2.4 Variation of Stimulation Parameters

The results from Section 9.2.3 show significant effects due to the frequency components at the repetition rate and its harmonics. This stimulus rate is required to ensure that a smooth tetanic contraction can be achieved. The relationship between sample rate, sample size and sample content defines how significant this effect is. These tests show how the choice of these parameters may be used to provide a more effective stimulus rate free frequency analysis.

With the current system software, the easiest method for showing the variations is by making use of the programmability of the stimulator. This would not be a suitable

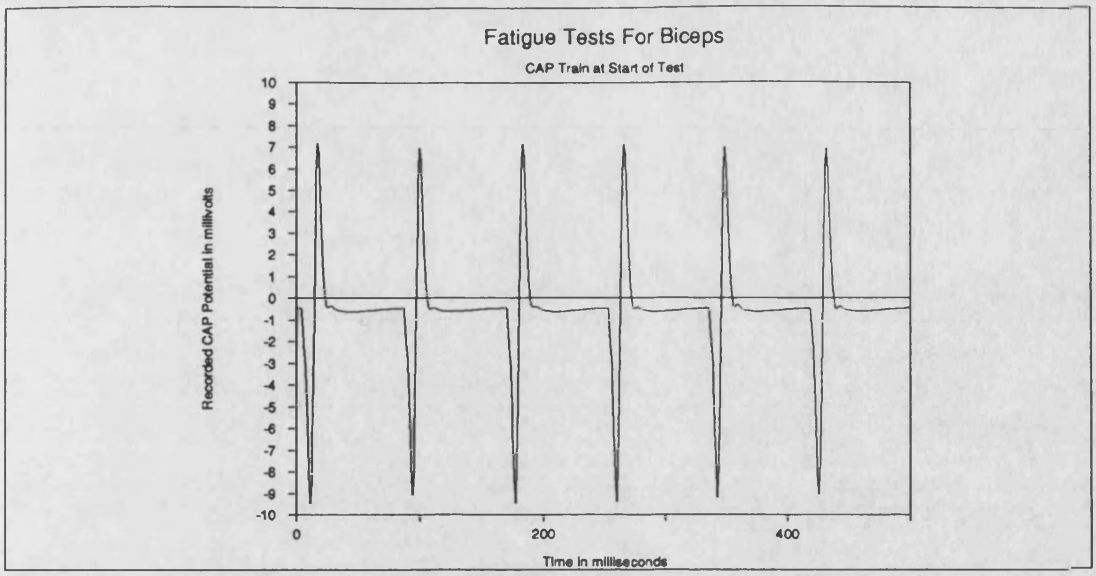

Figure 9.51 *CAP Train at the Start of the First Biceps Test on the Normal Male Subject*

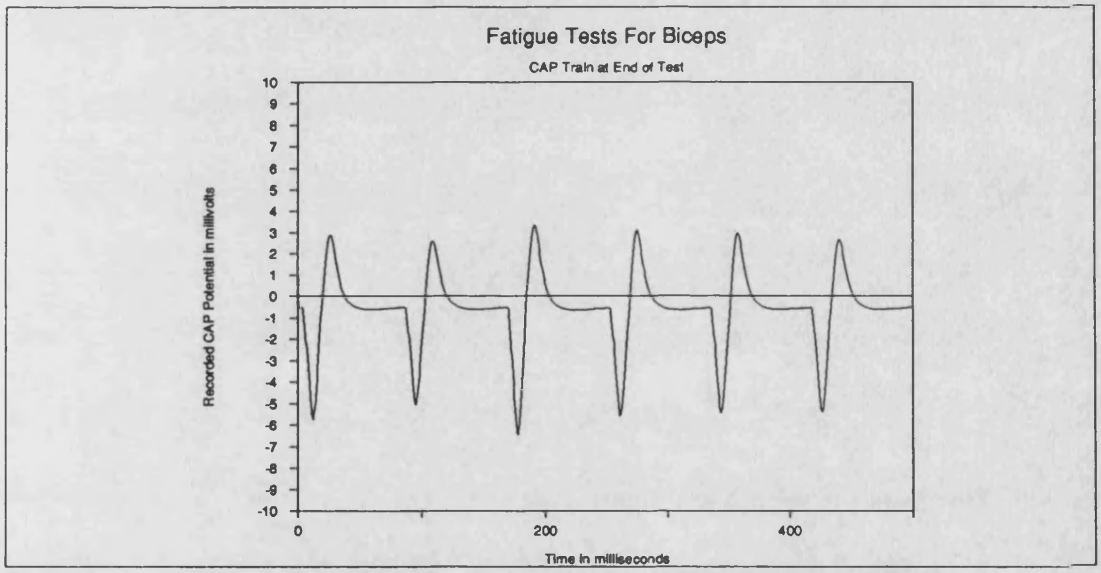

Figure 9.52 *CAP Train at the End of the First Biceps Test on the Normal Male Subject*

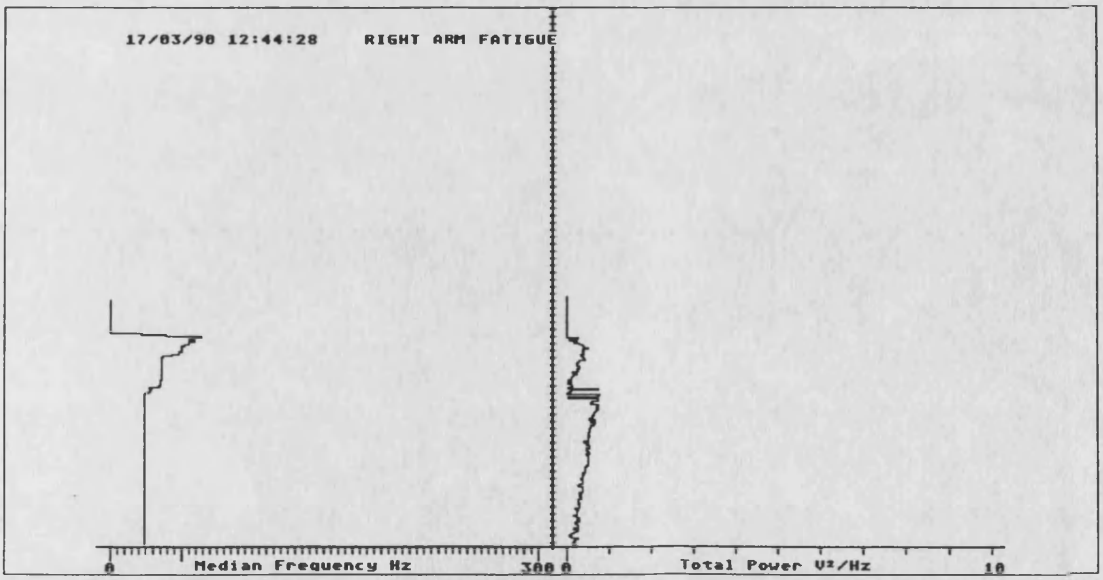

Figure 9.53 *Median Frequency and Power Results for the First Test on the Normal Male*

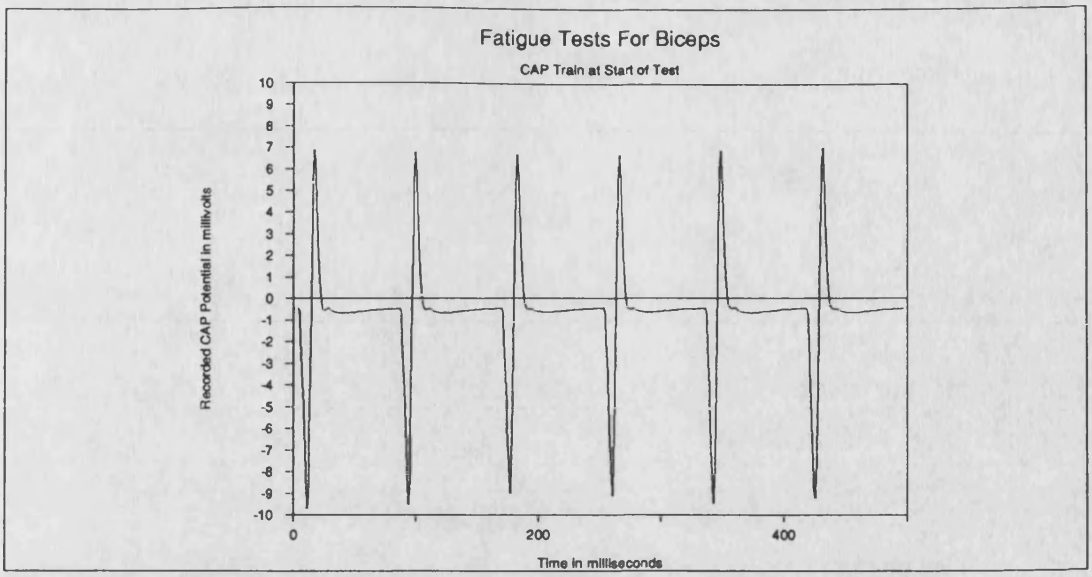

Figure 9.54 *CAP Train at the Start of the Second Biceps Test on the Normal Male Subject*

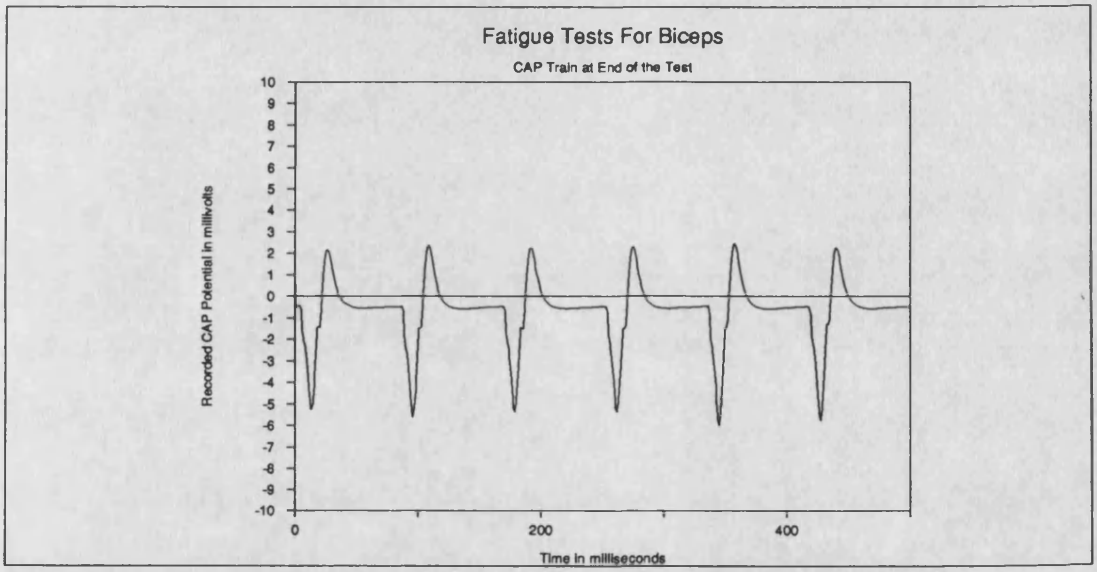

Figure 9.55 *CAP Train at the End of the Second Biceps Test on the Normal Male Subject*

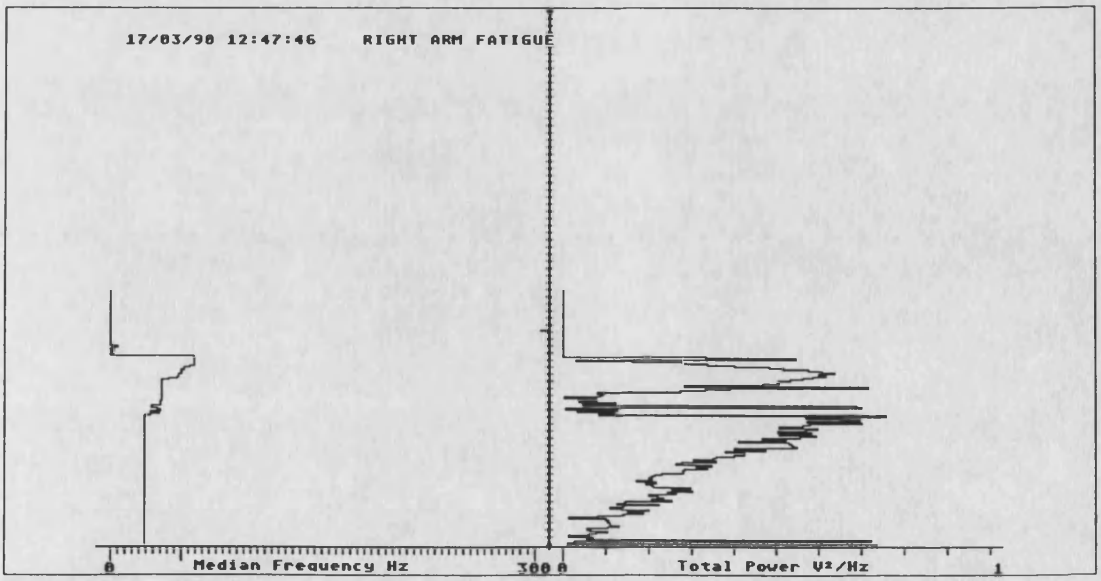

Figure 9.56 *Median Frequency and Power Results for the Second Test on the Normal Male*

technique for a sit/stand or walking system because of the lack of a fused contraction, however it will demonstrate how the frequency display can be tailored to provide only the information of interest.

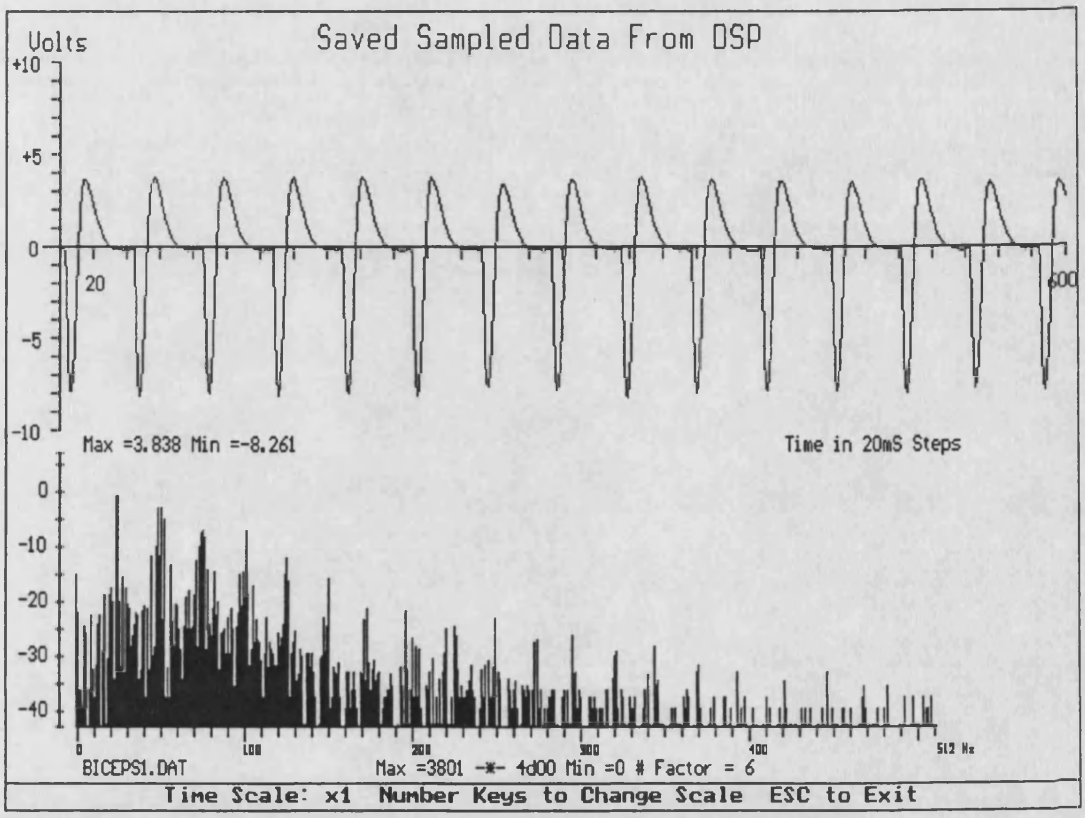

Figure 9.57 *CAP Train and Spectra for a Typical 300μs 40 ms IPI Stimulus*

9.2.4.1 Protocol

The test was carried out using a pulse width of 100μs and an IPI period that ranged from 100 ms to 1 second. Thus the number of CAPs in the window ranged from ten to one.

The basic protocol of the tests was as described previously; the EMG probe being placed along the muscle body between the stimulating electrodes on the biceps. The earth strap is connected to the wrist. The stimulus level is adjusted until a reasonable twitch or contraction is elicited.

9.2.4.2 Results

Seven sets of results are presented as screen dumps of generated displays from the display recorded data program on the IBM. Figure 9.57 shows the recorded results from a typical stimulus waveform of 300μs and 40 ms interpulse interval. In the top display the CAP train can be seen and in the bottom the DSP calculated spectrum. It should be noted that the CAP voltage scale does not take into account the amplifier

gain at the time of the recording. It is clear that the spectrum has a set of spectral lines associated with the stimulus rate and its harmonics.

In Figure 9.58 a similar plot is shown but this time the IPI has been increased to 100 ms and a pulse width of 100μs used. Here the CAP train shows little change except for the increased IPI whilst the spectrum has reduced spectral noise from the repetition rate but it still dominates the spectrum.

In Figure 9.59 the IPI is increased to 300 ms giving just 3 CAPs per sample period. The results of this are obvious in the spectrum at the bottom where the shape of the spectrum is no longer so dominated by the spectral lines due to the IPI.

In Figure 9.60 the IPI is increased still further to 500 ms giving just two CAPs per sample period. The results of this are obvious in the spectrum at the bottom where the shape of the spectrum is no longer dominated by the spectral lines due to the IPI. Now the shape is much more dependent on the CAP shape.

Figure 9.61 shows the typical results from an IPI of one second and pulse width of 100μs. Here the spectral lines actually occur at 1 Hz intervals so are completely hidden leaving the spectral shape to be controlled by the CAP shape.

Figures 9.62 and 9.63 show similar plots with an IPI of 1 second but this time stimulus pulse width is 300μs and two different CAP shapes have been recorded. From these it is clear that as the CAP shape changes the spectral shape changes quite dramatically.

9.3 Summary

This Chapter has presented results from two CAP analysis systems. The former system was limited by the hardware and processing system and the results from this system have been used to show that it is possible to detect the muscle CAPs elicited by muscle stimulation. It also showed that it is possible to detect the frequency shift commonly associated with fatigue in voluntary muscle responses in the CAP train. The test also showed that there is a variability in the frequency shift with fatigue. Results were presented that showed shifts in both directions and and in one case no shift at all during the fatigue test. These results have also been reported by other researchers.

The second section presented results from a new analysis system. These results showed that the analysis system could be used to record voluntary muscle fatigue trends. It compared the two designs of stimulator, showing that the operational amplifier output stage combined with the new suppression hardware provided a wider pulse width operating range. A set of tests were presented showing the systems ability

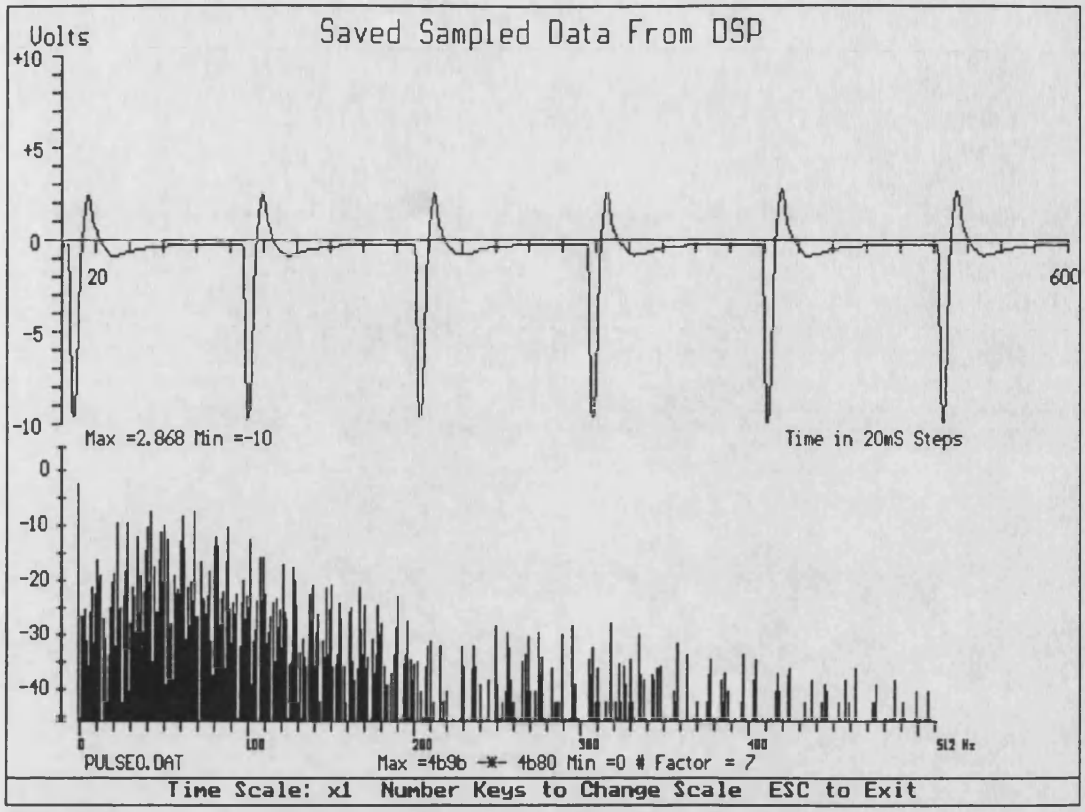

Figure 9.58 *CAP Train and Spectra for a 100µs 100 ms IPI Stimulus*

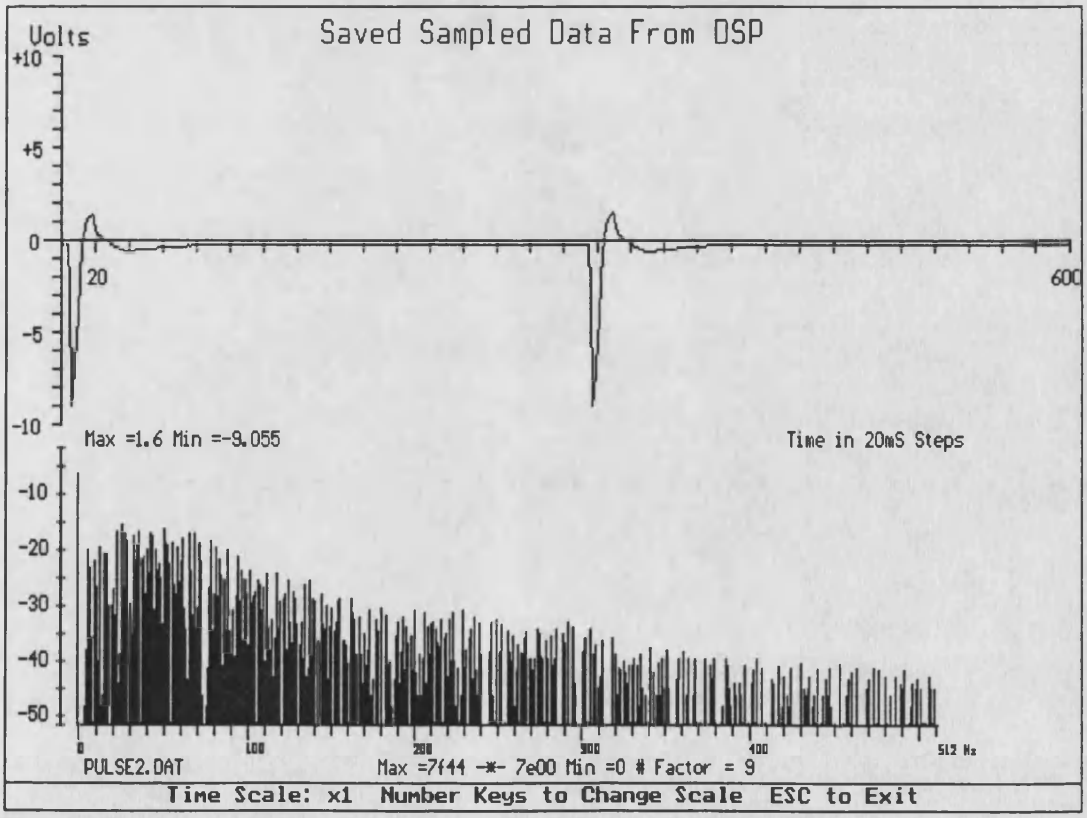

Figure 9.59 *CAP Train and Spectra for a 100µs 300 ms IPI Stimulus*

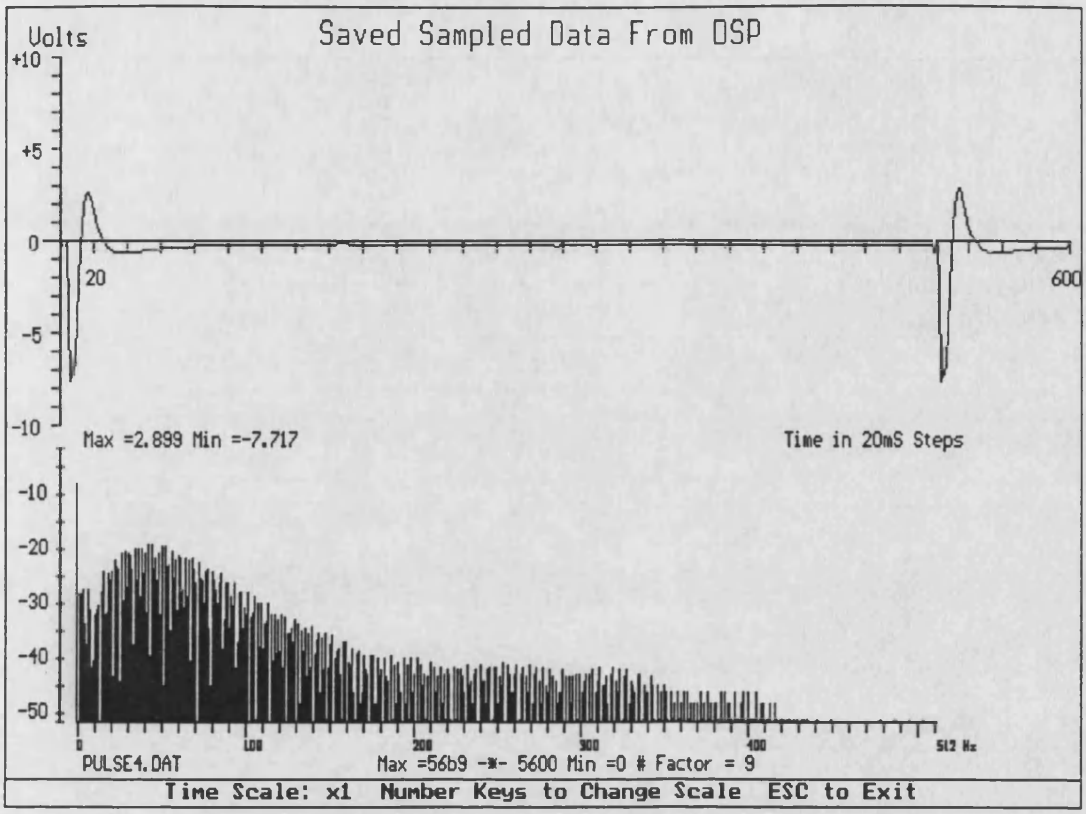

Figure 9.60 *CAP Train and Spectra for a 100μs 500 ms IPI Stimulus*

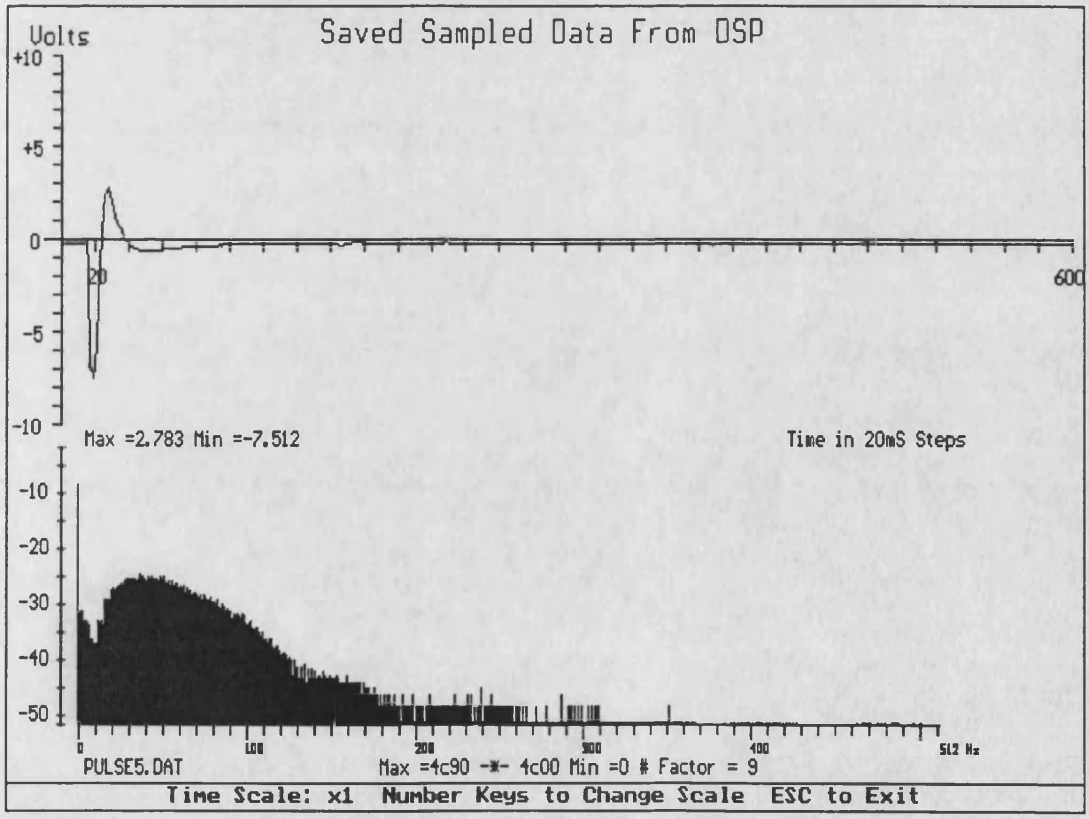

Figure 9.61 *CAP Train and Spectra for a 100μs 1 s IPI Stimulus*

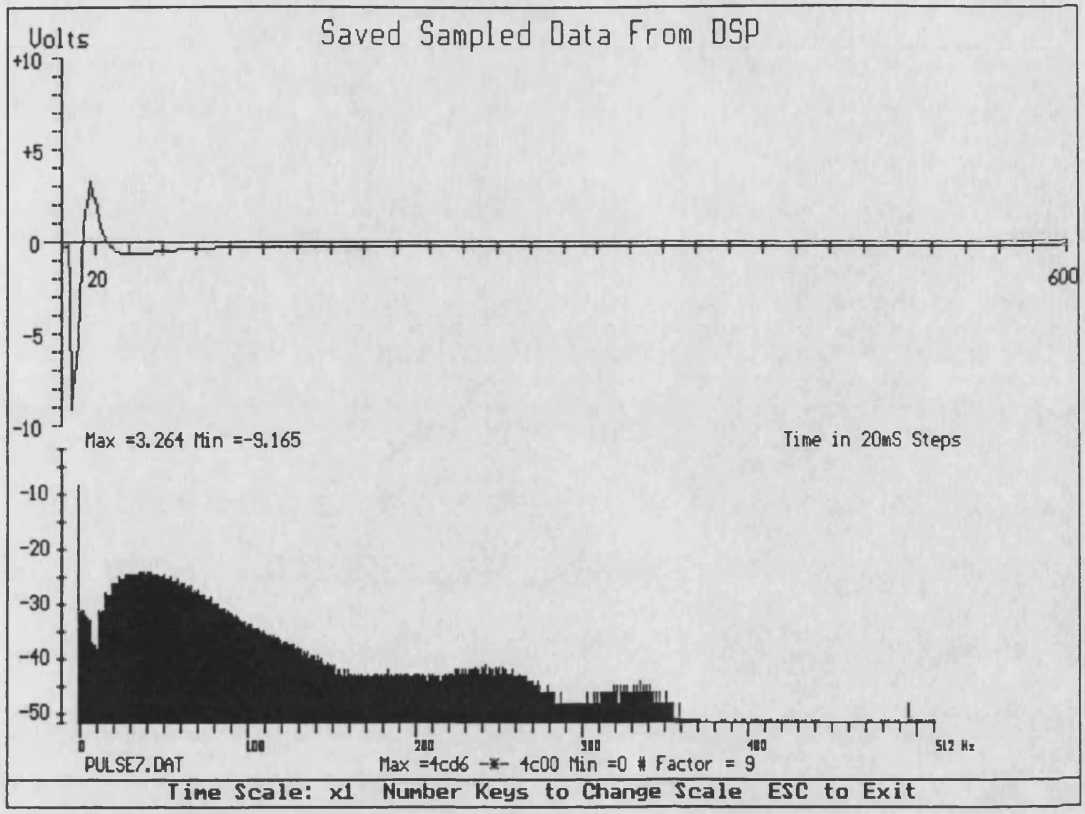

Figure 9.62 *CAP Train and Spectra for a 300µs 1 s IPI Stimulus*

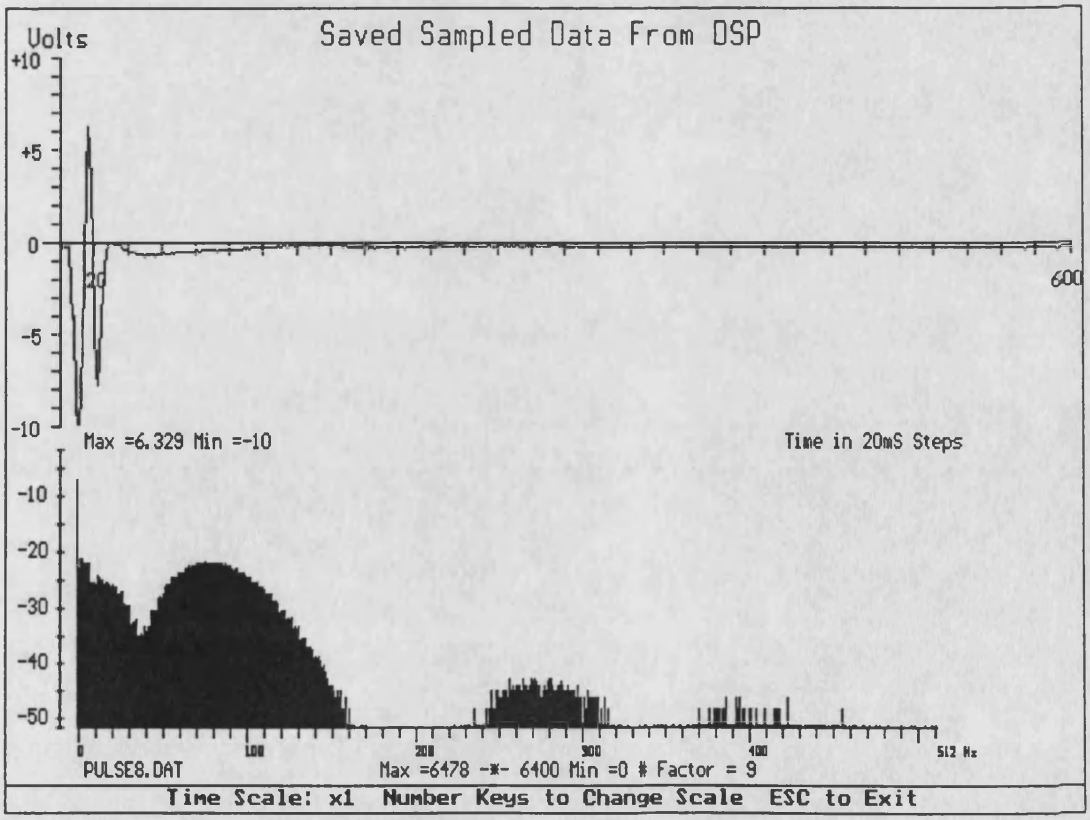

Figure 9.63 *CAP Train and Spectra for a 300µs 1 s IPI Stimulus*

to analyse CAP trains. These tests showed more repeatability than with the previous system but the lack of software filtering of the stimulus repetition rates meant that ultimately the median frequency would drop to the stimulus rate or a harmonic of it. The final set of tests showed how the changing of the stimulus repetition rate could hide the spectral effects of the repeating waveform. This could provide an alternative method for the reduction of the dominance of the stimulus repetition of the calculated spectrum.

The results for the new analysis system have also highlighted a number of shortcomings in the current software implementation on the analysis hardware. A number of improvements to overcome these faults are discussed in detail in Chapter 11.

Chapter 10

Conclusions

This thesis has presented a system for the detection, amplification and analysis of Compound Action Potentials elicited by functional electrical stimulation. The thesis has concerned itself mainly with the techniques required for artefact free recording of these muscle responses.

Some preliminary work has been carried out on the analysis of these signals and it is intended here to sum up the salient features and discuss their significance within the general field of Muscle Physiology instrumentation. The chapter is split using general headings to describe the instrumentation to be discussed.

10.1 The Original Atari System

As an analysis system the original system has been shown to work. It could detect and amplify voluntary muscle signals and transform them into their frequency domain spectra. The system could analyse both voluntary and stimulated muscle responses and produce median frequency plots for the sampled signal.

10.1.1 EMG Pre-Amplifiers

The early pre-amplifier designs were designed primarily as a means of detecting and amplifying muscle EMG. They were not designed with the suppression of artefacts as their primary objective. They functioned very well as basic EMG amplifiers and enabled the investigation of noise sources in basic EMG amplifier configurations.

The amplifiers proved usable for basic EMG detection and amplification but required modification when used to amplify CAP responses, since the recovery from saturation took considerable time and too high a gain in this stage resulted in almost permanent saturation of the pre-amplifier. As expected there was significant stimulus artefact contamination in the recorded CAP which would tend to disappear into the artefact as the muscle fatigued. These observations have been used by Graupe[96] as feedback in his stimulator systems.

These amplifiers suffered from a number of basic functional problems concerned with the combination of surface electrodes, electrode leads and amplifier input impedance. As a means for the initial investigation of CAP frequency response and identification of primary stimulation artefact sources and causes they served admirably. The various clamping forms of these amplifiers proved ineffective because the switching tended to introduce secondary transients. This leads to the EMG probe and isolation amplifier with sample and hold input. The EMG probe being used to

amplify the EMG signal to a level where small transients introduced by the sample and hold switching would be insignificant.

10.1.2 Frequency Analysis System

As has been described in Section 7.1, the early Atari frequency analysis system was aimed at primarily proving that frequency analysis could be used to identify changes in muscle response in much the same way as many researchers have reported for voluntary muscle. It is only recently that a number of researchers have started to publish findings based on the CAP responses from muscle stimulation[96, 102]. At the start of this research this information was unavailable and that which was available had not used the stimulation to provide functional use at the same time. This allowed the researchers to make use of reflex arcs such as the H-Reflex[30] to generate the CAP trains. The system also provided a platform for testing various techniques for the frequency analysis of contaminated muscle signals.

Though the system was limited by its simple design, it functioned reliably as can be seen from the results presented. With this system it was possible to remove the majority of the stimulus artefact via computer intensive processing in the frequency domain. The results clearly show there are significant changes in the median frequency and the total recorded power. This power figure is unscaled and is calculated from the filtered response and so reflects the changes in the CAP power. This has been shown by Graupe[96] to be a viable method of detecting the muscle power and on the results where this value was scaled to fit on the screen there is generally a distinct trend down in power.

The results show that three types of median frequency response are possible:

- The frequency can follow the pattern of voluntary muscle response but at a much accelerated rate.
- The median frequency shows no detectable change for the duration of the stand.
- The median frequency shows a frequency response in the opposite direction to that expected, based on the typical median frequency response obtained from voluntary muscle contractions.

These results were presented in a paper given at the 7th Congress of the International Society of Electrophysiological Kinesiology in Enschede; a copy of this paper appears in Appendix C.

At this conference these findings were confirmed by Merletti et al.[102] who suggested the cause for the differing results. In the original tests these differing trends were found to occur if the electrodes were moved between tests. The results were always consistent during a test if the electrodes were not adjusted as can be seen from

the results. The explanation given by Merletti et al. centres around the placement of the stimulating electrodes. Essentially the positioning of the active electrode with respect to the motor point will define the order in which the muscle fibres are recruited. That is whether the small diameter or large diameter fibres fire first. The fibre diameter, as discussed in Chapters 1, 2 and 3, defines the conduction velocity and thus the shape of the APs. It is the AP shapes summed randomly or synchronously depending on the stimulus source, that defines the spectrum that will be seen.

10.2 CAP Detection System

The discussion of the improved CAP analysis system can be conveniently separated into the separate hardware units involved. Discussion of the results obtained and the subsequent conclusions are discussed under the final section on the analysis system.

10.2.1 The EMG Probe

The initial results using EMG electrodes, flying electrode leads and a pre-amplifier unit proved functional but difficult to use and susceptible to noise and stimulus artefacts. As discussed in Chapter 4, the reduction of the basic extraneous noise requires the minimisation of the electrode impedance and reduction in electrode leads in order that the small muscle responses could be buffered as soon as possible.

The new EMG probe has shown that it reliably meets these requirements. The removal of an earth electrode and replacing it with a separate earth strap proved to be the key to mains interference problems, such that the EMG probe does not require any 50 Hz notch filter. The results from voluntary muscle responses recorded with the analysis system and with the muscle fatigue monitors described in Appendix B clearly show this improved detection and amplification capability.

There are limitations with these amplifiers when amplifying stimulated results as shown in Section 9.2.2. However a number of possible solutions are discussed in Section 11.2.5 of the Further Work Chapter. As the first part of a CAP reduction system the EMG probes have proved to be more than adequate.

10.2.2 The Artefact Suppression Hardware

The artefact suppression hardware itself combines with the anti-alias filters and isolation. This unit as described in Section 8.2.3 suffered from noise problems associated with the isolation amplifier design. After the re-design of this section the unit proved successful in reducing the stimulus artefacts across a reasonable range of stimulus pulsewidths.

As can be seen in the results of Section 9.2.2 effective suppression is limited by saturation effects to about 1 ms. The opamp stimulator results do suggest that the design of the stimulator output stage can lead to an improved working range. Each

stimulus pulsewidth required a careful choice of the hold time to give optimal results, as can be seen by the differing clamping times used as the pulsewidth increased. As the muscle fatigued it was almost always found necessary to increase these post pulse periods still further.

10.2.3 The Analysis and Display System

The potential of a DSP based frequency analysis system has been demonstrated. It has been used to show a number of features of the new stimulus artefact suppression and CAP detection technique. The system has shown to be effective in analysing both stimulated and voluntary muscle responses in real time. The tests have shown that the analysis software does require some changes to make it more effective at analysing the two types of signal.

The choice of analysis technique has been shown to have a significant effect on the spectrum produced by Fast Fourier methods. The potential of the single CAP technique for analysing CAP trains has been demonstrated but requires further work to implement a suitable algorithm for real time use of the method.

The use of separate display and analysis processors has been shown to offer significant speed advantages over the single processor approach. The use of the Fast Hartley Transform to carry out the time to frequency domain transformations has been shown to faster than the equivalent FFT routine. That is, less optimisation is required in an FHT to produce a fast transformation from the time to frequency domain.

10.3 Strength Duration Tester

The strength duration tester described in Appendix A shows a number of possible uses. It has been shown to be capable of carrying out a complete strength duration test in considerably less time than the equivalent manual test. The results show the system has a number of shortcomings. Most of these problems are attributable to the stimulator card as discussed in Section A.4.1. The system does provide a good match between manual results and automated recording, but suggests that some further development of the stimulator stage is a major factor in ensuring repeatable strength-duration tests.

Some other twitch detection techniques are discussed and the possible combination of these techniques with the strength duration tester are suggested. The combination of the CAP analysis system, described in the bulk of this thesis and the strength-duration tester is discussed and further work suggested to produce a system that combines these two elements in a single unit.

10.4 Muscle Fatigue Monitors

The muscle fatigue monitors are discussed in more detail in Appendix B. These systems monitor the muscle fatigue by tracking the median frequency. Unlike the system described in the main report these systems are currently only capable of tracking the median frequency from voluntary muscle responses. However they are both portable and battery powered.

The two systems are based on two differing techniques: one is analogue, the other digital. Extensive tests have been carried out on the analogue muscle fatigue monitor which have shown its effectiveness at monitoring voluntary muscle contractions as they fatigue. This system could lead to another useful piece of muscle physiology instrumentation.

10.5 Practical Application

This thesis has presented four pieces of muscle physiology instrumentation which could used almost immediately in the medical environment. Some further work is needed in all cases and this is discussed in the next chapter.

- A new design of muscle stimulator has been presented which is fully programmable and provides a number of synchronisation signals permitting synchronisation of analysis systems.
- A new technique for the suppression of stimulus artefacts has been presented which when combined with the new stimulator can provide a reliable means for recording CAP trains during functional electrical stimulations as well as the more traditional clinical tests.
- A means for automating the strength-duration test so that it is significantly faster than the manual technique has been presented. This could provide a great deal of extra information over and above the traditional strength-duration curve and has potential in the physiotherapy field. It also has application in the early detection and monitoring of muscle/nerve related diseases.
- A design for a simple muscle fatigue monitor which is portable and battery powered. This, as discussed in Appendix B, has many potential areas of application such as in the factory as part of ergonomic studies, on the sports field to aid with training schedules as well as within the hospital environment.

10.6 Summary

This thesis has presented methods for detecting and analysing muscle signals. The primary aim of this equipment has been to try and provide suitable surface feedback sensors for closed-loop FES systems. It has been shown that with the current techniques there is too much variability in the parameters for a reliable feedback

sensor. The reasons for this are attributable to the limitation of using surface stimulation and detection systems.

A number of the developments made during the course of this research have been shown to have practical applications in a number of areas of medical practice and research. Further work is required before these aims can be achieved and a number of suggestions have been made of how this could be done.

Chapter 11

Further Work

The new techniques presented in this thesis, for detecting and analysing a CAP train, still require considerable development before they can be used to provide a useful feedback signal. In this chapter a number of improvements to the system as it stands are discussed. The discussion of the possible improvements to the current system is split into two areas. These are software algorithm enhancements and hardware re-designs.

Appendix A and Appendix B give detailed descriptions of the Strength Duration Tester and Muscle Fatigue Monitors that have been designed as part of the work described in the main body of this thesis. Further work suggestions for these specific projects appear at the end of each of the appendices. A brief review of a few of the key issues is included here.

The chapter concludes with some suggestions as to the possible directions that this work could follow in the fields of feedback control of muscle stimulators for useful function and the automated analysis of CAPs and EMG signals.

11.1 Algorithm Improvements

In any real time analysis system it is the combination of efficient hardware and an integrated and optimised software package that ensures the displays provided are a true reflection of the current signal. The system that has been described in this thesis is not as yet fully optimised and integrated. There are various improvements that can be made that will improve the systems ability to both analyse and display the muscle signals. These improvements will be described under separate sub-headings.

11.1.1 Optimisation of Fourier Analysis

The present implementation of the FFT as described in Section 7.6.1 is not optimal. Currently this is not a significant disadvantage because of the various limitations caused by memory constraints. If, however, more memory is available, not only will it be possible to optimise the FFT algorithm by switching to an in line code algorithm, but the data need not be calculated on a block by block basis as is currently the case. That is 1024 samples are taken and the power spectrum calculated whilst the next 1024 samples are taken. This means that the spectrum from sample to sample can vary greatly because of both transient noise and the non-stationary nature of the muscle signal. As was suggested in Section 7.6.1 these factors are not so significant when the spectrum is further averaged to calculate the median frequency.

If the spectra of sets of samples are to be compared, the data will need to be averaged in the time or frequency domain in order that sudden fluctuations that may occur with a pseudo-stationary waveform do not significantly influence the spectrum. The provision of more data memory on the DSP card would permit the analysis software to average data in the frequency domain before transmitting it to the display processor.

11.1.2 Sliding FFT

This technique is an alternative form of the FFT often used in speech processing and permits the calculation of the FFT at rates more closely approaching the sampling frequency than the conventional algorithms allow. In the case of muscle signals the benefits could be twofold.

The sample rate is slow, so the benefits of this apparently fast algorithm could provide a greater resolution at the same time. It is only applicable to certain types of signals so is not generally used. However Springer[211] suggests that the voluntary muscle response is of the right form to make use of this technique. The speed increases likely can be seen by considering a 1024 point FFT where it takes 5120 complex multiplications and 10240 complex additions using a standard decimation in time algorithm. The sliding FFT requires only 1024 complex multiplications and 1025 complex additions. The technique is essentially recursive, deriving a new value from the previous N and the sample that has just been taken.

The second advantage of this technique is that it is well suited to non-specialised FFT processors or even hardware implementation. Assuming that the chosen spectral parameters can cope with the way the sliding FFT provides its data, this could provide a simple technique for a hardware based analyser.

11.1.3 DSP Based FHT

It was shown in Section 8.1.4 that the Fast Hartley Transform provided significant speed improvements in the original Atari system. It is conceivable that a similar improvement could be achieved with the DSP Card. The second advantage of the Hartley Transform is that the amount of storage memory required to calculate the transform is less than a Fourier Transform requires.

The DSP is optimised for FFT type algorithms, which in this case means there are instructions specifically for bitreversal and the type of multiply and add instructions common in the FFT algorithm. Since the FHT is similar to the FFT in its basic functioning it will also be able to take advantage of the specialised instructions.

The DSP also has a very low interrupt overhead in comparison to the Atari, thus it is unlikely that the effects of the sampling will degrade the algorithm as significantly as on the Atari system. Since the FHT is a relatively new technique, optimised

algorithms do not exist as they do for the FFT, so it is possible, that as was discussed in Section 7.4.2.3 , the improvements may not be as significant as a highly optimised FFT algorithm could provide.

11.1.4 Windowing

Windows were applied in the original Atari system with little detectable improvement in the performance of system when analysing compound action potentials. This is because the action potential trains tend to tail off naturally at the start and the end of the sample period, thus reducing the $\frac{sin(x)}{x}$ type windowing effect that a voluntary muscle signal is likely to be susceptible to.

The choice of window was discussed in Section 7.5.2 and from this it is obvious there are a large number of possible windows that could be applied. The choice will require further investigation, but should help to improve the ability of the DSP analysis system to analyse the less deterministic waveforms that are produced by voluntary muscle.

11.1.5 Sampling Technique Changes

The current system uses a continuous block sampling technique, thus a new frame of data is analysed each second and there is no overlap. As has been discussed above, under the smoothing sections, this not only is unreliable in its ability to reflect the true spectral content of a random signal but is susceptible to noise.

Overlapping sample blocks combined with averaging would enable the frequency spectrum to reflect more accurately the overall signal sample content. When only looking at the median frequency, which in itself is an average of the calculated spectrum, the improvement is unlikely to be any better than smoothing the median frequency samples. When trying to compare spectral plots of CAP trains and in particular the voluntary muscle signal, where the signal is not as deterministic as is the case with CAP trains, the smoothing effects could be very significant.

11.1.6 Other Techniques

Currently the only type of analysis software that has been considered for the analysis system has been frequency analysis. Graupe[96] has claimed some success using a simple shape analysis routine that seeks to monitor the CAP response above the stimulus artefact. This would be a much simpler algorithm, especially using the hardware described here where the CAP distortion is minimised. This would permit an analysis based on the CAP shape.

As has been described in Chapter 9 it is possible to combine the CAP analysis with the shape analysis by suitable combination of the CAP and stimulus rate. Since a tetanic contraction is required for effective muscle function, algorithms that could

make use of this would require the ability to separate the recorded CAP train into a format in which the stimulus cannot affect the output. This could be achieved by considering each sample as 512 CAP pairs or 1024 single CAP trains and then averaging the results.

With improved frequency analysis speed it may even be possible to carry out the frequency analysis during the IPI period on a CAP by CAP basis. This would permit a large amount of averaging to improve signal integrity but at no reduction in update rate which is currently set at one second.

11.1.7 Post -Processing

The Atari software that is currently being used takes full advantage of the software optimisations developed for the original Atari ST system. These include: special fast line drawing algorithms and optimised assembler code. Despite this, careful re-design could improve the system speed slightly but it is not considered that this is the most significant factor. As could be seen in Table 8.1the Atari ST system and the 68000 hardware is relatively slow in processing interrupts. The overheads caused by the technique currently being used to transmit the data is a significant drawback.

The software speed can really only be increased by using the direct access port provided as part of the IBM bus on the DSP card, which would permit a quick download of data with the overhead of only a single interrupt. Clearly this would provide more time for the post processing and analysis routines to process the data before it is displayed in a suitable form. This form has been assumed to be that which is common in the literature but further investigations may reveal that the detail provided by a frequency spectrum is far more than is required.

11.1.7.1 Smoothing

The main thrust of this report has been on the hardware necessary to be able to reliably detect muscle responses from stimulated muscle. Now that this has been achieved, albeit for a limited range of pulse widths, the analysis system requires significant improvement to ensure that it gives more statistically reliable frequency spectral estimates.

As has been discussed in Section 7.6.1, part of the system integrity is determined by the choice of frequency transform and data shaping. The system as configured currently does not have much free processing time due to the excessive interrupt overheads. Reducing this by the techniques described above will give the display software time to post-process the data.

The current median frequency does not use smoothing, as was introduced in the final versions of the Atari standalone system. This is because of the time constraints

involved. Addition of the smoothing routine would prevent the median frequency tracking from being seriously miscalculated due to some interference, such as transients caused by movements of the EMG probe relative to the muscle.

11.1.7.2 Averaging of Results

The second possible smoothing that could be added to the display processing is spectral averaging such that the display is the result of the past few spectra. This would have a similar effect to that described for the median frequency but across the entire spectral display. It is particularly important when considering voluntary muscle response. This smoothing could also be done at the DSP stage.

11.2 Hardware Improvements

The hardware as originally envisaged is fully integrated with the display processor, which in this case is the Atari Mega. As described in the thesis, this stage of integration has not been fully completed and thus the system is unable to run at its optimal speed. Thus on the hardware side there are two groups of improvements and further work that can be carried out to improve the system. Those aimed solely at improving the system integration and speed and those aimed at improving the effectiveness of the system in carrying out its task.

11.2.1 Improvement of DSP Display Processor Link

The DSP card provides, via its IBM compatible bus connector, the facility to read the DSP memory, directly removing most of the overhead that otherwise is entailed. The only overhead would be if the second processor tried to access at the same time as the DSP in which case wait states are introduced into the DSP. This link has been successfully used to produce a number of the results by grabbing the results and saving them to hard disk using the IBM host computer.

If this bus were provided by the Atari Mega expansion bus, the Atari display processor would be able to overcome the current problems caused by the slow link. This would reduce the interrupt overhead and speed up the display processing.

Currently, work is continuing on a fully integrated 68070 based display processor and TMS320C25 card to do this. The bus interface of the IBM is very simple and could readily be added to the current system configuration to take advantage of the software already written for this configuration and provide a number of the software improvements suggested above with little or no visible overhead.

11.2.2 Storage Facilities

The system currently has only two options for saving the data. These are screen dumps from the Atari system to a RAM disk which is later saved to floppy disk or via the DSP boot software running on the IBM which saves the data directly to hard disk.

Once again the time limitations are one of the main reasons the Atari does not provide more comprehensive saving facilities. The reason the real-time options are important is that the results obtained during a paraplegic stand differ quite markedly from those obtained by just stimulating the muscle. Clearly when recording information of this nature it is important to be able to see the changes and relate them directly to the action of the subject. The addition of a mass storage device such as a hard disk to the Atari would improve the reliability of the saving of data. More free processor time would allow results such as the calculated median frequency to be buffered in memory before saving to disk. This would permit more detailed analysis than is available from the screen dumps.

The Atari itself has 4 megabytes of memory permitting large buffers to be implemented so that later analysis of the stimulated muscle response can be carried out. These facilities are necessary to take the research on to the next stage, which is the identification of the parameters to follow in order to determine the muscle state as would be required in a feedback controlled stimulator.

An alternative option is the recording of the data with some form of time-coded video of the patients stimulated movements. This would allow considerably more complex post processing of the data on a mainframe. The calculated results could then be played back in real-time and synchronised with the video.

11.2.3 Use of IBM as Display Processor

Although the system has been designed around the Atari, the IBM AT computer which has hosted the DSP card has proved capable of fast displays in real time. This is mainly due to the fast 80386 processor that it uses. Since the IBM PC is a common sight in the medical environment, a CAP analysis system that can be plugged into an IBM expansion slot could be another possible area in which the analysis software could be made use of.

Clearly further hardware would be required in addition to the DSP card to provide the facilities for synchronisation and to link in the gain adjustment directly with the software scaling.

11.2.4 AGC techniques

One problem associated with the system is its reduced sensitivity with small input signals. The main reason for this reduction is the quantisation levels of the ADC combined with the fixed point integer arithmetic. As was described in Section 8.2.4.1 , there is a finite minimum of ADC values required to produce a meaningful result from the integer arithmetic FFT algorithm.

If the input gain could be automatically adjusted to make maximum use of the ADC range then the SNR of the system with low level signals would be dramatically improved. This would require that the DSP algorithm can identify the input gain required to do this, so that the correct scaling can be achieved.

The present amplifier configuration has a manual adjustment of the gain, which means the voltage scales do not reflect the true input signal but rather the signal seen at the ADC input. The addition of an amplifier whose gain can be controlled by the DSP card would enable the provision of the AGC function and ensure that the calculated results are a true reflection of the input signal.

11.2.5 EMG Probe Design

The EMG probe is currently the major limiting factor in the ability of the CAP analysis system to detect and amplify long pulses. The reasons appear to be due to various inherent system capacitances. Their precise source is unclear and seems to be mainly due to the amplifier integrated circuit used. If this design could be improved to reduce its saturation time constant still further, it is conceivable that this technique could usefully be applied to the strength-duration tester described in Appendix A.

Another area where the design could be improved is by including an earth contact as part of the electrode head. This would remove the need for the separate earth strap that is currently required. Some researchers have proposed using a metal case for their small EMG probes. This not only provided screening for the high gain amplifier but by bringing the casing edge down to the same level as the electrodes it provided an earth contact around the electrodes.

The addition of screening to the present configuration would further improve the noise rejection of the EMG probe. This could also help to reduce stray capacitance that is reducing the effectiveness of the EMG probes when amplifying CAP trains. Figure 11.1 shows two of the suggested EMG probe configurations in diagramatic

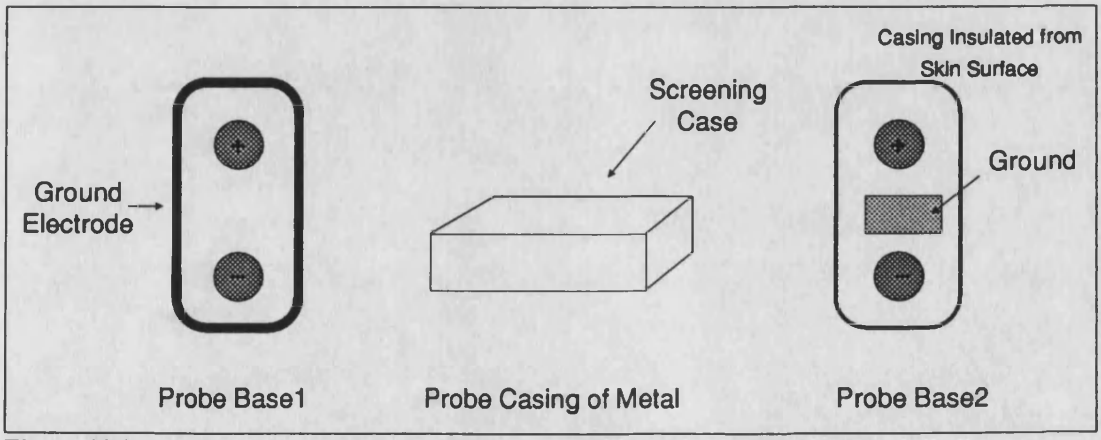

Figure 11.1 *Alternative EMG Electrode Configurations*

form. The circular electrodes represent the differential amplifier inputs and the other shaded blocks represent the ground electrode.

11.2.6 Stimulator Design

The stimulator is a key part of any CAP analysis system. As has been described, the present stimulator designs have serious limitations when trying to record artefact free CAP trains. It has been shown that by controlling the discharge rate of the stimulator a major contributor to the artefact content of the recorded CAP trains may be reduced sufficiently to allow the stimulus artefact to be removed by extra external hardware. The two stimulator designs both have drawbacks but it is clear that the operational amplifier based stimulator appears much more effective when artefact suppression is required.

The switch mode power supply based stimulator design is a very effective stimulator but has disadvantages because of both a limited pulse width range and because of its inability to actively switch off. This is clearly an area where much further work is required. The operational amplifier design, though proving effective, is a long way off being a medically safe stimulator, in that it does not conform to BS5274 and is only suitable for use within the laboratory.

Currently, work is continuing on improving the stimulator designs so that they are capable of fulfilling the requirements described above and of providing the complete pulse width range required by the strength duration tester.

None of the stimulator software takes advantage of the power down modes available with the CMOS processor. This means that although generally the processor card is doing nothing, it is still drawing about 80 mA. If the power down mode were added such that the processor is only active when outputting the stimulus pulse or a key is pressed, the overall power consumption should be significantly reduced. If it is assumed that the standard stimulus is being generated, that is, a 300μs pulse every 40 ms and the pre- and post-pulse hold times are of the order of 1 ms, then the processor need only be active for a twentieth of the time except when processing the keyboard. This would allow practical battery based stimulators to be made. The use of a battery as the power source makes compliance to British Standards for medical equipment considerably easier.

11.3 Practical Use of Systems

A number of potentially useful pieces of equipment could be derived from the various systems described in this report. Work is still required to ensure that the systems conform fully to the requirements of the various medical standards such as BS5274.

The original aim of this research, which was to produce EMG processing units suitable for use as feedback sensors, clearly requires a lot of further work. The work has shown that the use of surface electrodes to detect CAPs would be far too variable to be of great use as a feedback signal for a stimulation system. If, however, the signal quality could be guaranteed, as is the case with internal systems, then the use of frequency analysis to provide feedback could become a viable option. With the current technology the only practical use would be a technique similar to that used by Graupe based on the CAP amplitude.

The frequency analysis system, as has been suggested, requires extensive further work to make it a frequency analysis system suitable for both CAP potentials and voluntary EMGs. The current implementation provides a non-optimal means of translating signals to the frequency domain.

The two items that would require minimal further work to make them into useful products are described in Appendix A and B. The strength-duration tester described in Appendix A suffers a number of shortcomings due mainly to the stimulator design. Despite this the system performed quite reliably in the tests showing that it is possible to base an automated strength duration tester on accelerometer technology. The changes required are discussed in detail in Appendix A. Other detection techniques are also discussed and it is possible even more reliable results could be obtained from these with very little extra work.

The Muscle Fatigue Monitor described in Appendix B requires minimal extra work to transform the hardware into a suitable form for general use. It is in the software that improvements could be made to make the system more user friendly and provide it with better real-time analysis capabilities. These requirements would have to be met before the system could be used outside of the laboratory environment.

Acknowledgements

The author would like to thank Professor J. F. Eastham for the provision of facilities in the School of Electrical Engineering; Dr R. T. Lipczynski who supervised the research and provided valued advice and encouragement; Mr F. Burgum and Mr J. Sharp of Philips Components Application Laboratory for their advice and provision of components and the Science and Engineering Research Council and Philips Components for the provision of finances.

Thanks are also due to Mr L Grant of the Royal United Hospital for his valuable advice; the members of the Communications Research Laboratory for the provision of various pieces of test equipment with which some of the results were recorded and in particular Mr R. Mannings for his help, advice and encouragement; Mr A. Jenks and Dr Holbeche for the use of their laser printers and Mr R. Hill-Cottingham for the provision of storage scopes and PCB design software.

A special thanks to the members of the Medical Physics Department at Odstock Hospital, Salisbury; the members of the standing and walking research program at the Duke of Cornwall Spinal Injuries Unit, Odstock and Marie Thérèse House, St. Michael's Hospital, Hayle and many Students at the University of Bath for their willingness to try the equipment.

Lastly a special thanks to Fiona and Rob, my prof weeders, who spotted most of the mistooks.

Appendix A

Automated Strength Duration Curves

Strength-duration curve plotting is a technique often taught in physiotherapy schools but rarely used in clinical practice[30,213]. It is a plot of the strength of impulses of various durations required to just elicit a contraction in a muscle and is the most satisfactory method of routine testing of electrical reactions in peripheral nerve lesions. The shape of the curve gives an indication of the proportion of denervation, while a series of curves measured over a number of weeks shows changes in the condition. The test itself is simple and reliable but time consuming to carry out and in large muscles only a proportion of the fibres may respond.

The test is not generally used because of the time involved, about 30 minutes, and the requirement that the same physiotherapist carries out the test to ensure each curve has a consistent twitch level detection. The technique seems highly suited to automation as long as a reliable means of detecting the muscle response can be found.

This Appendix describes the work carried out to produce an automatic strength-duration tester. It first summarises a few of the features of the strength-duration curve and the application of such information, before going on to discuss various possible techniques that could be used to detect a muscle twitch.

A.1 The Strength Duration Curve

The only previous attempt to automate this test that could be traced was in 1963, by Thomas and Morton[214]. In their system they used a stimulator powered by 120V batteries with the switching circuitry being based on transistors triggered via an isolating transformer. The stimulating electrode was a probe electrode placed over the motor point of the muscle. The anode was a metal plate, 2.5cm x 5cm placed over a distal part of the muscle. The skin resistance was reduced with electrode jelly.

The muscle twitch was detected using electromyography using a double core needle electrode with the shaft earthed. This electrode was oriented such that it lay on equipotential lines in the field produced by the stimulating electrodes, in order to reduce the stimulating artefact. Identification of the twitch was done visually and was defined as the point at which the electrical activity that could be detected was clearly identifiable as being a motor unit.

The authors claim some success for their technique in identifying more details in the recorded strength duration curve, however the system was a long way off being fully automated and required considerable preparation. The use of needle electrodes, though

useful both for reducing artefacts and for giving a more detailed pickup, precludes the systems general use. This is especially true within the typical physiotherapy department, where qualified personnel are required to insert the needles.

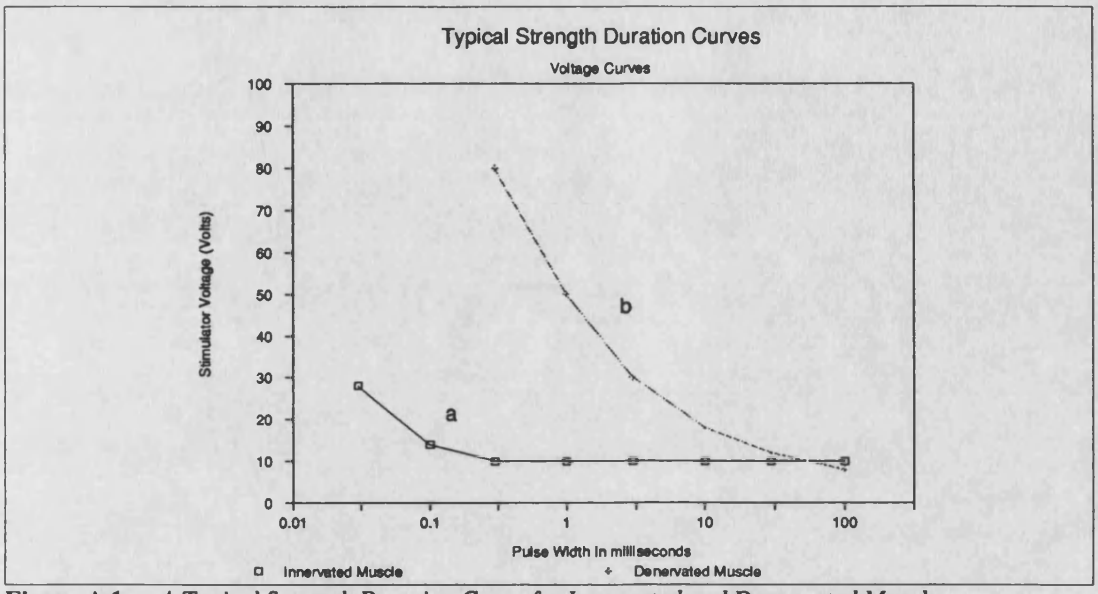

Figure A.1 *A Typical Strength Duration Curve for Innervated and Denervated Muscle*

A.1.1 The Basic Test

The test is carried out using either a constant-voltage or constant-current stimulator. Before the test is carried out the skin resistance is reduced by washing the skin over the muscle. The active electrode is placed over the belly of the muscle whilst the indifferent electrode is placed at some convenient point such as the origin of the muscle group. It is usually necessary to experiment to find the optimal positioning before commencing the actual test. Care must be taken not to fatigue the muscle whilst setting up.

The stimulation is started with the longest pulse width (100 or 300ms) and the intensity increased until a contraction is obtained. This contraction is usually detected by palpitation or visually. The procedure is repeated for each pulse width, noting the intensity required to just get a minimal contraction. It should be noted that generally the intensity increases when reducing the pulse width, thus usually only an increase is required. Figure A.1 shows typical strength-duration curves for innervated and denervated muscle.

A.1.2 Interpreting the Strength Duration Curve

Normal Innervation When all the nerve fibres supplying the muscle are intact, the strength-duration curve has the typical shape shown in Figure A.1a. The curve is this shape because the same strength stimulus is required to produce a twitch with all the larger pulse widths, while the narrower pulse widths require an increased stimulus each time the pulse width is reduced. The point at which the curve starts this rise

varies but is usually around 1 ms with a constant-current stimulator and 0.1 ms with the constant-voltage stimulator.

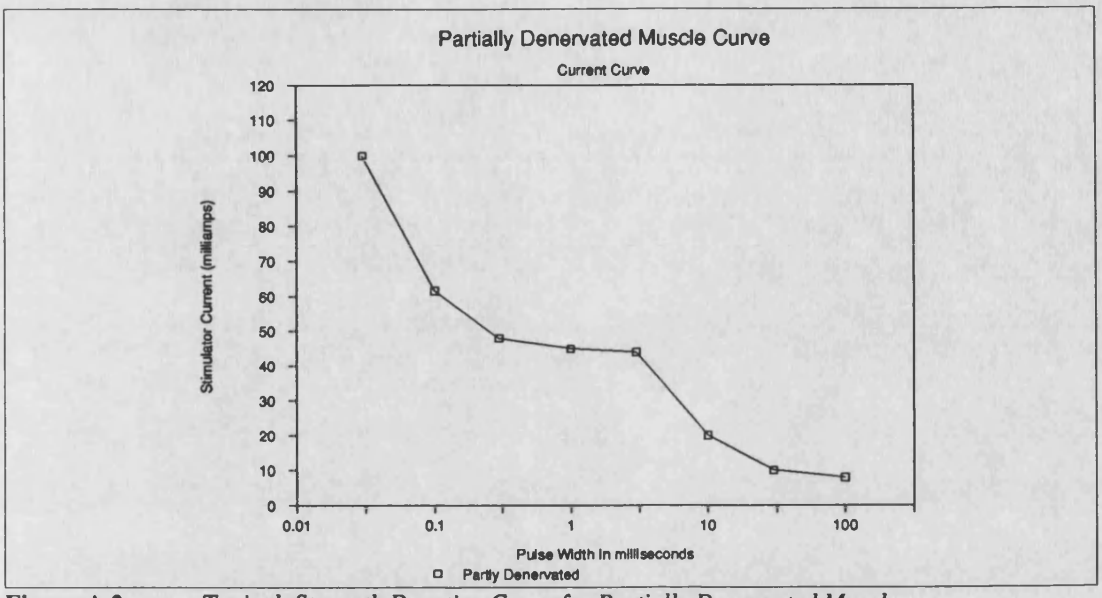

Figure A.2 *Typical Strength Duration Curve for Partially Denervated Muscle*

Complete Denervation When all the nerve fibres supplying a muscle have degenerated, the strength-duration curve has the typical shape shown in Figure A.1b. For all pulse widths of 100 ms or less the strength of the stimulus has to be increased each time the pulse width is reduced, and no twitch occurs for pulse widths of very short duration. This causes the curve to rise steeply and is further to the right than that of normally innervated muscle.

Partial Denervation When only some of the fibres supplying a muscle have degenerated while others are intact, the characteristic curve obtained clearly shows partial denervation, Figure A.2. The wider pulse widths stimulate both *innervated* and *denervated* muscle fibres, so a contraction is obtained with a low intensity stimulus. As the pulse width narrows the *denervated* fibres respond less readily, so that a stronger stimulus is required to produce a contraction and the curve rises steeply like that of denervated muscle. With the narrower pulse widths, the innervated fibres respond to a weaker stimulus than that required for denervated fibres, so contraction of denervated fibres is not obtained and the curve resembles that of the innervated muscle. Thus the right hand half of the curve is similar to a denervated muscle curve, the left hand part is similar to that of an innervated muscle curve and at the intersection there is a kink.

The shape of the curve indicates the proportion of denervation. If a large number of fibres are denervated, the curve rises steeply and the greater part of it resembles that of denervated muscle Figure A.3a. If the majority of the fibres are innervated, the curve is lower and flatter and is more like the innervated muscle curve Figure A.3b .

Changes in the shape of the strength-duration curve are often the earliest signs of the restoration of the nerve supply to a muscle. A kink appears in the curve and as re-innervation occurs, the curve moves down and to the left. Progressive denervation is indicated by the appearance of a kink, an increase in the slope and a shift to the right.

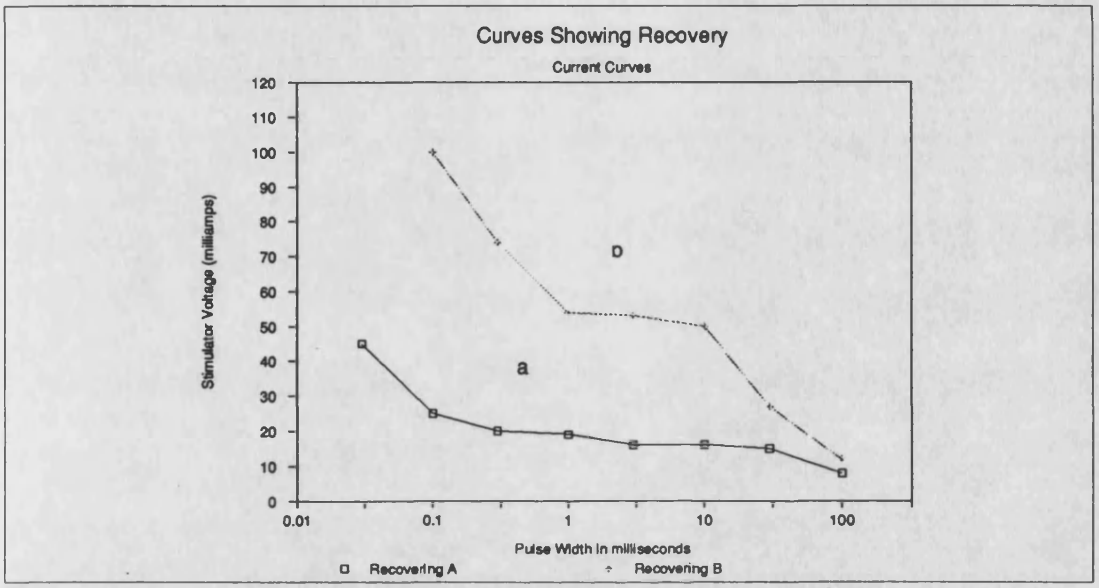

Figure A.3 *Strength-Duration curves of Partially Denervated Muscle , showing different degrees of Denervation*

Rheobase This parameter is still sometimes used and may be derived from the strength-duration curve. It is defined as the smallest current—voltage—that will produce a muscle contraction if the stimulus is of infinite duration; in practice a duration of 100 ms is used. In denervation, the Rheobase may be less than that for innervated muscle, and it often rises with re-innervation. Unfortunately these changes are not reliable enough to be useful in diagnosis.

Chronaxie This parameter is the duration of the shortest impulse that will produce a response with a current—voltage—of double the Rheobase. The chronaxie of innervated muscle is considerably less than that of denervated muscle. Usually less than 1 ms for innervated muscle and greater than 1 ms for denervated muscle if using a constant-voltage stimulator; constant-current stimulators produce higher values. Chronaxie is not useful for testing electrical reactions because it does not clearly distinguish between partially denervated muscle and innervated or denervated muscle, the chronaxie being that of the dominant fibres. That is, if a muscle had only twenty five per cent of its muscles innervated the chronaxie would be the same as for a completely denervated muscle.

A.2 Specification of the System

A.2.1 The Stimulator

The stimulators currently being used are manually operated, supplying square pulse trains with durations of 0.01, 0.03, 0.1, 0.3, 1, 3, 10, 30, 100, 300 ms. The interval between pulses and the intensity are both adjustable. Both constant-current and constant-voltage stimulators have been used, though there seems to be no significant difference in their respective results except a slight time shift in the curve.

A.2.2 The Detection System

The requirements for the detector are on the face of it fairly simple. The detector has to be able to detect the muscle response just as it occurs and then the controller needs to record the voltage—current—for that particular pulse width before switching to the next pulse width.

Three possible means of detection have been considered:

- An EMG amplifier
- Some form of sound detector
- An accelerometer

A.2.2.1 An EMG Amplifier

The use of an EMG amplifier would clearly provide a number of advantages. The effect of stimulation is to produce 'one large' compound action potential which lends itself readily to computer detection. The availability of a set of compound action potentials for a range of pulse widths for a particular muscle, could provide considerable further information about the muscle. This could include some indications of fibre type—slow or fast—if a suitable inverse model could be found, as discussed in Section 2.1.2.

There are however a number of problems. There is the basic one of a stimulation artefact that not only saturates the amplifier, but also could distort the picked up CAP, leading to misinterpretation of the twitch point by the twitch detector system. The second possible problem is that of the muscle response occurring whilst the stimulation is still present, which would be likely in the case of the long pulse stimulation. This would be fine as long as there is sufficient muscle activity after the pulse to allow reliable detection. Clearly moving the pickup so that it is more remote may solve this problem and also reduce the effects of the stimulation, but it would also require a larger CAP to overcome the body's natural filtering properties. The use of EMG will require a number of extra electrodes—at least three. This could be solved by building the amplifier into a unit containing the electrodes or even using the electrodes as the pickup as Graupe has done[96]. The final possible problem is the

detection of muscle signals from denervated muscle; because the muscle is being stimulated directly, a much smaller twitch and hence CAP is produced.

A.2.2.2 Sound Myography

That contracting muscles produce sounds has been known for almost two centuries, ever since Woolaston [215] 1810 and his Croonian lectures, though the first mention was by Grimaldi[216] in 1665. Muscles contracted by electrical stimulation were found to produce the same sound as those contracted voluntarily by Herroun and Yoe in 1885. They applied an electrical stimulus to a muscle every second and were struck by how the sound resembled that of heart sounds.

The muscle sounds are produced—it is thought—when the individual fibres tense—a cracking whip type of effect. The main frequencies of this sound are centred around 25 Hz. The effect of stimulation is to fire all the fibres practically simultaneously causing one loud crack which should be readily detectable.

The phenomenon of muscle sound has been largely neglected until recently because body sounds are usually detected with a mechanical stethoscope. This is typically maximally responsive to sounds around 200 Hz and is practically unresponsive at 20 Hz. It has not been until recently, when the newer transistorised stethoscopes became available, that interest in muscle sounds and their possible uses has been revived—Oster and Jaffe[217]. The other problem with the sounds is that their low frequency means that the sounds are readily confused with the ambient noise, such as that from machinery, footsteps and traffic noise, which is much harder to filter out than with high frequency noise. If the signal is periodic, such as is the case with stimulated muscle and to a lesser degree with voluntary muscle contractions, autocorrelation and other well known digital signal processing techniques may be used to enhance and extract the signal of interest.

Barry et al.[218] have investigated acoustic myography as a non-invasive monitor of motor unit fatigue. They found that the acoustic signal RMS amplitude increases with increasing force of contraction and shows an approximately linear relationship with increasing load. They present results which show that whilst the EMG shows only a small change with reducing muscle force—fatiguing—the acoustic RMS signal follows the reduction in force quite closely. They also were able to resolve individual motor units by monitoring both the acoustic and EMG signals and correlating the individual acoustic spikes. This shows that the result of stimulation should be readily detectable because of its similarity to the single motor unit.

Rhatigan et al.[219] have investigated the muscle sounds of healthy and diseased muscle. They concluded that there is significant differences between the sounds produced by healthy muscles and those with neuromuscular disorders. They also

found significant peaks in the power spectrum in the 5-12 Hz range and that as the contraction force increases these peaks shift up. They found for their normals a mean frequency of 15.1±4.2 Hz whilst Oster and Jaffe[217] obtained 25±2.5 Hz, though as they note their experimental procedures differed considerably.

Diemont and Figini et al.[220] have carried out comparisons of the sound myogram with the surface EMG signal for fatiguing muscle for voluntary contractions. They have found that the sound myogram displays similar properties to that reported in the literature for surface EMG; though they comment on finding a bimodal pattern in the sound myogram which suggests that more variables should be considered rather than just the mean frequency. In a more recent paper[221], where the cross-spectrum of muscular sound and surface EMG was considered, they found that the surface EMG still showed a more accentuated change with fatigue than the cross spectrum, though they did suggest that the sound myogram was suitable for following the firing pattern changes during sustained contraction.

With the advent of better sound amplification techniques the use of sound myography is increasing and showing potential in a number of different fields previously limited to electromyographic type studies. In the case of the strength-duration test there are some clear advantages over an EMG amplifier.

The stimulating voltage would not be able to affect the microphone which would be isolated from the stimulus. This would allow the recording of any event that may occur during the stimulation pulse without distortion. As suggested for the EMG amplifier it would be possible to combine the pickup with the stimulating electrodes so removing the need for a separate detector. There are some obvious problems with this approach. The sound frequencies are very low, which makes detection from the background noise harder, but as discussed above, because the stimulus produces a repetitive response, simple autocorrelation could be used to enhance the SNR before processing. The low frequencies also cause a second problem, that of finding suitable, cheap, transducers that have a frequency response that goes low enough.

A.2.2.3 Motion Detection

The accelerometer is another device which is finding renewed interest with the advent of modern electronics and signal processing. The accelerometer is based on the piezo-electric principle. When the piezo crystal is distorted by rapid movement of the crystal in the transducer, its output voltage is proportional to the deformation of the crystal. Hence it is possible to measure the acceleration of the object causing the rapid movement—in this case the muscle.

Itagaki et al.[222] have compared the accelerometer with a conventional force transducer for the evaluation of twitch responses. They found that it had some distinct

advantages over the conventional strain gauge, which requires a resting tension to ensure it has a constant baseline. Since the accelerometer responds to movement, stringent conditions on the movement direction and position are not required. They found the twitch responses almost identical to those from the force transducer. There was one distinct disadvantage of the accelerometer. This was that during tetanic contractions the transducer produced no output because it responds to movements that distort the crystal and not to the steady position response implied by the tetanic contraction.

Yoshida, Lamoreaux et al.[223] have used the accelerometer to replace EMG or force transducer measurements for assessing the patellar tendon reflex; a common test for spasticity. They found considerable advantages with the accelerometer; it does not prevent the normal reaction movement of the leg, it can be used with the extremities in any position, the accelerometer being light and small does not appreciably affect the reaction itself.

More recently, Willemsen, Alsté and Boom[224, 225] have been considering accelerometers for use in the feedback path of FES systems particularly for walking. They have shown theoretically that accelerometers can be used for the assessment of angle, velocity and angular acceleration of the different segments of an ideal multi-segment body.

The accelerometer shows a lot of promise as a twitch detector because, as with the sound myography, it is electrically isolated from the stimulus and patient. Itagaki et al.[222] have shown it functions well at twitch detection and all authors agree that positioning is not as stringent as in the case of EMG pickups. There is a potential problem in that the accelerometer is unable to detect tetanic contractions, but in the case of the strength-duration test this is not required.

A.3 System Design

Some initial work on this project has been carried out over the past three years by final year project students under the supervision of the author[226, 227]. Of these Lee[226] was the only one who managed to get some form of automated system going. The hardware was based on a muscle stimulator design in use within the medical electronics laboratory at the time and this was controlled by a BBC microcomputer using the 1 MHz expansion bus, which also had an ADC connected. The detection system made use of an accelerometer for the detection which was carried out by a BASIC program running on the BBC.

The design was neither reliable nor suitable for trials within the School of Physiotherapy at the Royal United Hospital here in Bath. The system that has now

been designed makes use of much of the circuitry and software already described in Chapter 5. It is self contained, portable, battery powered, and capable of interfacing directly to a micro-computer for the display and printing of the results. Figure A.4 is a block diagram of the complete system showing all the major components.

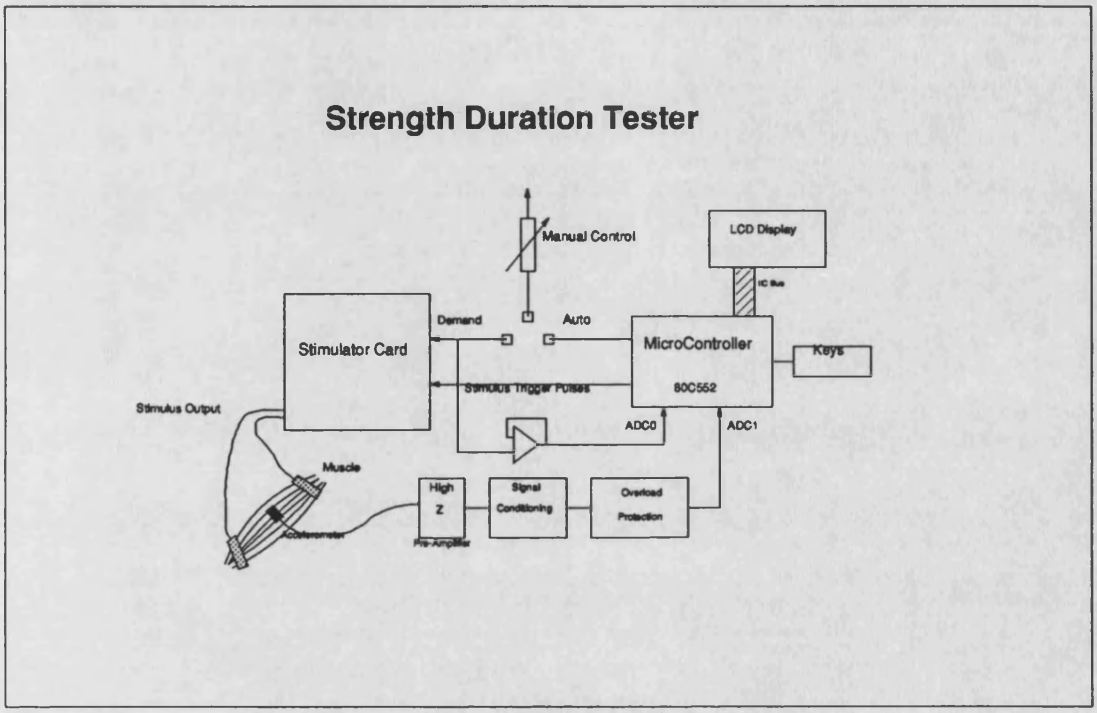

Figure A.4 *Block Diagram of the complete Strength-Duration Tester*

A.3.1 Hardware Configuration

As has been stated already, the circuitry is derived from the stimulator design used for the EMG system described in the bulk of this report. The design differs in a number of ways. Since the system was being built as a piece of test equipment, to compare results from the automatic tester and those obtained in the conventional manner, it has two modes: a Manual Mode and a Micro Mode. Both these modes have to produce voltage measurements based on the same scale, thus requiring the stimulator to have a voltage read-out. Simplicity of use is another important requirement, so a minimal keypad of four buttons is used combined with a beeper capable of a number of different types of beep to give audible feedback of mistakes and key clicks. In the Micro mode there is the possibility of the system failing to detect the twitch and continuing to ramp the stimulus up. In order to prevent this error causing serious injury an abort button is incorporated which will halt the test and zero the output of the stimulator.

A.3.1.1 The Stimulator

The stimulator card is based on the 2 channel walking system output card as described in Section 5.2.1. Figures G.36 and G.38 give the circuit diagram of this version. It is

functionally the same except that only one channel is actually brought out; the other channel remains as a spare should the one in use fail. The FET driving the output transformer is mounted on a heat sink since there is a chance that with the long pulse—100ms, 300ms—the FET will warm up considerably. The voltage clamp, Section 5.2.1, is provided and can be switched in or out as required allowing the system to be used with EMG pickups similar to those described in Section 6.3.

A.3.1.2 The Microcontroller

The microcontroller card is again functionally similar to those already described for the stimulators of Section 5.1.2. However a number of significant changes have been made. Figure G.37 gives the revised circuit diagrams for this card. The basic microcontroller configuration remains the same as in the standalone stimulators, with the stimulus signals and synchronising pulses being generated by VMOS FETs powered from the 10 V supply on the stimulator output card.

The main differences occur with the input keyboard and LCD display. On this controller card the LCD is a four digit eight segment display controlled via the I^2C bus. The keyboard, which consists of only four push to make buttons, connects directly to four port lines which are normally held high via 10kΩ pull-ups. Pushing one of the keys pulls its respective port pin low. The Abort/Enter and Mode keys connect to the INT 0 and INT 1 external interrupt pins, to allow their use as overrides via the interrupt function.

Inputs 0 and 1 of the ADC—P5.0 and P5.1—are used for the sampling of the demand signal in order to calculate the output voltage and the sampling of the detection signal from the pickup. Both these inputs are protected by clamps, which clamp the inputs between 0 and 5V, to prevent over voltage damage of the ADC.

A.3.1.3 The Battery Charger

The battery charger, Figure G.38, is a simple constant current source. It is combined with relay circuitry that prevents the unit being used if the mains is connected. This is achieved by relays that are powered by the battery charger such that the batteries are connected across the charger when mains is connected, and to the strength-duration circuitry when the mains is not.

A.3.1.4 The Twitch Detector Interface Circuitry

The twitch detection circuitry has been designed as a two stage interface. There is a buffer and amplifier stage that feeds into the clamp circuitry for P5.1. This circuitry is fed via the front panel 5 pin DIN socket. The signal into the socket, which also provides ±9V power, comes from an appropriate preamplifier which would depend on the detector. In the case of the system described here it is the accelerometer. This has a preamplifier giving a gain of ten, Figure G.35.

The signal in is AC coupled and DC shifted, to ensure it sits around 2.5 V for a zero volt input at the ADC input. The gain stage can be adjusted by a multi-turn preset to give a gain between 1 and 200.

A.3.1.5 The Detector

The detector used in this implementation is an accelerometer. This detector has a high impedance buffer and gain stage of ten which feeds into the strength-duration tester. Figure G.35 gives the circuit diagram for this stage.

From the circuit, it can be seen that there is a large input resistor of 1GΩ. If the typical leakage current for the BB3503 is 0.005 nA then one would expect a DC offset of at least 5 mV at its output. This coupled with the second stage amplifier which has a gain of 10, would give about 50 mV offset—worst case. Clearly this is unacceptable if a high gain is required to ensure very small twitchs are sufficient to trigger the twitch detector software. To overcome these problems the offset null circuitry shown in the circuit diagram has been added to the original configuration to eliminate this problem.

A.3.2 Software Configuration

As has already been described, the strength-duration stimulator is capable of two modes: Manual or Micro mode. The software is configured as two independent loops. One that deals solely with the Manual mode and one that deals solely with the Micro mode. The MAIN control routine executes the initialisation code then it jumps on the state of the Manual/Micro switch, P1.1; either the Micro mode or Manual mode control loop is entered. Each cycle through the Micro or Manual loop, the Manual/Micro switch is checked for a change of state and if detected a controlled exit of the current loop occurs and a controlled entrance into the other loop is made.

The default state for the stimulator in Manual mode is 300 μsecs pulse width and 40 ms IPI, with the clock switched off, that is, no stimulus output. A default display of OFF on the LCD display and the voltage LED lit.

The Micro mode defaults to 300 ms pulse width and a 1 s IPI which is the first pulse width required for the strength-duration test. The LCD display defaults to ---- and all LEDs are off.

Software debouncing is required for the function keys which connect directly to port pins. These four keys control all the functions of the tester except the output voltage, which is either controlled by a potentiometer in the case of Manual mode or by the processor via a DAC in Micro mode.

A.3.2.1 Software Concept

The software is based on state machine principles, that is each possible state can be represented by the value of a number of internal state variables. It is the value of these

variables that governs progress from one state value to another, thus ensuring that the software flows along a well defined path.

Two variables are used to control the states: an outer variable WMDE which determines which set-up/output mode the system is in, that is, Volts, IPI or PW for Manual mode. In the Micro mode a second state flag AMDE controls the progress around the automatic test routine until the Micro/Manual switch changes to Manual mode when WMDE takes over. When the mode state changes the machines will always exit their previous mode state and enter the new one via a clearly defined path, thus ensuring that the user does not suffer any unexpected stimulus. This requires checks that the output is zero and that the stimulator triggers are off.

Interpulse Interval	Permitted Pulse Widths (≈10%IPI)
40 ms	≤ 3 ms
100 ms	≤ 10 ms
500 ms	≤ 30 ms
1 s	≤300 ms

Table A.1 *Table Showing Permitted Pulse Widths for Manual Mode*

A.3.3 Manual Mode

Manual mode is the simplest of the modes to implement. It provides for the manual setting of the pulse width across the range required for the strength-duration test and adjustment of the IPI to allow for a sufficient delay between pulses for the larger pulse widths. The system defaults to the 'standard' tetanic type stimulus of 300 μs and an IPI of 40 ms to permit the initial locating of the electrodes. The control diagram is shown in Figure A.5. The three major states are the OFF/Voltage Display, IPI adjust and pulse width adjust. The switching between these states is achieved by the SET key, with the ARROW keys being used to change the values up or down for PW and IPI setting. Setting of the new values is achieved using the ENTER button which is used to switch on the stimulator output from the OFF/Voltage Display level. Output voltage level is controlled by the output potentiometer. If the output demand is not zero when an attempt is made to switch on the stimulus, the error buzzer is sounded and rEdu is displayed. The new values of PW and IPI will only be accepted if they satisfy the rules given in Table A.1. The checks are carried out by the routines CHKPW and CHKIPI in the module ERRORS. If the pulse width interpulse interval combination is not permitted, the routine returns to the OFF state but sounds the error buzzer instead of setting the new value. Whilst the processor is in the set IPI or set PW modes the stimulus trigger is off and may only be switched on after the setting has been completed and the display has returned to OFF.

A.3.4 Micro Mode

Micro mode is the most complex of the two control loops. In order to have as much

```
CODE                                        SUBROUTINE
Start
Initialise
    All LEDs Off
    Clear Internal and External RAM
    Set DACs to zero
    Set Up Default State Values
      STATE = 00H
      WMDE  = 00H
      AMDE  = 00H

;Manual Control Loop
Repeat
;Enter Key                                  ENTERFN
 If P3.2<>1
      If WMDE = 0 AND Demand = 0
        Turn on Stimulus Trigger
      Else
        Display rEdu                        BEEPL,ERRMSG
      Endif
      If WMDE = 1 AND CHKIPI                CHKIPI
        IPI=IPIN
      Endif
      If WMDE = 2 AND CHKPW                 CHKPW
        PW = PWN
      Endif
 EndIf
;Mode Key                                   CHNGEMDE
 If P3.3<>1
      Inc WMDE
        If WMDE = 3 Then WMDE = 0
 Endif
;Up Key                                     UPFN
 If P3.4<>1
      If WMDE = 0 Then Sound Buzzer         BEEPS,ERRMSG
      If WMDE = 1 Then Inc IPIN
        If IPIN = 4 Then IPIN = 0
      Endif
      IF WMDE = 2 Then Inc PWN
        If PWN = 10 Then PWN = 0
      Endif
 Endif
;Down Key                                   DWNFN
 If P3.5
      If WMDE = 0 Then Sound Buzzer         BEEPS,ERRMSG
      If WMDE = 1 Then DEC IPIN
        If IPIN = 255 Then IPIN = 3
      Endif
      IF WMDE = 2 Then Inc PWN
        If PWN = 255 Then PWN = 9
      Endif
 Endif
 Update LCD Display on WMDE                 SHOW,LCDIPI,LCDPW
Until Micro Mode ie P1.1<>1

Micro Mode Loop
```

Figure A.5 *Flow Diagram for the Control of the Manual Mode*

security in the system as possible, all possible states are coded even though, theoretically, some can never be reached. This is to allow for any spurious crash that may cause the system to suddenly jump into the wrong code section. Figure A.6 gives the pseudocode for the MICRO mode.

The default state is a superfluous level, which is there to ensure that the automatic testing can only be started by two distinct key presses, thus ensuring accidental triggering is minimised. Once again SET is used to take the system through the top level states, that is ----, tESt, Sho. With the Sho(w) state being the only state in which the ARROW keys serve a purpose. They are used to change up or down through the pulse widths, the ENTER key is used to toggle the display between the recorded voltage and pulse width. If the test was aborted and the pulse width not tested null is displayed in place of the recorded voltage.

The automatic test is started by the ENTER key from the tESt state. Once in the auto-test mode the system carries out the complete test unless aborted by the ABORT/ENTER key. The display gives an indication of what stage the test is at by passing through the messages, Strt, AVE, 300, 100, 30, 10, 3, 1, 300u, 100u, 30u, 10u, Sho. The SET key may be used to toggle the display to the voltage that is actually being outputted instead of the pulse width being tested. The keyboard functions during the test are achieved by using external interrupts instead of polling to ensure that aborting of the test can be guaranteed.

A.3.4.1 The Twitch Data

The twitch detector used for the system described here makes use of an accelerometer. This device is based on a piezo-electric crystal. Although this is electrically isolated from the stimulating circuitry it does suffer some interference, this appears to be capacitive coupling from the skin surface. This results in spikes at the stimulus points of the waveform Figure A.7. In order to avoid thi,s the sampling system only starts to sample the accelerometer response after the stimulus switches off by triggering on the edge of the sample and hold pulse. The sample and hold pulse, as described in Section 5.1.2, can be programmed such that it is active a pre-pulse period before the stimulus and continues to remain active until a post-pulse period after the stimulus. This allows the sampling of the muscle response to be as long as is necessary after the stimulus pulse is finished. Currently this period is preset to 128 μsecs after the stimulus pulse ends.

Figure A.7 shows some typical responses from the accelerometer for a threshold twitch. This may be compared with Figures A.8 and A.9, which show the noise signal and the response for a large twitch, respectively. It can be seen that the threshold twitch is easily distinguishable from the background noise suggesting that some

```
CODE                                          SUBROUTINE
Repeat
;Abort Key                                    ABORTFN
 If P3.2<>1
      If AMDE = 0
        AMDE = 3  ;Show Mode
        Display Sho on LCD                    LCDSHW,BEEPS
      Endif
      If AMDE = 1
        AMDE = 2  ;Test Mode
        Display Strt on LCD                   LCDMSG,BEEPS
        Do Strength Duration Test             DOTEST
      Endif
      If AMDE = 2
        AMDE = 4  ;Abort Test
        Display Abrt and Warble               ERRMSG,WARBLE
      Endif
      IF AMDE = 3
        Toggle F1 (PW or Volts Display)
        Display New Value                     LCDSHW
      Endif
 Endif
;Set Key                                      SETS
 If P3.3<>1
      If AMDE = 0
        Inc AMDE
        Display tESt                          LCDMSG
      Endif
      If AMDE = 1
        AMDE = 3; CLR F1; CPW = 9
        Display New Value                     LCDSHW
      ENDIF
      If AMDE = 2 Do Nothing
      If AMDE = 3
        AMDE = 0
        Display ----                          LCDMSG, BEEPS
      Endif
 Endif
;Up Key                                       UPAFN
 If P3.4<>1
   If AMDE=0 or AMDE=1 Display Err            ERRMSG, BEEPS
   If AMDE = 3
     CLR F!
     Inc CPW
       If CPW=10 Then CPW=0
     Display Value                            LCDSHW
   Endif
 Endif
;Down Key                                     DWNAFN
 If P3.5<>1
   If AMDE=0 or AMDE=1 Display Err            BEEPS,ERRMSG
   IF AMDE = 3
     CLR F1
     Dec CPW
       If CPW=255 Then CPW=9
     Display Value                            LCDSHW
   Endif
 Endif
 Update LCD Display on WMDE                   SHOW,LCDIPI,LCDPW
Until Micro Mode ie P1.1<>1

Goto Manual Loop
```

Figure A.6 *PseudoCode for the Control of the Micro Mode*

thresholding type algorithm would be suitable to detect the twitch. The second point to note is that the primary peak—after the stimulus spikes—is significantly larger than the second spike in the opposite direction. This would suggest that just checking for one half of this bi-phasic pulse is all that is required.

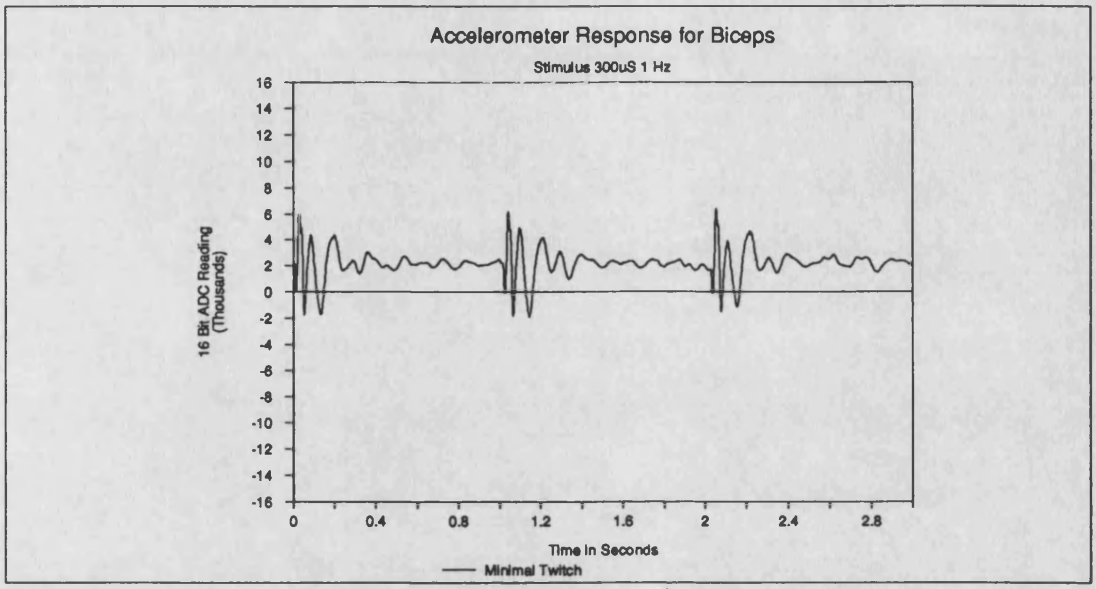

Figure A.7 *Typical Twitches from the Accelerometer*

Figure A.10 shows a histogram for the 8000 points in the noise sample of Figure A.9. From this it can be seen that the signal is reasonably normally distributed. Thus if a sample is taken initially that is large enough to not reflect the periodicity that may be present in the noise signal due to tremor, mains interference or vibrations, a reasonable estimate of the background noise is possible.

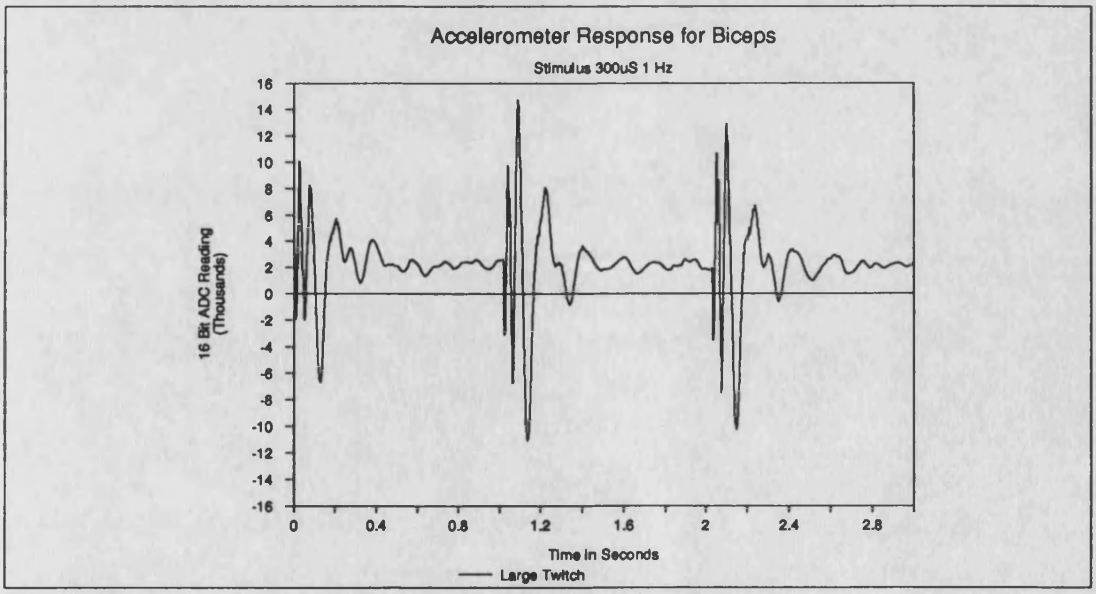

Figure A.8 *Large Twitches from Accelerometer*

The 80C552 is an 8 bit micro and this coupled with its very limited instruction set for accessing external memory makes the handling of data blocks greater than 256 very

expensive in terms of time to execute and assembler code. It was decided to try and implement the twitch algorithm based around a threshold sample set of 256.

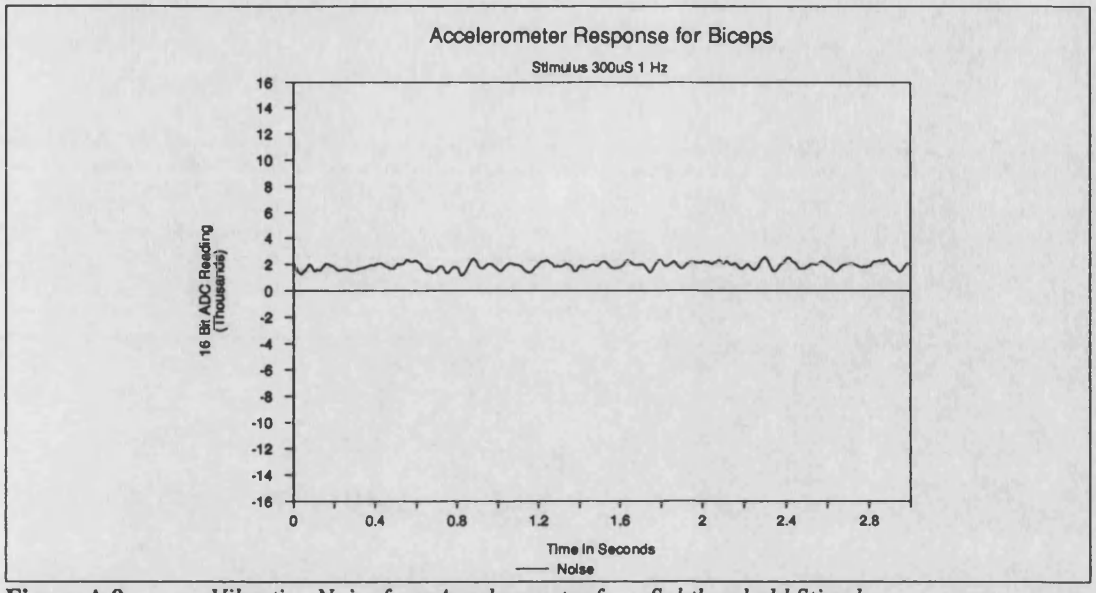

Figure A.9 *Vibration Noise from Accelerometer for a Subthreshold Stimulus*

The error in the sample values for a sample size of 256 is given[228] by:

$$e^2 = \frac{Z^2\sigma_x^2}{n} \qquad \text{A.1}$$

where e = *The Sampling Error*

σ_x^2 = *Variance of the Population*

Z = *Standardised Normal Random Variable*

n = *Sample Size*

The Standardised Normal Random Variable is defined by the required confidence limits from the standardised normal distribution. For a 99% confidence level, Z is 2.5758. For the large sample shown in Figure A.9 the variance σ_x^2 is 40326.7. Assuming a sample size of 256, equation A.1 gives the error e as 32 units on the 16 bit ADC used to record these results. Thus on the 8 bit ADC that is actually used this is equivalent to ±0.12 units; that is less than one bit. Hence 256 is a large enough sample to give a reasonable approximate of the noise assuming a normal distribution.

In order to approximate the maximum range that the noise signal takes based on the sample it is usual to calculate the standard deviation $\sigma_{\bar{x}}$. Then, assuming the noise is normally distributed, 99% of the values will be in the range:

$$\mu_{\bar{x}} \pm 2.5758 \times \sigma_{\bar{x}} \qquad \text{A.2}$$

where $\mu_{\bar{x}}$ = *Sample Mean*

$\sigma_{\bar{x}}$ = *Sample Standard Deviation*

2.5758 *is given by tables*

Calculation of the standard deviation requires quite a lot of processing time so to speed this up the interquartile range is used instead. The interquartile range (IQR) is the difference between the third and first quartiles. The third quartile is given by:

$$Q_3 = \mu_{\bar{x}} - 0.67\ \sigma_{\bar{x}} \qquad \text{A.3}$$

and the first quartile is given by:

$$Q_1 = \mu_{\bar{x}} + 0.67\ \sigma_{\bar{x}} \qquad \text{A.4}$$

Using equations A.3 and A.4 the interquartile range is given by:

$$\begin{aligned} IQR &= Q_3 - Q_1 \\ &= (\mu_{\bar{x}} + 0.67\ \sigma_{\bar{x}}) - (\mu_{\bar{x}} - 0.67\ \sigma_{\bar{x}}) \\ &\approx 1.33\ \sigma_{\bar{x}} \end{aligned} \qquad \text{A.5}$$

The interquartile range is a far easier parameter to find than the standard deviation. Thus using equation A.5 and assuming 99% confidence limits, the range of the noise thresholds for the sample is given by

$$\begin{aligned} Thresholds &= \mu_{\bar{x}} \pm 1.33 \times 2.5758 \times IQR \\ &= \mu_{\bar{x}} \pm 3.42\ IQR \end{aligned} \qquad \text{A.6}$$

where $\mu_{\bar{x}}$ = *sample mean*

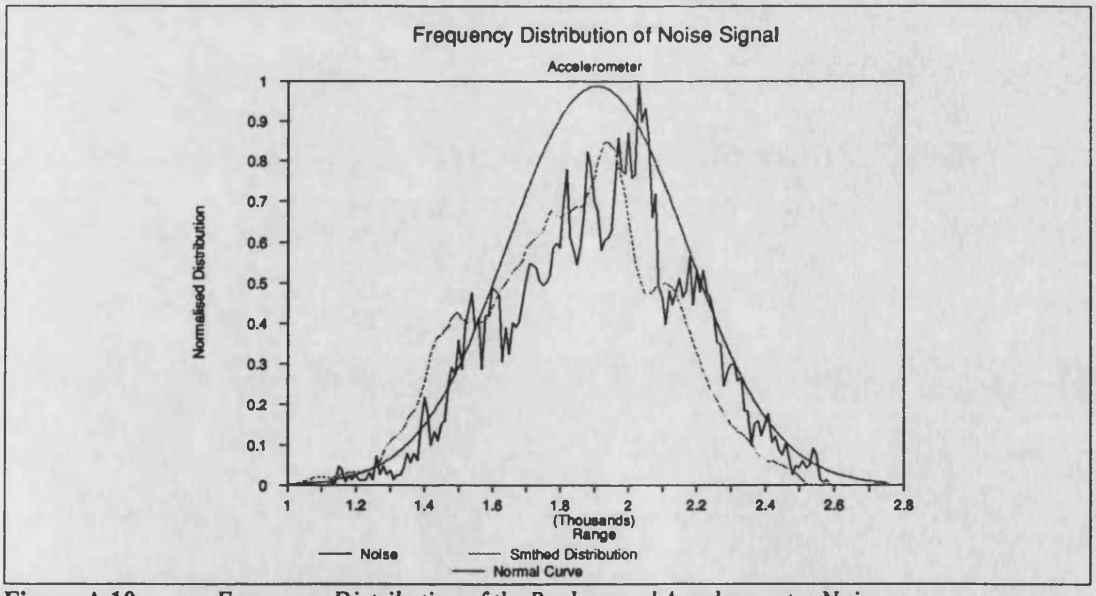

Figure A.10 *Frequency Distribution of the Background Accelerometer Noise*

A.3.4.2 Twitch Detection Algorithm

The twitch detection algorithm follows very closely the method used in the real test. Initially the voltage ramps up until a twitch is detected, then the stimulus is ramped down until it just disappears. A twitch is defined as ten consecutive samples over the threshold as defined by equation A.6. If some samples are found over the threshold but insufficient to meet the twitch criteria, then the software automatically repeats the

voltage to check the voltage level again. Similarly if a full twitch is detected, that is also repeated to ensure that it wasn't a coincidental movement of the subject.

A.3.4.3 Software Implementation

The interquartile range and median are found using the routines in the Module AVERAGE. The actual routine is thresh which first calls ssort which is a shell sort routine that puts the samples in sequential order. Then for the 256 samples, the lower quartile, mean and upper quartile are approximately given by the 64th, 128th and 192nd elements in the sequence.

Applying equation A.6 and using one decimal place in the calculations, the values for the upper and lower thresholds are found and stored in MAX and MIN respectively.

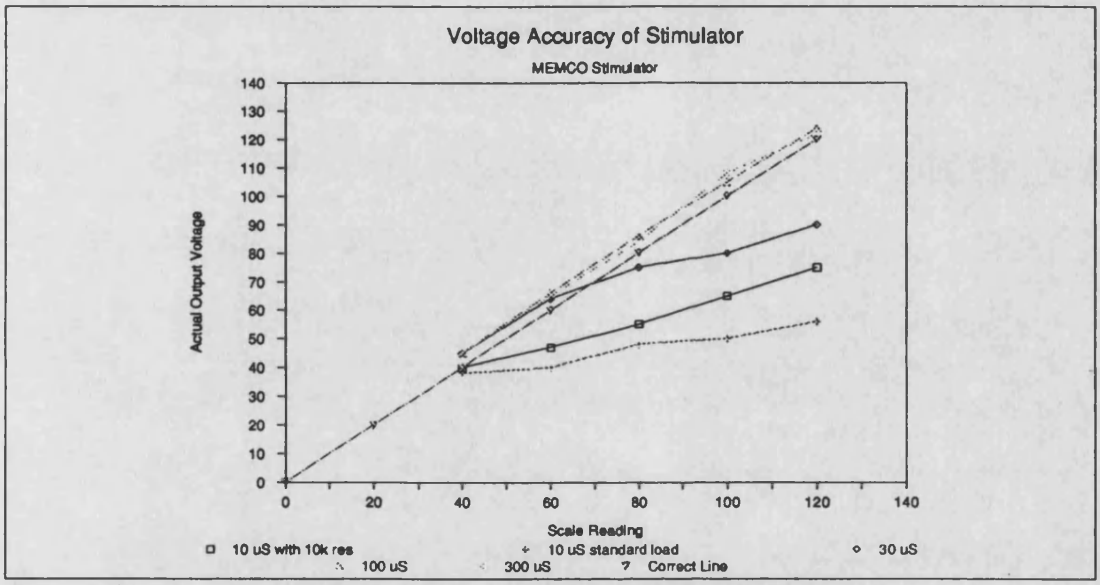

Figure A.11 *Linearity of a Typical Commercial Strength Duration Stimulator*

A.3.5 LCD Display Routines

Five routines are used to display information on the LCD display. Each uses a lookup table to translate the system variables into the appropriate message. LCDMSG is used to generate the various messages such as Strt, Fini, Abrt etc. This routine is entered with the accumulator containing the offset into the lookup table for the required message. LCDIPI is used for the translation of the current IPI as stored in the variable IPI into its time equivalent on the LCD. LCDPW does a similar job for the pulse width which is stored in the variable PW. LCDSHW translates the stored results from the automatic testing into the correct display voltage. The final routine is VOUTA which translate the demand signal as determined by the ADC into the 'correct' voltage for display.

A.4 System Calibration

Before discussing the calibration of the strength-duration stimulator it is important to consider what the linearity of the currently used stimulators is like. In order to do this

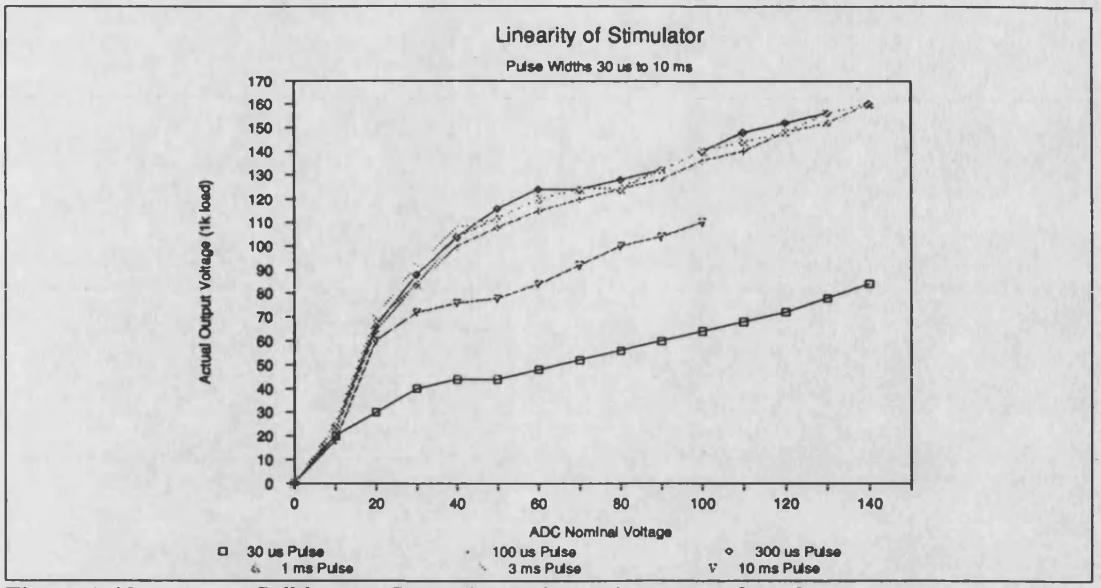

Figure A.12 *Callibration Curves for the Strength Duration Stimulator*

some typical stimulators used within the School of Physiotherapy at the RUH, Bath were tested. Using the standard load the output voltage was measured for each pulse width and compared with the reading on the meter. Figure A.11 shows some typical results obtained from a Memco Stimulator. From these results it is clear that the commercial stimulators do not display a true output voltage. This fact in itself is not significant if one is comparing the results from the same stimulator each time and considering the changes, rather than the absolute values. The fact that the true voltage is lower for the narrower pulse widths would suggest that the typical strength-duration curve may not rise quite as steeply as the recorded voltage would suggest.

A.4.1 Stimulator Output Voltage

The stimulator design that has been used does not provide an easy method for

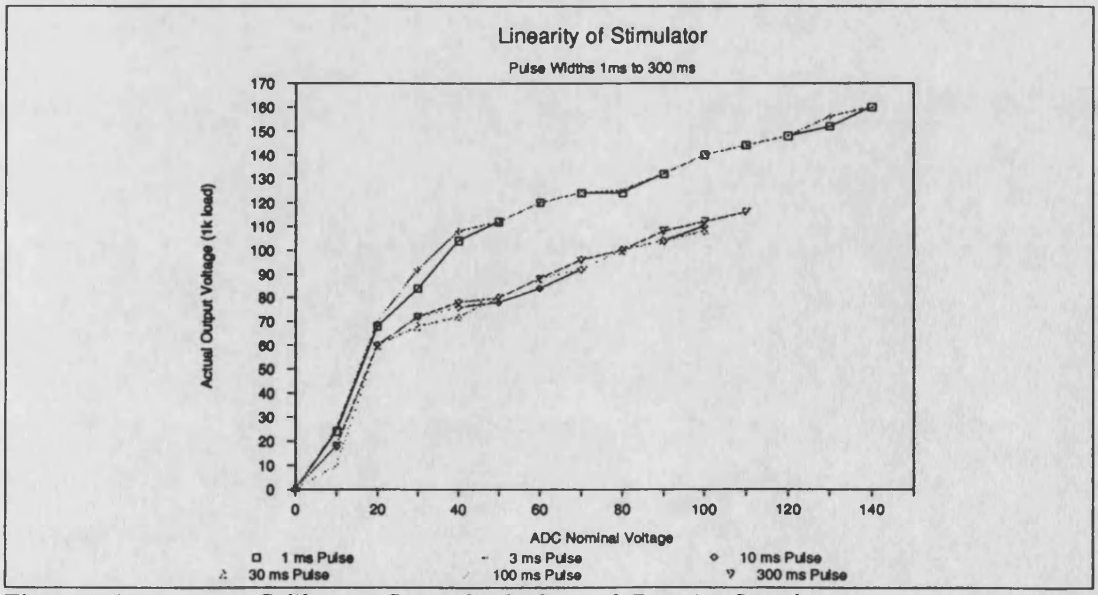

Figure A.13 *Calibration Curves for the Strength Duration Stimulator*

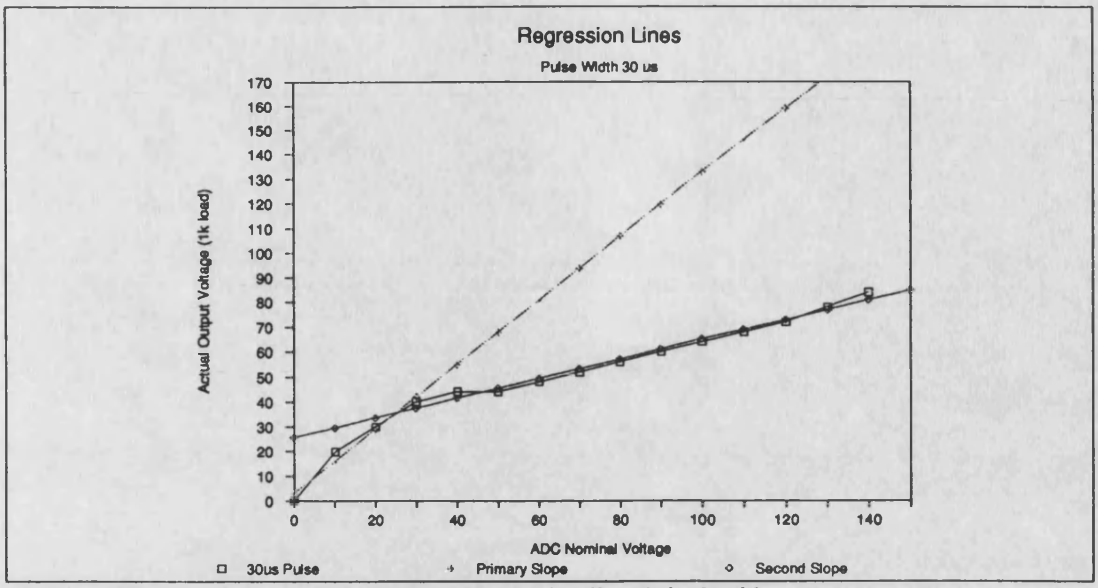

Figure A.14 *Regression Lines for Smallest Pulse Widths*

determining the actual output voltage level. In order to measure the output voltage, the processor samples the demand voltage that is used to set the output voltage. The relationship between the actual output voltage and the sampled demand signal is non-linear and varies with the pulse width. In order that the manual mode voltage display gives a reasonable indication of output voltage, the strength-duration tester has been calibrated using a standard load of 1kΩ in parallel with 0.1μF.

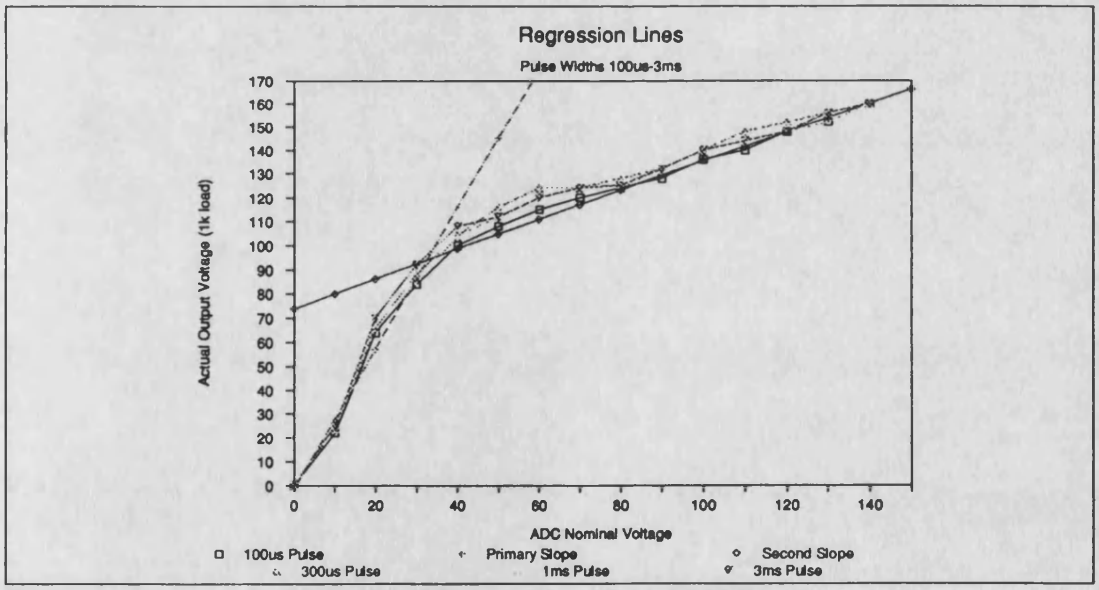

Figure A.15 *Regression Lines for Central Pulse Width Range*

As a first estimate to actual output voltage, the ADC value minus 100 was used. This gave a value between zero and 156 as a guide to the actual output. The value of 100 to subtract was found to be the approximate demand value at which the stimulator started to produce an output.

Figure A.12 and A.13 show the plots of the approximate value displayed and actual

voltage recorded across a standard load. From these graphs it can be seen that three distinct sets of curves exist. These three sets of curves were then each approximated using Linear Regression as two lines. Figures A.14, A.15 and A.16 show the curves and their respective regression lines. It is these values that are used in the conversion from Demand value to display voltage. The choice of which set of curves being determined by the pulse width value.

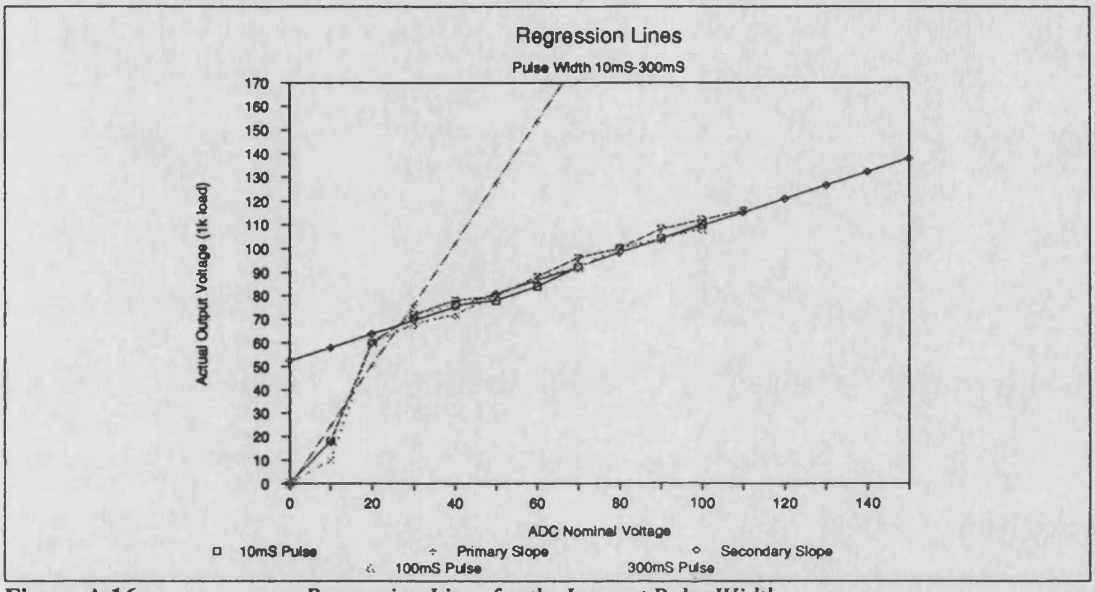

Figure A.16 *Regression Lines for the Largest Pulse Widths*

A.5 System Tests

The system has been boxed in a case similar to that used for the stimulator but a double height version of the box. Plates F.28 and F.29 show the final boxed system and front panel. Plate F.30 shows a view of the internals of the strength-duration tester. The complete system has been tested to show its ability to detect and record the strength-duration curve for a number of muscles and a number of subjects. The tests fall into three groups which will be described separately. The results are presented in tabular and graphical form.

A.5.1 Comparison of Manual and Auto Results

The strength-duration curves of four subjects were recorded. The tests were carried out using both the Micro mode and as a comparison, a Manual mode test was also carried out. The manual test used a visual twitch detection method. The tests were carried out on the biceps brachii of each of the subjects and the approximate time for the test was recorded. The results of these tests are presented in Table A.2. Comparative bar charts for the Manual mode and Micro mode are shown in Figures A.17 and A.18 respectively.

A.5.2 Repeatability

Strength-Duration curves were recorded from the biceps brachii of three subjects. Each subject was tested three times using the Micro mode of the strength-duration tester to see if there was a consistency in the results. Results for these tests are given in Table A.3. A comparative bar chart of the results for each of the subjects is given in Figures A.19, A.20 and A.21.

Pulse Width	Subject 1		Subject 2		Subject 3		Subject 4	
	Manual	Micro	Manual	Micro	Manual	Micro	Manual	Micro
10 µs	—	33	—	80	—	27	—	60
30 µs	21	27	19	36	30	06	18	16
100 µs	27	27	27	27	33	39	27	27
300 µs	27	27	24	27	30	33	27	27
1 ms	24	27	24	27	30	33	24	27
3 ms	22	27	22	18	27	29	22	24
10 ms	22	27	22	24	27	29	22	24
30 ms	22	27	22	24	27	29	22	24
100 ms	22	27	22	27	27	29	24	00
300 ms	22	24	22	24	24	24	22	27
Time in minutes	20	5	23	5	26	6	20	5

Table A.2 *Results of the Manual /Automatic Tests*

A.5.3 Tests on Different Muscles

The design work has been carried out using the biceps muscle as the primary test muscle. Clearly the position of the muscle will affect its ability to twitch and hence the effectiveness of the twitch detection algorithm.

Strength-duration tests were carried out using the Micro and Manual modes for two

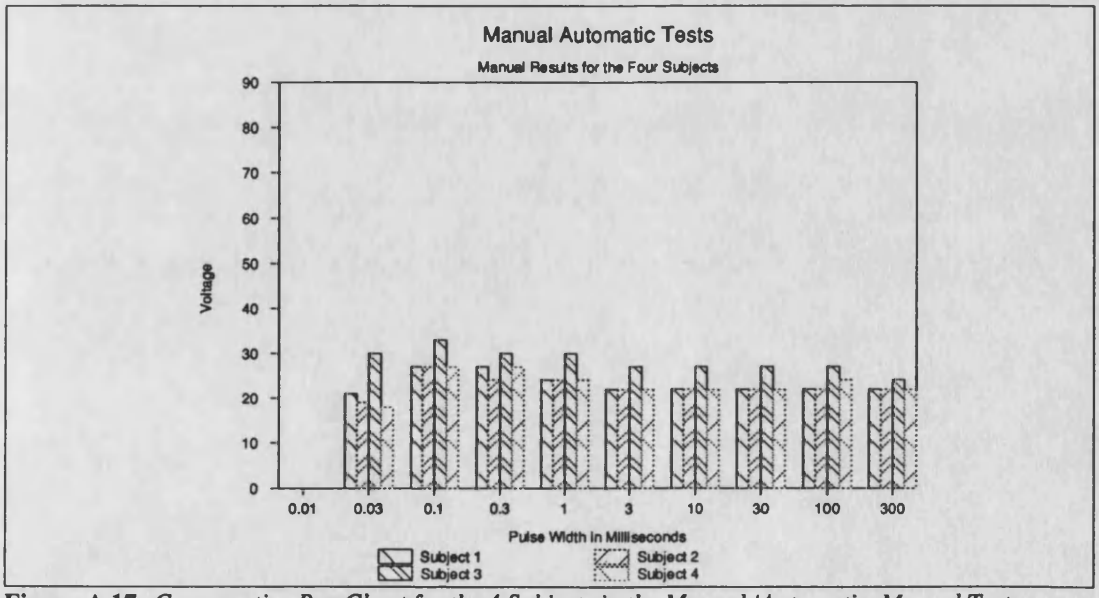

Figure A.17 *Comparative Bar Chart for the 4 Subjects in the Manual /Automatic Manual Test*

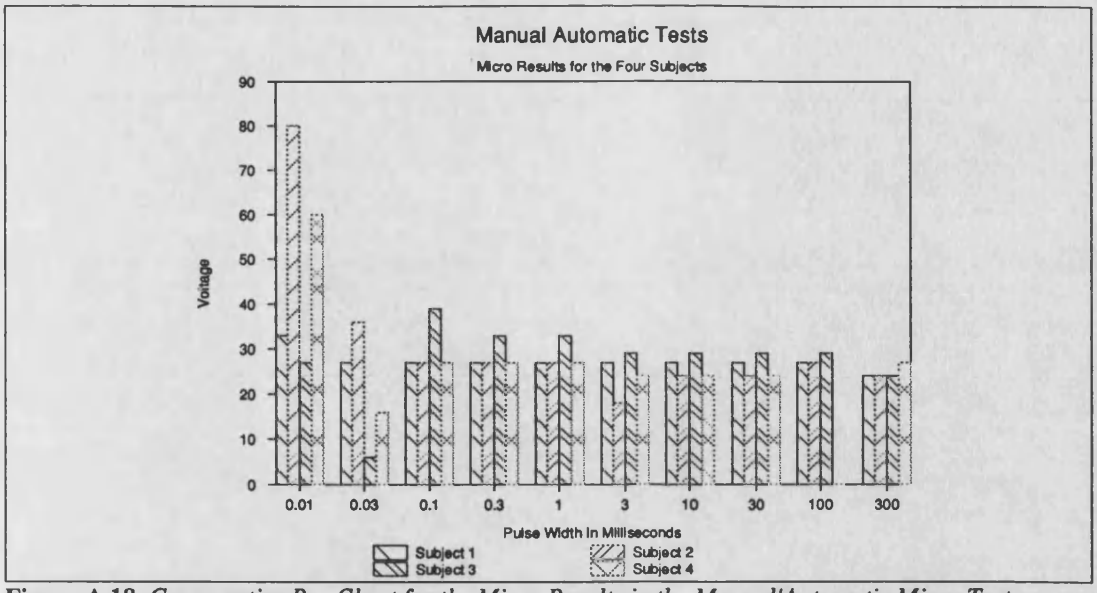

Figure A.18 *Comparative Bar Chart for the Micro Results in the Manual/Automatic Micro Test*

different muscles. The muscles chosen for the test were the extensor digitorum and anterior tibialis. The extensor digitorum in the forearm is one that does not have a very prominent twitch but does move the fingers/hand at the end of the arm. The anterior tibialis does have a reasonably prominent twitch and tends to cause the foot to tap. Thus these two muscles represent two different types of twitch for the detection algorithm to be tested on. Rather than use different subjects the tests were carried out on the left and right arm for the extensor digitorum muscle, and the left and right leg for the anterior tibialis muscle of the same subject. This would then present the system with two muscles for each limb which would be very similar, so the test would be on the algorithm and not how developed the muscle happened to be. The results of these tests are given in Table A.4. Comparative bar charts for the leg and arm results are given in Figures A.22 and A.23 respectively.

Pulse Width	Subject 1			Subject 2			Subject 3		
	First	Second	Third	First	Second	Third	First	Second	Third
10 µs	51	60	80	102	4	24	27	18	4
30 µs	36	39	36	36	18	27	06	48	48
100 µs	27	27	27	27	27	27	39	30	33
300 µs	27	27	27	27	27	27	33	30	30
1 ms	27	27	27	27	27	27	33	33	18
3 ms	4	27	18	27	24	27	29	27	27
10 ms	24	27	24	27	24	27	29	13	27
30 ms	00	27	24	00	24	27	29	1	27
100 ms	30	27	27	27	24	27	29	29	27
300 ms	24	22	24	24	24	24	24	27	00

Table A.3 *Repeatability of the Test on three Subjects*

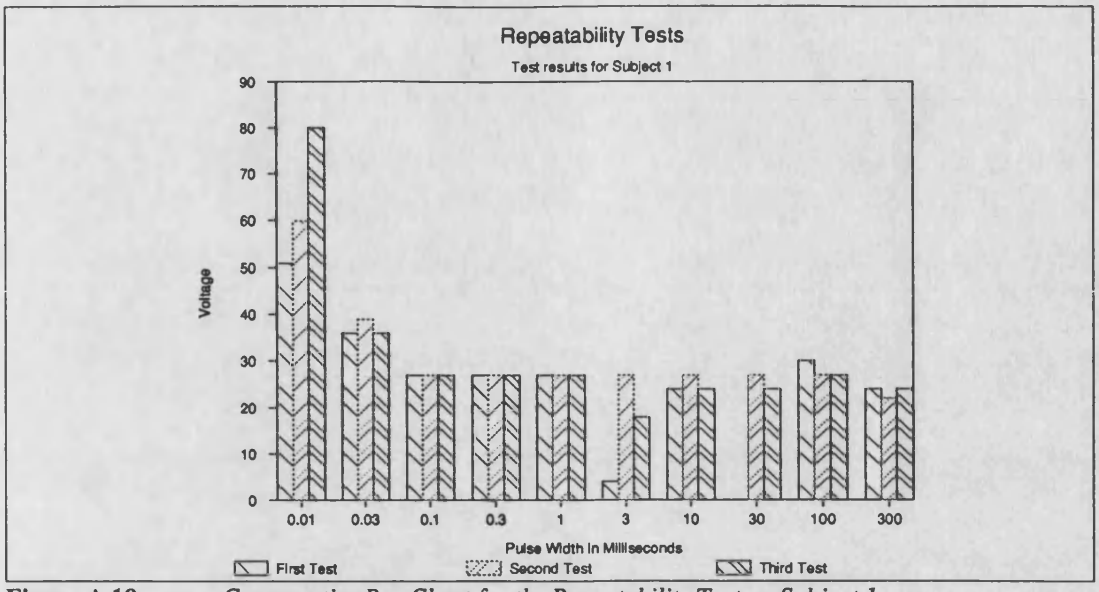

Figure A.19 *Comparative Bar Chart for the Repeatability Test on Subject 1*

A.6 Discussion

From the results it can be seen that the system is capable of producing a strength-duration curve that compares well with that obtained using the traditional manual test. There are some notable differences, particularly at the narrow pulse widths where the voltages are much lower. As has been discussed in section A.4 the stimulator design cannot produce 10 μs pulses and produces a very unstable 30 μs pulse width which explains the strange results obtained at these pulse widths. There are some obviously wrong results due to mis-triggering of the detection algorithm, except for those which can be eradicated by repeating the test. The correlation is good between manual and micro mode in the Automatic/Manual test.

Variations do occur and these are mainly due to the stimulator design which is in its

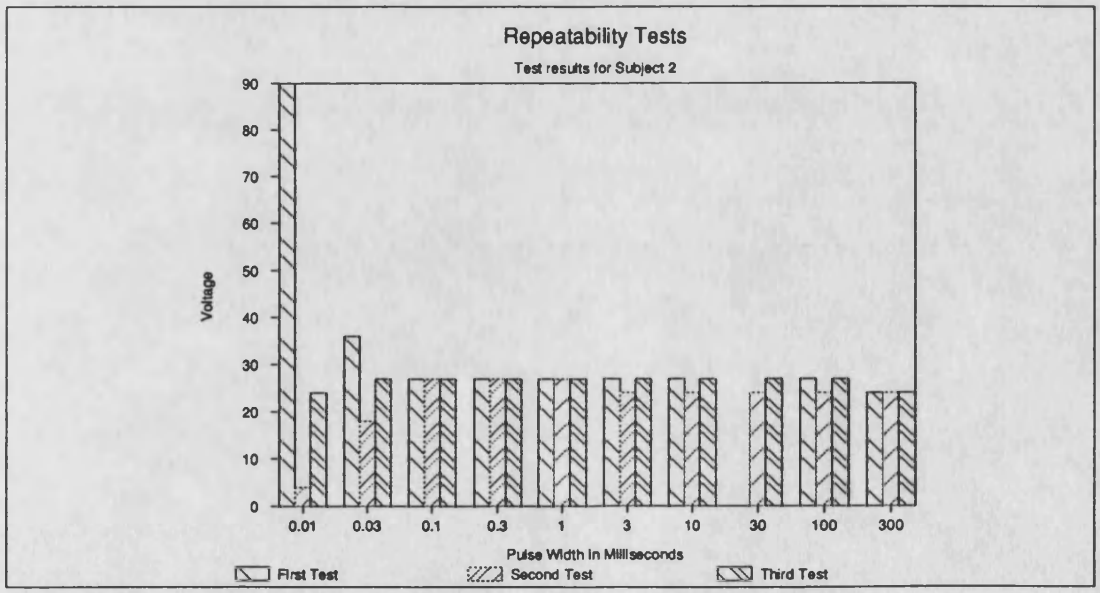

Figure A.20 *Comparative Bar Chart for the Repeatability Test on Subject 2*

most non-linear portion of its curve for most of the voltages of interest. On this part of the curve a single unit increase on the DAC can give a large change in the nominal output voltage. In the repeatability tests it can be seen that some false triggering has occurred. This could again be caused by the variability of the stimulator at low levels but it is always quite obvious that a spurious result has occurred and repeating the test usually ensures the results are corrected.

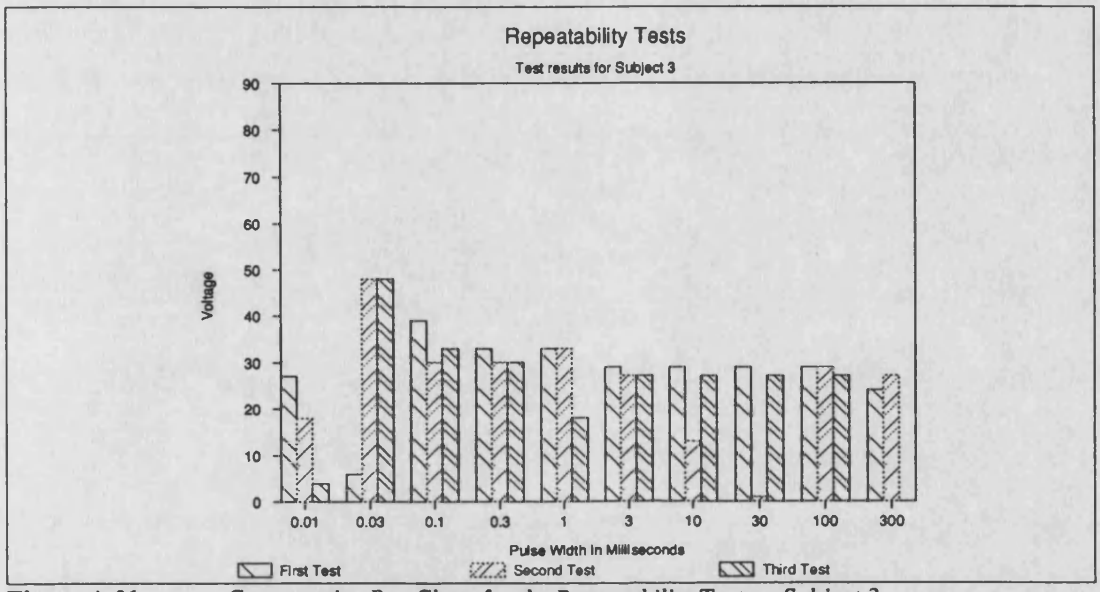

Figure A.21 *Comparative Bar Chart for the Repeatability Test on Subject 3*

The tests on the different muscles once again show good correlation between the Micro and Manual test. There is though, a notable difference between the left and right anterior tibialis muscle results. This is in fact due to damage to the right leg anterior tibialis. This shows the effectiveness of the strength-duration test in

Pulse Width	Left Side				Right Side			
	Extensor Digitorum		Anterior Tibialis		Extensor Digitorum		Anterior Tibialis	
	Micro	Manual	Micro	Manual	Micro	Manual	Micro	Manual
10 µs	77	—	105	—	77	—	105	—
30 µs	17	35	37	40	17	30	45	71
100 µs	27	33	51	54	27	27	80	93
300 µs	27	30	48	45	27	27	68	66
1 ms	27	30	48	45	27	27	68	66
3 ms	24	24	42	37	24	24	60	58
10 ms	24	24	42	37	24	24	52	50
30 ms	24	23	42	40	22	24	45	45
100 ms	24	24	42	37	27	23	40	47
300 ms	24	23	45	37	03	24	37	45

Table A.4 *Results for Different Muscles*

identifying muscle lesions such as this. Despite this obvious difference between right and left legs the results correlate well for extensor digitorum.

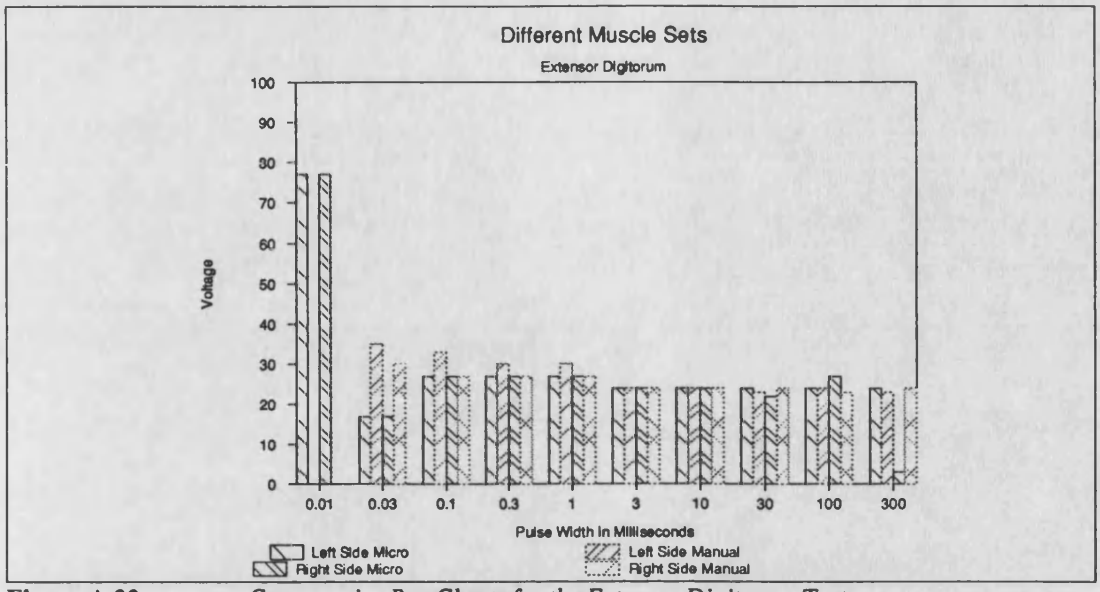

Figure A.22 *Comparative Bar Charts for the Extensor Digitorum Tests*

These tests show that the strength-duration tester is effective. It highlights a number of limitations which will have to be removed or improved before a system suitable for proper medical trials can be made available. The system is consistent in its results and has proved effective for a number of different muscle situations.

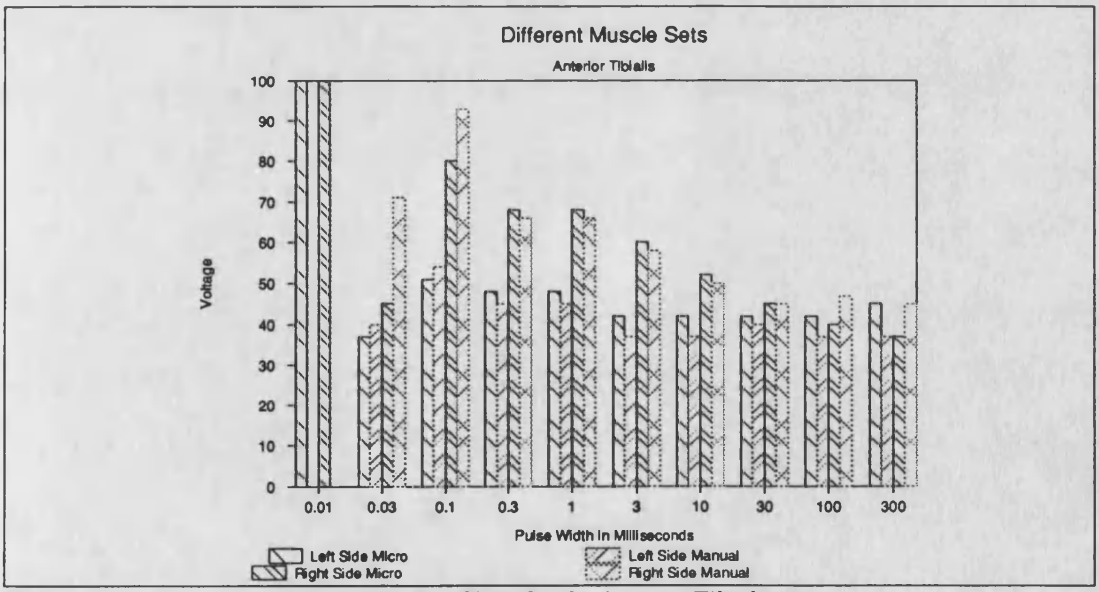

Figure A.23 *Comparative Bar Chart for the Anterior Tibialis Tests*

A.7 Further Work

The current strength-duration tester suffers a number of significant problems. Most of the problems can be attributed to the design of the stimulator card. This has a limited pulse width range, has no means for determining the true output voltage and has a

very non-linear output control. During the testing, a serious design fault became apparent in that if the wiper of the manual control potentiometer should momentarily not make contact with the resistive track, the output of the stimulator is immediately set to maximum. On narrow pulse widths the effect of this is not noticeable but when testing the longer pulses the subject can be subjected to a painful pulse. This design fault is readily corrected by rewiring the potentiometer. The best solution to these problems is to redesign the stimulator with a better output voltage control response, more stable narrow pulse widths and a means of determining the true output voltage. This last requirement would then ensure that the recorded voltage is a true representation of the output voltage rather being based on the assumption all humans present a load of 1 kΩ in parallel with 100 nF.

The current system uses the 3M electrodes that are used for the standing system as the stimulating electrodes. These electrodes, though convenient for the standing system and for initial tests, are not suitable for practical use in the physiotherapy department. The usual electrodes used by the physiotherapist are held on the muscle under test. Clearly since the current implementation uses movement as a means of detection the traditional method is unsatisfactory because of the variability in electrode contact. A possible solution would be to re-design the electrode and accelerometer combination into a single unit. This would have to allow for the complete range of muscles that could require testing so could entail having more than one size. The combination of electrodes and accelerometer would also make the system easier to use, since just a single strap could be used to hold the detection/stimulation device. This would ensure the twitch detection would only be required to detect the difference between patient movement and muscle movement and not the physiotherapists movement which would be introduced if the physiotherapist held the detector on the muscle.

Further work is required on the use of both EMG pickups and sound pickups. The current EMG systems described in Chapter 6 only have a limited range of pulse widths over which they don not saturate which precludes their use in the strength-duration tester except over the narrower pulse range. As has been discussed in section A.2.2.2 muscle sounds could be the best solution and would allow the traditional method of applying the electrodes. Since the microphones currently available in the laboratory do not have a low enough frequency response to test these theories it is hoped that when a suitable microphone is identified, a muscle sounds based detector can be tried.

The new Siemens SAB80C517 microcontroller offers greater speed capabilities over the PCB80C552. A switch to this processor, which is essentially an enhanced PCB80C552, could provide further system enhancements. Not only in terms of speed,

but in ease of programming particularly, the taking of more than 256 sample blocks should enhance the detection algorithm and eradicate the odd mis-triggering that currently occurs.

The current software does not make use of any of the power down modes of the processor. This means that the system currently draws around 80 mA continuously when running, which significantly limits the time between charges. The reason no power down mode has been introduced was to ensure that a working system could be built before introducing the power saving options. This is why the software is interrupt driven except for when the whole keyboard is being used. It is a fairly trivial matter to link the keyboard polling into an interrupt such that the processors normal state becomes powered down. This would lead to significant power consumption reductions since generally the processor is idling. The other major contributor to this high current consumption is the eprom. From the circuit diagram in Figure G.37 it can be seen that the chip enable is always active. If the circuitry were adjusted so that the chip enable was only enabled for an access the power consumption of the EPROM would be reduced to its standby current of 1mA alot of the time.

An area that has not been considered as yet is the storage and display of multiple results. Whether this is carried out by a separate microcomputer linked via the RS423 or whether the tester itself should provide a parallel printer output to directly plot results requires further investigation. It is envisaged that if a separate microcomputer is used it would have to have a simple to use user-friendly application to deal with the gathering, plotting, storing and retrieval of results. A simple input system would be required, particularly in the physiotherapy out-patients environment, such as a mouse, lightpen or roller ball. Building the whole unit into a single monitor style case such that the results can be displayed on the screen and then printed would seem the best option.

A possible system under consideration would be based on the Philips SCC68070 microcore board combined with a small monitor and running the GEM operating system. The whole system would then be capable of being powered by batteries, ensuring patient isolation. GEM could provide an icon based multi-window interactive display and analysis environment.

Appendix B

Muscle Fatigue Monitors

In recent years a number of authors have published their designs for muscle fatigue monitors. These nearly all seem to have evolved from the original Muscle Fatigue Monitor (MFM) published by Stulen and De Luca[79,229]. This system, as with almost all subsequent ones, tracks the median frequency of the EMG signal picked up from the muscle under test. The median frequency has been used because it is one of the more reliable muscle parameters that changes with fatigue.

In this chapter a review of a number of published muscle fatigue monitors is given. These fall into two basic categories, digital and analogue. These categories essentially describe the technique that is used to determine the median frequency. Two median frequency monitoring Muscle Fatigue Monitors have been built as part of this work. One is based on analogue techniques similar to those used by Stulen and De Luca, the other uses a single chip microcontroller to implement a digital Muscle Fatigue Monitor that is similar to those described by Basano et al.[230].

B.1 Review of Published Designs

B.1.1 The Stulen and De Luca Muscle Fatigue Monitor

The original MFM was a purely analogue device. Figure B.1 gives a block diagram of the system. The EMG signal is initially buffered by a preamplifier then fed into two filters: one is a sharp rolloff high-pass filter, the other a sharp rolloff low-pass filter. These filters are modulated filters with their respective cut-offs set to be the same such that increasing the cut-off of one of the filters causes a matching rise in the other. The modulation control is derived from the integral of the difference between the RMS outputs of the two filters. When the outputs from the two filters are the same the cut-off frequency of the filters equals the median frequency of the EMG signal.

This original system required two filters that were closely matched and had very sharp rolloffs to ensure that an accurate estimate of the median frequency could be obtained, so that the filters could be considered orthogonal. This system was improved by using the system shown in Figure B.2. The system has since been improved by Gilmore and De Luca[231] to produce a marketable Second Generation MFM. This version has only one modulated filter, a sharp cut-off low-pass filter and instead of comparing the output with that of another filter it is compared with that of a –3dB attenuator. This system has the advantage that it greatly simplifies the circuitry. Also, it not only provides the median frequency value, but also produces the RMS amplitude of the whole ME signal. There is however a significant disadvantage; the control law

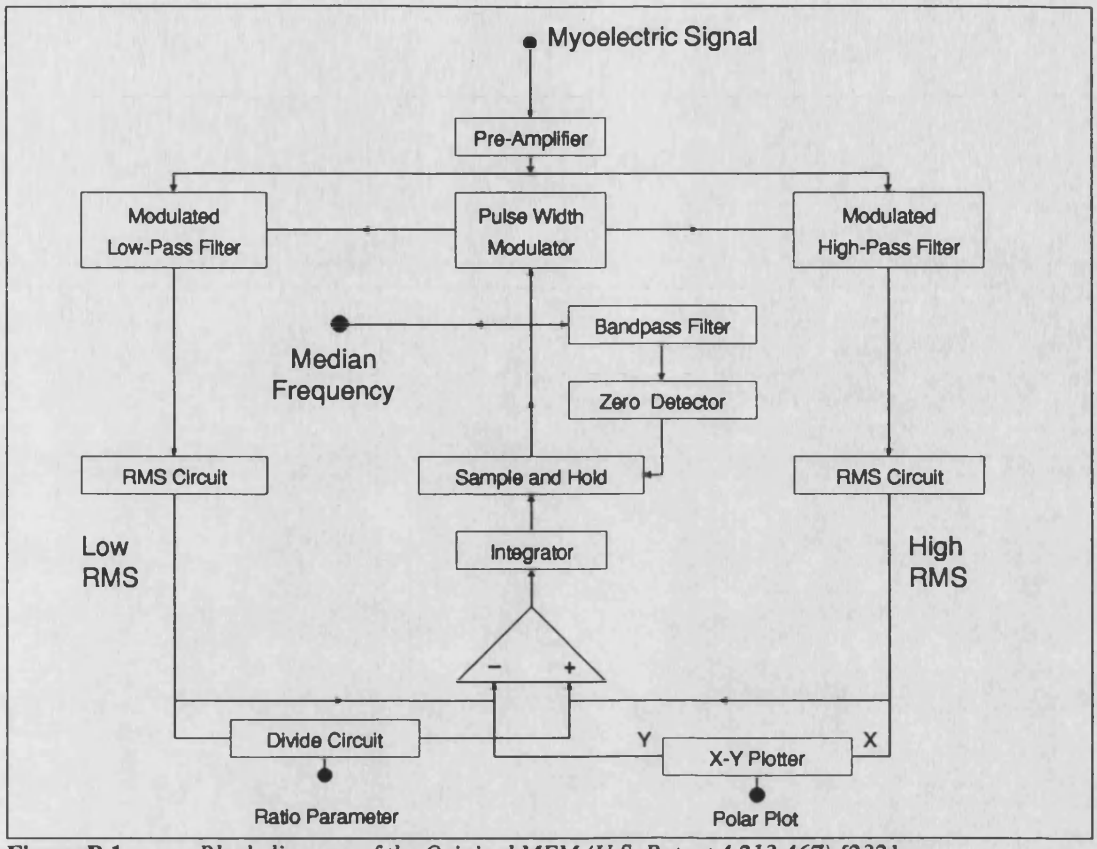

Figure B.1 *Block diagram of the Original MFM (U.S. Patent 4 213 467) [232]*

is not symmetric. This causes the tracking to be faster when the current median frequency is below the actual detected median frequency than when it is above.

B.1.2 The Voltage Controlled Filter

This method from Manchester University[234] is similar to the technique of Stulen and De Luca but makes use of a Voltage Controlled Filter (VCF). It has the advantage of having both high-pass and low-pass outputs available at no extra cost and uses operational transconductance amplifiers as an alternative to the switched capacitor method. The advantage of transconductance amplifiers is that they can be controlled directly by a voltage, thus eliminating the need for a VCO or pulsewidth modulator.

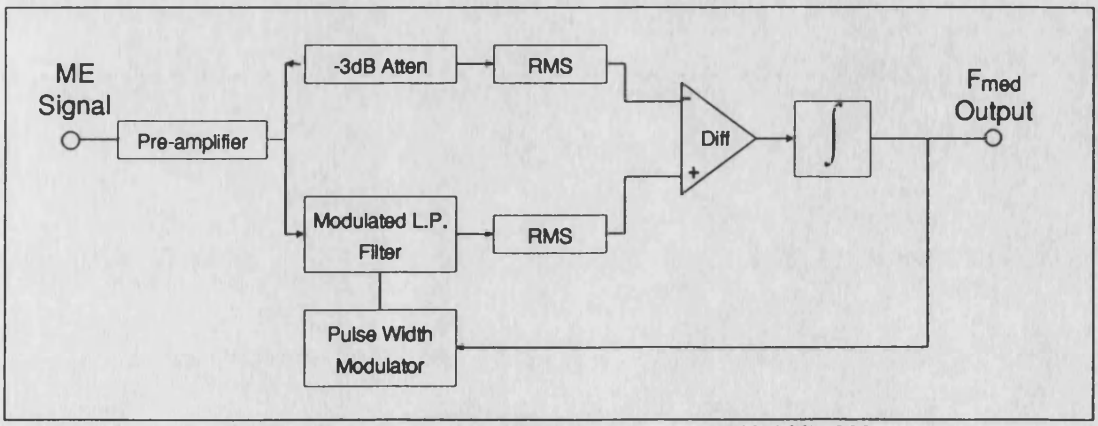

Figure B.2 *Modified First Generation MFM (U.S. Patent 4 213 466) [233]*

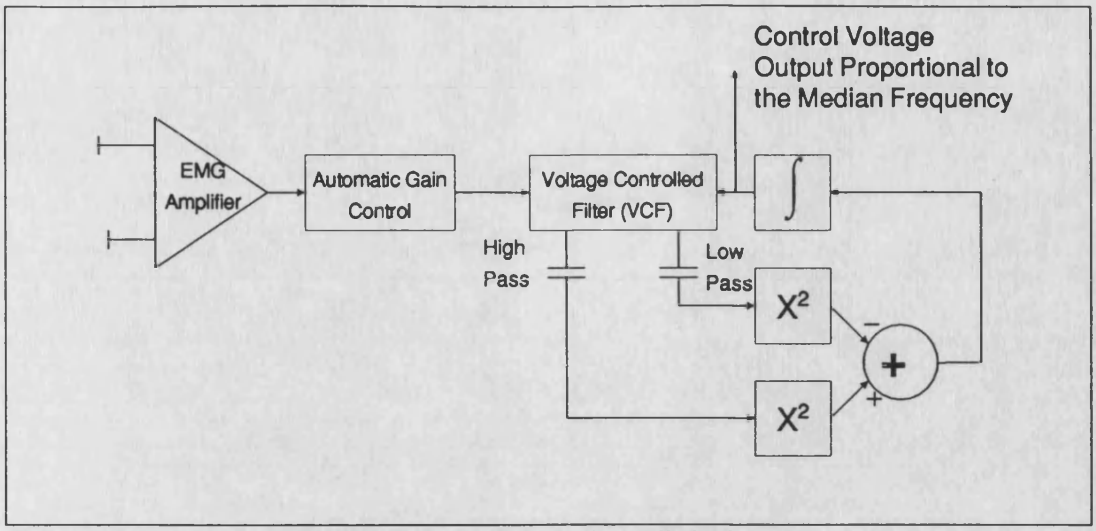

Figure B.3 *Block Diagram of the Voltage Controlled Filter MFM*

A block diagram of the system is given in Figure B.3. The EMG signal is band-pass filtered between 10 Hz and 1 kHz to limit noise and reduce artefacts due to body movements. An automatic gain control amplifier, with a time constant of 0.5 s ensures that the VCF has a constant average power. The high- and low-pass outputs of the VCF are then both squared. The difference between these squares is then integrated and fed back to control the cut-off frequency of the VCF. As a result, the integrator varies the cut-off frequency, until equal average power is detected from both the high- and low-pass outputs. The control voltage of the VCF can then be used to measure the median frequency of the signal. The speed of response of the circuit is determined by the time constant of the integrator in the feedback path and by the size of the input signal to the VCF.

B.1.3 Differentiated Integrated Power Ratio Technique

This technique has been proposed by Kramer et al.[235] who have made a small electronic device which operates in real time and online. The signal is derived from the whole EMG signal spectrum. Its operation is shown in block diagram form in Figure B.4

The EMG signal is first band filtered and processed by two separate sections. One section amplifies and differentiates the signal, and then squares and smoothes the signal by a low-pass filter. The other section amplifies and integrates the signal then squares and smoothes the output using a similar circuit to that used for the first section. The outputs from these two sections are estimates of the power of the differentiated signal and the power of the integrated signal. The output of the two sections are then scaled and divided to produce a differentiated integrated power ratio. The second part of the block diagram represents a simple mean EMG amplitude circuit.

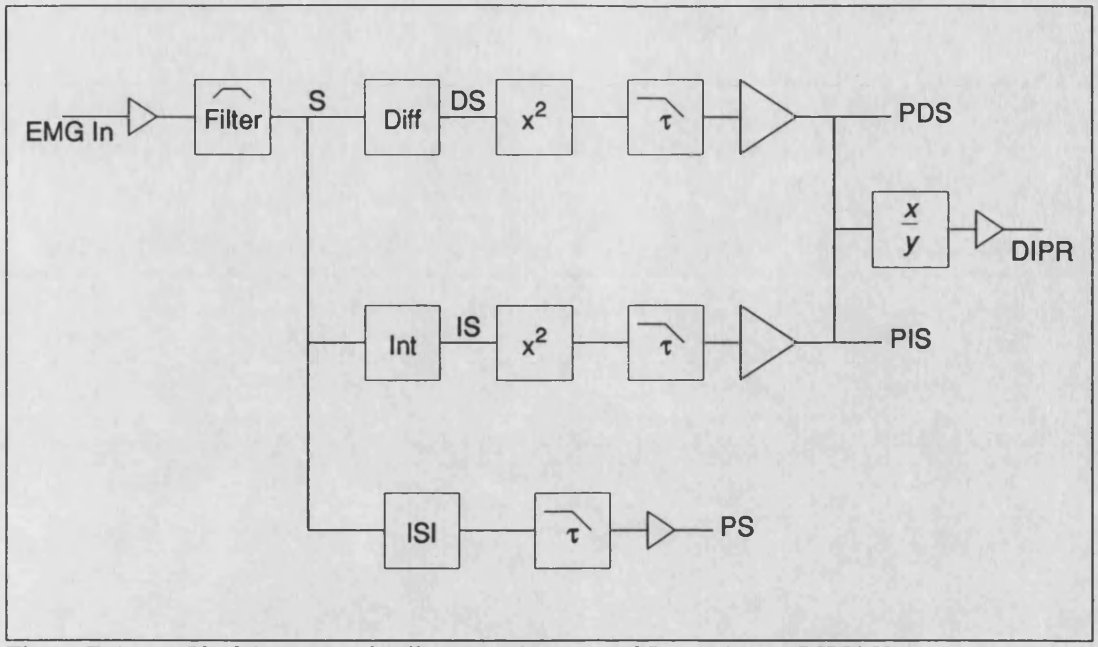

Figure B.4 *Block Diagram of Differentiated Integrated Power Ratio (DIPR) Unit*
S = signal after bandpass-filter ; DS = differentiated signal S; IS = integrated signal S;
τ = time-constant integrating low-pass filter.

The authors choose the time constants for the filters to track changes in fast fatiguing muscles such as masseter muscles which fatigue in about 1 s. The output from the system provides a signal that drops as the muscle fatigues. They claim it performs comparable to or better than other techniques that have been reported in the literature.

B.1.4 The "Analogue" Microprocessor Approach

This technique[166,167] used the now obsolete Intel 2920 microprocessor to monitor the median frequency of the input signal. Despite the obsolete component it is worthy of mention because it uses an alternative technique for determining the median frequency. Unfortunately the simplicity of the solution relied heavily on the Intel "Analogue" processor to implement the algorithm.

The algorithm uses a fixed frequency high-pass filter and a shifting ME spectrum obtained by amplitude modulating the ME signal with a sine wave carrier. The operating principle of this technique is shown in Figure B.5. A unity amplitude sine wave carrier is multiplied by the input signal generating an output whose power spectrum is shown in Figure B.5c. The resulting signal is applied to a fixed cut-off high-pass filter and a feedback mechanism adjusts the carrier frequency so that the output from the filter has a power equal to ⅛th the power of the input signal P_x. This occurs when the difference between the carrier frequency f_c and the ideal filter cut-off frequency f_f matches the median frequency.

The factor of an ⅛th is derived by considering a signal $x(t)$ which has a power spectrum of $S_{xx}(t)$ in the positive frequency domain. Then, given a unity amplitude

sine wave with a frequency f_c, the product of the two signals has a power spectrum given by $\frac{1}{4}S_{xx}(f-f_c)+\frac{1}{4}S_{xx}(f_c-f)$.

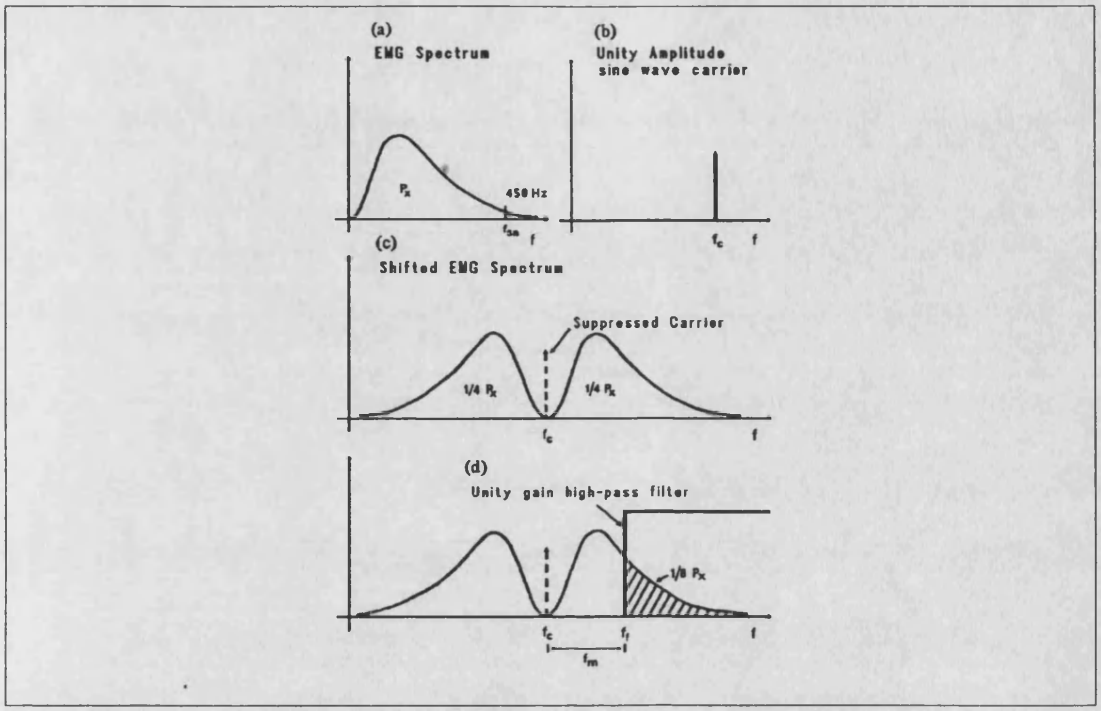

Figure B.5 *Principle of Operation of the Analogue Microprocessor MFM*

If the total power of $x(t)$ is P_x, $\frac{1}{4}P_x$ will be in the lower sideband with respect to the suppressed carrier. Therefore, when the output of the high pass filter is $\frac{1}{8}P_x$, the following equation is satisfied:

$$f_f - f_c = f_m \qquad \text{B.1}$$

where f_f *is the Filter Cut-off Frequency*

f_c *is the Carrier Frequency*

f_m *is the Median Frequency*

The values of f_{sn} (Maximum Frequency of the ME Signal), f_c and f_f must match the following conditions to prevent a fold back of the lower sideband of the modulated signal into the filter passband:

$$f_{sn} \le f_{m(max)} + 2f_{c(min)} \qquad \text{B.2}$$

That is

$$f_{sn} \le f_f + f_{c(min)} \qquad \text{B.3}$$

The algorithm has been totally implemented (except for the AGC and anti-aliasing filter) in software using the Intel 2920 which is well suited to the implementation of digital filters, thus giving a high-pass filter with much sharper cut-off than analogue techniques permit. The technique does have a drawback in that because of the digital nature of the system, quantisation error occurs giving a non linear error that is worst at lower frequencies.

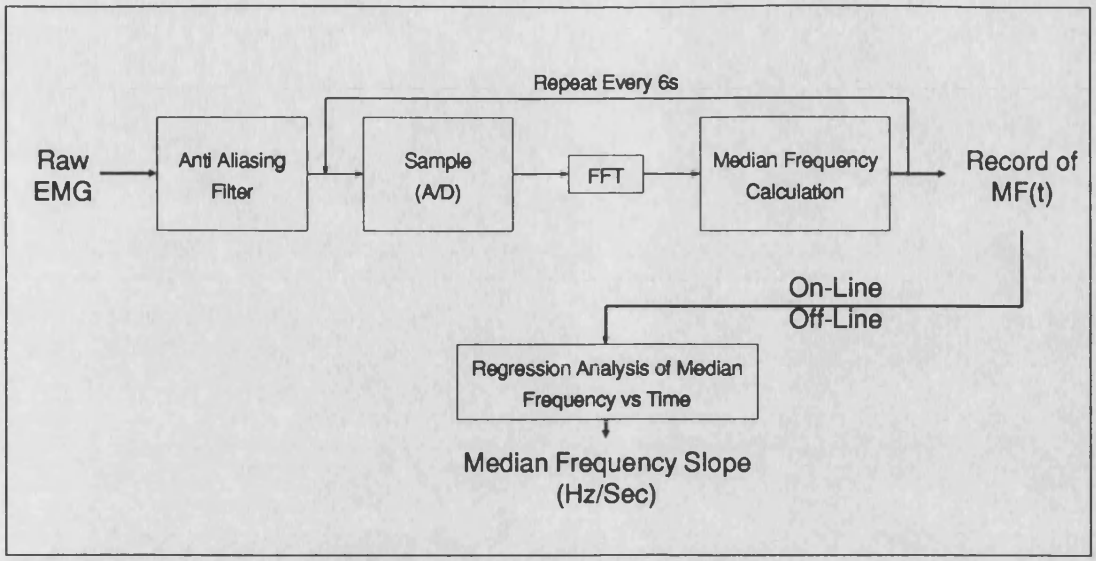

Figure B.6 *Block Diagram of the Seroussi et al. System*

B.1.5 Fully Digital Methods

All the digital techniques reported in the literature[230,236] rely on the computation of a Fast Fourier Transform. Two descriptions of this technique have been found in the literature. Basano et al.[230] made use of a Texas Instruments TMS32010 digital signal processor which has a 16 x 16 multiplier and 144 bytes of internal RAM which allow very fast on chip evaluation of 64-point Fourier Transforms. The data is bit reversed on input and "windowed" using a Hamming Window. A 64 point complex decimation in time FFT is used to find the power spectrum and hence the median frequency f_m. This is defined as the first value of f for which the relation

$$\sum_{i=0}^{f} P_i \geq \frac{1}{2} \sum_{i=0}^{31} P_i \qquad \text{B.4}$$

is satisfied. Each value output by the device is an average of 16 previous calculations with a new value being output each second. The resolution of the device is 16 Hz, which is defined by its 1000 samples/second sampling rate.

The system described by Seroussi et al.[236] makes use of an IBM PC to do the calculations. A block diagram is given in Figure B.6. The system samples the data for 2s at 512 Hz after first anti-alias filtering to 220 Hz with a 4 pole butterworth filter. It then performs a 1024 point FFT, giving a resolution of 0.5 Hz. Finally the Median Frequency is calculated. This is repeated every 6s, 2s for sampling and 4s are used for the FFT and median frequency calculation. After collecting the data for a muscle contraction it is then post-processed to yield a slope, Hz/second and a coefficient of determination for comparison of sets of results.

B.2 Bath University Muscle Fatigue Monitor

Various prototypes of the current system have been investigated all of which have been designed using a similar technique to that used by Stulen and De Luca[229,231] in their later generation MFM. The current design makes use of an analogue front end with the comparator function and generation of the modulating signal being carried out by a PCB80C552 microprocessor. A block diagram of this system is given in Figure B.7.

The system has two 4 digit LCD displays controlled via the I^2C bus to display the median frequency and input signal power. The median frequency is also available via an RS423 serial link, which is opto-isolated by the box described in Section 5.5. Analysis software to make use of this data has been written for use on an Atari ST computer. This software permits the logging and analysis of the median frequency against time.

B.3 Implementation

The use of the microcontroller allows considerable flexibility in the eventual configuration. At this stage all analysis of the data is carried out by the Atari based software. Clearly this can eventually be moved to the MFM microcontroller once the routines required have been ascertained. The boxed MFM is shown in Plates F.31 and in more detail in Plates F.32 and F.33.

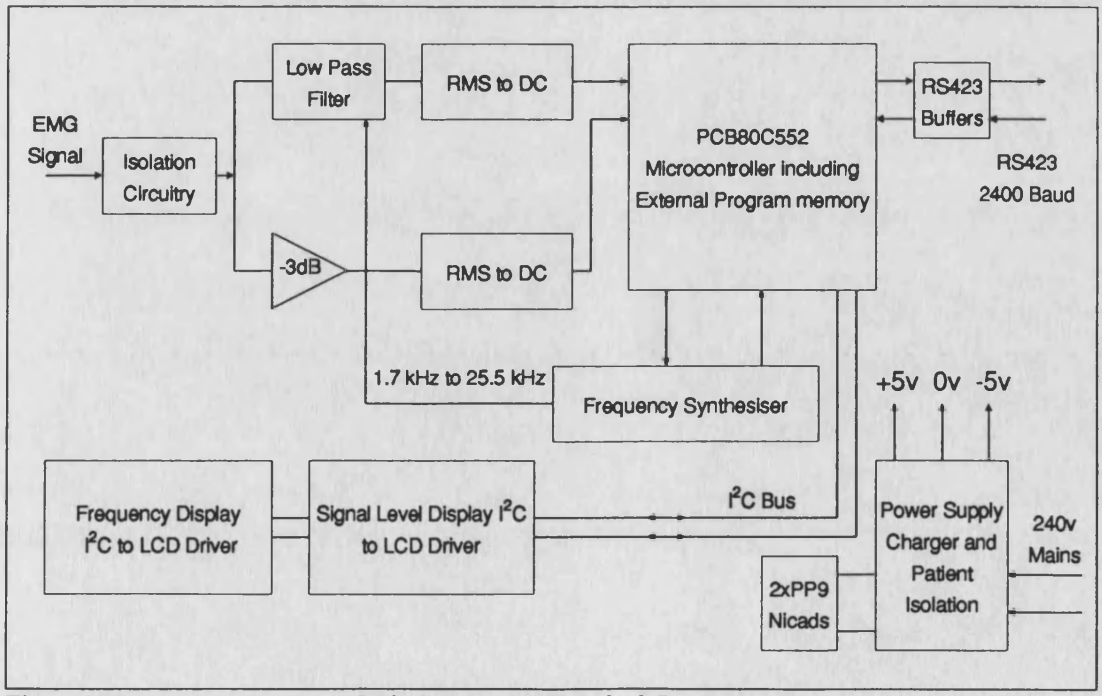

Figure B.7 *Bath University MFM Block Diagram*

B.3.1 Analogue Circuitry

Figure G.39 gives the circuit diagram for the MFM system. The system uses two MF10 switch capacitor filters configured as an eighth order unity gain Butterworth filter to give a sharp rolloff. The MF10s are configured to have their cut-off frequency equivalent to 1/100th of the input clock signal.

The –3db attenuator U1a,b is configured as a non-inverting amplifier with U1a giving the gain of –3dBs and the second half acting as a unity gain inverting amplifier with a preset to allow for attenuator calibration.

The RMS to DC converters on the outputs of the –3dB amplifier and filter are the key to the systems accuracy. The RMS to DC converters are currently based on standard discrete opamp designs with unity gain, U1c and U2c.

B.3.2 Digital Circuitry

The microcontroller, Figure G.40 requires a fixed frequency 12 MHz clock; the filter requires an equal mark space ratio clock in the range 0 to 25.5 kHz. If the filter clock has a resolution of 100 Hz the filter has a cut-off frequency between 0 and 255 Hz. By using a 4059 divide-by-n divider, frequencies in the range 1.7 kHz to 25.5 kHz in 100 Hz steps may be achieved, thus setting the lower frequency of the filter cut-off at 17Hz. The 12 MHz clock is generated from a standard crystal oscillator circuit and feeds both the microcontroller and the divide-by-n divider. The divider does not necessarily produce an output with equal mark space ratio so it is used to generate a clock of twice the required rate which is then divided by 2 using a D-type latch to give an equal markspace ratio.

The divide-by-n counter is controlled by 16 JAM codes and 3 pre-divider bits. The pre-divider is set to give a division of two and the 16 JAM codes are controlled by the microprocessor, port pins P4.0-P4.7, P1.0-P1.5, P3.2 and P3.3.

The two 4 digit LCD displays use two PCF8577 I^2C to LCD driver chips. These have on board all the necessary driving and control logic for the LCD requiring only a resistor and capacitor for the oscillator. The PCF8577 is a slave device with a fixed I^2C address of 01110100B. To select between multiple devices a 3 bit sub-address is used. This is set by three pins on the PCF8577. The device is selected in sofware by the control byte device sub address field. This gives a maximum of 7 devices per I^2C bus. The frequency display LCD is configured to reside at device sub address 0 and the signal level display LCD is configured to reside at device sub address 4.

The microcontroller, PCB80C552, is configured with 8 kbytes of rom via an external eprom, 27C64, and an RS423 compatible serial interface. The two analogue signals, from the –3dB attenuator and MF10 filter, are fed into the ADC ports 0 and 1, P5.0

and P5.1, respectively. The ADC is configured for voltages between 0 and 5V giving a theoretical resolution of 4.9mV ($5V/2^{10}$)

B.3.3 Power Supply and Charger

To ensure that the subject being tested has no chance of being connected to the mains the system is run from two PP9 ni-cad batteries. These are combined with a mains powered battery charger Figure G.39. The battery charger when powered up, closes relays that disconnect the batteries from the MFM circuitry and connects them to the charger. It also disconnects the input thus isolating the subject under test should the charger inadvertently be connected.The batteries are regulated from ±9V to ±5V to power the processor and analogue circuitry.

B.4 Control Software

The pseudo code for the main control loop is given in Figure B.8 along with the names of the main subroutines used to carry out the functions.

B.4.1 Main Control and Averaging Loop

This sets up the user defined flags and initialises the required system registers on power up. It then enters the loop that calculates and outputs the median frequency. Within the main loop there is a smaller averaging loop. In this loop the analogue to digital conversion and adjustment of the output frequency is carried out. The resulting frequency is then output via the RS232 port.

Every ten times round this loop a new average frequency is calculated and if it is different from that currently being displayed it is displayed. A new value for the signal power is also calculated and displayed if different from that being displayed. The choice of 10 for the loop COUNT is a reasonable compromise between display 'flicker' and response time of the unit to frequency changes. Having done the various LCD changes, the flags are reset and the program repeats from the averaging loop.

Before displaying the frequency it is 'corrected' by the subroutine CAL. This correction is required because it was found in initial accuracy tests that the MFM had a constant error. Adjustment of the presets on the RMS to DC converter gave an improvement, making the error approximately 9%. Figure B.9 shows plots of the accuracy before and after the software correction. The correction involves multiplying the frequency by 1.09. The cause of this seems to be the RMS to DC converters which are not true RMS converters. It should be *noted* that the *value output* via the RS232 is *not corrected*, so any post processing software must allow for this error.

```
CODE                                        SUBROUTINES
Start
Initialise Variables                        INIT,IICINIT,RSINIT,ADINIT
Repeat
 While COUNT not zero
   Do ADC Conversions                       ADGET,ADCINT(Interrupt)
   Alter Frequency                          ALTFREQ,SETFREQ
   Output Frequency via RS4234              RSFREQ
   Calculate new Average Frequency
 Endwhile
 Correct FREQ                               CAL
 while NUMBYTMST <> 0
   Endwhile
 Output new FREQ to LCD                     FREOUT
 Compare ADCA with ADCAA
 If difference < 4
   While NUMBYMST <>0
     Endwhile
   Output new ADCA to LCD                   SIGPWR
 Endif
Reset FREQUB,FREQLB to 0
Reset COUNT to 10
Update ADCAA with ADCA
Update FREQ with FREQUB
Until False
```

Figure B.8 *Pseudocode of the Main Control loop of the MFM*

B.4.2 Analogue to Digital Conversion

The ADC is a 10 bit converter of which only the most significant 8 bits are used at this stage. Channel 0 is used for the attenuated signal and Channel 1 for the filtered signal. The routine called to do the ADC conversions is ADGET. The reduction of the ADC accuracy to 8 bits simplifies the software but increases the minimum detectable voltage change from 4.9 mV to 19.5 mV.

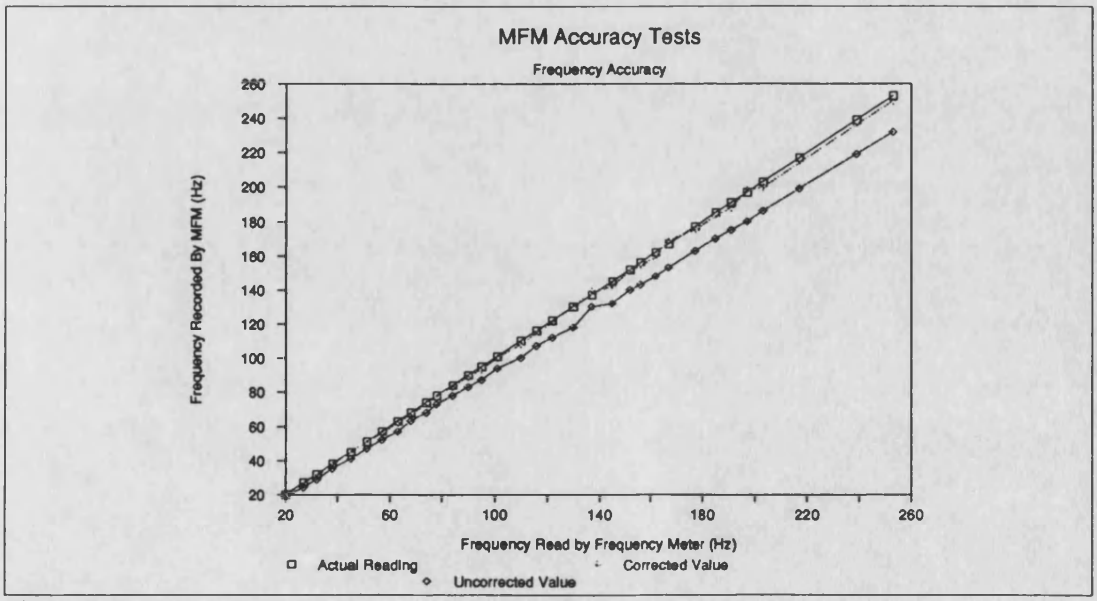

Figure B.9 *Frequency Accuracy*

B.4.3 Alteration of Filter Cut-off Frequency

To track the median frequency changes in the input signal, the results of the analogue conversions are compared and the control frequency for the switch capacitor filter adjusted accordingly. This is carried out by the subroutine ALTFREQ and is called from within the averaging loop.

The amplitudes of the two conversions are compared and if they differ by more than 78 mV the cut off frequency is adjusted. The 78 mV of hysteresis is necessary to prevent the system oscillating wildly about the median frequency of the EMG signal and is a compromise between accuracy and size of oscillations. The hysteresis is obtained by ignoring the two least significant bits of the difference between the ADC values, which is equivalent to four times the minimum step size of 19 mV.

B.4.4 Control of the Frequency Synthesiser

Once the new frequency has been calculated by ALTFREQ, SETFREQ is used to generate the necessary JAM codes for the divide-by-n counter. The calculation is carried out by a lookup table. SETFREQ looks up the JAM code for the required frequency and splits it up for output to the various ports. As discussed earlier the frequency generated is twice that required, to allow for the divide by two stage.

B.4.5 Median Frequency Output

The median frequency is output to the RS232 link by the subroutine RS232. This routine takes the median frequency converts it to BCD and thence to ASCII and outputs the three characters followed by a CR and LF.

The data is transmitted at 2400 baud, which is the maximum rate that still meets the RS232 specification when using a 12 MHz clock for the processor. The routine waits for each byte to be sent thus introducing a delay of about 2.5ms into the loop. This delay is required whether an RS232 output is required or not to stabilise the median frequency tracking.

B.4.6 Median Frequency Display

The LCD display is written to by FREOUT. This takes the corrected median frequency and transmits it serially via the I^2C bus. The data is sent as 6 bytes, a slave address, control byte and four bytes corresponding to the four digits of the display. The routine splits the frequency up into hundreds, tens and units, then converts these to the data required to display the numbers on the LCD with a leading zeros as required.

B.4.7 Calculation and Display of the Signal Power

The MFM also displays the mean square of the input signal. This is calculated by doubling and then squaring the signal obtained from the attenuated channel analogue to digital conversion. The subroutine that does this is SIGPWR. The input value, an

eight bit number, is then scaled and multiplied using 16 bit integer maths to produce the final displayed value.

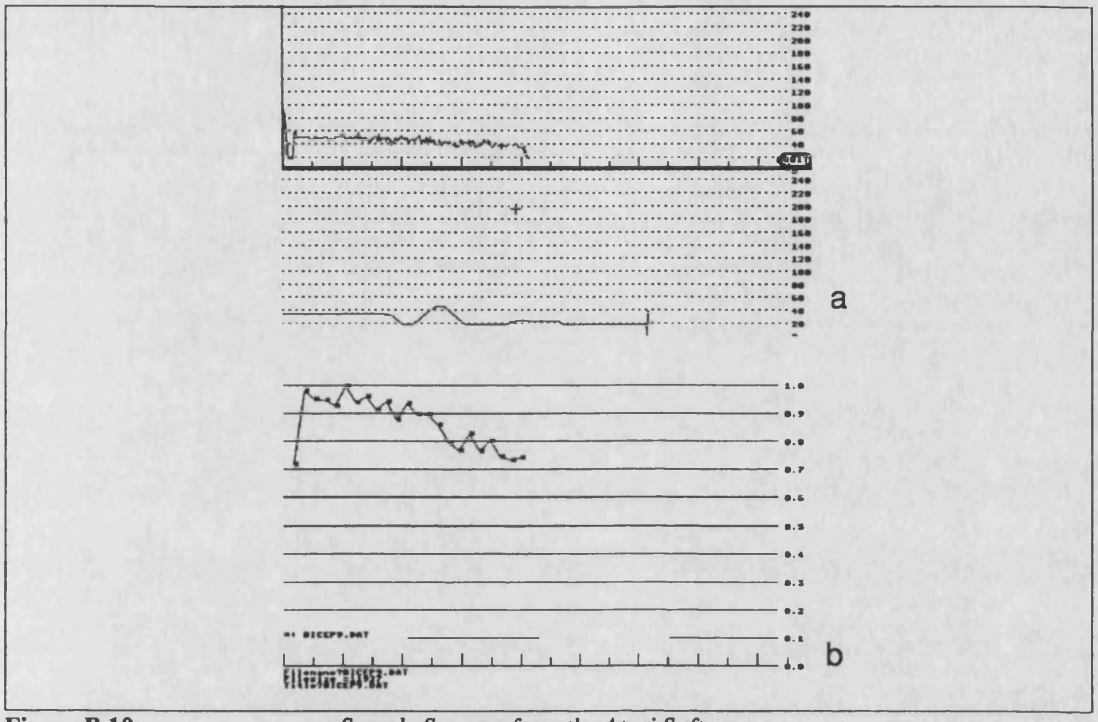

Figure B.10 *Sample Screens from the Atari Software*
a) Capture Software b) Post -Capture Smoothing Software

The power display is referenced to the input of the MFM so that the EMG preamplifier gain does not need to be known. This means to convert the displayed value to true muscle power it needs to be divided by the gain of the preamplifier used.

B.5 Analysis Software

The basic MFM unit as described carries out no processing or storage of the median frequency. Software to capture and display the data in real time, and to post process recorded results has been written using FastBasic running on an Atari ST computer.

B.5.1 Data Capture Routine

This program, MFM.BSC, captures and displays up to eight minutes of median frequency data. It produces a long term and short term plot of the MFM on the screen in real time. Figure B.10 shows a sample plot of some typical data. The top half of the screen is the long term plot and the lower half is the short term plot. Once data capture is complete it may be saved to disc.

This routine has the option of being able to re-load previously saved data and re-plot it on the screen. Then, using the mouse, any part of the long term display may be chosen to be displayed in the detailed display below.

B.5.2 Post-processing Routine

This program, GRAPH.BSC, allows the comparison of sets of recorded results. The routine allows for the normalisation of the results as well as the display of the results against an absolute frequency scale. Up to six sets of results may be displayed at once; each can be smoothed by a running average over a chosen 'window' size and either displayed as normalised data or on an absolute scale.

On running the program it asks for the required window size for smoothing; this size is used for all sets of data. Figure B.11b shows the typical data of Figure B.11a normalised and averaged with a window size of 1500 samples by GRAPH.BSC.

B.6 System Calibration

Figure B.11 shows the block diagram for the test equipment for the calibration tests. It consists of a signal generator 2, that can be modulated by a second signal generator 1. The output of signal generator 2 is a swept frequency centred around the frequency set on signal generator 2, sweeping at the frequency set by signal generator 1.

B.6.1 Accuracy of the Frequency Measurement

For this test, signal generator 1, the modulator, was set to produce a sinusoid of 1 MHz which produces a so called white noise spectrum at the output of signal generator 2. This signal was then fed to a frequency meter and on to the MFM unit.

The test was carried out by adjusting the frequency of signal generator 2 and then allowing the MFM frequency display to stabilise. The MFM reading was then recorded. The correct median frequency was taken to be that recorded by the frequency meter when the modulating generator was connected.

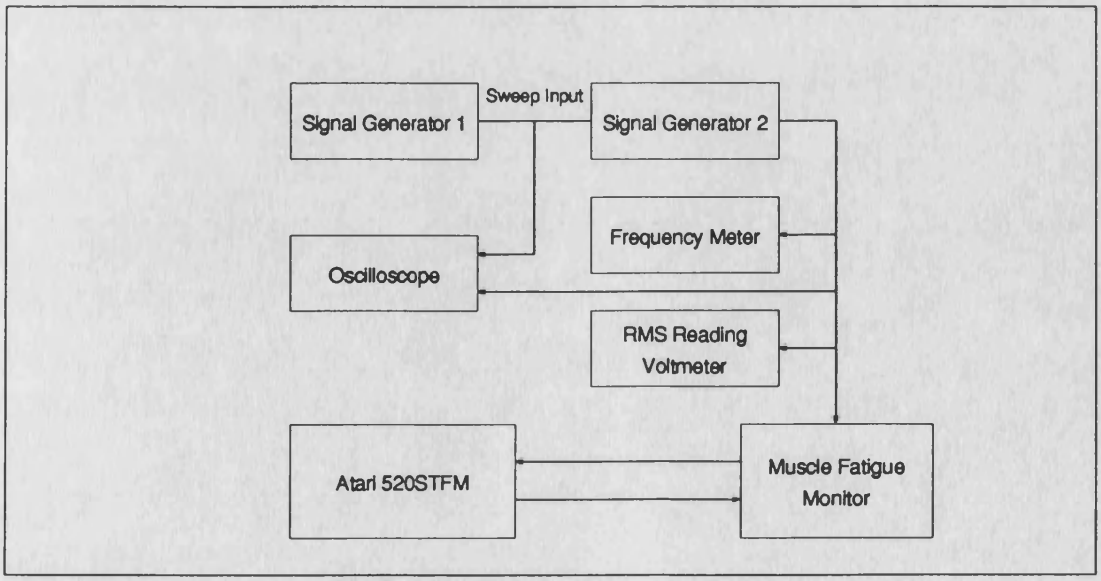

Figure B.11 *Block Diagram of the Calibration Set-up*

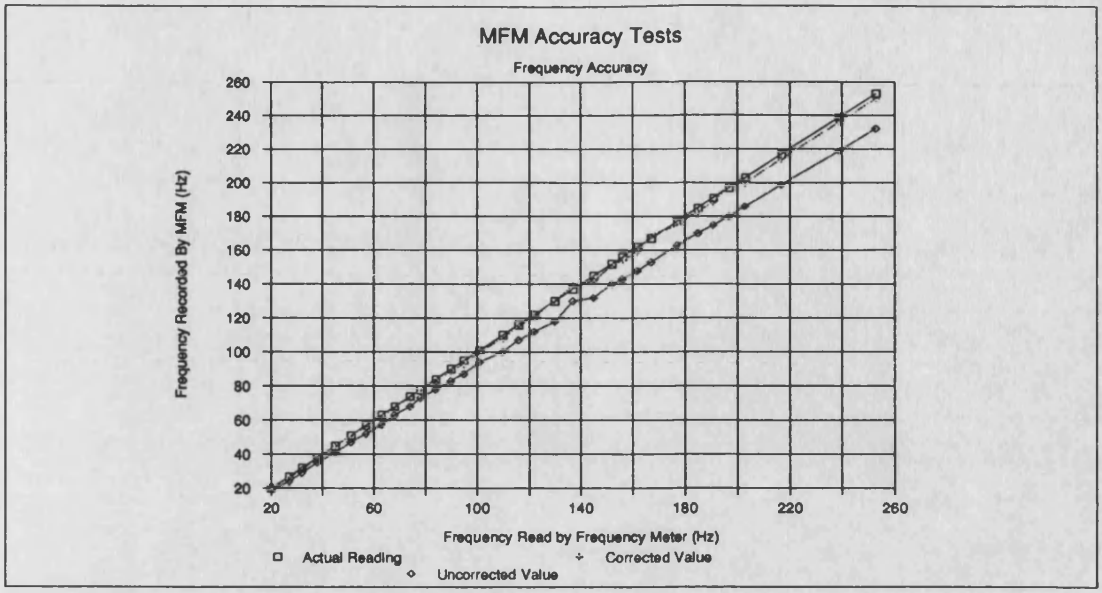

Figure B.12 *Results of the Frequency Accuracy Test*

Initial tests were carried out taking the unmodulated frequency from signal generator 2 to be the correct median frequency. These tests produced results showing that the MFM reading had a greater inaccuracy near the extremes of the signal generator frequency range. This was clearly a function of the test set up and was traced to a non symmetrical spectrum being produced from signal generator 2 due to the modulating signal sweeping the frequency of signal generator 2 beyond its range. Thus the measurement described above was used as the median frequency.

Figure B.12 shows the plot of the accuracy of measurement of the MFM unit along with that after correcting, assuming a 9% error.

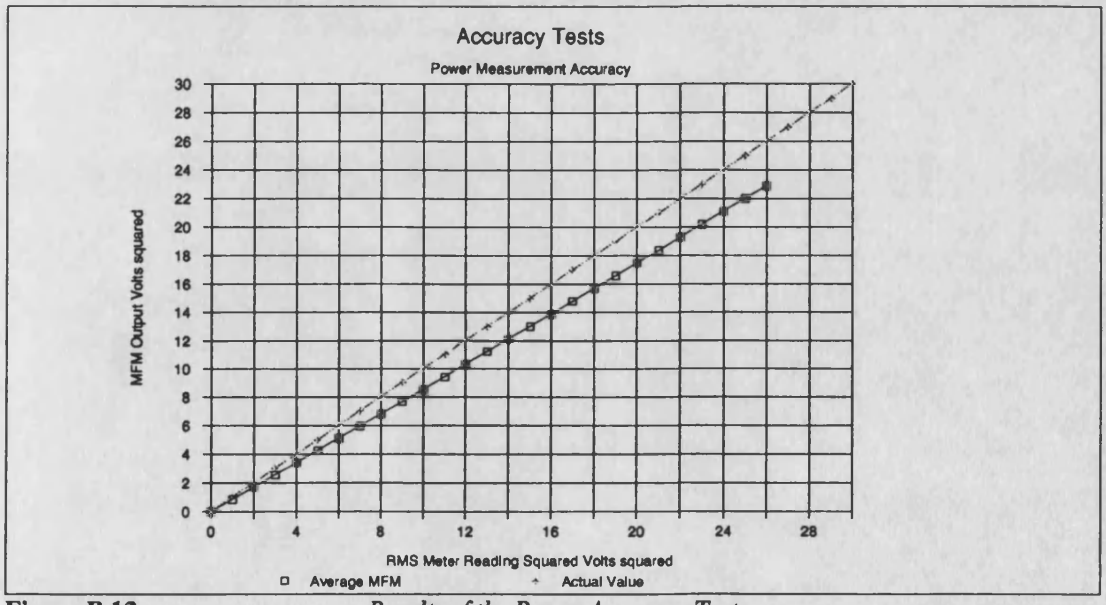

Figure B.13 *Results of the Power Accuracy Test*

B.6.2 Accuracy of Signal Level Measurement

The test as described above in section B.6.1 was repeated but this time the RMS voltage as measured by an RMS voltage meter was compared with the reading of the unit. The tests were carried out at three frequencies 52 Hz, 89 Hz, and 161 Hz. In each test the input signal amplitude was varied from 0 to 5v RMS.

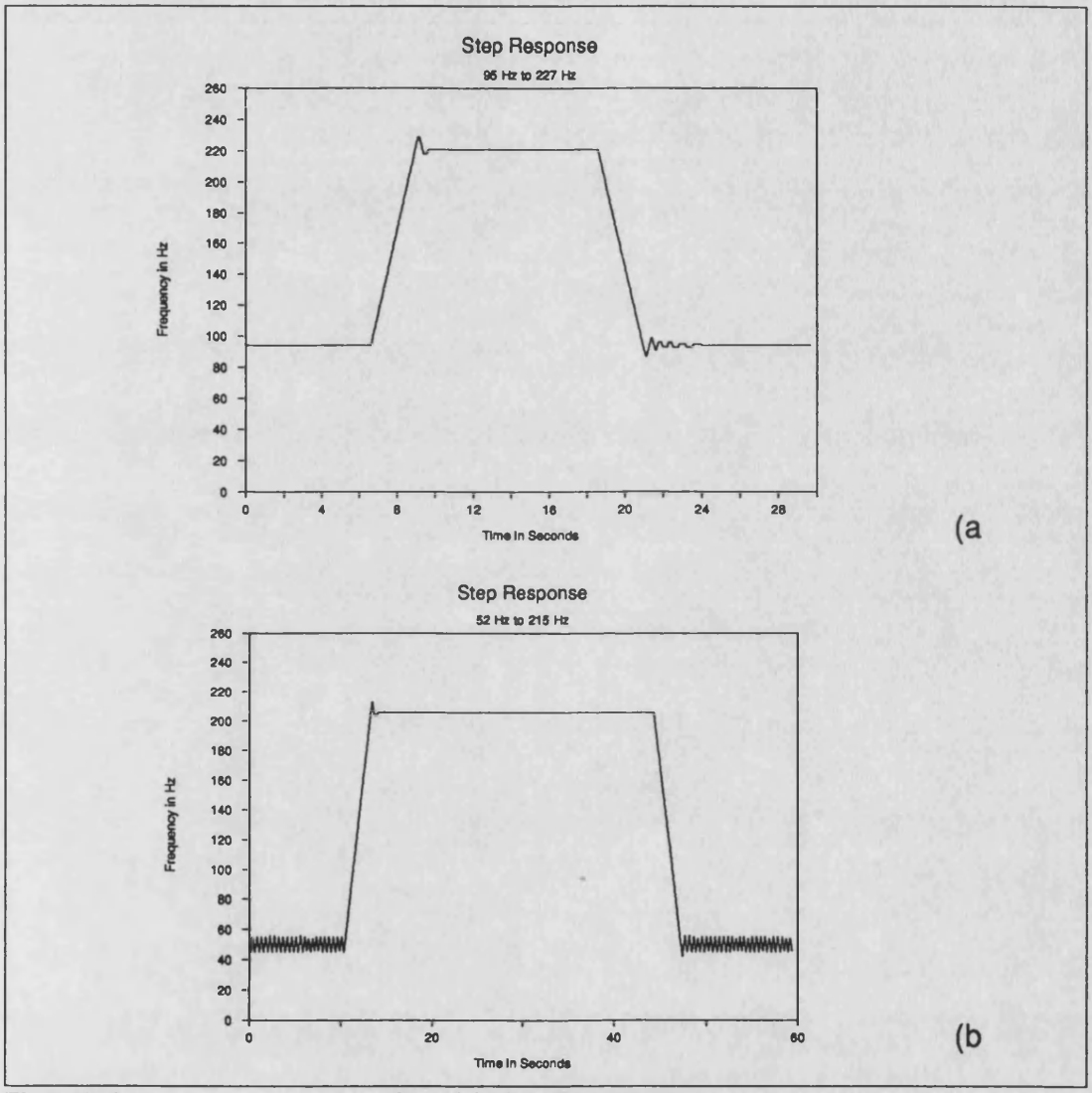

Figure B.14 *Plots of the Step Response Tests*

The actual displayed signal is power so the graph of Figure B.13 plots the MFM reading against the meter reading squared. The error is approximately 10% and is constant at the frequencies chosen and over the input test range. Figure B.13 also shows thresholds between which the MFM will function correctly. The values of 0.15 V and 4.05 V RMS are the limits inside of which the signal of the EMG probe output must fall in order to ensure reliable results from the MFM unit.

B.6.3 Step Response of the System

To test the step response of the system, signal generator 1 was set to produce a square wave of very low frequency, thus causing signal generator 2 to switch between two frequencies. By adjusting the offset and amplitude of signal generator 1 the two frequencies that are stepped between may be adjusted. Figures B.14a and b show the resulting plots for two different step sizes.

The plots show that there is some overshoot on the step response when the input frequency is increasing; this overshoot is recovered in less than 5s. At low frequencies, there is a steady state ripple of 4 Hz which does not decay. At higher frequencies above 65 Hz there is an undershoot which takes between 5 and 15 seconds to decay away.

Sample Number	Sex	Biceps Weight Used	Quadricep Weight Used
1	Male	4.4 kg	2.2 kg
2	Male	4.4 kg	2.2 kg
3	Male	4.4 kg	s
4	Male	4.4 kg	e
5	Female	2.2 kg	s
8	Female	4.4 kg	1.1 kg
9	Male	4.4 kg	s
10	Female	4.4 kg	1.1 kg
11	Male	4.4 kg	2.2 kg*
12	Female	e	1.1 kg
13	Female	4.4 kg	s
14	Male	4.4 kg*	2.2 kg

Key:
e - Equipment Errors prevented valid results being taken
* - Equipment Errors Affected part of the results.
s- Subject unwilling or unable to take part in tests

Table B.1 *Table of Subjects taking Part in Tests*

B.7 Muscle Fatigue Tests

To test the systems effectiveness in monitoring real fatigue signals a series of tests were carried out on a set of volunteers. These tests involved isometric contractions whilst monitoring the muscle signal. Two separate tests were carried out on a total of twelve subjects. The two tests were on the biceps muscle and the quadriceps muscle group.

In addition to the isometric tests mentioned above, repeatability tests were carried out. The same set of isometric tests were carried out on the same two subjects at the same time for a period of four days to see if any significant variations could be found.

B.7.1 The Test Subjects

A group of twelve subjects were taken, six males and six females. The subjects were all between the ages of 18 and 23 years, with their physical fitness ranging from unfit to fit sports people. The subjects carried out the tests at a time of their own choosing within the laboratory. Table B.1 gives details of the subjects.

B.7.2 Equipment Configuration

The EMG amplifier used had a fixed gain of 1000 and is as described in Section 6.3 with two stainless steel electrodes 2 cm apart. This was attached over the belly of the muscle being tested, with a separate saline soaked earth strap being connected to a convenient neutral point, such as wrist or ankle, of the subject. The pre-amplifier output was then amplified by a further amplifier with a gain of x5, before being fed into the MFM. If necessary this was increased or decreased to ensure the signal level remained within bounds. The RS423 output from the MFM was then fed via an opto-isolating RS232 box to the Atari ST which carried out a real time plot of the frequency data being received as well as allowing the data to be stored for further analysis.

During the initial tests the subjects were able to see the Atari screen showing the plot, some subjects then used this as a biofeedback signal and tried to keep their medians artificially high. For the second series of tests on the repeatability, the subjects were not permitted to see the screen until the test was completed.

B.7.3 Test 1 The Biceps

The purpose of this test was to track the fatigue curve of the biceps muscle whilst a subject maintained an isometric contraction. The protocol for the test was simple. The subjects were required to stand upright whilst holding a 4.4 kilogram dumb-bell in their dominant hand. The forearm was required to be maintained at the horizontal for the duration of the test, meaning the arm was bent at right angles at the elbow. The test was stopped by the subject when he/she was unable to keep the forearm horizontal. The end point was decided by the subject and not the researcher.

The pickup electrode was placed over the belly of the biceps brachii muscle while the earth strap was attached to the wrist. The position on the muscle was determined by asking the subject to flex their arm and then the pickup was placed on the belly of the muscle such that a good EMG signal was seen on the scope. Figures B.15 and B.16 give the normalised plots of the results from these tests.

B.7.4 Test 2 The Quadriceps

The purpose of this test was to track the fatigue curves of the quadriceps. The protocol for this test was that the subject sat in a chair with their thigh on the chair, and the rest

of their leg extended out straight such that the knee was the fulcrum. Weights to a total of 2.2 kilograms were attached to the ankle and the subject was required to maintain a straight leg for as long as possible. Once again it was the subject who decided that they were too fatigued to continue.

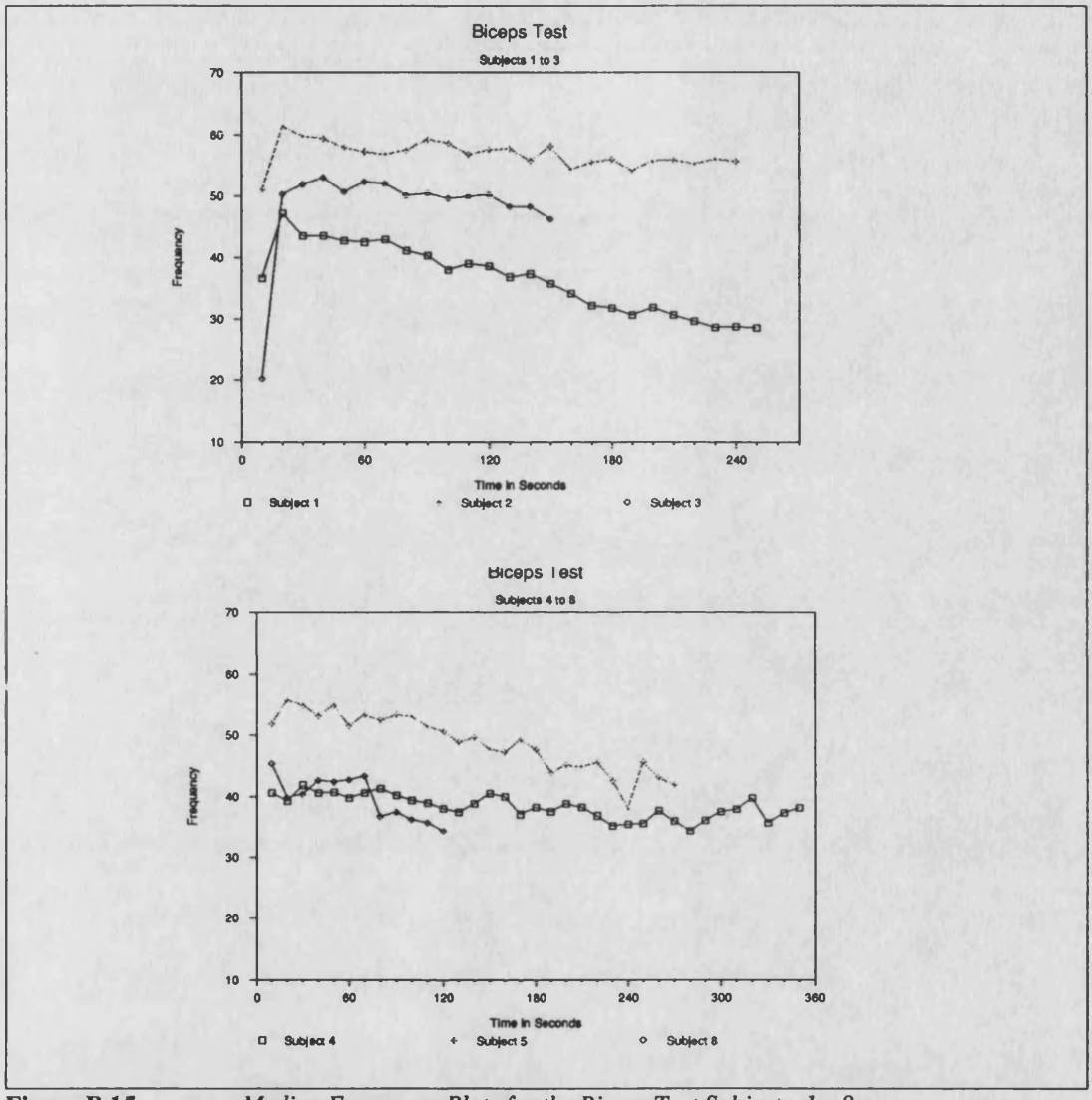

Figure B.15 *Median Frequency Plots for the Biceps Test Subjects 1—8*

The EMG pickup for this test was placed over the vastus lateralis and rectus femoris muscles, with most of the pickup being from the vastus lateralis. The muscles were located by asking the subject to flex their leg muscles and then locating the probe over the belly of the now prominent muscles. The earth strap was placed around the ankle. Figure B.17 gives the results from these tests.

B.7.5 Test 3 Repeatability

The purpose of this test was to check the repeatability of the measurements from day to day. Two subjects repeated the same exercise at the same time of day for four days.

The test carried out was test 1 described in section B.7.1 except that the subjects were not allowed to view the results on the monitor during the test. The results from these tests are given in Figure B.18.

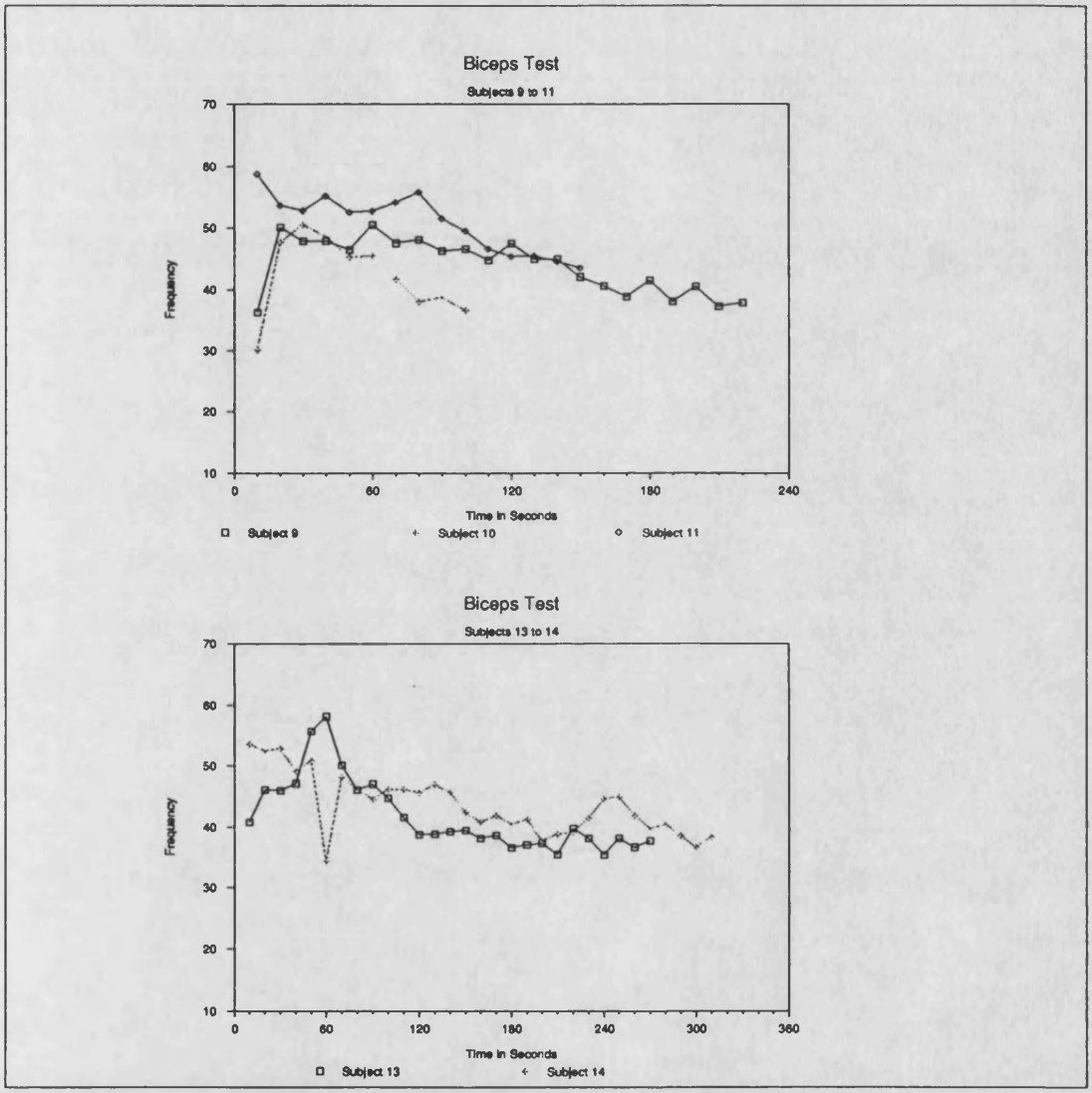

Figure B.16 *Median Frequency Plots for the Biceps Test Subjects 9 -14*

B.8 Analysis of Results

The purpose of these tests has been to assess the effectiveness of the Muscle Fatigue Monitor to give an indication of fatigue and see if any quantifiable measures can be found. The results will be considered both quantitatively and qualitatively.

B.8.1 Validity of Results

The two main assumptions made for these tests have been that muscular fatigue is a function of time for which the weight was supported and that the muscles being monitored were the main muscles involved, that is, the muscles being monitored were working hardest.

The first assumption is essentially correct; fatigue is a function of the time a contraction is maintained, although as suggested earlier other psychological and physiological factors may be involved.

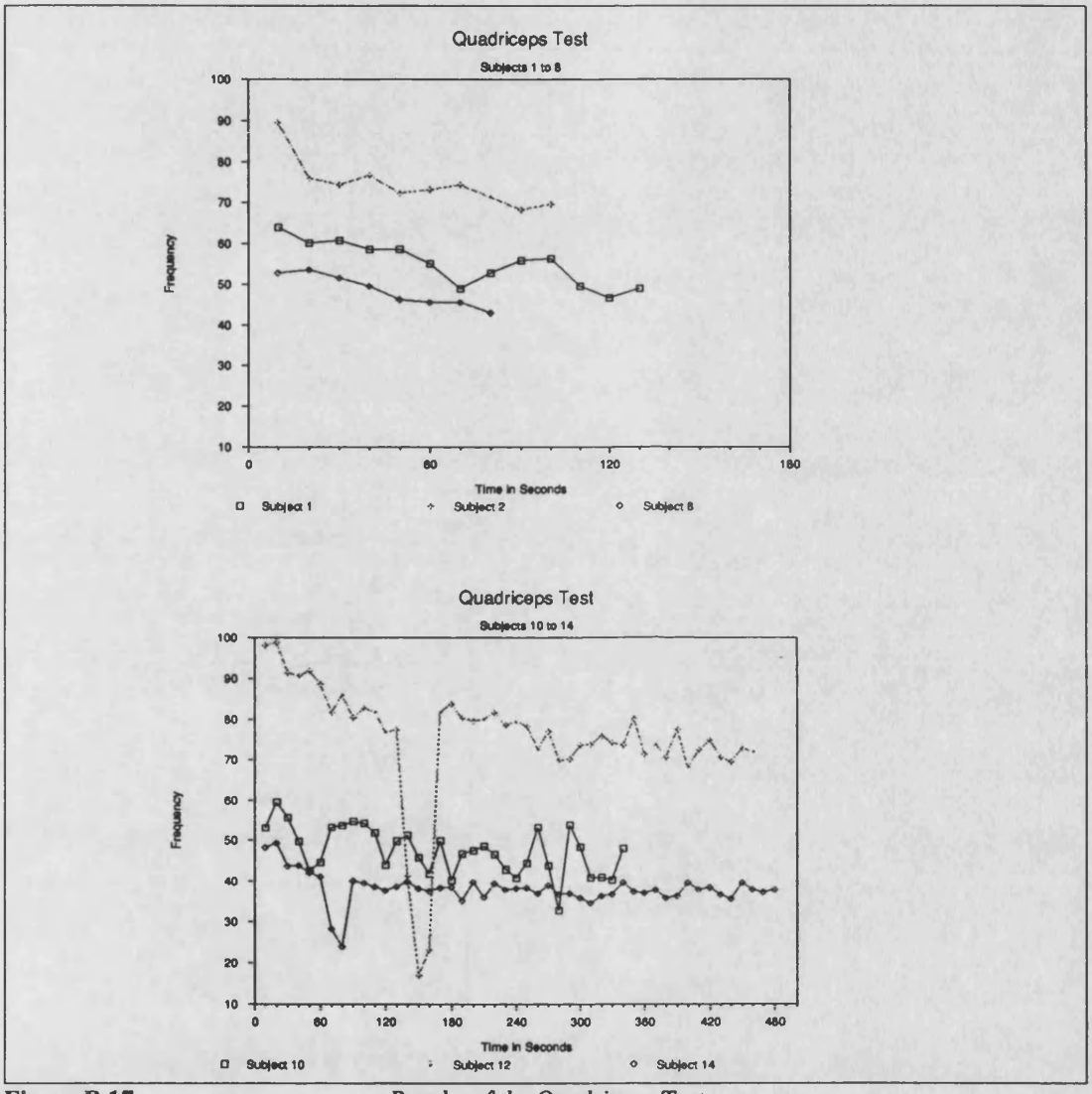

Figure B.17 *Results of the Quadriceps Test*

The second assumption is not necessarily correct. In test 1 the biceps muscle is certainly one of the major contributing muscles but it works in antagonism with the triceps brachii and this, combined with the subjects posture, can seriously affect the amount of effort the biceps brachii is required to exert. In test 2 there is more ambiguity as to which muscle is the major contributor to the leg extension used for the test. As has already been stated it was assumed that the vastus lateralis and to a lesser extent the rectus femoris were the main quadricep muscles involved. This clearly is not necessarily so, but for the purposes of these tests appears to be a reasonable assumption.

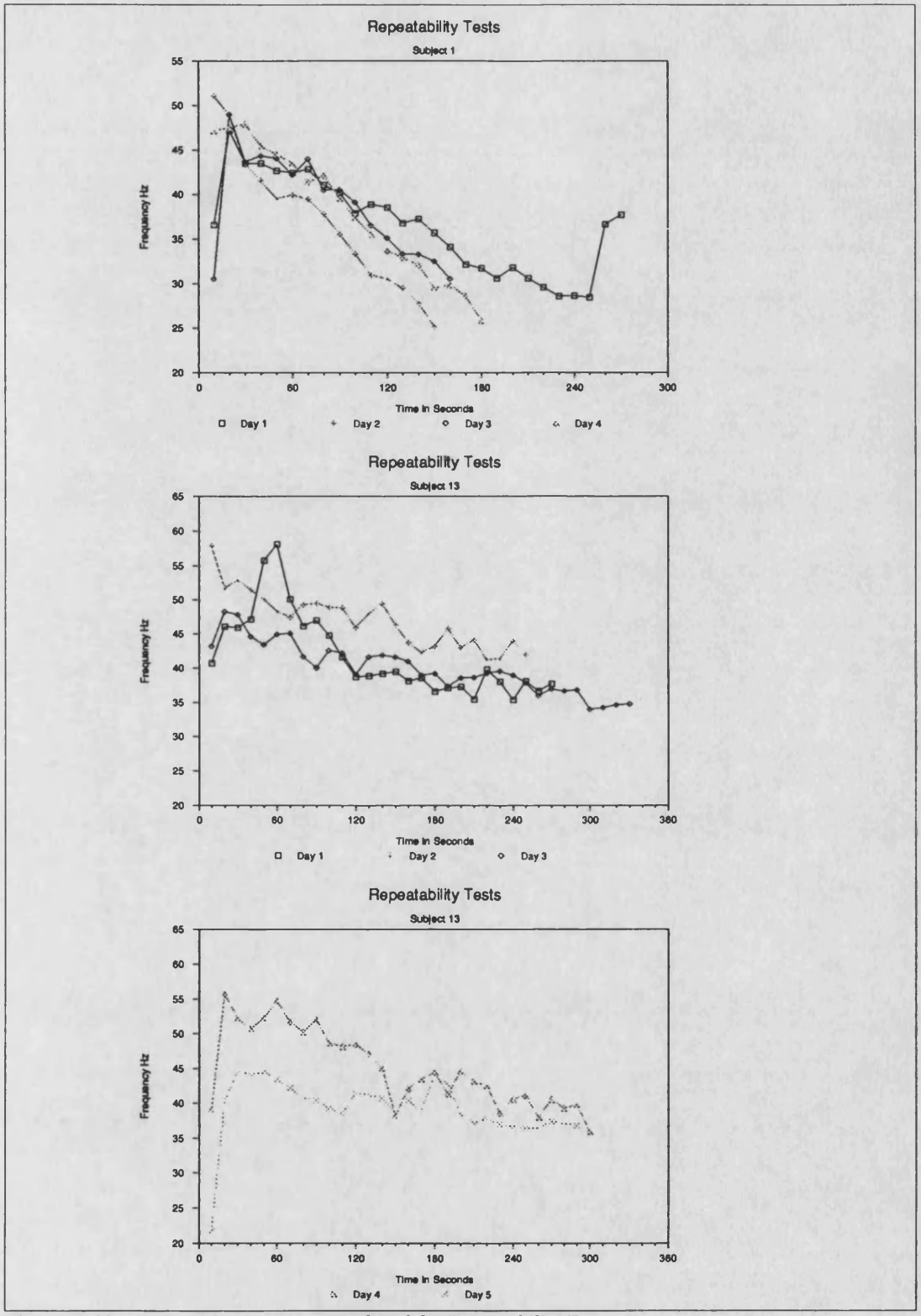

Figure B.18 *Results of the Repeatability Test*

B.8.2 Qualitative Analysis of Results

The simplest way to do a qualitative comparison of the results is to plot the median frequency against time for each subject. These are shown in Figures B.15 and B.16. It should be noted that the results have been smoothed with a window of 500 samples (≈10s) before plotting.

In all cases the median frequency does reduce with time as expected hence the median frequency may be considered a measure of fatigue. From the results of Figure B.17 the results of the quadriceps do not decay as fast and appear to have a higher median frequency than those from the biceps. Also it can be seen that each muscle displays a wide frequency variation between subjects.

The graphs of Figure B.18 show the results of the repeatability tests. It is clear from these graphs that, with the exception of the first day for subject 13, there is a greater similarity in the results obtained from the same muscle and subject. This suggests that quantifying muscle fatigue may be possible for individuals if previous data on the subject is known.

B.8.3 Quantitative Analysis of Results

A number of indices for each curve have been calculated to try and characterise them. The indices used are mean median frequency over the test period, the median frequency at the start of the test, the slope of the curve, and the time for which the weight was supported.

The mean median frequency was calculated over the whole duration of the test except the first 500 samples. These first few samples were discarded because this is the time during which the subject picked up the weight and therefore it is not part of the fatiguing curve. The starting frequency was taken as the average of the first 100 samples of median frequency after the initial transient period of 500 samples.

The gradient of the curve was calculated assuming the curve to be linear and then applying linear regression using a least squares method of best fit. The results are in Hz/minute. To assess the measure of fit, the correlation coefficient was also calculated, which has a value of one if it fits the data perfectly, decreasing to zero for no fit.

The time for which the test lasted was calculated assuming a sample rate of 50.5 samples per second and was calculated from the sampled data taking the point of failure as when the subject was unable to continue the test.

These results are given in Table B.2. The indices were further analysed by taking the means and standard deviations of each index for each set of results. The results were

separated into five groups; the biceps results, the quadriceps results, the repeatability test for subject thirteen, and the repeatability test for subject one.

Sample	Mean	Start	Gradient	r	t
B1	36.3	48.3	-4.721	0.714	4.24
B2	56.9	60.4	-1.230	0.959	4.08
B3	50.0	53.3	-2.427	0.962	2.53
B4	38.0	38.7	-0.773	0.979	5.91
B5	48.3	57.7	-3.558	0.636	4.60
B8	38.9	43.9	-4.585	0.944	2.06
B9	43.9	46.3	-3.733	0.718	3.79
B10	43.4	52.6	-10.02	0.834	1.68
B11	50.0	53.6	-5.412	0.873	2.55
B13	41.8	45.7	-3.721	0.833	4.53
B14	43.1	53.9	-2.236	0.916	5.23
Y1	41.8	45.7	-3.721	0.833	4.53
Y2	46.4	52.8	-2.740	0.876	4.22
Y3	39.7	47.6	-2.173	0.862	5.60
Y4	45.0	53.8	-3.682	0.766	5.03
Y5	39.7	43.6	-1.530	0.938	4.99
A1	36.3	48.3	-4.721	0.714	4.24
A2	35.9	50.9	-9.446	0.636	5.09
A3	38.8	48.9	-6.888	0.753	5.82
A4	36.9	50.3	-8.103	0.655	5.90
Q1	54.2	61.2	-6.643	0.794	2.18
Q2	72.7	81.0	-5.243	0.822	1.69
Q8	47.8	54.0	-9.370	0.743	1.36
Q10	47.3	59.6	-1.824	0.908	5.72
Q11	74.7	96.8	-1.449	0.980	7.68
Q12	37.9	52.2	-0.315	0.993	8.04
Q14	45.0	57.5	-2.891	0.461	4.57

Key:
Bx Biceps Test x
Yx Day x Test on Subject 13
Ax Day x Test on Subject 1
Qx Quadricep Test x
r Correlation Coefficient
t Time for which test lasted in minutes

Table B.2 *Indices Calculated for Each Test Carried Out*

Since the standard deviation is a function of magnitude of the samples a comparison has been carried out using the coefficient of variation which is independent of sample magnitude. A value of zero implies that the results have no variation and a value of one indicates a large variation. These results are given in Table B.3 .

From Table B.3 the mean median frequency of the quadriceps results is 54 Hz and that for the biceps is 43 Hz. The coefficient of variation for the repeatability tests are

0.07 and 0.03 in comparison to 0.14 for the biceps test, itself showing that results are repeatable between times for one subject but that between subjects considerably more variation occurs.

		Set B	Set Y	Set A	Set Q	B+Y+A
MEAN	μ	44.60	42.52	36.98	54.23	42.94
	σ_{n-1}	6.17	3.07	1.28	14.15	5.69
	n	11	5	4	7	18
	c/v	0.14	0.07	0.03	0.26	0.13
START	μ	50.40	48.70	49.60	66.05	50.13
	σ_{n-1}	6.41	4.45	1.21	16.54	5.34
	n	11	5	4	7	18
	c/v	0.13	0.09	0.02	0.25	0.11
GRAD	μ	-3.85	-2.76	-7.30	-3.97	-4.27
	σ_{n-1}	2.52	0.94	2.00	3.24	2.73
	n	11	5	4	7	18
	c/v	-0.65	-0.34	-0.27	-0.82	-0.64

Table B.3 *Analysis of Indices for Sets of Results*

The start frequency, not surprisingly, is higher for the biceps test than for the quadriceps, 66 Hz as against 50 Hz. Once again the coefficient of variation is higher for the biceps group in comparison to the repeatability tests, 0.13 as against 0.09 and 0.02. The results for the gradient give an average of –4.27 Hz/min for the biceps and –3.97 Hz/min for the quadriceps. It is difficult to draw any conclusions from these results. Once again the repeated tests have a lower coefficient of variation.

B.9 Conclusions

These sections of the appendix have described a system that is capable of tracking the median frequency of an EMG signal. The system is self contained and battery powered making it safe and portable. Recording of the results is possible via the RS232 port.

Tests of the system have been carried out on twelve volunteers which show that the characteristic median frequency of quadriceps is higher than that of the biceps. This frequency difference may be explained by considering the fibre content of the muscles involved as discussed in Section 1.1.3. Both muscle groups displayed a decrease in median frequency with fatigue as has been suggested by many authors.

The variation in results for the twelve subjects suggest that absolute comparisons of median frequency cannot be made between different people because of the wide variation. This again may be attributed to the type of muscle fibres present, which would be dependent on the type of use they put their muscles too; whether they are sports persons or not. The repeatability tests suggest that comparisons between the

same person over several days is possible and may be a reasonable method for quantifying the state of fatigue of a person given a known reference set.

The performance of the MFM could be improved in several ways; the software could be rewritten such that the updating is timer controlled and the RS423 is interrupt driven so that an accurate set of samples is taken with minimal inter-sample interval variation. Checks could be incorporated to indicate overload, and hence incorrect readings, and use of another ADC input could be used to provide a battery check.

The analogue circuitry at the moment is made of discrete devices which contribute significant errors particularly in the rms-dc converters. If true RMS to DC converter integrated circuits are used it is likely that significant accuracy improvements could be achieved.

The data capture and analysis software could be improved to provide a full set of statistical functions for result analysis and result plotting routines.

Clearly the simple tests discussed here could be improved to include things like force measurement. If this was combined with suitable protocols that ensure the muscles of interest are the only muscles involved in the test, more accurate fatigue tests could be carried out.

B.10 Digital MFM

The TMS32010 MFM design by Basano et al.[230] provided the initial concept for the all Digital Muscle Fatigue Monitor described here. Instead of using a microprocessor specifically designed for digital signal processing, this system makes use of the PCB80C552 described in Section 5.1.1. When compared with the TMS32010 it could be considered equivalent to an eight bit DSP with built in A/D with a instruction clock of 1 MHz.

The reason for building the device was to prove the feasibility of using the PCB80C552, with minimal extra hardware, as a low resolution MFM.

B.11 The Hardware

Figures G.41 and G.42 give the circuit diagrams and Plates F.34 and F.36 show the final boxed Digital Muscle Fatigue monitor. The circuit may be divided into three distinct sections; the processor unit, the input filter and buffering and the I^2C controlled 4 digit LCD display.

B.11.1 Processor Card

The processor card is the standard external RAM and EPROM configuration of the 80C552 that has been used previously. It contains a 32 kbyte EPROM and 8k × 8 static RAM. An RS423 compatible serial port is provided using the usual 25 D-Type connector for debugging and future enhancements.

Port 4 of the 80C552 is used to control the attenuator circuitry described in Section B.11.3. The input signal from this is fed into ADC0, P5.0. Port 1 bits 2 and 3 are used to control the overload LEDs. These LEDs are lit if there is an overload condition on the input attenuator, that is the output is greater than 5V or less than 0V relative to the ADC ground (after the signal has been level shifted).

The anti-alias filtering is carried out by an MF10 digital filter. The configuration used requires a clock signal that is 100 times the cut-off frequency of the filter. This clock is generated by the T0 timer of the 80C552 toggling P1.1. This signal is also fed to the event input of Timer T2 which acts as a divider to generate the actual sample clock used to initiate each ADC sample. Thus the anti-aliasing filter cut-off is automatically adjusted to an appropriate value to match the sample rate in use.

B.11.2 I^2C to LCD Interface

The LCD is controlled by a PCF8577 I^2C to LCD driver chip. This is configured to the decode at the default address of 01110100B, with a sub-address of 0H. This display is built on a separate card in order that it can be mounted in the display area of the box as can be seen on the left of Plate F.35.

B.11.3 Input Filter and Buffer

The input filter and buffers consist of a computer controllable attenuator, 4th order Butterworth anti-aliasing filter, a clamp and DC offset stage. It will take an input signal in the range ±9 V and attenuate and offset it to be sampled by the ADC which has an input range of 0 to 5 V. All stages are powered by the ±9 V dual PP3 based power supply except the MF10 digital filter, which has a maximum rail voltage of ±7 V so a special rail of ±6.2 V is derived from the batteries to power the filter such that it can output a full ±5 V signal.

The output of the filter is fed via a divide-by-two buffer which offsets the ±5V filter output to 0 and 5V then via a DC clamp that protects the ADC input from spikes and thence to P5.0 the ADC0 input.

The digital attenuator is based on two DAC0800 and a summing amplifier. This attenuator provides 256 linear steps worth of attenuation which is more than sufficient to attenuate a maximal input signal of ±9 V to the 0 to 5V range required. Connectors provided on the unit are a standard audio phono connector and the laboratory standard 5 way DIN connector which provides ±9 V rails to power the EMG probe described in Section 6.3.

B.12 The Software

The software is run as a linear loop, that is, the input signal is sampled, the FFT is carried out, the median is calculated and displayed, and then the process repeats itself. Sampling for the next data set is started on entry to the routine to calculate the median frequency and display edit. This ensures there is minimal waiting for the sampling to finish.

The initialisation and control is carried out by a single routine which checks the overload or underload counts which are generated by the sample software and adjusts the attenuator appropriately. Adjustment only occurs if more than 10 values in the set of samples of 64, meet the overload condition. An underload is flagged but not acted on since it is assumed that if an overload occurs there is equal likely hood of underload so there is no need to do anything other than check the presence of underload.

Having dealt with the displaying of underload and overload conditions and taken the appropriate action, the main control routine then calls the FFT routine BITREV, followed by the median calculation and display routine MEDIAN. It then loops back to a routine that waits for the sampling to complete to ensure it does not try processing the sample data before it is all available.

```
CODE                                          SUBROUTINES
Start
Set Attenuation to max 0FFH on P4
Clear Internal RAM
Clear External RAM
Set up Timers T0 for Filter Clock
              T1 for RS232                    DEBUG
              T2 for Sampling
Initialise I2C                                IICINIT
;Main Control Loop
Repeat
 Repeat
 Until Sampling Finished GF0=0
 If OVERL  10
      If Attenuation <> 0FFH INC Attenuation
      Set P1.2 Overload LED
 Endif
 If OVERL1  10
      Set P1.3 Underload LED
 Endif
 OVERL = 0
 OVERL1 = 0
 Do Bitreversal                               BITREV
 Calculate Fourier Transform                  BITREV
 Calculate Median Frequency and Display       MEDIAN
Until FALSE
```

Figure B.19 *Pseudocode for the Digital MFM*

B.12.1 Sampling Routine

As described above the sampling process is interrupt driven. A Timer T2 interrupt starts a conversion which completes in 50 μs, then an end of conversion interrupt is used to store the sample in external RAM. The sample routine, STORE, that is called by the end of conversion interrupt, converts the sample data to a twos complement 8 bit number before storing it in the external RAM. It then increments the counts for overload and underload if required. Overload is defined as a sample value of 0FFH and underload is defined as a sample value of 00H. When the 64th sample is taken the routine turns off timer T2 thus preventing further interrupts until the sampling is re-enabled within the MEDIAN routine.

In order to flag the completion of sampling, the general purpose flag GF0 is set. This flag is cleared by the software that initiates the sampling.

B.12.2 FFT Algorithm

The FFT routine used in this system is a 64 point complex FFT which runs entirely in the top 128 bytes of internal RAM from address 080H through 0FFH, of the 80C552 processor. The type of FFT routine implemented here is a radix-2 decimation in time in place algorithm.

The routine first reads the real data samples, stored in external RAM, and loads them into the internal RAM of the 80C552 in a bitreversed order. The imaginary array is filled with 00H. Real data is stored in internal RAM locations 80H to 9FH, imaginary data in locations 0A0H to 0FFH. This is carried out by the routine called BRTABL using a lookup table for the bit reversal addresses.

The actual FFT is carried out by the routine FFT and continues with no further external RAM accesses to ensure maximum speed of execution. To prevent overflow and ensure the full 8bit are used, overflow is detected after each ADD and SUBB instruction. A lookup table is used for the sine and cosine multipliers.

B.12.3 Median Calculation

Once the FFT has been calculated, the results are left in the internal RAM as real and imaginary components. The main routine then passes control to the subroutine MEDIAN.

The MEDIAN routine first converts the real and imaginary results to power by squaring and adding. The power results are stored as 16 bit integers in external RAM at 0300H to 04FFH. It is at this point that the taking of the next set of samples is started by enabling timer T2.

The power components are now summed and the sum used to find the half sum. Then the power components are subtracted one by one from the half sum until the result is zero or negative. The number of the power spectral component at which this occurs is then said to be the median. This value is converted to its equivalent frequency and displayed, using the I^2C interface software derived from detailed description given in the PCB83C552 User Manual[190]. At this point control returns to the main routine.

B.13 Setting Up and Testing

The resolution of the current implementation is only 16 Hz which means this MFM would not serve much practical use in monitoring a fatiguing muscle since the usual change in the median frequency is usually not much more than 16 Hz. It is because of these facts that the system has been tested with the aim being to show its functionality rather than practical application. It is envisaged that further development of the same basic circuit could lead to a more practical version.

The FFT software was first tested by using the sine lookup table as the input data for the FFT routine. The results from a correctly functioning FFT routine would be to produce a single component in the first spectral bin of the output array. Correct placing of the data was monitored by the serial monitor program described in

Chapter 5. Once the main processing routine had been checked as functioning the other routines required were added and the system functioning corrected.

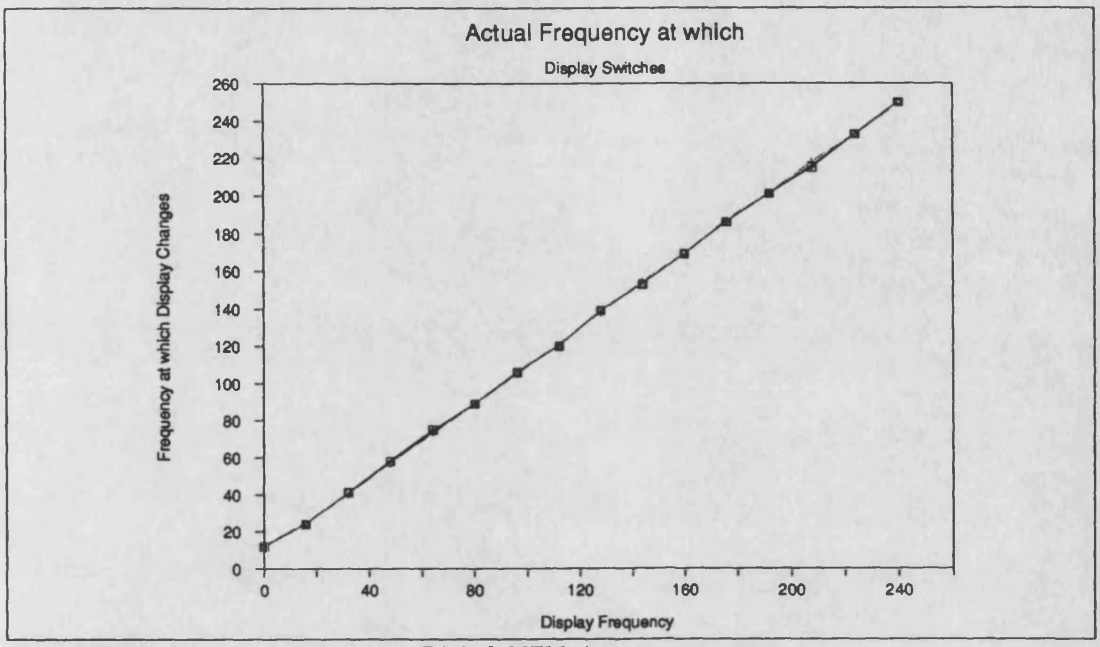

Figure B.20 *Digital MFM Accuracy*

B.13.1 Accuracy

With a resolution of 16 Hz this system has a fairly wide margin for error. The software is configured to switch to the next displayed frequency ±8 Hz away from the current display. So for a display frequency of 96 Hz it would be expected to change over to 112 Hz at an input frequency of 104 Hz, or to change to the 80 Hz display at 88 Hz. To check the linearity of this the input frequency from a sine wave generator was varied from 0 to 256 Hz and the frequency at which the display changed recorded. This was repeated across the active range of the system, which is from 0.6V pk-pk to 10V pk-pk, to check the linearity across the input range. The results of these tests are plotted in Figure B.20. From the curve it can be seen that the attenuator does not unduly affect the systems functioning.

B.13.2 System Timings

By using a spare port pin it is possible to measure the time the software spends in each section of the code whilst looping. The software loops every 350 ms, that is a new result is available every 0.35 seconds. This breaks down into 64 ms sampling time, 25 ms for BITREV, 250 ms for FFT and 75 ms for MEDIAN. The actual control loop takes about 0.2 ms. It is clear from this that the bottle-neck is the FFT routine.

B.14 Results and Discussion

The results show a small handheld digital median frequency meter can be made from a PCB80C552 and a minimum of extra components. The system is consistent and

accurate within the expected limits considering the low resolution that can be achieved with the 64 point FFT. Though the low resolution precludes practical use in the required medical application it is possible that its low resolution would not be significant in other industrial uses.

The slowness of the main FFT of 260 ms when compared to the approximate value based on normal instruction timings of 26 ms clearly shows that the current system does not make optimal use of the processor. The source of the slowing down is the interrupt routine used to calculate and generate the clock signals for the filter and sampling. The problem is not the length of the code but the frequency of the interrupts. A re-design of this stage should reduce the interrupt overheads to an acceptable level providing a faster repetition rate. Although the FFT is the slowest routine, all the routines are affected by the slowing down due to excessive interrupts. It is likely that if the overheads are reduced a repetition rate of the order of 64 ms should be possible where almost half the time is awaiting the completion of sampling; that is, the effective time for the current software to execute would be around 35 ms.

For a practical MFM the resolution would have to be increased and a proper windowing function applied to the sampled data to reduce any picket fence effects. If a Hartley Transform is used instead of the FFT, it would not directly increase the resolution but would increase the speed of calculation including the accuracy, since integer multiplications are used. It is worth noting that the FFT takes a disproportionate amount of time and it is probable that with optimisation an improved speed can be achieved. Siemens have produced a new processor very similar to the 80C552 but giving a number of new features which could enable a speeded up FFT or FHT routine to be implemented. The Siemens 80C517 can handle 32 bit multiplication and division, 8 data pointers for external RAM access and a 12 input A/D.

If these improvements are coupled with a more structured set of software subroutines a faster and higher resolution digital muscle fatigue analyser should be possible. The current system makes no use of the power information inherently present in the FFT data nor does it provide any facilities via the RS423 compatible serial port. The inclusion of these facilities and even some simple programmable options using the serial port would make the system much more useful.

As with the strength duration system of Appendix A no use is made of the power down mode. With the present configuration there is no processing time when the processor is idling but if the improvements suggested for the software are included it is possible that idle time will exist. Changes to the decode of the CMOS eprom such that $\overline{CE}$ is only active when accesses are required would reduce the continuous drain of current from about 30 mA to 1 mA except when the EPROM is being accessed.

Clearly the saving here will only be significant if significant power down time exists but even so some savings can be expected.

This system, when compared to the DSP based system of Basano et al.[230] is not as efficient. However, as a low cost system with minimal components as would be required for feedback sensors, this type of approach shows promise. With the newer 16 bit microcontrollers that are now appearing, even faster 'single chip' digital MFMs should be possible.

B.15 Applications of the Muscle Fatigue Monitors

A Muscle Fatigue Monitor is of use in a number of fields within research and the 'real world'. It is intended here to give a brief resumé of some potential applications of the systems described. In this section a number of applications are suggested, some of which are only concepts and will require experimental verification, whilst others are extensions of techniques that are already analysing the spectral changes.

The median frequency varies between; the same muscle in different subjects, different muscles in the same subject, and with different electrode positions on the same muscle. However, when care is taken to ensure the electrode positioning on a given muscle of a subject is kept constant, the median frequency is repeatable. Clearly this means that the Muscle Fatigue Monitors may best be applied to situations where changes in a particular muscle are to be observed and a number of median frequency measurements taken over a period of time for comparison. Generally single measurements of the median frequency have little application.

B.15.1 Fundamental Research

The use of the changes in median frequency has numerous possible applications. The localised fatiguing of muscle is a complex process and requires a large number of techniques for its study. The use of the median frequency is a reasonably new non-invasive technique that has a direct and indirect relationship to the physiological, anatomical, and biochemical events in the muscle[64]. Investigations of the median frequency changes with temperature and ischemic conditions have been reported. Some investigators have reported a relationship between the median- and mean-frequencies and the fibre type composition giving an application of this technique as a non-invasive muscle biopsy[64].

B.15.2 Physical Therapy

In rehabilitation involving muscle re-education and exercise it is often necessary to assess the effectiveness of the treatment or the amount of recovery. Currently manual muscle tests are used to determine the muscular strength and the progression or regression of strength. These tests like the strength duration test are subjective and

depend on the clinician carrying out the test[237,238]. Edwards and Hyde[237] stated that there are no quantitative methods for measuring muscle function in clinical use today for the diagnosis and management of patients complaining of weakness.

Whilst the patient is undergoing physiotherapy it may be possible to assess the response from the impaired muscle from its median frequency. If the median frequency drops then it is being fatigued by the therapy. If, as may happen, the frequency does not change, it may indicate that the muscle is not being adequately exercised and/or the unaffected synergistic muscles are providing most of the force. This is a documented feature associated with muscle weakening, where there is a shift in muscle control to enable synergist muscles to provide the required force and is known as *muscle substitution*. This effect prevents the impaired muscle from having the required exercise and is difficult to detect using standard manual tests. Muscle substitution might be detected by observing modifications in the behaviour of the median frequency. That is the median frequency dropping, then suddenly levelling off or rising without the force decreasing. This would suggest that other muscles were now providing the force allowing the weakened muscle to relax.

The effectiveness of the treatment might be assessed by observing the changes in the behaviour of the median frequency during a series of treatment sessions. If the muscle is atrophied at the start of the treatment it is likely that the initial value of the median frequency will change significantly between sessions.

B.15.3 Diagnosis of Neuromuscular Disorders

Larsson[101] has already carried out studies on neuropathies induced by lesions of the peripheral motorneurons. His results suggest that detectable changes occur in the frequency spectrum, that is, a reduction in frequency for neuropathies (of at least 6 months) and an increase for myopathies. Since neuropathies and myopathies can be identified by the changing shape of the MUAPs and the median frequency reflects these it could be possible to monitor the development of disorders with the Muscle Fatigue Monitors.

For measurement of the median frequency to be of use in the diagnosis and prognosis of either type of disorder, the frequency shift must be measurably different to that obtained from a normal muscle. If the disease is known to be present then the changes in median frequency could be an effective means of monitoring the progress.

B.15.4 Athletic Training

The effects of exercise and athletic training on the muscle architecture and muscle fibre metabolism is a subject of much research[3]. Many studies have concluded a number of conflicting results[3]. Whatever changes may occur, as discussed in

Chapter 3, the modifications that occur in the muscle will be accompanied by observable changes in the median frequency properties.

B.15.5 Industrial Applications

Changes in the median frequency as an indicator of localised muscle fatigue has already been applied to the field of Ergonomics. Tests on the fatigue of the shoulder and arm in elevated arm positions have been carried out using the median frequency to monitor the fatigue effects[64].

The use of median frequency monitoring has an obvious application in aiding in the distinguishing between physiological fatigue due to the effort of work and physiological fatigue due to boredom.

Appendix C

ISEK Congress Paper

Copy of the paper presented at the 7th Congress of the International Society of Electrophysiological Kinesiology, held in Enschede, the Netherlands, 20-23 June 1988.

SPECTRAL ANALYSIS OF STIMULATED MUSCLE EMGS TO PROVIDE FEEDBACK IN CLOSED LOOP FES SYSTEMS

T.L. WHITLOCK*, D.J. EWINS*, P.N. TAYLOR**, I.D. SWAIN**, R.T. LIPCZYNSKI*
*School of Electrical Engineering, University of Bath, Bath, England
**Medical Physics Department Odstock Hospital, Salisbury, England

Well documented features of Electromyograms (EMGs) from voluntary muscle contractions are the spectral shift with fatigue and the change in power being a measure of force exerted. This paper discusses the techniques being developed to identify these features quantitatively from surface EMGs to provide feedback for a computer controlled stimulator. This stimulator is being designed to provide practical standing and walking functions for paraplegics. The EMGs arising from the stimulating signal show marked periodicity due to the synchronisation inherent in the Motor Unit Action Potential Trains (MUAPT). This permits the consideration of the EMG as much more of a deterministic process than is possible with voluntary muscle contractions. The work involves the design of a number of differing EMG amplifiers which have been designed to reduce the saturation caused by the stimulating voltage while still providing a large gain to amplify the actual EMG signal. The EMGs are analysed by Fast Hartley Transforms in 'real-time' using a 68000 microprocessor system which is being replaced by a fast microcontroller. In the frequency domain the signals are filtered to remove effects due to mains interference and stimulating artefacts.

INTRODUCTION

Muscle fatigue is probably the greatest problem limiting the use of FES systems for prolonged function because fatigue occurs faster than during voluntary contractions. The fatigue is faster because the same muscle fibres are constantly activated whereas in voluntary muscle the contraction is maintained by the activation of differing groups of fibres. Knowledge of the state of fatigue of a given muscle or group of muscles would be of use as a feedback parameter for computer controlled FES systems [2]. The state of fatigue could provide early warning of the point of failure ensuring the user does not collapse. Many researchers have identified changes that may be observed in the EMG from a voluntary muscle contraction as fatigue occurs[1]. One of the most quoted is the spectral shift that occurs in the EMG as the muscle fatigues[3]. A number of methods have been suggested for monitoring this shift of which the Median frequency is one of the most reliable[1]. Other associated features that have been observed are a peaking in the overall power of the EMG and synchronisation between individual MUAPTs. Only qualitative use of these features for measuring fatigue has been found. The most often used quantitative feature is the power(amplitude) of the EMG signal (RMS peak etc.)[1,4,5]. This is related to the force being exerted by the muscles from whom the signal was picked up. The relationship of this power to force depends on the investigator[6,7] but the law may simply be stated as the greater the signal the greater the force. This signal is most often used to control prostheses. In stimulated muscle the use of the Compound Action Potential (CAP) to identify fatigue and force parameters does not appear to have been quantified. The system described here is an attempt to do this by taking the parameters most often described in the literature for voluntary muscle contractions and monitoring them for the stimulated case. The surface EMG is typically less than 2mV whilst the stimulus voltage (constant voltage) is greater than 80V - the majority of this voltage is dropped across the electrode skin interface though. The effect of this stimulus on a normal EMG amplifier leads to artefacts appearing in the recorded signal which not only reduce the signal integrity but may hide it altogether[9]. For the work being carried out here the pickups have to work in conjunction with the stimulator systems already developed, of the constant voltage type. The pickups need to be close to the stimulating site to ensure

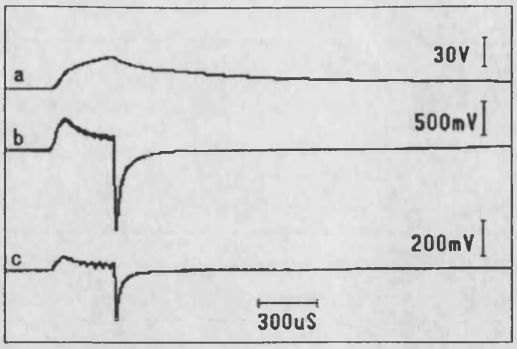

Figure 1. Stimulating Pulse (a) and associated voltage difference seen at the EMG Electrodes; (b) Electrodes not on an equipotential line; (c) Electrodes on an equipotential line.

only the muscles of interest are recorded since future systems may require more channels being active on the limb at once. This paper covers the problems of detecting the CAP with minimised artefact contamination; the sampling and processing of the signal produced from the stimulation to try and identify fatigue and force.

ARTEFACT SOURCES

The main source is the voltage difference between the recording electrodes which is seen as a saturating pulse on the output of the amplifier when the stimulus is present. This pulse is followed by a fast tail due to the subsequent discharge of the electrodes through the limb (Fig 1b). This tail is particularly noticeable when using with a low output impedance stimulator - after a stimulus pulse from a high output impedance stimulator the skin capacitance discharges through the skin resistance and no current flows through the limb but a low output impedance stimulator the skin capacitance discharges through the stimulator[8,9]. A second source of artefact is the effect of the stimulus spike passing through the amplifiers high-pass filter, this causes a slow exponential tail. If the signal is large enough to cause saturation in the amplifier the tail becomes more severe. If this occurs in one of the early stages of amplification the recovery from saturation could take several milliseconds. The size of the tail may also be decreased by lowering the cut-off of the high pass filter[6]. Other sources of artefacts are; any common mode voltage at the recording site, capacitative coupling between the recording and stimulating leads. In both of these cases if there is an electrode imbalance the common mode signals - assuming equal coupling into each lead- would produce artefacts proportional to the imbalance.

Methods of Artefact Reduction

Some of the artefacts can be reduced to insignificant levels by proper placement of the electrodes. Placing the electrodes on an equipotential line reduces the voltage differences[9] at the recording electrodes (Fig 1c). Moving the pickup electrodes so that they are further from the stimulus will reduce the effect of the stimulus and increase the CAP latency time. This will reduce the amplitude of the CAP and information may be lost by the filtering that occurs due to the skin (Figs. 2a,2b).The use of a constant voltage stimulator means that there is a large artefact[8] due to the discharge current that flows when the stimulator switches off. The design of this particular stimulator means that it has quite a high output impedance (like a constant current stimulator). Despite this the best option would seem to be to reduce the electrode charge quickly after the stimulus by clamping the output (Figs. 3a,3b). This generates a large voltage spike on the falling edge which can be removed by one of the modifications

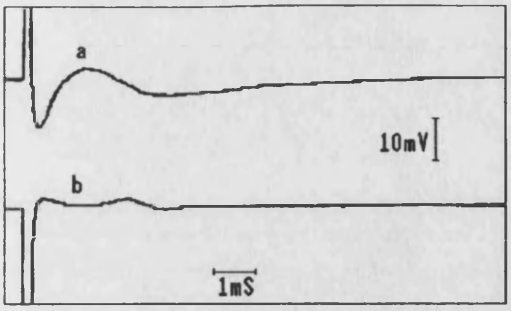

Figure 2. (a) Stimulating Artefact and CAP between Stimulating electrodes. (b) Stimulating artefact and reduced CAP when pickup is remote from Stimulation

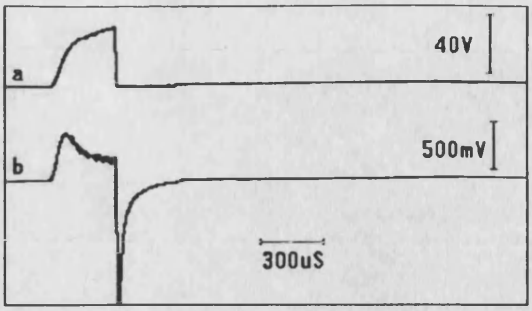

Figure 3 (a) Clamped Stimulating Pulse (b) Resulting Voltage seen at EMG Electrodes.

described for the EMG amplifiers. Isolation of the amplifier during the stimulating pulse prevents the amplifier from saturating[7,8]. This can be achieved in a number of ways:

A sample and hold on the input to the differential amplifier isolates the amplifier and keeps the amplifier close to the voltage that is present when the switch reconnects. To do this a differential sample and hold is necessary.

Switching off the differential amplifier stage when the stimulus is present prevents the stimulus passing through but will not necessarily cause another artefact when it is switched back on, because the chip capacitances will not have discharged in the time the amplifier is off.

Computer Artefact Reduction

Any use of the computer system to remove the artefacts will inevitably reduce the rate at which it can update the results. Two obvious options are available: Time Domain or Frequency Domain 'filtering'. Most time domain methods rely on a test being done to get an artefact only signal and then subtracting a scaled version of this from the contaminated CAP. In the frequency domain the effects of the stimulus appear as spectral lines at the stimulus frequencies and its harmonics. Mains interference appears at 50Hz (60Hz). Tests on the spectrum of a subthreshold signal indicate that major components are limited to these frequencies. These effects can be removed by deconvolution or by just ignoring the frequency components at the stimulus frequency and its harmonics.

THE SAMPLING AND PROCESSING SYSTEM

The sampling of EMGs assumes that the wave form may be considered stationary. It has been found that EMGs can be considered quasi-stationary over periods of 0.5 to 1.0s[4]; these figures of course apply to voluntary muscle EMGs. In this case, the wave form is periodic, which therefore means that the sampling must be synchronised to the stimulus pulse. It does not necessarily imply that the statistics of the signal itself has changed[11]. The sampling is synchronised by means of a pulse train from the stimulator that is fed into an input port of the computer and the sampling routine waits for this pulse before starting a set of samples. The processing system is a 68000 based computer running at 8MHz. The A/D is a simple 8 bit converter which is continuously converting at 50kHz. The actual sample rate is set by the rate at which the data is read. For surface EMGs the bandwidth of the signal is about 500Hz[1,6] so theoretical minimum sample rate of 1kHz is required. The rates chosen are 1024Hz and 2048Hz. Analysis of the data is carried out by Fast Hartley Transform (FHT)[10] which is faster in calculating the Power Spectrum than the equivalent FFT routine. For the sample rates mentioned and

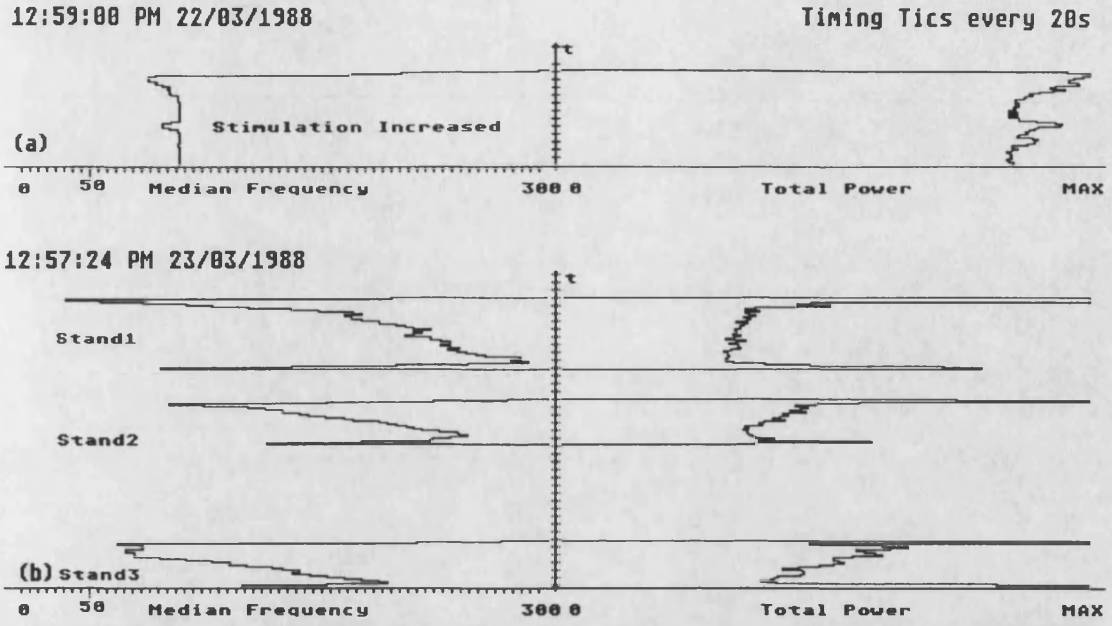

Figure 4. Plots of the Smoothed Median Frequency and Power from Stimulated Muscle EMGs (a) Showing Slight frequency drops just before the stimulus is increased to maintain stand (b) Showing median frequency rising during each stand whilst the overall power drops more rapidly.

using a 1024 point FHT gives a frequency resolution of 1 and 2 Hz respectively. The routines use 16 bit signed integer arithmetic returning a spectrum every 600 mS.

DISCUSSION

At the time of writing full quantitative results are not available. However the tests so far carried out do provide some information. Tests carried out on the muscles of people with full voluntary control seem to differ from those carried out on paraplegics. This may be explained by the differing fibre compositions skin condition etc. The clamping amplifiers described above have not been available for the initial tests so the removal of the major artefacts is done in the frequency domain by ignoring the stimulus frequency and its harmonics. The tests have been carried out on a number of paraplegics all of whom are part of a standing program. The tests have been carried out at two distinct stages either during stands or once they are too fatigued to maintain long stands. Two example curves are shown in Figure 4 where it can be seen that the spectral shift downwards occurs in one just at the point at which the stimulus is increased (Figure 4a). In Figure 4b the spectral shift is in the opposite direction though for each of the stands the force drops more rapidly. As yet there is insufficient evidence to support the validity of these curves, however it has been observed on a number of patients that the curve follows that suggested in the voluntary muscle contraction case initially, i.e. spectral shifts downwards, power drops. As the patient does more stands the curve appears to reverse as in Figure 4b. The power starting level increases but falls faster with the later stands. This would be expected since it increases stimulus and therefore some extra muscle fibres are recruited to maintain the stand, whilst the muscle fibres involved in the earlier contractions would fatigue faster.

REFERENCES

1. J.V. Basmajian and C.J. De Luca "Muscles Alive Their Functions Revealed By Electromyography" Fifth Edition Williams and Wilkins 1985 ISBN 0-683-00414-X

2. D.J. Ewins, P.N. Taylor, S.E. Crook, R.T. Lipczynski and I.D. Swain "Practical Low Cost Stand/Sit System for Midthoracic Paraplegics" J. Biomed Eng. Vol 10 pp 184-188 April 1988

3. C.J.De Luca "Myoelectrical Manifestations of Localized Muscular Fatigue in Humans" CRC Critical Reviews in Biomed. Eng. Vol 11 No 4 pp251-279

4. G.F. Inbar and A.E. Noujaim "On Surface EMG Spectral Characterization and its application to diagnostic Classification" IEEE Trans. Biomed. Eng. BME-31 No. 9 pp597-604 Sept. 1984

5. J.J. Woods and B. Bigland-Ritchie "Linear and Non-Linear Surface EMG/Force Relationships in Human Muscles" Amer. J. of Phys. Med. Vol 62 No 6 pp287-299 1983

6. V.O. Andersen and F.Buchthal "Low Noise Alternating Current Amplifier and Compensator to Reduce Stimulus Artefact" Med. & Biol. Engng. Vol 8 pp501-508 1970

7. R.J. Roby and E. Lettich "A Simplified Circuit for Stimulus Artifact Suppression" Electroenceph. and Clin. Neurophysiol. Vol 39 pp85-87 1975

8. T.L. Babb, E. Mariani, G.M. Strain, J.P. Lieb, H.V. Soper and P.H. Crandall "Sample and Hold Amplifier System for Stimulus Artifact Suppression" Electroenceph. and Clin. Neurophysiol. Vol 44 pp528-531 1978

9. K.C. McGill, K.L. Cummins, L.J. Dorfman, B.B. Berlizot, K. Luetkemeyer, D.G. Nishimura and B. Widrow "On the Nature and Elimination of Stimulus Artifact in Nerve Signals Evoked and Recorded Using Surface Electrodes" IEEE Trans. Vol BME-29 No 2 pp129-137 Feb. 1982

10. R.N. Bracewell "The Hartley Transform" Oxford Science Publications 1986 ISBN 0-19-503969-6

11. D.E. Newland "An Introduction to Random Vibrations and Spectral Analysis" Second Edition Longamn Group Ltd 1984 ISBN 0-582-30530-6

Appendix D

Glossary of Medical Terms

Accommodation Curve see *Strength Duration Curve*.

Acetylcholine A reversible acetic acid ester of choline important in the transfer of a nerve impulse across a synapse.

Action Current The electrical currents associated with an Action Potential.

Action Potential The brief, regenerative, all-or-nothing electrical potential that propagates along a single axon or muscle fibre membrane. See also Compound Action Potential.

Active Electrode Electrode from which the current flows, the Negative Terminal or Cathode.

Afferent Leading to the centre, applied to the lymphatic vessels and to sensory nerves.

Agonist Muscle One which initiates a contraction.

Amplitude With reference to an *action potential*, the maximum voltage difference between two points, usually baseline to peak or peak to peak. By convention, the amplitude of the *compound muscle action potential* is measured from the baseline to the most negative peak. In contrast, the amplitude of a *compound sensory nerve action potential, motor unit potential*, and most other *action potentials* is measured from the most positive to the most negative peak.

Anisometric Contraction A contraction during which the length of the contracting muscle may vary.

Anodal Block A local block of nerve conduction caused by *hyperpolarisation* of the nerve cell membrane by an electrical stimulus.

Antagonist Muscle A muscle that actively provides a negative contribution to a particular function during a contraction.

Anterior Situated in front of; forward part of.

Artefact A voltage change generated by biological or nonbiological sources other than the ones of interest. The *stimulus artefact* is the potential recorded at the time the stimulus is applied and includes the *electrical* or *shock artefact*, which represents the cutaneous spread of stimulating current to the recording electrode. The stimulus and shock artefacts usually precede the activity of interest. A *movement artefact* refers to a change in the recorded activity caused by movement of the recording electrodes.

Average Firing Rate The average firing rate of a motor unit over a given period of time. It is measured in units of pulses per second and is usually calculated as the reciprocal of the average Interpulse Interval.

Axon A single nerve-cell process, usually long, that conducts impulses away from the cell body of a neurone as a rule .

Ballistic Contraction A contraction that is executed with the greatest speed physiologically possible.

Baseline The potential recorded from a biological system while the system is at rest.

Biphasic Action Potential An Action Potential with two phases.

Bipolar Electrode System Either a pickup or stimulating system consisting of two electrodes whose relation to the tissue currents is roughly symmetrical.

Chronaxie See *Strength Duration Curve.*

Compound mixed nerve Action Potential A compound nerve action potential is considered to have been evoked from afferent and efferent fibres if the recording electrodes detect activity on a mixed nerve with electrical stimulus applied to a segment of the nerve that contains both afferent and efferent fibres.

Compound Muscle Action Potential A compound nerve action potential is considered to have been evoked from efferent fibres to a muscle if the recording electrodes detect activity only in a motor branch of a mixed nerve, or if the electrical stimulus is applied only to such a nerve or a ventral root.

Compound Muscle Action Potential The summation of nearly synchronous muscle fibre action potentials recorded from a muscle commonly produced by stimulation of the nerve supplying the muscle either directly or indirectly.

Compound Nerve Action Potential The summation of nearly synchronous nerve fibre action potentials recorded from the nerve trunk, commonly produced by stimulation of the nerve directly or indirectly.

Concentric Needle Electrode A *recording electrode* that measures an electrical potential difference between the bare tip of an insulated wire, usually stainless steel, silver, or platinum, and the bare shaft of a steel cannula through which it is inserted. The bare tip of the central wire (recording electrode) is flush with the tip of the cannula (reference electrode).

Conduction Block Failure of an action potential to be conducted past a particular point in the nervous system, whereas conduction is possible below the point of the block.

Conduction Distance See *Conduction Velocity.*

Conduction Time See *Conduction Velocity.*

Conduction Velocity Speed of propagation of an *action potential* along a nerve or muscle fibre. The nerve fibres studied (motor, sensory, autonomic, or mixed) should be specified. For a nerve trunk, the maximum conduction velocity is calculated from the *latency* of the evoked potential (muscle or nerve) at maximal or supramaximal intensity of stimulation at two different points. The distance between the two points (*conduction distance*), is divided by the difference between the corresponding latencies (*conduction time*). The calculated velocity represents the conduction velocity of the fastest fibres and is expressed as metres per second (m/sec.). As commonly used the *conduction velocity* refers to the *maximum conduction velocity.*

Contraction A voluntary or involuntary reversible shortening that may or may not be accompanied by *action potentials* from the muscle. This term should be contrasted with the term *contracture*, which refers to a condition of fixed muscle shortening.

Denervated Deprived of nerve supply.

Distal Away from the centre of the body.

Dorsal A position more toward the back of an object of reference.

ECG Abbreviation for Electrocardiogram.

EEG Abbreviation for Electroencephalogram.

Efferent Conveying from the centre, *e.g.* the motor nerves which convey impulses from the brain and the spinal cord to muscles and glands. *cf.* afferent.

Electrical Artefact See *Artefact*.

EMG Electromyogram.

Evoked Potential Electrical waveform elicited by and temporally related to a stimulus, most commonly an electrical stimulus delivered to a sensory receptor or nerve, or applied directly to a discrete area of the brain, spinal cord, or muscle.

Facilitation The brief rise of excitability above normal either after a response or a series of subthreshold stimuli.

Faradic Current An asymmetrical alternating current obtained from or similar to that obtained from the secondary winding of an induction coil operated by repeatedly interrupting a direct current in the primary.

Faradisation The use of a faradic current to stimulate muscles and nerves.

Fasciculation The random, spontaneous twitching of a group of muscle fibres or a motor unit. This twitch may produce movement of the overlying skin. The electrical activity associated with the spontaneous contraction is called the *Fasciculation Potential.*

Firing Rate See *Average Firing Rate.*

Galvanic Uninterrupted current derived from a chemical battery.

H Wave A compound muscle action potential having a consistent latency evoked regularly, when present, from a muscle by an electrical stimulus to the nerve. It is regularly found in only a limited group of physiologic extensors, particularly the calf muscles. The reflex is most easily obtained with the cathode positioned proximal to the anode. Compared with the maximum amplitude M wave of the same muscle, the H wave has a smaller amplitude, a longer latency, and a lower optimal stimulus intensity. A stimulus intensity sufficient to elicit a maximal amplitude M wave reduces or abolishes the H wave. The H wave is thought to be due to a spinal reflex—Hoffmann reflex—with electrical stimulation of afferent fibres in the mixed nerve to the muscle and activation of motor neurones to the muscle through a monosynaptic connection in the spinal cord. The reflex and wave are named in honour of Hoffmann's description.

Hoffmann Reflex See *H wave.*

Inferior Situated or directed below.

Innervation Supply of nerves or the conveyance of nervous impulses to or from a part. *Reciprocal Innervation* One set of muscles contracts whilst those opposing it relax.

Interpulse Interval In the context of muscle signals it is the time between adjacent discharges of a motor unit. It is a semi-random quantity. In the context of muscle stimulators it is the time between stimulating pulses.

Isometric Contraction A contraction during which the length of the contracting muscle remains constant. Generally, the muscle length is assessed by monitoring the angle of the joint being affected.

Latency Time delay between stimulus and response.

Latency of Activation The time required for an electrical stimulus to depolarise a nerve fibre (or bundle of fibres as in a nerve trunk) beyond threshold and to initiate a regenerative action potential in the fibre(s). This time is usually of the order of 0.1 msec or less.

Lateral A position more toward the side of flank.

M Response See synonym *M Wave.*

M Wave A *compound action potential* evoked from a muscle by a single electrical stimulus to its motor nerve. By convention, the M wave elicited by supramaximal stimulation is used for motor nerve conduction studies. By convention the recording electrodes are placed such that the initial deflection is negative. The *amplitude* (mV) is

the baseline-to-peak amplitude of the first negative phase unless otherwise specified. The *duration* (msec) refers to the duration of the first negative phase.

Maximal Stimulus See *Stimulus.*

Motor Point The point over a muscle where a contraction of a muscle may be elicited by the minimal-intensity, short-duration electrical stimulus. The motor point corresponds anatomically to the location of terminal portion of the motor nerve fibres (end-plate zone).

Maximal Voluntary Contraction The greatest amount of effort that an individual may exert. Usually, the effort is concentrated on one muscle or on one joint. It is generally measured by monitoring the force torque output.

Monopolar Electrode System See *Unipolar Electrode System.*

Motor Unit The anatomical unit of an anterior cell, its axon, the neuromuscular junctions, and all of the muscle fibres innervated by the axon.

MUAP Abbreviation for *Motor Unit Action Potential.*

MUP Abbreviation for *Motor Unit Potential.*

Muscle Action Potential term commonly used to refer to a *Compound Muscle Action Potential.*

Muscle Fibre Action Potential Action potential recorded from a single muscle fibre.

Muscle Fibre Conduction Velocity The speed of propagation of a single muscle fibre action potential, usually expressed as metres per second. The muscle fibre conduction velocity is usually less than most nerve conduction velocities, varies with the rate of discharge of the muscle fibre, and requires special techniques for measurement.

MVC Abbreviation for Maximal Voluntary Contraction.

Nerve Action Potential Action potential recorded from a single nerve fibre.

Neurapraxia Failure of nerve conduction, usually reversible.

Polarisation As used in neurophysiology, the presence of an electrical potential difference across an excitable cell membrane.

Pronation Turning of the palm downwards or backwards such that the radius and ulna are crossed.

Proximal Toward the centre of the body.

Recruitment The successive activation of the same and additional motor units with increasing strength of voluntary muscle contraction.

Refractory Period The *absolute refractory period* is the period following an *action potential* during which no stimulus, however strong, evokes a further response. The *relative refractory period* is the period following an *action potential* during which a stimulus must be abnormally large to evoke a second response. The functional refractory period is the period following an *action potential* during which a second *action potential* cannot yet excite the given region.

Relative Refractory Period See *Refractory Period.*

Repolarisation See *Polarisation.*

Resting Membrane Potential Voltage across the membrane of an excitable cell at rest. See *Polarisation.*

Rheobase See *Strength-Duration Curve.*

Sensory Nerve Conduction Velocity See *Conduction Velocity.*

SFEMG Abbreviation for *Single Fibre Electromyography.*

Silent Period A pause in the electrical activity of a muscle such as seen after a rapid unloading of a muscle.

Spinal Evoked Potential Electrical waveforms of biological origin recorded over the sacral, lumber, thoracic, or cervical spine in response to electrical stimulation or physiological activation of peripheral sensory fibres.

Stimulus Any external agent, state , or change that is capable of influencing the activity of a cell tissue, or organism. The electrical stimulus is usually defined in absolute terms by a duration (msec), a waveform (such as square, exponential, linear etc.), and a strength or intensity measured in voltage (V) or current (mA). Alternatively it may be described in terms of the evoked potential as subthreshold, threshold, submaximal maximal, or supramaximal. A *threshold stimulus* is that stimulus just sufficient to produce a detectable response. Stimuli less than the threshold stimulus are termed *subthreshold.* The *maximal stimulus* is the stimulus intensity after which a further increase in the stimulus intensity causes no increase in the amplitude of the evoked potential. Stimuli of intensity below this level but above threshold are *submaximal.* Stimuli of intensity greater than the maximal stimulus are termed *supramaximal.* Ordinarily, supramaximal stimuli are used for nerve conduction studies.

Stimulus Artefact See *Artefact.*

Strength-Duration Curve Graphic presentation of the relationship between the intensity (Y axis) and various durations (X axis) of the threshold electrical stimulus for a muscle with the stimulating cathode positioned over the *motor point.* The *rheobase* is the intensity of an electrical current of infinite duration necessary to produce a

minimal visible twitch of a muscle when applied to the motor point. In clinical practice, a duration of 100 or 300 msec is used to determine the rheobase. The *chronaxie* is the time required for an electrical current twice the *rheobase* to elicit the first visible muscle twitch.

Submaximal Stimulus See *Stimulus.*

Subthreshold Stimulus See *Stimulus.*

Superior Situated or directed above.

Supination The turning of the palm upwards.

Suprathreshold Stimulus See *Stimulus.*

Synchronisation The term used to describe the tendency of a motor unit to discharge at or near the time that another motor unit discharges. It describes the interdependence or entrainment of two or more motor units.

Synapse The point at which a nervous impulse passes from one neurone to another. They have the property of one-way propagation.

Synergist Muscle A muscle that actively provides an additive contribution to a particular function during a contraction.

Tetanic Contraction The contraction produced in a muscle through repetitive maximal direct or indirect stimulation at a sufficiently high frequency to produce a smooth summation of successive maximum twitches. The term may also be applied to maximum voluntary contractions in which the firing frequencies of most or all of the component motor units are sufficiently high that successive twitches of individual motor units fuse smoothly. Their tensions all combine to produce a steady, smooth maximum contraction of the whole muscle.

Tetanus The continuous contraction of muscle caused by repetitive stimulation or discharge of nerve or muscle.

Unipolar Electrode System Either a pickup or stimulating system, consisting of one active and one dispersive electrode.

Appendix E

Muscle Anatomy

E.1 Muscles of the Arm

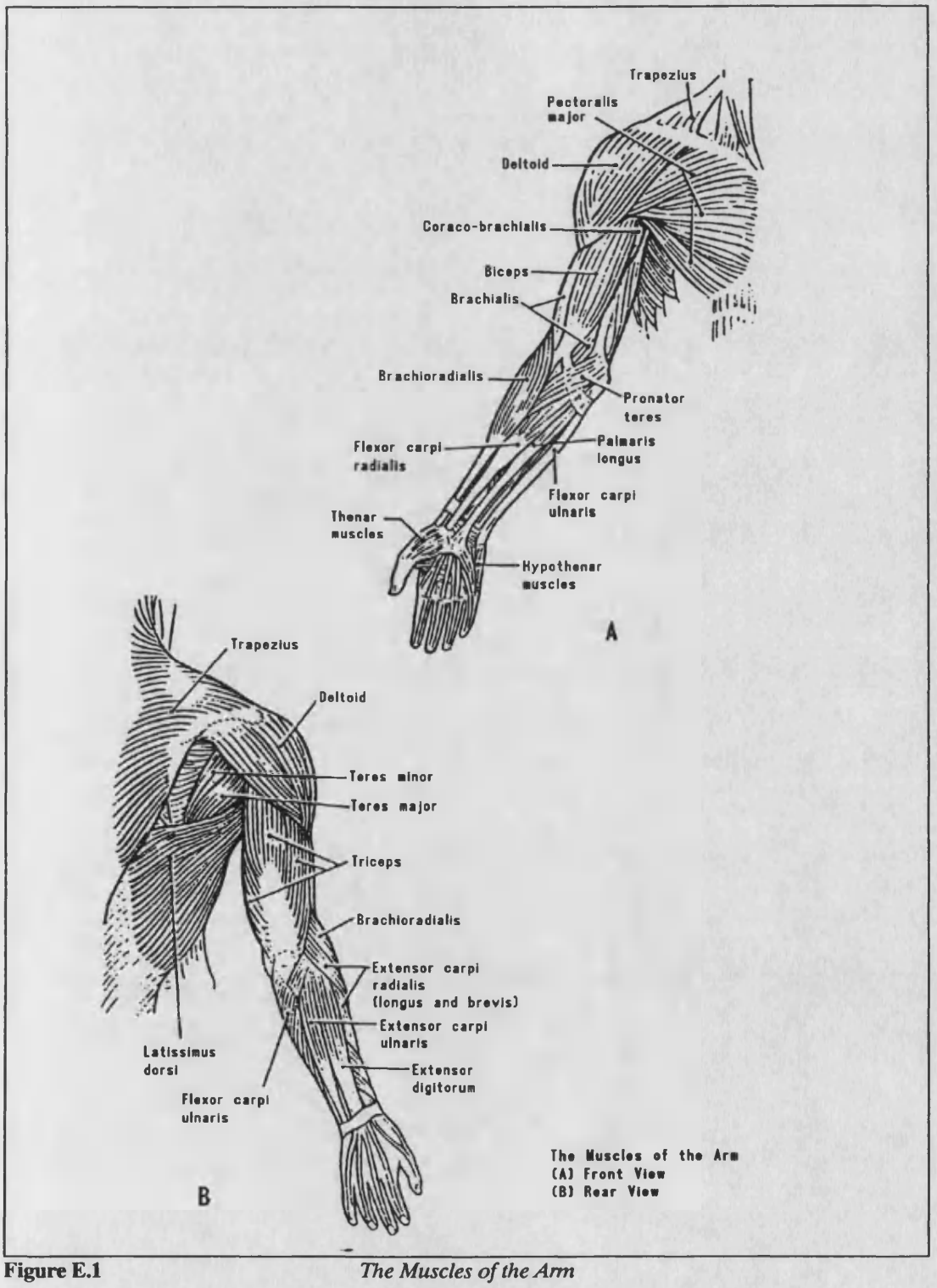

Figure E.1 *The Muscles of the Arm*

E.2 Muscles of the Leg

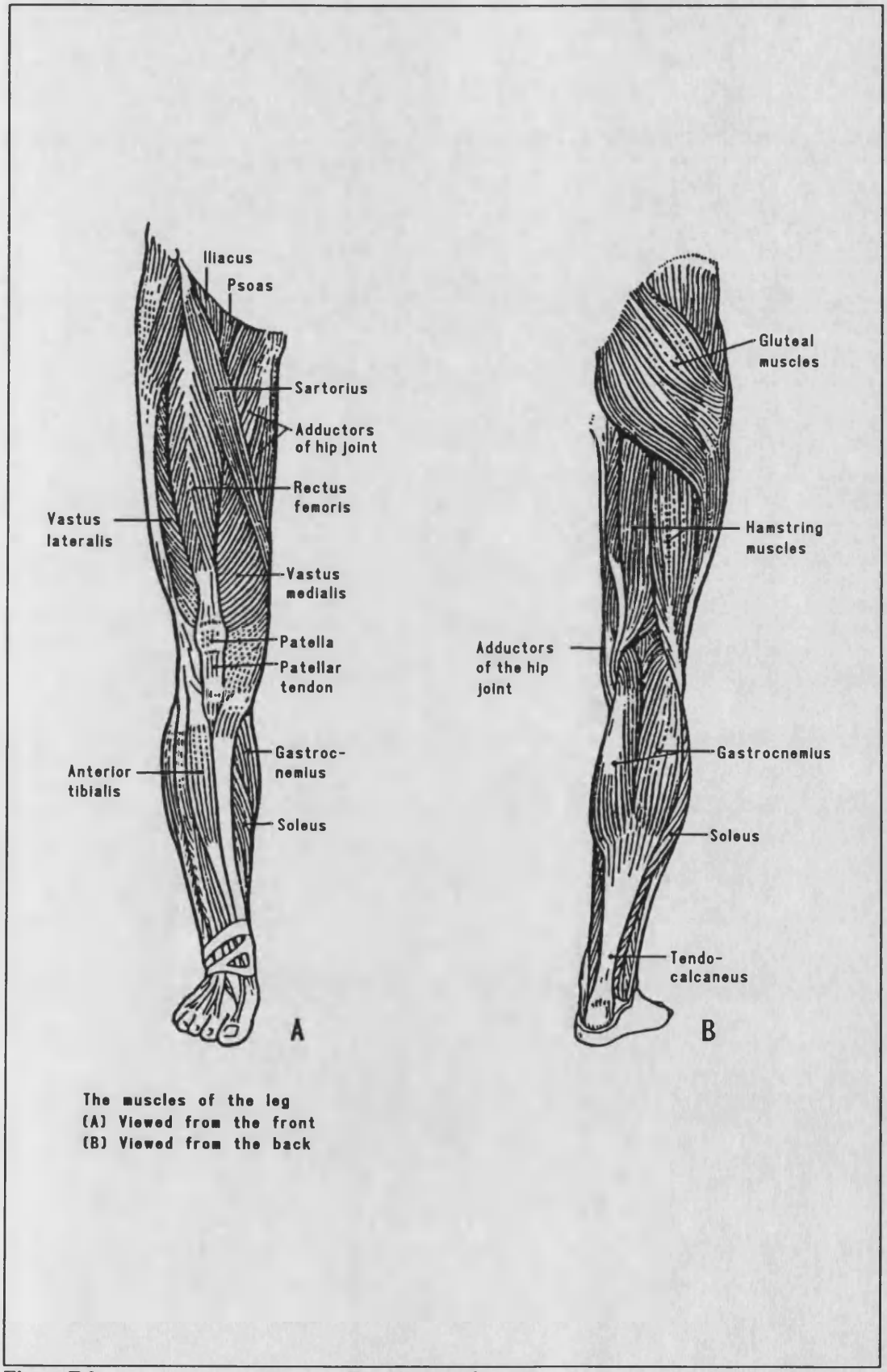

Figure E.2 *The Muscles of the Leg*

Appendix F

Photographs of the Equipment

The photographs show the various pieces of equipment that have been built, showing both their outside casing and where appropriate the internal boards.

F.1 Muscle Stimulators

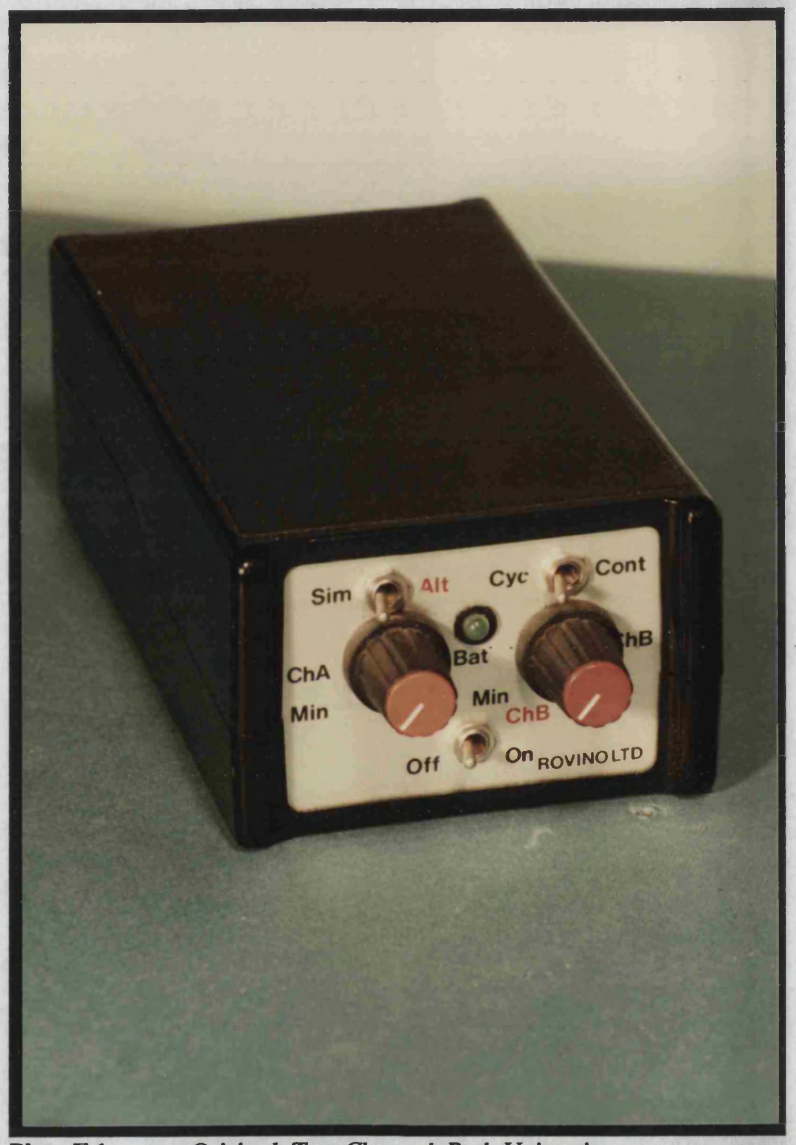

Plate F.1 *Original Two Channel Bath University Exercise Stimulator*

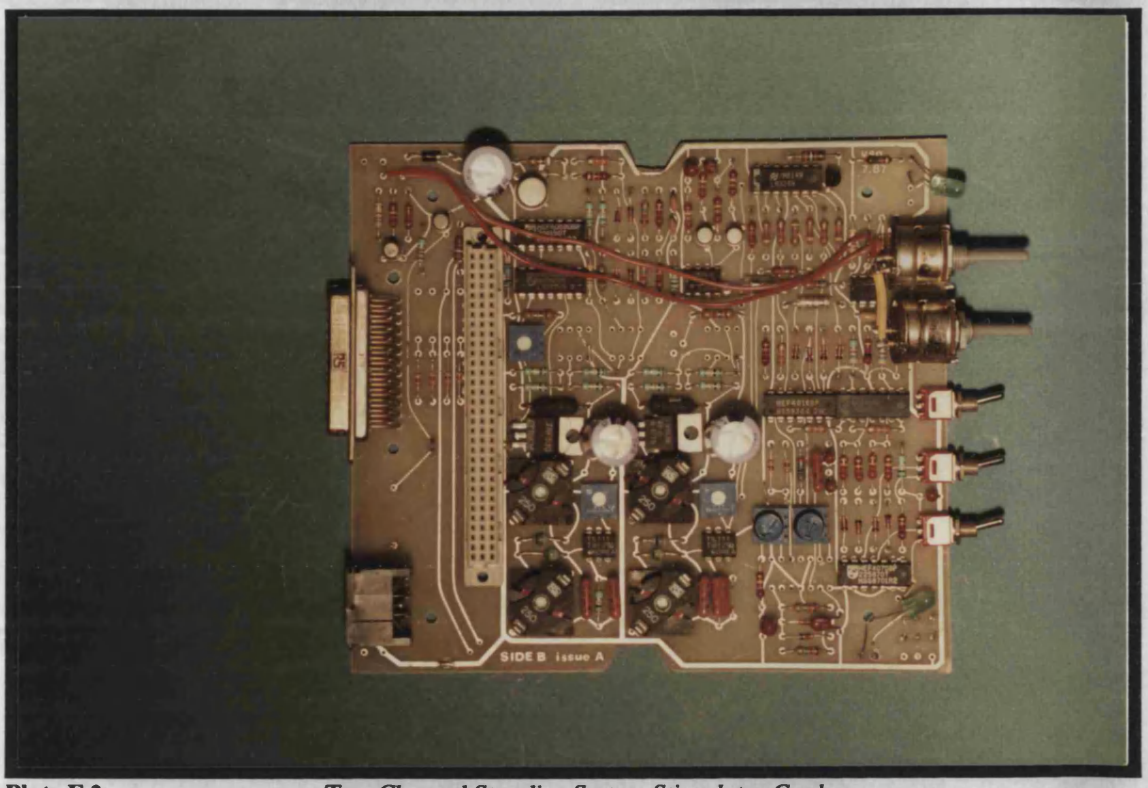

Plate F.2 *Two Channel Standing System Stimulator Card*

Plate F.3 *New Programmable Two Channel Stimulator using Standing System Stimulator*

Plate F.4 *Two Channel Programmable Stimulator Front Panel*

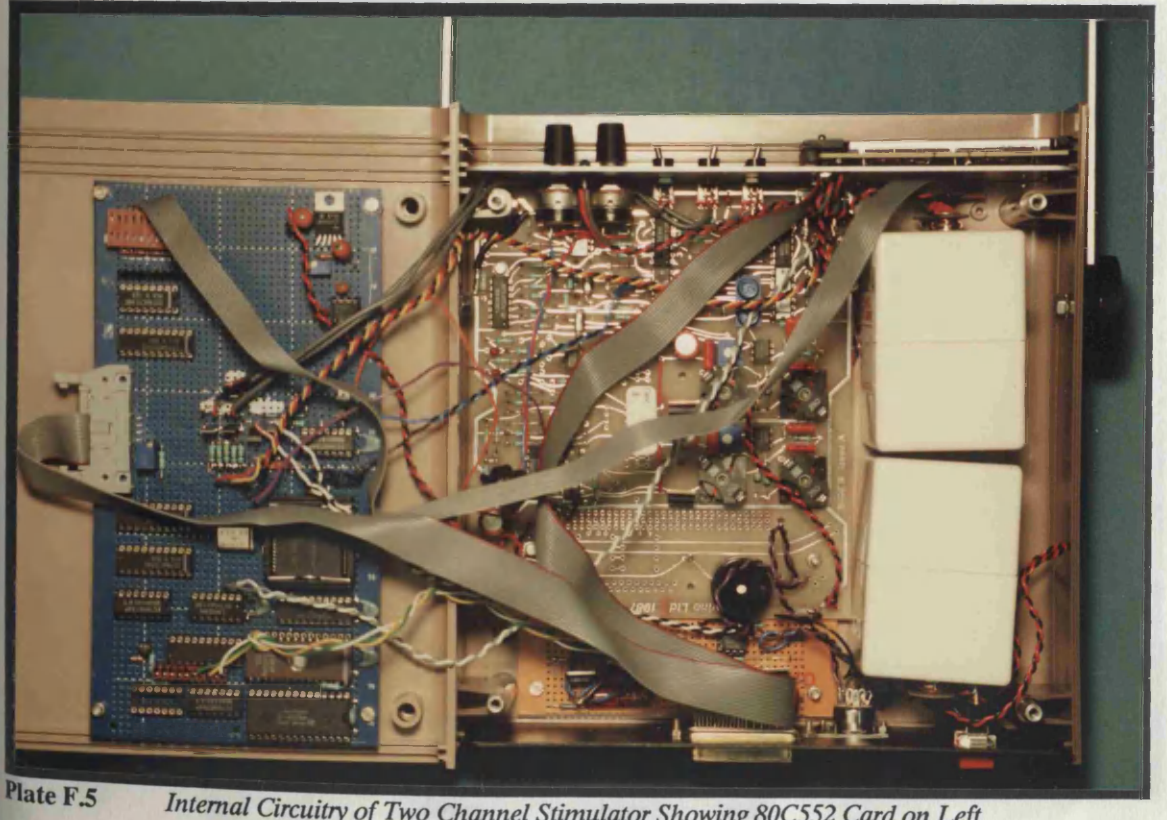

Plate F.5 *Internal Circuitry of Two Channel Stimulator Showing 80C552 Card on Left*

Plate F.6 *Two Channel Programmable Stimulator showing the Display when Programming a New Pulse Width*

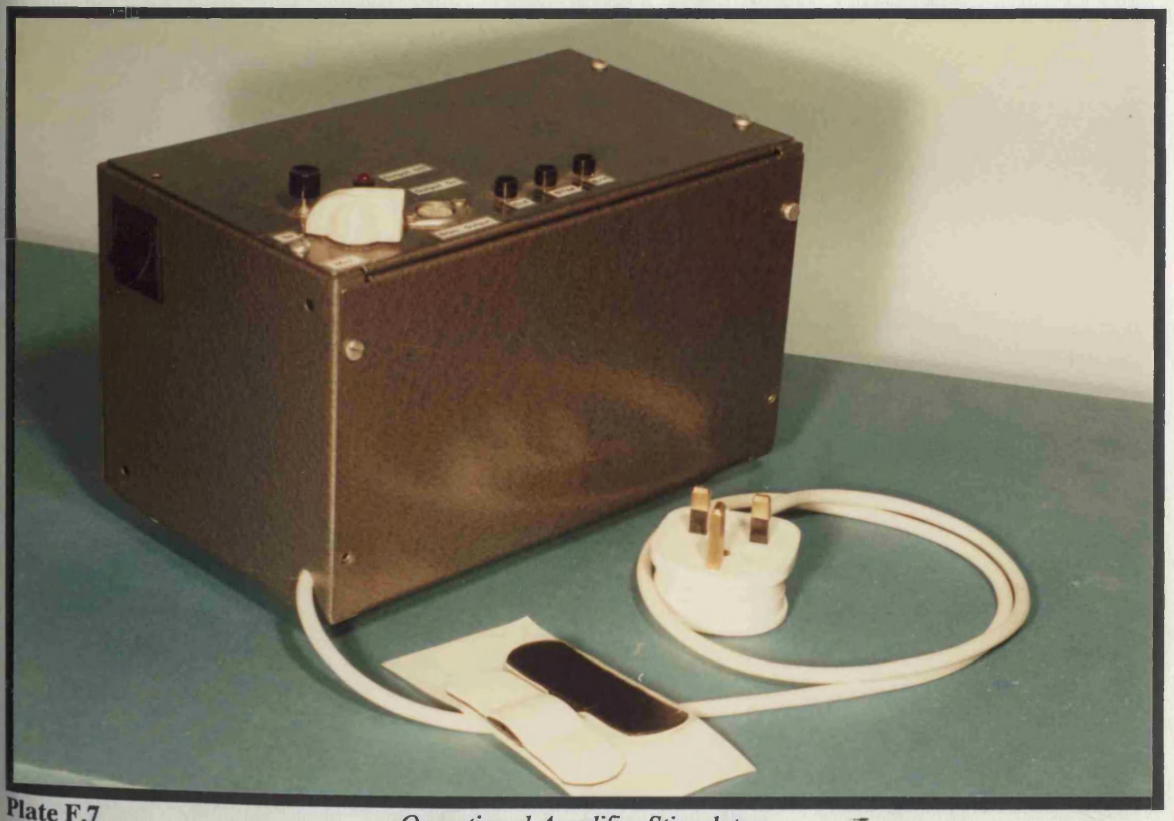

Plate F.7 *Operational Amplifier Stimulator*

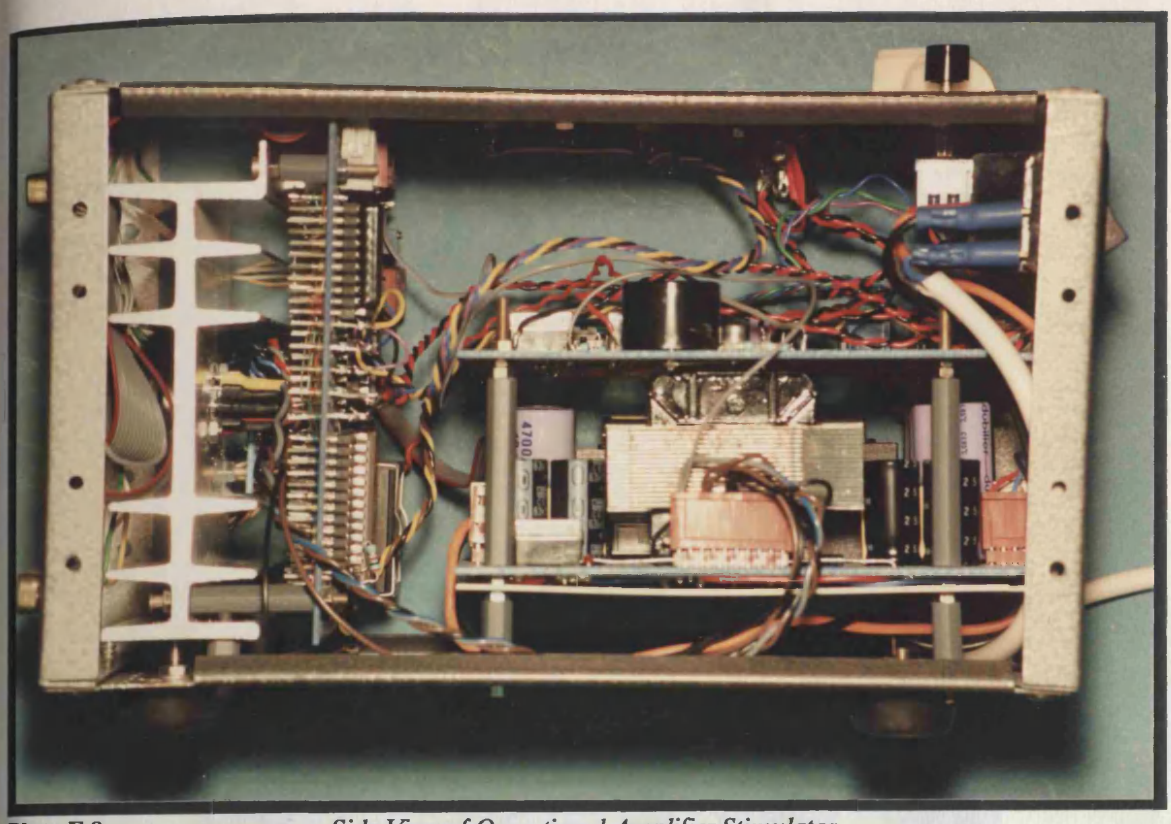

Plate F.8 *Side View of Operational Amplifier Stimulator*
Showing Heatsink with Operational Amplifier mounted on it, the Processor Card beside it on the Left and the Isolating Power Supply mounted on the Base.

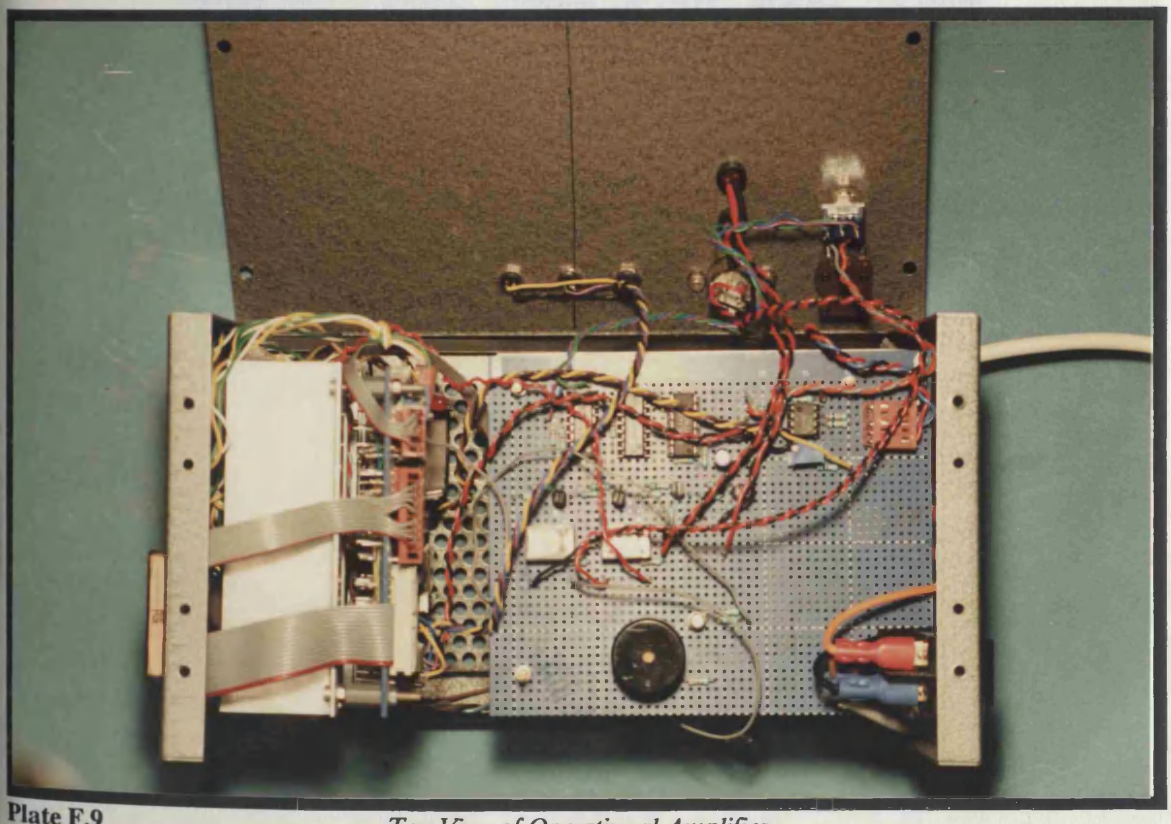

Plate F.9 *Top View of Operational Amplifier*
Showing Start up Circuitry and Output Level Control

Plate F.10 *Hand held Keyboard and LCD Display for programming Operational Amplifier Stimulator*

Plate F.11 *Top Panel of the Power Amplifier Stimulator*

F.2 EMG Amplifiers

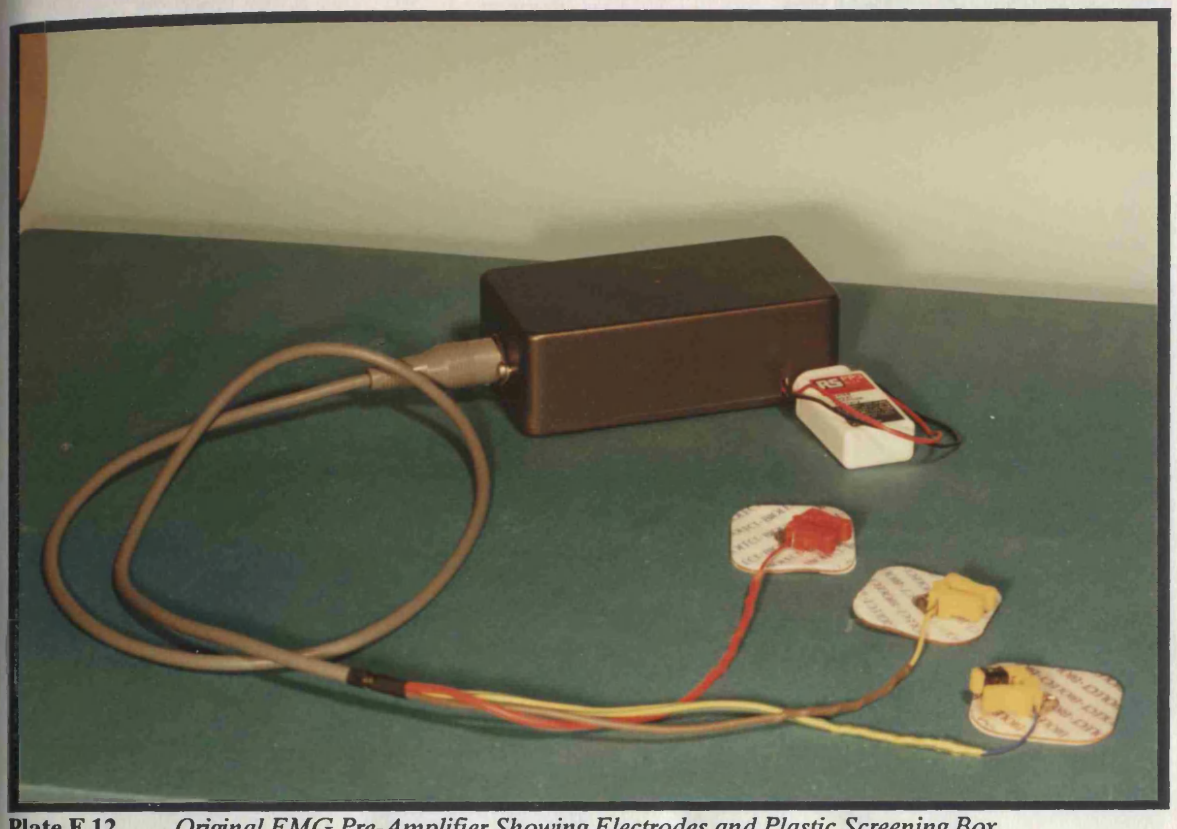

Plate F.12 *Original EMG Pre-Amplifier Showing Electrodes and Plastic Screening Box*

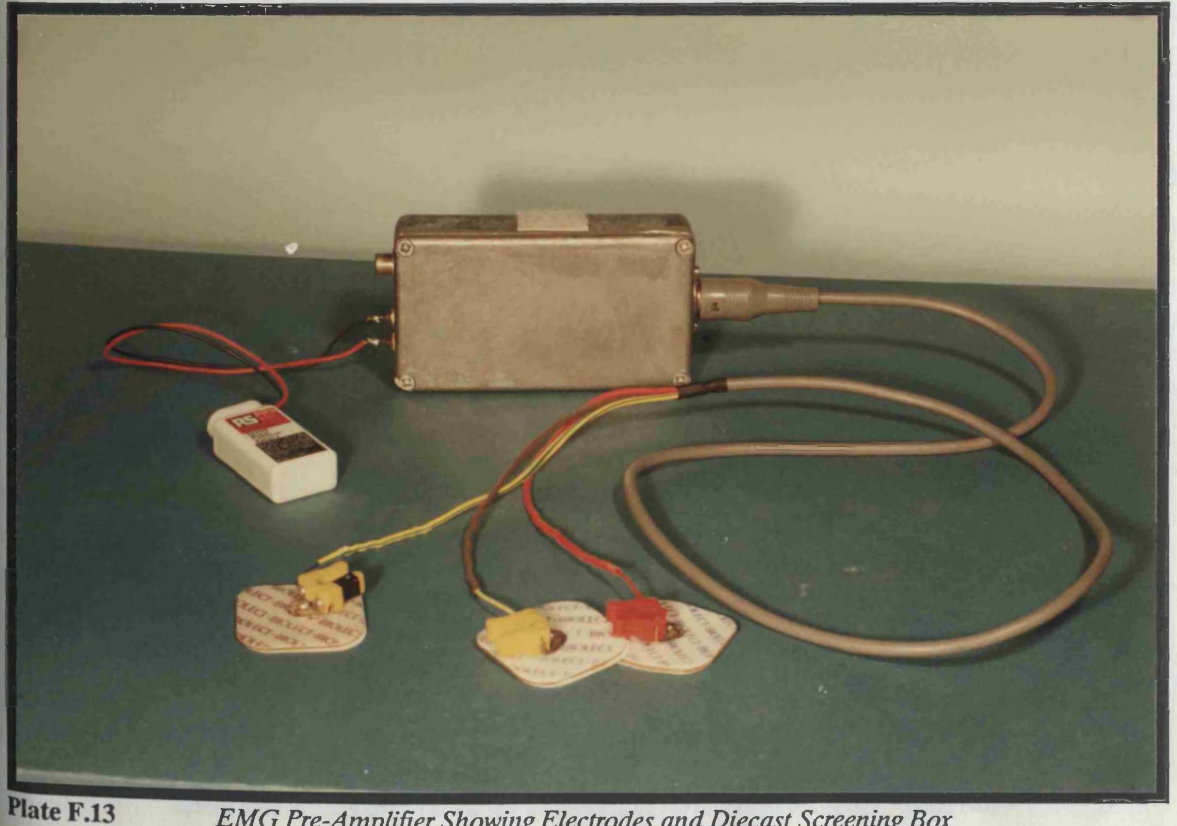

Plate F.13 *EMG Pre-Amplifier Showing Electrodes and Diecast Screening Box*

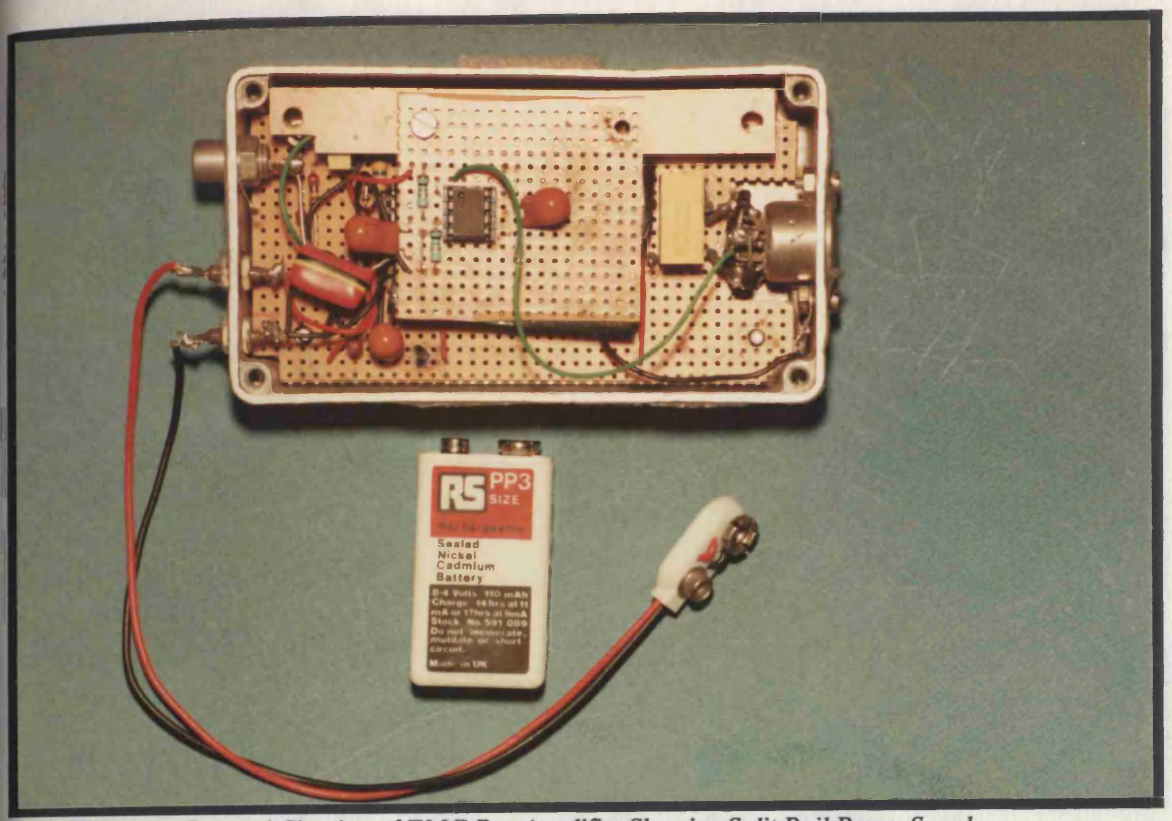

Plate F.14 *Internal Circuitry of EMG Pre-Amplifier Showing Split Rail Power Supply*

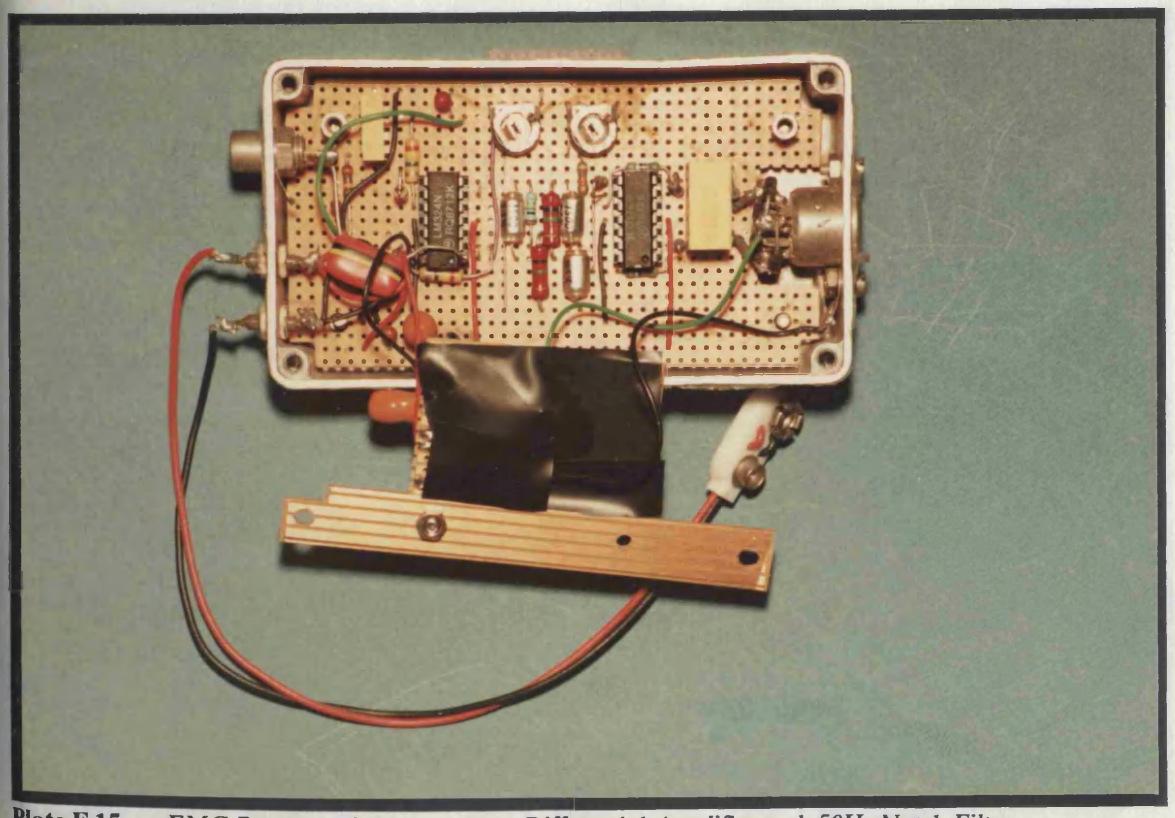

Plate F.15 *EMG Pre-Amplifier showing the Differential Amplifier and 50Hz Notch Filter*

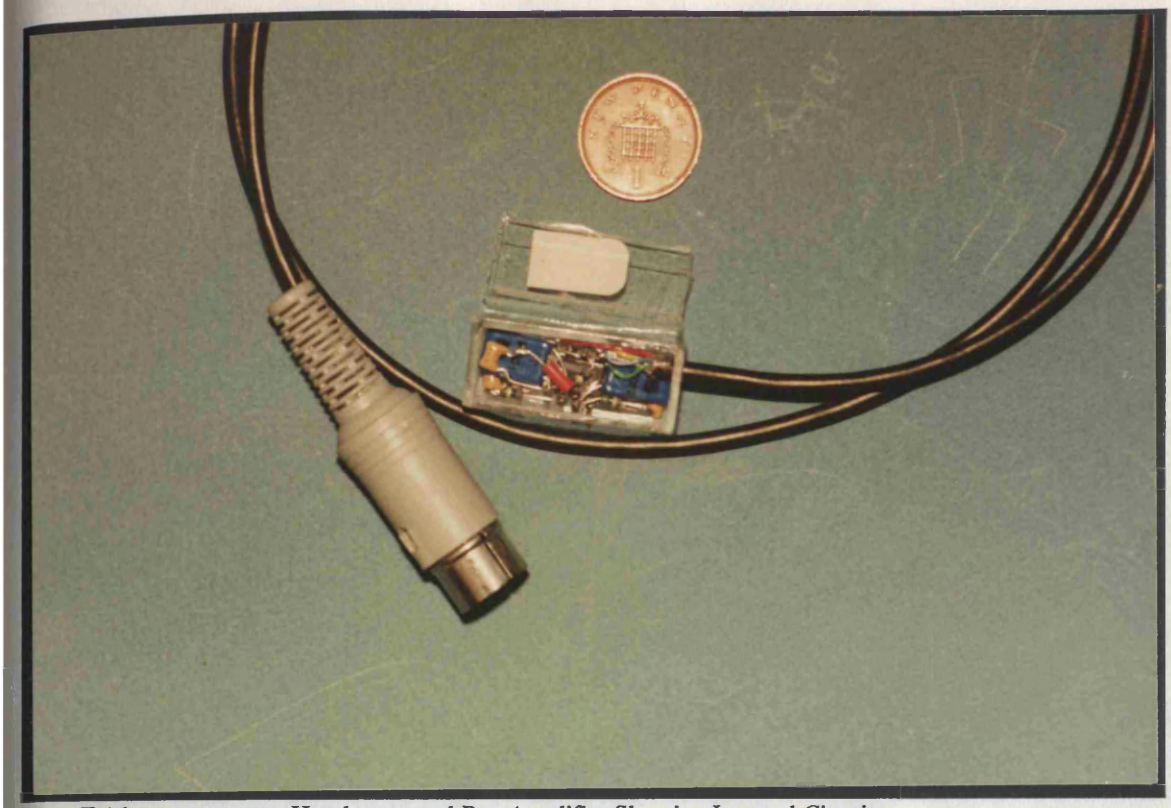

Plate F.16 *Head-mounted Pre-Amplifier Showing Internal Circuitry*

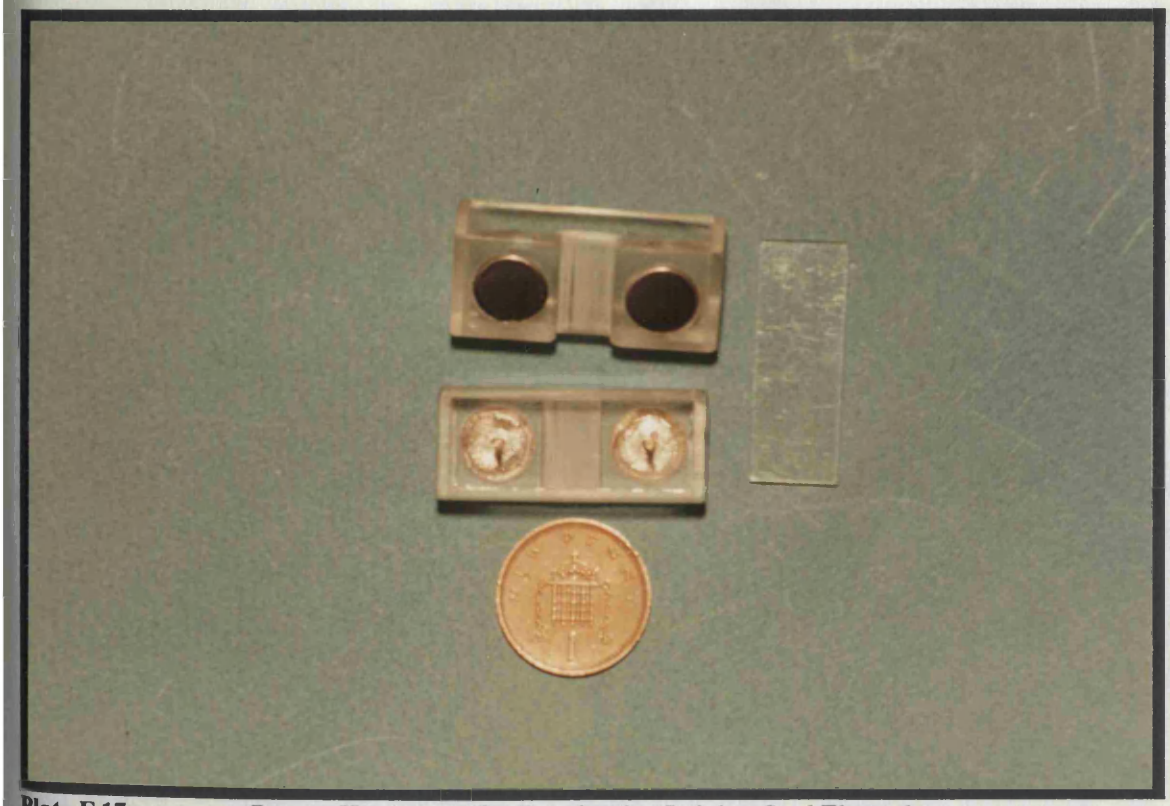

Plate F.17 *Perspex Head Amplifier Box showing Stainless Steel Electrodes*

Plate F.18 *Isolation Amplifier and Filter showing Front Panel*

Plate F.19 *Isolation Amplifier showing Rear Panel*

F.3 Signal Processing Hardware

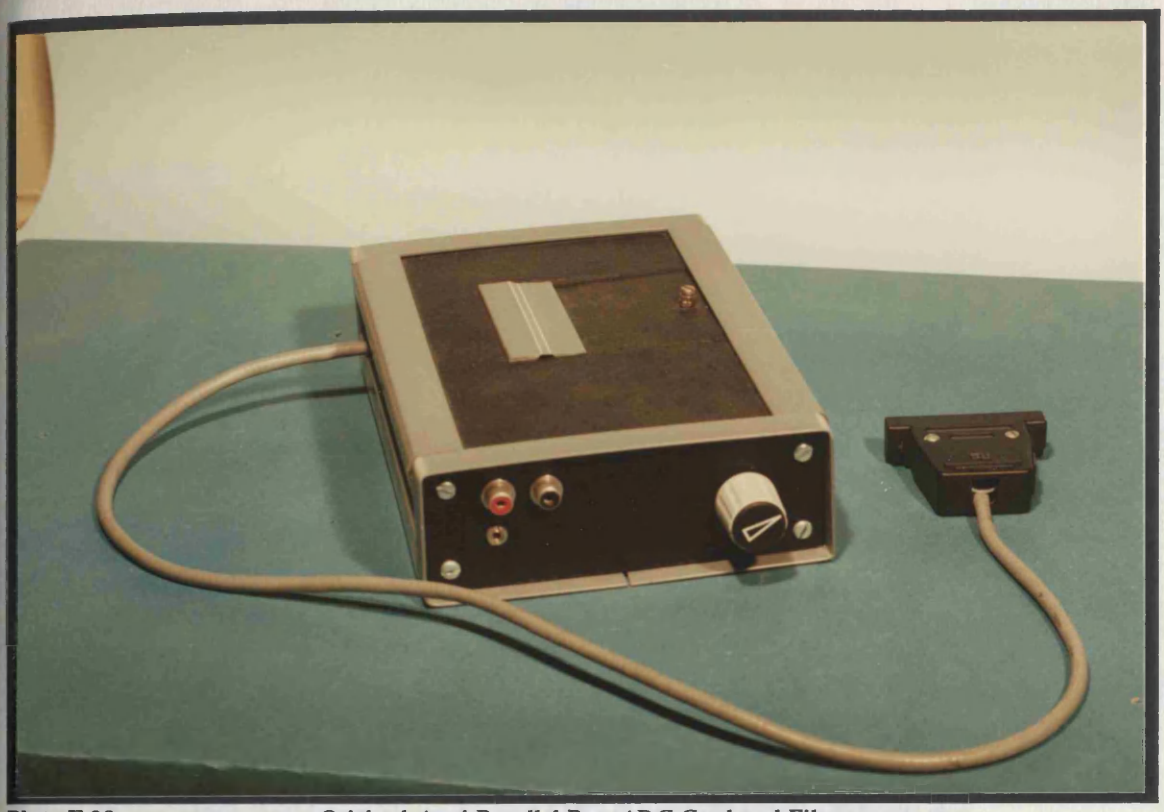

Plate F.20 *Original Atari Parallel Port ADC Card and Filter*
Showing Dual Input Phonos and Synchronisation Input Jack with Filter Switch on the right.

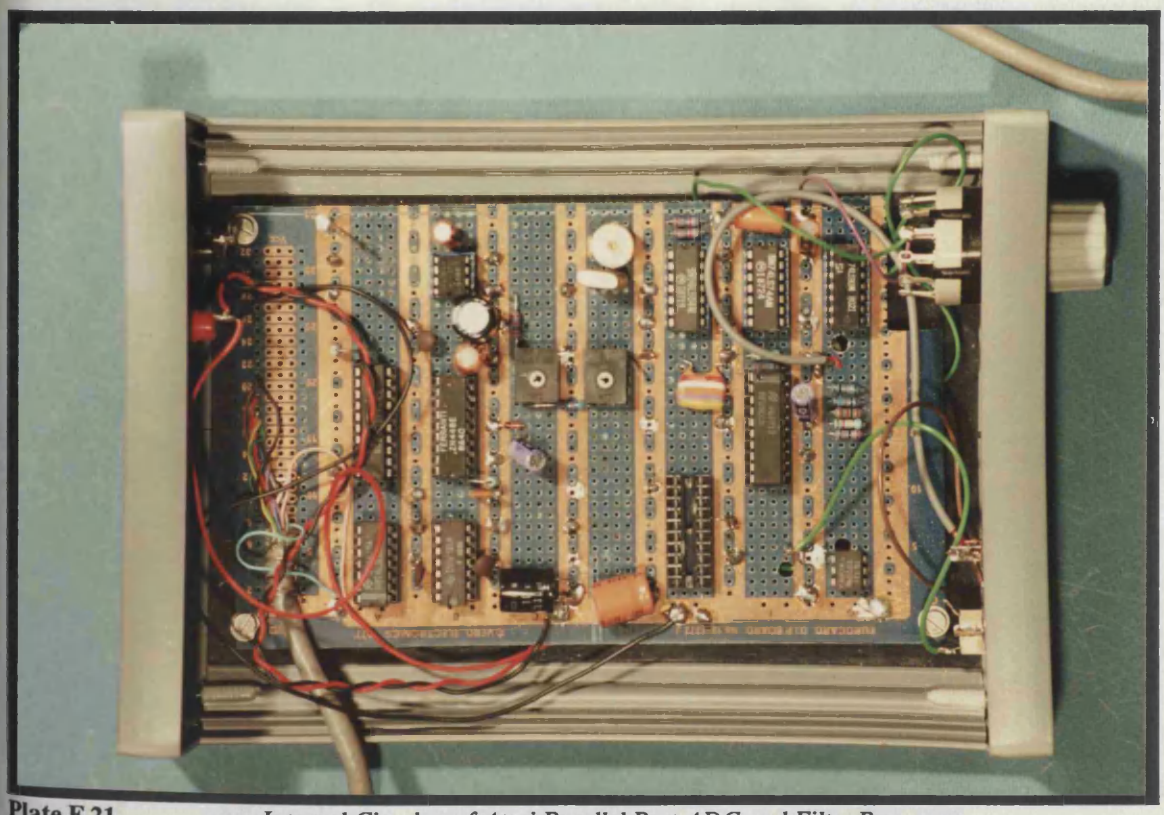

Plate F.21 *Internal Circuitry of Atari Parallel Port ADC and Filter Box*

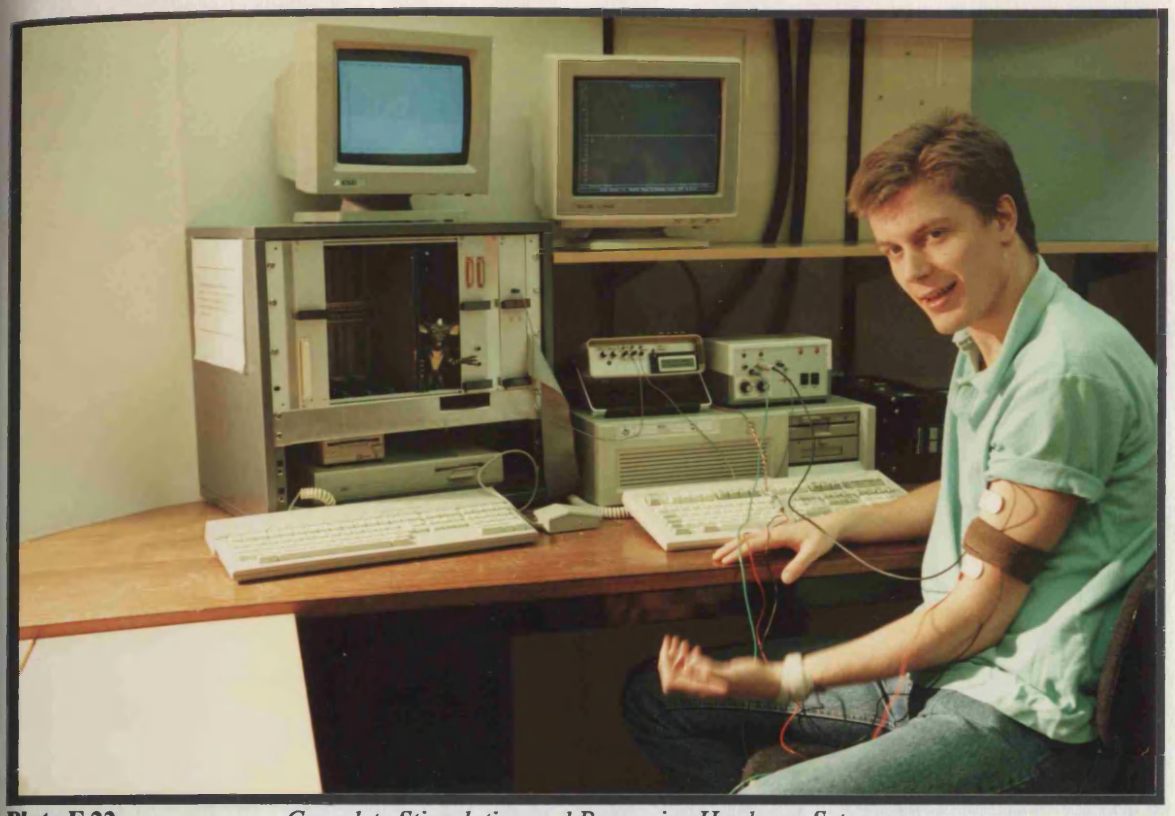

Plate F.22 *Complete Stimulating and Processing Hardware Set-up*
Showing Atari Mega on the Left with expansion cards above; IBM Computer Hosting the DSP card right;
Programmable Stimulator and Isolation amplifier on the IBM case;
and Stimulating Electrodes and EMG Pre-amplifier on the Subjects arm.

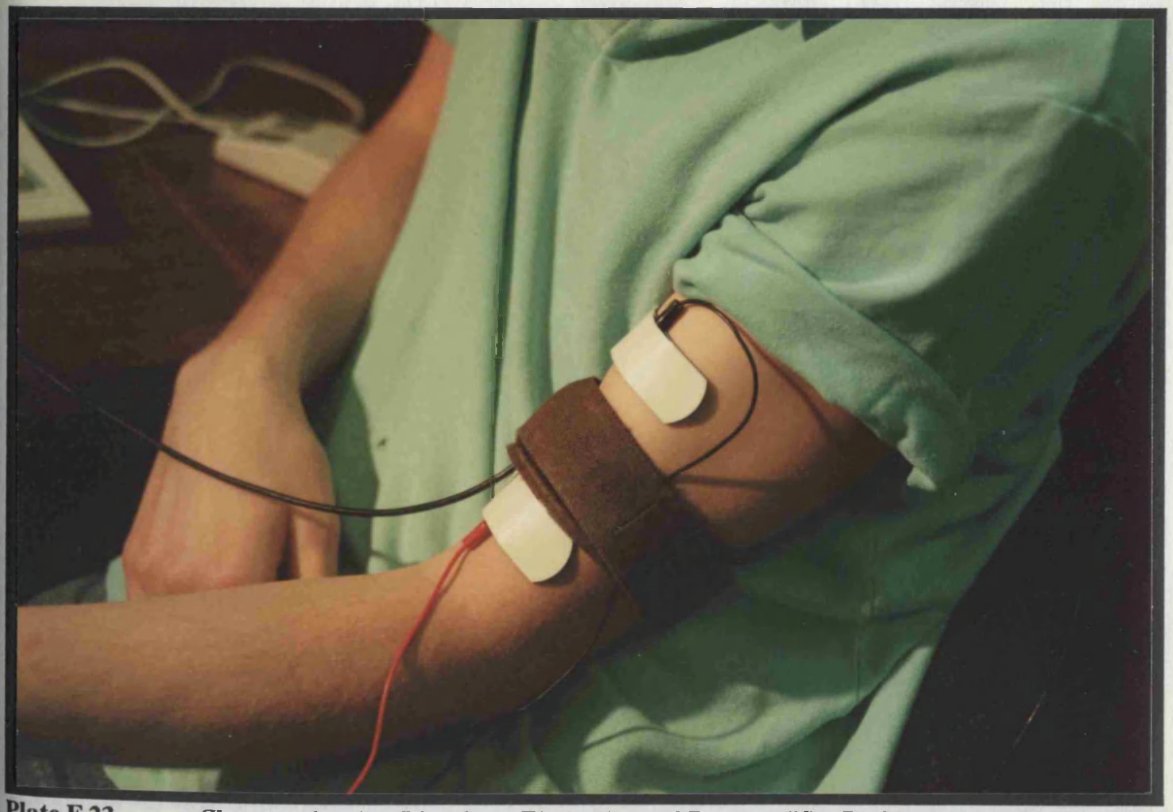

Plate F.23 *Close-up showing Stimulator Electrodes and Pre-Amplifier Positioning*
for the Biceps

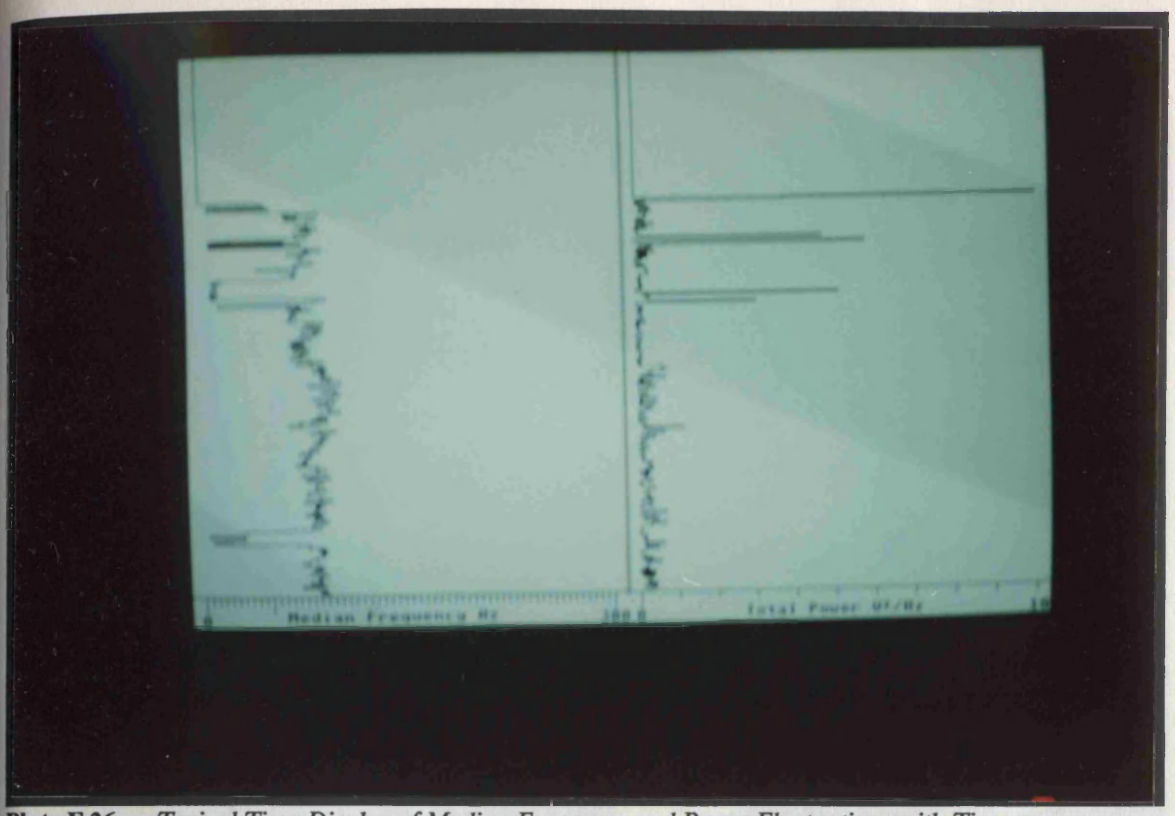

Plate F.26 *Typical Time Display of Median Frequency and Power Fluctuations with Time*

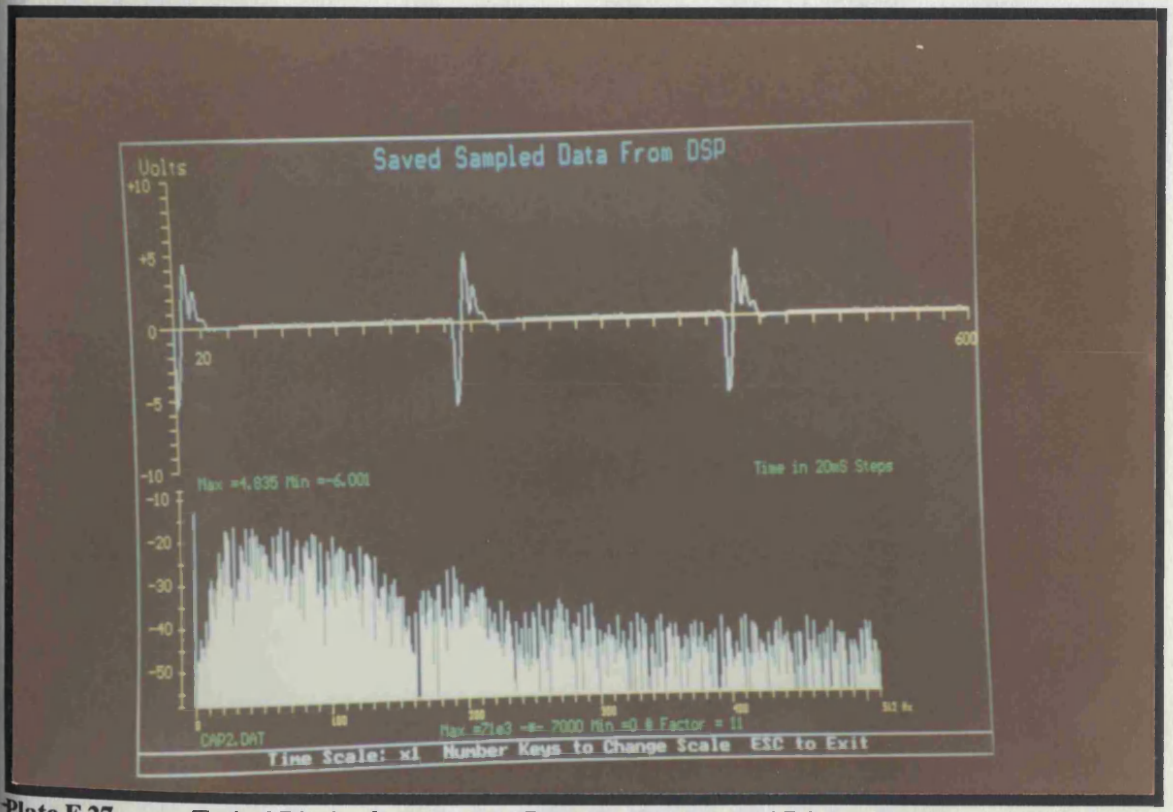

Plate F.27 *Typical Display from the Post-Recording Display and Printing Program on the IBM*

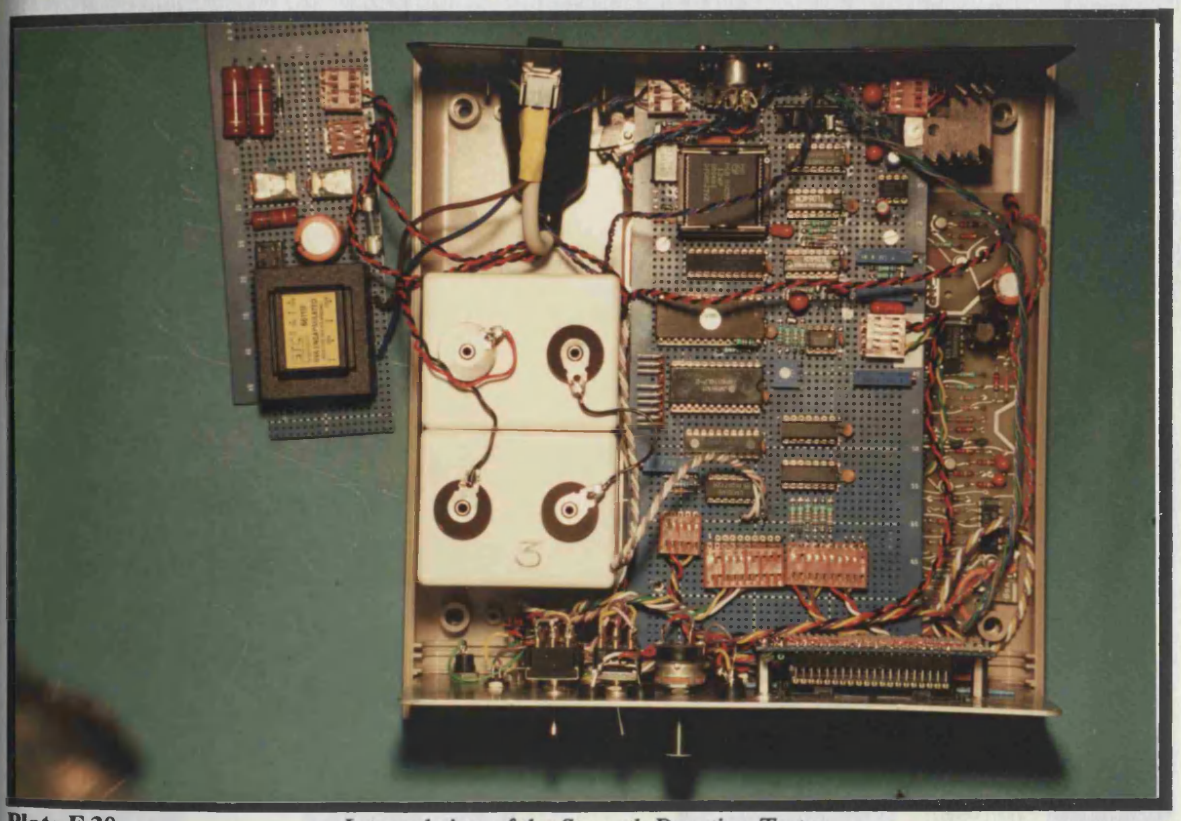

Plate F.30 *Internal view of the Strength Duration Tester*
Showing Battery Charger (left); Processor Card Mounted above Stimulator Card

F.5 The Analogue Muscle Fatigue Monitors

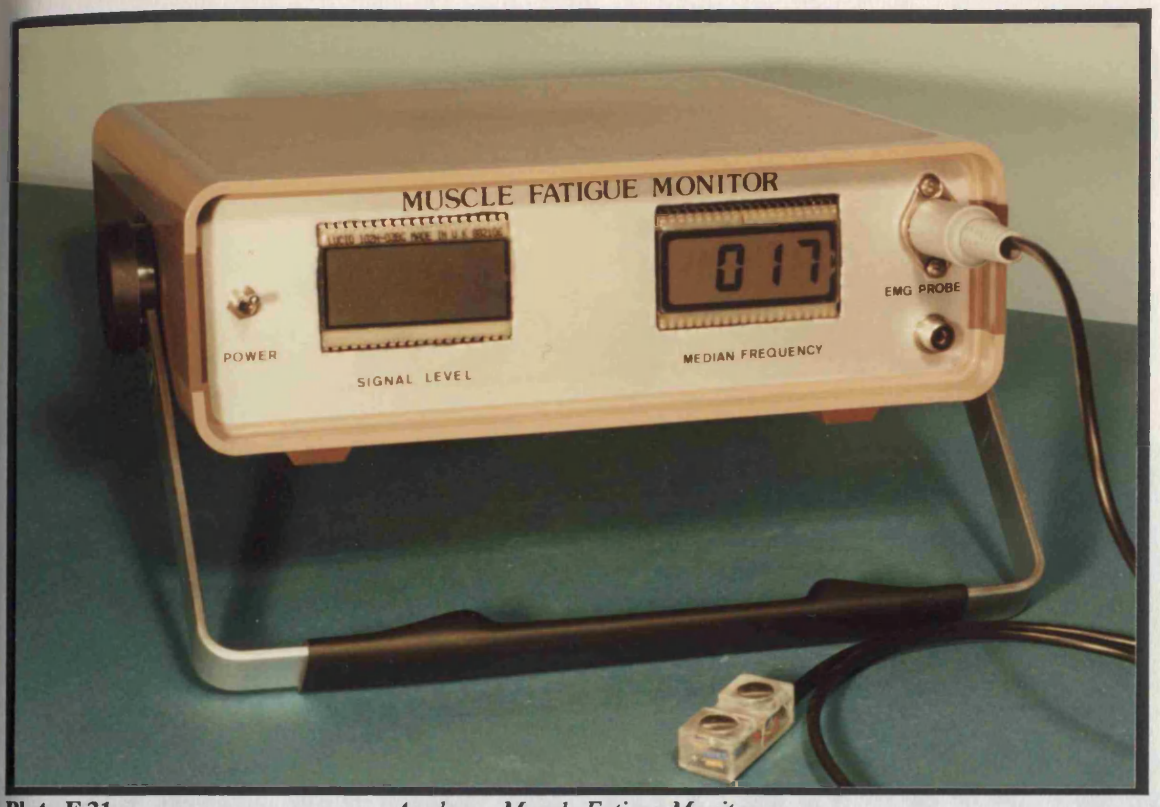

Plate F.31 *Analogue Muscle Fatigue Monitor*
Showing EMG Electrode Mounted Pre-Amplifier

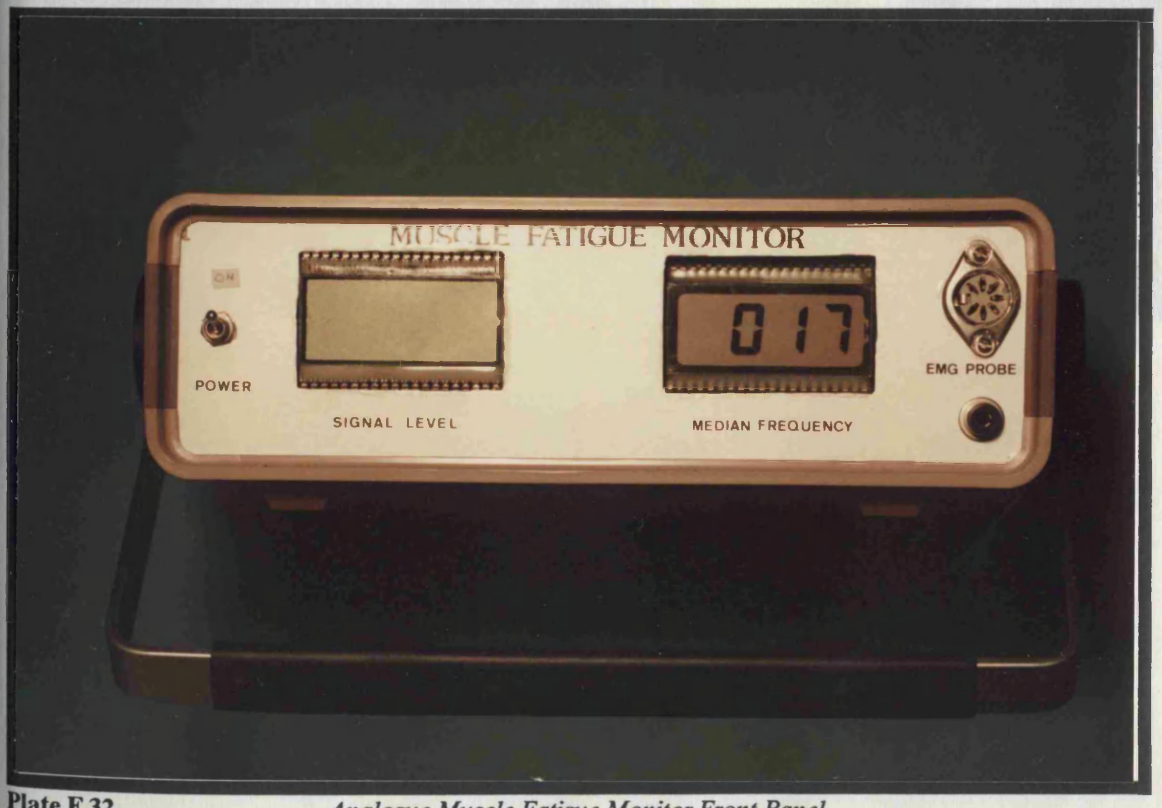

Plate F.32 *Analogue Muscle Fatigue Monitor Front Panel*

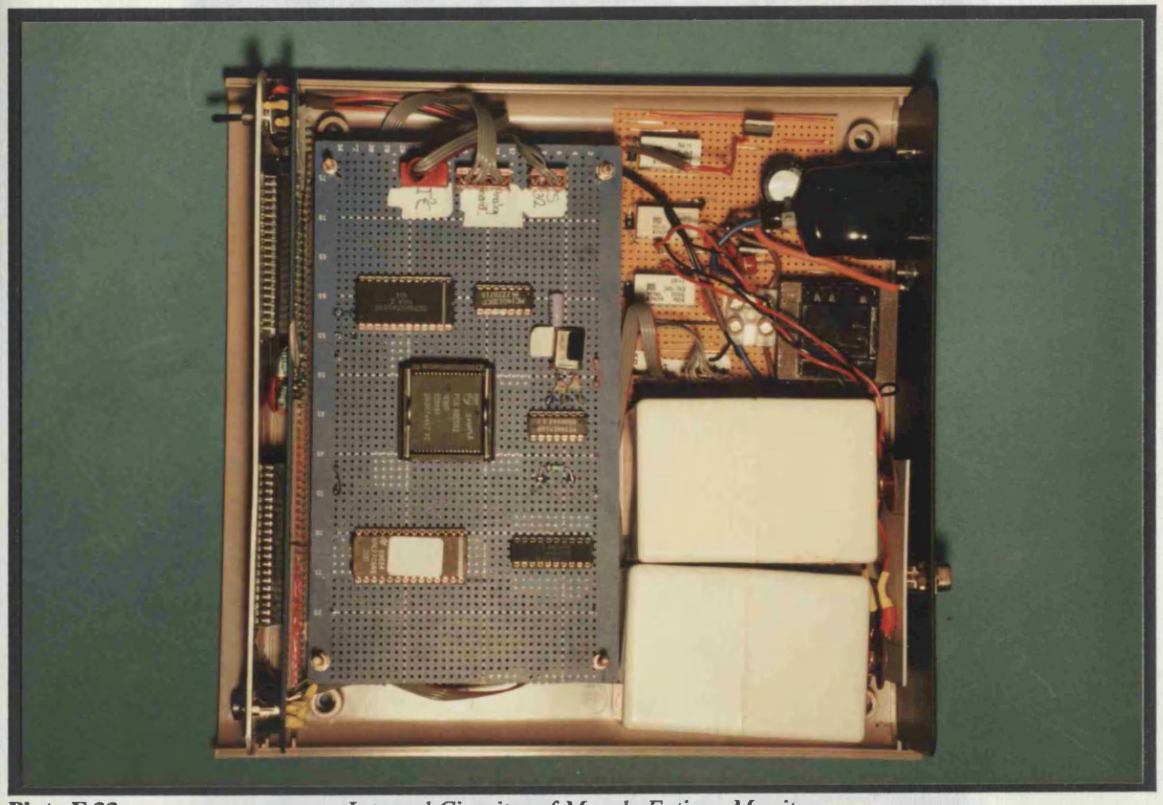

Plate F.33 *Internal Circuitry of Muscle Fatigue Monitor*
Showing Display Processor above the Analogue Processing Section

F.6 The Digital Muscle Fatigue Monitor

Plate F.34 *Digital Muscle Fatigue Monitor*
Showing The Electrode Mounted Pre-Amplifier in the Foreground

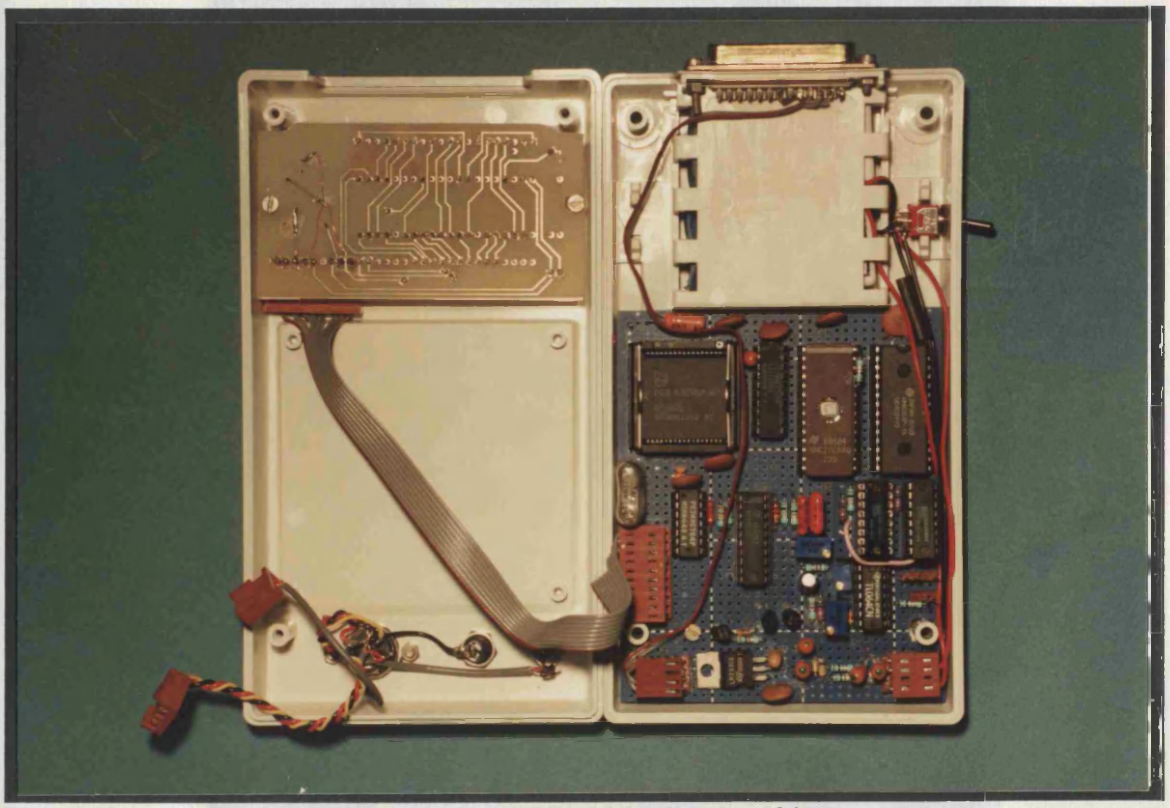

Plate F.35 *Internal Circuitry of Digital Muscle Fatigue Monitor*

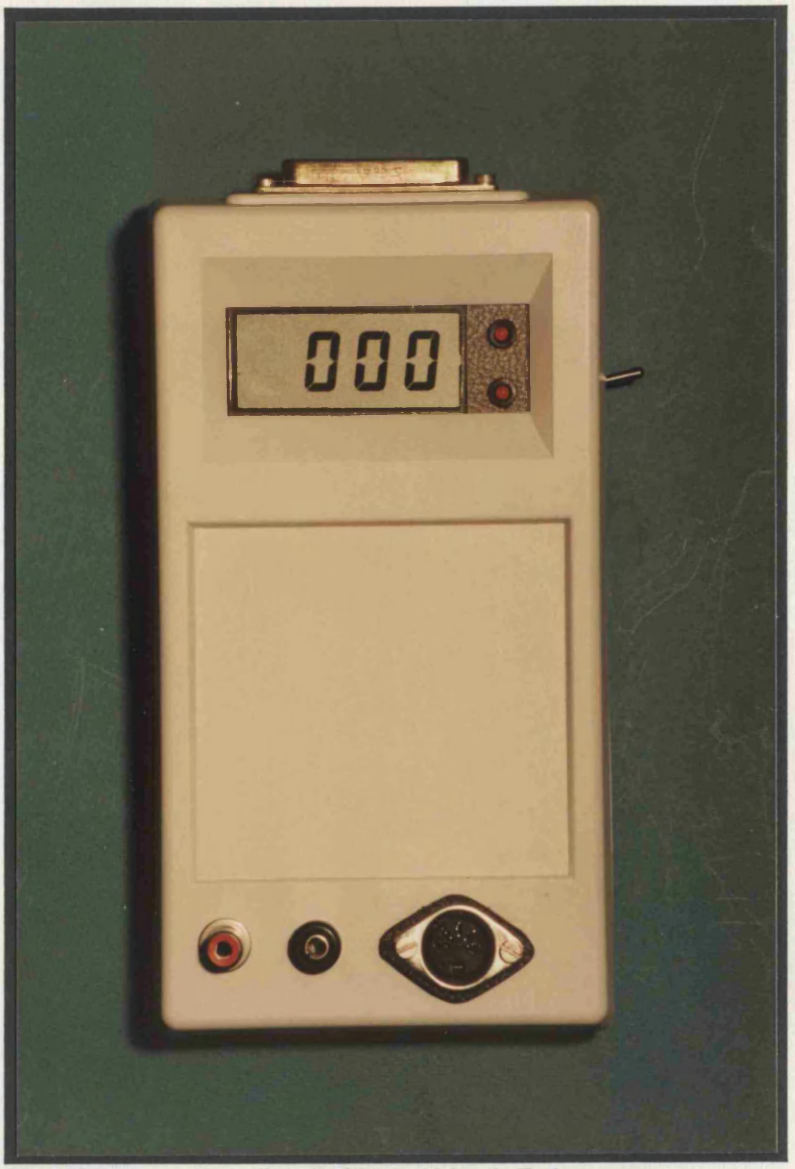

Plate F.36 *Front Panel of Digital Muscle Fatigue Monitor*

Appendix G

Circuit Diagrams

The circuit diagrams for the circuits described in Chapters 5, 6, 7, Appendix A and Appendix B are presented in the following pages. The order matches the order in which they are described in the text.

Appendix G

Circuit Diagrams

The circuit diagrams for the circuits described in Chapters 5, 6, 7, Appendix A and Appendix B are presented in the following pages. The order matches the order in which they are described in the text.

G.1 Bath University Stimulator

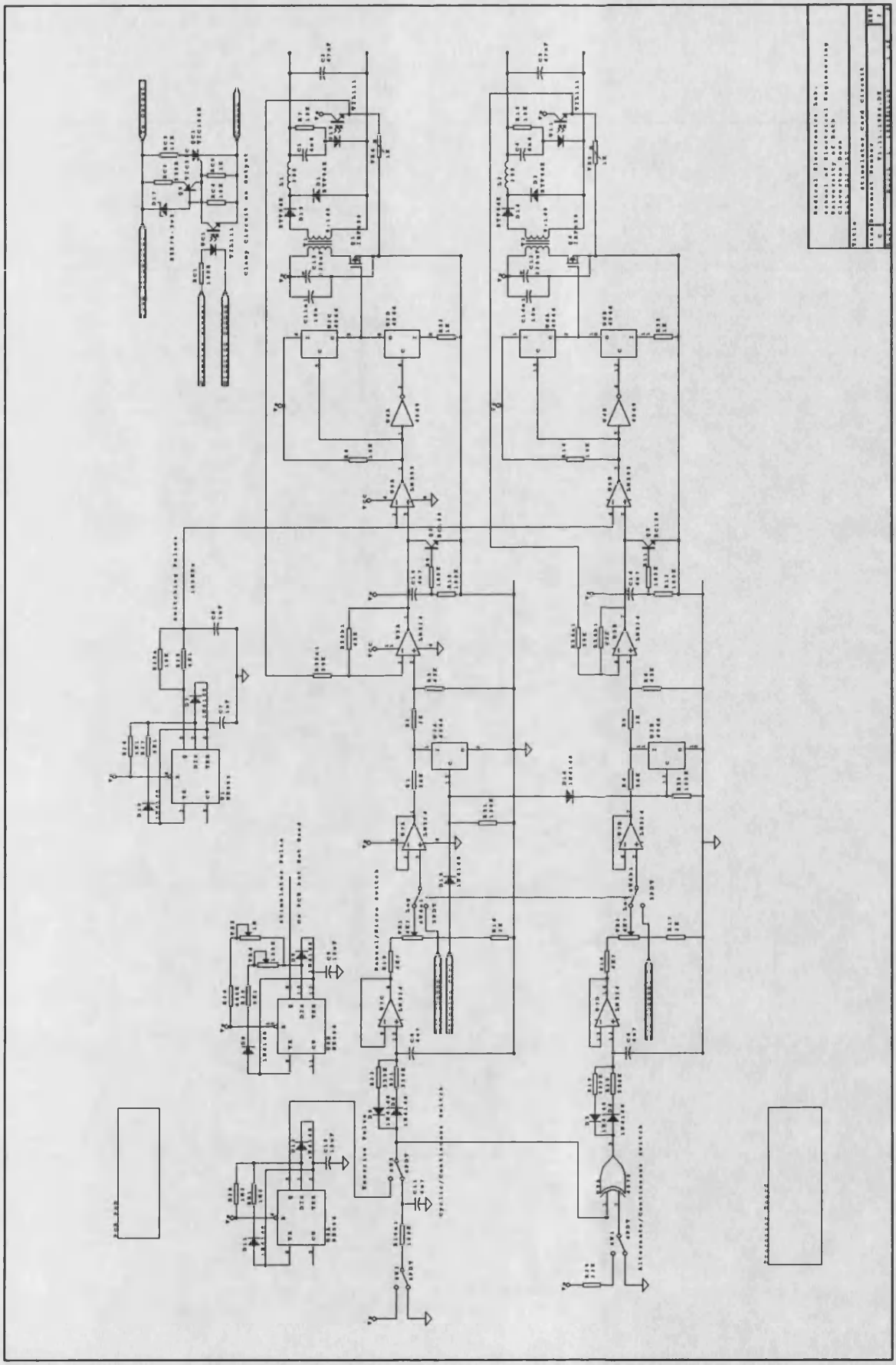

Figure G.1 *Standing Stimulator Card with Output Clamp*

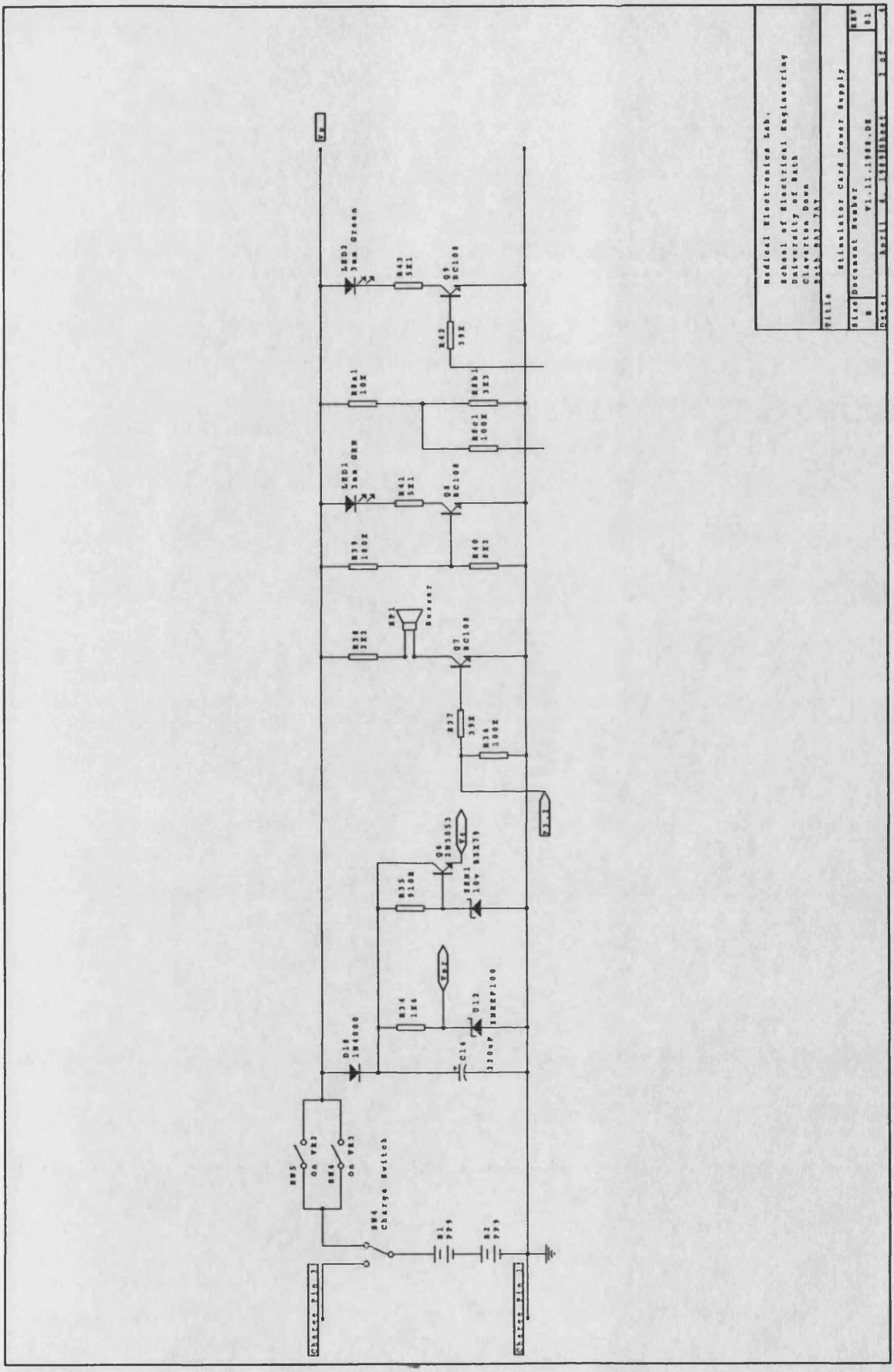

Figure G.2 *Stimulator Card Power Supply and Buzzer Circuitry*

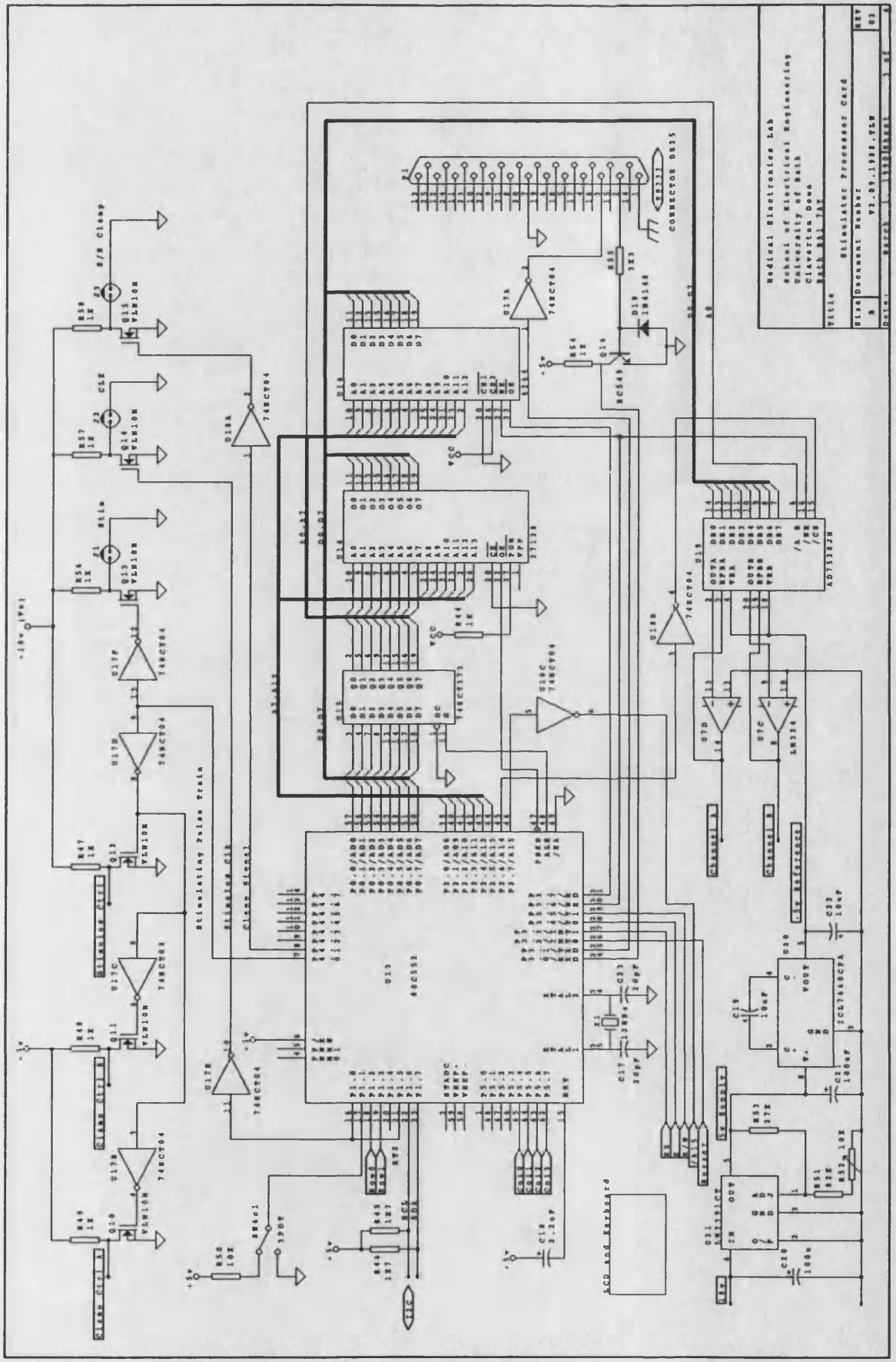

Figure G.3 *Stimulator Processor Card*

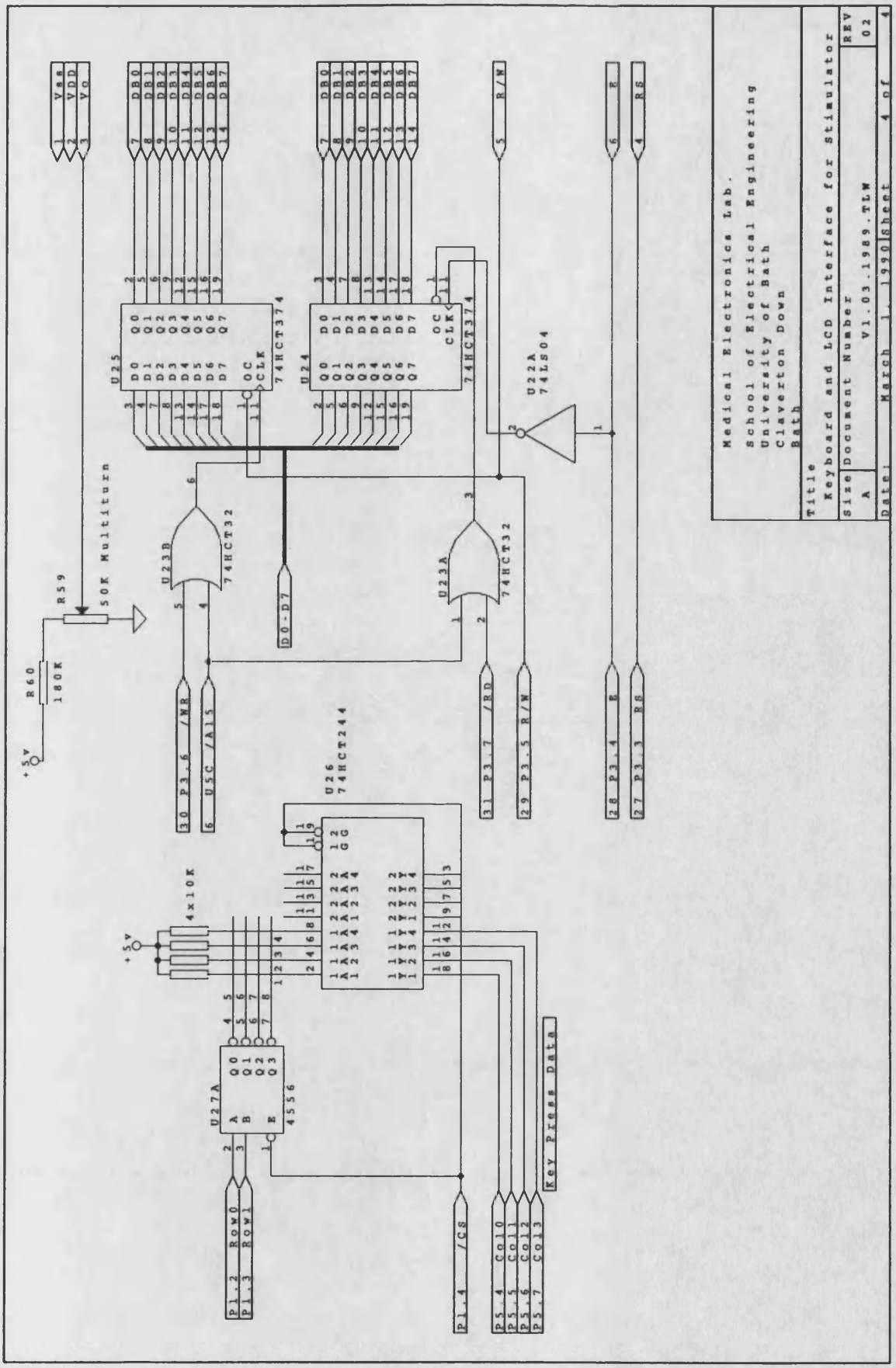

Figure G.4 *Keyboard and LCD Interface for Bath University Stimulator*

G.2 Operational Amplifier Stimulator

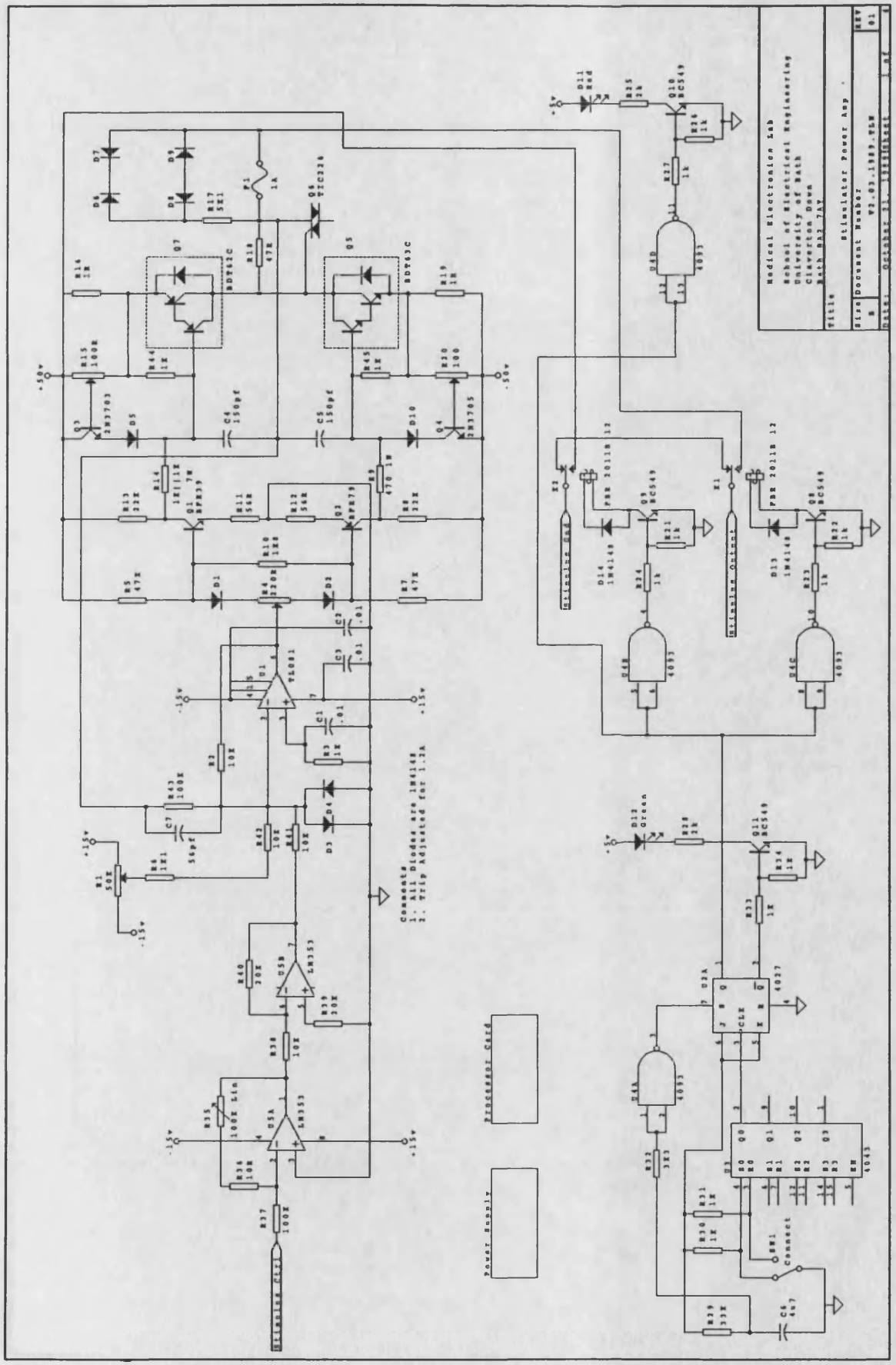

Figure G.5 *Mark 1 Power Amplifier Stimulator and Reset Circuitry*

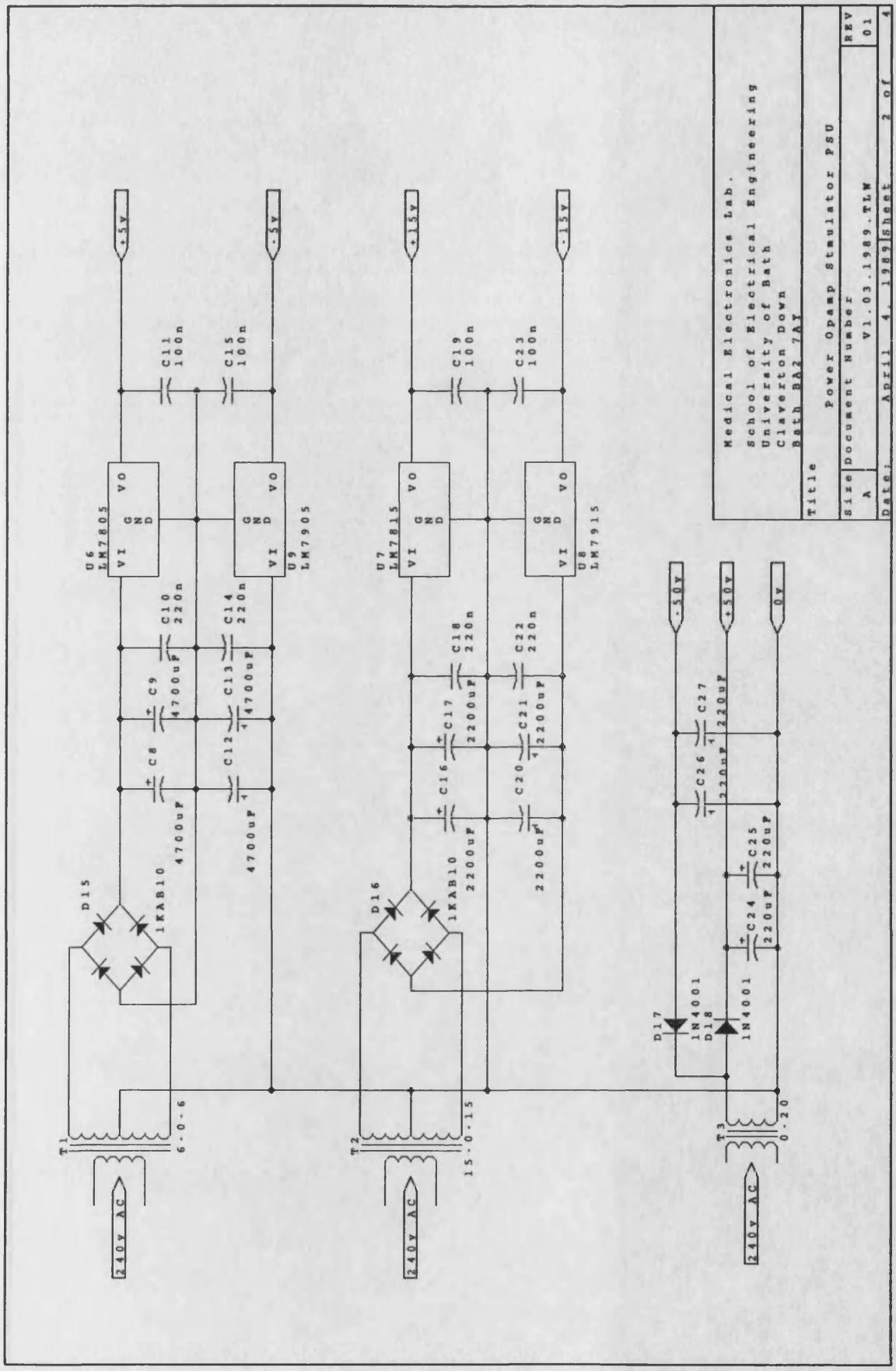

Figure G.6 *Power Amplifier Stimulator Power Supplies*

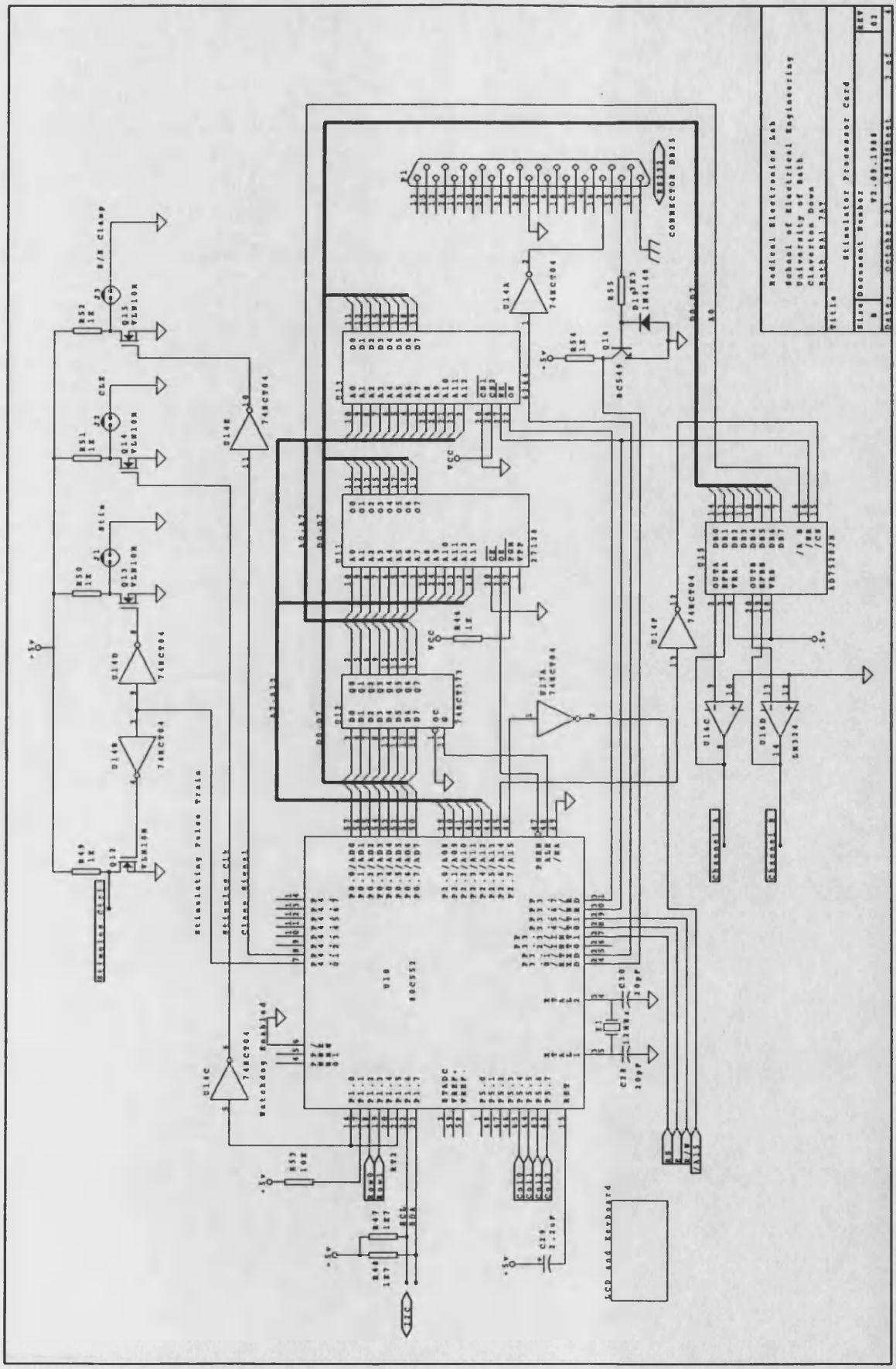

Figure G.7 *Processor Card for Power Amplifier Stimulator*

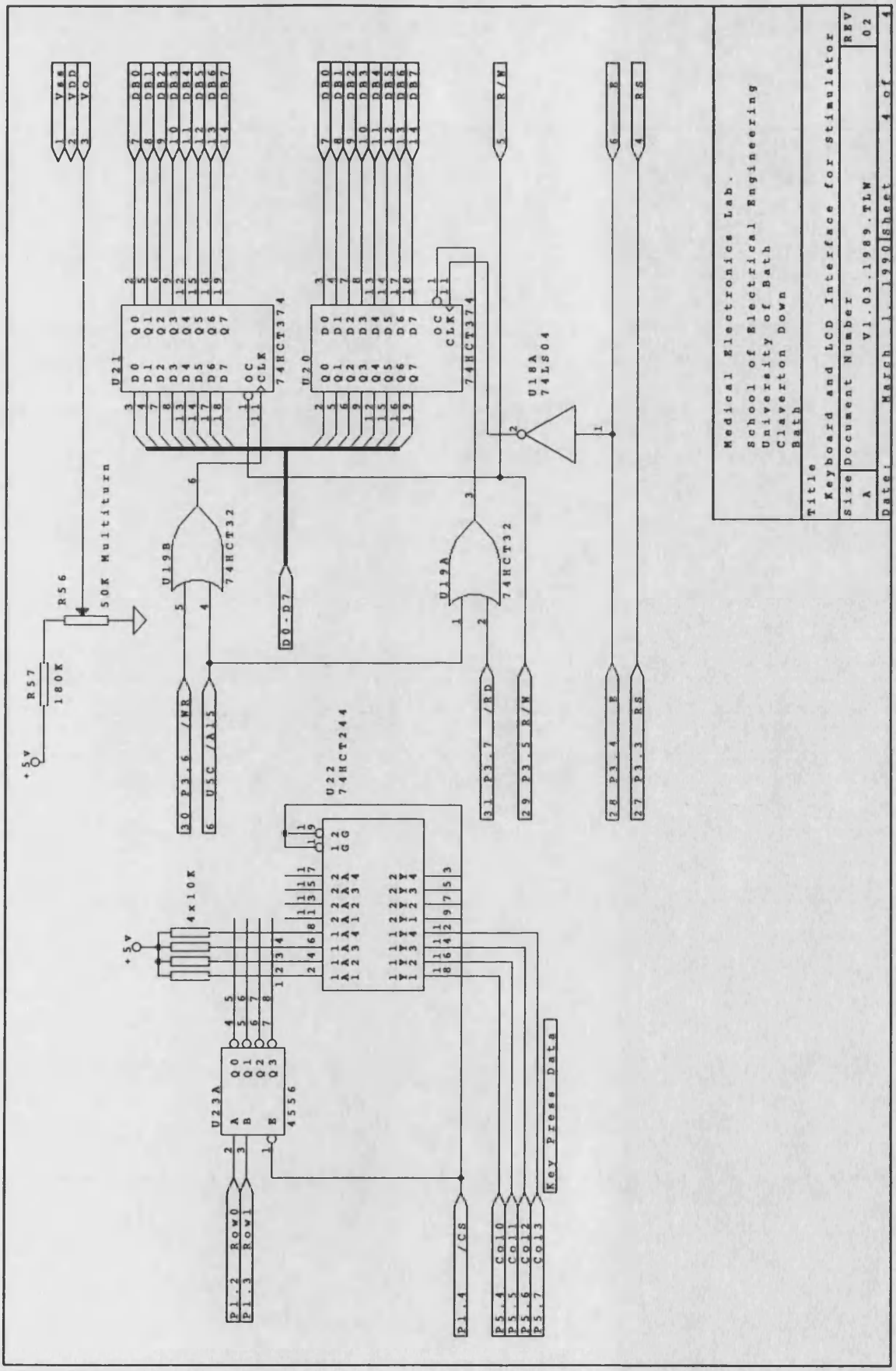

Figure G.8 *Keyboard and LCD Display interface for Power Amplifier Stimulator*

G.3 Revised Operational Amplifier Stimulator

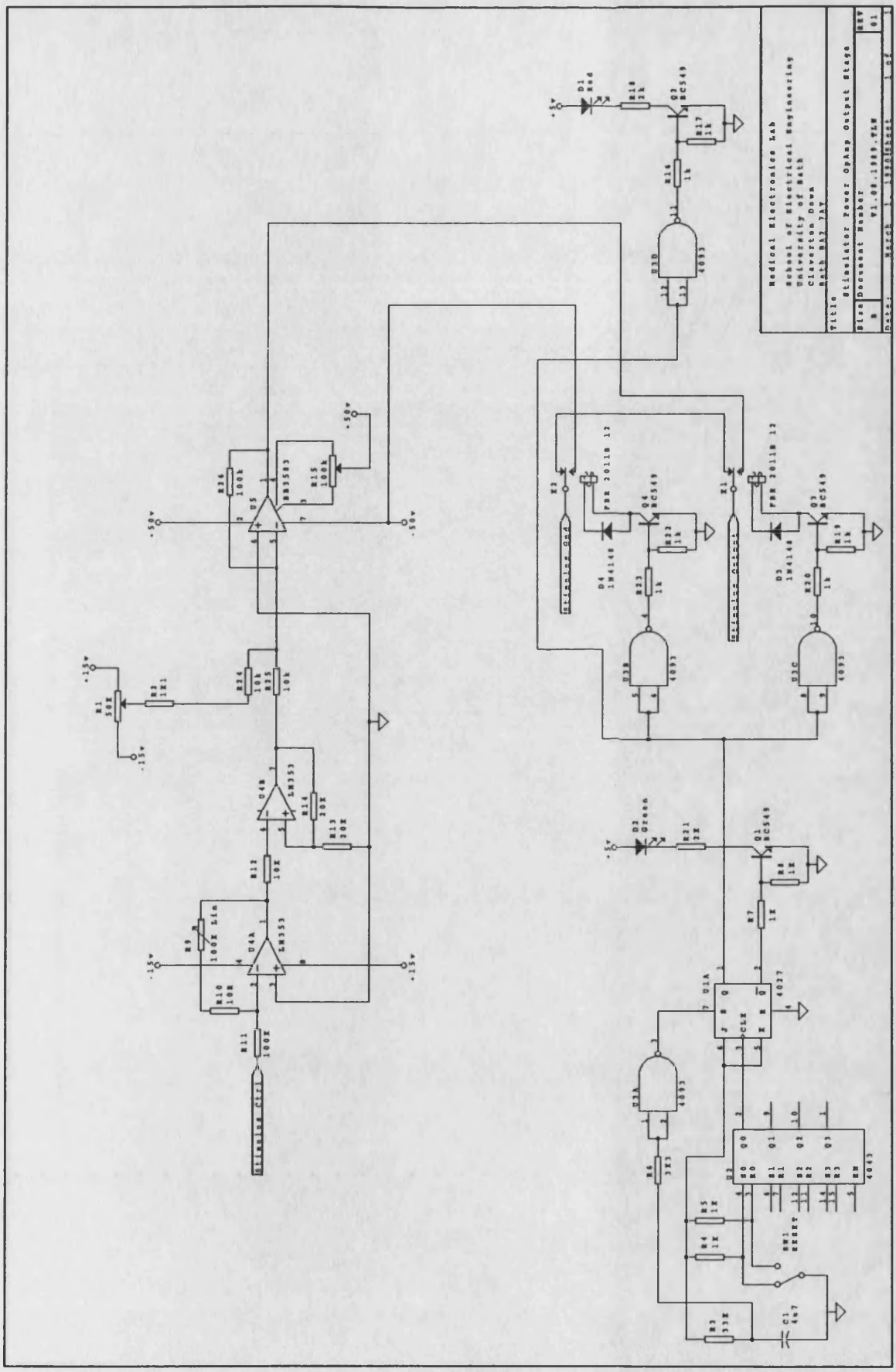

Figure G.9 *Mark II Power Amplifier Stimulator Output Stage, other sections as Mark I*

G.4 RS232 Isolation Box

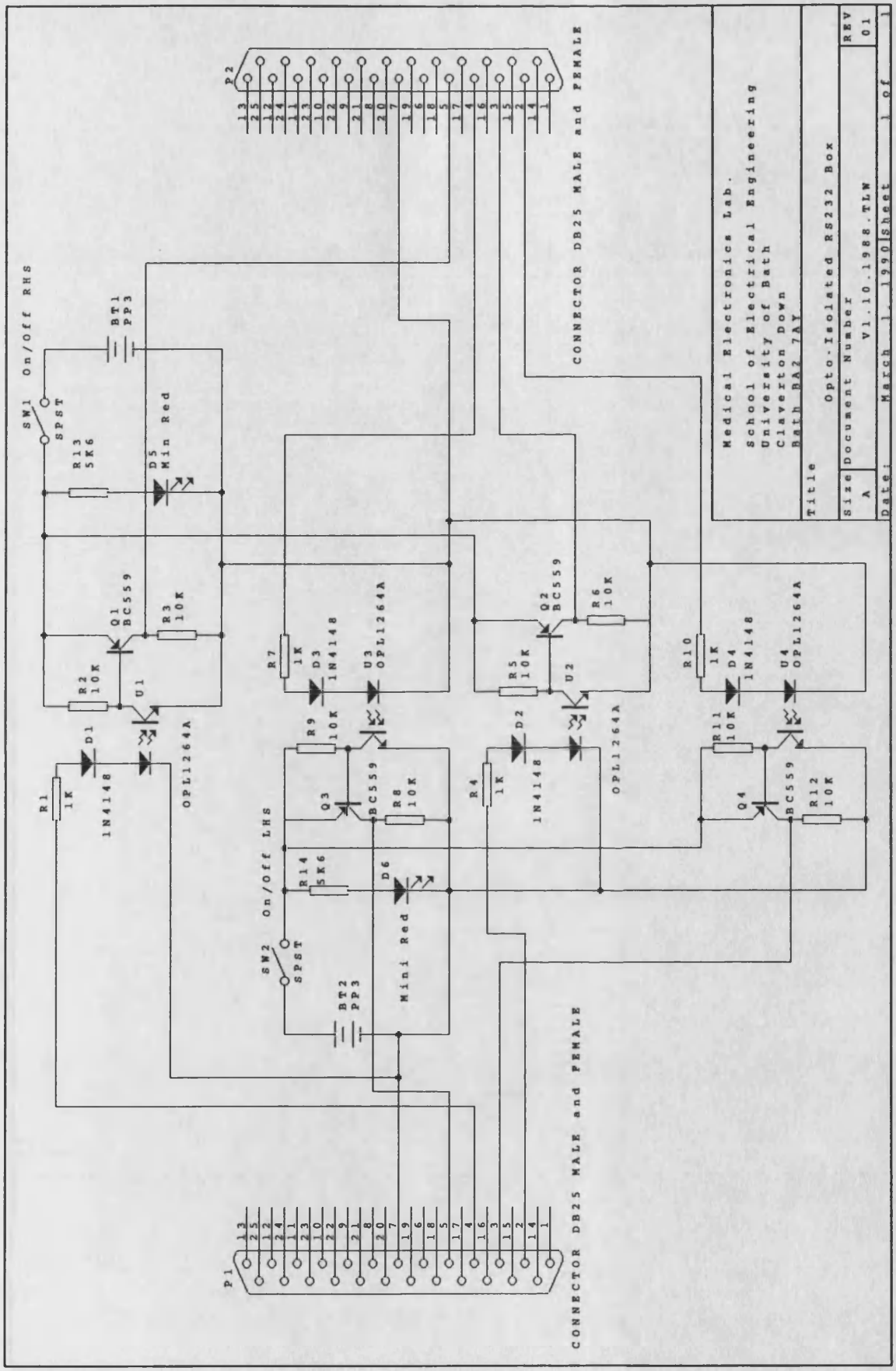

Figure G.10 *Opto-Isolated RS232 Box*

G.5 EMG Amplifiers

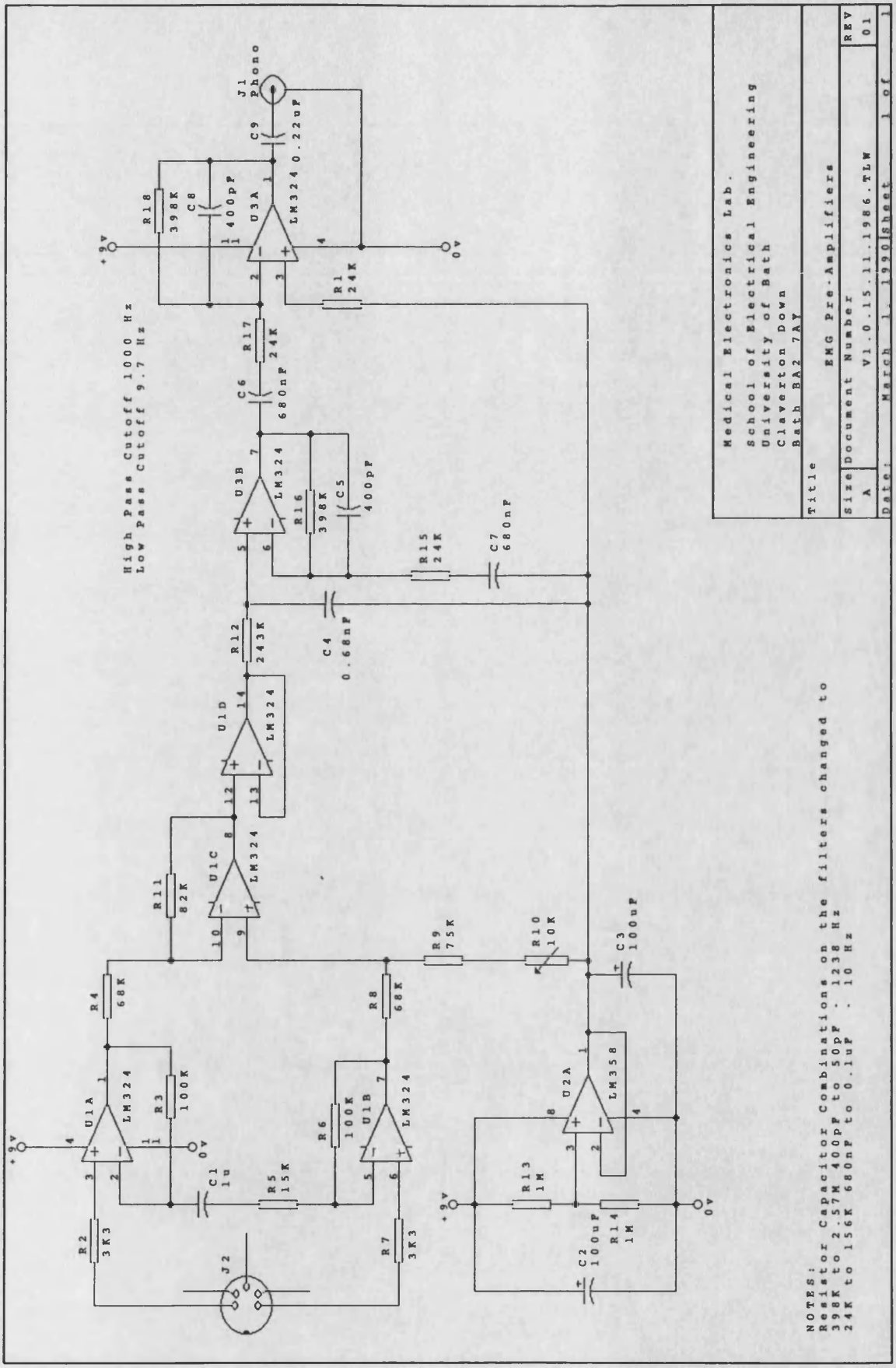

Figure G.11 *Initial EMG Pre-Amplifier Design*

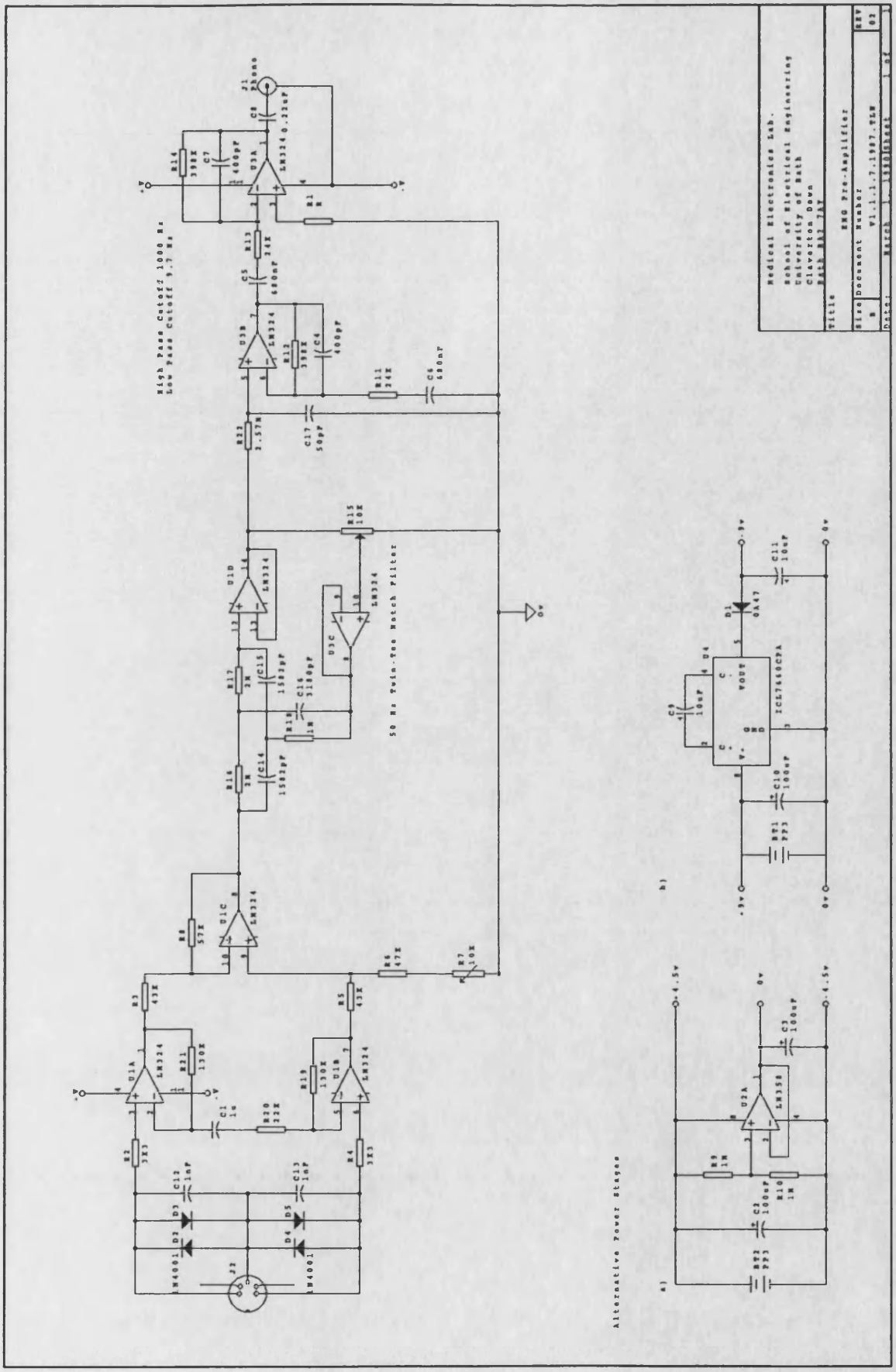

Figure G.12 *Initial EMG Amplifier Variations*

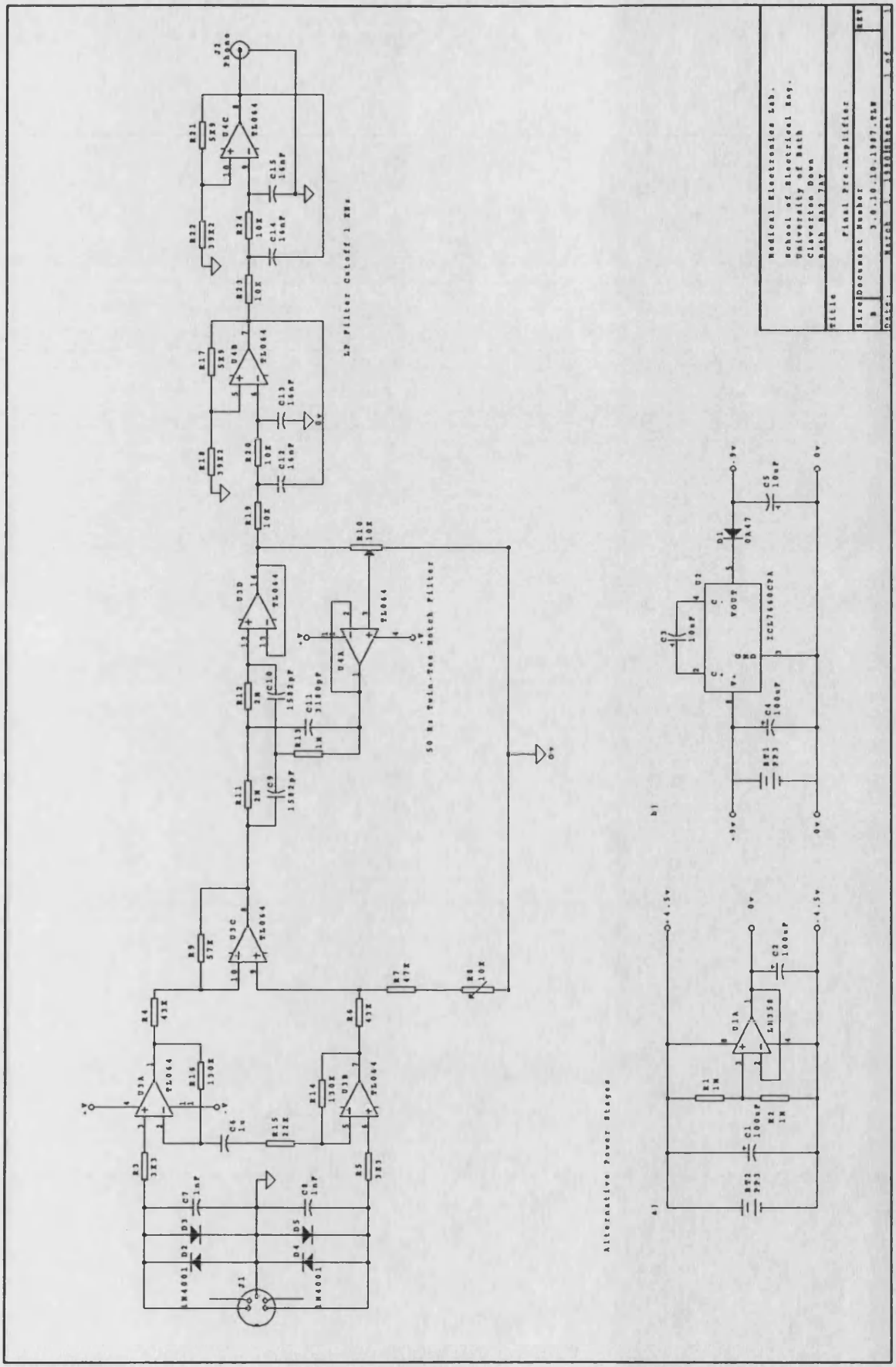

Figure G.13 *Final Pre-Amplifier Design*

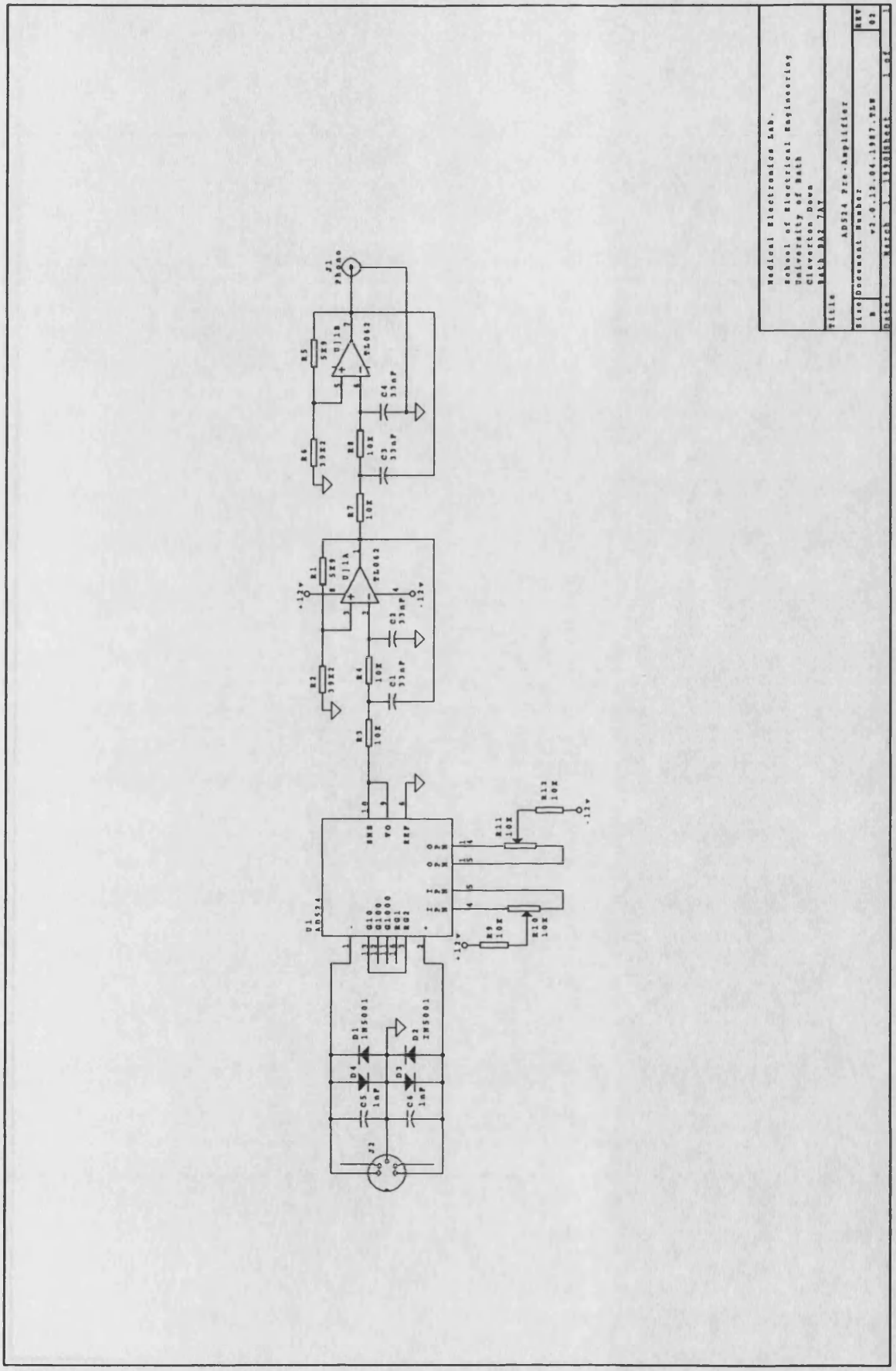

Figure G.14 *AD524 Based Pre-Amplifier*

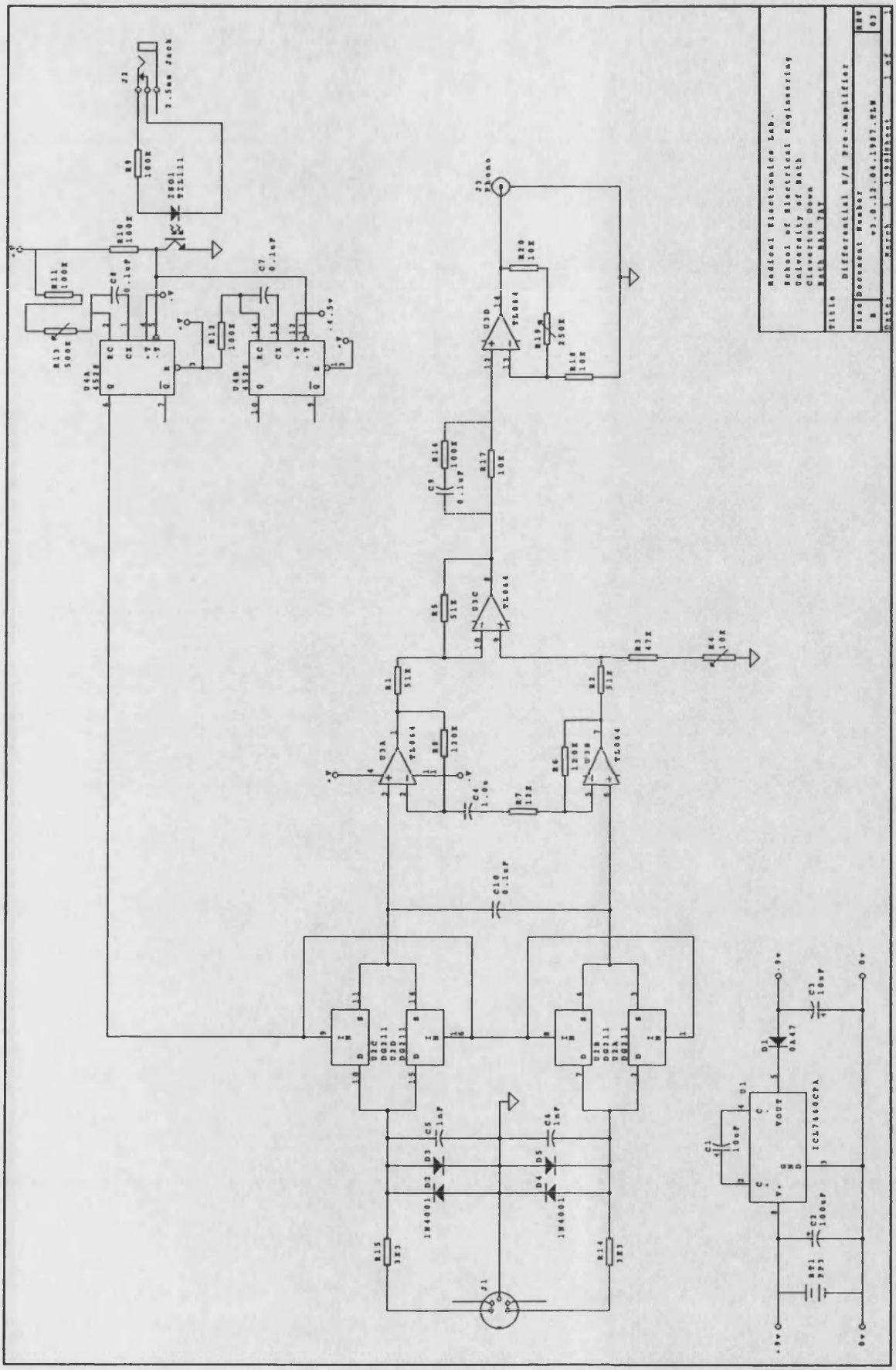

Figure G.15 *Differential S/H Pre-Amplifier*

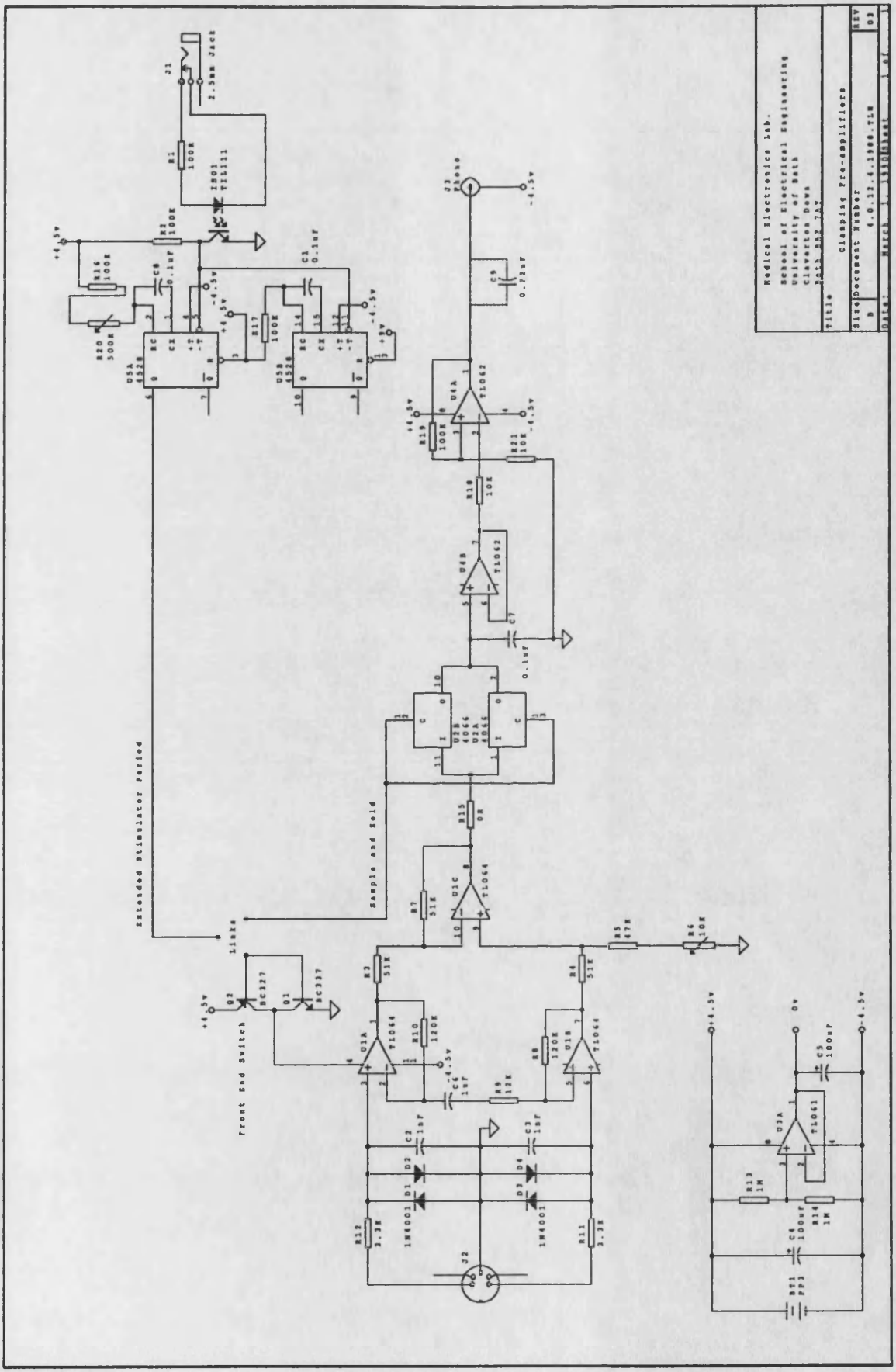

Figure G.16 *Clamping Pre-Amplifier*

G.6 EMG Probes

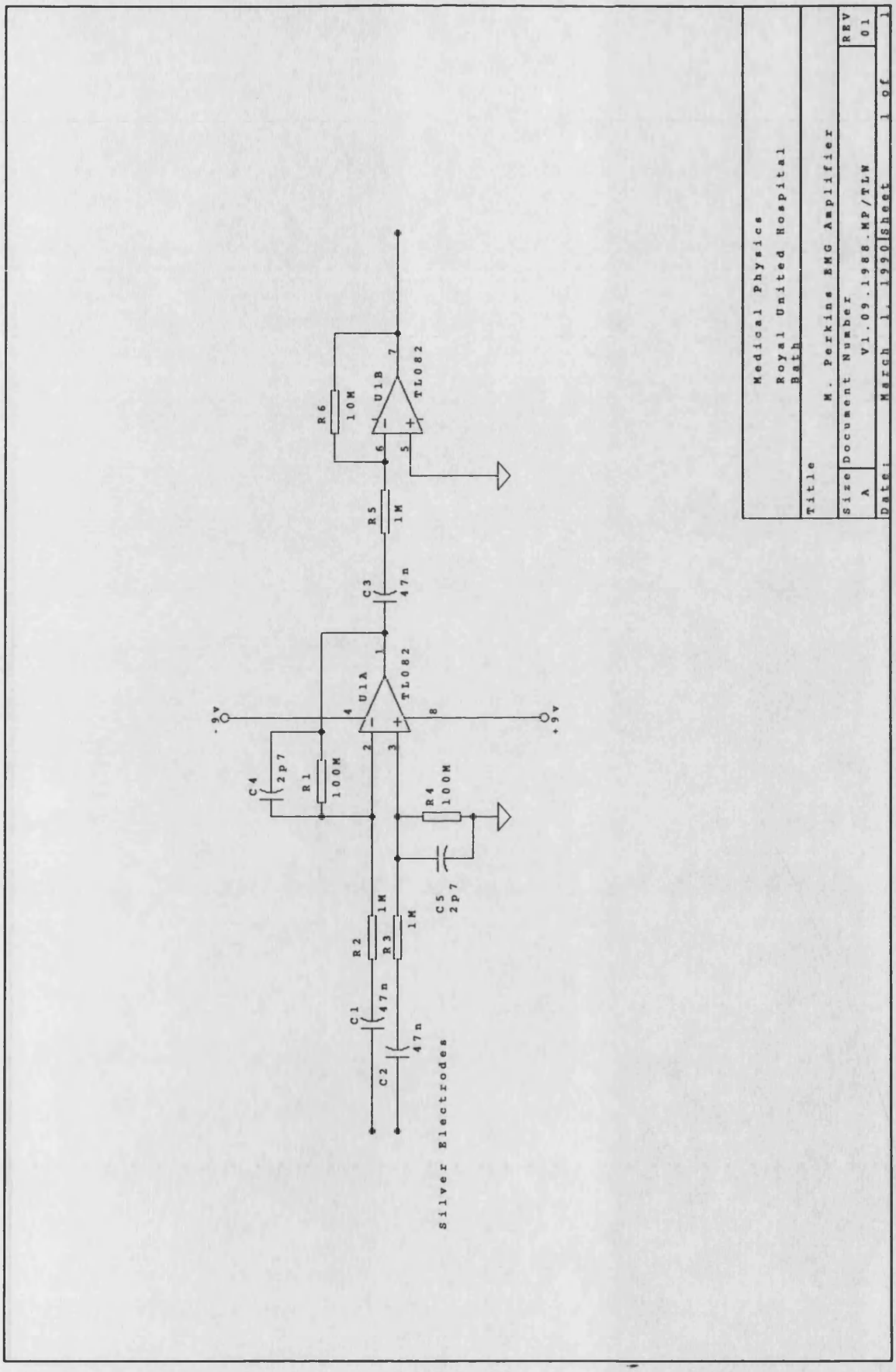

Figure G.17 *RUH EMG Amplifier*

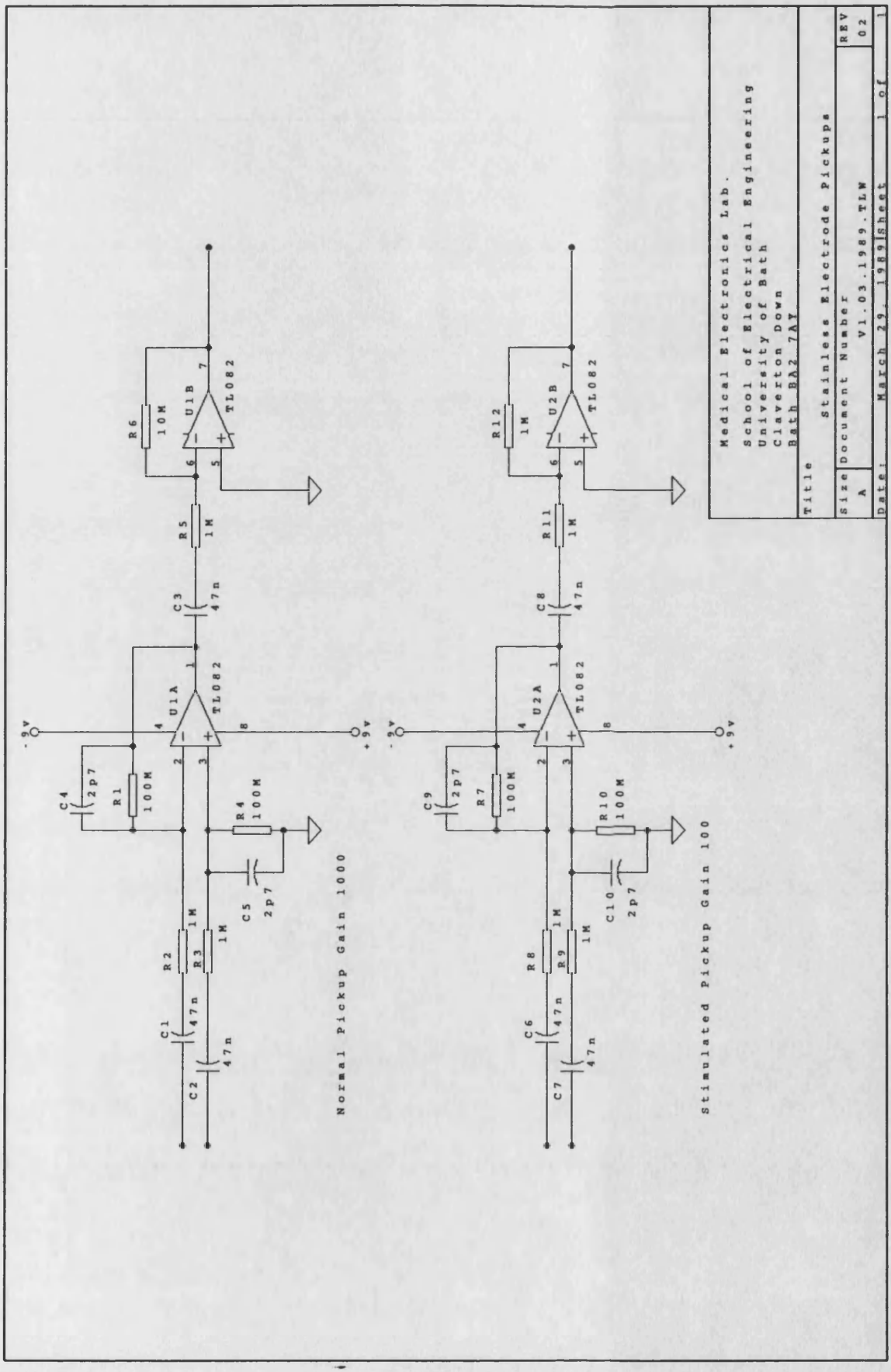

Figure G.18 *Stainless Steel Electrode Pickups*

G.7 Switchable Gain Amplifier

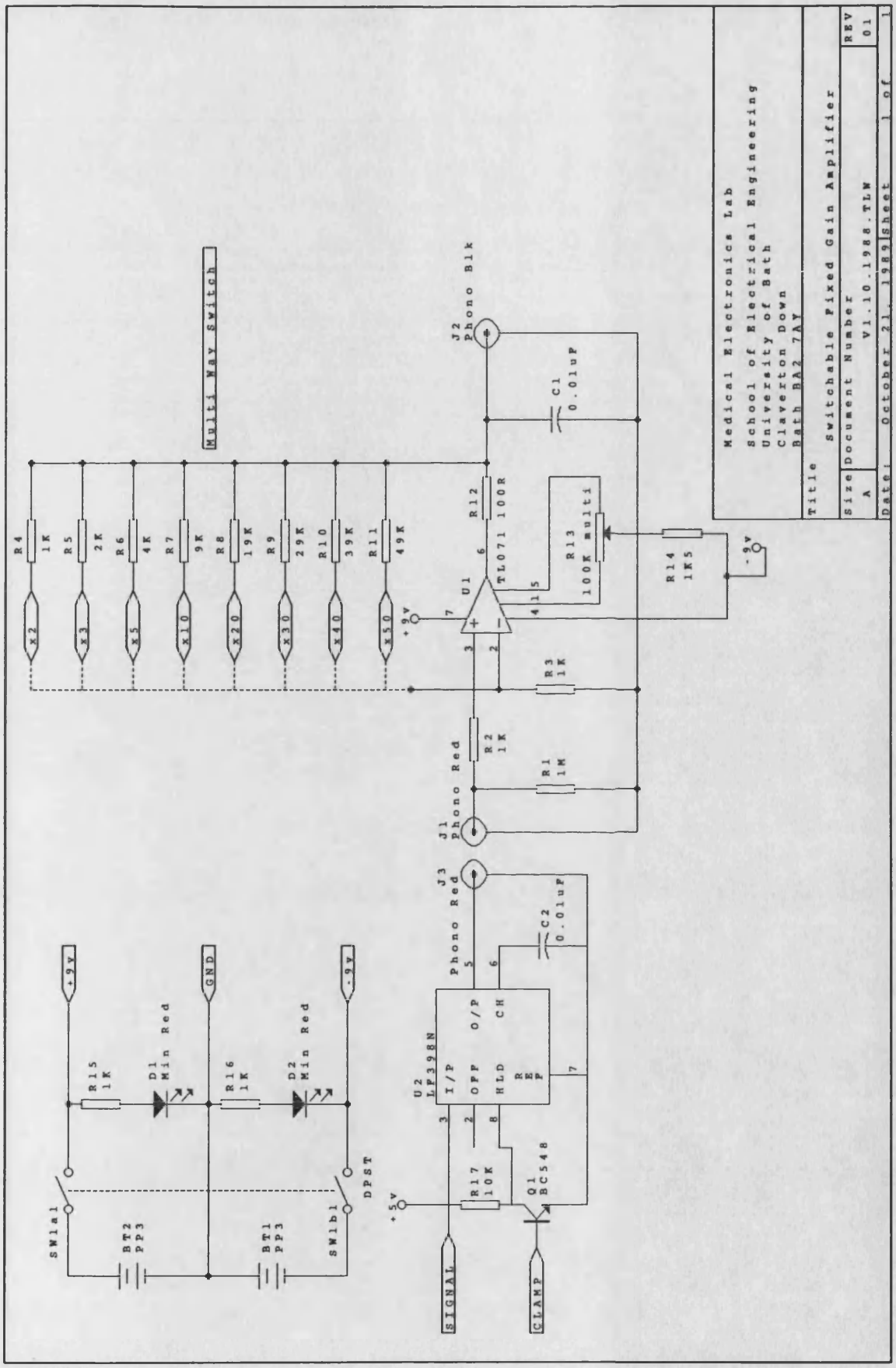

Figure G.19 *Switchable Gain Amplifier*

G.8 Isolation Amplifier

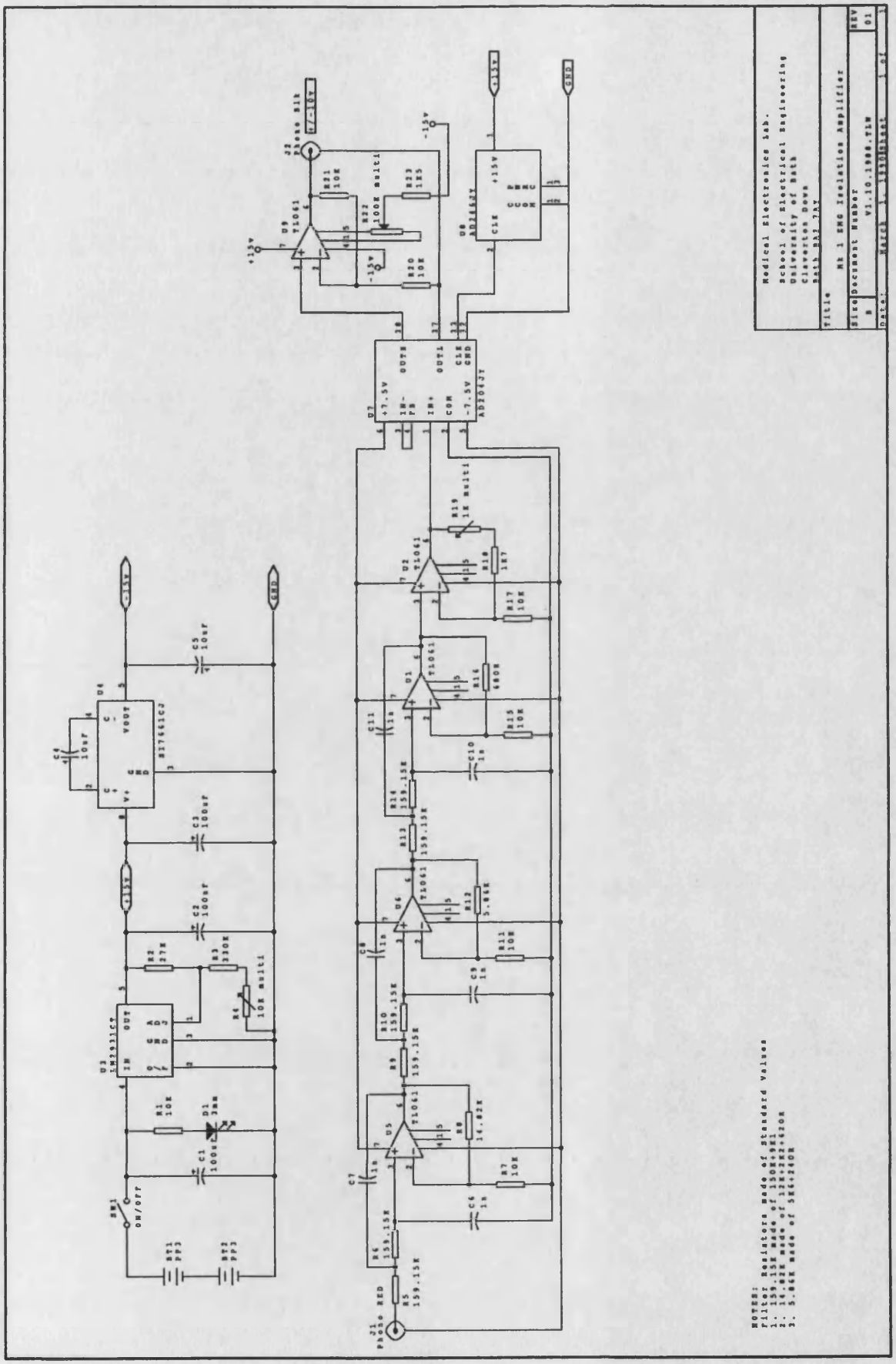

Figure G.20 *EMG Isolation Amplifier*

G.9 Combined Isolation and Gain Unit

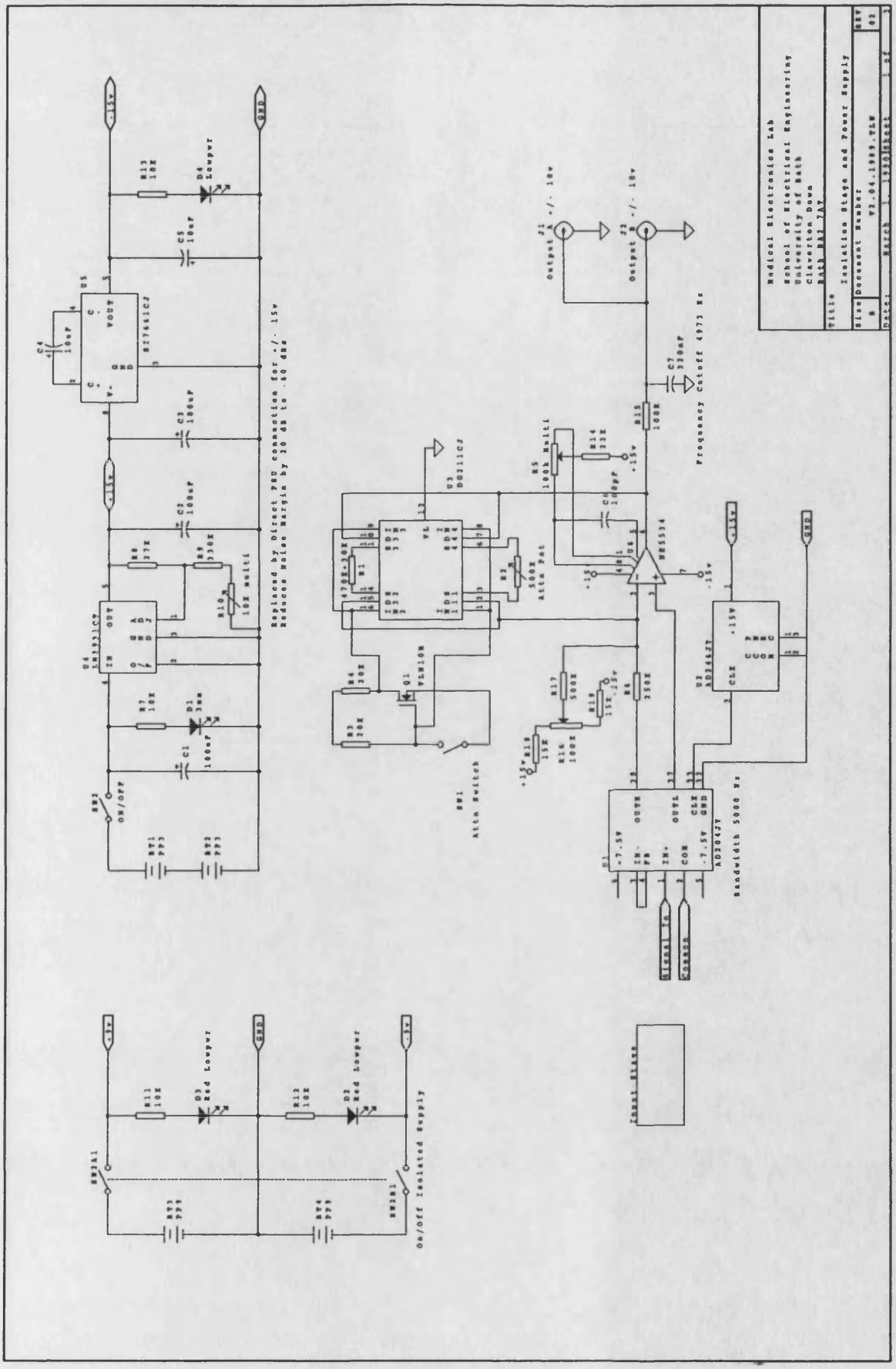

Figure G.21 *Isolating Stage and Power Supply*

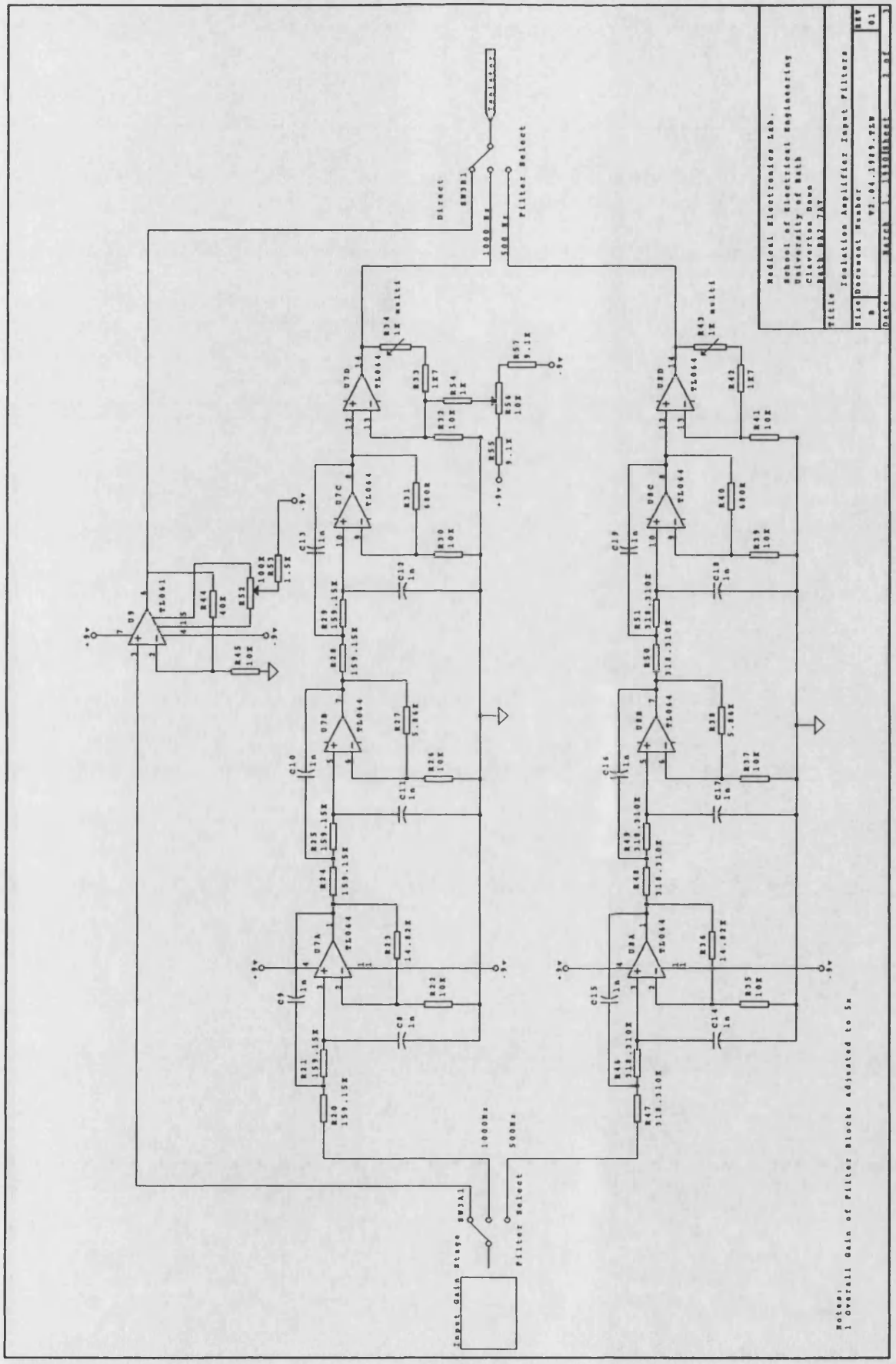

Figure G.22 *Input Filters*

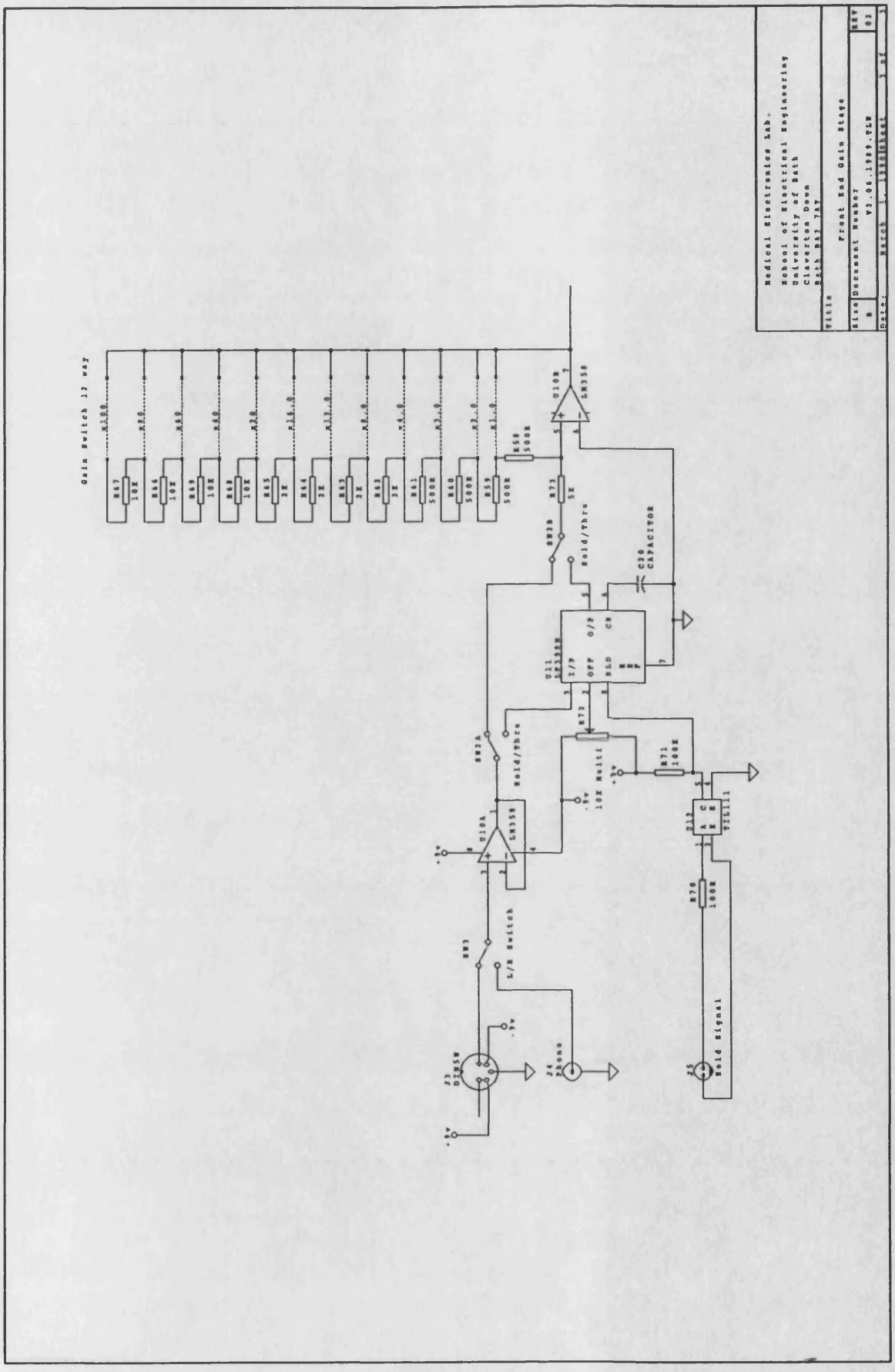

Figure G.23 *Front End Gain Stage*

G.10 Initial System

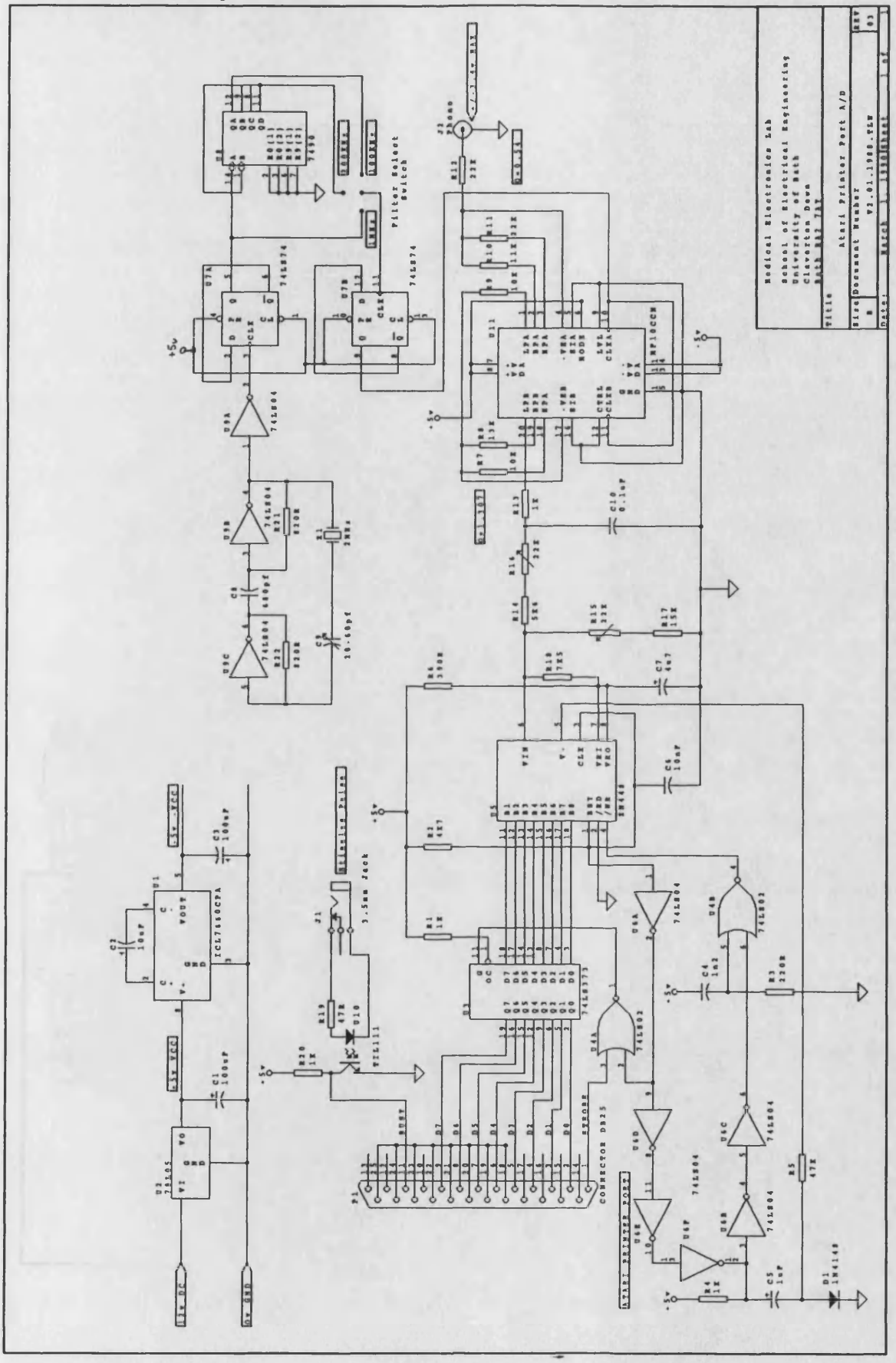

Figure G.24 *Atari Printer Port ADC*

G.11 Mega Expansion

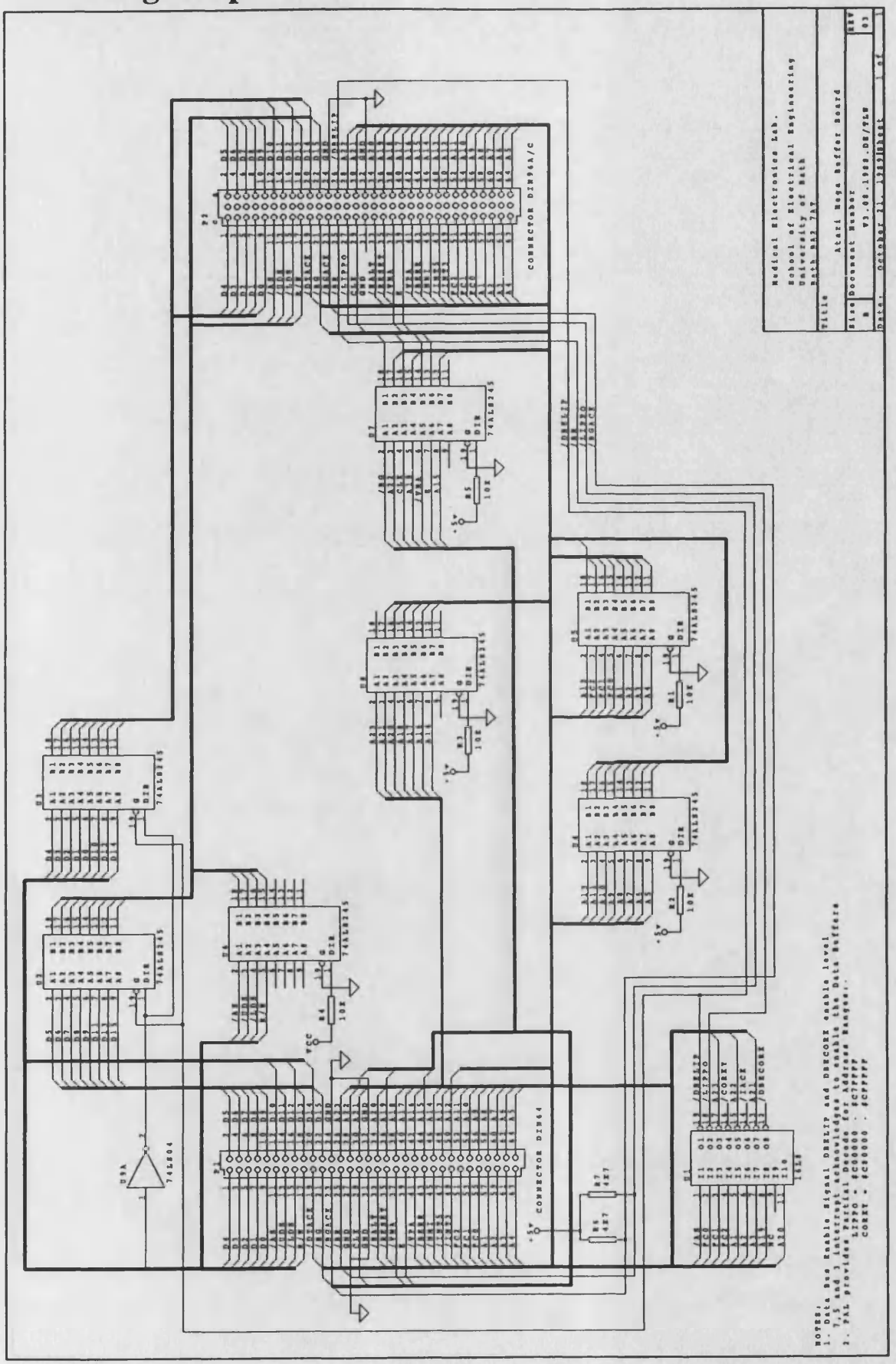

Figure G.25 *Atari Mega Internal Buffer Board*

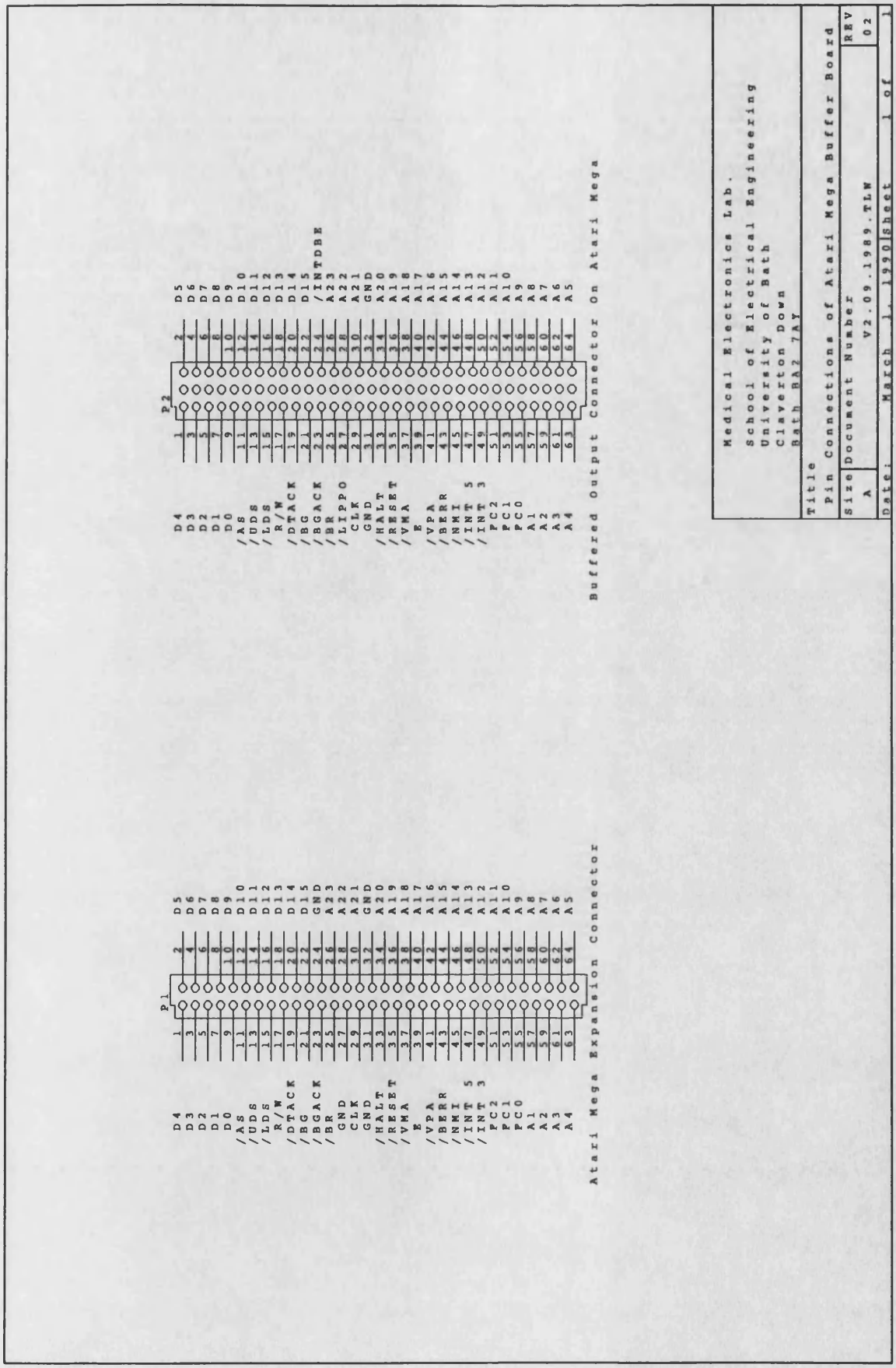

Figure G.26 *Pinouts for the Mega ST Connectors*

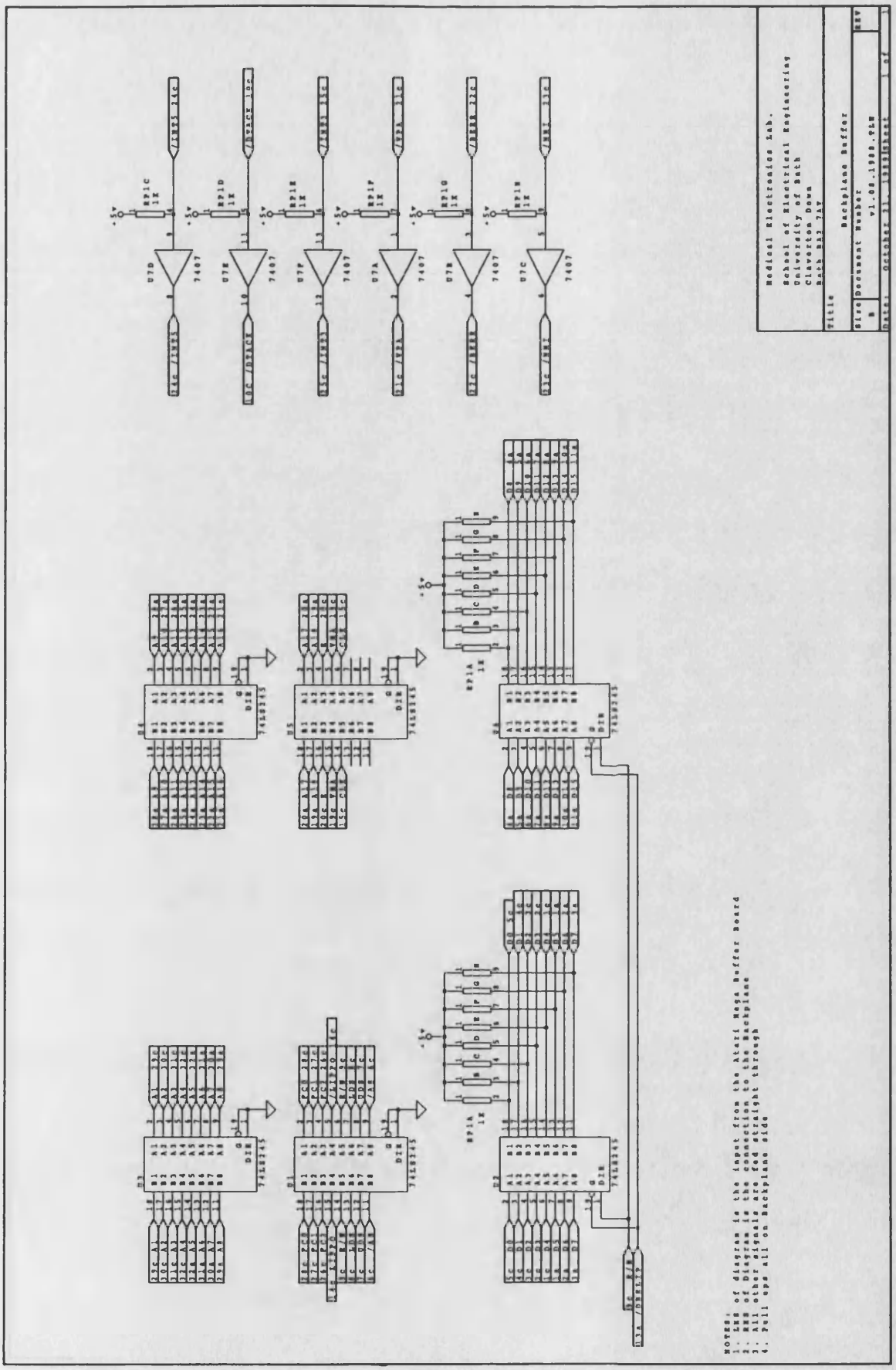

Figure G.27 *Buffering on to the Backplane of Rack*

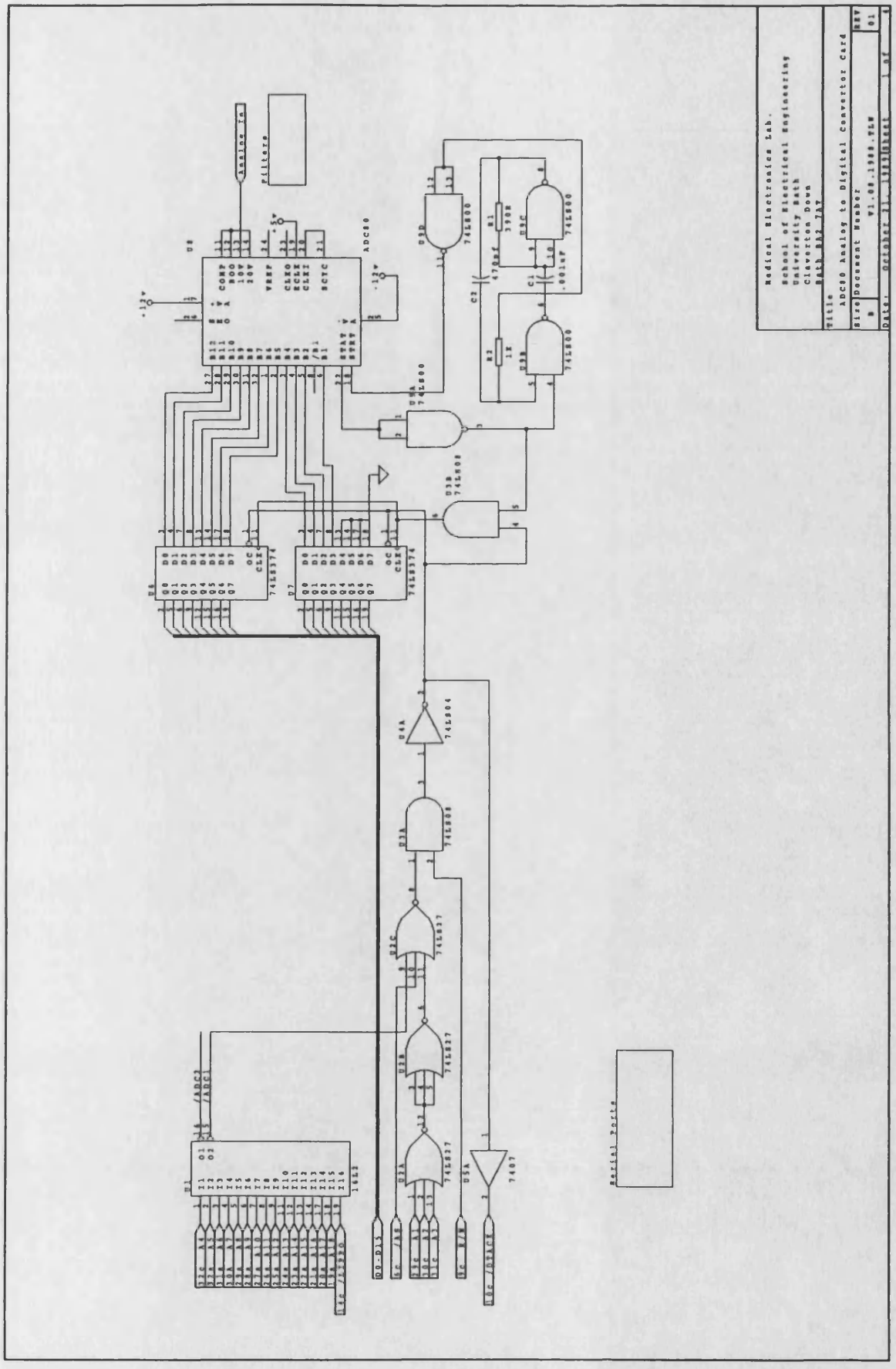

Figure G.28 *Expansion Bus ADC Card*

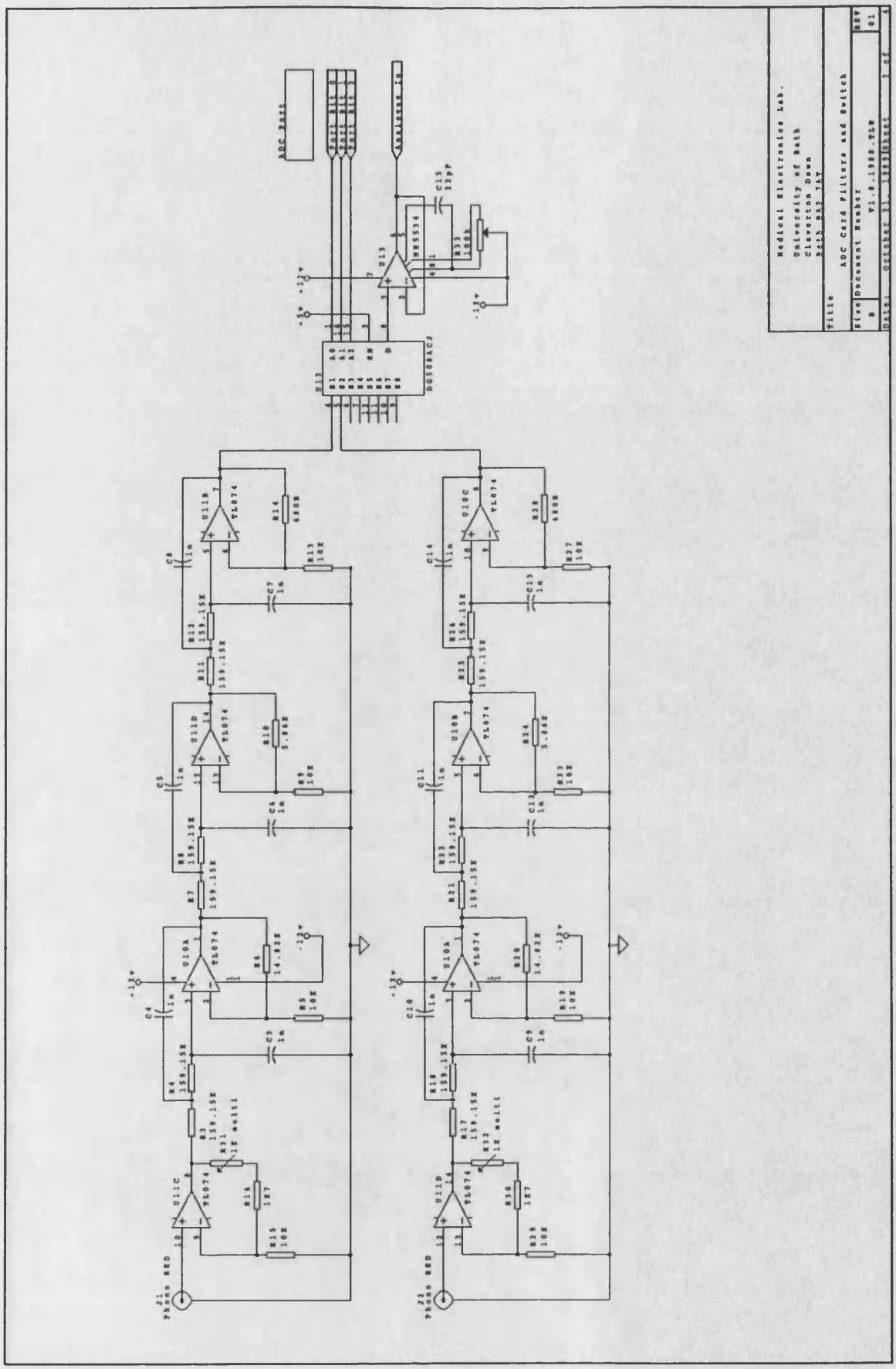

Figure G.29 *ADC Card Filters*

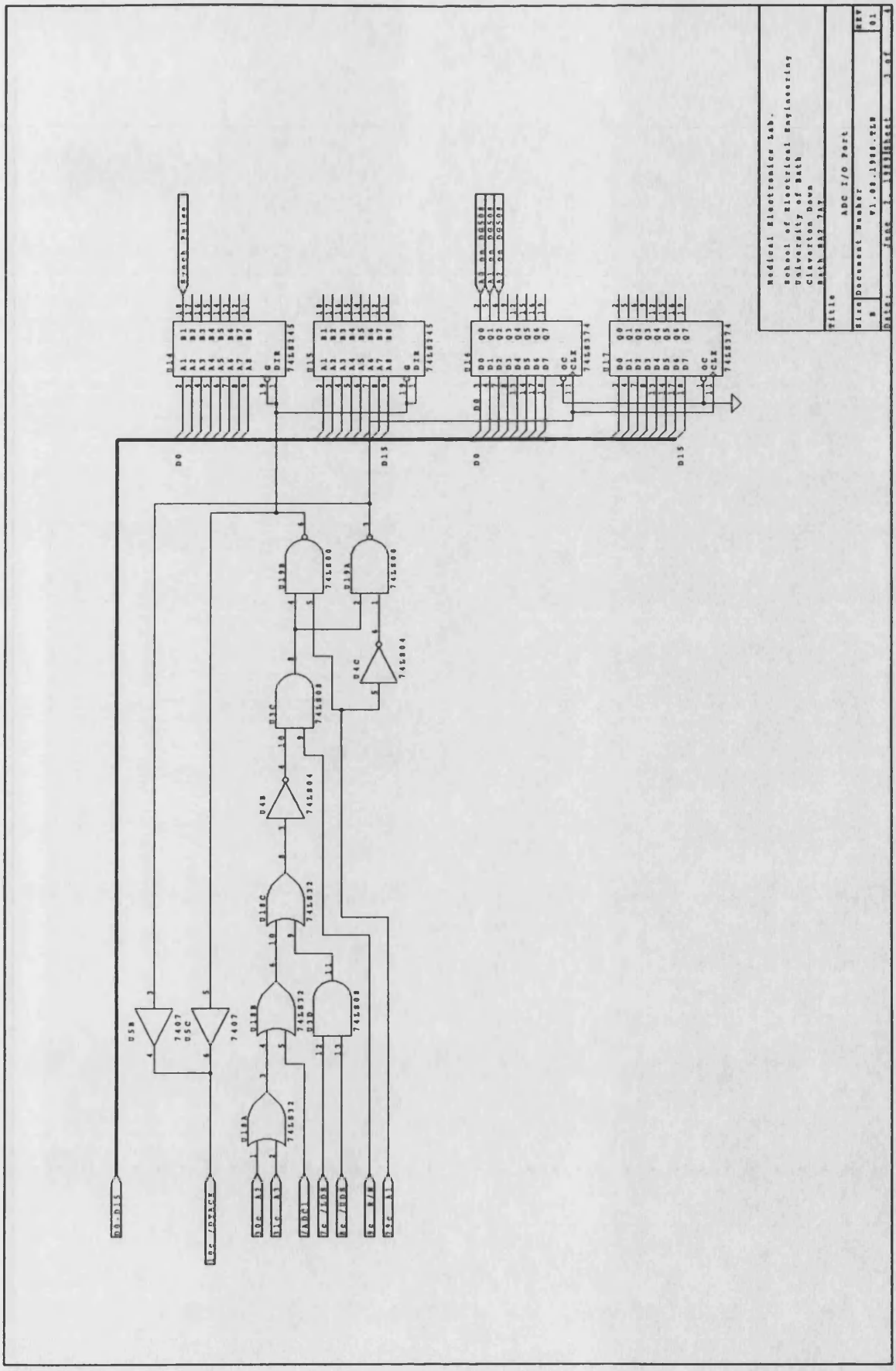

Figure G.30 *ADC I/O Port*

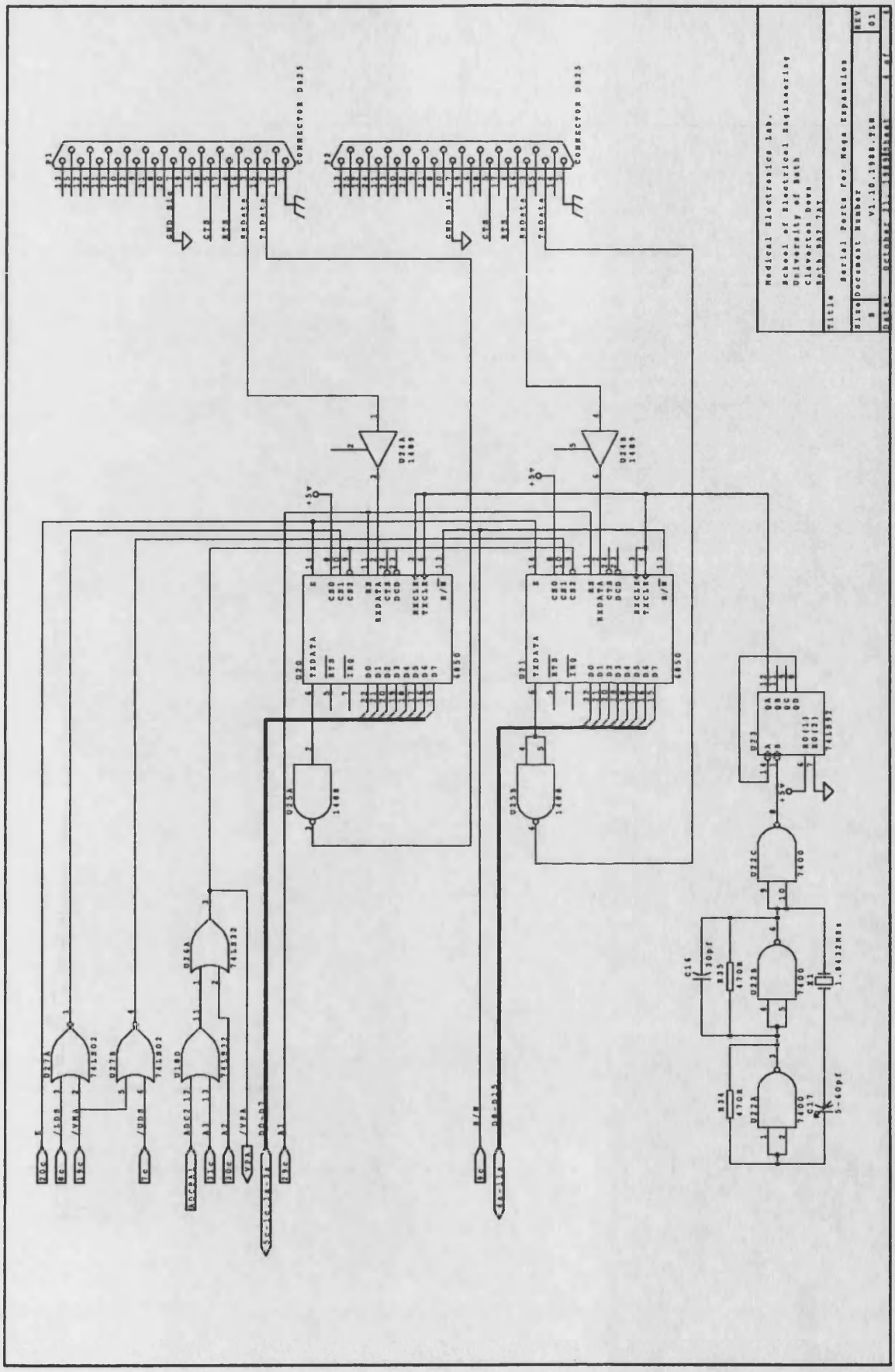

Figure G.31 *Expansion Bus Serial Ports*

G.12 DSP Interface Circuitry

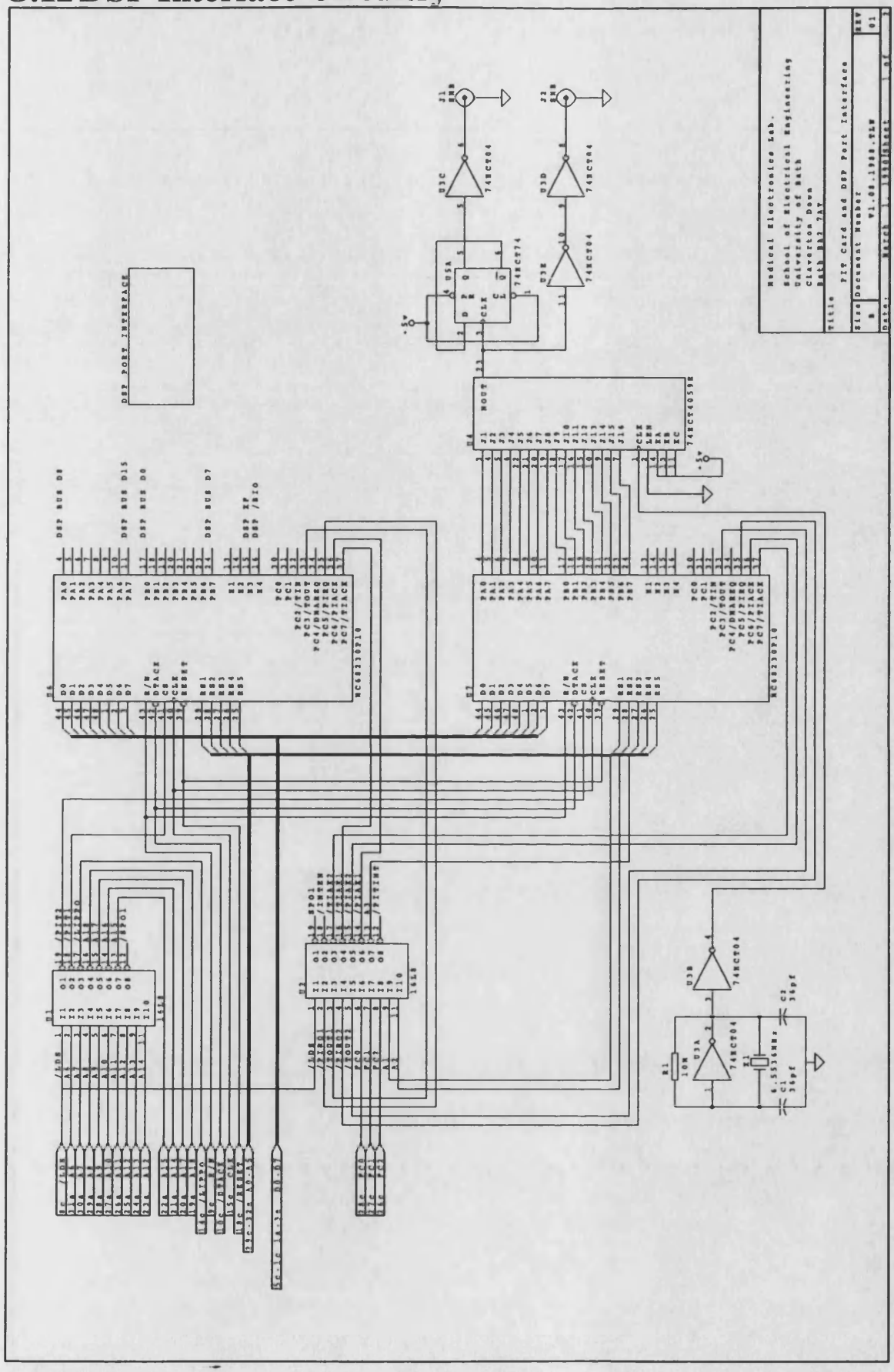

Figure G.32 *Expansion Bus PIT Card*

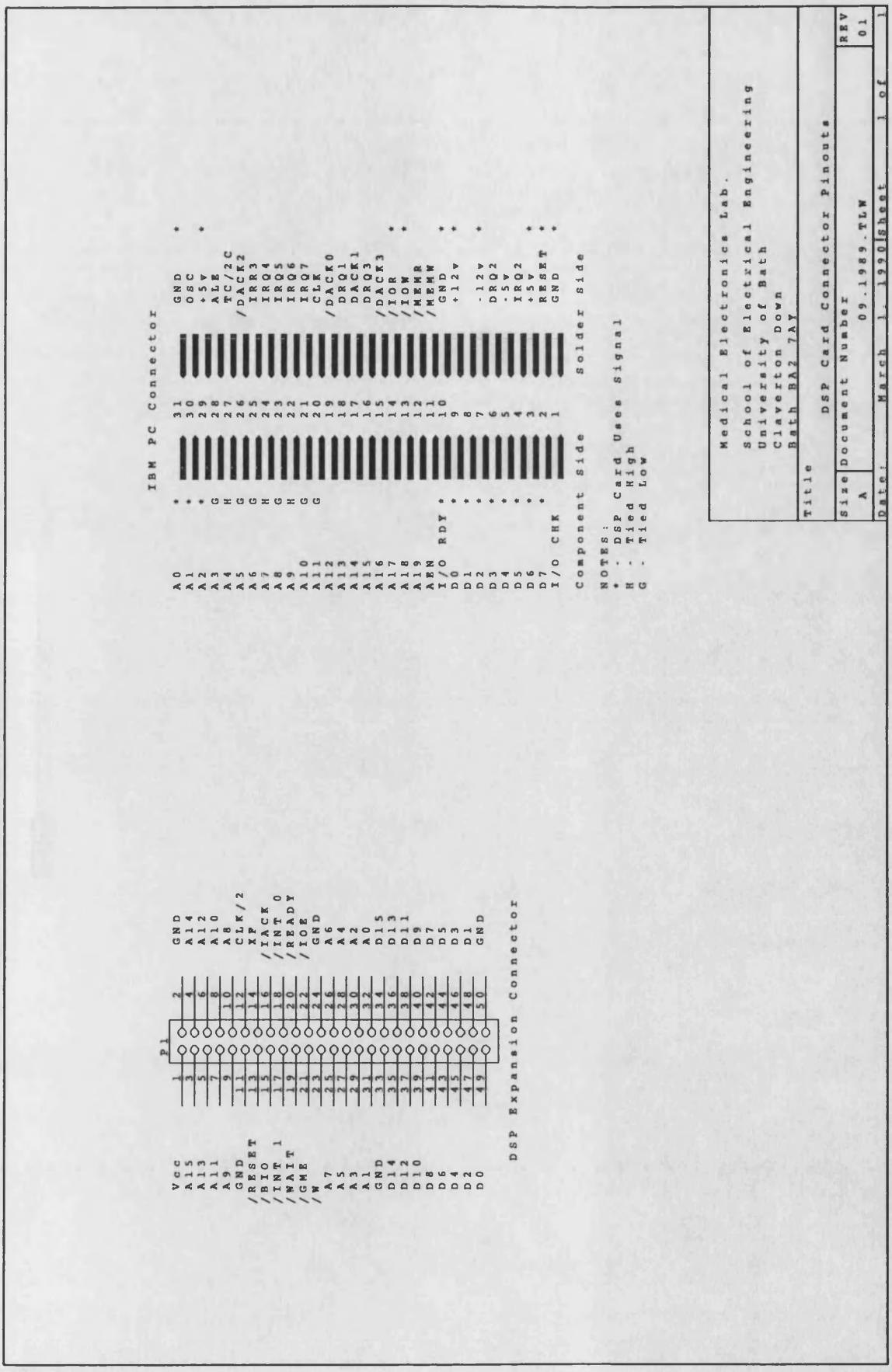

Figure G.33 *Interface Connections on DSP Card*

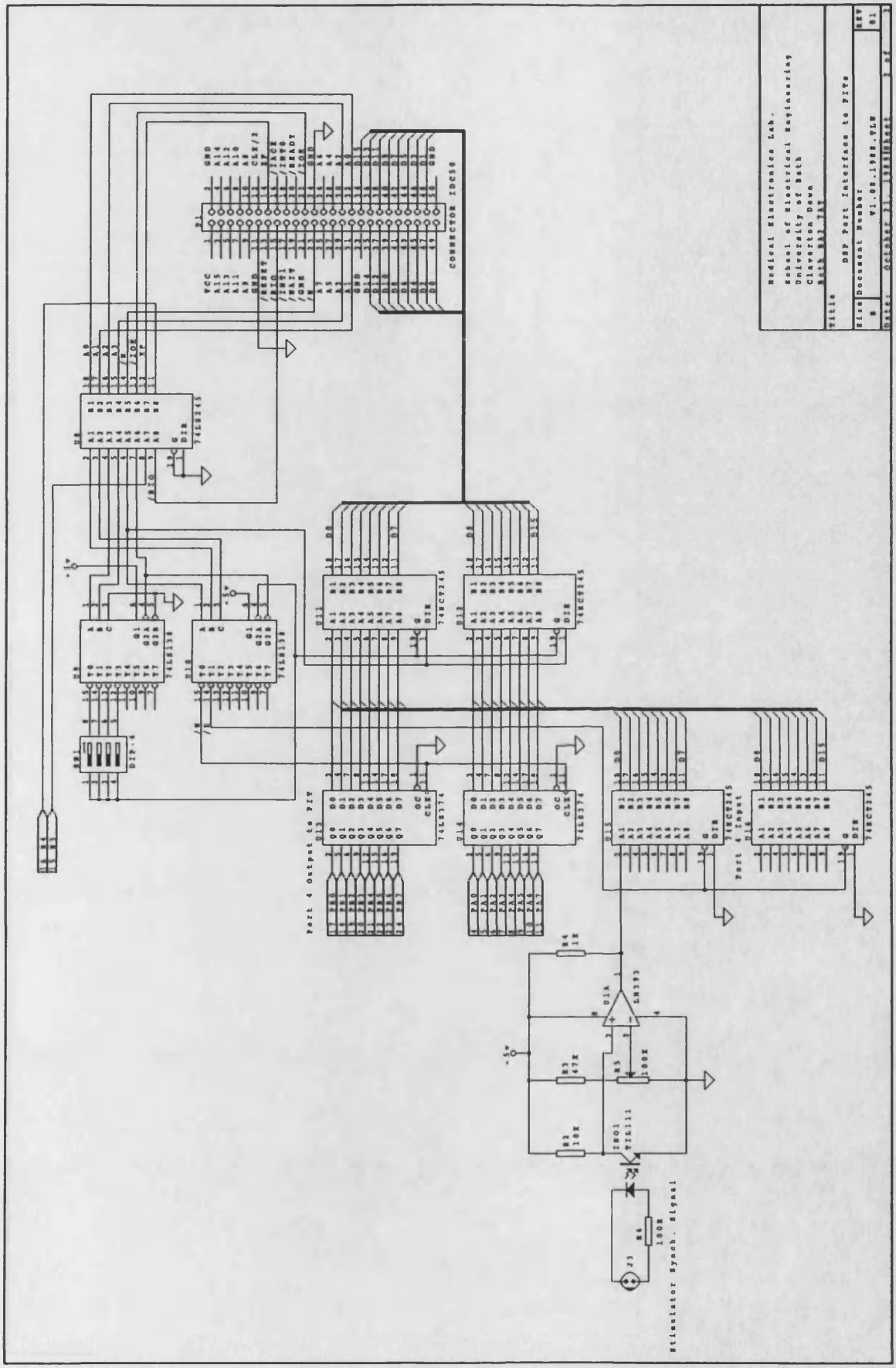

Figure G.34 *DSP Expansion Port Interface to PITs*

G.13 Strength Duration Tester

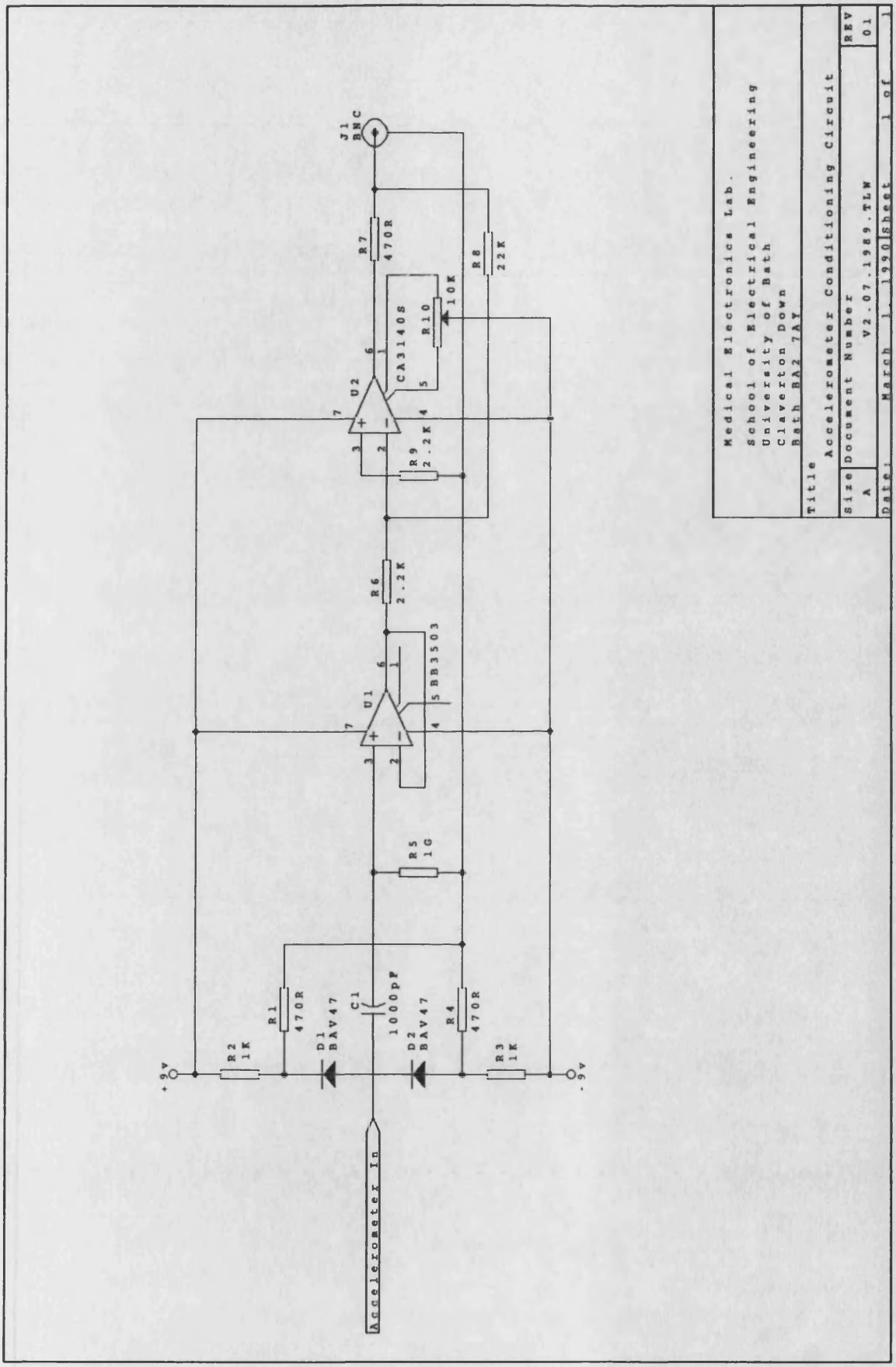

Figure G.35 *Accelerometer Conditioning Circuit*

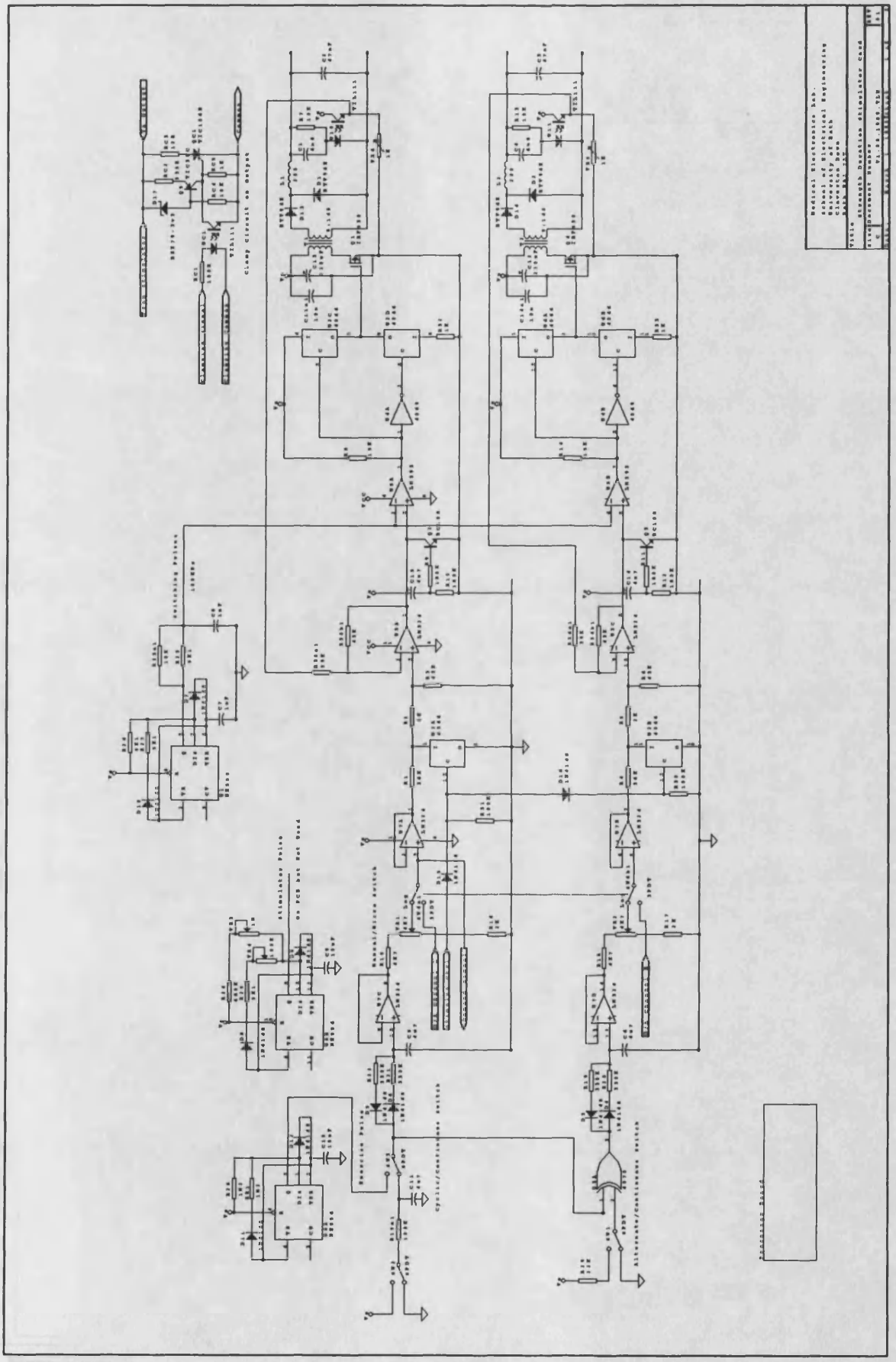

Figure G.36 *Strength-Duration Stimulator Card*

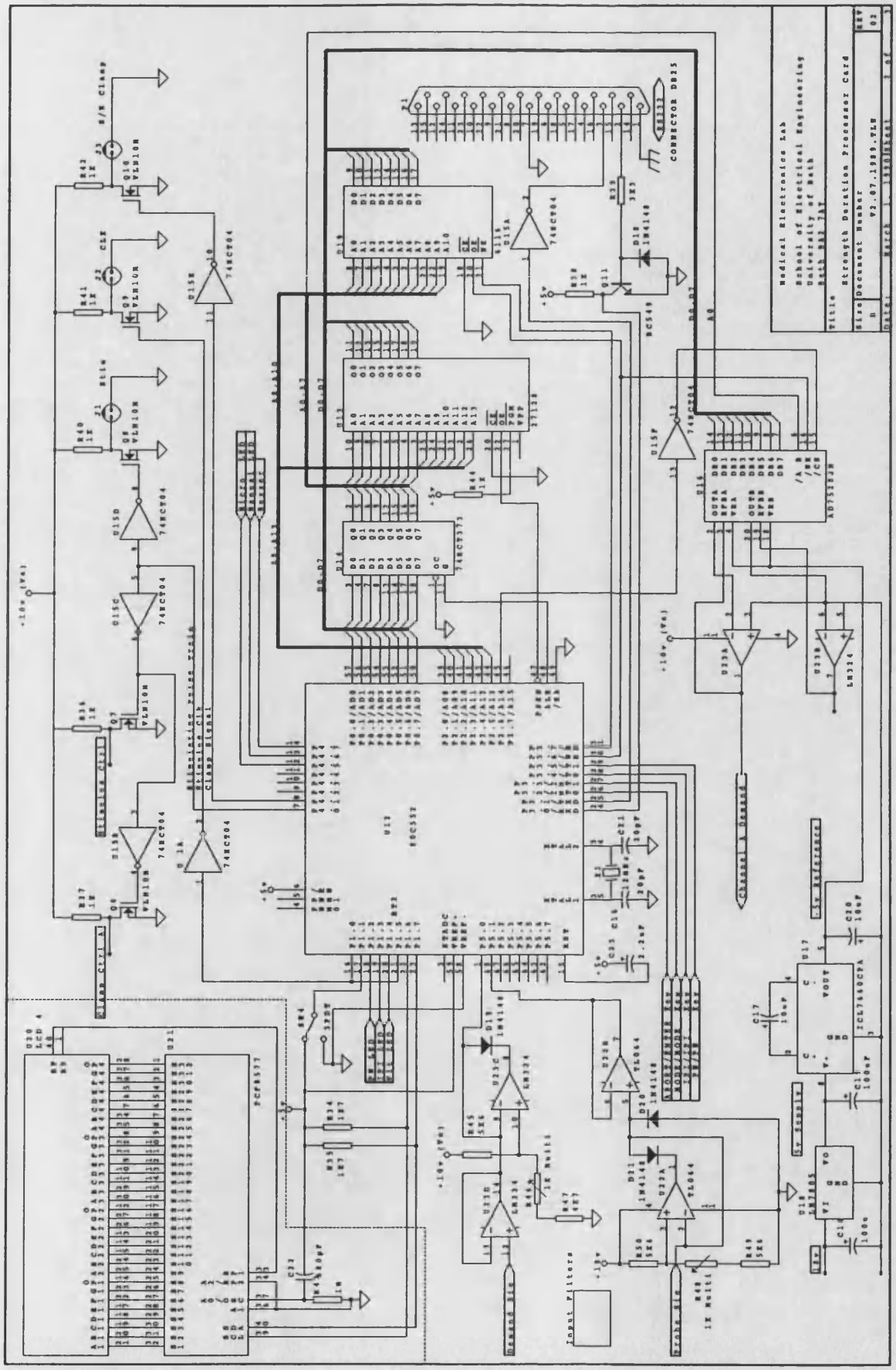

Figure G.37 *Strength -Duration Processor Card*

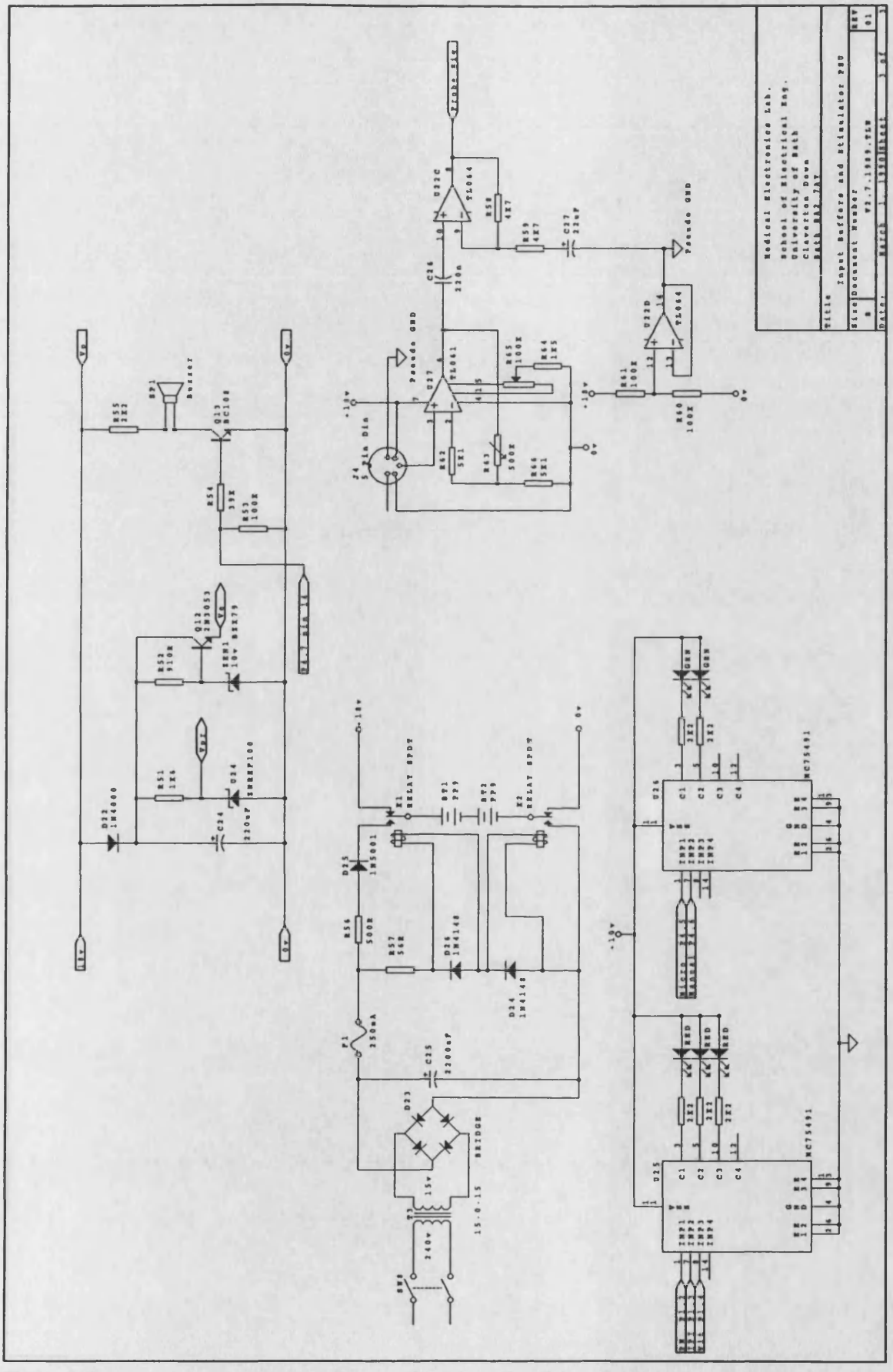

Figure G.38 *Input Buffers and Stimulator Power Supply*

G.14 Analogue Muscle Fatigue Monitor

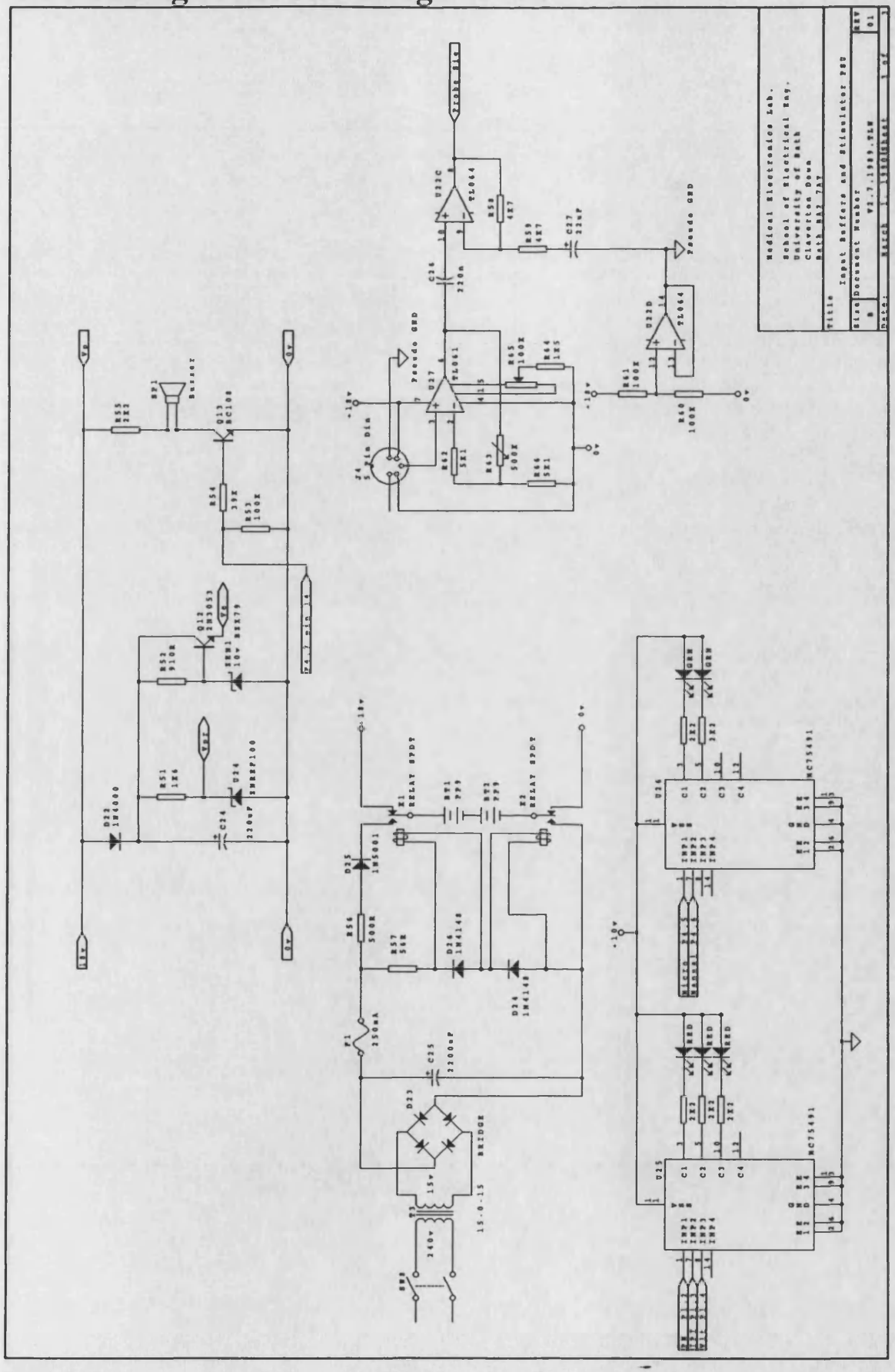

Figure G.39 *Power Supply and Input Filter Section*

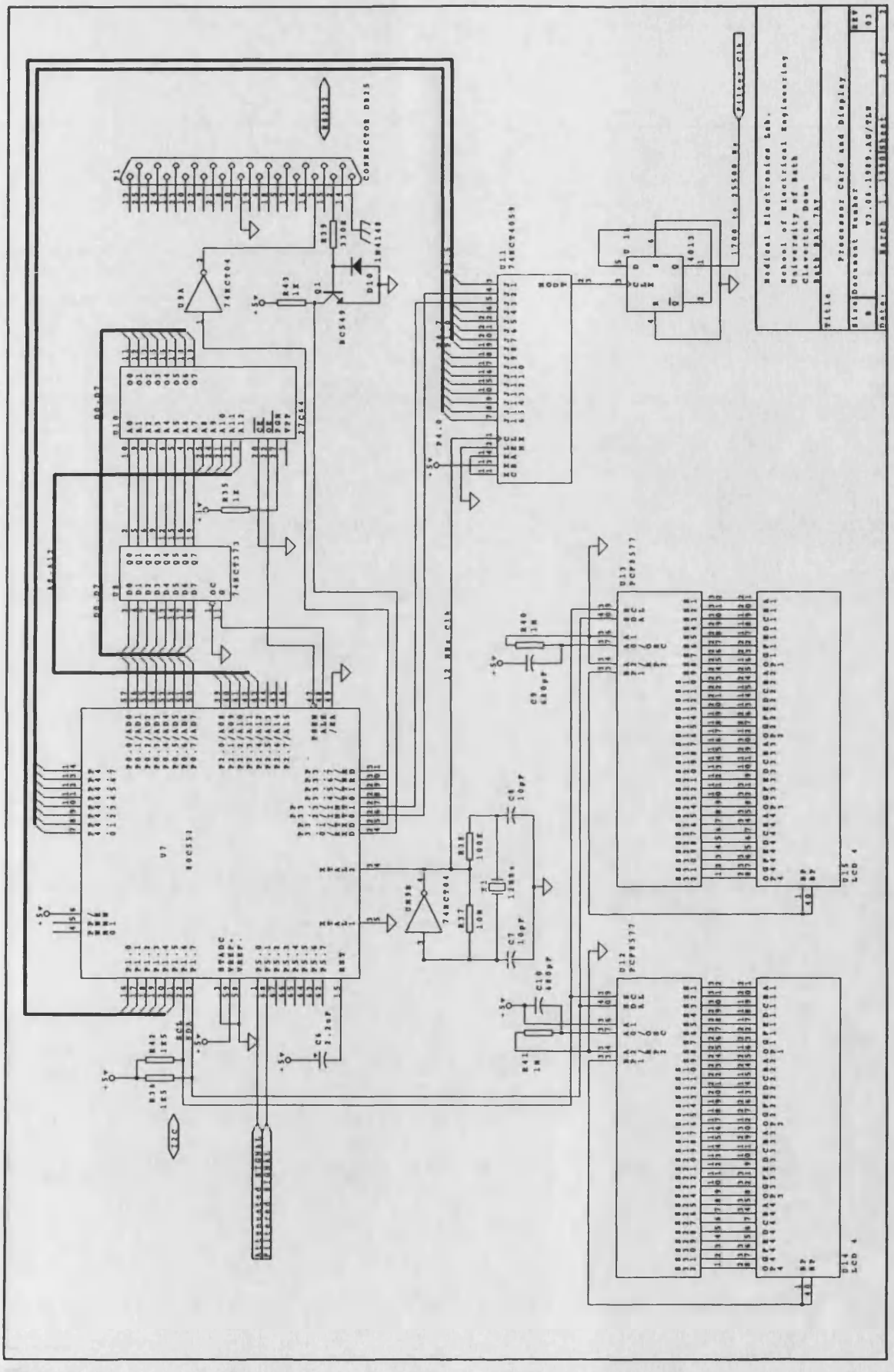

Figure G.40 *Microprocessor Control Card and Display Circuits*

G.15 Digital Muscle Fatigue Monitor

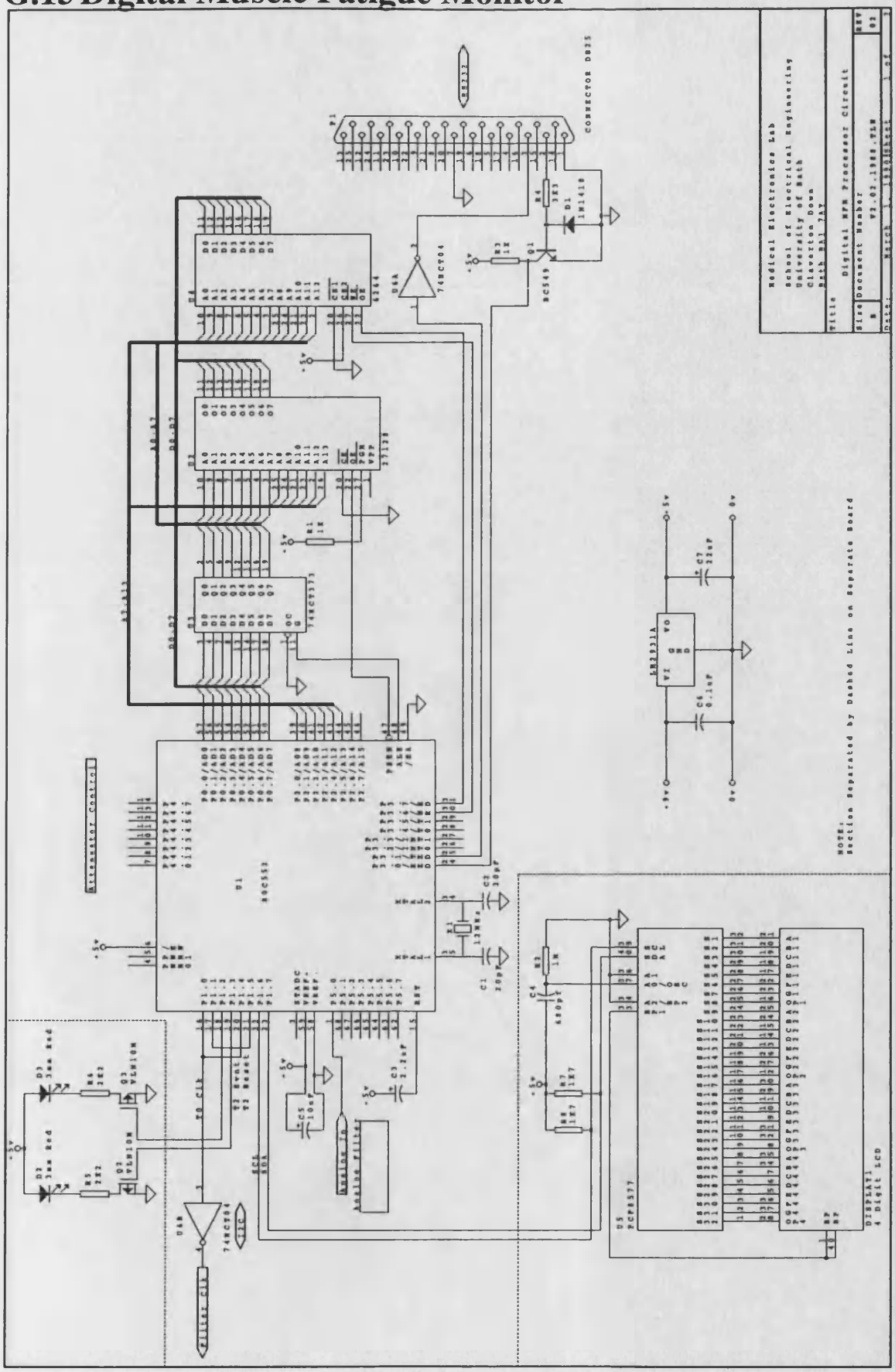

Figure G.41 *Digital Muscle Fatigue Processor Card and LCD Display*

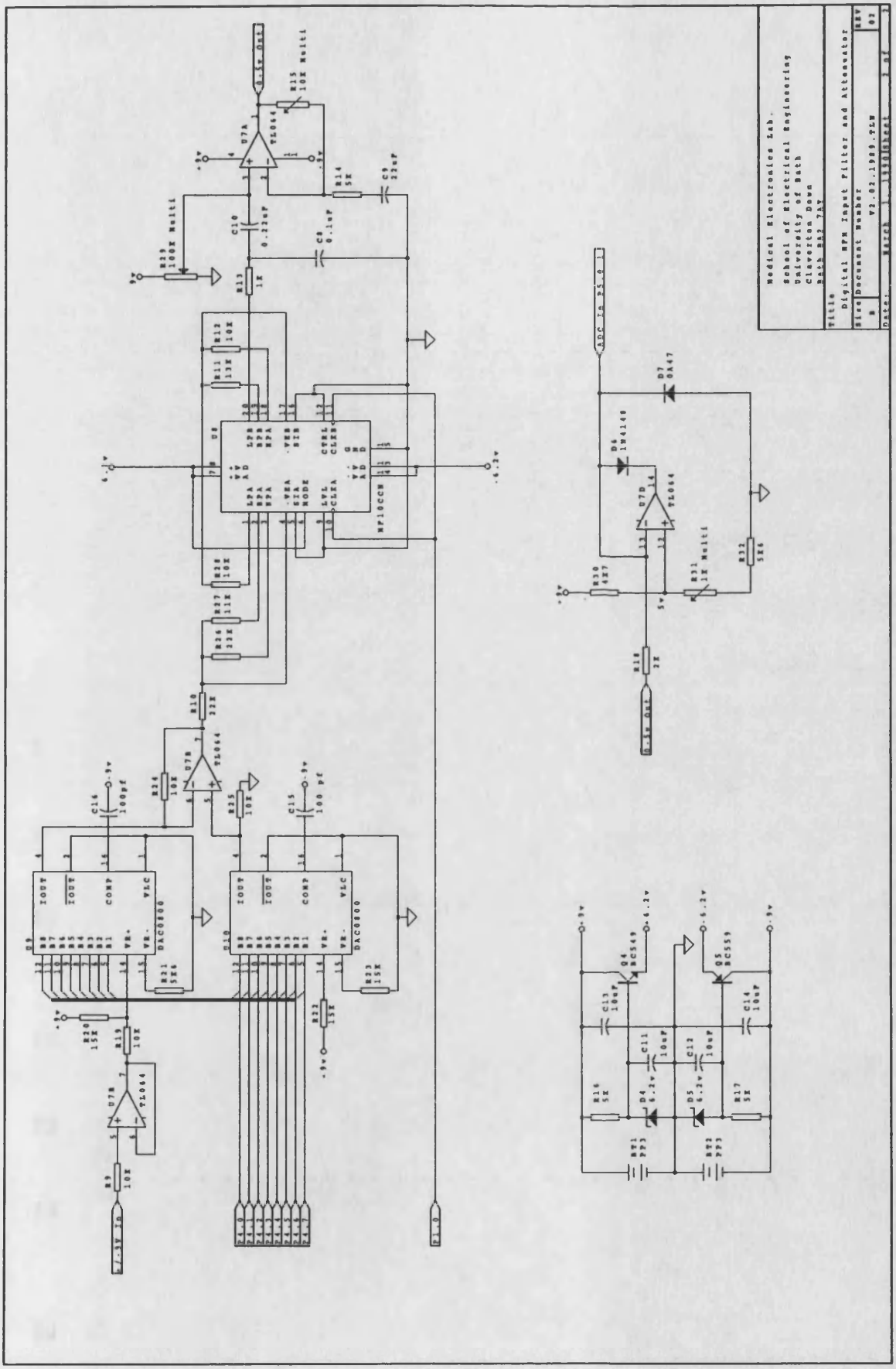

Figure G.42 *Input AGC , Filter Sections and ADC conditioning Circuits*

References

Chapter 1

1 A. Galvani "Deviribus electricitatis inmotu musculari" Commentarius De Bononiensi Scientarium et Artium Instituto atque Academia Commentarii vol. 7 p363 1791

2 A. Volta "On electricity excited by the mere contact of conducting substances of different kinds" Phil. Trans. vol. 90 p403 1800

3 J. V. Basmajian and C. J. De Luca "Muscles Alive Their Functions Revealed By Electromyography" Fifth Edition Williams and Wilkins 1985 ISBN 0-683-00414-X

4 D. Ottoson "Physiology of the Nervous System" The Macmillan Press Ltd. London 1983 ISBN 0-333-19464-0

5 H. Piper "Electrophysiologie Menschlicher Muskeln" Verlag von Julius Springer pp125-127 1911

6 C. Coërs and A. L. Woolf "The Innervation of Muscle, a Biopsy Study" Blackwell Scientific Publications, Ltd., Oxford and Charles C. Thomas, Springfield Ill. 1959

7 L. Reudi "Some Observations on the Histology and Function of Myoelectric Signals" Eds. P. Herberts Charles C. Thomas Springfield Ill. 1974

8 E. Bors "Ueber das Zahlenverhältnis zwischen Nerven—und Muskelfasern" Anat. Anz. vol. 60 pp14-416 1926

9 B. Feinstein, B. Lindegård, E. Nyman and G. Wohlfart "Morphological studies of motor units in human muscles" Acta Anat. vol. 23 pp127-142 1955

10 E. Stålberg and B. Theale "Motor Unit Fibre Density in the Extensor Digitorum Communis Muscle; Single Fibre Electromyographic Study in Normal Subjects at Different Ages" J. Neurol. Neurosurg. Psych. vol. 38 pp874-880 1975

11 F. Buchthal, C. Gould and P. RosenFalck "Multielectrode Study of the Territory of a Motor Unit" Acta Physiol. Scand vol. 39 83-104 1957

12 H. S. Milner-Brown and R. B. Stein "The Relation between the Surface Electromyogram and Muscular Force" J. Physiol. vol. 246 549-569 1975

13 L. Edström and E. Kugelberg "Histochemical Composition Distribution of Fibers and Fatigueability of Single Motor Units" J. Neurol. Neurosurg. Psychiatry vol. 31 pp424-433 1968

14 W. K. Engel "Fiber-Type Nomenclature of Human Skeletal Muscle for Histochemical Purposes" Neurology vol. 24 pp344-348 1974

15 R. E. Burke, D. N. Levine, F. E. Zajac, P. Tsairis, and W. K. Engel "Mammalian Motor Units: Physiological-Histochemical Correlation in Three Types in Cat Gastrocnemius" Science vol. 12 pp709-712 1971

16 M. A. Johnson, J. Polgar, D. Weightman and D. Appleton "Data on the Distribution of Fibre Types in Thirty-Six Human Muscles an Autopsy Study" J. of the Neurological Sciences vol. 18 pp111-129 1975

17 V. R. Edgerton, J. L. Smith and D. R. Simpson "Muscle Fibre Type Populations of Human Leg Muscles" Histochemical Journal vol. 7 pp259-266 1975

18 E. D. Adrian and D. W. Bronk "The Discharge of Impulses in Motor Nerve Fibres. Part II. The Frequency of Discharge in Reflex and Voluntary Contractions" J. Physiol. vol. 67 pp119-151 1929

19 E. Henneman, G. Somjen and D. O. Carpenter "Functional Significance of Cell Size in Spinal Motorneurons" J. Neurophysiol. vol. 28 pp560-580 1965

20 E. Henneman, and C. B. Olson "Relations Between Structure and Function in the Design of Cell Size in Spinal Motorneurons" J. Neurophysiol. vol. 28 pp581-598 1965

21 H. S. Milner-Brown, R. B. Stein, and R. Yemm "The Orderly Recruitment of Human Motor Units During Voluntary Isometric Contractions" J. Physiol. vol. 246 pp549-569 1973

22 L. Grimby and J. Hannerz "Firing Rate Recruitment Order of Toe Extensor Motor Units in Different Modes of Voluntary Contraction" J. Physiol. vol. 264 pp865-879 1977

23 H. S. Milner-Brown, R. B. Stein, and R. Yemm "Changes in Firing Rate of Human Motor Units During Linearly Changing Voluntary Contractions" J. Physiol vol. 230 pp371-390 1973

24 A. Gydikov, and D. Kosarov "Some Features of Different Motors Units in Human Biceps Brachii" Pflugers Arch. Ges. Physiol. vol. 347 pp75-88 1974

25 H. P. Clamann "Statistical Analysis of Motor Unit Firing Patterns in a Human Skeletal Muscle" Biophysical Journal vol. 9 pp1233-1251 1969

26 H. S. Milner-Brown, R. B. Stein, and R. Yemm "The Contractile Properties of Human Motor Units During Voluntary Isometric Contractions" J. Physiol. vol. 228 pp285-306 1973

27 R. S. LeFever, A. P. Xenakis, and C. J. De Luca "Firing Rate Modulation of Concurrently Active Motor Units" Proc. 4th Cong. of the Int. Soc. of Electrophysiol. Kinesiol. pp202-203 Aug. 1979

28 C. J. De Luca "A Model for a Motor Unit Train Recorded During Constant Force Isometric Contractions" Biol. Cybernetics vol. 19 pp159-167 1975

29 M. J. Aminoff "Electromyography in Clinical Practice" Churchill Livingstone Inc. NY 1987 ISBN 0-443-08419-X

30 A. Forster and N. Palastanga "Claytons Electrotherapy Theory and Practice" Ninth Edition Bailliere Tindall 1985 ISBN 0-7020-1100-2

Chapter 2

31 V. Dunfield and E. Shwedyk "Digital e.m.g. processor" Med. & Biol. Eng. & Comput. vol. 16 pp745-751 Nov. 1978

32 A. Thusnetapan and G. I. Zahalak "A Practical Electrode-Array Myoprocessor for Surface Electromyography" IEEE Trans. vol. BME-36 No. 2 pp295-299 Feb. 1989

33 D. Graupe, J. Magnussen and A. A. Beex "A Microprocessor System for Multifunctional Control of Upper-Limb Prostheses via Myoelectric Signal Identification" IEEE Trans. Auto. Con. vol. AC-23 No. 4 pp538-552 Aug. 1978

34 R. J. Triolo, D. H. Nash and G. D. Moskowitz "Application of Box-Jenkins criteria to the Identification of Time Serie Models of Lower Extremity EMG for the Control of Prostheses" Proc. 6th Annu. Conf. IEEE EMBS Los Angeles, CA pp597-602 Sept. 1984

35 R. J. Triolo, D. H. Nash and G. D. Moskowitz "The Identification of Time series Models of Lower Extremity EMG for the Control of Protheses Using Box-Jenkins Criteria" IEEE Trans. Biomed. Eng. vol. 15 No. 8 pp584-594 Aug. 1988

36 D. Graupe, J. Salahi and D. Zhang "Stochastic Analysis of Myoelectric Temporal Signatures for Multifunctional Single-site Activation of Protheses and Orthoses" J. Biomed. Eng. vol. 7 pp18-29 Jan. 1985

37 R. W. Fields "Electromyographically Triggered Electric Muscle Stimulation for Chronic Hemiplegia" Arch. Phys. Med. Rehabil. vol. 68 pp407-414 July 1987

38 G. Hefftner, W. Zucchini, and G. G. Jaros "The Electromyogram (EMG) as a Control Signal for Functional Neuromuscular Stimulation—Part I: Autoregressive Modeling as a Means of EMG Signature Discrimination" IEEE Trans. Biomed. Eng. vol. BME-35 No. 4 pp230-237 April 1988

39 G. Hefftner and G. G. Jaros "The Electromyogram (EMG) as a Control Signal for Functional Neuromuscular Stimulation—Part II: Practical Demonstration of the EMG Signature Discrimination System" IEEE Trans. Biomed. Eng. vol. BME-35 No. 4 pp238-242 April 1988

40 L. H. Lindström and R. I. Magnusson "Interpretation of Myoelectric Power Spectra: A Model and Its Applications" Proc. of the IEEE vol. 65 No.5 pp653-662 May 1977

41 R. Schoonhoven, D. F. Stegeman, A. Van Oosterom and G. F. M. Dautzenberg "The Inverse Problem in Electroneurography—I: Conceptual Basis and Mathematical Formulation" IEEE Trans. Biomed. Eng. vol. 35 No. 10 pp769-777 Oct. 1988

42 D. F. Stegeman, R. Schoonhoven, G. F. M. Dautzenberg, and J. Moleman "The Inverse Problem in Electroneurography—II: Computational Aspects and Evaluation Using Simulated Data" IEEE Trans. Biomed. Eng. vol. 35 No. 10 pp778-788 Oct. 1988

43 J. Allin and G. Inbar "FNS Control Schemes for the Upper Limb" IEEE Trans. Biomed. Eng. vol. BME-33 No. 9 pp818-828 Sept. 1986

44 H. J. Hermens, T. A. M. v. Bruggen, W. L. C. Rutten, G. Wilts, K. L. Boon, W. Wallinga- De Jonge and G. Zilvold "A Stochastic Model for Simulation of Surface EMG Patterns" Proc. 7th Cong. of Int. Soc. of Electrophysiol. Kinesiol. Enschede pp231-234 June 1988

45 M. H. Sherif, R. J. Gregor and J. Lyman "Effects of Load on Myoelectric Signals: The ARMA Representation" IEEE Trans. Biomed. Eng. vol. BME-28 No. 5 pp411-416 May 1981

46 J. L. F. Weytjens and D. van Steenberghe "The Effects of Motor Unit Synchronization on the Power Spectrum of the Electromyogram" Biol. Cybern. vol. 51 pp 71-77 1984

47 O. Paiss and G. F. Inbar "Autoregressive Modeling of Surface EMG and Its Spectrum with Application to Fatigue" IEEE Trans. vol. BME-34 No. 10 pp761-770 Oct. 1987

48 P. C. Doerschuk, D. E. Gustafson and A. S. Willsky "Upper Extremity Limb Function Discrimination using EMG Signal Analysis" IEEE Trans. Biomed. Eng. vol. BME-30 No. 1 pp18-28 Jan. 1983

49 M. H. Sherif, R. J. Gregor and J. Lyman "Comments on 'Upper Extremity Limb Function Discrimination Using EMG Signal Analysis'" IEEE Trans. Biomed. Eng. vol. BME-31 No. 5 pp440-441May 1984

50 R. J. Triolo and G. D. Moskowitz "Comments on 'Upper Extremity Limb Function Discrimination Using EMG Signal Analysis' and the Relationship Between Parallel-Filtering and Hypothesis-Testing Limb Function Classifiers" IEEE Trans. Biomed. Eng. vol. BME-32 No. 3 pp239-241 Mar. 1985

51 G. Balestra, M. Knaflitz and R. Merletti "Stationarity of Voluntary and Electrically Elicited Surface Myoelectric Signals" Proc. 7th Cong. of Int. Soc. of Electrophysiol. Kinesiol. Enschede pp275-278 June 1988

52 E. Kwatny, D. H. Thomas and H. G. Kwatny "An Application of Signal Processing Techniques to the Study of Myoelectric Signals" IEEE Trans. Biomed. Eng. vol. BME-17 No. 4 pp303-313 Oct. 1970

53 G. F. Inbar and A. E. Noujaim "On the Surface EMG Spectral Characterization and its Application to Diagnostic Classification" Trans. IEEE Biomed. Eng. vol. BME-31 No. 9 pp597- 604 Sept. 1984

54 J. S. Bendat and A. G. Piersol "Measurement and Analysis of Random Data" John Wiley and Sons Inc 1966

55 J. S. Bendat and A. G. Piersol "Random Data Analysis and Measurement Procedures" Wiley-Interscience 1971 ISBN 0-471-06470- X

56 E. Shwedyk, R. Balasubramanian and R. N. Scott "A Nonstationary Model for the Electromyogram" IEEE Trans. Biomed. Eng. vol. BME-24 No. 5 pp417-424 Sept. 1977

57 A. T. Barker, B. H. Brown and I. L. Freeston "Modeling of an Active Nerve Fiber in a Finite Volume Conductor and Its Application to the Calculation of Surface Action Potentials" IEEE Trans. Biomed. Eng. vol. BME-26 No.1 pp53-56 Jan. 1979

58 T. H. J. M. Gootzen, H. M. Vingerhoets and D. F. Stegeman "Volume Conductor Modeling of Motor Unit Action Potentials in the Surface Electromyogram" Proc. 7th Cong. of Int. Soc. of Electrophysiol. Kinesiol. Enschede pp227-230 June 1988

59 R. Schoonhoven, D. F. Stegeman, and A. Van Oosterom "The Forward Problem in Electroneurography II: Comparison of Models" IEEE trans. Biomed. Eng. vol. BME-33 No. 4 pp327-334 Mar. 1986

60 K. L. Cummins, L. J. Dorfman and D. H. Perkel "Nerve Fiber Conduction-Velocity Distributions II Estimation Based on Two Compound Action Potentials" Electroenceph. and Clin. Neurophys. vol. 46 pp647-658 1979

61 R. Schoonhoven, D. F. Stegeman, and J. P. C. De Weerd "The Forward Problem in Electroneurography I: A Generalised Volume Conductor Model" IEEE Trans. Biomed. Eng. vol. BME-33 No. 4 pp327-334 Mar. 1986

62 C. J. De Luca "Physiology and Mathematics of Myoelectric Signals" Trans. IEEE Biomed. Eng. vol. BME-26 No. 6 pp313-325 June 1979

63 T. W. Calvert and A. E. Chapman "The Relationship Between the Surface EMG and Force Transients in Muscle: Simulation and Experimental Studies" Proc. IEEE vol. 65 No. 5 pp682-689 May 1977

64 C. J. De Luca "Myoelectrical Manifestations of Localized Muscular Fatigue in Humans" CRC Critical Reviews in Biomed. Eng. vol. 11 No. 4 pp251-279

65 N. B. Jones and P. J. A. Lago "Spectral Analysis and the Interference EMG" IEE Proc. vol. 129 Pt. A No. 9 pp673-678 Dec. 1982

66 C. J. De Luca and W. J. Forrest "Some Properties of Motor Unit Action Potential Trains Recorded during Constant Force Isometric Contractions in Man" Kybernetik vol. 12 pp160-168 1973

67 C. J. De Luca and E. J. Vandyk "Derivation of some Parameters of Myoelectric Signals Recorded During Sustained Constant Force Isometric Contractions" Biophys. J. vol 15 pp1167-1180 1975

68 R. S. Le Fever and C. J. De Luca "The Contribution of Individual Motor Units to the EMG Power Spectrum" 29th ACEMB Boston p56 Nov. 1976

69 F. Q. Xiong and E. Shwedyk "Some Aspects of Nonstationary Myoelectric Signal Processing" IEEE Trans. Biomed. Eng. vol. BME- 34 No. 2 pp166-172 Feb. 1987

70 L. A. Bernotas, P. E. Crago and H. J. Chizeck "A Discrete-time model of electrically Stimulated Muscle" IEEE Trans. Biomed. Eng. vol. BME-33 No. 9 pp829-838 Sept. 1986

71 L. A. Bernotas, P. E. Crago and H. J. Chizeck "Adaptive Control of Electrically Stimulated Muscle" IEEE Trans. Biomed. Eng. vol. BME-34 No. 2 pp140-147 Feb. 1987

72 M. S. Hatwell and G. F. Inbar "A Model of the Leg Joints under Electrical Stimulation" IEEE Eighth Ann. Conf. of the Eng. in Med. and Biol. Soc. pp667-669 1986

73 Y. Iguchi, K. Kubo, N. Itakura and H. Minamitani "On the Multi-Joint Control of Lower Extremity using Functional Electrical Stimulation" Proc. 7th Cong. of Int. Soc. of Electrophysiol. Kinesiol. Enschede pp117-120 June 1988

74 J. Allin and G. Inbar "FNS Parameter Selection and Upper Limb Characterization" IEEE Trans. Biomed. Eng. vol. BME-33 No. 9 pp809-817 Sept. 1986

75 D. J. Ewins "Standing and Walking Systems for Paraplegics" PhD Thesis Bath University 1990.

76 D. Graupe, K. H. Kohn, A. Kralj and S. Basseas "Patient Controlled Electrical Stimulation via EMG Signature Discrimination for Providing certain Paraplegics with Primative Walking Functions" J. Biomed. Eng. vol. 5 pp220-226 July 1983

77 D. Graupe "Above-Lesions' EMG Pattern-Mapping for Controlling Electrical Stimulation of Paraplegics to Facilitate Unbraced Walker-Supported Walking" J. Orthopedic Surg. Tech. p61 1986

78 P. E. Crago, J. T. Mortimer and P. H. Peckham "Closed-Loop Control of Force During Electrical Stimulation of Muscle" IEEE Trans. vol. BME-27 No. 6 pp306-312

79 F. B. Stulen "A Technique for Monitoring Localized Muscular Fatigue using Frequency Domain Analysis of the Myoelectric Signal" Ph.D. Dissertation Massachusetts Inst. Technol. Cambridge, M.A. 1980

80 F. B. Stulen and C. J. De Luca "Frequency Parameters of the Myoelectric Signal as a Measure of Muscle Conduction Velocity" IEEE Trans. Biomed. Eng. vol. BME-28 No. 7 pp515-523 July 1981

81 D. Hary, M. J. Belman, J. Propst and S. Lewis "A statistical analysis of the spectral moments used in EMG test of endurance" J. Appl. Physiol. vol. 53 pp773-783 1982

Chapter 3

82 "Applied Neural Control Part 1" Special Issue IEEE Eng. in Med. and Biol. Magazine pp12-36 June 1983

83 "Applied Neural Control Part 2" Special Issue IEEE Eng. in Med. and Biol. Magazine pp29-49 Sept 1983

84 P. E. Crago, H. J. Chizeck, M. R. Neuman, and F. T. Hambrecht "Sensors for Use with Functional Neuromuscular Stimulation" IEEE Trans. Biomed. Eng. vol. BME-33 No. 2 pp256-268 Feb. 1986

85 N. Hogan and R. W. Mann "Myoelectric Signal Processing: Optimal Estimation Applied to Electromyography—Part I: Derivation of the Optimal Myoprocessor" IEEE Trans. Biomed. Eng. vol. BME-27 No. 7 pp382-395 July 1980

86 N. Hogan and R. W. Mann "Myoelectric Signal Processing: Optimal Estimation Applied to Electromyography—Part II: Experimental Demonstration of Optimal Myoprocessor Performance" IEEE Trans. Biomed. Eng. vol. BME-27 No. 7 pp396-410 July 1980

87 C. J. De Luca "The Common Drive of Motor Units" Proc. 7th Cong. of Int. Soc. of Electrophysiol. Kinesiol. Enschede pp35-38 June 1988

88 D. A. Winter, G. Rau, R. Kadefors, H. Broman and J. De Luca "Units, Terms and Standards in the Reporting of EMG Research" Report by the Ad Hoc Committee of the Int. Soc. of Electrophysiol. Kinesiol. Aug. 1980

89 J. J. Woods and B. Bigland-Ritchie "Linear and Non-Linear Surface EMG/Force Relationships in Human Muscles" Amer. J. of Phys. Med. vol. 62 No. 6 pp287-299 1983

90 J. H. Lawrence and C. J. De Luca "Myoelectric Signal versus Force Relationship in Different Human Muscles" Amer. Physiol. Soc. pp1653-1659 1983

91 C. W. Heckathorne and D. S. Childress "Relationships of the Surface Electromyogram to the Force, Length, Velocity and Contraction Rate of the Cineplastic Human Biceps" Amer. J. Phys. Med. vol. 60 No. 1 pp1-19 1981

92 A. J. Lloyd "Surface Electromyography during Sustained Isometric Contractions" J. Appl. Physiol. vol. 30 No. 5 pp713-719 May 1971

93 M. Solomonow, R. Baratta, B. H. Zhou, H. Shoji and R. D'Ambrosia "The EMG-Force Model of Electrically Stimulated Muscle: Dependence on Control Strategy and Predominant Fiber Composition" IEEE Trans. Biomed. Eng. vol. BME-34 No. 9 pp692-703 Sept. 1987

94 M. Solomonow, B-H Zhou, R. Barrata, H. Shoji and R. D'Ambrosia "EMG-Force Realtionships of a Skeletal Muscle as a Function of Recruitment Range" Proc. of 8th Annu. Conf. of the EMBS pp500-502 1986

95 D. Graupe, S. Basseas and J. Deng "EMG Response to Electrical Stimulation of Quadriceps in Upper-Motor-Neuron Paraplegics and its Employment to Control Levels of Stimulation at Onset of Fatigue" J. Orthopedic Surg. Tech. p61 1986

96 D. Graupe "EMG Pattern Analysis for Patient-Responsive Control of FES in Paraplegics for Walker-Supported Walking" IEEE Trans. Biomed Eng vol BME-36 No 7 pp711-720 July 1989

97 D. Hary, G. A. Bekey, and D. J. Antonelli "Circuit Models and Simulation Analysis of Electromyographic Signal Sources—I: The Impedance of EMG Electrodes" IEEE Trans. Biomed. Eng. vol. BME-34 No. 2 pp91-97 Feb. 1987

Correction to "Circuit Models and Simulation Analysis of Electromyographic Signal Sources—I: The Impedance of EMG Electrodes" IEEE Trans. Biomed. Eng. vol. BME-34 No. 9 p758 Sept. 1987

98 M. Maranzana Figini, G. Prato and R. Merletti "Repeatability of Surface E.M.G. Spectral Parameters in Normal Subjects" Proc. of 3rd Mediterranean Conf. on Biomed. Eng., Portoroz, Yugoslavia paper 1.4 1983

99 K. R. Mills "Power Spectral Analysis of Electromyogram and Compound Muscle Action Potential during Muscle Fatigue and Recovery" J. Physiol vol 326 pp401-409 1982

100 G. F. Inbar, J. Allin and H. Kranz "Surface EMG Spectral Changes with Muscle Length" Med. & Biol. Eng. & Comput. pp 683-689 Nov. 1987

101 L. Larsson "On the Relation between the EMG Frequency Spectrum and the Duration of Symptoms in Lesions of the Peripheral Motor Neuron" Electroenceph. and Clin. Neurophysiol. vol. 38 pp69-78 1975

102 R. Merletti, M. Knaflitz and C. J. De Luca "Muscle Fiber Conduction Velocity and EMG Spectral Parameters in Voluntary and Stimulated Contractions" Proc. 7th Cong. of Int. Soc. of Electrophysiol. Kinesiol. Enschede pp35-38 June 1988

103 P. A. Merton, D. K. Hill and H. B. Morton "Indirect and Direct Stimulation of Fatigued Human Muscle" 1981 Human Muscle Fatigue:Physiological Mechanisms. Pitman Medical London (Ciba Symposium 1982) pp120-129

104 B. Bigland-Ritchie "EMG and Fatigue of Human Voluntary and Stimulated Contractions" 1981 Human Muscle Fatigue:Physiological Mechanisms. Pitman Medical London (Ciba Symposium 1982) pp130-157

105 P. H. Veltink, J. A. van Alsté "Electrical Nerve Stimulation: Experiments and Simulations" Proc. 7th Cong. of Int. Soc. of Electrophysiol. Kinesiol. Enschede pp85-88 June 1988

106 H. Broman, G. Bilotto and C. J. De Luca "Myoelectric signal conduction velocity and spectral parameters: influence of force and time" J. Appl. Physiol. vol. 58 No. 5 pp1428-1437 1985

107 S. H. Roy, C. J. De Luca, and J. Schneider "Effects of Electrode Location on Myoelectric Conduction Velocity and Median Frequency Estimates" J. Appl. Physiol. vol. 61 No. 4 pp1510-1517 April 1986

108 G. R. Cybulski, R. D. Penn, and R. J. Jaeger "Lower Extremity Functional Neuromuscular Stimulation in Cases of Spinal Cord Injury" Neurosurgery vol. 15 No.1 pp132-146 1984

109 L. Lindström, R. Magnusson and I. Petersén "Muscular Fatigue and Action Potential Conduction Velocity changes Studied with Frequency Analysis of EMG Signals" Electromyography No. 4 pp341-356 1970

110 M. Naeije and H. Zorn "Estimation of the Action Potential Conduction Velocity in Human Skeletal Muscle using The Surface EMG Cross-Correlation Technique" Electromyogr. clin. Neurophysiol. vol. 23 pp73-80 1983

111 T. Bajd, A. Kralj, R. Turk, H. Benko and J. Šega "Use of Functional Electrical Stimulation in the Rehabilitation of Patients with Incomplete Spinal Cord Injuries" J. Biomed. Eng. vol. 11 pp96-102 Mar. 1989

112 P. E. Crago, P. Hunter Peckham and G. B. Thrope "Modulation of Muscle Recruitment During Intramuscular Stimulation" IEEE Trans. Biomed. Eng. vol. BME-27 No. 12 pp679-684 Dec. 1980

113 M. Malezic, U. Stanic, M. Kljajic, R. Acimovic, J. Krajnik, N. Gros and M. Stopar "Multichannel Electrical Stimulation of Gait in Motor Disabled Patients" Orthopedics vol. 7 No. 7 pp1187-1195 July 1984

114 J. Holle, M. Frey, H. Gruber, H. Kern, H. Stöhr and H. Thoma "Functional Electrostimulation of Paraplegics Exprerimental Investigations and First Clinical Experience with an Implantable Stimulation Device" Orthopedics vol. 7 No. 7 pp1145-1155 July 1984

115 D. J. Ewins, P. N. Taylor, S. E. Crook, R. T. Lipczynski and I. D. Swain "Practical Low Cost Stand/Sit System for Midthoracic Paraplegics" J. Biomed. Eng. Vol. 10 pp184-188 April 1988

116 D. J. Ewins, P. N. Taylor, T. L. Whitlock, B. A. Fox, R. T. Lipczynski and I. D. Swain "Practical closed loop stand/sit and walking systems for mid thoracic Paraplegics" Electrophysiological Kinesiology Proc. of the 7th Cong. of the Int. Soc. of Electrophysiological Kinesiology Enschede pp113-116 June 1988

117 A. J. Mulder, H. J. Hermens, J. A. van Alsté and G. Zilvold "An Improved Strategy to Minimize Muscle Fatigue during FES-Induced Standing" Proc. 7th Cong. of Int. Soc. of Electrophysiol. Kinesiol. Enschede pp109-112 June 1988

118 M. Pournezam, B. J. Andrews, R. H. Baxendale, G. F. Phillips and J. P. Paul "Reduction of Muscle Fatigue in Man by Cyclical Stimulation" J. Biomed. Eng. vol. 10 pp196-200 April 1988

119 G. L. Kidd and J. A. Oldham "An Electrotherapy based on the Natural Sequence of Motor Unit Action Potentials: A Laboratory Trial" Clinical Rehab. vol. 2 pp125-138 1988

120 J. H. Dale "Eutrophic Electrostimulation and Strengthening Exercises for Rehabilitation" Proc. BES Conf. on 'Electrical Stimulation of Muscle' Hexham General Hospital Jan. 1989

121 J. H. Dale Private Communication Jan. 1989

122 M. Solomonow, A. King, R. D'Ambrosia and H. Shoji "Dynamic Control of Muscle Force by High Frequency Electrostimulation" paper 1.2

123 M. Solomonow, B-H. Zhou, R. Baratta, H. Shoji. and R. D'Ambrosia "A New technique for Physiological Stimulation of Skeletal Muscle" Eighth Ann. Conf. of the Eng. in Med. and Biol. Soc. pp664-666 1986

124 B. H. Zhou, R. Baratta and M. Solomonow "Manipulation of Muscle Force with Various Firing Rate and Recruitment Control Strategies" IEEE Trans. Biomed. Eng. vol. BME-34 No. 2 pp128-139 Feb. 1987

Chapter 4

125 L. A. Geddes "Electrodes and the Measurement of Bioelectric Events" Wiley-Interscience 1972 ISBN 0-471-29490-X

126 H. A. Miller and D. C. Harrison (Eds) "Biomedical Electrode Technology theory and Practice" Academic Press Inc. NY 1974 ISBN 0-12-496850-4

127 L. A. Geddes "Interface Design for Bioelectrode Systems" IEEE Spectrum vol. 9 pp41-48 Oct. 1972

128 L. Cromwell, F. J. Weibell and E. A. Pfeiffer "Biomedical Instrumentation and Measurements" Prentice-Hall, Inc. 2nd Ed. 1980 ISBN 0-13-076448-5

129 G. E. Loeb and C. Gans "Electromyography for Experimentalists" Univ. of Chicago Press 1986 ISBN 0-226-49014-9

130 J. G. Webster, editor "Medical Instrumentation Application and Design" Houghton Mufflin Company Boston 1979 ISBN 0-395-25411-6

131 R. S. C. Cobbold "Transducers for Biomedical Measurements: Principles and Applications" J. Wiley & Sons, Inc. 1974 ISBN 0-471-16145-4

132 S. W. Johnson, P. A. Lynn, J. S. G. Miller and G. A. L. Reed "Miniature Skin Mounted Preamplifier for Measurement of Surface Electromyographic Potentials" Med. & Biol. Eng. & Comput. vol. 15 pp710-711 Nov. 1977

133 G. Rau, H. Reucher, J. Schneider and J. Silnay "Design and Application of Spatially Filtering EMG Electrode Configurations" Eighth Ann. Conf. of the Eng. in Med. and Biol.Soc. pp522-525 1986

134 G. E. Bergey, R. D. Squires, and W. C. Sipple "Electrocardiogram Recording with Pasteless Electrodes" IEEE Trans. vol. BME-18 No. 3 pp206-211 May 1971

135 W. H. Ko, M. R. Neuman, R. N. Wolfson and E. T. Yon "Insulated Active Electrodes" IEEE Trans. Ind. Elect. Contrl. Instr. IECL-17 pp195-197 1970

136 R. Nencini and E. Pasquali "Manganese Dioxide Electrodes for Stimulation and Recording" (Technical Note) Med & Biol. Engng. vol. 6 pp193-197 1968

137 P. C. Richardson "The Insulated Electrode" Proc. Ann Conf. Eng. Med. Biol. 1967 paper 15.7

138 C. J. De Luca, R. S. Le Fever and F. B. Stulen "Pasteless Electrode for Clinical Use" Med. & Biol. Eng. & Comput. vol. 17 pp387-390 May 1979

139 H. Reucher, G. Rau, and J. Silny "Spatial filtering of Noninvasive Multielectrode EMG:Part I-Introduction to Measuring Technique and Applications" IEEE Trans. Biomed. Eng. vol. BME-34 No. 2 pp98-105 Feb. 1987

140 H. Reucher, G. Rau, and J. Silny "Spatial Filtering of Noninvasive Multielectrode EMG:Part II—Filter Performance in Theory and Modeling" IEEE Trans. Biomed. Eng. vol. BME-34 No. 2 pp106-113 Feb. 1987

141 J. G. Webster Editor-in-Chief "Encylopedia of Medical Devices and Instrumentation" John Wiley & Sons, Inc. 1988 ISBN 0-471-82936-6

142 Y. Yamamoto, T. Yamamoto and T. Ozawa "Characteristics of Skin Admittance for Dry Electrodes and the Measurement of Skin Moisturisation" Med. & Biol. Eng. & Comput. vol. 24 pp71-77 Jan 1986

143 A. S. Berson and H. V. Pipberger "Skin-electrode impedance problems in electrocardiography" Amer. Heart J. vol. 76 No. 4 pp514-525 Oct. 1968

144 D. E. Wood "An AC coupled Skin Impedance Meter" B.Eng Project Report Dept. of Electronics and Computer Science University of Southampton May 1989

145 K. C. McGill, K. L. Cummins, L. J. Dorfman, B. B. Berlizot, K. Luetkemeyer, D. G. Nishimura and B. Widrow "On the Nature and Elimination of Stimulus Artifact in Nerve Signals Evoked and Recorded Using Surface Electrodes" IEEE Trans. vol. BME-29 No. 2 pp129-137 Feb. 1982

146 H. W. Tam and J. G. Webster "Minimizing Electrode Motion Artifact by Skin Abrasion" IEEE Trans. Biomed. vol. BME-24 No. 2 pp134-139 Mar. 1977

147 J. Rosell, J. Colominas, P. Riu, R. Pallas-Areny and J. G. Webster "Skin Impedance from 1 Hz to 1 MHz" IEEE Trans. Biomed. Eng. vol. BME-35 No. 8 pp649-651 Aug. 1988

148 A. M. Dymond "Characteristics of the Metal-Tissue Interface of Stimulation Electrodes" IEEE Trans. Biomed. Eng. vol. BME-23 No. 4 pp274-280 July 1976

149 T. Masuda H. Miyano and T. Sadoyama "The Position of Innervation Zones in the Biceps Brachii Investigated by Surface Electromyography" IEEE Trans. Biomed. Eng. vol. BME-32 No. 1 pp36-42 Jan 1985

150 P. Zipp "Effect of Electrode Parameters on the Bandwidth of the Surface EMG Power Density Spectrum" Med. & Biol. Eng. & Comput. vol. 16 pp537-541 Sept. 1978

151 W. D. McLeod, H. N. Nunnally and P. E. Cantrell "Dependence of EMG Power Spectra on Electrode Type" IEEE Trans. Biomed. vol. BME-23 pp172-175 No. 3 Mar. 1976

152 J. A. de Kreek, J. Harlaar and H. Bakker "Surface EMG: The Effect of Electrode Configuration Parameters" Proc. 7th Cong. of Int. Soc. of Electrophysiol. Kinesiol. Enschede pp235-239 June 1988

153 P. A. Lynn, N. D. Bettles, A. D. Hughes and S. W. Johnson "Influence of Electrode Geometry on Bipolar Recordings of the Surface Electromyogram" Med. & Biol. Eng. & Comput. vol 16 pp651-660 Sept. 1978

154 P. Strong "Biophysical Measurements" Textronic Inc. 1973

155 W. G. Crosier and R. C. Lee "Multipurpose EOG/ECG/EMG Electrophysiological Amplifier" IEEE Fronitiers of Eng. and Comput. On Health Care pp327-330 1984

156 L. L. Huntsman and G. L. Nichols "A Low-Cost High-Gain Amplifier with Exceptional Noise Performance" (Short Commun.) IEEE Trans. Biomed. vol. BME-18 pp301-302 July 1971

157 M. Solomonow, R. Baratta, T. Miwa, H. Shoji and R. D'Ambrosia "A Technique for Recording the EMG of Electrically Stimulated Skeletal Muscle" Orthopedics Vol 8 No.4 pp492-495 Apr. 1985

158 J. G. Webster "Interference and Motion Artifact in Biopotentials" IEEE Region 6 Conference Record pp53-64 1977

159 M. L. Wolbarsht and H. Spekreijse "Biological Instrumentation" in Advan. Biomed. Eng. Med. Phys. vol 2 pp206-242 1968.

160 B. B. Winter and J. G. Webster "Reduction of Interference Due to Common Mode Voltage in Biopotential Amplifiers" IEEE Trans. Biomed. Eng. vol. BME-30 No. 1 pp58-62 Jan. 1983

161 M. Solomonow, R. Baratta, H. Shoji, and D. D'Ambrosia "The Myoelectric Signal of Electrically Stimulated Muscle during Recruitment: An Inherent Feedback Parameter for a Closed-Loop Control Scheme" IEEE Trans. Biomed. Eng. vol. BME-33 No. 8 pp735-745 Aug. 1986

162 J. Li, E. Zheng and C. Peng "A Multichannel Low-Level-Signal Amplifier for SHBE" Procs.of the Eighth Ann. Conf. of Eng. in Med. and Biol. Soc. p497-499 1986

163 H. W. Smit, K. Verton and C. A. Grimbergen "A Low-Cost Multichannel Preamplifier for Physiological Signals" IEEE Trans. Biomed. Eng. vol. BME-34 No. 4 pp307-310 Apr. 1987

164 C. G. Burgar and J. D. Rugh "An EMG Integrator for Muscle Activity Studies in Ambulatory Subjects" IEEE Trans. Biomed. Eng. vol. BME- 30 No. 1 pp66-70 Jan. 1983

165 M. Knaflitz and R. Merletti "Suppression of Stimulation Artifacts from Myoelectric-Evoked Potential Recordings" IEEE Trans. Biomed. Eng. vol. BME-35 No. 9 pp758-763 Sept. 1988

166 R. Merletti, D. Biey, M. Biey, G. Prato and A. Orusa "A Monitor of Surface EMG Median Frequency" IEEE Frontiers of Eng. and Comput. in Health Care pp170-174 1983

167 R. Merletti, D. Biey, M. Biey, G. Prato and A. Orusa "On-Line Monitoring of the Median Frequency of the Surface EMG power Spectrum" IEEE Trans. Biomed. Eng. Vol BME-32 No 1 pp 1-7 Jan. 1985

168 J. C. Huhta and J. G. Webster "60-Hz Interference in Electrocardiography" IEEE Trans. Biomed. Eng. vol. BME-20 No. 2 pp91-101 Mar. 1973

169 M. A. Tooley, L. J. Grant and A. R. Davies "A Microprocessor Based Instrument for the Spectral Analysis of the EEG in Anaesthesia" Clin. Phys. Physiol. Meas. vol. 5 No. 4 pp303-311 1984

170 W. J. Tompkins and J. G. Webster (eds) "Design of Microcomputer Based Medical Instrumentation" Prentice-Hall Inc. 1981 ISBN 0-13-201244-8

171 B. B. Winter and J. G. Webster "Driven Right-Leg Circuit Design" IEEE Trans. Biomed. Eng. vol. BME-30 No. 1 pp62-66 Jan. 1983

172 A. Miller "Coupling Circuit with Driven Guard" Mar. 4 1980 U.S. Patent 4 191 195 1985

173 J. S. Coombs "Some Methods of reducing Interference caused by Stimulus Artifacts" in D. R. Curtis and A. K. McIntyre (Eds) Studies in Physiology Springer-Verlag New York pp29-33 1965

174 R. Baratta, M. Ichie, S. Hwang and M. Solomonow "Method for Studying Muscle Properties under Orderly Stimulated Motor Units with Tripolar Nerve Cuff Electrode" J. Biomed.Eng. vol. 11 pp141- 147 Mar. 1989

175 H. Broman, G. Bilotto and C. J. De Luca "A note on noninvasive estimation of muscle fiber conduction velocity" IEEE Trans. Biomed. Eng. vol. BME-32 No. pp341-344 1985

176 A. Peper and C. A. Grimbergen "EEG Measurement During Electrical Stimulation" IEEE Trans. Biomed. Eng. vol. BME-30 No. 4 pp231-234 Apr. 1983

177 F. Del Pozo and J. M. R. Delgado "Hybrid Stimulator for Chronic Experiments" IEEE Trans. vol. BME-25 No. 1 pp92-94 Jan. 1978

178 C. Guld "The Reduction of Stimulus Interference in Electrophysiology" Proc. of Third Int. Conf. on Med. Electronics pp103-105 July 1960

179 V. O. Andersen and F. Buchthal "Low Noise Alternating Current Amplifier and Compensator to Reduce Stimulus Artefact" Med. & Biol. Engng. vol. 8 pp501-508 1970

180 D. D. Walker and J. Kimura "A Fast-Recovery Electrode Amplifier for Electrophysiology" Electroen. and Clin. Neurophysiol. vol. 45 pp789-792 1978

181 J. A. Freeman "An Electronic Stimulus Artifact Suppressor" Electroenceph. and Clin. Neurophysiol. vol. 31 pp170-172 1971

182 R. J. Roby and E. Lettich "A Simplified Circuit for Stimulus Artifact Suppression" Electroenceph. and Clin. Neurophysiol. vol. 39 pp85-87 1975

183 T. L. Babb, E. Mariani, G. M. Strain, J. P. Lieb, H. V. Soper and P. H. Crandall "A Sample and Hold Amplifier System for Stimulus Artifact Suppression" Electroenceph. and Clin. Neurophysiol. vol. 44 pp528-531 1978

184 E. Roškar and A. Roškar "Microcomputer based Electromyographic Recording System with Stimulus Artefact Suppression" III Mediterranean Conf. on Biomed. Eng. pp1.6-1.7 Portoroz 1983

185 Z. L. Kovacs "Filtering the Stimulus Artefact in Recordings from Nerves" Procs. of 31st ACEMB Atlanta Georgia p269 Oct. 1978

186 D. E. Newland "An Introduction to Random Vibrations and Spectral Analysis" Second Edition Longamn Group Ltd 1984 ISBN 0-582-30530- 6

187 A. Papoulis "Probability, Random Variables, and Stochastic Processes" Second Edition McGraw-Hill Inc. 1984 ISBN 0-07-048468-6

188 G. R. Cooper and C. D. McGillem "Probalisitic Methods of Signal and System Analysis" Second Edition CBS Publishing Japan Ltd. 1986 ISBN 0-03-910734-5

Chapter 5

189 "Single-Chip 8-Bit Microcontrollers User Manual" 1988 Philips Technical Publication No. 9398 638 20011

190 "Single-Chip 8-Bit Microcontrollers PCB83C552 User Manual" 1988 Philips Technical Publication No. 9398 637 90011

Chapter 7

191 "TMS320C25 PC Board User Manual" Issue 3 Loughborough Sound Images Ltd Feb. 1988

192 G. D. Bergland "A Guided Tour of the Fast Fourier Transform" IEEE Spectrum pp41-52 July 1969

193 W. T Cochran, J. W. Cooley, D. L. Favin, H. D. Helms, R. A. Kaenal, W. W. Lang, G. C. Maling, D. E. Nelson, C. M. Radar and P. D. Welch "What is the Fast Fourier Transform ?" IEEE Trans. Audio Electroacoust. vol. AU-15 pp 45-55 June 1967

194 R. N. Bracewell "The Fast Hartley Transform" Procs. IEEE vol. 72 No. 8 pp1010-1018 Aug. 1984

195 R. V. L. Hartley "A More Symmetrical Fourier Analysis Applied to Transmission Problems" Proc. IRE vol. 30 pp144-155 Mar. 1942

196 R. N. Bracewell "The Hartley Transform" Oxford Science Publications 1986 ISBN 0-19-503969-6

197 R. Williams "The Hartley Transform: What's All the Fuss ?" Intelligent Instruments and Computers pp81-84 Mar. 1988

198 M. A. O'Neill "Faster than Fast Fourier" Byte pp293-300 April 1988

199 J. I. Agbinya "Fast Interpolation Algorithm Using Fast Hartley Transform" Proc. IEEE vol. 75 No. 4 pp523-524 April 1987

200 G. E. J. Bold "A Comparison of the Time Involved in Computing Fast Hartley and Fast Fourier Transforms" Proc. IEEE vol. 73 No. 12 pp1863-1864 Dec. 1985

201 C. S. Burrus and T. W. Parks "DFT/FFT and Convolution Algorithms Theory and Implementation" Wiley-Interscience 1985 ISBN 0-471- 81932-8

202 J. Prado "Comments on 'The Fast Hartley Transform' " Proc. IEEE vol. 73 No. 12 pp1862-1863 Dec. 1985

203 A. H. Nuttall "Some Windows with very Good Sidelobe Behavior" IEEE Trans. on Accoustics, Speech and Signal processing Vol. ASSP-29 No.1 pp84-91 Feb. 1981

204 F. J. Harris "On the Use of Windows for Harmonic Analysis with the Discrete Fourier Transform" Proc. IEEE Vol. 66 No. 1 pp51-83 Jan. 1978

205 P. I. Richards "Computing Reliable Power Spectra" IEEE Spectrum pp83-90 Jan. 1967

206 P. D. Stigall, R. E. Ziemer, and L. Hudec "A performance Study of 16-bit Microcomputer-implemented FFT Algorithms" IEEE Micro pp61-66 Nov. 1982

207 R. H. Lord "Fast Fourier for the 6800" Byte pp 108-119 Feb. 1979

208 D. Shear "EDN's DSP Benchmarks" EDN Vol. 33 No. 20 pp126-148 Sept. 29 1988

209 "Digital Signal Processing Applications with the TMS320 Family" Texas Instruments 1986 ISBN 2-86886-009-5

Chapter 9

210 J. G. Welch "A Four Channel Muscle Stimulator Unit" Final Year Project Report No. 87/87 University of Bath May 1987.

Chapter 11

211 T. Springer "Sliding FFT computes frequency spectra in real time" EDN Vol. 33 No. 20 pp161-170 Sept. 29 1988

212 P. Meehan and J. Reidy "FFT Techniques give Birth to Digital Spectrum Analyzer" Electronic Design Vol. 136 No. 18 pp117-122 Aug. 11 1988

Appendix A

213 L. A. Geddes and J. D. Bourland "The Strength-Duration Curve" IEEE Trans. Biomed.Eng. vol BME-32 No 6 pp458-459 June 1985

214 P. K. Thomas and H. B. Morton "The Electromyographic Recording of Intensity-Duration Curves" Electroenceph. clin. Neurophysiol. vol 15 pp691-698 1963

215 G. Oster "Muscle Sounds" Sci. Amer. vol 250 No. 3 pp80-90 1984

216 F. V. Brozovich and G. H. Pollack "Muscle Contraction Generates Discrete Sound Bursts" Biophys. J. vol 41 pp35-40 Jan. 1983

217 G. Oster J. S. Jaffe "Low Frequency Sounds From Sustained Contraction of Human Skeletal Muscle" Biophys. J. vol 30 pp119- 128 Apr. 1980

218 D. T. Barry S. R. Geiringer and R. D. Ball "Acoustic Myography: A Noninvasive Monitor of Motor Unit Fatigue" Muscle & Nerve Mar/Apr 1985 pp 189-194.

219 B. A. Rhatigan K. C. Mylrea E. Lonsdale and L. Z. Stern "Investigation of Sounds Produced by Healthy and Diseased Human Muscular Contraction" IEEE Trans. Biomed. Eng. vol. BME-33 No 10 pp967-971 1986

220 B. Diemont, M. Maranzana Figini, C. Orizio, R. Perini, A. Veicsteinas "Compared Spectral Analysis of Muscular Sound and Surface EMG at Fatigue" Eighth Ann. Conf. of the Eng.in Med. and Biol. Soc. pp526-528 1986

221 B. Diemont, M. Maranzana Figini, C. Orizio, R. Perini, A. Veicsteinas "A Study of Fatigue by Cross Spectrum of Muscular Sound and Surface EMG" Proc. 7th Cong. of Int. Soc. of Electrophysiol. Kiniseology Enschede pp295-298 June 1988.

222 T. Itagaki, K Tai, N. Katsumata and H. Suzuki "Comparison between a New Acceleration transducer and a conventional Force Transducer in the Evaluation of Twitch Responses" Acta Anaesthesiol Scand. vol. 32 pp347-349 1988

223 M. K. Yoshida, L. W. Lamoreaux, M. E. Johanson, R. St. Helen, S. R. Skinner and R. K. Ashley "Quantitative assessment of Patellar Tendon Reflex using an Angular Accelerometer" Proc. 7th Cong. of Int. Soc. of Electrophysiol. Kiniseology Enschede pp371-376 June 1988.

224 A. Th. M. Willemsen, J. A. van Alsté, and H. B. K. Boom "Measuring FES Feedback Parameters with Accelerometers" IEEE Eighth Conf. of the Eng. in Med. and Biol. Soc. pp671-674 1986

225 A. Th. M. Willemsen, J. A. van Alsté, and H. B. K. Boom "Accelerometers and Functional Electrical Stimulation" Proc. 7th Cong. of Int. Soc. of Electrophysiol. Kiniseology Enschede pp105-108 June 1988.

226 J. Lee "Application of Electronics to the Automation of Strength-Duration Curve Measurements" Final Year Project Report No. 53/87 University of Bath May 1987

227 S. Kane "Electronic Intensity-Duration Testing using Kinetic Myology" Final Year Project Report No. 45/89 University of Bath May 1989

228 M. L. Berenson, D. M. Levine and D. Rindskopf "Applied Statistics A First Course" Prentice-Hall Inc. 1988 ISBN 0-13-041476-X 01 pp159-265

Appendix B

229 F. B. Stulen and C. J. De Luca "Muscle Fatigue Monitor: A Noninvasive Device for Observing Localized Muscular Fatigue" IEEE Trans. Biomed. Eng. Vol BME-29 No 12 pp760-768 Dec. 1982

230 L. Basano and P. Ottonello "Real-Time FFT to Monitor Muscle Fatigue" IEEE Trans. Biomed. Eng. vol. BME-33 No 11 pp1049-1051 Nov. 1986

231 L. D. Gilmore C. J. De Luca "Muscle Fatigue Monitor (MFM): Second Generation" IEEE Trans. Biomed. Eng. Vol BME-32 No 1 pp 75-78 Jan. 1985

232 F. B. Stulen and C. J. De Luca "Monitoring Myoelectric Signals" July 22 1980 U.S.Patent 4 213 467

233 F. B. Stulen "Monitoring Myoelectric Signals" July 22 1980 U.S. Patent 4 213 466

234 A. J. Peyton "Circuit for Monitoring the Median Frequency of the Spectrum of the Surface EMG Signal" IEEE Trans. Biomed. Eng. Vol. BME-34 No. 5 pp391-394 May 1987

235 C. G. S. Kramer, T. Hagg and B. Kemp "Real-Time Measurement of Muscle Fatigue Related Changes in Surface EMG" Med. & Biol. Eng. & Comput. pp627-630 Nov. 1987

236 R. Seroussi, M. H. Krag, P. Wilder, and M. H. Pope "The Design of a Microcomputerized Real-Time Muscle Fatigue Monitor Based on the Medial Frequency Shift in the Electromyographic Signal" IEEE Trans. vol. BME-36 No.2 pp284-286 Feb. 1989

237 R. H. T. Edwards and S. Hyde "Methods of Measuring Strength and Fatigue" Physiotherapy vol. 63 No. 2 pp51-53 Feb. 1977

238 H. S. Milner-Brown, M. Mellenthin and R. G. Miller "Quantifying Muscle Strength, Endurance and Fatigue" Arch. Phys. Med. Rehabil. vol. 67 pp530-535 Aug. 1986

Bibliography

239 "The Developers Toolkit" Atari Corporation, Sunnyvale Ca. July 1986

240 K. Geritis, L. Englisch, R. Bruckmann "Atari ST Internals The authoritative insider's guide" Data Becker GmbH 1985 ISBN 0-916439-46-1

241 "MC68000, MC68008, MC68010/12 Programming Pocket Reference Guide" Motorola Ltd. Semiconductor Products Group 1986

242 "ST FastBasic the Basic Interpreter For the Atari ST ROM Cartridge Manual" Computer Concepts 1st Ed. 1986

243 W. A. Triebel and A. Singh "The 68000 Microprocessor Architecture, Software, and Interfacing Techniques" Prentice-Hall 1986 ISBN 0- 13-811357-2

244 "TMS320C025 Users's Guide Preliminary" Texas Instruments 1986 ISBN 2-86886-014-1

245 A. Bateman and W. Yates "Digital Signal Processing Design" Pitman Computer Systems Series 1988 ISBN 0-273-02787-5

246 M. Schwartz and L. Shaw "Signal Processing Discrete Spectral Analysis Detection and Estimation" Mcgraw-Hill Book Company 1975 ISBN 0-07-055662-8